Disclaimer

The ABCB and the Participating Governments are committed to enhancing the availability and dissemination of information relevant to the built environment. Distortional Buckling Behaviour of Cold-formed Steel Compression Members at Elevated Temperature (the Report) is designed in making such information easily available. However neither the ABCB, the Participating Governments, nor the groups or individuals which have been involved in the development of the Report, accept any responsibility for the use of the information contained in the Report and make no warranty or representation whatsoever that the information is an exhaustive treatment of the subject matters contained therein or is complete, accurate, up-to-date or relevant as a guide to action for any particular purpose. Users are required to exercise their own skill and care with respect to its use. In any important matter, users should carefully evaluate the scope of the treatment of the particular subject matter, its completeness, accuracy, currency and relevance for their purposes, and should obtain appropriate professional advice relevant to the particular circumstances.

In particular, and to avoid doubt, the use of the Report does not:

- guarantee acceptance or accreditation of a material by any entity authorised to do so under any law;
- mean that a material complies with the BCA; or
- absolve the user from complying with any State, Territory or Commonwealth regulatory requirements.

The ABCB does not hold any responsibility for the accessibility of the Report or related documents under Web Content Accessibility Guidelines (WCAG 2.0).

DISTORTIONAL BUCKLING BEHAVIOUR OF COLD-FORMED STEEL COMPRESSION MEMBERS AT ELEVATED TEMPERATURES

THANUJA RANAWAKA

Distortional Buckling Behaviour of Cold-Formed Steel Compression Members at Elevated Temperatures

By

Thanuja Ranawaka

School of Urban Developments
Queensland University of Technology

A THESIS SUBMITTED TO THE SCHOOL OF URBAN DEVELOPMENTS
QUEENSLAND UNIVERSITY OF TECHNOLOGY IN PARTIAL
FULFILLMENT OF REQUIREMENTS FOR THE DEGREE OF
DOCTOR OF PHILOSOPHY

SEPTEMBER   2006

KEYWORDS

Light gauge cold-formed steel, distortional buckling, compression members, elevated temperatures, axial compression load, reduced yield strength, reduced elasticity modulus, stress-strain model, fire safety design, fire test, finite element analysis.

ABSTRACT

In recent times, light gauge cold-formed steel sections have been used extensively in residential, industrial and commercial buildings as primary load bearing structural components. This is because cold-formed steel sections have a very high strength to weight ratio compared with thicker hot-rolled steel sections, and their manufacturing process is simple and cost-effective. However, these members are susceptible to various buckling modes including local and distortional buckling and their ultimate strength behaviour is governed by these buckling modes. Fire safety design of building structures has received greater attention in recent times due to continuing loss of properties and lives during fires. Hence, there is a need to fully evaluate the performance of light gauge cold-formed steel structures under fire conditions. Past fire research has focused heavily on heavier, hot-rolled steel members. The buckling behaviour of light gauge cold-formed steel members under fire conditions is not well understood. The buckling effects associated with thin steels are significant and have to be taken into account in fire safety design. Therefore, a research project based on extensive experimental and numerical studies was undertaken at the Queensland University of Technology to investigate the distortional buckling behaviour of light gauge cold-formed steel compression members under simulated fire conditions.

As the first phase of this research program more than 115 tensile coupon tests of light gauge cold-formed steels including two steel grades and five thicknesses were conducted at elevated temperatures. Accurate mechanical properties including the yield strength, elasticity modulus and stress-strain curves were all determined at elevated temperatures since the deterioration of the mechanical properties is one of the major parameters in the structural design under fire conditions. An appropriate stress-strain model was also developed by considering the inelastic characteristics. The results obtained from the tensile coupon tests were then used to predict the ultimate strength of cold-formed steel compression members.

In the second phase of this research more than 170 laboratory experiments were undertaken to investigate the distortional buckling behaviour of light gauge cold-formed steel compression members at ambient and elevated temperatures. Two types

of cross sections were selected with various thicknesses (nominal thicknesses are 0.6, 0.8, and 0.95 mm) and both low and high strength steels (G250 and G550 steels with minimum yield strengths of 250 and 550 MPa). The experiments were conducted at six different temperatures in the range of 20 to 800°C. A finite element model of the tested compression members was then developed and validated with the help of experimental results. The degradation of mechanical properties with increasing temperatures was included in finite element analyses.

An extensive series of parametric analyses was undertaken using the validated finite element model to investigate the effect of all the influential parameters such as section geometry, steel thickness and grade, mechanical properties and temperature. The resulting large data base of ultimate loads of compression members subject to distortional buckling was then used to review the adequacy of the current design rules at ambient temperature. The current design rules were reasonably accurate in general, but in order to improve the accuracy further, this research has developed new design equations to determine the ultimate loads of compression members at ambient temperature. The developed equation was then simply modified by including the relevant mechanical properties at elevated temperatures. It was found that this simple modification based on reduced mechanical properties gave reasonable results, but not at higher temperatures. Therefore, they were further modified to obtain a more accurate design equation at elevated temperatures. The accuracy of new design rules was then verified by comparing their predictions with the results obtained from the parametric study.

This thesis presents a description of the experimental and numerical studies undertaken in this research and the results including comparison with simply modified current design rules. It describes the laboratory experiments at ambient and elevated temperatures. It also describes the finite element models of cold-formed steel compression members developed in this research that included the appropriate mechanical properties, initial geometric imperfections and residual stresses. Finally, it presents the details of the new design equations proposed for the light gauge cold-formed steel compression members subjected to distortional buckling effects at elevated temperatures.

PUBLICATIONS

(a) Conference Papers

1. Ranawaka, T. and Mahendran, M. (2004) Design of Cold-Formed Steel Compression Members Subject to Distortional Buckling at Elevated Temperatures, Proceedings of the 17th International Speciality Conference, Cold-Formed Steel Structures, Orlando, Florida, pp. 225 - 240

2. Ranawaka, T. and Mahendran, M. (2004) Distortional Buckling Test of Cold-Formed Steel Compression Members at Elevated Temperatures, Proceedings of the 18th Australian Conference on the Mechanics of Structures and Materials, Perth, Western Australia, pp. 583 - 588

3. Ranawaka, T. and Mahendran, M. (2005) Fire Safety of Light Gauge Cold-formed Steel Buildings, Proceedings of the Postgraduate Research Conference, Smart Systems, QUT, Brisbane, Australia, pp. 1 - 16

4. Ranawaka, T. and Mahendran, M. (2006) Experimental Investigation of Cold-formed Steel Columns Subject to Distortional Buckling under Simulated Fire Conditions, Proceedings of the 4th International Workshop, Structures in Fire, Aveiro, Portugal, pp. 29 - 40

5. Ranawaka, T. and Mahendran, M. (2006) Mechanical Properties of Thin Steels at Elevated Temperatures, Proceedings of the 4th International Workshop, Structures in Fire, Aveiro, Portugal, pp. 53 – 62

6. Ranawaka, T. and Mahendran, M. (2006) Finite Element Analyses of Cold-formed Steel Columns Subject to Distortional Buckling under Simulated Fire Conditions, Proceedings of the International Colloquium on Stability and Ductility of Steel structures, Lisbon, Portugal, pp. 747 – 755

7. Ranawaka, T. and Mahendran, M. (2006) Cold-formed steel columns under simulated fire conditions, Proceedings of the 19th Biennial Conference on the Mechanics of Structures and Materials, University of Canterbury, Christchurch, New Zealand, pp. 485 – 491

(b) Journal Papers

1. Ranawaka, T. and Mahendran, M. (2006) New Design Equation for the Mechanical Properties of Light gauge Cold-formed Steels at Elevated Temperatures, Fire Safety Journal, (Submitted for review)

2. Ranawaka, T. and Mahendran, M. (2006) Experimental Studies of Light gauge Cold-formed Steel Compression Members Subjected to Distortional Buckling at Elevated Temperatures, Journal of Constructional Steel Research, (Submitted for review)

3. Ranawaka, T. and Mahendran, M. (2006) Numerical modelling of Light gauge Cold-formed Steel Compression Members Subjected to Distortional Buckling at Elevated Temperatures, Thin-Walled Structures, (In preparation)

4. Ranawaka, T. and Mahendran, M. (2006) New Design Methods for Light gauge Cold-formed Steel Columns Subjected to Distortional Buckling at Ambient and Elevated Temperatures, Engineering Structures, (In preparation)

TABLE OF CONTENTS

LIST OF FIGURES

LIST OF TABLES

ABBREVIATIONS

A	cross sectional area
A_e	effective cross section area
b	plate width or (flange width)
b_e	effective plate width
BMT	Base Metal Thickness
C_p	Correction factor depending on the number of tests
d	lip length
E (E_{20})	elasticity modulus at ambient temperature
E_T	elasticity modulus at temperature T
f_{crl}	local buckling stress
F_m	mean of the fabrication factor
f_n	ultimate stress
f_{od}	distortional buckling stress
f_{odT}	distortional buckling stress at temperature T
f_{pT}	proportional limit at temperature T
f_u	ultimate tensile stress
f_y (f_{y20})	yield strength at ambient temperature
f_{yT}	yield strength at temperature T
h	web height
k_{ET}	reduction factor of elasticity modulus
k_{yT}	reduction factor of yield strength
L	length
m	degree of freedom (n-1)
M_m	Mean of the material factor
n	number of tests
N	Section capacity
N^*	design axial compression force
P_E	elastic buckling load
P_i	buckling load of imperfect plate
P_m	mean value of the tested to predicted load ratio
P_n	nominal axial load
P_{nT}	nominal axial load at temperature T
P_{od}	distortional buckling load
P_{odT}	distortional buckling load at elevated temperature
P_p	buckling load of perfect plate
P_u	applied axial load

P_y	crushing load
r	radius of gyration
s	stiffener length
T	temperature
t	thickness
TCT	Total Coating Thickness
V_f	coefficient of variation of the fabrication factor
V_m	coefficient of variation of the material factor
V_p	Coefficient of variation of the tested to predicted load ratio
V_q	coefficient of variation of load effect
$\varepsilon_{T\pi}$	strain at the proportional limit at temperature T
α	residual stress reduction factor
β	constant for Ramberg-Osgood model
$β_0$	Target reliability index
Δ	magnitude of initial imperfection
$δ$	out-of-plane displacement
$δ_U$	displacement at 85% of the ultimate load on the descending curve
$δ_Y$	displacement of the specimen at yield)
ε	strain
ε_{ln}^{pl}	logarithmic plastic strain
ε_{nom}	nominal strain
ε_T	strain at temperature T
ε_y	strain at yield stress
ε_{yT}	strain at yield stress at temperature T
$η_T$	parameter for Ramberg-Osgood model at temperature T
$λ$	slenderness ratio
$ρ$	ratio of effective width to actual width of the plate
$σ$	stress
$σ_{nom}$	nominal stress
$σ_{true}$	true stress
Φ	the capacity reduction factor

STATEMENT OF ORIGINAL AUTHORSHIP

The work contained in this thesis has not been previously submitted for a degree or diploma at any other higher education institution. To the best of my knowledge and belief, the thesis contains no material previously published or written by another person except where due reference is made.

Signed: _____

Date: _____

ACKNOWLEDGEMENTS

1 Introduction

1.1 General

In recent times, light gauge cold-formed steel sections have been used extensively in residential, industrial and commercial buildings (see Figure 1.1 (a)) as primary load bearing structural components. Cold-formed steel sections have a very high strength to weight ratio compared with thicker hot-rolled steel sections. The manufacturing process of cold-formed steel sections is very simple. A thin flat sheet element is converted to different shapes of cross sections (see Figure 1.2) at room temperature, and substantial rigidity, strength and necessary structural qualities are obtained without increasing the thickness. Three methods are used as roll forming, press break operation and bending break operation to manufacture cold-formed steel sections. Roll forming method is used to produce large quantities from one section while press braking method is used to produce small quantities from various sections. The initial cost of roll forming method is higher than the press braking method. However, it is economical to produce large amounts of one shape from roll forming method.

The use of cold-formed steel sections leads to innovative designs for specific architectural purposes, civil and structural work (see Figure 1.1 (b)), and is an economical design solution. Recent research and development works have found hot-rolled steel structures to be less economical when compared with light gauge cold-formed steel structures. Furthermore, light gauge cold-formed steel sections have the following advantages:

- Ease of prefabrication and mass production
- Uniform quality
- Low self weight
- Economy in transportation and handling
- Fast and simple erection or installation
- Improved technology of manufacture and corrosion protection
- Non-shrinking and non-creeping at ambient temperature

♦ Improved production of complex shapes (since modern rolling lines are computer controlled, the highly accurate complex sections can be made.)

(a)   Residential uses (from AISI, 2003)

(b)   Architectural and structural uses (from AISI, 2003)

Figure 1.1   Uses of Light Gauge Cold-formed Steel Members

These advantages have led to cold-formed steel structures replacing conventional hot-rolled steel structures in many cases in the building construction industry. Development and usage of cold-formed steel structural members came to use in building construction in about the 1850s in the United States and Great Britain. However, they were not widely used in building structures until 1940 (Yu, 2000). Today most developed countries increasingly use cold-formed steel framing systems

for houses and other low-rise constructions. Pekoz (1999) states that in the USA 500 homes were built in light gauge steel in 1992, 15,000 in 1993 and 75,000 in 1994. Further, it continues to increase.

(a)   Studs or joist

(b)   Other shapes
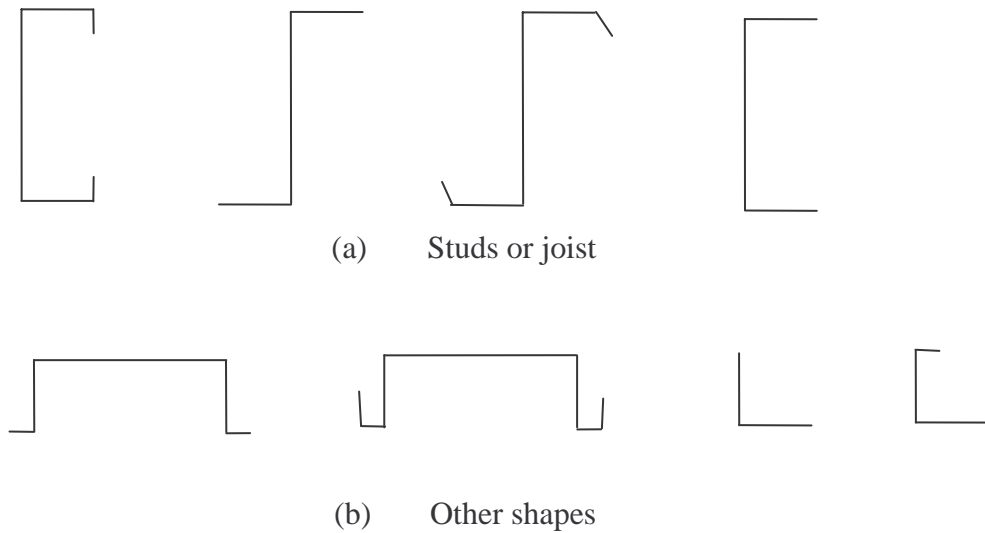
Figure 1.2   Cold-formed Steel Cross Sections

With the rapidly increasing usage of cold-formed steel structures, research into their applications and understanding of their structural behaviour have increased significantly since the first specification of cold-formed steel design was issued by the American Iron and Steel Institute (AISI) in 1946. The light gauge cold-formed steel members encounter some design problems not normally seen in the traditional thicker hot-rolled steel members. For example, buckling is a serious issue leading to their failure modes.

1.2 Properties of light gauge cold-formed steel

Light gauge cold-formed steel sheets have thicknesses ranging from 0.4 to 6.4 mm (Yu, 2000). The nominal yield strength of available cold-formed steels ranges from 250 to 550 MPa. The yield strength of cold-formed steel is determined based on 0.2% proof stress (see Figure 1.3). The modulus of elasticity is determined from the slope of the graph and it is approximately 200,000 MPa.
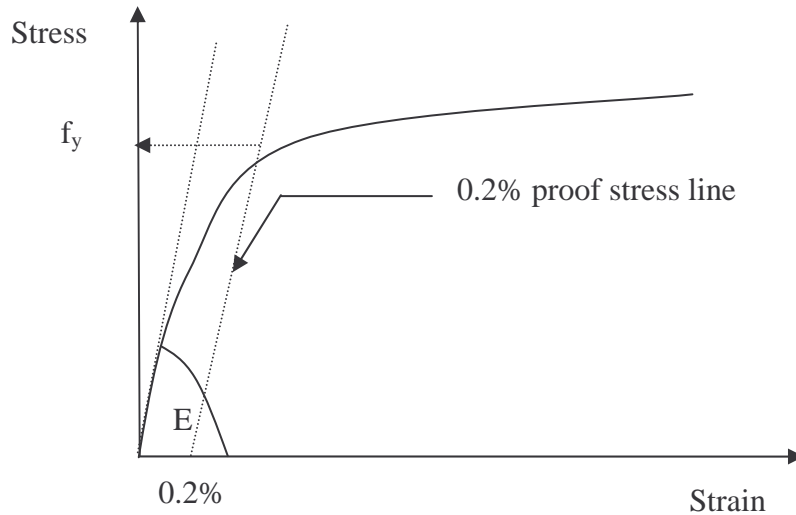
Figure 1.3   Stress-strain Curve of Cold-formed Steel

1.3 Compression members

Unfortunately, the behaviour of cold-formed steel structures is more complex than that of traditional hot-rolled steel structures. Research between 1940 and 1950 has highlighted that cold-formed steel members are subjected to various buckling modes including local, distortional and global modes, and their ultimate strength behaviour is governed by these buckling modes. As an example, a short concentrically loaded C-section almost always fails because of a combination of local buckling of thin plate elements and distortional buckling of the edge stiffeners while the failure mode of longer columns is often governed by a combination of global buckling and local or distortional buckling. Although cold-formed steel members have been researched for a long time, the stability problem is not fully understood.

Previously, most research has been concerned with local and global buckling modes and there is a wealth of knowledge on this aspect at ambient temperature. This knowledge and understanding is reflected in the various design rules in national or international design standards or specifications required to achieve an economical and safe design. Many solutions have been presented in some national and international standards such as Eurocode 3: Part 1.3 (ECS, 1993), British Standard Part 5 (BSI, 1990), Australian/New Zealand Standard, AS/NZS 4600 (SA, 1996) and

American Specification (AISI, 1996), and in many research papers. However, there is a lack of research on the relatively new distortional buckling mode of cold-formed steel members and its interaction with other modes. Further, no exact method has been finalised yet to design light gauge cold-formed compression members failing from distortional buckling mode.

1.4   Fire damages

The structural design to withstand fire effects came to prominence with the great fire in London in 1666. Unfortunately structures can accidentally catch fire or be deliberately set on fire which can cause loss of life and property, not only because of fire but also due to the structural failure of buildings (see Figures 1.4 and 1.5). However, fire damage of low-rise buildings and dwelling units is greater than the fire damage of high-rise buildings. On the other hand, cold-formed steel structures are mainly used for low-rise building and dwelling units. Light gauge cold-formed steel structures heat up quickly and reduce their stiffness and strength under fire conditions due to the thinness of materials. Therefore, the fire safety design of building structures has received greater attention in recent times and there is a need to assess the performance of light gauge cold-formed steel structures under fire conditions.

Figure 1.4   Failure of Structures due to Fire (from http://www.twin-towers.net/collapse.htm)
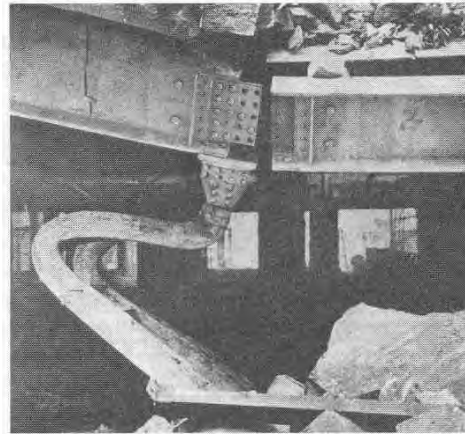
Figure 1.5   Local and Global Buckling of Columns under Fire

Although some past research has focussed on fire, it has focused predominantly on heavier, hot-rolled steel members, and not on light gauge cold-formed steel structures. On the other hand, the mechanical properties of cold-formed steel at elevated temperatures are different from hot-rolled steel. Although cold-formed steel has a strengthening effect at normal temperature, it is reduced with the temperature rise. According to Feng et al. (2003a) cold-formed steel shows 20% higher reduction of strength at elevated temperature than hot-rolled steel. Further, most thin-walled members are exposed to fire on one side due to the nature of the fire protection design methods of buildings. Thus, the temperature distribution of thin-walled steel members is highly non-uniform and different from hot-rolled steel members. Further, fire design methods of light gauge cold-formed steel structures are mainly based on the results of the manufacturers' standard fire tests and hence, it is expensive. The buckling behaviour of cold-formed steel structures becomes more complicated at elevated temperatures due to the non-linear stress-strain relationship of cold-formed

steel. Thus, it is very important to investigate the structural behaviour of cold-formed steel structures at elevated temperatures.

1.5 Problem definition

The structural behaviour of light gauge cold-formed steel members under fire conditions is not well understood. Distortional buckling effects of these members are significant and have to be taken into account in fire safety design. However, the effects of fire conditions on the distortional buckling behaviour of such members are not known. Currently there is little research on the relatively new distortional buckling mode of light gauge cold-formed steel members even at ambient temperatures. Therefore this research will include both experimental and numerical analyses to investigate the distortional buckling behaviour of light gauge cold-formed steel compression members under fire conditions.

In addition, the mechanical properties of cold-formed steel at elevated temperatures were not investigated accurately. Although Lee et al. (2003) presented some design equations at elevated temperatures, their experimental methods were not adequate and therefore their equations should be further modified and improved.

Although Feng et al. (2003a and b) have carried out some experiments of distortional buckling of cold-formed steel members at elevated temperatures, they were unable to achieve the required results due to some practical difficulties. Their research was not aimed at developing design rules for fire conditions and also did not consider higher strength steels that are commonly used in Australia.

Australian/New Zealand Standard, AS/NZS 4600 (SA, 1996) has addressed cold-formed steel members subject to distortional buckling effects. However, it is limited to some specific sections and only considered ambient temperature. The British Standard for fire resistance design of steel structures, BS 5950 Part 5 (BSI, 1990) has addressed the design of cold-formed steel structures. But there are no specific rules or specifications regarding the distortional buckling behaviour of cold-formed steel members at elevated temperatures or even at ambient temperature.

Further, the direct strength method proposed by Schafer and Pekoz (1998) addressed the distortional buckling mode of cold-formed steel compression members. However, it is limited to ambient temperature and only pin-end conditions are considered.

The current Australian Standard, AS 4100 (SA, 1998), has addressed the variation of material properties at elevated temperatures, but only for thicker hot-rolled steel, and is too conservative for the light gauge cold-formed steel. Although Eurocode 3 Part 1.2 (ECS, 1993) has addressed the material properties of cold-formed steel at elevated temperatures, there is no difference between the reduction factors of hot-rolled and cold-formed steels. It does not include any design rules for distortional buckling failures.

Kesti and Davies (1999) carried out the analysis of distortional buckling with respect to different end conditions. However they have not addressed it for elevated temperatures nor provided any exact method to determine the distortional buckling behaviour of compression members.

The well known buckling analysis program Thin-wall is only applicable for simply supported conditions, and hence does not permit the analysis of distortional buckling behaviour of steel compression members with other end conditions.

Some researchers argued that a high post-buckling strength exists after the elastic distortional buckling failure whereas others argued that the post-buckling capacity for distortional mode is very small. However, it should be further investigated.

Chapter 2 "literature review" suggests that the above problems have still not been solved yet.

1.6 Objectives

Overall objective

The overall objective of this research is to develop suitable design rules for the safe and economical design of light gauge cold-formed steel compression members under fire conditions with respect to the relatively new distortional buckling failure mode of two types of cold-formed steel sections.

Specific objectives

- To investigate the mechanical properties for low (f_y<450 MPa) and high (f_y≥450 MPa) strength light gauge cold-formed steels at ambient and elevated temperatures and develop new design equations so that the reduced mechanical properties can be used in the design rules for the fire safety of cold-formed steel structures. Additionally, to develop the stress-strain characteristics of light gauge cold-formed steels at ambient and elevated temperatures.

- To develop suitable experimental designs including test sections, end supports, and test set-up for the buckling tests of light gauge cold-formed steel compression members under ambient and elevated temperatures and undertake the required distortional buckling tests.

- To conduct a comparative study of distortional buckling behaviour of light gauge cold-formed steel compression members with respect to the pin-end and fixed-end conditions.

- To develop buckling analysis results based on the well known finite strip analysis program Thin-wall that can be used to develop suitable test geometry and to validate finite element models.

- To develop advanced finite element models capable of simulating the elastic buckling and non-linear ultimate strength behaviour of light gauge cold-

formed steel compression members under ambient and elevated temperatures using the finite element program ABAQUS and validate them using experimental results.

♦ To investigate the distortional buckling behaviour of light gauge cold-formed steel members at ambient and elevated temperatures under axial compression loads using simulated fire tests and numerical modelling.

♦ To undertake a detailed parametric study using the validated finite element model to extend the database on the structural performance of light gauge cold-formed steel compression members involving distortional buckling at both ambient and elevated temperatures.

♦ To investigate the influence of various parameters on the behaviour of distortional buckling mode at both ambient and elevated temperatures.

♦ To investigate the applicability of current design equations in predicting the ultimate loads of cold-formed steel compression members subjected to distortional buckling at both ambient and elevated temperatures

♦ Using the extended data base of ultimate loads obtained from the parametric study and the associated improved knowledge and understanding on the topic, to develop improved and more accurate design equations for light gauge cold-formed steel compression members subjected to distortional buckling at both ambient and elevated temperatures for possible inclusion in national and international cold-formed steel structures and fire safety codes.

1.7   Contents of the Thesis

The outline of this thesis is as follows:

Chapter 1 presents the general introduction of cold-formed steel structures and their behaviour at ambient and elevated temperatures; fire damage of steel

structures and fire behaviour. Further, it defines the current situation of light-gauge cold-formed steel compression members with respect to the distortional buckling behaviour and the objectives of this research.

Chapter 2 presents the literature review findings based on this investigation. It describes the distortional buckling behaviour of cold-formed steel members at ambient temperature as well as at elevated temperatures, fire effects on the mechanical properties of cold-formed steel and testing methods of compression members at ambient and elevated temperatures.

Chapter 3 presents the experimental investigation of mechanical properties at ambient and elevated temperatures. Both compression and tension coupon tests were included at ambient temperature while only tension coupon test results were presented at elevated temperatures. New design equations were presented including the range of thicknesses and steel grades used in this research.

Chapter 4 presents the experimental investigation of distortional buckling of compression members at ambient and elevated temperatures.

Chapter 5 presents the details of finite element analyses and validation of the finite element model. The results are compared with experimental test results and presented.

Chapter 6 presents the detailed parametric study for two types of steel sections and the development of new design rules.

Chapter 7 presents the significant findings from this research and recommendations for further research.

2 Literature Review

2.1 Behaviour of Cold-formed Steel Structures at Ambient Temperature

2.1.1 General Buckling Modes

Mainly, three types of buckling behaviour can be observed in cold-formed steel compression members. They are called, local, distortional and flexural or flexural torsional buckling. In addition to these three main types their interactions can also occur as local and distortional, local and flexural, distortional and flexural, and local distortional and flexural. The Thin-wall computer program which was developed at the University of Sydney and CUFSM software which was developed by Schafer (2002) can be directly used to observe these buckling modes (see Section 2.1.3).

2.1.1.1 Local buckling

Local buckling occurs in the slender plate elements without changing the position of longitudinal edges of compression members. On the other hand, it occurs due to the buckling of individual plate elements. Local buckling is a common buckling failure in compression members, which is made of slender plate elements. The cross section and the typical failure mode are shown in Figure 2.1. The half-wave-length of the local buckling mode is the shortest one among the other failure modes. Since local buckling has a higher post buckling range, it is not considered as failure of the whole column when columns buckle locally. However, if the column is pin-ended it might have an additional moment after local buckling due to the shift in the line of axial force.

Longitudinal edges have not moved

(a)   Analytical result   (b)   Experimental result
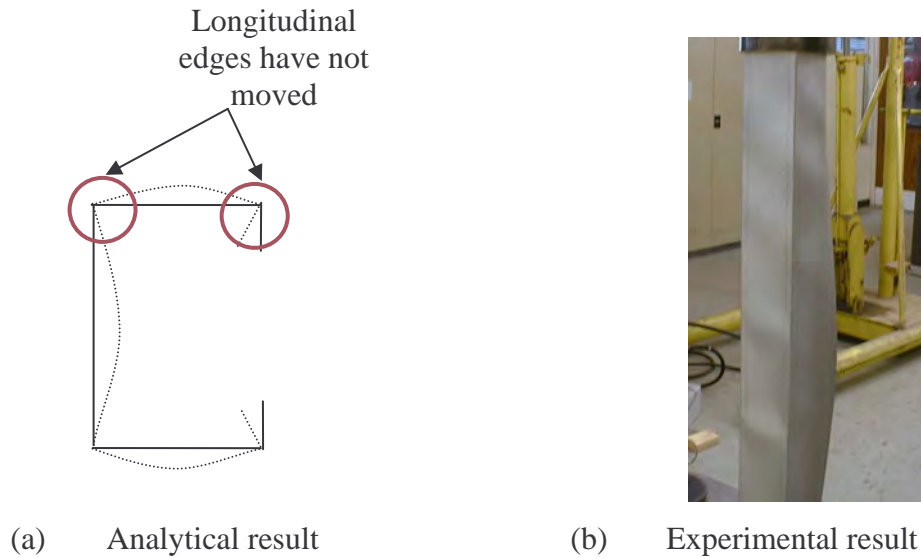
Figure 2.1   Local Buckling Mode of Compression Members

2.1.1.2   Distortional buckling

Distortional buckling mode is a relatively new and less researched buckling mode compared to the other buckling modes. It is also known as stiffener buckling or local-torsional buckling. It occurs due to the rotation of the flange at the flange-web junction for the members with edge stiffeners (see Figure 2.2) and displacement of the intermediate stiffeners normal to the plane of the element for the intermediately stiffened members. However, the buckling of lipped channels with narrow flanges show lateral bending of the whole cross section while the flange web junction of the buckling of lipped channels with wide flanges remain nearly straight. Distortional buckling exists at an intermediate half-wave-length between local buckling and flexural or flexural torsional buckling. However, the distortional buckling can be safely ignored if members are designed to achieve significantly lower local buckling stress than the distortional buckling stress. Most probably, members with narrow flanges fail by local buckling mode since, the web is much slender and buckles locally first, while members with wide flanges buckle distortionally. However, by introducing the stiffeners to the web, narrow flange members can buckle distortionally.
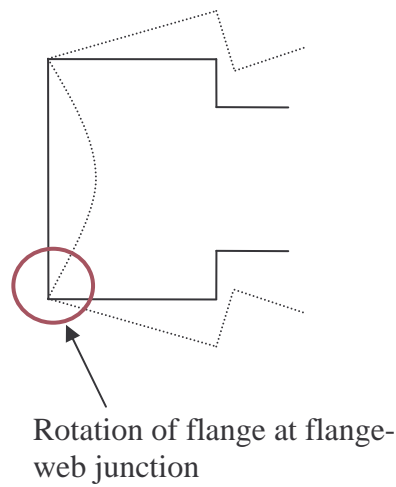
| (a) | Analytical result | (b) | Experimental result |

Figure 2.2   Distortional Buckling Mode of Compression Members

2.1.1.3   Flexural buckling

Most commonly flexural buckling mode is known as global buckling. Since the behaviour is similar to the behaviour of beams this is known as flexural or flexural torsional buckling. In flexural buckling, the cross sectional shape remains unchanged and it has only lateral or lateral torsional movements (see Figure 2.3). This buckling mode is sometimes called rigid-body buckling since the cross section remains the same at any given section after global buckling occurs. The lateral deflection of the flexural mode is larger than the local and distortional mode. The half-wave-length of the flexural mode is the largest among the buckling modes. The half-wave-length is equal to full column length if it is pin-ended and half of the full length if it is fixed-ended.

This research was focussed on investigating the relatively new and less researched distortional buckling mode of light gauge cold-formed steel compression members. The literature review is therefore aimed at determining the current situation of the knowledge of distortional buckling behaviour. Thus, the following section describes the previous research on distortional buckling.

(a) Flexural
buckling

(b) Flexural
torsional buckling

(c) Flexural failure of
column
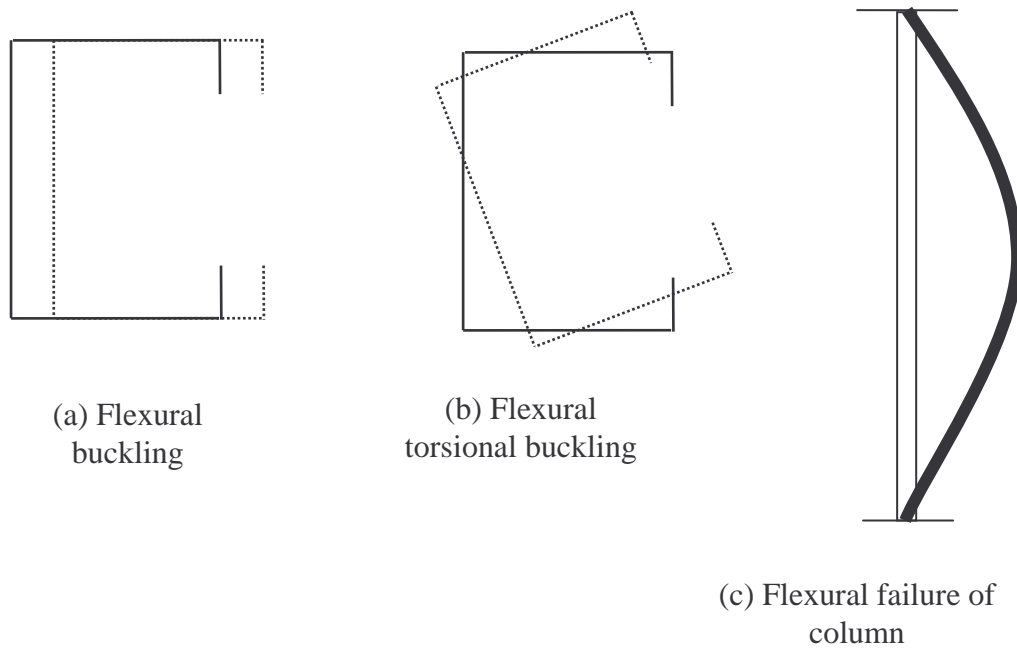
Figure 2.3   Flexural Buckling Mode of Compression Members

2.1.2   Previous Research on Distortional Buckling

Thomasson (1978) tested 0.63 mm lipped channel sections with two stiffeners in the web and observed the uncommon failure mode of the intermediate stiffeners buckling in distortional mode (see Figure 2.4). Hancock (1998) has stated that cold-formed steel members show stability problems which are uncommonly encountered in normal structural design. Although cold-formed steel members have been researched for a long time, their stability problem is still not well understood.
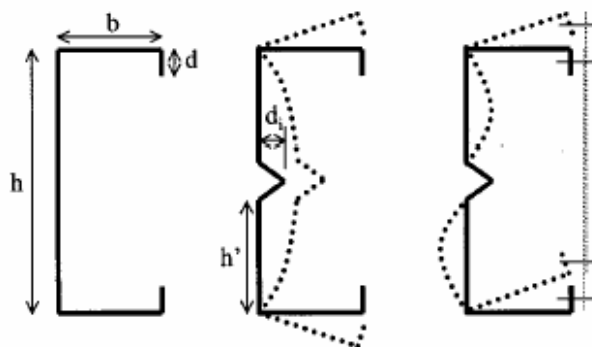
Figure 2.4   Cross Sections Tested by Thomasson (1978)-(from Schafer 2002)

Most experiments regarding distortional buckling failure were carried out at the University of Sydney by Lau and Hancock (1987) and Kwon and Hancock (1992a and b), and are summarised in Hancock et al. (1994). They have considered various types of cross sections: a) lipped channels, b) rack column uprights, c) rack column uprights with additional outward edge stiffeners, d) hats and e) lipped channels with web stiffeners (see Figure 2.5).
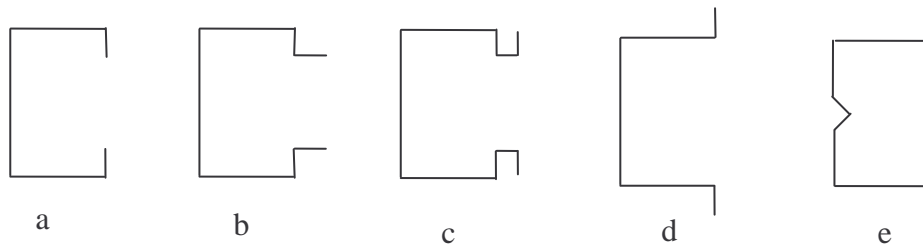
Figure 2.5   Sections used by the University of Sydney Researchers

Hancock (1985) presented a series of experimental results for lipped channel sections in compression by considering all the buckling modes: local, distortional and flexural. He showed that distortional buckling controls the design of some geometric sections with rear flanges or lipped rear flanges. Further, he has presented a detailed design chart to compute the critical distortional buckling stress of channel columns for the geometries of simple lipped channel, rack column upright with rear flanges and rack column upright with rear flanges with additional lip stiffeners.
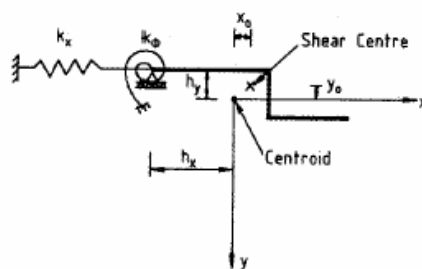
Figure 2.6   Effect of Web on the Flange Behaviour
(from Lau and Hancock, 1987)

Lau and Hancock (1987) used Hancock's (1985) design charts and presented some expressions to determine the elastic distortional buckling stress of channel columns, which were included in the Australian / New Zealand design code (SA, 1996). Since

distortional buckling mainly occurs due to the rotation and lateral bending of the flanges, these expressions have been derived by considering only the flanges. The effect of the web on the flanges has been considered as a lateral spring and a rotational spring as shown in Figure 2.6 to derive those expressions.

Further, Lau and Hancock (1988) have proposed an equation to determine the inelastic distortional buckling stress based on the assumption of a parabolic relation between inelastic buckling stress and column slenderness ratio. The proposed design formula is expressed as follows (Equation 2.1).

$$f_n = f_{od} \qquad\qquad\qquad \text{for} \quad f_{od} < \frac{f_y}{2}$$

$$f_n = f_y\left(1 - \frac{f_y}{4f_{od}}\right) \qquad\qquad \text{for} \quad f_{od} \geq \frac{f_y}{2}$$

(2.1)

where, f_{od} and f_n are the elastic and inelastic distortional buckling stresses, respectively.

Lau and Hancock (1988) further showed that the post buckling capacity is very low when the elastic failure occurs by distortional mode. Schafer and Pekoz (1998) also supported this statement. They stated that distortional buckling failures have a lower post-buckling capacity than local buckling failures. Distortional buckling may control the failure mechanism even though the elastic distortional buckling stress is higher than the elastic local buckling stress and distortional buckling failure has higher imperfection sensitivity. The analysis of lipped channel columns Schafer (1997) also supports this conclusion. However, Kwon and Hancock (1993) argued that significant post-buckling strength exists after the elastic distortional buckling failure in a similar manner to local buckling. However this phenomenon may depend on the geometry of the section and it should be further investigated.

Kwon and Hancock (1992b) have studied the behaviour of simple lipped channels and lipped channels with intermediate stiffeners under fixed boundary conditions. They showed that the design equations in the American Specification (AISI, 1996) are unconservative for predicting the distortional buckling strength of channel sections made of high strength steel and there should necessarily be an alternative

method for distortional buckling. Further, Kwon and Hancock (1992b) suggested that the load carrying capacity of the compression members is greatly reduced with the presence of initial imperfection, in particular, on both the magnitude and mode of geometric imperfection. If the stresses of the various buckling modes are close to each other, the buckling behaviour is more complicated with the presence of imperfection.

Figure 2.7   Sections used by Kwon and Hancock (1992b)

Further, Kwon and Hancock (1992b) described the application of theoretical methods to predict the post buckling behaviour and the influence of interaction of various buckling modes including imperfection sensitivity by using the test results of channel columns used by Kwon and Hancock (1992a). A non-linear elastic spline finite strip method was used for these theoretical predictions. The results obtained from the experiments show good agreement with the analytical results, which were obtained from the spline finite strip method for some sections while others have variations. However, only limited cold-formed steel sections (see Figure 2.7) made of 1.1 mm thickness and grade G500 steel were considered in their experimental and analytical investigations.

Kwon and Hancock (1992a) expanded Lau and Hancock's (1988) equation (Equation 2.1) to determine the distortional buckling stress or the interaction of local and distortional buckling for thin steel slender sections, which was included in AS/NZS 4600 (SA, 1996). They allowed considerable post buckling strength for distortional or interaction modes. Their expression for the ultimate stress, σ_{max} is given by Equation 2.2. However, they considered limited cross sections and high strength steels with 1.2 mm thickness. Figure 2.8 shows the comparison of test results and Equation 2.2 as given in Kwon and Hancock (1992a). As shown in Figure 2.8, they used limited number of test results to develop their equations. Therefore the validity of their equations to other sections should be investigated.
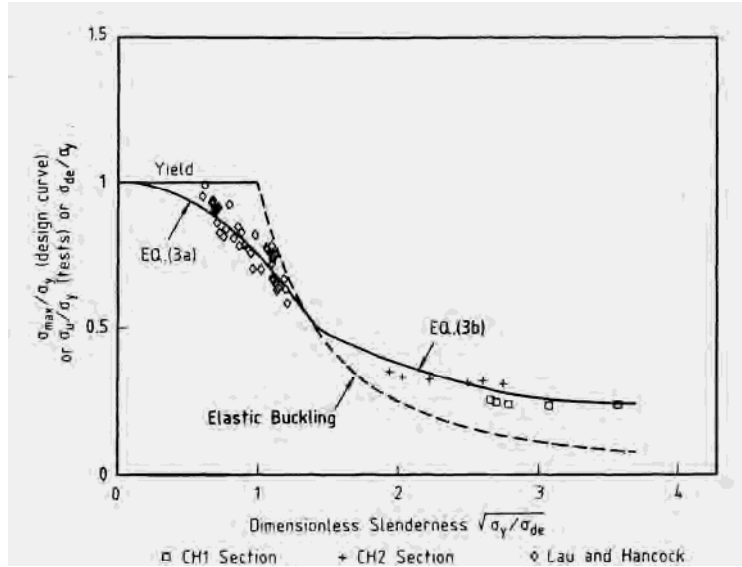
**Figure 2.8   Comparison of Equation 2.2 with Test Results
(Kwon and Hancock, 1992a)**

$$f_n = f_y \left(1 - \frac{f_y}{4 f_{od}} \right) \qquad\qquad f_{od} \geq \frac{f_y}{2}$$

$$f_n = f_y \left(0.055 \left(\sqrt{\frac{f_y}{f_{od}}} - 3.6 \right)^2 + 0.237 \right) \qquad \frac{f_y}{13} \leq f_{od} \leq \frac{f_y}{2}$$

(2.2)

where, f_{od} :- Elastic distortional buckling stress or elastic buckling strength for the interaction of local and distortional modes

In addition Kwon and Hancock (1992a) proposed an alternative effective width formula based on Winter formula to design for distortional buckling and is given by Equation 2.3. However, AS/NZS 4600 recommends only Equation 2.2 and used gross cross sectional area rather than effective area. The direct strength method proposed by Schafer (2000) is similar to Equation 2.3 (see Section 2.1.5.2).

$$\frac{b_e}{b} = 1 \qquad\qquad \lambda \leq 0.561$$

$$\frac{b_e}{b} = \left(\frac{f_{od}}{f_y} \right)^{0.6} \left(1 - 0.25 \left(\frac{f_{od}}{f_y} \right)^{0.6} \right) \qquad \lambda \geq 0.561$$

(2.3)

$$\text{where, } \lambda = \sqrt{\frac{f_y}{f_{od}}}$$

The strength of pin-end column is clearly lower than that of the fixed-end column when the column fails by local buckling mode. This is because of the additional moments in the case of pin-end columns due to the shift of the line of action of the internal force when the section is locally buckled. However, this is only for local buckling and the effect on the behaviour of distortional buckling under pinned and fixed-end conditions is not known. According to Young and Rasmussen (1995), research work has been carried out for pin-end channel columns between 1970 and 1980. Kloppel and Bilsten (1976) and Rhods and Harvey (1977) have carried out some tests for pin-end cold-formed plain channel columns while Rasmussen and Hancock (1989) carried out tests on welded plain channel columns.

Young and Rasmussen (1995) described the experimental behaviour of pin-end and fixed-end lipped channel columns with respect to pure local buckling, distortional buckling, overall flexural buckling and flexural torsional buckling modes. However, their research was limited to two geometric lipped channel sections and G450 steel with 1.5 mm thickness. According to their research, a column, which buckles distortionally gives nearly the same strengths for pin-end and fixed-end conditions.

On the other hand, Kesti and Davies (1999) conducted research into the local and distortional buckling behaviour of thin-walled short columns. They compared the minimum elastic distortional buckling stresses obtained using different methods, and demonstrated the influence of support conditions on the strength of short columns with C, hat and rack upright.

Analytical and numerical methods were used to determine the elastic distortional buckling stress of singly symmetric cross sections. Two analytical methods have been presented:

1. Eurocode 3 (ECS, 1993) method – based on the flexural buckling of the stiffener.
2. Model developed by Lau and Hancock (1987) – based on flexural torsional buckling of a simple flange including a stiffener (used in AS/NZS 4600).

These methods show that the end boundary conditions have a significant influence on the distortional buckling behaviour and compression capacity of short columns. The analysis was based on Generalised Beam Theory (GBT), which showed that the elastic distortional buckling stress of the fixed-end column is much greater than that of the pin-end column.

Kwon and Hancock (1992a) have tested channel sections under fixed-end conditions. A much higher buckling stress was observed for fixed-end conditions than the simply supported conditions. However, the effect of fixed-end decreased with the increasing of number of half wave buckles. Yang and Hancock (2003) and Young and Hancock (2003) also agreed with this and they mentioned that the end effect is little for long columns with small lips. Further, Kwon and Hancock (1992a) showed that the local buckling strength of lipped channels can be increased by introducing the longitudinal stiffeners to the web and then the failure is governed by distortional buckling. The experimental results of Thomasson (1978) also supported this argument. Schafer (2000) proved this with lipped C-sections. Kesti (2000) has also proved this by using C-sections and showed that a number of distortional buckling modes occur due to additional stiffeners in the web.

Davies and Jiang (1996) suggested that distortional buckling has weak interaction with other modes and the interaction between local and distortional buckling should be taken into account. Davies and Jiang (1998) used the Generalised Beam Theory to analyse the various buckling modes either separately or in selected combinations. However, their analysis work was not aimed at developing equations.
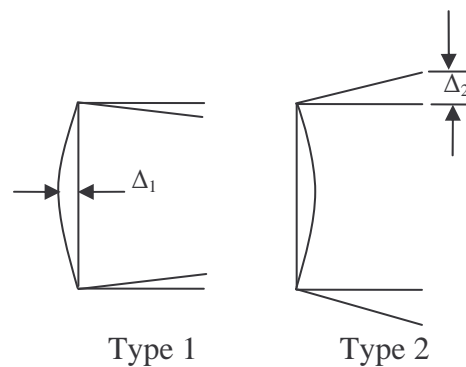
Figure 2.9   Definition of Geometric Imperfections

Geometric imperfection is the deviation of a section from its perfect geometry. According to Kwon and Hancock (1992a), initial geometric imperfection shows considerable influence on the distortional buckling behaviour. Schafer and Pekoz (1998) describes the geometric imperfection and residual stresses of cold-formed steel members based on the data from previous research. The initial imperfection was presented in two ways as shown in Figure 2.9. They are only for cold-formed steel members with a thickness less than 3 mm.

Type 1 Maximum local imperfection in a stiffened element

Type 2 Maximum deviation from straightness for a lip stiffened or unstiffened flanges

The maximum initial imperfection of Type 1 is given as $\Delta_1 = 6te^{-2t}$ or $\Delta_1 = 0.006b$ (b = width of the plate and t = thickness) while the maximum initial imperfection of Type 2 is approximately equal to the plate thickness. However, according to Ala-Outinen and Myllymaki (1995) and Kaitila (2002) the maximum initial imperfection is about b/200. Further, Walker (1975) presented an expression to determine the initial imperfection, which is given here as Equation 2.4.

$$\Delta = 0.3b\sqrt{\frac{12f_y\left(1-\nu^2\right)}{k\pi^2 E}}$$
(2.4)

However, Walker's equation and that used by Ala-Outinen and Myllymaki (1995) and Kaitila (2002) did not consider thickness of cold-formed steel members although the thickness plays an important role in the initial imperfection due to the cold-forming process. Hence, it is better to use the measured initial imperfection values for analyses. There is a need to develop acceptable initial imperfection levels for numerical analyses of cold-formed steel members. Further, more details of initial imperfections are presented in Chapter 5 of this thesis.

Local buckling behaviour is relatively straightforward so that when the width-to-thickness ratio increases local buckling stress declines. However, there is no specific trend in the distortional buckling behaviour. Therefore, Schafer (2000) examined a series of lipped C-sections to study the behaviour of distortional buckling stress with

respect to the flange width, lip length and web depth separately. He observed that too narrow (flange width less than approximately 1/6 of the web height) or too wide (flange width greater than approximately 3/4 of the web height) flange gives lower distortional buckling stresses for C-sections. When the flange is too narrow the local buckling of the web and the distortional buckling of the flange show nearly equal half wave lengths thus, distortional buckling can form at low stresses. Further, when the flange is excessively wide distortional buckling forms at low stresses. The maximum buckling stress is given when the b/h ratio is about 1/3 (b = flange width, h = web height). Further, he observed that the longer lips are usually better and the maximum distortional buckling stress can be achieved when the lip length is nearly equal to the flange width (d/b ≈ 1, d = lip length). He also observed that the distortional buckling stress is reduced for deeper webs. Further, he showed that when h/t < 100, the failure mode of typical C and Z-sections is governed by distortional buckling. In this study the distortional buckling stress was calculated using closed-formed expressions derived by Schafer (1997). However, he could not adequately investigate the distortional buckling behaviour with respect to the interaction of flange, web and lip elements due to its complex nature.
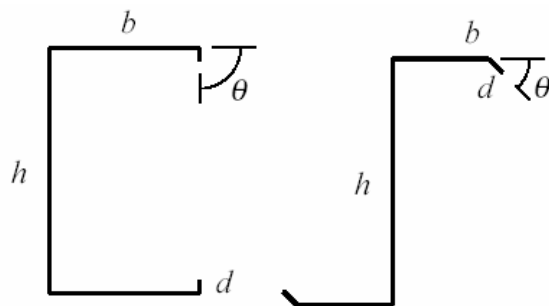
Figure 2.10   Cross Sections used by Schafer (from Schafer, 2000)

Schafer (2000) presented the new direct strength method. He carried out a parametric study of 170 cross-sections (see Figure 2.10) to determine the accuracy of available hand methods in predicting the local, distortional and global buckling modes. Groups of C's and Z's were studied including the sections listed in AISI (1996) and commercially available dry wall studs. Schafer's (1997), Lau and Hancock's (1987) and AISI (1996) methods were used to predict the elastic distortional buckling stress and it was found that the existing AISI method is unconservative while the other two

are reasonable. However, according to Schafer (2000), distortional buckling predictions of Schafer's method show slightly more accurate, but less conservative results when compared with Lau and Hancock's (1987) method. Further, Schafer argued that if failure mode is known as distortional, the ultimate strength can be predicted correctly from the elastic distortional buckling stress. The parametric study was continued further by introducing stiffeners to the web of the section and it was shown that the elastic local buckling stress increases while the failure is governed by distortional buckling mode.

Kesti (2000) investigated the local and distortional behaviour of flange and web stiffened compression members. He stated that the method given in Eurocode 3 (ECS, 1993) gives some inaccurate results for estimating the elastic distortional buckling stress of both C-sections and intermediate stiffened plates while methods developed by Lau and Hancock (1987) correlate better with the numerical results for C-section.

Narayanan and Mahendran (2002) described the distortional buckling behaviour of a series of innovative cold-formed steel columns with complex geometries. The experiments were a part of a design project of civil engineering undergraduates at The Queensland University of Technology. Sixteen innovative 1000 mm long columns (see Figure 2.11) were tested with the thicknesses of 0.8 and 0.95 mm for G550 steel and 0.96 and 1.14 mm with G250 steel. Column 1 (see Figure 2.11) was tested with various lengths as 1000, 875, 675, 475, 275, 130 and 100 mm. The sections and buckling properties were obtained using the finite strip analysis program, Thin-wall. The non-linear ultimate strength was determined using the finite element analysis program ABAQUS. Four nodded, 3-D quadrilateral shell elements (S4R5) were used. The measured base metal thickness and yield stress were used. 5 mm x 5 mm mesh size was used for most of the sections. The influence of the rounded corners was neglected since it has not shown considerable effect. Four different types of finite element models were considered and their details are given as follows.

1. Full length and half length models were studied by using multi-point constraints (MPC).

2. Full length and half length models were studied by using rigid body elements (R3D4).

3. Half-wave length model based on half wave buckling length of the column was studied by using MPC.

4. Half-wave length model based on half wave buckling length of the column was studied by using R3D4.
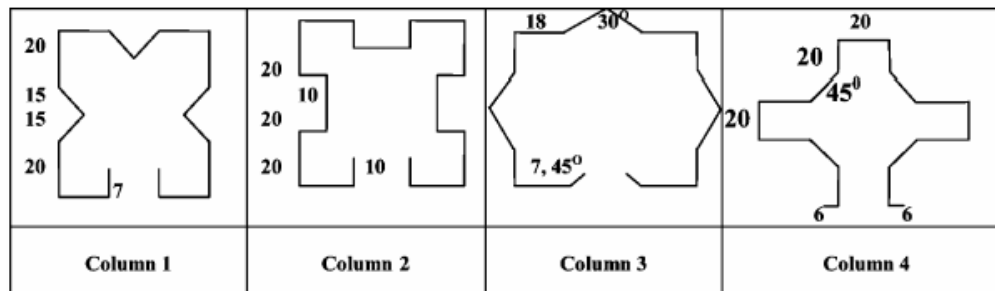
Figure 2.11   Geometry of Members used by Narayanan and Mahendran (2002)

The initial imperfection used was b/167 and 2b/167 (b = width of the section). An average residual stress of $17\%f_y$ was applied uniformly to the section and it was found that the residual stresses have a very small effect on the ultimate load. All the columns buckled distortionally except the 130 and 100 mm length columns, which failed in local buckling.

Nevertheless, they showed that AS/NZS 4600 (SA, 1996) over-predicts the ultimate load of G550 steel columns. However, when $0.75f_y$ was used for G550 steel with the thickness less than 0.9 mm the predicted results from AS/NZS 4600 were improved.

Yang and Hancock (2003) describes a series of compression tests of lipped channels with intermediate stiffeners in the web and flanges (see Figure 2.12). Cold-reduced high strength steel was used with a nominal yield stress of 550 MPa and 0.42 mm thickness. The column lengths were varied from 360 to 2000 mm (360, 800, 1300, 2000). Fixed-end conditions were used for all the experiments since pin-ended singly symmetric compression members cause additional moments after local buckling due to the shift of their line of centroidal axis.
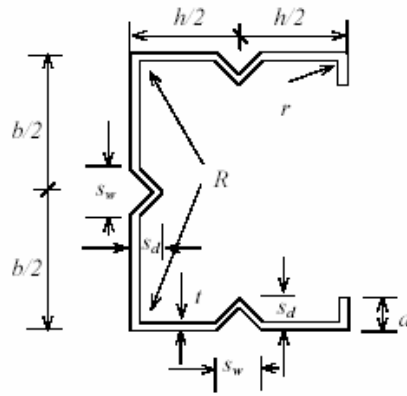
Figure 2.12   Section used by Yang and Hancock (2003)

Yang and Hancock (2003) investigated the effects of local buckling, distortional buckling and the interaction between them. Long columns (800, 1300 and 2000 mm length) were tested to study the behaviour of distortional buckling and interaction of distortional and local buckling. Stub columns (360 mm length) were tested to determine the local buckling behaviour. Thin-wall program and the Spline Finite Strip Method (SFSM) were used to determine the geometry of sections. The SFSM can be used to analyse the fixed-end column accurately. However, the distortional buckling stress obtained from SFSM with fixed-end conditions showed higher values than the distortional buckling stresses which were obtained from Thin-wall program. But this is only up to 1500 mm length and after that the stresses were nearly the same. They selected the 2000 mm length column to reduce the effect of end boundary conditions for distortional buckling mode. The stub columns showed very high post local buckling strength. Some strange behaviours were observed with the long columns. There was no difference between the results of 1300 mm and 2000 mm columns. Different failure modes have been observed for 2000 mm long column as one column failed as a result of the flange lips moving inwards and another one failed by flange lips moving outwards. However, the column, which failed with flange lips moving inward showed lower strength than the other column. Further, three different types of failure modes have also been observed in stub columns: two flanges moved outward, two flanges moved inward and one flange moved outward while the other one moved inward. But Yang and Hancock (2003) did not describe any reason for those different types of failure.

Test results were compared with the North American Specifications (NAS, 2001) and AS/NZS 4600 (SA, 1996). Both showed unconservative predictions since distortional buckling and interaction of local and distortional buckling are not adequately accounted in these specifications.

Yan and Young (2003) describe the experimental investigation of cold-formed steel channel columns with complex stiffeners and varying column lengths (see Figure 2.13) compressed under fixed-end conditions. Test results were compared with the predicted design strengths from the direct strength method, American Specification (AISI, 1996) and Australian/ New Zealand Standard, AS/NZS 4600 (SA, 1996) for cold-formed steel structures.
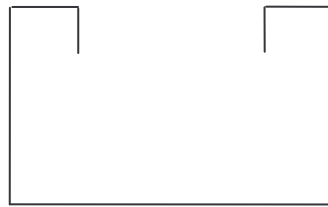
Figure 2.13   Test Specimen used by Yan and Young (2003)

The purpose of Yan and Young's (2003) research was to compare the test strength and the failure mode of fixed-end columns with the design strength and failure mode obtained by the direct strength method, which was calibrated for the pin-end conditions. G450 structural steel sheets with a nominal yield strength of 450 MPa were used for the experiments. Nominal thicknesses were 1.5 mm and 1.9 mm while the varying column lengths were in the range of 500 to 3500 mm.

Yan and Young (2003) showed that the strength predicted by the direct strength method was generally accurate for the series which had the slender flanges and conservative for others which had less slender flanges. AISI predicted values showed the unconservative results while AS/NZS Standard shows conservative results for most tests. The predicted failure modes are generally in agreement with the long columns but not for short and intermediate columns.

Young and Hancock (2003) described a series of fixed-end cold-formed channels with inclined simple edge stiffeners (see Figure 2.14) subjected to compression. Grade 450 steel sheets were used having a nominal yield strength of 450 MPa. The plate thicknesses used were 1.5, 1.9 and 2.4 mm and the column length was 1500 mm.
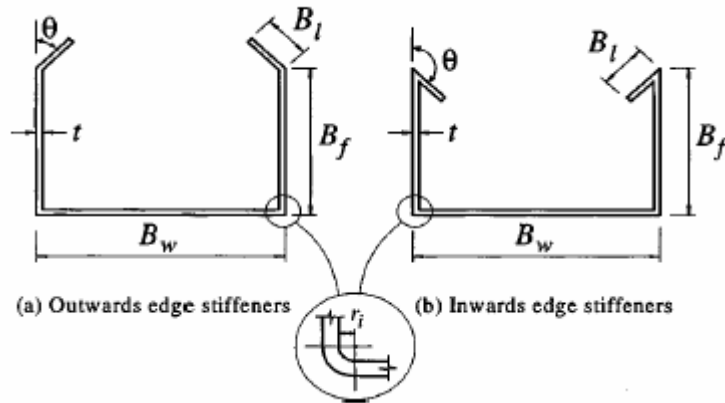
Figure 2.14   Geometry of Sections used by Young and Hancock (2003)

Young and Hancock (2003) has observed the distortional buckling mode for all the columns near the ultimate load. Experimental results were compared with the unfactored design strength predicted from North American Specification (NAS 2001), American Iron and Steel Institute Specification (AISI, 1996) and Australian New Zealand Standard, AS/NZS 4600 (SA, 1996). The elastic distortional buckling stress was determined by using the Thin-wall computer program and was used to predict the ultimate buckling load with the assumption of there being no influence of end effects. The design strengths predicted from the AS/NZS 4600 are conservative for all columns when compared with test results. However, the predicted strengths from the other two specifications are conservative for some columns and unconservative for others when compared with results. Finally, Young and Hancock (2003) explained that the end effects can increase the test load for compression members which failed due to distortional buckling and the effect is little for long columns with small lips.

Young and Yan (2004) carried out experimental investigation of fixed-end cold-formed steel channel columns with complex edge stiffeners (see Figure 2.15). The test results were compared with direct strength method predictions. They stated that

the direct strength method is generally accurate for fixed-end cold-formed steel channels with complex edge stiffeners for sections having slender flanges and conservative for sections having less slender flanges. However the reduction factor Φ was considered as 0.85 for this investigation. In addition they used G450 steel with a nominal yield strength of 450 MPa with the thicknesses of 1.5 and 1.9 mm. Therefore the accuracy of direct strength method for compression members made of very thin steels and with fixed-end should be further investigated.
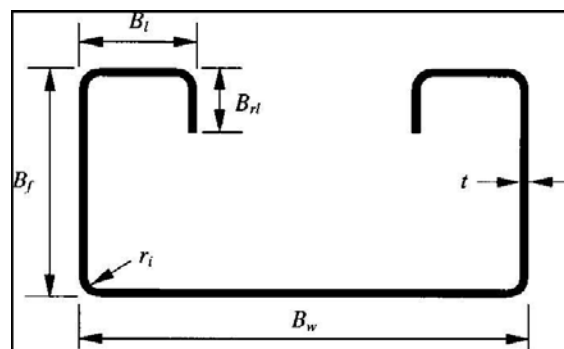
Figure 2.15   Geometry of Sections used by Young and Yan
(From Young and Yan, 2004)

2.1.3 Analysis Methods

Numerous analysis methods are currently available. Lau and Hancock (1987) and Schafer and Pekoz (1999) have introduced manual calculation methods for elastic distortional buckling with respect to simple C and rack sections. Finite strip and finite element methods can be used as different elastic distortional buckling analysis tools. Finite strip method is simpler and takes a very short time to analyse members while finite element method is more complicated and takes a long time. However, the finite element method can be used for any type of end boundary conditions and column lengths. Finite strip method is generally based on simply supported end boundary conditions and hence the member length should be long enough to include multiple half-wave lengths.

The Generalised Beam Theory is another effective method to analyse the compression members. The analysis time of Generalised Beam Theory is also short and any type of boundary conditions can be analysed. Non-linear elastic spline finite strip method is another method to predict the theoretical buckling strength of thin-walled sections, which was developed in the University of Sydney (Kwon and Hancock 1992a and b). Geometric imperfections, residual stresses and complex end boundary conditions of the section can be taken into account in the analysis. If local and distortional buckling modes occur simultaneously at different half wave lengths, they can be observed by using this method. The analysis has different convergence criteria as strip sub-division and longitudinal sub-section hence it can be used with reliable convergence criteria. The accuracy of this method is governed by the number of strips and the number of sub-sections used. The spline finite strip method is more powerful than the semi analytical finite strip method since it can handle the various boundary conditions. Further, it is more efficient than the finite element method in terms of computational efficiency.

As a more common and simple method, the finite strip program Thin-wall is used to analyse compression members and thus, a short description of the Thin-wall program is presented here. Further, the finite element program ABAQUS is used to analyse the results obtained from experiments and current design standards. Hence a short description of ABAQUS is also presented here.

2.1.3.1   Thin-wall program

The Thin-wall computer program can be used to investigate different modes of buckling in thin-walled structures. The analysis is based on the finite strip method, which subdivides the thin-walled sections into longitudinal strips. It examines only the simply supported end conditions for columns. Any steel section can be analysed using Thin-wall program and the appropriate column length can be obtained to suit the desired buckling mode. The buckling modes can be obtained as shown in Figure 2.16 (a). The buckling stress versus buckling half wave length plot can also be obtained from this program (see Figure 2.16 (b)).
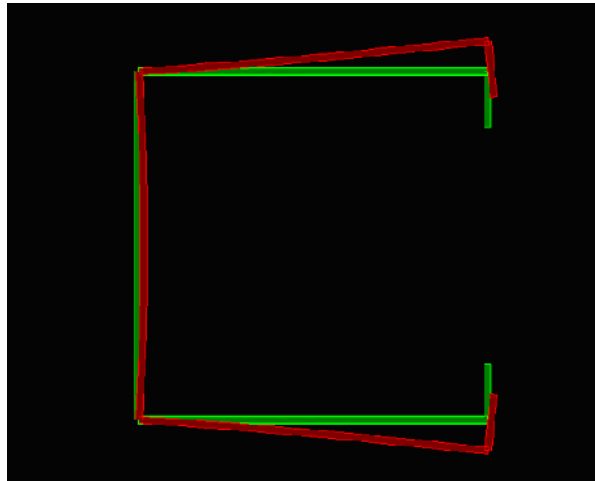
(a)   Distortional buckling mode
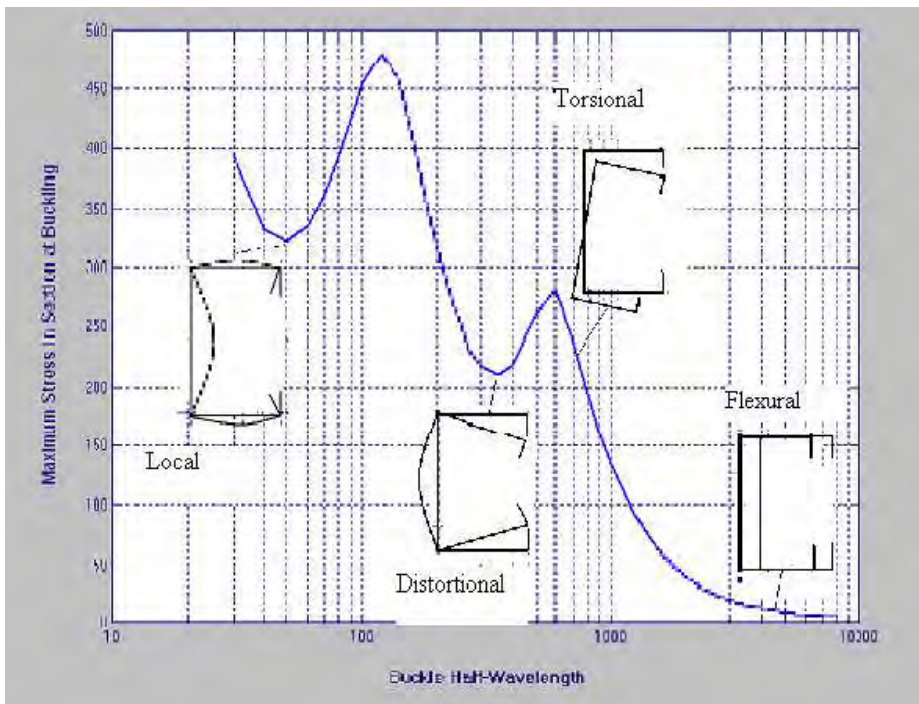
(b)   Buckling stress versus half wave buckle length

Figure 2.16   Buckling Results based on Thin-wall Program

Figure 2.16 (b) shows the results from a finite strip analysis of purely compressed lipped C-section. The minima of the curve represent several buckling modes which exist in the member. It is clear that the distortional buckling occurs at intermediate half wave-lengths between local and flexural or flexural torsional half-wave lengths. According to this graph, the elastic local buckling stress is higher than the elastic

distortional buckling stress. If the member length is between 200 mm to 800 mm its failure is governed by distortional buckling mode. On the other hand, if it is less than 200 mm, it is local buckling mode, while if it is greater than 800 mm it is flexural or flexural torsional buckling.

2.1.3.2 Finite element analysis program ABAQUS

The finite element analysis program (ABAQUS) is a very efficient tool to analyse the behaviour of steel structures. Light gauge cold-formed steel compression members can be modelled and analysed under different types of boundary conditions and temperature levels. However, the finite element method is not a new technique. It was first introduced in 1950 and there are many new techniques added to it. Today any type of problems can be analysed by using this finite element program ABAQUS although it is complex. However, finite element analysis is playing an important role in engineering practice since it has some excellent features. It is relatively inexpensive and time efficient compared with physical experiments.

The finite element analysis process can be divided into the following basic steps.
- Pre-processing the model, i.e. discretisation of the problem into selected elements
- Calculation of the element matrices and vectors
- Assembly of the element matrices and vectors to give the global (or system) equations
- Incorporation of the boundary conditions into the global equations
- Solution of the equation to find the unknown nodal values of the field variables
- Post-processing of the results to give strains/stresses, heat flows and so on

2.1.4 Experimental Method

Mainly fixed-end (which prevents end rotations and produce upper bounds for the column strength) and pin-end (which produce lower bounds for the strengths of

concentrically loaded column) column testing methods can be observed as they are used in the practical situations. However, most of the researchers have considered the fixed-end method to carry out the distortional buckling tests and there is a need to compare the fixed-end and pin-end methods. According to Young and Rasmussen (1995) there is no overall bending of fixed-end columns after local buckling while pin-end columns show overall bending. They mentioned that there is a shift of line of action of internal force in the uniformly buckled channel section (see Figure 2.17) and hence it leads to an eccentricity of the applied load in pin-end channels (see Figure 2.18). However, this does not occur in the fixed-end channel columns since the shift in the line of action of internal force is balanced by the shift in the line of action of external force (see Figure 2.19). However, this is only for local buckling failure and there have not been any investigations for distortional buckling.
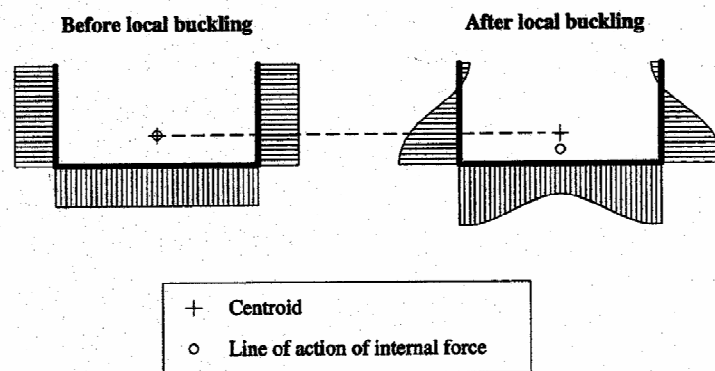
Figure 2.17   Stress Reductions in Channel Section under Uniform Compression
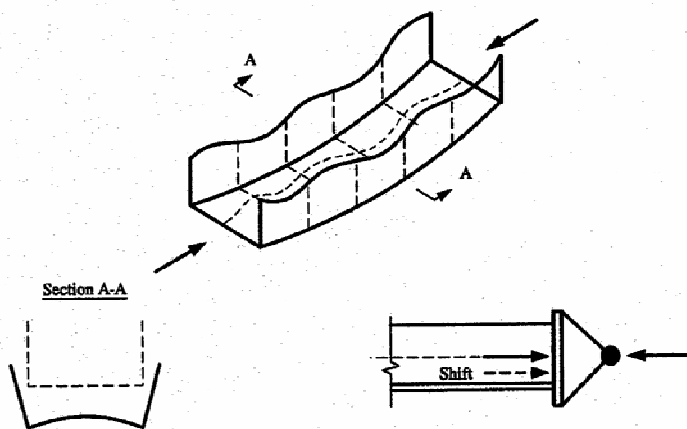
Figure 2.18   Pin-end Column after Local Buckling
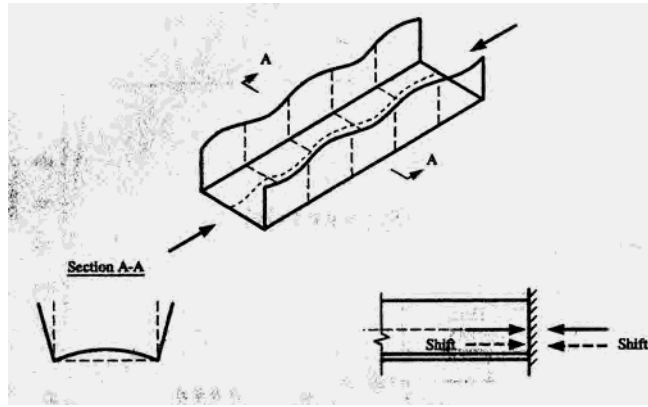
Figure 2.19   Fixed-end Column after Local Buckling
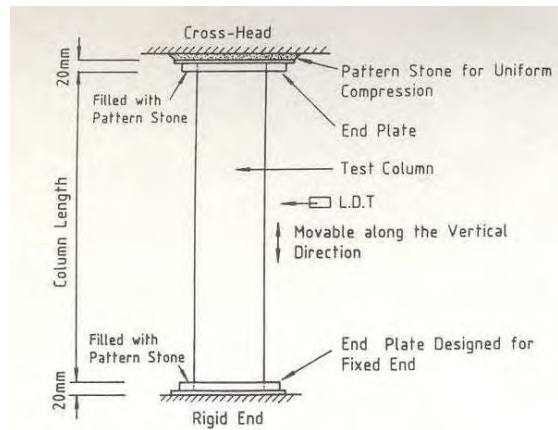
(a)   Compression test arrangement
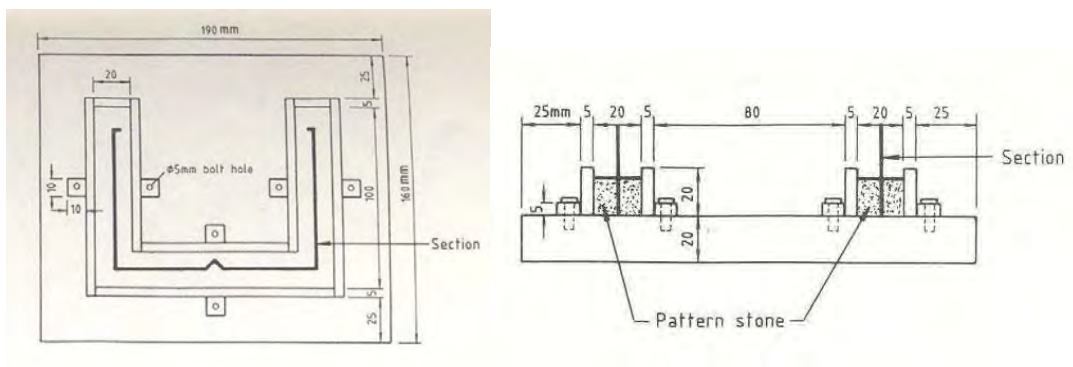
(b)   End plate

Figure 2.20   Compression Test Arrangement and End Plate used by Kwon and Hancock (1992a)

Kwon and Hancock (1992a) used fixed-end boundary conditions by using pattern stone (see Figure 2.20). However, Kwon and Hancock (1992b) mentioned that this system cannot be considered as fully fixed-end condition since there might be a small longitudinal displacement at the end of the section because the galvanised section can slide in the pattern stone.

(a)   End plate before inserting the specimen

(b)   Specimen on end plate filled with pattern-stone
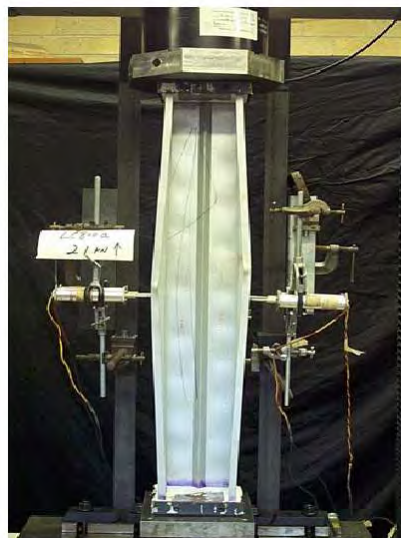
(c)   Testing of specimen

Figure 2.21   Testing Method used by Yang and Hancock (2003)

Yang and Hancock (2003) also used fixed-end conditions in their experiments on compression members as a modified method used by Kwon and Hancock (1992a). A Sintech/MTS-300 kN testing machine was used with fixed-end bearings. The bottom bearing was kept adjustable to orient the specimen vertically before the bearing was

locked for testing. Specially designed end plates were filled with pattern-stone (see Figure 2.21) to guarantee perfect fixed-end boundary conditions. According to Yang and Hancock (2003) this method acts as a fully fixed-end condition.
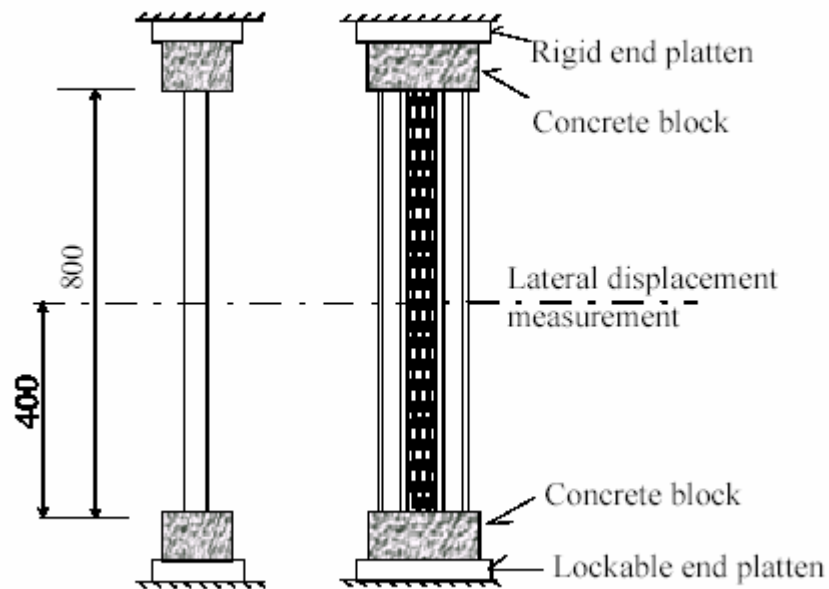
Figure 2.22   Testing Method used by Kesti (2000)

In addition, Kesti (2000) also used fixed-end conditions for all of his specimens. He used concrete to cast each end of the specimens to end plates to ensure perfect fixed conditions. A 500 kN hydraulic testing machine equipped with a lockable plate at one end was used for his experiments. The loading rate used was 4 kN/min. His test set-up is shown in Figure 2.22.

However, among these methods, the method used by Yang and Hancock (2003) can be considered as fully fixed-end and an easier method than the others. But his experiments were carried out only at ambient temperature and pattern-stone cannot be used at elevated temperatures. Thus, a modified Yang and Hancock (2003) method is needed to achieve the perfect fixed-end boundary conditions by introducing a different grout, which can withstand elevated temperatures.

2.1.5 Current Design Rules at Ambient Temperature

Unlike local or global buckling behaviour of light gauge cold-formed steel compression members, there is a lack of design rules for the distortional buckling behaviour. The following sections clearly demonstrate that the distortional buckling behaviour and associated design rules should be further investigated.

2.1.5.1 Effective width method

Effective width method was first proposed by von Karman (1932) and calibrated for cold-formed steel members by Winter (1947). The post buckling strength is predicted by considering the reduced plate width at design stress. The current column design rules are mainly based on the effective width method. This method is used in American and Australian/ New Zealand Standards (AISI, 1996; SA, 1996). However this method becomes more tedious when calculating the effective width for cross sections with complex shapes such as lips having some additional return lips (for more complex sections see Figure 2.11). In this method, the buckling coefficient (k) is given as 4.0 for stiffened elements, (supported at two edges) such as web of channel sections and k is considered as 0.43 for unstiffened elements, (supported only at one edge) such as flange of unlipped channel sections. AS/NZS 4600 (SA, 1996) presents the equations of the effective widths (b_e) of uniformly compressed elements as follows (Equation 2.5). However, these equations are valid only for local buckling failures. But when the compression members fail by the interaction of local and distortional buckling the suitability of these equations should be investigated.
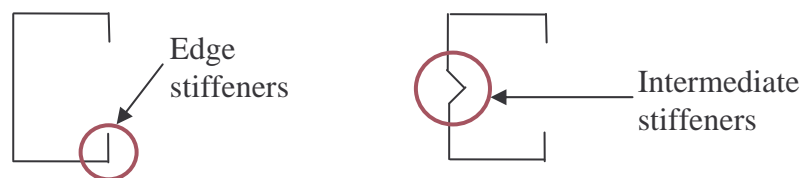
Figure 2.23   Elements with Stiffeners

For $\lambda \leq 0.673$: $b_e = b$

For $\lambda > 0.673$: $b_e = \rho b$

Where, b = flat width of element excluding radii

$$\rho = \text{effective width factor} = \frac{\left(1 - \dfrac{0.22}{\lambda}\right)}{\lambda} \leq 1.0 \qquad (2.5)$$

The slenderness ratio λ is determined as follows

$$\lambda = \left(\frac{1.052}{\sqrt{k}}\right)\left(\frac{b}{t}\right)\left(\sqrt{\frac{f^*}{E}}\right)$$

Where,

      k = plate buckling coefficient

      t = thickness of the uniformly compressed element

      f* = design stress in the compression element

      E = Young's modulus of elasticity

When the elements are considered as partially stiffened elements (element with an intermediate stiffener or element with an edge stiffener) (see Figure 2.23), the value of k is between 0.43 and 4.0. Mainly three cases are considered to determine the value of k (see Equations 2.6 (a) and (b)).

Elements with an intermediate stiffener

Case I: $\dfrac{b_2}{t} \leq S$:- $I_a = 0$ (no edge stiffener is required), $b_e = b$, $A_s = A_{se}$

Case II: $S < \dfrac{b_2}{t} < 3S$:- $\dfrac{I_a}{t^4} = \dfrac{50\left(\dfrac{b_2}{t}\right)}{S} - 50$, $k = 3\left(\sqrt{\dfrac{I_s}{I_a}}\right) + 1 \leq 4$, $A_s = A_{se}\left(\dfrac{I_s}{I_a}\right) \leq A_{se}$

$$\text{2.6(a)}$$

Case III: $\dfrac{b_2}{t} \geq 3S$:- $\dfrac{I_a}{t^4} = \left[\dfrac{128\left(\dfrac{b_2}{t}\right)}{S}\right] - 285$, $k = 3\left(\dfrac{I_s}{I_a}\right)^{1/3} + 1 \leq 4$,

$$A_s = A_{se}\left(\frac{I_s}{I_a}\right) \leq A_{se}$$

Elements with an edge stiffener

Case I: $\dfrac{b}{t} \leq \dfrac{S}{3}$:- $I_a = 0$ (no edge stiffener is required) $\quad b_e = b$,

$\qquad\qquad$ $d_s = d_{se}$ (for simple lip stiffener) $\quad A_s = A_{se}$ (for other stiffener shapes)

Case II: $\dfrac{S}{3} < \dfrac{b}{t} < S$:- $\qquad$ $\dfrac{I_a}{t^4} = 399\left[\dfrac{\left(\dfrac{b}{t}\right)}{S} - \sqrt{\dfrac{k_u}{4}}\right]^3$ $\qquad$ $k = C_2^{\frac{1}{2}}(k_a - k_u) + k_u$

Case III: $\dfrac{b}{t} \geq S$:- $\qquad$ $\dfrac{I_a}{t^4} = \left[\dfrac{115\left(\dfrac{b}{t}\right)}{S}\right] + 5$ $\qquad\qquad\qquad$ 2.6(b)

where, $s = 1.28\sqrt{\dfrac{E}{f^*}}$, $k_a = 5.25 - 5\left(\dfrac{B_l}{b}\right) \leq 4.0$, $k_u = 0.43$,

$\qquad$ $C_2 = \dfrac{I_s}{I_a} \leq 1$ $\qquad\qquad\qquad$ $C_1 = 2 - C_2$

I_a is the adequate second moment of area of the stiffener, I_s is the second moment of area of the full stiffener about its own centroidal axis parallel to the element to be stiffened, B_l is the overall width of the lip and C_1 and C_2 are coefficients. For more details, refer Clause 2.4 of Australian/ New Zealand Standard 4600 (SA, 1996). Further, when there are more stiffeners the expressions become more complicated (see clause 2.5 of AS/NZS).

However, the effective width method considers each element separately. The rotational restraint of the adjacent elements is not taken into account and hence it may be less accurate. To overcome these disadvantages Schafer and Pekoz (1998) have developed the new direct strength method.

2.1.5.2   Direct strength method

The direct strength method was proposed by Schafer and Pekoz (1998b) for laterally braced flexural members undergoing local or distortional buckling modes. Afterwards it was developed for pin-end compression members to determine the

local, distortional or overall buckling and interaction of local and overall buckling, and distortional and overall buckling modes. The direct strength method has been calibrated using the test results of concentrically loaded pin-end cold-formed steel columns for certain cross-sections including simple lipped channel, lipped channel with web stiffeners, Z section, rack upright section and hat section. The direct strength method uses the whole section instead of individual elements separately. Equation 2.7 describes the column design rules for the interaction of local and overall buckling and the interaction of distortional and overall buckling.

$$
\begin{aligned}
P_{DSM} &= f_{min} A \\
f_{min} &= \min \left(f_{nl}, f_{nd} \right) \\
f_{nl} &= f_n \quad \text{for } \lambda_l \leq 0.776 \\
f_{nl} &= \left(1 - 0.15 \left(\frac{f_{crl}}{f_n} \right)^{0.4} \right) \left(\frac{f_{crl}}{f_n} \right)^{0.4} f_n \quad \text{for } \lambda_l \rangle 0.776 \\
f_{nd} &= f_n \quad \text{for } \lambda_l \leq 0.561 \\
f_{nd} &= \left(1 - 0.25 \left(\frac{f_{od}}{f_n} \right)^{0.6} \right) \left(\frac{f_{od}}{f_n} \right)^{0.6} f_n \quad \text{for } \lambda_l \rangle 0.561
\end{aligned}
\tag{2.7}
$$

where,

$$
\lambda_l = \sqrt{\frac{f_n}{f_{crl}}} \quad \text{and} \quad \lambda_d = \sqrt{\frac{f_n}{f_{od}}}
$$

f_{nl} = limiting stress for interaction of local and overall buckling

f_{nd} = limiting stress for interaction of distortional and overall buckling

A = gross cross sectional area

P_{DSM} = nominal or unfactored design column strength

f_{crl} = critical elastic local buckling stress

f_{od} = critical elastic distortional buckling stress

f_n = elastic overall buckling stress

Recently, Schafer (2002) suggested equations to consider the distortional buckling alone by ignoring the interaction of distortional and overall buckling since distortional buckling shows weak interaction with flexural buckling. The nominal

strength for distortional buckling mode for compression members is then determined as shown in Equation 2.8.

$$f_{nd} = f_y \qquad \lambda \leq 0.561$$

$$f_{nd} = f_y \left[1 - 0.25\left(\frac{f_{od}}{f_y}\right)^{0.6}\right]\left[\frac{f_{od}}{f_y}\right]^{0.6} \qquad \lambda > 0.561 \qquad (2.8)$$

where, $\qquad \lambda = \sqrt{\dfrac{f_y}{f_{od}}}$

2.1.5.3   AS/NZS 4600

Australian/New Zealand Standard, AS/NZS 4600 (SA, 1996) for cold-formed steel structures has design rules for the singly-symmetric sections subjected to distortional buckling such as lipped channels with additional rear flanges. The elastic distortional buckling stress (f_{od}) is mainly calculated for the following situations:

- General channels in compression
- Simple lipped channels in compression
- Simple lipped channels or Z-sections in bending about the axis perpendicular to the web

The design compressive axial force N* is given as follows (Equation 2.9 (a)) (see clause 3.4.1 of AS/NZS 4600)

$$N^* \leq \phi_c N_s \qquad , \qquad N^* \leq \phi_c N_c \qquad\qquad 2.9(a)$$

Where,

ϕ_c = Capacity (strength reduction) factor for members in compression (see Table 1.6 of AS/NZS 4600)

N_s = Nominal section capacity in compression = $A_e f_y$

$\qquad A_e$ = Effective area at yield stress (f_y) which takes into account the effects of local buckling

N_c = Nominal member capacity in compression = $A_e f_n$

$\qquad A_e$ = Effective area at the critical stress (f_n)

f_n = Critical global buckling stress and determined from Equations 3.4.1 (3) or 3.4.1 (4) in AS 4600 which calculate flexural and flexural torsional buckling stresses (f_{ox}, f_{oz}, f_{oxz})

The above equations are used to allow for local and global buckling effects. When singly symmetric sections are subjected to distortional buckling effects, the ultimate load (Af_n) is obtained as follows (see Equations 2.9 (b)):

- For $f_{od} > f_y/2$:

$$Af_n = Af_y\left(1 - \frac{f_y}{4f_{od}}\right)$$

2.9(b)

- For $f_y/13 \leq f_{od} \leq f_y/2$:

$$Af_n = Af_y\left[0.055\left(\sqrt{\frac{f_y}{f_{od}}} - 3.6\right)^2 + 0.237\right]$$

f_{od} can be calculated using finite strip analysis Thin-wall program for simply supported end conditions and finite element analysis ABAQUS for both pin and fixed-end conditions or Appendix D of AS/NZS 4600 for standard sections.

A = Area of the full cross-section

However, it does not discuss the interaction of local and distortional buckling modes. By replacing A (area of full cross section) with A_e (effective area as mentioned above), Equations 2.9 (b) can be modified, but the accuracy of such modification is not known.

2.1.5.4   Other specifications

The current Australian standard for steel structures, AS 4100 (SA, 1998) has not addressed light gauge cold-formed steel sections. It focuses only on heavier hot-rolled steel sections. The American Specification (AISI, 1996) does not explicitly treat distortional buckling as a separate mode of failure, and interaction of distortional mode with other modes is not considered. Therefore the use of existing AISI equations is inadequate to predict the distortional buckling for a large variety of common members. Further, Schafer (2000) discussed lipped C and Z sections and proved that the AISI method is not significant enough to predict the distortional buckling stress separately. However the new edition (AISI, 2004) has included direct

strength method as Appendix 1 to the specification to determine the ultimate load of compression members which buckle distortionally.

Eurocode 3: Design of steel structures Part 1.3 (ECS, 1993) addresses the behaviour of cold-formed steel members and sheeting, but does not include the distortional buckling effects. It only discusses the local buckling and flexural or flexural torsional buckling effects. British Standard Part 5: code of practice for the design of cold-formed thin-gauge sections (BSI, 1990) has addressed the design of light gauge cold-formed steel members, but not the distortional buckling failure mode. British Standard Part 5 also presents expressions for local and flexural or flexural torsional buckling modes. Current North American Design Specification (NAS, 2001) for cold-formed steel columns has not included the explicit checks for distortional buckling and does not consider the interaction of local and distortional buckling.

2.2 Fire Safety Design

2.2.1   General

Unfortunately, fires can occur in almost any kind of building and cause thousands of deaths and property losses each year. However, most of the fire design has been based on prescriptive building codes. The designers are limited to taking a rational engineering approach for fire safety. The primary objectives of fire safety are to provide life safety, property protection and environmental protection. The balance between life safety and property protection varies in different countries depending on the type of building and occupancy. The safety of the occupants in the building mainly depends on the collapse of the building and the spreading of fire. The general method of providing life safety is to ensure safe escape. To achieve this, it is necessary to alert people to the fire, provide suitable escape paths, which are not affected by fire or smoke while escaping. People in the adjacent buildings should also be protected. In addition, safety paths should be provided to the people who enter the building for fire control. The property protection depends on the protection

of the structure, fabric of the building and movable things in the building under fire. There are mainly four strategies considered in relation to fire safety engineering.

1. Detection and warning system

2. Escape

3. Controlling of ignition and fire

4. Structural protection

   ♦ Time determination

   ♦ Critical temperature

   ♦ Member capacity design

2.2.2 Behaviour of Fire

The behaviour of fire can be clearly seen in Figure 2.24. It shows the variation of temperature with time if there is no fire control, and Table 2.1 clearly shows the periods of typical fire development.
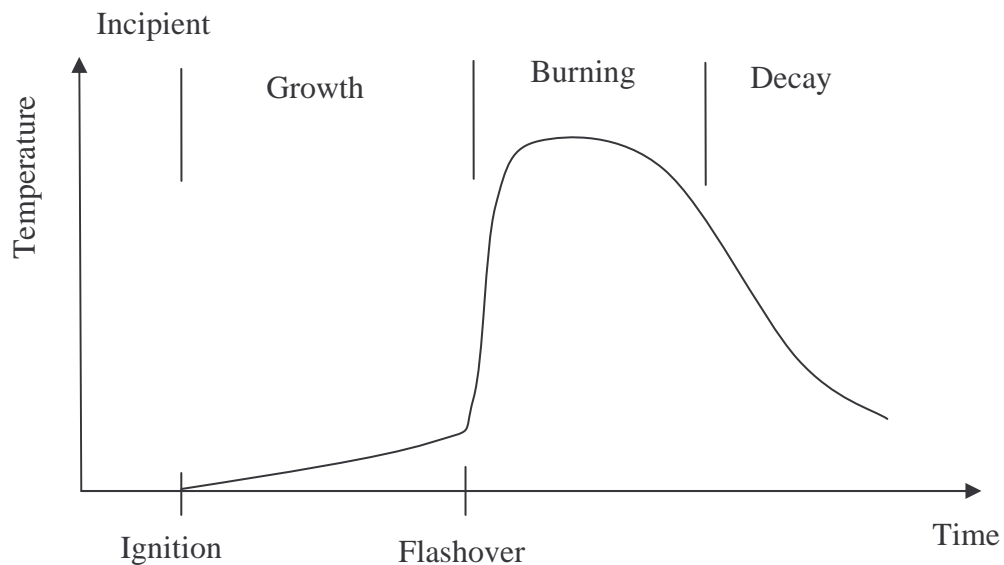
Figure 2.24   Temperature-Time Curve for Fire

Mainly there are four periods: incipient, growth, burning and decay. Heating of fuel is taking place in the incipient period of fire and then it transfers to the growth period with the start of fire. Ignition is the start of flaming combustion. In the growth period the spreading of fire is not difficult. When the upper layer temperature reaches

600°C the burning rate increases rapidly with the transition to burning period. Finally, the temperature drops and it transfers to the decay period. However, if there is control against fire these periods can be changed and the fire can be stopped before reaching the burning period without having much damage to the building.

Table 2.1   Summary of Periods of Typical Fire Development

	Incipient period	Growth period	Burning period	Decay period
Fire behaviour	Heating of fuel	Fuel controlled burning	Ventilation controlled burning	Fuel controlled burning
Human behaviour	Prevent ignition	Extinguish by hand, escape	Death	
Detection	Smoke detectors	Smoke detectors, heat detectors	External smoke and flame	
Active control	Prevent ignition	Extinguish by sprinklers or fire fighters; control smoke	Control by fire fighters	
Passive control		Select materials with resistance to flame spread	Provide fire resistance; contain fire, prevent collapse	

2.2.3 Fire Control

Fire control can be mainly categorised in two ways: active and passive. In active control, people or automatic devices take an action against fire. The automatic sprinkler system is the best fire protection active control system hence it sprays water over a local area. Sprinkler systems turn-off most of the fires at their early stages. However, it should operate early since it is designed for limited water supply.

Smokes can be removed with the operation of fans. Nevertheless, it should be ensured that the toxic gases are removed safely. Passive control can be defined as the material of building, which prevents the spreading of fire. On the other hand passive control can control the fire without any interference from people or fire fighting equipment (see Table 2.1).

2.2.4 Design of Buildings Against Fire

Buildings are designed with a number of elements such as walls, floors and roofs which are supported by members like beams and columns. The collapse of the building may happen due to the failure of one structural member under fire. Therefore when designing a building structure, each and every structural member should be designed against fire. However, some complex structures behave in a stable way although there are structural failures of some members. On the other hand design for fire has many variations compared to the design for normal condition. The following facts should be taken into account when designing a structure against fire:

- Applied loads are less
- Internal forces may be induced by thermal expansion
- Strength of material may be reduced by elevated temperatures
- Cross sectional area may be reduced by charring or spalling
- Smaller safety factor can be used
- Deflections are not important (unless they affect strength)
- Different failure mechanisms are to be considered

However, the above factors may be different for different materials. As an example, Figures 2.25 (a) and (b) show the failure of simply supported steel and timber beams separately. There is a reduction of material strength in steel while there is an increase of stress in timber. The stress on steel beams is not changed since there is no reduction in the cross sectional area of steel beam. But the cross sectional area of timber beam is reduced during fire, resulting in a higher stress in it.

(a) Steel   (b) Timber
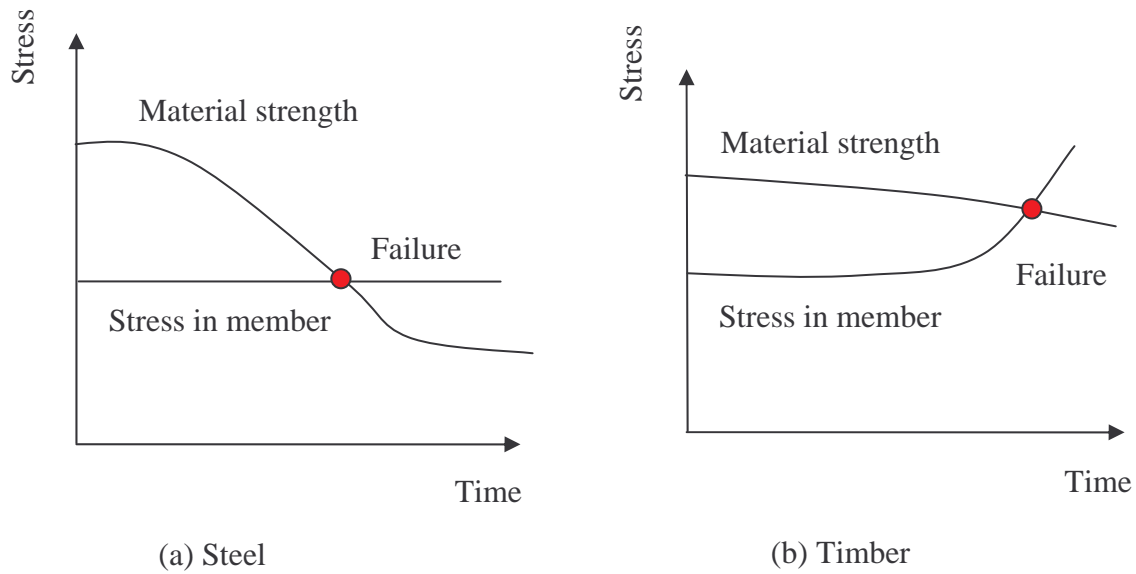
Figure 2.25   Failure of Different Types of Members

Table 2.2   Design Combinations of Dead and Live Loads

	Dead load	Permanent live load	Other live load
New Zealand (SNZ,1992)	G	0.6Q	0.4Q
Eurocode (ECI, 1993)	G	0.9Q	0.5Q
USA (ASCE, 1995)	1.2G	0.5Q	0.5Q
Ellingwood and Corotis (1991)	G	0.5Q	0.5Q
British Standard (BSI, 1990)	G	Q	0.8Q

Note:- G = Dead load and Q = Live load

Further, the applied loads in a fire situation are much lower than the maximum design loads specified for normal conditions. Therefore, different load combinations are used for designing against fire (see Table 2.2). The following fundamental equation should be satisfied when designing a building or any structure against fire.

Fire resistance ≥ Fire severity

Fire resistance of the structure (resistance to collapse, spread of fire or any failure) should be greater than fire severity of structure. The fire engineer who designs structures against fire must have a good understanding of the relationship between fire resistance and fire severity. Mainly there are three methods to compare fire severity and fire resistance. Table 2.3 provides an outline of this.

Table 2.3   Methods of Comparing Fire Resistance with Fire Severity

Domain	Units	Fire Resistance	≥Fire severity
Time	minutes or hours	Time to failure	≥ Fire duration as calculated or specified by code
Temperature	$^\circ$C	Temperature to cause failure	≥ Maximum temperature reached during the fire
Strength	kN or kNm	Load capacity at elevated temperature	≥ Applied load during the fire

The following equation (Equation 2.10) is used when designing a building in accordance with fire conditions.

$$U_{fire} \leq \Phi_f \, R_{fire} \qquad\qquad (2.10)$$

where,

U_{fire} = Design action from the applied load in the fire (This can be axial force N_{fire}, bending moment M_{fire}, shear force V_{fire} or a combination of them).

R_{fire} = Nominal load capacity under fire situation.

Φ_f =   Strength reduction factor for fire design (However, most national and international codes consider $\Phi_f = 1.0$)

More details on Structural Design for Fire Safety are given in Buchanan (2001).

2.2.5 Fire Resistance

This is a measurement of the building's ability to resist fire. The objectives of fire resistance should be identified before designing a building against fire. The following main objectives have been identified.

Prevent internal spread of fire :- Fire barriers can be provided to separate the building into fire compartments, which delay the spread of fire. Further, the following advantages can be seen with the introduction of fire compartments or fire cells: they increase the available time for escape, limit the area of possible losses, reduce the fire impact on the structure and protect escape routes.

Reduce the probability of fire spread to other buildings :- Boundary walls can be provided which delay the spread of fire to other buildings.

Prevent structural collapse:- Materials which are used for structural elements should have sufficient strength at elevated temperatures. This should be mainly considered for main load bearing elements and secondary elements, which provide stability to main members.

The spread of fire can be mainly categorised as follows: within the room of origin, adjacent rooms, other stories and other buildings. Fire spread within the room of origin can happen to vertical and horizontal direction and the spreading rate depends upon the combustible material used in the room. The spreading of fire can be reduced by limiting the usage of combustible material. After ignition occurs, fire safety of the building depends upon the fire spreading rate. Fires in rooms can be mainly divided into pre-flashover fire and post-flashover fire. There should be a good understanding of pre-flashover fire when designing a building against fire. Pre-flashover fire has the most influence on life safety.

Spreading of fire and smoke to the adjacent rooms happens mainly due to the openings (doors). By introducing fire barriers to doors, the spreading of smoke and toxic gases can be prevented hence, spreading of fire can be reduced or delayed. The

spreading of fire to other storeys mainly depends upon the voids of the building: service ducts, lift shaft and stair ways. By introducing fire barriers to these openings the spreading of fire can be reduced. Fire can be spread to the adjacent buildings due to the contact of flame if it is very close; by radiant heat transfer if it is further away or by flaming brands. This can be prevented by designing a building with sufficient distance or by introducing fire barriers.

2.2.6 Steel in Fire

When steel structures are exposed to fire, strength and stiffness are decreased with increasing temperature. The structure is then deformed and the deformation depends upon the applied load and support conditions. The severity of fire, the exposed area to the fire and applied fire protection are the governing factors for increasing steel temperatures. Due to the higher thermal conductivity and thinner members, the increase of temperature of steel is much higher than other materials such as concrete and timber. Due to the rapid temperature rise the structure can collapse with loss of strength of members (see Figure 2.26). However, steel members can be protected by using some low thermal transfer material surrounding the members. However, full scale fire tests and some actual fire situation have proven that well designed steel structures can behave without collapsing under some fire conditions although there are unprotected main load bearing members. Unprotected steel members show large deformation due to fire whereas well protected members usually exhibit no damage. However, steel members, which were exposed to fire, can be reused without further investigation if they do not show any deflection after cooling (Tide, 1998). Further, there is a large temperature difference between the fire side and the other side of the steel structural members due to the fire compartment of the building. Normally the temperature difference can be around 200°C to 300°C. Therefore, the temperature distribution of steel structures is a very important phenomenon due to two main reasons: degradation of material properties of the heated zones and the thermal elongation (axial compressive force is induced due to thermal elongation). However, as a simple design method, an even distribution of temperature across the cross section and along the length of the member is considered. But this method gives

inaccurate results or is conservative. Degradation of mechanical properties is an important phenomenon and is presented in the next section.

Figure 2.26   Steel Structural Failure due to Fire

2.2.7 Mechanical Properties of Steel at Elevated Temperatures

Unlike hot-rolled steel members, cold-formed steel shapes are formed at room temperature. The two main methods used for cold-forming are press-braking and roll-forming. When a member is cold-formed from a flat sheet or plate, the yield strength, and to a lesser extent the ultimate strength, are increased as a result of this cold working. Therefore, at elevated temperatures the variation of mechanical properties of cold-formed steel is not the same as the mechanical properties of hot-rolled steel.

Eurocode 3: Part 1.2 (ECS, 1993) has addressed the mechanical properties of cold-formed steel with respect to temperature. The reduction factor (see Table 2.4) has been defined for mechanical properties at elevated temperatures with respect to the mechanical properties at 20°C. However, according to Table 2.4 there is no difference between the reduction factors of cold-formed and hot-rolled steels at elevated temperatures. Further, it does not consider the reduction factors for low strength and high strength steels separately. For heating rates between 2 and 50°C/min, the strength and deformation properties of steel at elevated temperatures can be obtained based on Figure 2.27.

Table 2.4   Reduction Factors for Mechanical Properties of Steel at Elevated Temperatures (from Eurocode 3 Part 1.2 (ECS, 1993))

Steel Temperature T (^{o}C)	for cold-formed and hot-rolled thin-walled sections (relative to f_y)	for cold-formed and hot-rolled sections (relative to E)
20	1.00	1.000
100	1.00	1.000
200	1.00	0.900
300	1.00	0.800
400	1.00	0.700
500	0.78	0.600
600	0.47	0.310
700	0.23	0.130
800	0.11	0.090
900	0.06	0.068
1000	0.04	0.045
1100	0.02	0.022
1200	0.00	0.000
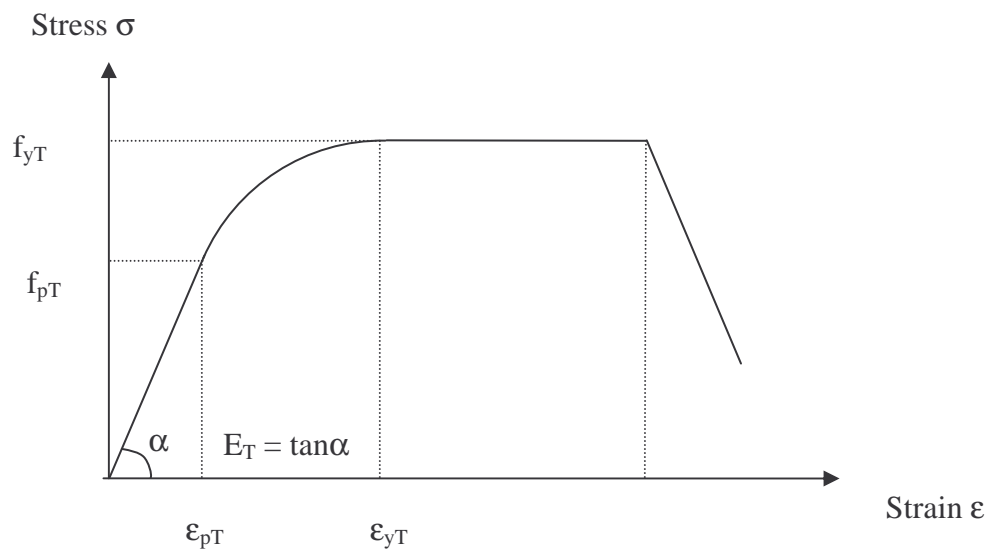
Figure 2.27   Stress-strain Relationship for Steel at Elevated Temperatures

where,

f_{yT} = Effective yield strength

f_{pT} = Proportional limit

E_T = Slope of the linear elastic range = elasticity modulus

ε_{pT} = Strain at the proportional limit

ε_{yT} = Yield strain

Based on Figure 2.27 the following reduction factors have been calculated relative to the appropriate value at 20°C for elevated temperatures:

Reduction factor for yield strength: $k_{yT} = f_{yT}/f_y$

Reduction factor for proportional limit: $k_{pT} = f_{pT}/f_y$

Reduction factor for elasticity modulus: $k_{ET} = E_T/E$

British Standard Part 8: Code of Practice for Fire Resistant Design (BSI, 1990) has also addressed the strength reduction factors for light gauge cold-formed steel at elevated temperatures (see Table 2.5), but only for a temperature range of 200°C to 600°C and for yield stresses corresponding to 0.5, 1.5, and 2.0% strain levels even though 0.2% proof stress is commonly used. Further, it does not discuss the reduction factors for elasticity modulus. The American Specification (AISI, 1996) does not present any detail relating to such reduction factors.

Table 2.5   Yield Strength Reduction Factors for Cold-formed Steel
(from BS 5950 Part 8)

Strain	Temperature (°C)								
%	200	250	300	350	400	450	500	550	600
0.5	0.945	0.890	0.834	0.758	0.680	0.575	0.471	0.370	0.269
1.5	1.000	0.985	0.949	0.883	0.815	0.685	0.556	0.453	0.349
2.0	1.000	1.000	1.000	0.935	0.867	0.730	0.590	0.490	0.390

The study of steel structures in fire conditions has been carried out at the Helsinky University of Technology since 1994. They have measured the material properties of various structural steels at elevated temperatures (Outinen et al., 2000).   Their research was mainly focused on transient state tensile test method while the steady

state method was used to create a proper basis for the analysis of test results. Mainly four kinds of materials were considered: S350 GD + Z (cold-formed steel with 2 mm thickness), S355 (cold-rolled steel with 4 mm thickness), S460 M (high strength steel with 20 mm thickness) and S355 J2H. However, the reduction factors for yield strength of S350 GD + Z did not agree with Eurocode 3 values while other material types showed better agreement with Eurocode 3 values. Table 2.6 shows the proposed reduction factors for S350 GD + Z by Outinen and Makelainen (2001).

Ala-Outinen and Myllymaki (1995) and Ranby (1998) recommended the use of 0.2% proof stress to determine the yield stress at elevated temperatures. However, according to the Steel Construction Institute's recommendation, the 0.5% proof stress should be used to determine the yield strength of members which fail due to buckling and 1.5% which fail due to bending. This is a very important issue in fire research and design that require further investigation.

Table 2.6   Reduction Factors for Yield Strength of S350 GD + Z Proposed by Outinen and Makelainen (2001)

Temperature (^{o}C)	Proposed reduction factor for f_y	Proposed reduction factor for E
20	1.000	1.000
100	0.970	1.000
200	0.932	0.900
300	0.895	0.800
400	0.857	0.700
500	0.619	0.600
600	0.381	0.310
700	0.143	0.130
800	0.105	0.090
900	0.067	0.068
1000	0.029	0.045

Lee et al. (2003) describes the details of an experimental study, the results, the empirical equations for the reduction factors of mechanical properties and stress-strain model for light gauge cold-formed steels at elevated temperatures. They examined the deterioration of mechanical properties of thin steels at different strain levels and temperatures. Three steel grades G550, G500 and G250 (minimum yield stresses of 550, 500, 250 N/mm^2) with the thicknesses of 0.4, 0.6, 1.0 and 1.2 mm were used. Temperature levels from 100°C to 800°C at intervals of 100°C with heating rates of 15-20 ^{o}C/min were considered. Tests were limited to a maximum temperature of 800°C since the reduced yield strength is less than 10% when the temperature is above 800°C. Steady state method (constant temperature with increasing static loads) was used due to its simplicity and accuracy of the results rather than transient state and ISO test methods (both methods are based on constant load with temperature variation). The yield strength results are shown in Figure 2.28.
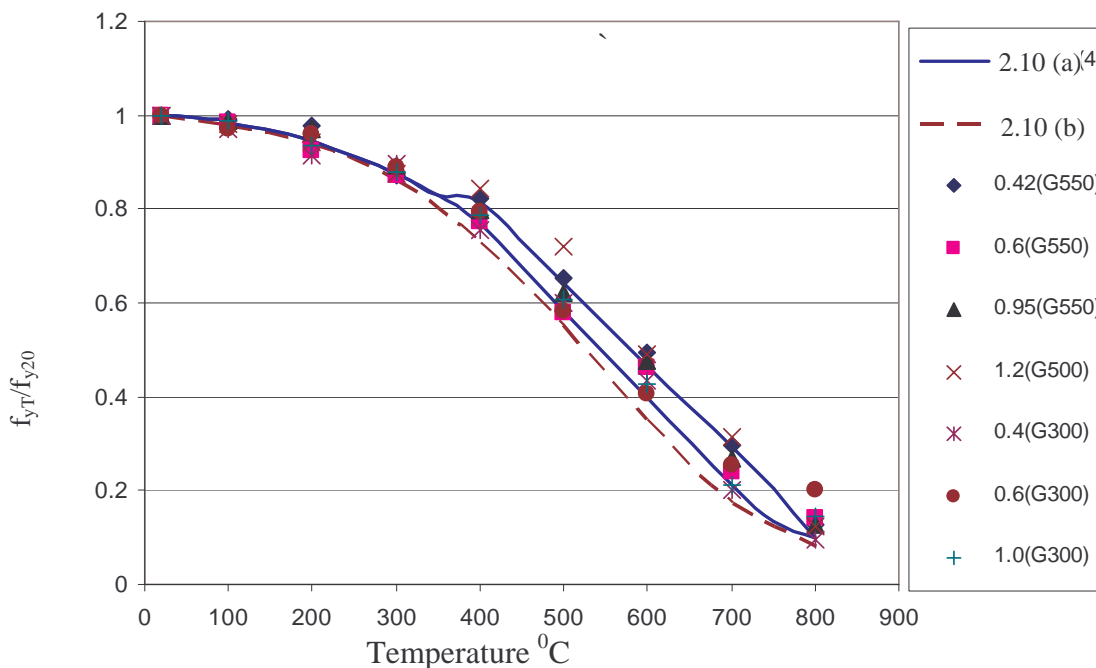
Figure 2.28   Variation of Yield Strength with Temperature

The strength or 0.2% proof stress was measured according to the different strain levels such as 0.2, 0.5, 1.0, 1.5 and 2.0%. Reduction factors for yield strength were calculated as the ratio of yield strength at elevated temperatures to that at ambient temperature (20°C). Since the modulus of elasticity is also an important factor in

determining the buckling stress of thin-walled steel members, the reduction factor for modulus of elasticity was also determined. Test results showed that the influence of the thicknesses on the mechanical properties is negligible, however, it was found that there are some differences between low strength and high strength steel grades in the range of 400-750 °C and this difference is about 10%.

According to Lee et al.'s (2003) results, the variation of yield strength can be categorised into four stages (see Figure 2.28). There is no variation up to 100°C. The reduction rate of the yield strength shows nearly equal values from 100°C to 350°C and from 400°C to 750°C. After around 800°C it shows another rate and the reduction factor is very small. As an example the reduction factors for yield strength and modulus of elasticity of 0.42 mm thickness with G550 cold-formed steel members have been presented here (see Table 2.7). Therefore, the variation of the yield strength with respect to the temperature should be taken into account when selecting the temperature ranges for experiments.

The following equations (Equations 2.11 (a) to (c)) for the reduction factors have been derived by Lee et al. (2003):

◆ Reduction factors for yield strength at temperature T, f_{yT}

$$\frac{f_{yT}}{f_{y20}} = 1.0 \qquad\qquad\qquad\qquad\qquad 20\,℃ \le T < 100\,℃$$

$$\frac{f_{yT}}{f_{y20}} = 0.964 + 0.00045T - 3.08 \cdot 10^{-6}T^2 + 1.969 \cdot 10^{-9}T^3 \qquad 100\,℃ \le T \le 350\,℃$$

$$\frac{f_{yT}}{f_{y20}} = 1.514 - \frac{0.0144 \times T}{f_{y20}^{1/5} + 4.72} \qquad\qquad 400\,℃ \le T \le 750\,℃$$

2.11(a)

$$\frac{f_{yT}}{f_{y20}} = 0.1 \qquad\qquad\qquad\qquad\qquad T = 800\,℃$$

They also developed another equation as follows, which can be used safely for both low and high strength light gauge steels in the temperature range from 20°C to 800°C. These equations are also included in Figure 2.28 which shows a good agreement with experimental data.

$$\frac{f_{yT}}{f_{y20}} = 1.0065 - 0.0004T + 2 \times 10^{-6}T^2 - 10^{-8}T^3 + 7.9 \times 10^{-12}T^4 \quad 20^{\circ}\text{C} \le \text{T} \le 800^{\circ}\text{C} \qquad 2.11\text{(b)}$$

◆ Reduction factors for Elasticity modulus, E_T

$$\frac{E_T}{E_{20}} = 1.0 \qquad\qquad\qquad\qquad 20\,^{\circ}\text{C} \le \text{T} \le 100\,^{\circ}\text{C}$$

$$\frac{E_T}{E_{20}} = 1 - 0.0014\,(T - 100) \qquad\qquad 100\,^{\circ}\text{C} < \text{T} \le 500^{\circ}\text{C} \qquad 2.11\text{(c)}$$

$$\frac{E_T}{E_{20}} = \frac{1 - \dfrac{T}{1200}}{0.00122\,T + 0.3} - 0.203 \qquad\qquad 500\,^{\circ}\text{C} < \text{T} \le 800\,^{\circ}\text{C}$$

Table 2.7   Reduction Factors for Yield Strength and Elasticity Modulus at 0.2% Proof Stress for 0.42mm Thickness G550 Steel (Lee et al., 2003)

Temperature (^{o}C)	Yield strength	Modulus of elasticity
20	1.000	1.000
100	0.993	1.000
200	0.977	0.894
300	0.872	0.702
400	0.821	0.583
500	0.652	0.473
600	0.491	0.238
700	0.297	0.114
800	0.127	0.072

Finally, they observed that the use of reduction factors given in the current steel design specifications for thicker hot-rolled steels is unconservative for light gauge cold-formed steels. However, Lee et al. presented their reduction factors for low and high strength steels with various thicknesses based on an extensive experimental study. But it was subsequently found that there were some errors in the temperature measurements in their study. Therefore, Lee et al.'s (2003) equations should be further investigated by comparing with the others results.

Chen and Young (2004) also studied the mechanical properties of cold-formed steel at elevated temperatures by using steady state and transient state method. They used G550 and G500 steel with the plate thickness of 1.0 and 1.9 mm, respectively. However they used only G500 cold-formed steel with plate thickness of 1.9 mm specimen for transient state test method. They undertook experiments up to 1000°C. Reduction factors of yield strengths were determined at elevated temperatures based on different strain levels of 0.2%, 0.5%, 1.5% and 2%. Figure 2.29 shows the reduction factors of yield strength of both steel grades used by Chen and Young (2004). However, according to their results there is a considerable difference between the reduction factors obtained from G500 and G550 cold-formed steels. But they have presented an unified equation to obtain the reduction factors of 0.2% strain level for both steel grades (see Equation 2.12 (a)). The coefficients a, b, c and n are presented in Table 2.8. They also proposed an equation to obtain the reduction factors of elasticity modulus under transient state conditions for G500, 1.9 mm thick cold-formed steel as shown in Equation 2.12 (b). The coefficients are given in Table 2.9.
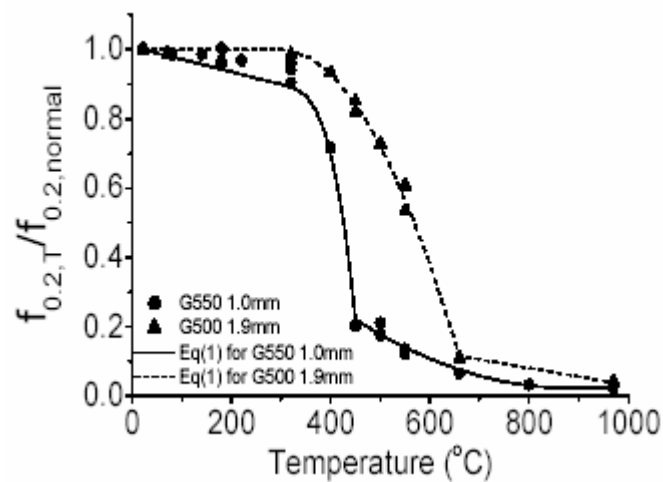
Figure 2.29   Reduction Factors of 0.2% Yield Strength

(Chen and Young, 2004)

$$\frac{f_{0.2,T}}{f_{0.2}} = a - \frac{(T-b)^n}{c}$$

2.12(a)

Table 2.8   Coefficients for Equation 2.12 (a) (Chen and Young, 2004)

	Temperature (°C)	$22 \leq T < 300$	$300 \leq T < 450$	$450 \leq T < 1000$
G550 1.0mm	a	1.0	0.9	0.02
	b	22	300	1000
	c	2.78×10^3	4.8×10^6	9×10^8
	n	1	3	3
	Temperature (°C)	$22 \leq T < 300$	$300 \leq T < 650$	$650 \leq T < 1000$
G500 1.9mm	a	1.0	0.95	0.105
	b	22	300	650
	c	5.56×10^3	1.45×10^5	5×10^3
	n	1	2	1

$$\frac{E_T}{E} = a - \frac{(T-b)^n}{c}$$

2.12(b)

Table 2.9   Coefficients for Equation 2.12 (b) (Chen and Young, 2004)

	Temperature (°C)	$22 \leq T < 450$	$450 \leq T \leq 650$
G500 1.9mm	a	1.0	-0.11
	b	22	860
	c	1.25×10^3	-2.2×10^5
	n	1	2

However, most of the researchers agree that reduction factors for hot rolled steels are not the same as for cold-formed steels. The reduction factors based on 0.2% proof stress presented by various authors and standards are compared in Figure 2.30 for yield strength and Figure 2.31 for elasticity modulus. According to the figures the reduction factors presented by various authors and standards show considerable differences among them. Therefore the mechanical properties reduction factors at elevated temperatures for light gauge cold-formed steel should be further investigated.
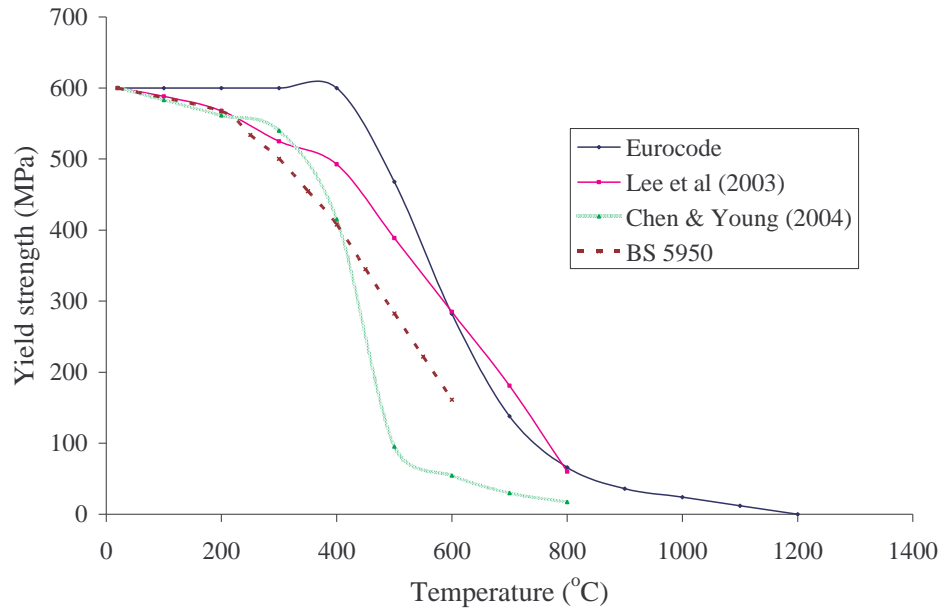
(a)   High strength steel
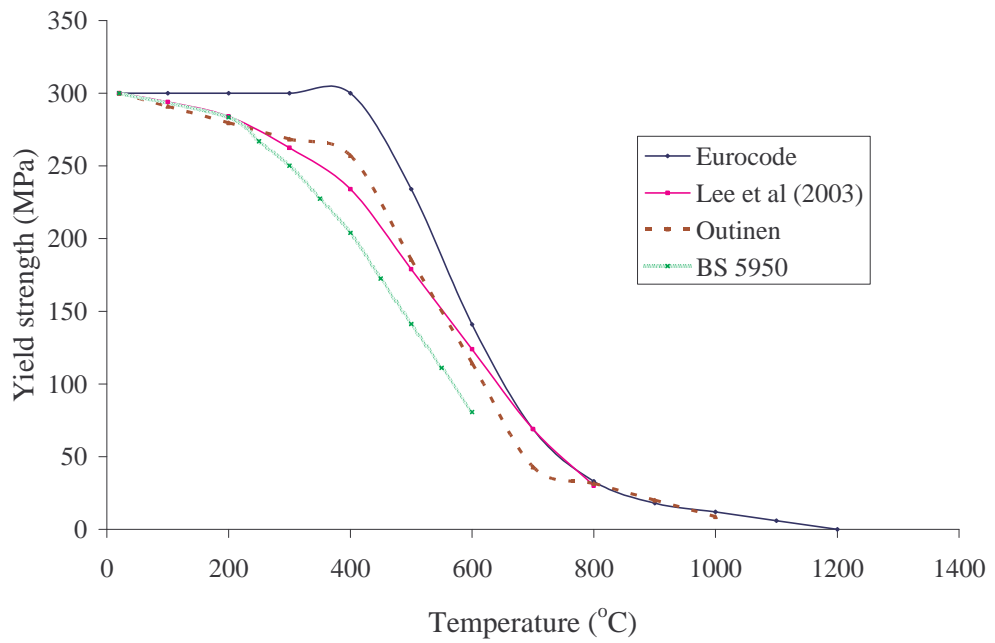
(b)   Low strength steel

Figure 2.30   Comparison of Reduction Factors for Yield Strength
(0.2% proof stress)
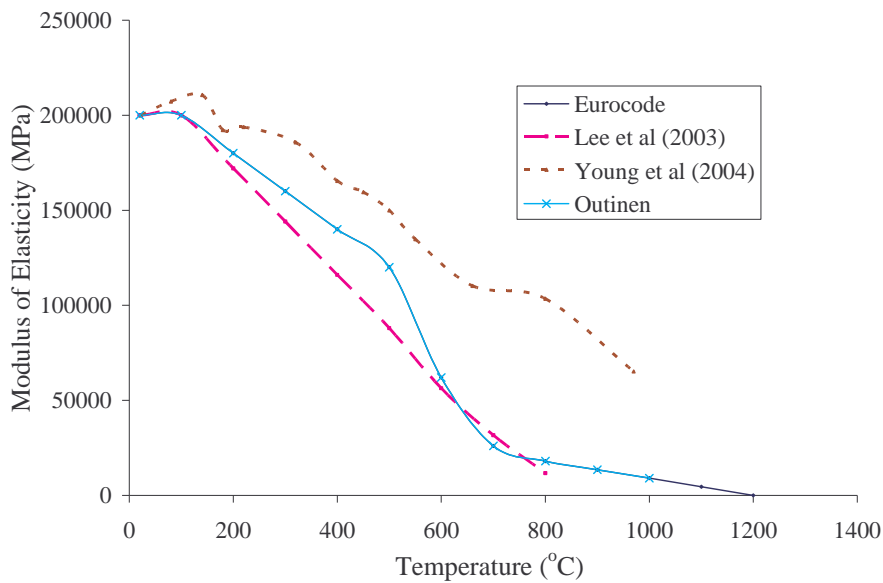
Figure 2.31   Comparison of Reduction Factors for Elasticity Modulus

2.3   Behaviour of Steel Structures at Elevated Temperatures

Due to the reduction of the mechanical properties of cold-formed steels at elevated temperatures, the buckling stress is also reduced. However the buckling behaviour of light gauge cold-formed steel members at elevated temperatures has received little attention in the literature.

2.3.1 Previous Research

Limited research work has been carried out to investigate the behaviour of cold-formed steel structures in a fire situation. Some work has been carried out in Finland, Sweden, The United Kingdom, New Zealand and Australia during the 1990s (Kaitila, 2002).

Klippstein (1978) examined the strength of cold-formed steel wall studs exposed to fire and developed an expression to determine the failure load in a fire situation. However, this expression is limited to regular C-sections and does not include distortional buckling phenomenon. Gerlich (1995) has given another expression to

predict the resistance of steel stud walls. The corresponding stresses under load in the hot inner flange and the cooler outer flange can be calculated for the C-sections in a fire situation.

Based on extensive tests and finite element modelling, Ranby (1998) argued that the basic equations of Eurocode 3, Part 1.3 (ECS, 1993) can be directly used in fire design by simply applying the reduced mechanical properties as a function of temperature. However, he has not considered distortional buckling mode in his studies.

Kaitila (2002) carried out research to compare the Eurocode 3 predictions with finite element analysis results for simply supported plate and lipped channel sections for elastic buckling and ultimate loads. His analysis was carried out for both ambient and elevated temperatures. However, his research was limited to local, flexural and flexural torsional buckling modes.

Ala-Outinen and Myllymaki (1995) carried out experimental and numerical analyses of local buckling behaviour of cold-formed rectangular hollow section (RHS) members in fire conditions. They used the transient state test method for this purpose and found that a concentrically loaded column lost its capacity at the middle of the column due to the local buckling effect while an eccentrically loaded column lost its capacity due to the local buckling failure at the top of the column. Low strength steel (S350) was used in their investigations. They concluded that the effective widths at elevated temperature can be accurately calculated by using the effective width formula of Eurocode 3: Part 1.3 (ECS, 1993) by simply using the reduced mechanical properties.

Lee (2004) carried out a series of experiments to study the local buckling behaviour of cold-formed steel members at elevated temperatures. He has investigated the local buckling behaviour of cold-formed unstiffened and stiffened elements made of low and high strength steel grades with various thicknesses at elevated temperatures. The design equations available in AS/NZS 4600 (SA, 1996) did not predict the ultimate loads at elevated temperatures correctly. Therefore, those equations were modified by simply using the reduction factors of yield strength and modulus of elasticity.

However, these modifications were found to be valid only for low strength steel compression members and hence, new design rules were developed for high strength steel compression members to determine the accurate effective width at elevated temperatures (see Equations 2.13 (a) to 2.13 (c)). The tests carried out under steady and transient state conditions showed that there is no significant difference between the local buckling behaviour with respect to these two methods.

Method 1- Theoretical design method

$$\frac{b_{e,T}}{b} = \sqrt{\eta_T} \sqrt{\frac{f_{cr,T}}{f_{y,T}}}$$
2.13(a)

Method 2 – Semi empirical design method

$$\frac{b_{e,T}}{b} = \frac{0.16}{\lambda_T} \left[1 + \frac{7.96}{\beta_T} - \frac{6.77}{\beta_T^2} + \frac{1.99}{\beta_T^3}\right]$$
2.13(b)

Method 3 – Simplified design method

$$\frac{b_{e,T}}{b} = 0.745(1 - 0.00063T)\sqrt{\frac{f_{cr,T}}{f_{y,T}}}$$
2.13(c)

where f_{yT} and $f_{cr,T}$ are the yield strength and critical buckling stress at temperature T respectively and $\eta_T = \frac{E_{t,T}}{E_T}$, $\lambda_T = \sqrt{\frac{f_{y,T}}{f_{cr,T}}}$ and $\beta_T = 1.052\left(\frac{b}{t}\right)\sqrt{\frac{f_{y,T}}{E_T}}$

Feng et al. (2003a) also investigated the behaviour of short light gauge cold-formed steel channel columns at elevated temperatures based on experimental studies, design calculations and numerical analysis. Their focus was on the experimental behaviour and to determine the physical behaviour and failure modes of cold-formed steel channel sections. Strength tests were carried out using lipped channels with and without service holes, and unlipped channels. Two types of tests were carried out: ambient temperature tests and elevated temperature tests. In the elevated temperature tests, the experiments were carried out under steady state conditions. The column length was chosen as 400 mm as they considered that it was long enough to minimise the end effects while being short enough to eliminate overall buckling.

All the unlipped channel members failed due to local buckling, while lipped channel members failed due to a combination of local and distortional buckling and bending

modes. From the final failure mode of the column, it can be assumed that the behaviour of the column at elevated temperatures is similar to the behaviour of columns at ambient temperature. But since the elevated temperature tests were carried out in a kiln only the final deformed shape was observed and the actual behaviour of columns during the testing was not known. However, as they expected the stiffness of the columns was reduced with temperature increase. Furthermore, some initial imperfections and practical difficulties have meant that this research has not given a clear understanding of distortional buckling behaviour at elevated temperatures. This research was also limited to low strength light gauge cold-formed steel members with a steel grade of S350 GD + Z (minimum yield strength = 350 MPa) and thicknesses of 1.2, 1.5 and 2.0 mm.

Feng et al. (2003b) have modified the current design rules to enable the distortional buckling at elevated temperatures for short columns under uniform temperatures. They modified an expression to determine the effective width of the flange when the section failed by distortional buckling. The well known effective width formula for local buckling was modified to suit distortional buckling (see Equation 2.14). However, this equation is limited for flanges of lipped channel sections.

$$\frac{b_{eff,de}}{b} = 1 \qquad \text{for } \lambda \leq 0.673$$

$$\frac{b_{eff,de}}{b} = \sqrt{\frac{\sigma_{de}}{f_y}}\left(1 - 0.22\sqrt{\frac{\sigma_{de}}{f_y}}\right) \qquad \text{for } \lambda \geq 0.673$$

(2.14)

where,

$b_{eff,de}$ = effective width of the flange plate for distortional buckling

σ_{de} = elastic distortional buckling stress

$$\lambda = \sqrt{\frac{f_y}{\sigma_{de}}}$$

The test results were compared with the modified values with respect to British Standard BS 5950 Part 5 (BSI, 1990), Eurocode 3 Part 1.3 (ECS, 1993) and the American Specification (AISI, 1996). By including the reduction factors for 0.2% proof stress from Outinen (1999) and Eurocode 3 Part 1.2, they showed that the predicted failure loads are close to test failure loads. The use of the reduced yield strength based on 0.2% proof stress and the reduced elastic modulus, the ambient

temperature design formula can be extended to elevated temperatures. But since there were many shortcomings in the experiments reported by Feng et al. (2003a), their results should be further investigated.

Feng et al. (2004) carried out a numerical study to determine the influence of initial imperfections on the ultimate strength of cold-formed steel compression members by considering rectangular hollow sections at elevated temperatures. The stress-strain relationship at elevated temperatures was used based on Outinen (1999) model, ENV1993-1-2-(2001) and an elastic perfectly plastic stress-strain representation. They showed that the local buckling imperfection has a significant effect on the ultimate strength of the columns, which buckle locally while global imperfection has a significant effect on the ultimate strength of the columns, which buckles globally. They have studied these compression members under uniformly heated conditions. According to their studies, initial imperfection has a significant influence on the load carrying capacity of light gauge cold-formed steel compression members under uniform heating.

Further, Feng et al. (2004) investigated the influence of stress-strain relationship of cold-formed steel compression members at elevated temperatures. Since there is no specific method to determine the stress-strain relationship of cold-formed steel, the available methods as Outinen (1999), ENV1993-1-2 and perfect elastic-plastic methods were used to see the column failure load at various temperatures such as ambient, 400°C and 600°C. They showed that the stress-strain relationship also affect the column failure load regardless of temperature. However, this investigation considered both local and global buckling behaviours but not the distortional buckling behaviour of light gauge cold-formed steel at elevated temperatures. On the other hand the exact mechanical properties of light gauge cold-formed steel were not used since they were not available. Therefore distortional buckling behaviour of light gauge cold-formed steel compression members should be examined by using accurate mechanical properties at elevated temperatures.

Extensive research work has been carried out on conventional hot-rolled steel structures at elevated temperatures and the relevant results have been included in steel design standards and specifications for economical and safer design (Valente

and Neves, 1999). However, they are not applicable to light gauge cold-formed steel structures.

Gardner and Nethercot (2006) discussed the design of stainless steel members at ambient temperature. They proposed new design equations (see Equations 2.15 (a) to (c)) which are different from the carbon steel design methods. Carbon steel design equations are based on elastic perfect plastic stress-strain behaviour. However stainless steel exhibits a rounded stress-strain curve. According to the previous research on cold-formed steel, the cold-formed steel shows rounded stress-strain behaviour at high temperatures. Therefore Gardner and Nethercot's (2006) method should be considered in developing the new design rules at elevated temperatures for light gauge cold-formed steel members. However, they considered the local buckling behaviour of compression members, but distortional buckling behaviour was not considered. In Gardner and Nethercot's (2006) method, the cross-sectional slenderness was defined as follows

$$\beta = \left(\frac{b}{t}\right)\sqrt{\frac{\sigma_{0.2}}{E_0}}\sqrt{\frac{4}{k}} \quad \text{for SHS and RHS} \qquad \text{2.15(a)}$$

Local buckling strain at ultimate load was defined as

$$\frac{\varepsilon_{LB}}{\varepsilon_0} = \frac{7.07}{\beta^{2.13+0.21\beta}} \chi^{-0.3\beta^{0.5}} \qquad \text{2.15(b)}$$

χ is cross-section aspect ratio for RHS subjected to pure compression and is taken as 1.0 for all the other cases.

$$\varepsilon_0 = \frac{\sigma_{0.2}}{E_0} \qquad \text{2.15(c)}$$

The ultimate local buckling stress, σ_{LB}, was then obtained from the stress-strain curve for stainless steel based on the determined values of ε_{LB} and $\sigma_{0.2}$.

2.3.2 Analysis Method

As for the structural investigations at ambient temperature, the finite strip analysis program Thin-wall and finite element analysis program ABAQUS can be used to

analyse the distortional buckling behaviour of light gauge cold-formed steel members at elevated temperatures. However, unlike for ambient temperature the reduced mechanical properties must be used for elevated temperatures.

2.3.3 Experimental Methods

Lee (2004) carried out a series of full scale tests to investigate the local buckling behaviour of light-gauge cold-formed steel members at elevated temperatures. All the tests were carried out using the specially designed electric furnace by him (see Figure 2.32). Displacement control method was used to apply the compression load. Thermocouples were used to examine the temperature in the furnace and the test specimen. The furnace was electrically heated by using glow bars. Further, an automatic temperature controller was used to ensure the upper limit of temperature correctly. As shown in Figure 2.32 an extensometer was used to measure the horizontal displacement of the flange. He considered the following test methods for his experiments: Elevated temperature tests using steady state test method and transient state test method.

Feng et al. (2003a) also carried out a series of tests on short channel columns at elevated temperatures. Their tests were also carried out in an electrically heated kiln (see Figure 2.33). Five thermocouples were used to measure the temperature in test columns. Four displacement transducers (two at the top and two at the bottom) were used to measure the longitudinal displacements of columns. They used four temperature levels of 250, 400, 550 and 700$^{\text{o}}$C. The steady state method was used to carry out all the tests. First, the kiln temperature was increased up to the desired level and then it was kept constant for about twenty minutes to allow the specimen to reach uniform temperature. The thermal expansion of the specimen was totally free and hence, no induced compression force was present on the specimen until the load was applied. Load control method was used to apply the compression load
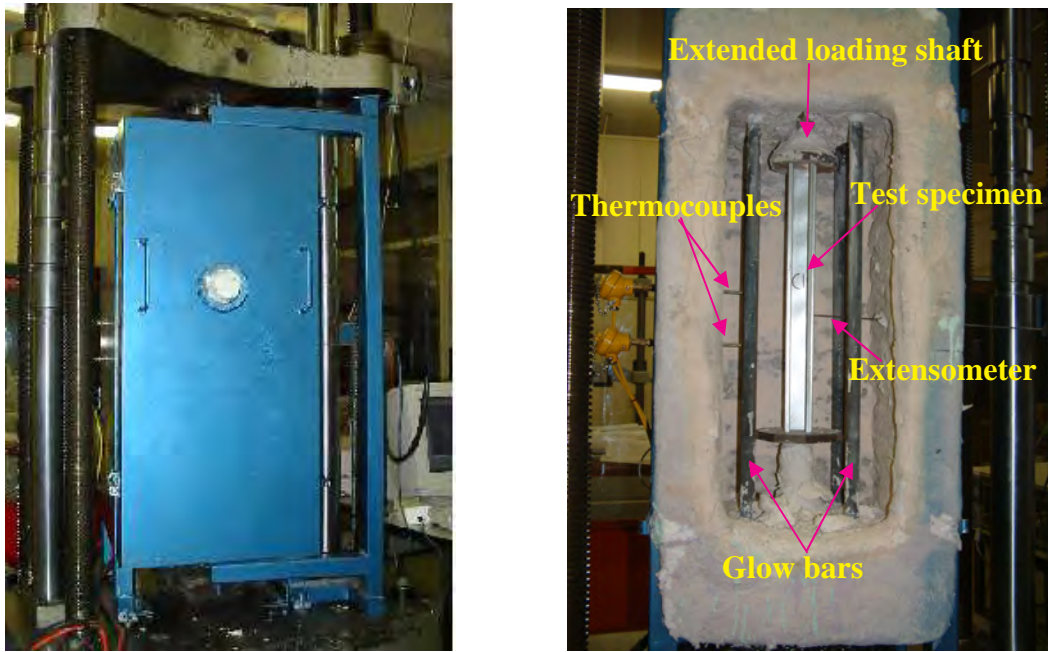
Figure 2.32   Elevated Temperature Test Rig used by Lee (2004)
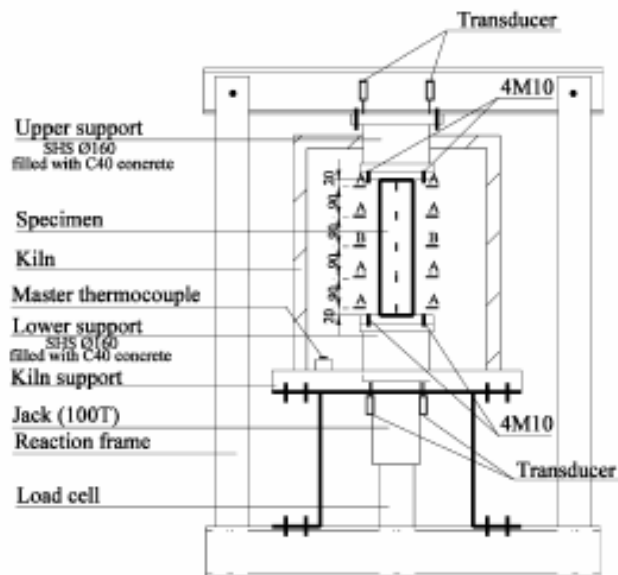
Figure 2.33   Elevated Temperature Test Rig used by Feng et al. (2003a)

Among these two, the method used by Lee (2004) is more advanced than that of Feng et al. (2003a). Only the vertical displacement can be measured in the method used by Feng et al. (2003a) since it has displacement transducers at the top and bottom. But in Lee's method, an extensometer was used to measure the horizontal displacement of the flange. Since flange movement is a major issue in distortional

buckling mode, measurement of horizontal displacement is more important. Further, there is an automatic temperature controller in Lee's method, which controls the upper limit of temperature correctly. Lee (2004) used displacement control method while Feng et al. (2003a) used load control method to apply compression load. However, the displacement control method is safer than the load control method since it avoids sudden failure.

2.3.4 Current Design Rules at Elevated Temperatures

Many design specifications have not addressed the distortional buckling behaviour at elevated temperatures for light gauge cold-formed steel members. Following paragraphs clearly prove that there is not a current standard or specification regarding the distortional buckling behaviour of cold-formed steel members at elevated temperatures.

Although the current Australian standard for steel structures, AS 4100 (SA, 1998) has addressed the design for fire conditions, it has not considered light gauge cold-formed steel sections nor their distortional buckling behaviour. Instead it has concentrated on the variation of mechanical properties such as yield stress and the modulus of elasticity of steel at elevated temperatures. Since they were determined only for heavier, hot-rolled steel members, they could not be used for cold-formed steel structures. If these design values are used for light gauge cold-formed members, it may lead to overly conservative designs.

The British and European design standards (BSI, 1990; ECS, 1993) discuss fire design of light gauge cold-formed steel members; however, they present the reduction factors for mechanical properties (see Section 2.2.7) and rules for local and flexural buckling modes. On the other hand, the American Specification (AISI, 1996) does not discuss fire design at all. Although Australian/New Zealand Standard AS/NZS 4600 (SA, 1996) has included distortional buckling of cold-formed steel sections it is limited to ambient temperature.

2.4   Literature Review Findings

It is clear that light gauge cold-formed steel members are more useful than the conventional hot-rolled steel members both economically and structurally. However, there is still limited knowledge of them. Specific rules and regulations regarding distortional buckling behaviour are not widely included in the current standards and specifications. AS/NZS 4600 (SA, 1996) has addressed the distortional buckling behaviour of cold-formed steel members and included design equations. However, these equations are limited to specific shapes and do not address the distortional buckling behaviour at elevated temperatures.

The current Australian Standard AS 4100 (SA, 1998) focuses only on heavier hot-rolled steel sections and cannot be used for light gauge cold-formed steel sections. Eurocode 3: Design of Steel Structures Part 1.3 (ECS, 1993) and British Standard Part 5 (BSI, 1990) have addressed the behaviour of cold-formed steel members. However, their design equations are limited to local and flexural or flexural torsional buckling behaviour. Further, none of these standards have addressed the distortional buckling failure mode at elevated temperatures.

Although extensive research has been carried out all around the world in the field of cold-formed steel structures, there is inadequate knowledge about the distortional buckling mode of cold-formed steel structures. A number of researchers has focussed their attention on various aspects of the distortional buckling mode but due to some experimental difficulties, results are not conclusive. Furthermore, the knowledge of distortional buckling behaviour at elevated temperature is very little while there is limited knowledge of it at ambient temperature.

Most experiments regarding distortional buckling failure were carried out at the University of Sydney and relevant design equations have been developed. However, they were limited to specific sections and ambient temperature condition. Therefore their validity for more sections should be investigated and the validity at elevated temperatures should be investigated based on the results obtained.

Lau and Hancock (1988) and Schafer and Pekoz (1998) stated that the post buckling capacity is very low when the elastic failure occurs by distortional mode while Kwon and Hancock (1993) argued that significant post-buckling stress exists after the elastic distortional buckling failure. However, this may depend on the geometry of the section and should be further investigated.

Effect of pin-end and fixed-end conditions on the distortional buckling behaviour was not fully understood. Young and Rasmussen (1995) stated that there is no significant effect due to the end conditions while Kesti and Davies (1999) and Kwon and Hancock (1993) argued that the failure load under fixed-end conditions is higher than that of pin-end conditions. However, based on Yang and Hancock's (2003) and Young and Hancock's (2003) results, the end effects are negligible for longer columns. Therefore this should be further investigated by using various types of sections.

Schafer and Pekoz (1998) have proposed a direct strength method to obtain the distortional buckling strength at ambient temperature. However this method is limited to pin-end conditions and some specific cross-sections and should be further investigated.

Geometric imperfections can have a considerable influence on the ultimate load when the failure of compression members is governed by distortional mode. Many researchers have presented some explanations to determine the geometric imperfections but there are some contradictions between them. Therefore it is recommended that the measured imperfection values are used when determining the ultimate loads. Further research is needed to develop guidelines on the more likely levels of geometrical imperfections for cold-formed steel structures.

Elevated temperatures influence the mechanical properties of cold-formed steels significantly. Research has already been carried out by Lee et al. (2003) and they have proved that the reduction of yield strength depends upon the steel grades. Further they developed reliable equations to determine the reduction factors of mechanical properties at elevated temperatures. Nevertheless, the reductions factors were presented for various steel grades and thicknesses based on 0.2% proof stress,

0.5%, 1.5% and 2.0% strain levels. However, their equations cannot be further used due to some limitations of the experimental methods used by them. Therefore the mechanical properties of light gauge cold-formed steels at elevated temperatures should be investigated.

Ranby (1998) stated that the basic equations of Eurocode 3 (ECS, 1993) can be used in fire design by applying the reduced mechanical properties. However, his research was limited to local, flexural and flexural torsional buckling. Ala-Outinen and Myllymaki (1995) also stated that the effective width at elevated temperatures can be accurately determined from the effective width formula of Eurocode 3 (ECS, 1993) by simply using the reduced mechanical properties. However, this research was limited to low strength steels. Further, Lee (2004) also agreed with this observation relating to the effective width equations of AS/NZS 4600 (SA, 1996). However, he showed that AS/NZS 4600 (SA, 1996) equations cannot be used to predict the ultimate load of high strength steel compression members by simply using the reduced mechanical properties. Further, his research was limited to local buckling behaviour. This phenomenon should be investigated for available distortional buckling equations or any new distortional buckling equations which will be developed at ambient temperature.

Following their experiments on local and distortional buckling modes at ambient and elevated temperatures, Feng et al. (2003a and b) stated that the design equations of BS 5950 (BSI, 1990), Eurocode 3 (ECS, 1993) and American Specification (AISI, 1996) can be used to predict the ultimate load at elevated temperatures by using the reduced mechanical properties. However, their research was limited to low strength steels and specific sections. Further, due to the many limitations in the experiments as reported by Feng et al. (2003a and b), their results should be further investigated.

In summary, it is clear that distortional buckling behaviour of light gauge cold-formed steel compression members at ambient and elevated temperatures should be further investigated. There is limited knowledge and understanding of distortional buckling behaviour at elevated temperatures. In addition, the mechanical properties of light gauge cold-formed steels should be determined at elevated temperatures.

3 Mechanical Properties of Light Gauge Cold-formed Steels

3.1 Mechanical Properties at Ambient Temperature

The structural behaviour of light gauge cold-formed steel compression members depends mainly on their mechanical properties. These properties are also essential for finite element and finite strip analyses under various temperatures. Therefore a good knowledge of the mechanical properties of light gauge cold-formed steel is very important. The yield strength (f_y) and the ultimate tensile strength (f_u) of cold-formed steel directly depend upon the amount of cold work. The yield strength and the ultimate strength of the cold-formed steel can be increased with the increasing of cold working while the ductility of steel is decreasing.

(a) Sharp yielding

(b) Gradual yielding
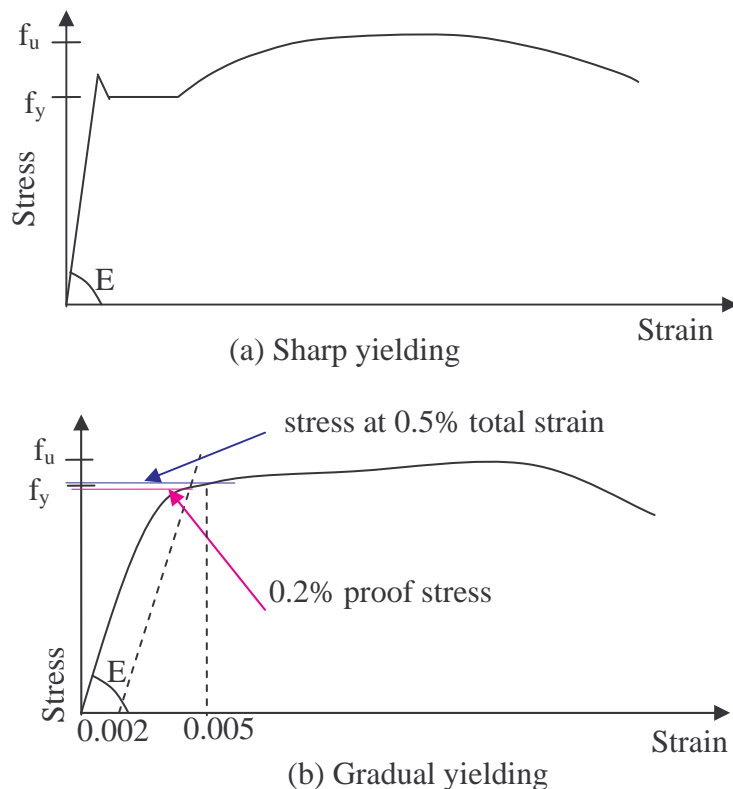
Figure 3.1   Stress-strain Curves

The mechanical properties of steel are determined from the stress-strain curves obtained from tension or compression coupon tests. Two main types of stress-strain curves can be observed: a sharp yielding type and a gradual yielding type (see Figure 3.1). In the sharp yielding type, the yield point can be defined easily. The level at which the stress-strain curve becomes horizontal is defined as the yield point. In the gradual yielding type, the yield point is defined by the off-set method or the strain-under load method. In the off-set method the yield point is defined by 0.2% proof stress while in the strain-under load method, it is the stress corresponding to 0.5% of total strain (see Figure 3.1). However, the yield points determined by these two methods are similar in most cases.

On the other hand, the mechanical properties may depend upon the test method used (tension or compression coupon test). Therefore, a series of coupon tests was carried out to determine the mechanical properties of light gauge cold-formed steels under compression and tension loads.

3.1.1 Tension Coupon Tests

Tension coupon tests were carried out for both low (G250 with a nominal yield strength of 250 MPa) and high strength (G550 with a nominal yield strength of 550 MPa) steel specimens. Tension test coupons were taken from the same batch of steel which was used to cut compression coupons and buckling test specimens. They were cut in the longitudinal direction of the steel sheets.
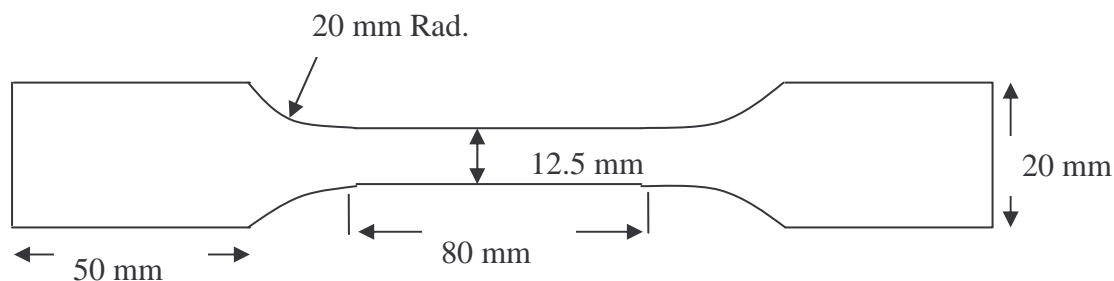
(a)　　Dimensions of tension test coupon in mm

Figure 3.2　　Tension Test Coupons and Dimensions

(b)   Tension test coupons

Figure 3.2   Tension Test Coupons and Dimensions
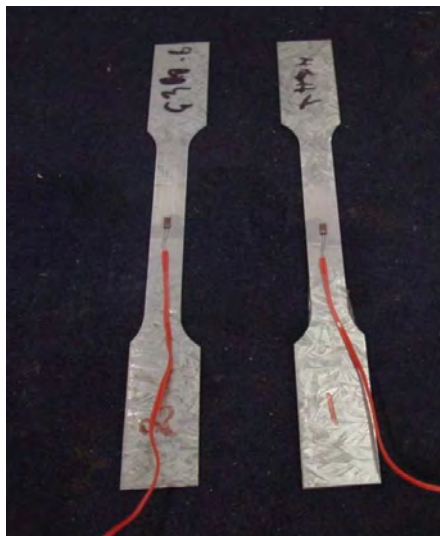
(a) Strain gauge arrangement
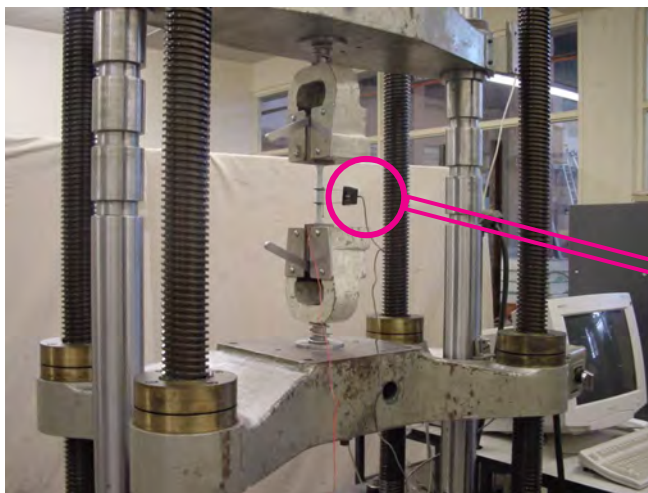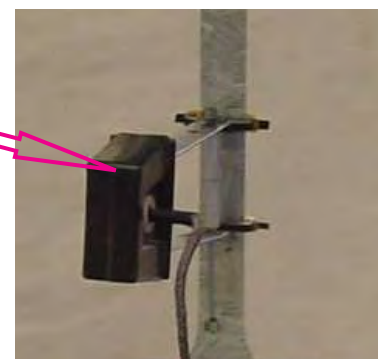
(b) Test method   (c) Extensometer

Figure 3.3   Tension Test Arrangement

All the tests were carried using the method specified in the Australian Standard AS 1391 (SA, 1991). The dimensions of the tension coupons (see Figure 3.2) were decided as specified in AS 1391 (SA, 1991). A 2 mm strain gauge on each side of the coupon (see Figure 3.3) and a 25 mm gauge length extensometer were used at the middle of the specimen to measure the strain more accurately. The tests were carried out by using a Tinius Olsen testing machine in the QUT Structural Testing Laboratory (see Figure 3.3). A displacement control method was used to apply the tension load at a rate of 0.5 mm per minute. Specially made plates were attached to the cross head of the tension test machine to prevent the slippage of test specimens when the load was applied. The tension force was applied until a fracture occurred in the specimen (see Figure 3.4). The dimensions of the specimens were measured prior to the experiments. The total coating thickness and the base metal thickness were measured using a micrometer screw gauge. The coupons were immersed in a 1:1 diluted hydrochloric acid basin to remove the steel coating. These measured dimensions were then used to calculate the tensile stress.
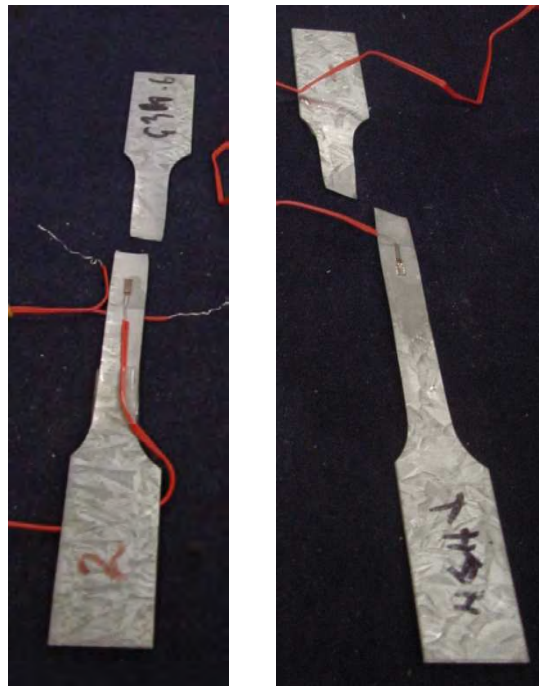
Figure 3.4   Failure Patterns of Tension Coupons

The load and strain were automatically recorded at one second intervals by using a data logger. All the experiments were repeated twice in order to obtain better results.

Typical stress-strain curves derived from these results are shown in Figures 3.5 (a) and (b) for G250 and G550 steels, respectively. As shown in Figure 3.5, a yield point with a yield plateau exists for G250 steel while it does not exist for G550 steel. This happens because the G550 steel undergoes cold reducing (hard rolling) during the manufacturing process. Further the linearity of the stress-strain curve of G550 steel does not continue up to the yield point.
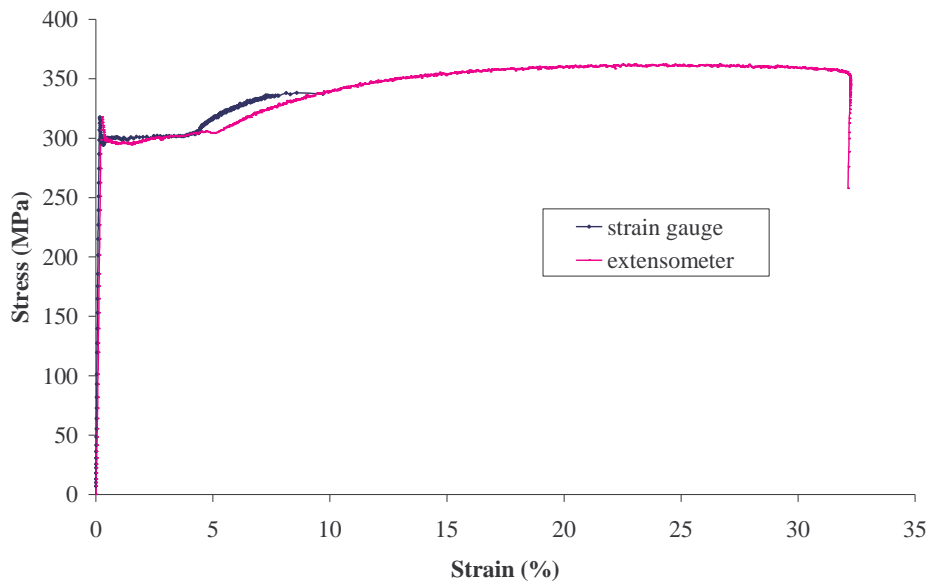
(a)   0.8 mm G250 steel
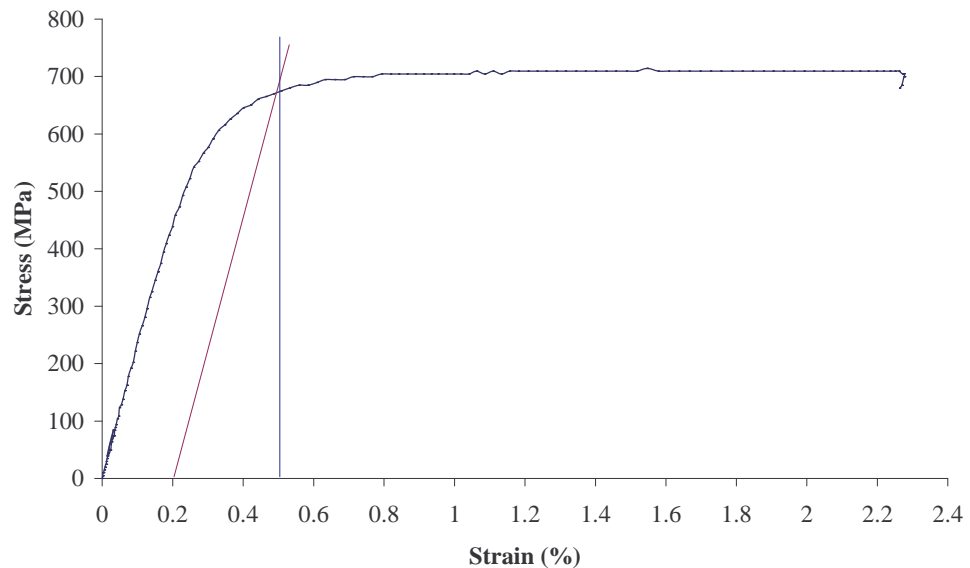
(b)   0.6 mm G550 steel

Figure 3.5   Typical Stress-strain Curves from the Tension Coupon Tests

The yield strength and the elasticity modulus were measured for both grades of steel. The measured values of yield strength and Young's modulus of steel are shown in Table 3.1. The slope of the initial linear elastic part of the stress-strain curve was taken as the elastic modulus. The yield strength of low strength steel was measured directly from the stress-strain graph while the yield strength for high strength steel was measured based on both the 0.2% proof stress and the 0.5% total strain methods. As can be seen in Figure 3.5 (b), the tension yield strengths (f_y) obtained from the 0.2% proof stress and the 0.5% total strain methods for high strength steel are about the same. Hence Table 3.1 includes only the yield strength obtained from the 0.2% proof stress method. The ultimate tension strength was also measured. The difference between the tension yield (f_y) and ultimate (f_u) strengths for high strength steel is small (around 1 to 3%) while low strength steel shows considerable difference (around 13 to 22%).

Table 3.1   Mechanical Properties of Cold-formed Steel

Steel Grade	Measured thickness (mm)		Tension yield strength f_y (MPa)	Tension ultimate strength f_u (MPa)	Elasticity modulus E (MPa)	f_u/f_y
	TCT	BMT				
G250	0.59	0.54	320	370	200000	1.16
	0.80	0.75	300	365	200000	1.22
	0.96	0.91	320	361	200000	1.13
G550	0.67	0.60	678	700	220336	1.03
	0.85	0.80	648	670	201785	1.03
	1.00	0.95	618	625	200000	1.01

Note: TCT – Total coating thickness, BMT – Base metal thickness

3.1.2 Compression Coupon Tests

Hancock (1998) stated that the tension yield strength and the compression yield strength of cold-formed steels are different due to the Bauschinger effect with respect to both longitudinal and transverse directions. He mentioned that the

longitudinal tension yield strength is greater than the compression yield strength while the transverse tension yield strength is smaller than the compression yield strength in the same steel with the same cold work.

In addition, according to AS/NZS 4600 (SA, 2003), a reduction factor has to be applied to the yield strength of light gauge G550 steel since it has lower ductility than other steels. When the steel thickness is less than 0.95 mm, the reduction factor is 0.90 whereas it is 0.75 for steel thickness less than 0.6 mm. However, only tension yield strength has been tested in the past and a good understanding of yield strength under tension and compression loads is very limited. Further only AS/NZS 4600 includes such reduction factors for design purposes.

Therefore a series of compression coupon tests was also undertaken to determine the yield strength of light gauge cold-formed steel members. The high strength steel G550 was used with various thicknesses: 0.42, 0.6, 0.8 and 0.95 mm. Unlike the tension coupon tests there were no standard specifications for the compression coupon tests. Therefore the test method and the dimensions of the compression coupon had to be decided prior to the tests. The dimensions of the compression test coupons were selected by limiting their l/r ratio to less than 20 (l = length of the testing part and r = radius of gyration) to avoid member buckling. Test coupons were 5 mm width x 105 mm length rectangular pieces cut in the longitudinal direction of the steel sheet.

At least three specimens were tested for each thickness. A specially designed test assembly made of stainless steel was used for the compression coupon tests (see Figure 3.6). Stainless steel was used to prevent any frictional force when the specimen slid down. Although the specimen length was 105 mm, only a 5 mm gap was provided without any clamping to avoid failure due to buckling. Further three coupon plates were glued with epoxy in the case of 0.42 mm thick steel and two plates were glued for 0.6 and 0.8 mm thick steels to eliminate member buckling failures.

The dimensions of specimens and the coating were measured prior to tests. The Tinius Olsen testing machine which was used for tension coupon tests was also used

for this series of tests. The compression force was applied under displacement control at a rate of 0.3 mm/min.
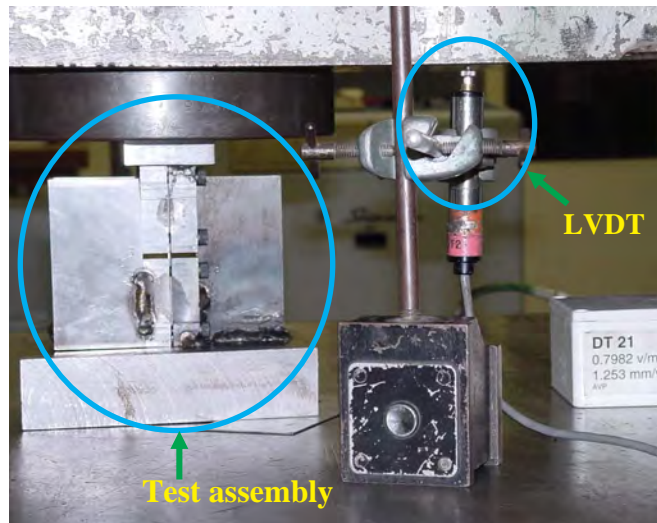
(a) Test photograph
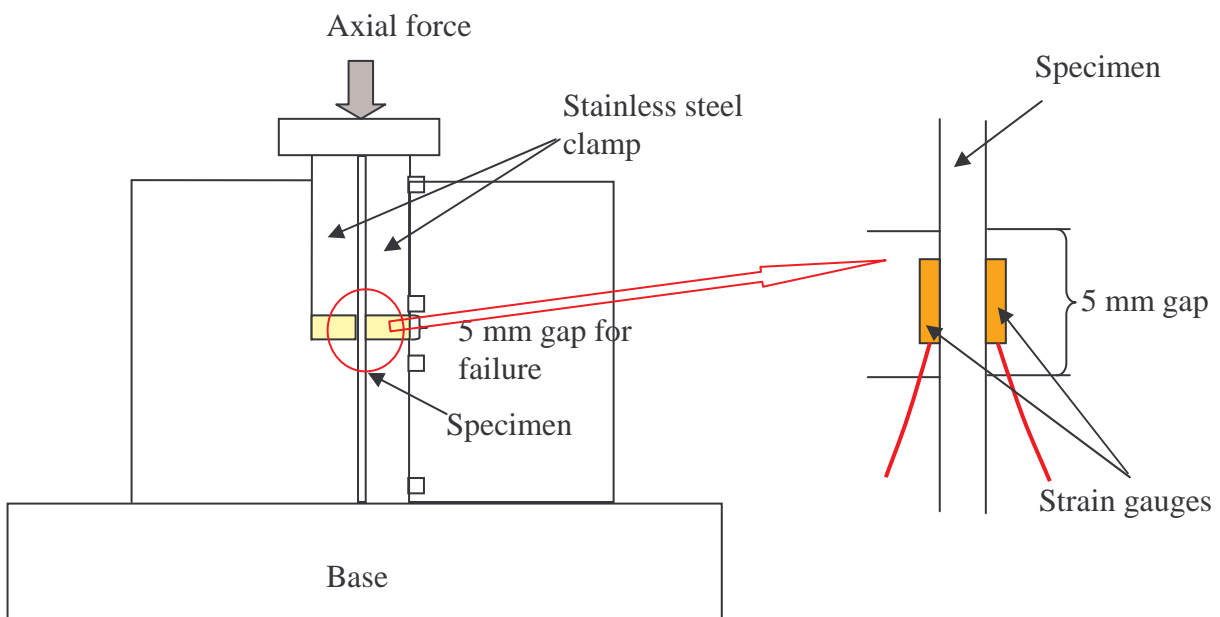
(b) Schematic diagram

Figure 3.6   Compression Coupon Test Arrangement
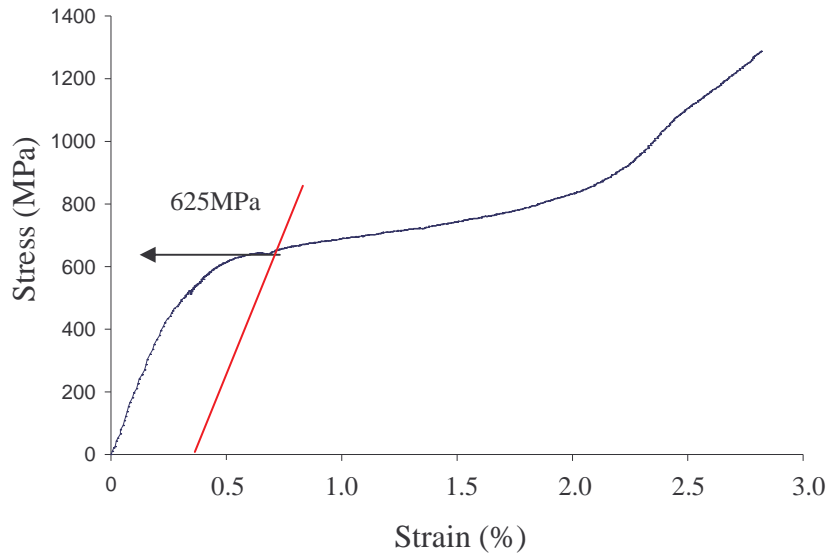
Figure 3.7   Typical Stress-strain Curve from the Compression Coupon Test of 0.95 mm G550 Steel obtained using LVDT Measurements

(a) Specimen before failure

(b) Specimen after failure
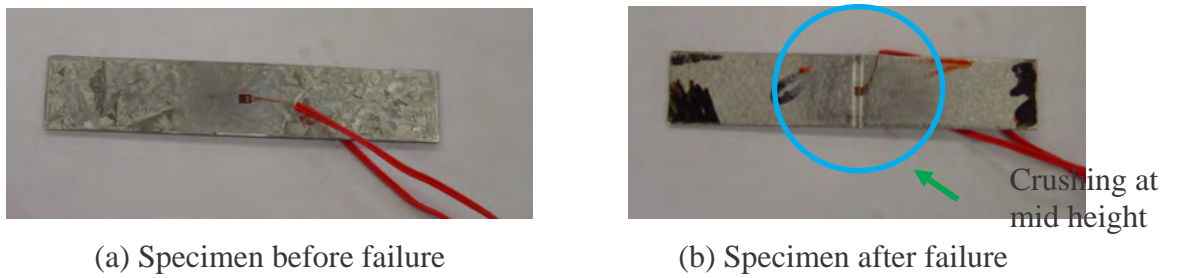
Figure 3.8   Compression Coupons with 0.2 mm Strain Gauges
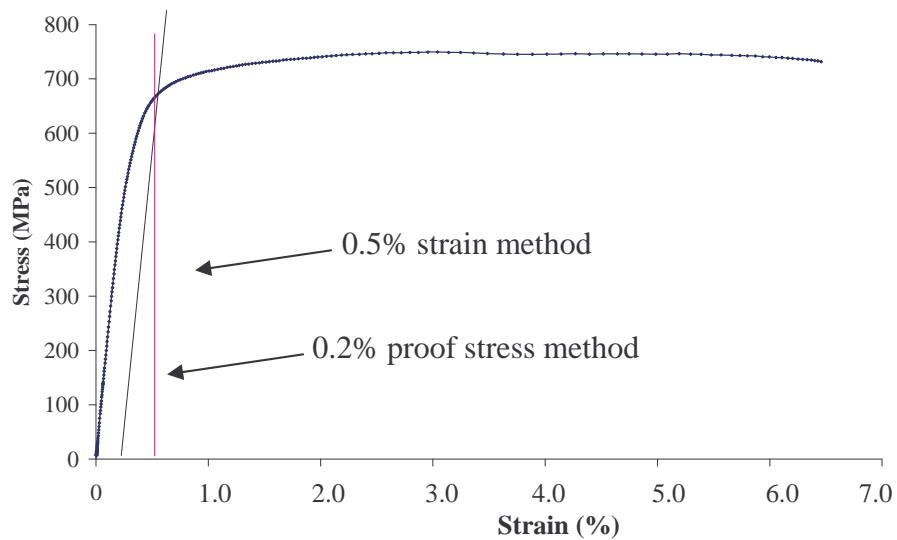
Figure 3.9   Typical Stress-strain Curve from the Compression Coupon Test of 0.6 mm G550 Steel using Strain Gauges

Initially a 5 mm LVDT (Linear Variable Displacement Transducers) was used to measure the shortening of the specimen. The failure mode of the specimen was a crushing failure. Stress-strain curves were derived from the results as shown in Figure 3.7. The yield strength based on the 0.2% proof stress method and the elasticity modulus (ratio between stress and strain in the linear elastic region) were calculated. The values of compression yield strengths were close to tension yield strength values. However, the elasticity modulus obtained from this method appeared to be inaccurate. Moreover, the accuracy of results acquired from the compression coupon tests depends upon the accuracy of LVDT used and there was an undesirable effect from the initial settlement of the specimen. The accuracy of 5 mm LVDT which was used for the compression coupon test was about 5%. Thus, further compression coupon tests were undertaken using strain gauges, a more accurate method. The strain gauges had a gauge length of 0.2 mm and were attached to both sides of the specimen as shown in Figure 3.8.

The yield strengths were measured by using both the 0.2% proof stress and the 0.5% total strain methods as shown in Figure 3.9. Unlike in the tension coupon test, it was difficult to determine the ultimate failure load from the compression coupon tests since crushing was at the mid point of the specimen and the stress was still increasing at the failure of strain gauges.

3.1.3 Comparison of Compression and Tension Coupon Test Results

The mechanical properties obtained from the compression coupon tests for high strength steel were then compared with those obtained from the tension coupon tests (see Table 3.2). Further, the available tension coupon test results from the past research at QUT were also compared with the compression coupon test results.

However, as can be seen in Tables 3.2 and 3.3 there is a good agreement between the yield strengths obtained from tension and compression coupon tests for 0.42 mm and 0.95 mm thickness specimens while 0.8 mm thickness specimen showed a lower value for the compression coupon test.

Table 3.2   Tension and Compression Coupon Test Results

Measured BMT (mm)	Compression coupon				Tension coupon			
	f_y (MPa)		E (MPa)		f_y (MPa)		E (MPa)	
	Measured	Average	Measured	Average	Measured	Average	Measured	Average
0.42	700 690	695	231818 214285	223051	700	700	233000	233000
0.60	680 640 662 655 620	651	218918 211764 211764 200000 220000	212489	675 680	678	220673 220000	220336
0.80	600 580 565 550 580 580 555	573	214285 216000 200000 200000 200000 205128 205128	205791	650 645	648	203571 200000	201785
0.95	605 610 600 620 625	612	222222 222222 214285 225000 200000	216745	610 625	618	200000 200000	200000

Table 3.3   Comparison of Tension and Compression Coupon Test Results

Measured BMT (mm)	Tension yield strength / Compression yield strength
0.42	1.007
0.60	1.041
0.80	1.131
0.95	1.010
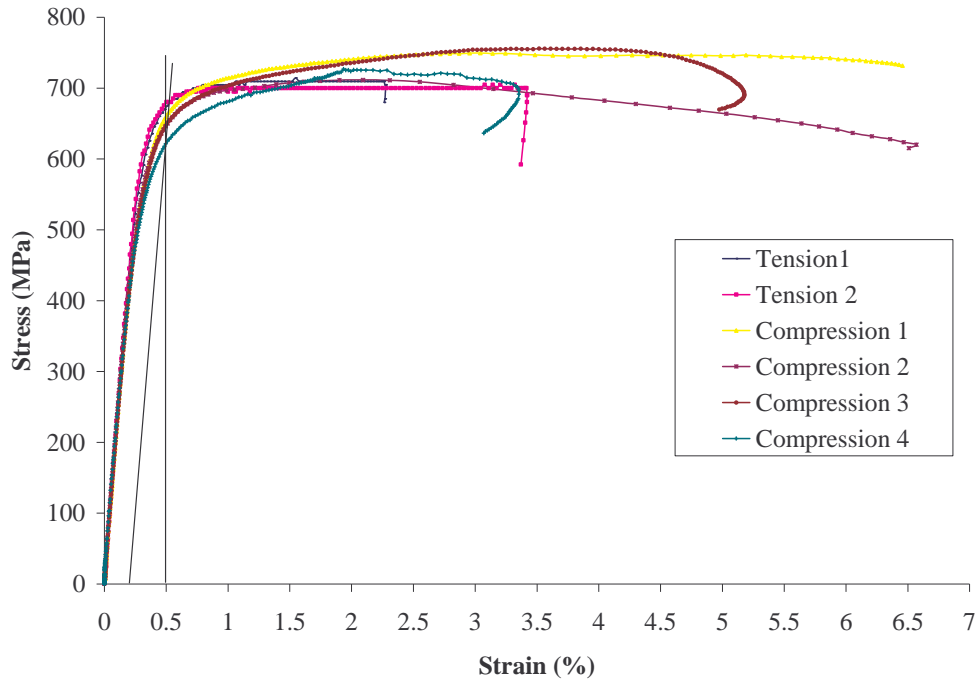
(a)   0.6 mm thick G550 steel
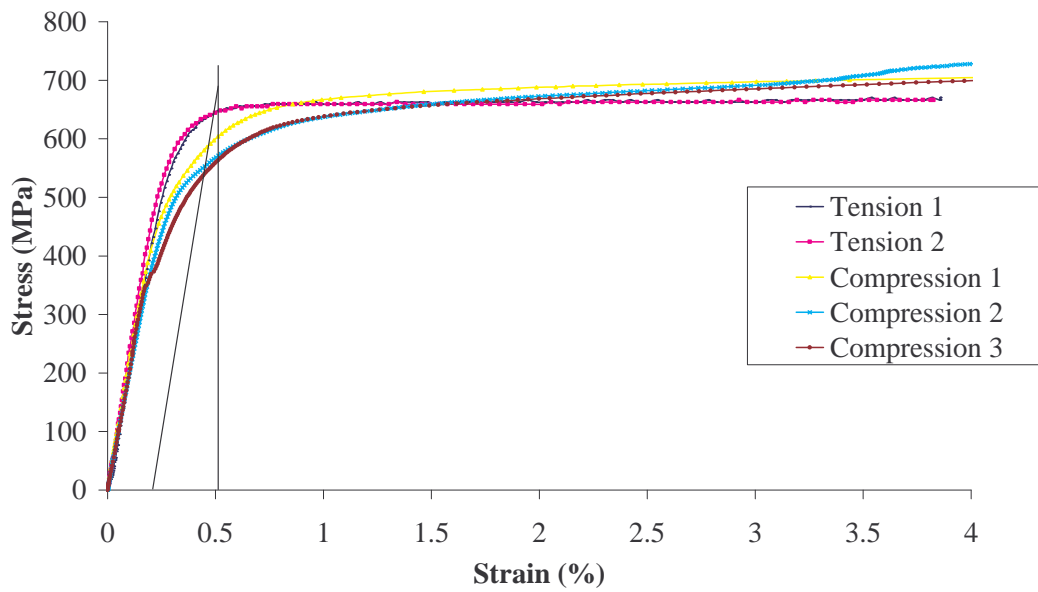
(b)   0.8 mm thick G550 steel

Figure 3.10   Comparison of Tension and Compression Stress-strain curves

The compression coupon test curves were then compared with the tension coupon test curves to observe the behaviour under compression and tension forces. According to Figure 3.10 the ultimate compression failure strength is higher than the ultimate tension failure strength. On the other hand the compression yield strength is always lower than the tension yield strength. However, the compression yield strength shows a considerable difference for 0.8 mm thick steel when compared with the tension yield strength. This observation is not present for the other thicknesses. This could be because of the different grain structures and manufacturing methods. Therefore, the mechanical properties under compression and tension forces should be further investigated by considering grain structure and manufacturing methods. Further, both tension and compression stress-strain curves should be used in finite element analyses to investigate the effect of different mechanical properties from both cases on the strength of columns.

Table 3.4   Comparison of Coupon Test Results with Other Researchers

Steel thickness and grade	Tension elasticity modulus/Compression elasticity modulus	Tension yield strength/Compression yield strength
1.7 mm HR340	1.216	0.968
2.0 mm HR2 (Lau and Hancock, 1988)	1.049	1.014
2.4 mm G450	1.125	1.020
2.5 mm (Macadam et al.,1988)	-	1.187
2.0 mm 304	1.032	1.037
1.2 mm 430 (Lecce and Rasmussen, 2004)	0.959	1.074
2.0 mm 3Cr12	0.938	0.997
0.42 mm G550	1.121	1.007
0.6 mm G550	1.037	1.041
0.8 mm G550 This research	0.981	1.131
0.95 mm G550	0.923	1.010

The results from this study were further investigated by comparing with available results from other researchers as shown in Table 3.4. Lau and Hancock (1988) carried out some compression and tension coupon tests for cold-reduced zinc coated steel and hot-rolled rimming steel with thicknesses of 2.4, 2.0 and 1.7 mm with a nominal yield strength of 450 MPa, 200 MPa and 340 MPa, respectively. Macadam et. al. (1988) undertook both tension and compression coupon tests for 2.5 mm thick steel which was treated using hot rolling and light cold-rolling. Lecce and Rasmussen (2004) also undertook tension and compression coupon tests of austenitic 304 and ferritic 430 cold-formed stainless steel and ferritic-like 3Cr12 chromium weldable steel. The nominal thicknesses used were 2.0 mm for 304 and 3Cr12 material and 1.2 mm for 430 materials.

According to the available results, the results obtained from light gauge cold-formed steels show no significant difference to those of other researchers' results. But compression yield strength values are lower than the tension yield strength values in most cases. However, there is no clear relationship between tension and compression coupon test results. Therefore this phenomenon should be further investigated by considering the material properties and grain structures of steel. The conversion and the effect of grain structure with respect to the tension and compression forces should be investigated by considering the type and thickness of steel.

3.1.4 Summary

The coupon test results in this research showed that the compression yield strength is lower than the tension yield strength. This can occur due to the anisotropy of single elements in the specimen. Mainly there are three regions that can be seen in a stress-strain curve: elastic region, transition region (elastic to plastic) and plastic region. The elastic region is linear and the transition region is nonlinear. The measured 0.2% proof stress and the stress corresponding to 0.5% total strain were in that transition region. The limit of the transition region depends upon the behaviour of grains in the structure. The elastic constant (elastic modulus) of the two neighbouring grains is the same while having the different elastic limits (yield strength), which undergo the same strain in one direction. Plastic deformation can occur in the grain which has

lower elastic limit when the strain level is sufficiently higher. In that occasion one grain has deformed plastically while other one behaves elastically so that transition period can commence. However, these grain structures can vary in the different thicknesses of the same steel. There is a compact grain structure in the very thin steel while there are some voids in the thicker steel. Therefore the behaviour of grain structure can be influenced by the test method. According to this research, compression test coupons show earlier commencement of transition period than tension coupons. Therefore the yield strength determined from compression force was lower than that of tension force. On the other hand 0.8 mm thick steel shows a considerable difference between tension and compression yield strengths.
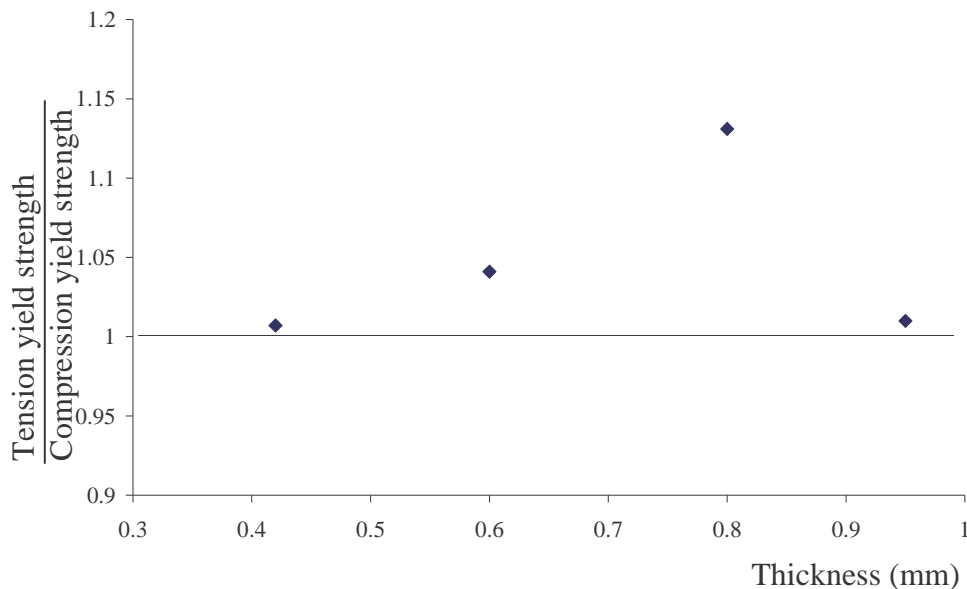
Figure 3.11   Comparison of Tension and Compression Yield Strengths with respect to the Thickness

Figure 3.11 shows the comparison of tension and compression yield strengths with respect to the thickness. The very thinner (0.42 mm) and thicker (0.95 mm) steels show the same compression to tension yield strength ratio while 0.8 mm thick steel shows a considerable difference between them. As discussed earlier the 0.42 mm thick steel has a compact grain structure while the 0.95 mm thick steel has a grain structure with some voids. The elastic limit and the elastic constant of the

neighbouring grains can be changed due to the condition of the grain structure. The grain structure changes from more compact to less compact when the thickness of steel is increased. Therefore the commencement of the transition region is affected by steel thickness. On the other hand that region can also be affected by the direction of the applied force. According to Figure 3.11 the behaviour under compression and tension forces has been affected by the changing grain structure. The difference between compression and tension yield strength has increased and then decreased with respect to the grain structure (thickness of steel).

3.2 Mechanical Properties at Elevated Temperatures

A greater understanding of the mechanical properties of steel enables the development of accurate and cost effective fire design methods for steel structures. The mechanical properties of light gauge cold-formed steel reduce significantly with increasing temperatures. The deterioration of the mechanical properties, yield strength and elasticity modulus, affects the strength of the cold-formed steel structures significantly. Sidey and Teague (1988) stated that the reduction in strength for cold-formed steel is 10-20% more than hot-rolled steel. However, the reason for this difference is not yet understood thoroughly. It is partly due to the metallurgical composition and molecular surface effects.

The deterioration of the mechanical properties of light gauge cold-formed steels at elevated temperatures has not been investigated adequately. This is despite the fact that light gauge cold-formed steels are commonly used in Australia. Therefore an improved knowledge and understanding of mechanical properties at elevated temperatures is required to improve the available design methods or to develop new design methods. In other words, the reduction of mechanical properties at elevated temperatures requires further detailed investigation. Hence an extensive experimental study into the deterioration of mechanical properties for light gauge cold-formed steels at elevated temperatures was conducted to derive accurate reduction factors of mechanical properties. Both low and high strength steels (G250 and G550) were considered with thicknesses varying from 0.6 mm to 1.0 mm.

3.2.1 Experimental Investigation

Lee et. al. (2003) undertook a series of tensile coupon tests at elevated temperatures. As discussed in Chapter 2 they developed valuable equations to determine the reduction factors of mechanical properties of light gauge cold-formed steels at elevated temperatures. Although they have used appropriate methods to develop their equations by using their test results, the reduction factors determined from their equations seem to be incorrect. Therefore their experimental methods were investigated first to determine whether there were any shortcomings. It was observed that their strain measuring method they adopted in the experiments is not adequate. As shown in Figure 3.12 they used a modified extensometer to measure the strains of tensile specimens. But the accuracy of that extensometer is inadequate to determine the strains correctly. On the other hand the furnace temperature measuring device also had a limitation and hence their measured temperatures were not accurate. Therefore the yield strength and the elasticity modulus values and equations obtained from Lee et al's research cannot be considered as accurate. Improved test methods and devices should be used in this research to determine the stress-strain curves at elevated temperatures accurately.

Modified extensometer with long rods
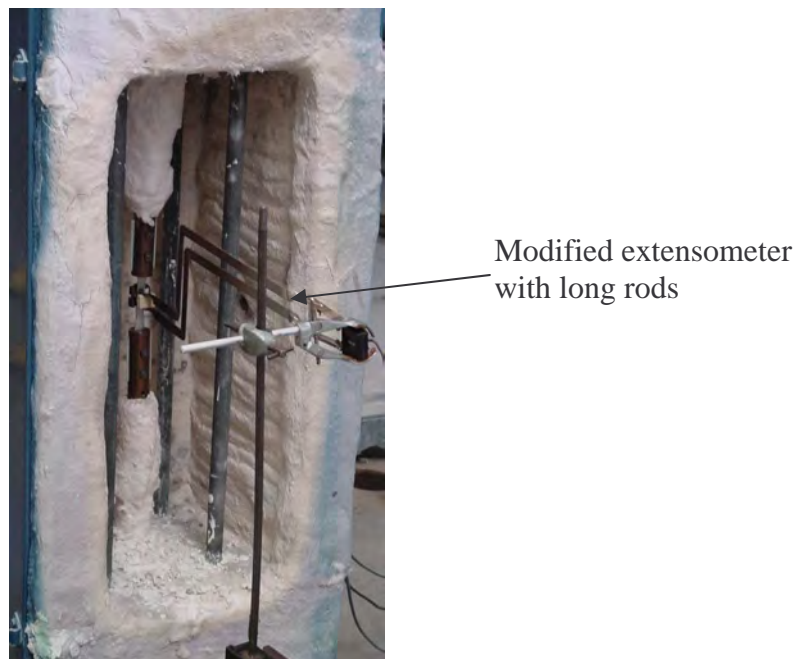
Figure 3.12   Test Rig used by Lee et al. (2003)

Strain gauge or extensometer can be attached to the tensile coupons at ambient temperature. However, these two methods show some drawbacks at elevated temperatures. Strain gauges cannot function at high temperatures and only the clip-on extensometer can be used at high temperatures. Extensometers with long rods should be used for high temperature tests since all the tests should be carried out inside the furnace. But the available extensometers do not consist such long rods and hence they cannot be used inside the furnace. The extensometer modified by Lee et al. (2003) (see Figure 3.12) is not accurate to be used in the high temperature tests. On the other hand the conventional clip-on extensometers can be used only on rigid materials. But the steels used in this research were very thin and it was difficult to set such a long rod extensometer on the specimen. In addition, most of the extensometers have limited amount of travel which is not sufficient at elevated temperature tests and have to be removed from the specimen prior to failure.

In order to eliminate these shortcomings, a contact free Laser Speckle Extensometer which was developed by the Austrian Company Messphysik Gmbh was selected in this research. This new expensive device is very sensitive and gives accurate results when the overall test set-up is made properly. It contains two cameras and two laser beams and gives accurate results. This instrument is being used in Australia for the first time. More details of this instrument are presented in Section 3.2.1.3.

3.2.1.1   Test method

Three types of test methods are currently used to investigate the behaviour of steel structures under fire conditions, namely, steady-state test, transient-state test and ISO test (ISO, 1999). Both the transient state and ISO test methods are based on temperature variations under a constant load while the steady state method is based on a constant temperature with increasing load. A steady state test method was used to determine the mechanical properties of light gauge cold-formed steels due to its simplicity and accurate data acquisition. Many other researchers have also used the steady state test method for the same reasons (Feng et al., 2003a, Outinen, 1999). However, Chen and Young (2004) stated that the transient state test method is more realistic than the steady state method since it simulates the temperature rise as in a

real fire. They conducted experiments under both transient and steady state methods for 1.9 mm G500 cold-formed steel. They did not compare the transient state and steady state test results for yield strength. However, they stated that there is a considerable difference between the transient state and steady state test methods with respect to the elasticity modulus results. In addition to that, Chen and Young (2006) conducted experiments on stainless steel at elevated temperatures to determine its mechanical properties considering both transient and steady state methods. In this case, they stated that the test results obtained from the transient and steady state tests are similar.

On the other hand some researchers argued that the transient state test method should be used as it simulates the creep effect that occurs in building fires (Lee et. al., 2003). However, creep effects are time dependent and are influenced by applied load and temperature. But since both steady state and transient state tests can be completed within an hour the creep effect can be considered to be negligible. On the other hand, there are no accepted theories available to define creep behaviour accurately. The creep tests are usually undertaken under constant load or constant temperature.

Outinen (1999) carried out both steady state and transient state tests using zinc-coated low strength light gauge steels. He found that the difference between steady state and transient state test results is negligible. In addition Lee et al. (2003) carried out experiments of light gauge cold-formed steels using both steady state and transient state test methods and showed that the difference is negligible. Therefore the experimental investigation in this research was based on steady state test method due to its simplicity.

3.2.1.2   Test specimens

The dimensions of tensile test specimens were decided based on AS 1391 (SA, 1991) as shown in Figure 3.13. Two holes were provided at each end as shown in Figure 3.13 to fix the specimen to the loading shafts located at the top and bottom ends of the furnace. The dimensions of the two ends and the holes were designed so

that there was no premature failure at the holes. The first series of tests was conducted at ambient temperature to determine the accuracy of test methods since the mechanical properties at ambient temperature are already known. The results showed the same mechanical properties as for the earlier method, which indicated that there were no effects from the end holes on the failure load or failure mode.
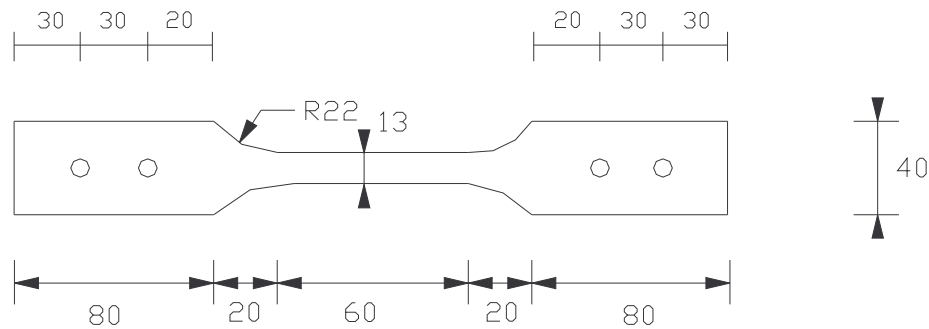
Figure 3.13   Dimensions of Tensile Test Specimens

All the specimens were cut from the same batch of cold-formed steel sheets which were used in other experiments (tensile coupon tests at ambient temperature, compression coupon tests at ambient temperature and column buckling tests). Further, the test specimens were taken in the longitudinal direction of the cold-formed steel sheet since the mechanical properties of light gauge cold-formed steel can vary depending on the direction, ie., longitudinal or transverse.

All the required dimensions of specimens were measured prior to testing. Table 3.5 shows the details of the tensile test specimens. Both high strength steel with a nominal yield strength of 550 MPa and low strength steel with a nominal yield strength of 250 MPa were considered with the thicknesses as shown in Table 3.5. All the experiments were repeated two or three times so that the accuracy of results could be increased. Temperatures were selected from 20°C to 800°C at different intervals for elevated temperatures based on previous research results (Lee et al., 2003). A total of 115 tests was undertaken in this study.

Table 3.5   Details of Tensile Test Specimens

Steel Grade	Minimum yield strength (MPa)	Nominal thickness (mm)	Test temperature	Measured base metal thickness (mm) *	Measured width (mm) *
G250	250	0.6	20	0.55	12.94
			100	0.55	12.94
			200	0.55	12.95
			350	0.55	12.95
			500	0.55	12.95
			650	0.55	12.94
			800	0.55	12.94
		0.8	20	0.75	12.86
			100	0.75	12.87
			200	0.75	12.87
			350	0.75	12.88
			500	0.75	12.88
			650	0.75	12.86
			800	0.75	12.87
		1.0	20	0.94	12.95
			100	0.94	12.97
			200	0.94	12.95
			350	0.94	12.98
			500	0.93	12.97
			650	0.94	12.94
			800	0.94	12.95
G550	550	0.6	20	0.60	13.02
			100	0.60	13.01
			200	0.60	13.01
			350	0.60	12.96
			500	0.60	12.95
			600	0.59	12.95
			650	0.59	12.94
			800	0.60	13.00
		0.8	20	0.79	13.11
			100	0.79	13.06
			200	0.78	13.07
			350	0.79	13.06
			500	0.80	13.06
			600	0.80	13.07
			650	0.79	13.06
			800	0.80	13.07
		0.95	20	0.94	13.10
			100	0.94	13.10
			200	0.94	13.11
			350	0.94	13.12
			500	0.94	13.12
			600	0.94	13.11
			650	0.94	13.12
			800	0.94	13.10

Note: * Mean value based on two or three specimens

The total thickness of each specimen was measured accurately using a micrometer. A special coating thickness gauge was then used to measure the thickness of the zinc/aluminium coating. From these two measurements, the base metal thickness was determined. Further, the coating of the specimens was removed by immersing them in diluted hydrochloric acid (acid to water = 1:3) and the specimen thicknesses were measured to obtain the base metal thickness with greater accuracy. The base metal thickness (BMT) was used in the calculations of mechanical properties.

3.2.1.3   Test rig and procedure

All the tensile coupon tests were carried out in the Structures Laboratory at the Queensland University of Technology under both ambient and elevated temperatures. The available electrically heated furnace was used for the simulated fire tests in this research project. Figure 3.14 shows the test specimen inside the electrical furnace and the methods of load application and measurement. The tensile load was applied by using two end rods. The bottom rod was fixed while top rod was moved upwards. Four glow bars were set inside the furnace so that the specimen was heated uniformly. Two thermocouples were used to measure the inside temperature. An additional thermometer was attached to the specimen to measure the specimen temperature during testing.

The elevated temperatures selected in this study were 100°C, 200°C, 350°C, 500°C, 650°C and 800°C. The heating rates were set between 10°C/min and 25°C/min. When the temperature reached the pre-selected value, it exceeded the pre-selected value by a small margin, but the difference was less than 1% at the higher temperatures of 650°C and 5% at lower temperatures of 200 and 350°C. However, the furnace temperature reached its required value quickly.   The specimen temperature measured by thermometer and the air temperature measured by thermocouples were observed during the test period. It was observed that the air temperature measured by the thermocouples and the specimen temperature measured by the thermometer were the same.
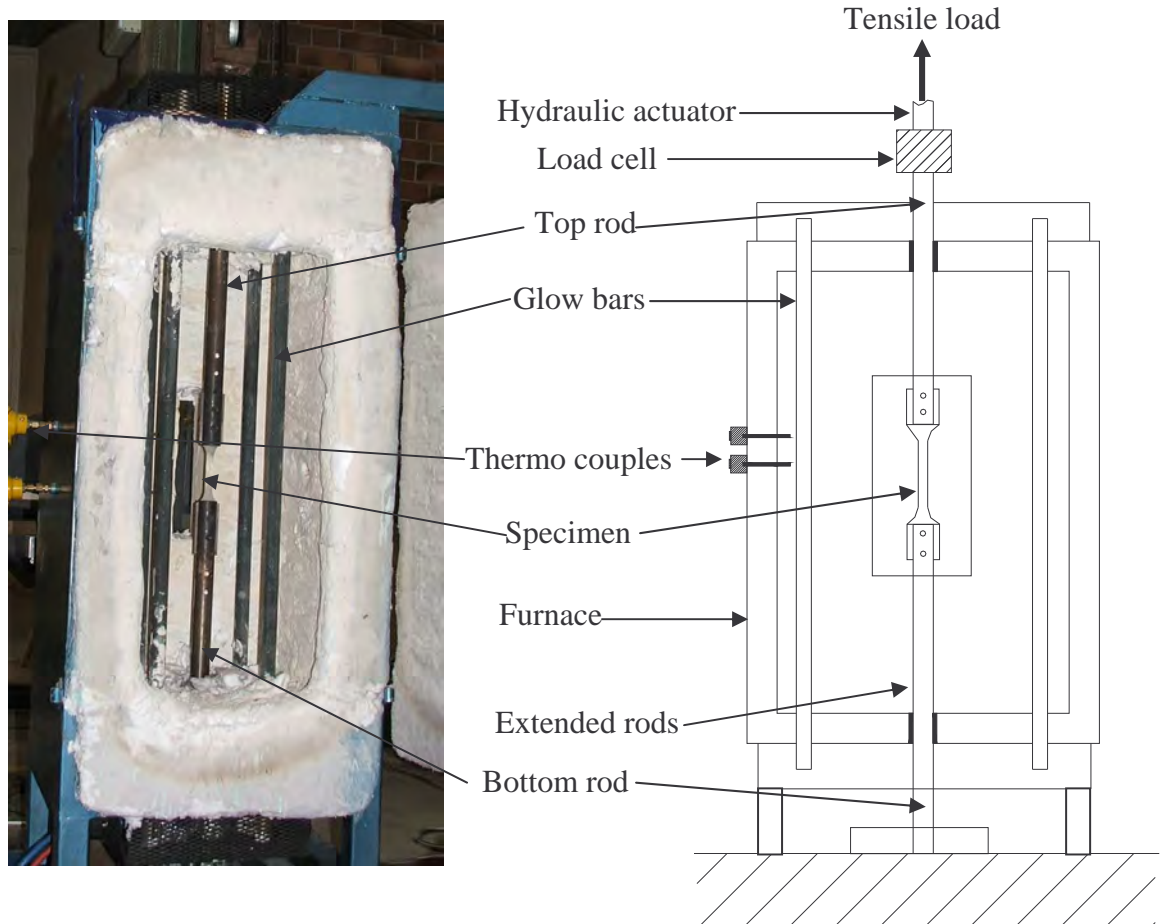
Figure 3.14   Test Rig

All the tensile coupon tests were carried out based on the steady state test method. Firstly the temperature inside the furnace was increased to a pre-selected temperature with the specimen inside the furnace. The specimen was then kept for 15 to 20 minuets at this constant temperature until it reached the steady state condition. The specimen was allowed to freely expand during this process by allowing the top rod to move upwards. The specimen was then loaded in tension until failure while maintaining the pre-set temperature. There are two main methods used to carry out the steady state tests at elevated temperatures: load control or displacement (strain) control. The strain rate should be kept constant in the strain control test while the loading rate should be kept constant in the load control test. The strain rate should be within the range of 0.00002/s to 0.00005/s and the upper limit of stress rate is 30MPa/s according to AS 2291 (SA, 1979). In this study displacement control was used with a displacement rate of 0.4 mm/min throughout the test. This is equivalent

to a strain rate of 0.000048/s and thus satisfies the requirements of AS 2291 (SA, 1979).

Figure 3.15 shows details of the main test set-up. A hydraulic actuator was used to apply the tensile load to the specimens with the help of MultiPurpose TestWare (MTS) system. A load cell connected to the top rod was used to measure the tensile load. Alignment of the test set-up is one of the most important factors when measuring the strain using the laser speckle extensometer. Therefore the alignments of both the top and bottom rods were checked prior to all the tests. The bottom rod of the test set-up was fixed at the base (see Figure 3.15 (c)) while the top rod was pinned at the top (see Figure 3.15 (a)). The alignment of the test set-up was then checked by applying a pre-tensile load of 200 N and removing it.

A laser beam speckle extensometer developed by an Austrian Company Messphysik GmbH was used in this study to measure the strains. It was located behind the furnace as shown in Figure 3.15 and was used to measure the strains in the middle of the specimen while the tensile load was being applied. The fire resistant glass window allowed the viewing of the specimen with the use of laser beams. The laser speckle extensometer contains a computer based video processor to measure the strains. The extensometer continuously measures the displacement of the two speckle patterns as shown in Figure 3.16, recorded by two video cameras in a master-slave configuration. Typical speckle outputs before and during the test are shown in Figures 3.16 (a) and (b), respectively. The selected specimen gauge length was 50 mm as specified in AS 1391 (SA, 1991). The strains were then calculated and recorded in another computer simultaneously with the stress results from the MTS system as discussed earlier.

10 kN "S" shape load cell

Pin connection

(a) Top End

(b) Side View of Laser Speckle Extensometer with cameras

Bottom rod
(fixed to the plate)

(c) Bottom End

(d) Specimen inside the furnace
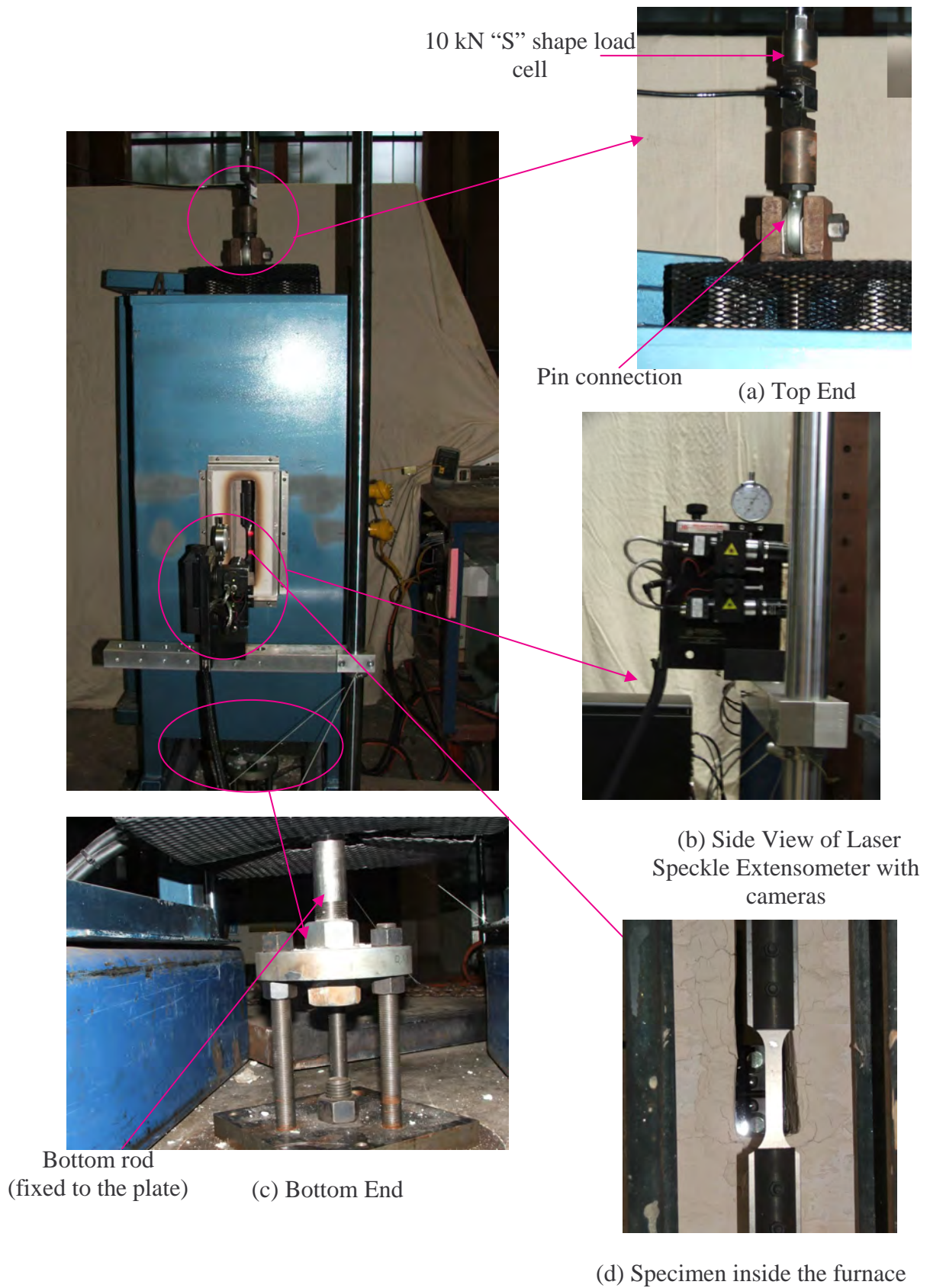
Figure 3.15   Test Set-up Showing Load Application and Strain Measurements
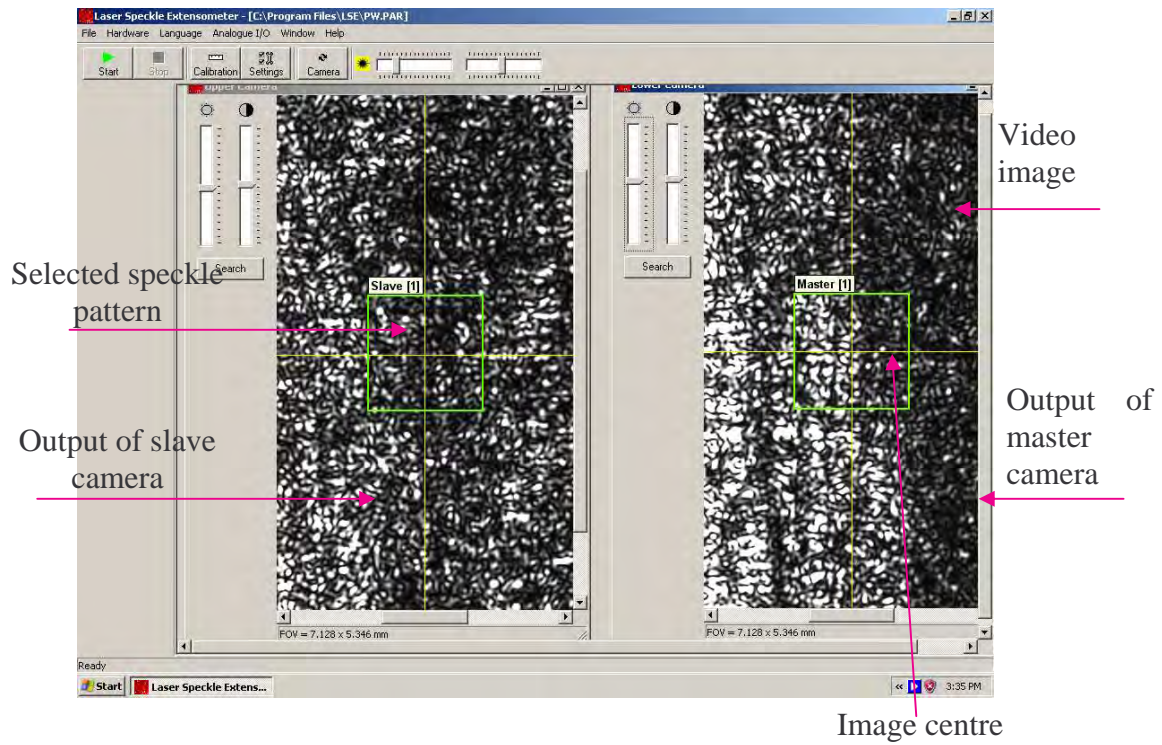
(a)　　　Speckle output before the test
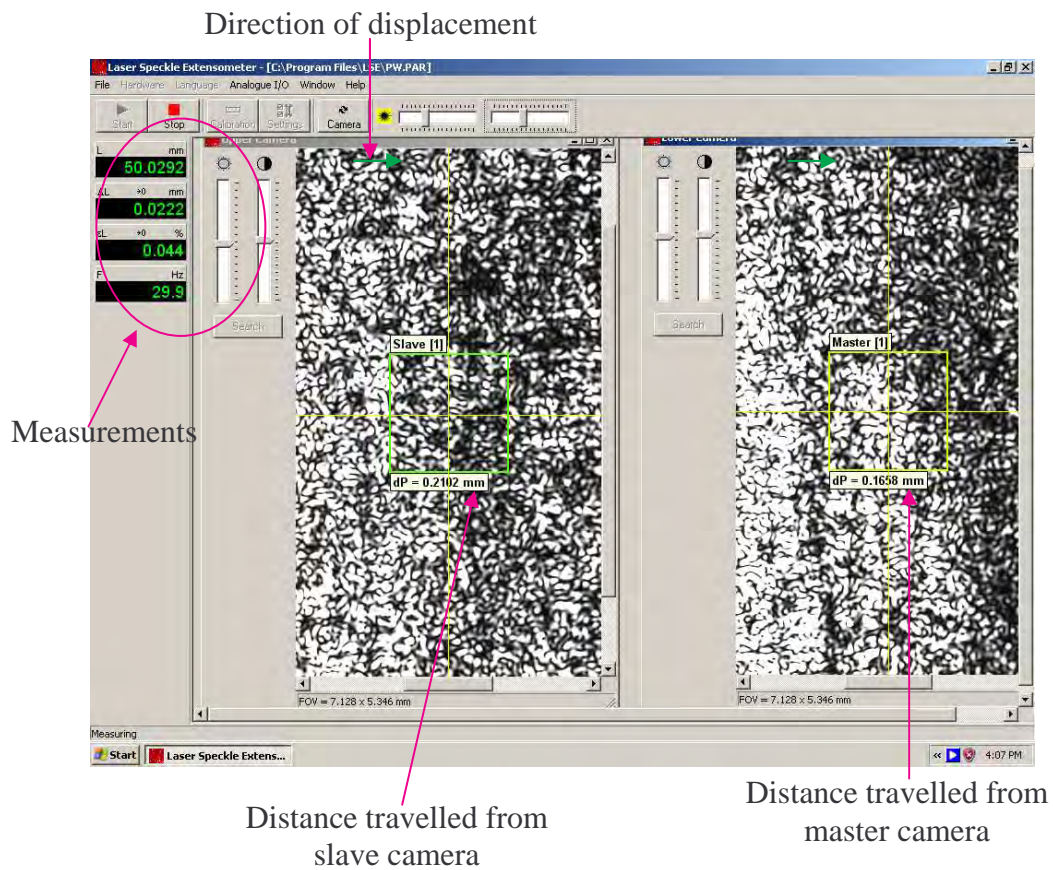
(b)　　　Speckle output during the test

Figure 3.16　　Speckle Output for Strain Measurements
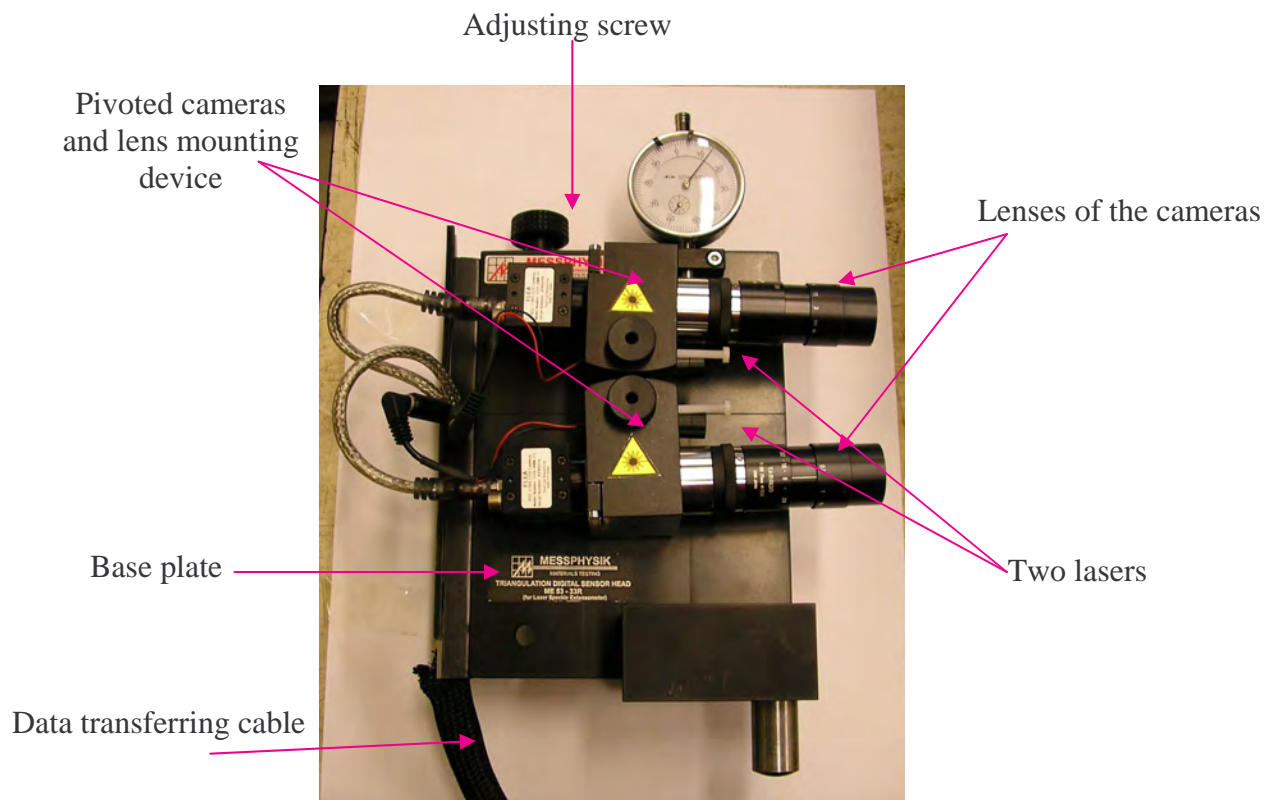
Figure 3.17   Laser Speckle Extensometer

The components of the laser speckle extensometer are laser diodes, video cameras, lenses, frame grabber, video processor, DA converter and Application software. This instrument includes two red laser diodes (class 3A). When the temperature is above $500^{\circ}C$, interference filters were used to eliminate infra-red radiation emitted by the hot specimen and hence speckle pattern can be seen clearly. Details of camera can be seen in Figure 3.17.

There are two cameras and two laser beams targeting the specimen as shown in Figure 3.18 in this process. The upper camera was named as slave while the lower camera named as master. The measuring principle of the extensometer is as follows. When a coherent laser beam hits the optical rough surface, the light will be dispersed in many different directions. As a result of this the laser speckle pattern can be observed as shown in Figure 3.16 (a). As shown in Figure 3.18, the two cameras are directed towards the two points of the specimen. When a tensile load is applied, theses two points move slightly and new materials or new surfaces come to these

relevant positions. Therefore the speckle pattern changes as relevant to this new surface. The video processor is able to measure the travelled distance (see Figure 3.16 (b)) of earlier speckle pattern. Both master and slave cameras can measure the movement of reference speckle patterns. The special calibration method was undertaken prior to experiments as specified in the manual. Since the distance between the two cameras (gauge length) has already been measured from this particular calibration method and stored in the program the processor can calculate the strain at any given time. Equation 3.1 presents the strain measurements (ε) from laser speckle extensometer.

$$\varepsilon = \frac{\sum d_{Slave} - \sum d_{Master}}{l_o} \quad \text{------------------------- (3.1)}$$

where,

$\sum d_{Slave}$ ------------------- Sum of displacement on slave system

$\sum d_{Master}$ ------------------- Sum of displacement on master system

l_o ------------------------- Distance of initial reference patterns (gauge length)
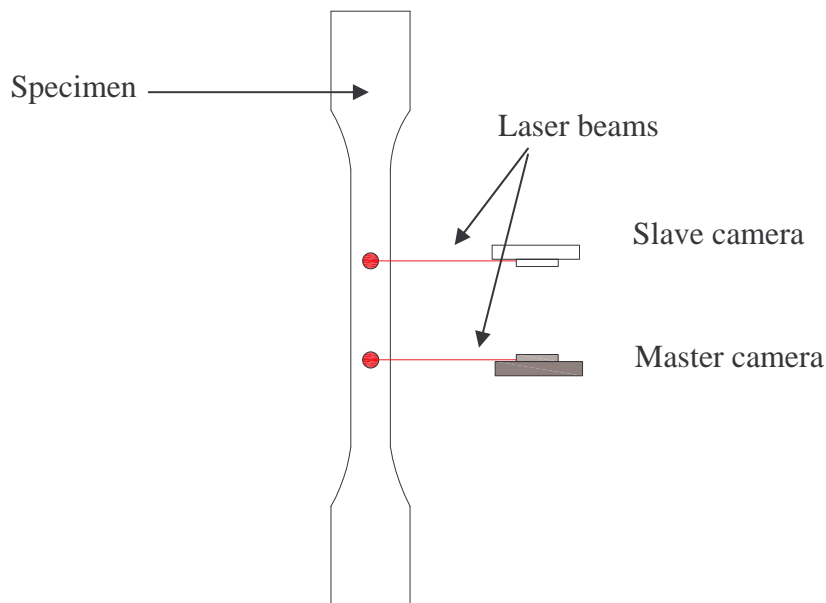
Figure 3.18   Strain Measurements

The laser speckle extensometer can give accurate results as discussed earlier. However, this instrument has never been used in Australia and therefore its accuracy must be checked by using known methods. Therefore all the experiments were first undertaken at the ambient temperature since the mechanical properties at ambient

temperature are already known. In addition, 10 mm strain gauges were also used in the ambient temperature test to determine the accuracy of the speckle system. Figure 3.19 presents the stress versus strain curves of 0.6 mm G550 steel test results at ambient temperature by using both the strain gauges and the laser speckle extensometer. It shows a very good agreement between them. Therefore all the elevated temperature tests were then undertaken by using a laser speckle extensometer to measure strains.

The yield strength, the elasticity modulus and the ultimate strength were obtained from the tensile test results. Three computers were used for data acquisition purposes. The applied tensile load was measured by one computer while the strain was measured by the other. Both load and strain data were then transferred to the third computer. Hence the stress-strain graph was available on the third computer while the test was progressing. The overall test set-up is shown in Figure 3.20.
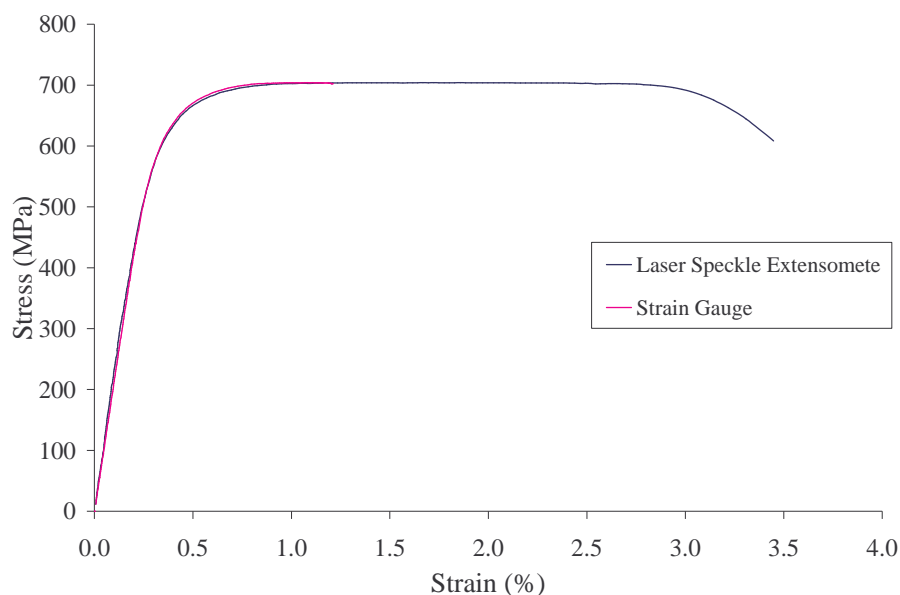
Figure 3.19 **Stress-strain Curve for 0.6 mm G550 Steel at 20°C**

In order to determine the error band for the measured stress and strain data, a simple analysis was undertaken based on the estimated error bands for the independent variables that could have affected the measured values of stresses and strains. These factors were considered to be the load (P) the thickness (t) and the width (b) of the specimen while they were the initial and final gauge lengths (l) for strain. The error band was determined as follows.

Error band (stress) $= \sqrt{\left(\dfrac{\Delta P}{P}\right)^2 + \left(\dfrac{\Delta t}{t}\right)^2 + \left(\dfrac{\Delta b}{b}\right)^2}$ Error band (strain) $= \sqrt{\left(\dfrac{\Delta l}{l}\right)^2}$

Based on the manufacturers' data for the errors in the measurements of P, t and b are 1%, 0.1%, and 0.001%, respectively, the error band for stress was determined as 1.01%. Similarly, it was determined as 1% for strain based on the error band for gauge length measurements. These error bands are quite small and thus demonstrate the good accuracy of stress-strain data reported in this chapter.
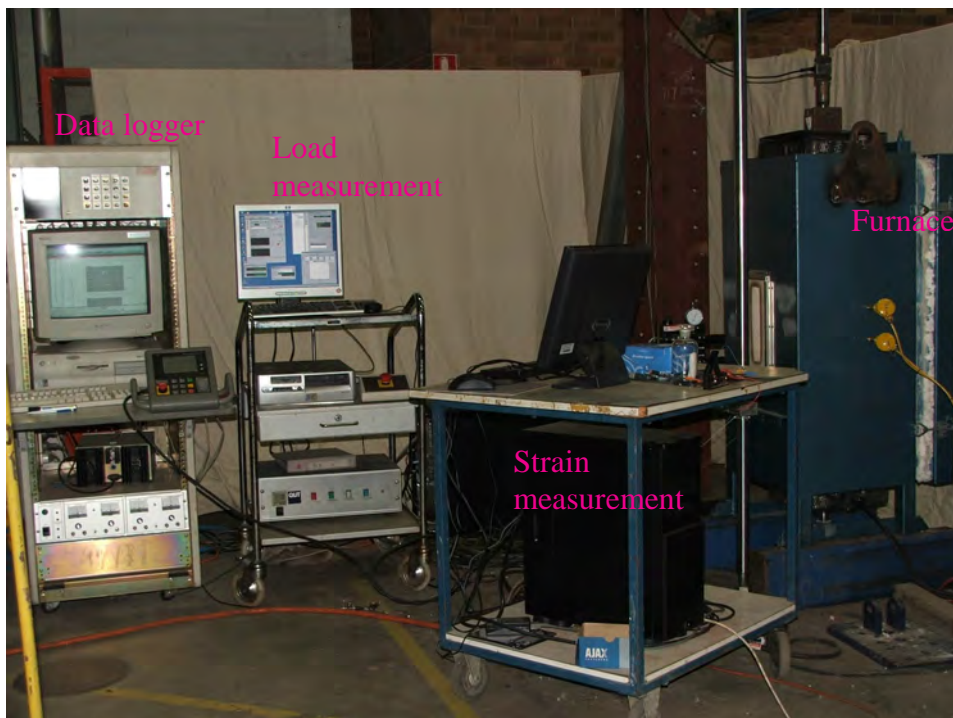
Figure 3.20   Overall Test Set-up

3.2.2 Deterioration of Mechanical Properties with Increasing Temperatures

3.2.2.1 Determination of yield strength and elasticity modulus

Normally the 0.2% proof stress method was used to determine the yield strength of steel at ambient temperatures. Most researchers used the 0.2% proof stress method while some of them used 0.5%, 1.5% and 2.0% of total strain to determine the yield

strength at elevated temperatures. Therefore all of these methods were used in this study to determine the yield strength of light gauge cold-formed steels at elevated temperatures and the results were compared to determine the difference between them. Mainly the British Standard BS5950 (BSI, 1990) provides the yield strength reduction factors at three strain levels of 0.5, 1.5 and 2.0%. It allows the use of 1.5 and 2.0% strain levels in a limited way provided structural stability remains in-tact at these levels of strain.

(a) Yield strength   (b) Elasticity modulus
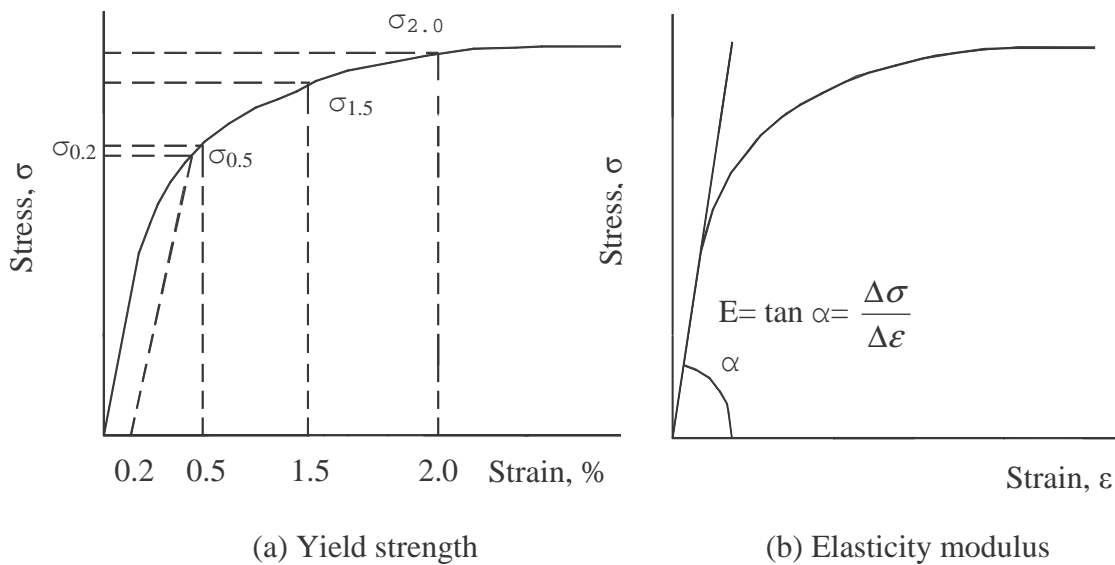
Figure 3.21   Determination of Mechanical Properties

In this research, the 0.2% proof stress values were used in further studies. The reason for this is that the 0.2% proof stress is commonly used while other stresses are not accepted widely. The elasticity modulus was obtained from the stress-strain curve as described in the ambient temperature test. Figure 3.21 shows the determination of mechanical properties.

3.2.2.2   Yield strength

Figures 3.22 (a) to (d) show the typical stress-strain curves obtained for low and high strength steels at ambient and elevated temperatures. Other stress-strain curves are given in Appendix A. These stress-strain curves were used to determine the yield strengths. The yield strength based on the 0.2% proof stress method was measured

from the intersection of the stress-strain curve and the proportional line off-set by 0.2% strain level. The strengths at 0.5%, 1.5% and 2.0% strain levels were measured from the intersection of stress-strain curve and the non-proportional vertical line specified at given strain values (see Figures 3.22 (a) to (d)).
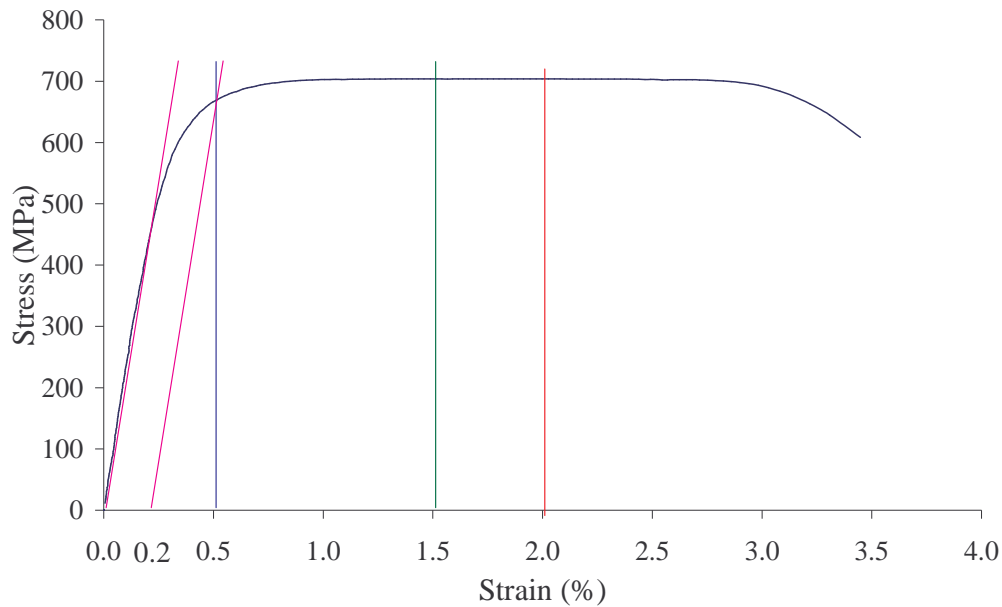
(a) 0.6 mm G550 steel at 20°C
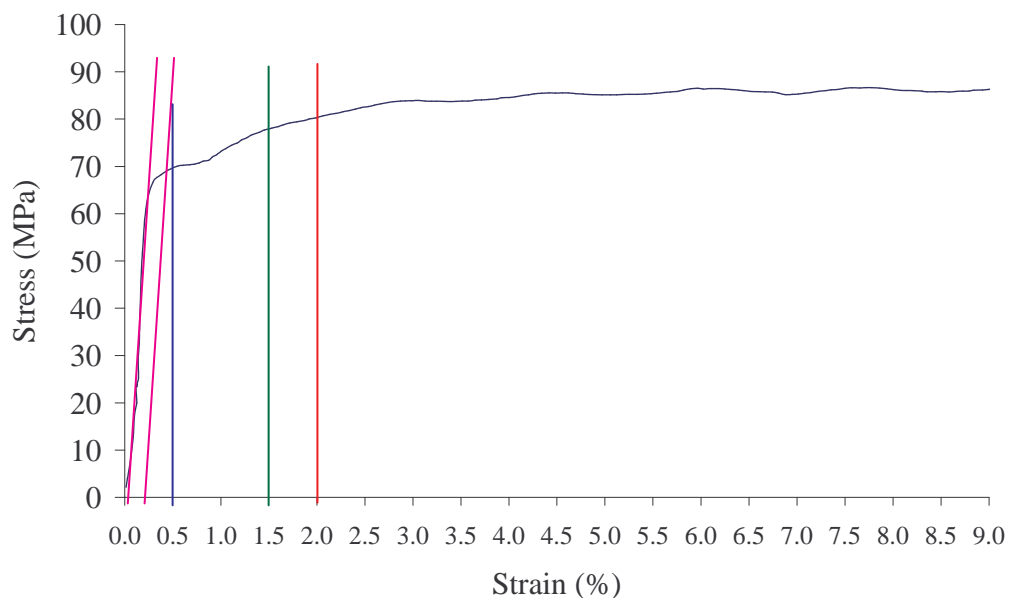
(b) 0.6 mm G550 steel at 650°C

Figure 3.22   Determination of Yield Strength at Various Strain Levels and Different Temperatures for Low and High Strength Steels
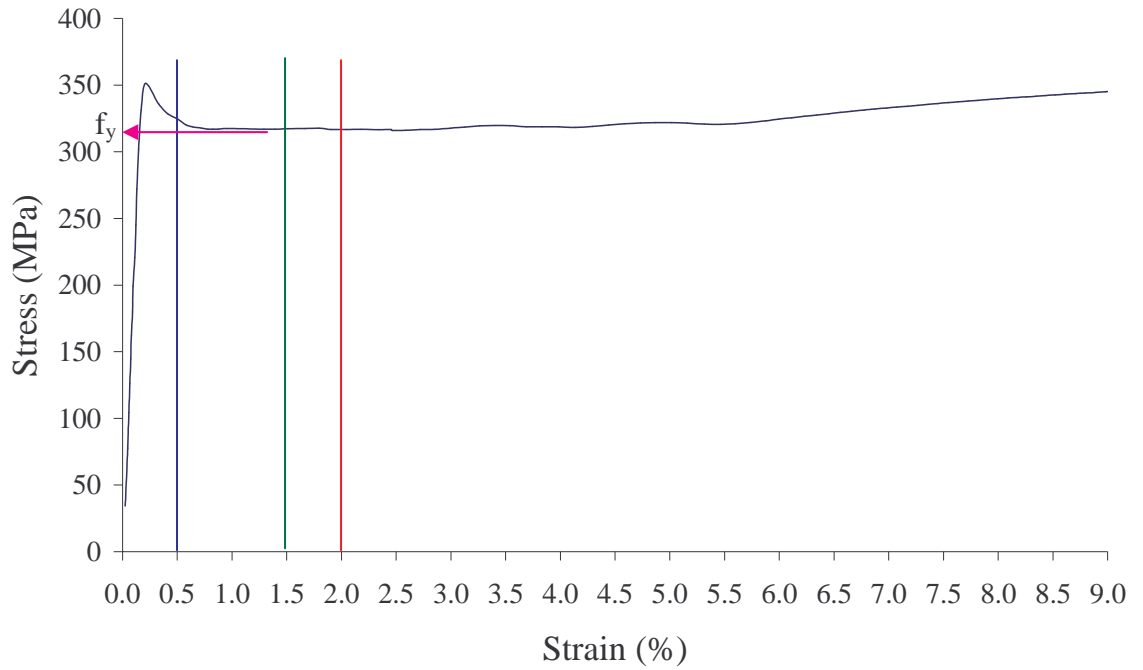
(c) 0.6 mm G250 steel at 20°C
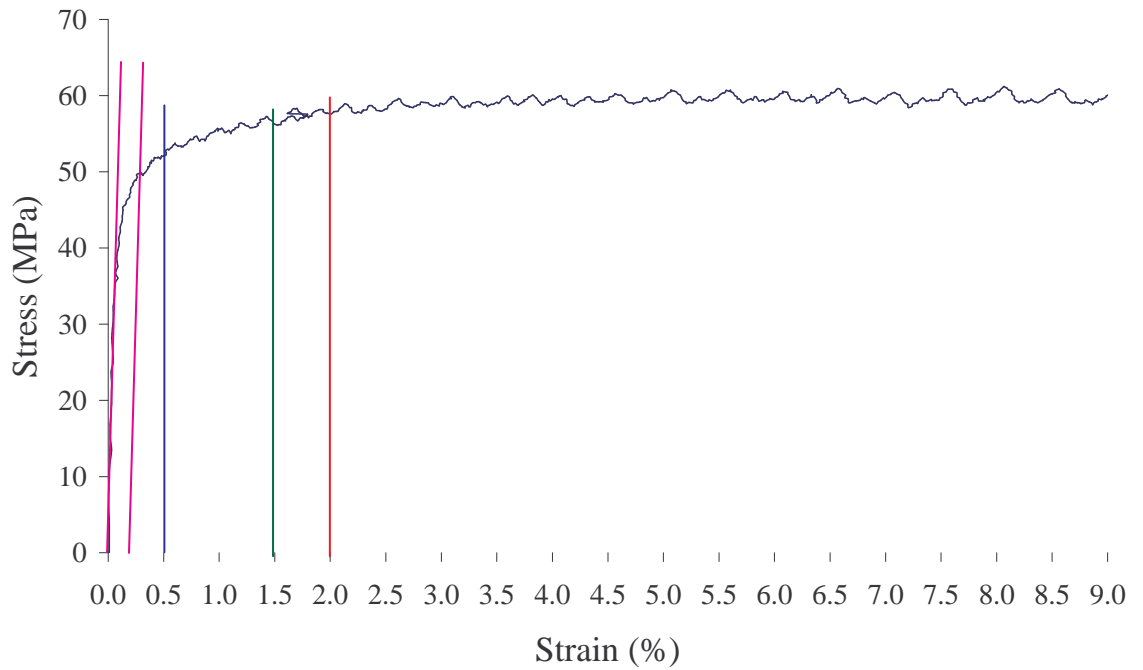
(d) 0.6 mm G250 steel at 650°C

Figure 3.22   Determination of Yield Strength at Various Strain Levels and Different Temperatures for Low and High Strength Steels

Table 3.6   Yield Strength Reduction Factors (f_{yT}/f_{y20}) based on Various Strain Levels

Temperature	0.60 mm G550 steel				0.60 mm G250 steel			
(°C)	0.2%	0.5%	1.5%	2.0%	0.2%	0.5%	1.5%	2.0%
20	1.000	1.000	1.000	1.000	1.000	1.000	1.000	1.000
100	0.970	0.968	1.000	1.000	0.937	0.935	0.958	0.978
200	0.956	0.947	0.996	0.994	0.922	0.901	0.938	0.965
350	0.838	0.814	0.897	0.896	0.526	0.539	0.711	0.758
500	0.403	0.402	0.461	0.471	0.323	0.338	0.398	0.413
600*	0.118							
650	0.097	0.099	0.105	0.107	0.163	0.166	0.179	0.183
800	0.030	0.030	0.031	0.031	0.036	0.036	0.37	0.037

Temperature	0.80 mm G550 steel				0.80 mm G250 steel			
(°C)	0.2%	0.5%	1.5%	2.0%	0.2%	0.5%	1.5%	2.0%
20	1.000	1.000	1.000	1.000	1.000	1.000	1.000	1.000
100	1.000	1.000	0.990	0.990	0.960	0.958	0.968	0.965
200	0.992	1.004	0.978	0.980	0.918	0.922	0.947	0.943
350	0.876	0.870	0.899	0.901	0.586	0.629	0.786	0.844
500	0.429	0.425	0.464	0.469	0.360	0.383	0.443	0.455
600*	0.123							
650	0.093	0.102	0.111	0.114	0.180	0.187	0.200	0.202
800	0.051	0.050	0.055	0.056	0.081	0.082	0.085	0.086

Temperature	0.95 mm G550 steel				0.95 mm G250 steel			
(°C)	0.2%	0.5%	1.5%	2.0%	0.2%	0.5%	1.5%	2.0%
20	1.000	1.000	1.000	1.000	1.000	1.000	1.000	1.000
100	0.976	0.976	0.985	0.988	0.906	0.906	0.910	0.921
200	0.963	0.963	0.970	0.977	0.823	0.865	0.855	0.930
350	0.877	0.861	0.944	0.953	0.510	0.565	0.715	0.774
500	0.471	0.450	0.537	0.541	0.327	0.355	0.411	0.427
600*	0.113							
650	0.082	0.089	0.105	0.108	0.164	0.175	0.185	0.189
800	0.044	0.045	0.055	0.056	0.059	0.061	0.067	0.067

Note: 0.60, 0.80 and 0.95 mm are nominal thicknesses and * indicates that limited tests were undertaken to obtain the yield strength of G550 steel.

The reduction factors at elevated temperatures were calculated as the ratio of yield strength at elevated temperatures (f_{yT}) to yield strength at ambient temperature (f_{y20}). They were determined based on various strain levels and the determined values are presented in Table 3.6. Figure 3.23 shows the deterioration of yield strength with temperature for both low and high strength steels of different thicknesses. According to Figure 3.23, high strength steel shows higher reduction factors at low temperatures than low strength steels. Low strength steels lose its strength more rapidly at lower temperatures than high strength steels. There is a considerable difference in the degradation of yield strength between low and high strength steels in the range of 200°C to 500°C. However, when the temperature increases beyond 400°C, high strength steel loses its strength more rapidly than low strength steel. Hence both low and high strength steels have closer yield strengths at higher temperatures. However, the steel thickness does not appear to have a significant influence on the reduction factors.
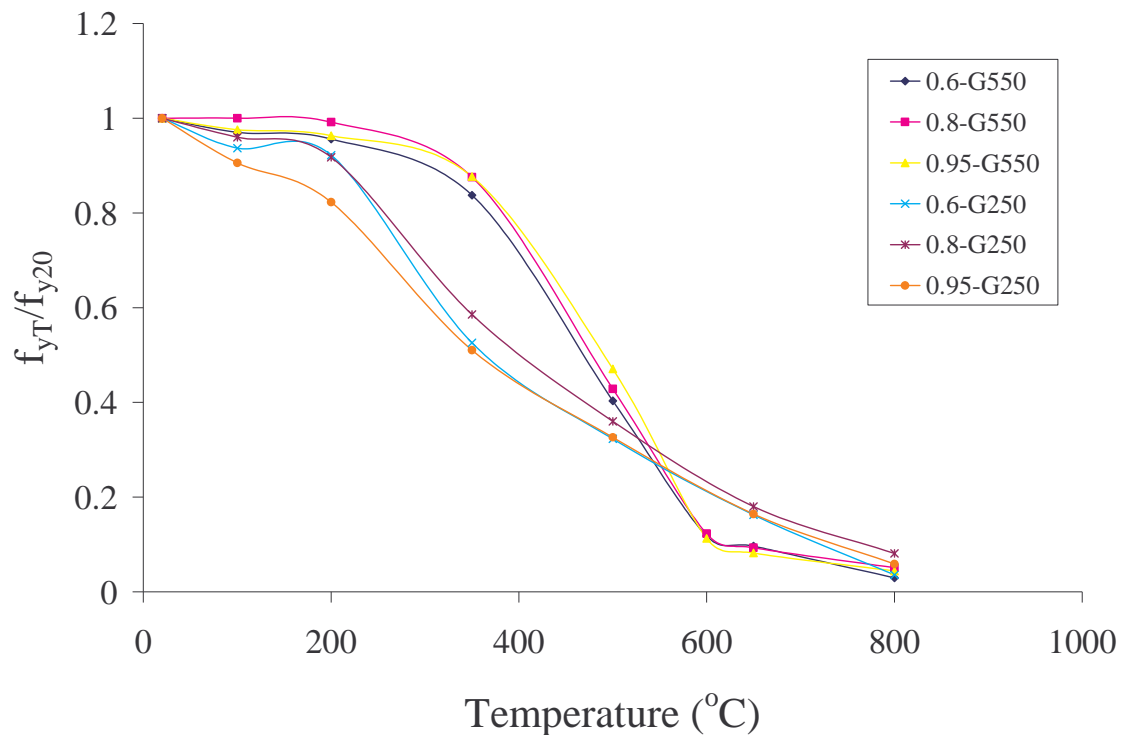
Figure 3.23   Yield Strength Reduction Factor versus Temperature for Different Steel Grades and Thicknesses
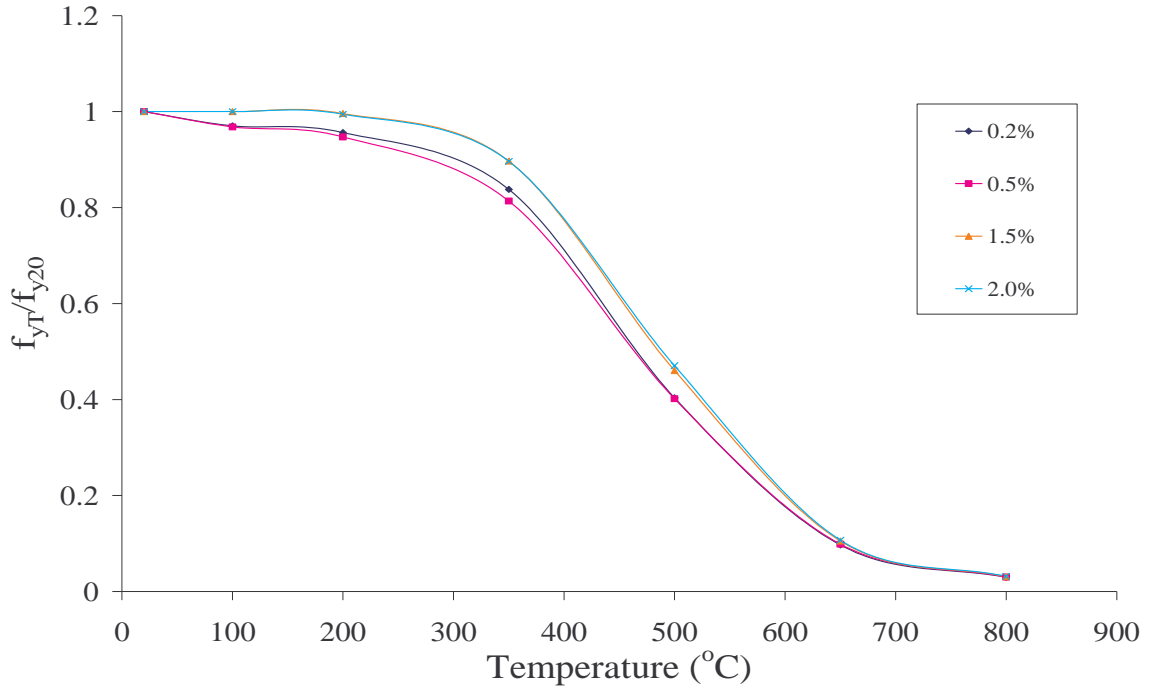
(a) 0.6 mm G550 Steel
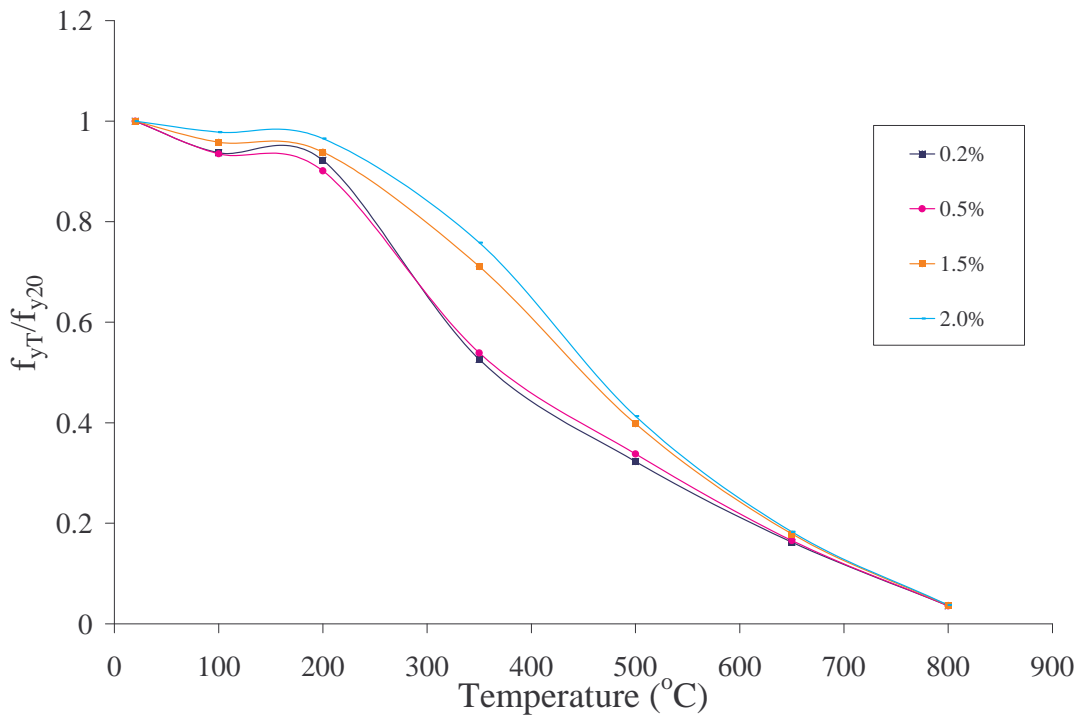
(b) 0.6 mm G250 Steel

Figure 3.24   Yield Strength Reduction Factor versus Temperature for Different Strain Levels for 0.6 mm Steels

Figures 3.24 (a) and (b) show the variation of reduction factors with respect to the different strain levels for both low and high strength steels. Both low and high strength steels show higher reduction factors at higher strain levels (strain levels at 1.5% and 2.0%). However, the reduction factors of low strength steels at higher strain levels are more than the reduction factors of high strength steels. The strength at 2% strain level is very close to the ultimate strength in some cases. Therefore the use of 0.2% proof stress can be recommended for elevated temperatures as for the ambient temperature.

Figure 3.25 also shows the ratios of yield strength reduction factors at the strain levels of 0.2, 0.5, 1.5, and 2.0% to the 0.2% proof stress. The values shown in this figure are the average values for all the temperatures. It clearly shows that there are some effects of using different strain levels to determine the yield strength reduction factors. As shown in the figure, reduction factors obtained at 0.5% strain level method are closer to those from the 0.2% proof stress method for high strength steel. However, the reduction factors obtained from the 0.5% strain level method for low strength steel are higher than the reduction factors obtained from the normal method. In addition all the low strength steels show higher reduction factors at higher strain levels than the high strength steels.
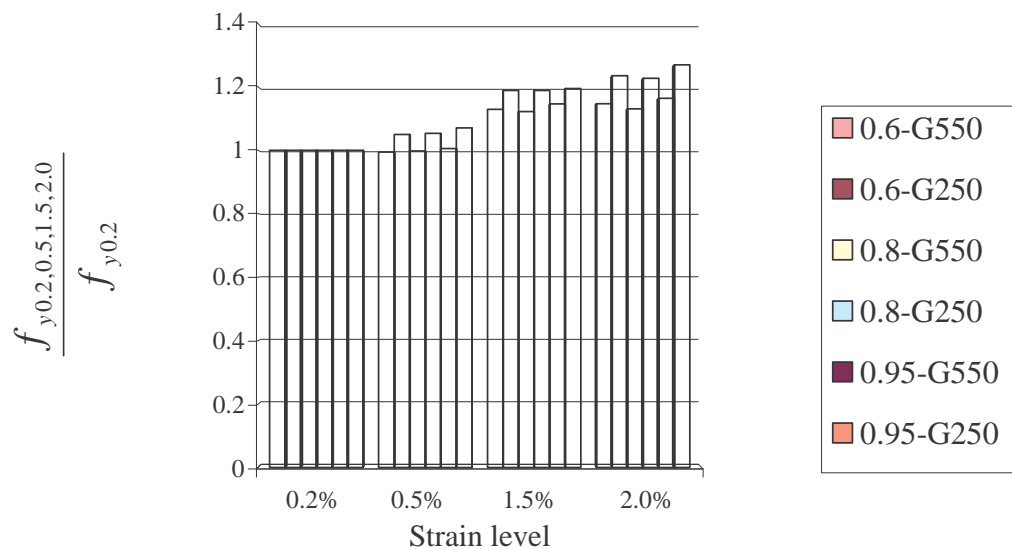
Figure 3.25   Comparison of Yield Strength Reduction Factors Based on Different Strain Levels
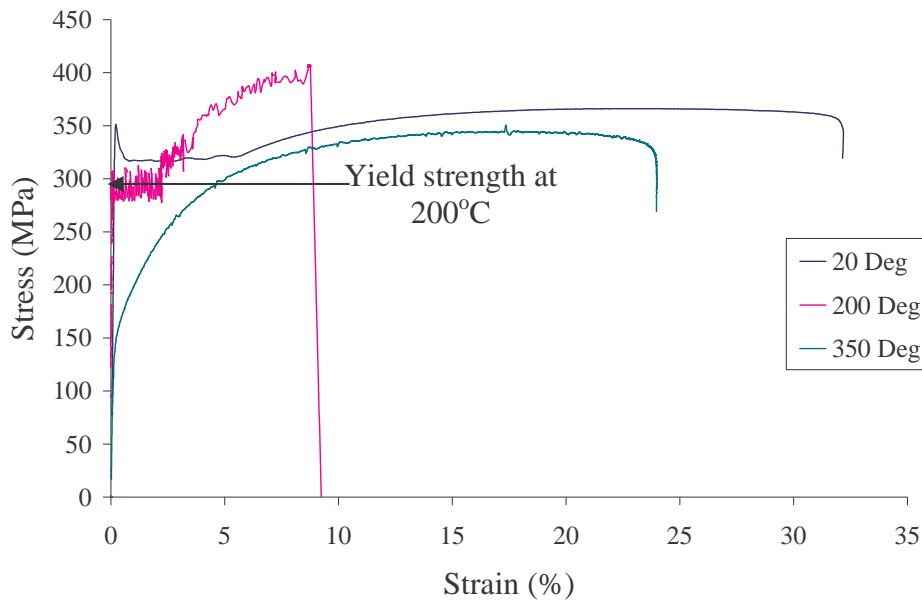
Figure 3.26   Stress-strain Curves for 0.6 mm G250 Steel at Selected Temperatures

As described earlier, the stress-strain graph of low strength steel shows a linear elastic portion followed by a flat yield plateau and then a smooth curve at ambient temperature. This behaviour changed when the temperature was 200°C and it did not show a clear flat yield plateau or smooth curvature. Therefore yield strength at 200°C was determined based on the average value of the lower values as shown in Figure 3.26. However, when the temperature is at 350°C the flat yield plateau does not exist and a smooth curve can be seen as shown in Figure 3.26. Therefore the 0.2% proof stress method was used to determine the yield strength of low strength steel at elevated temperatures.

3.2.2.3   Elasticity modulus

Elasticity modulus is also one of the most important mechanical properties needed in cold-formed steel design for fire safety. As for the yield strength of steel, elasticity modulus also deteriorates with elevated temperature. Therefore the elasticity modulus reduction factors were measured with respect to the temperatures. The elasticity modulus was determined from the initial slope of the stress-strain curves.

The reduction factors were then calculated as the ratio of the elasticity modulus at elevated temperature (E_T) to that at ambient temperature (E_{20}). The average reduction factors are given in Table 3.7 while the measured values and the stress-strain curves are presented in Appendix A.

Table 3.7   Elasticity Modulus Reduction Factors

Steel Temperature (^{o}C)	0.60 mm		0.80 mm		0.95 mm	
	G550	G250	G550	G250	G550	G250
20	1.000	1.000	1.000	1.000	1.000	1.000
100	1.000	0.998	1.000	1.000	1.000	1.000
200	0.822	0.948	0.854	0.890	0.863	0.925
350	0.652	0.630	0.710	0.550	0.688	0.627
500	0.396	0.468	0.398	0.488	0.392	0.488
650	0.264	0.265	0.310	0.343	0.322	0.350
800	0.058	0.047	0.130	0.038	0.140	0.096
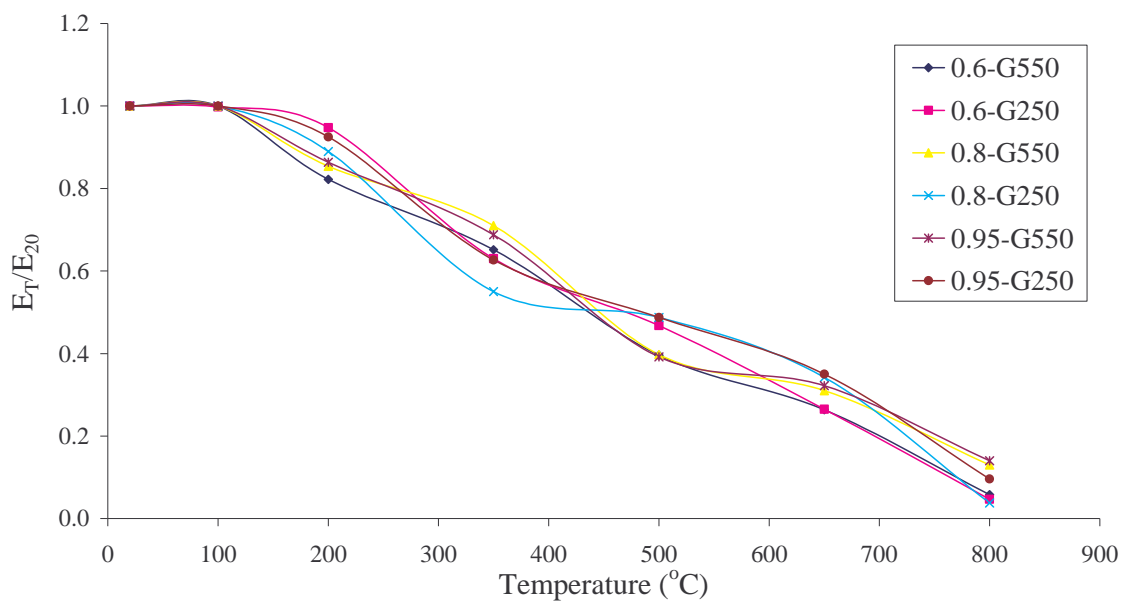
Figure 3.27   Elasticity Modulus Reduction Factors versus Temperature for Different Steel Grades and Thicknesses

Figure 3.27 shows the reduction factors of elasticity modulus versus temperature for both low and high strength steels. According to Figure 3.27 the variation of the reduction factors for low and high strength steels is not the same. Elasticity modulus

of high strength steel decreased significantly when the temperature is 200$^\text{o}$C than in low strength steel. However, when the temperature reaches 350$^\text{o}$C the low strength steel reduces its elasticity modulus at a higher rate than high strength steel. However, the difference is less than 10% in most cases. The reduction factors were also compared with respect to steel thickness. It can be seen that the variation of reduction factors with steel thickness is negligible in most cases.

3.2.3 Ultimate Strength

The ultimate strength is also an important mechanical property in steel design. Therefore the tensile tests were carried out until specimen failure. The reduction factors were then calculated as the ratio of ultimate strength at elevated temperature (f_{uT}) to that at ambient temperature (f_{u20}). Table 3.8 shows the reduction factors of ultimate strength with increasing temperature while Figure 3.28 shows the variation of reduction factors with temperature.

The results show that the behaviour of low strength steel is totally different from high strength steel at lower temperatures. At 200$^\text{o}$C the low strength steel shows an unusual behaviour. Figure 3.29 shows the behaviour at ambient temperature and 200$^\text{o}$C for both low and high strength steels of 0.6 mm thickness. The ultimate strength of high strength steel at 200$^\text{o}$C is also much closer to that at ambient temperature. But low strength steel shows a considerable difference compared to high strength steel from ambient temperature to 200$^\text{o}$C. This phenomenon can be discussed in relation to the chemical composition of cold-formed steel. Table 3.9 gives the typical chemical composition of cold-formed steel (BlueScope Steel, 2005). When the temperature increases from ambient level to 200$^\text{o}$C, chemical reactions occur in the steel base. The strength of the steel can increase due to these chemical reactions. Therefore the ultimate strength at 200$^\text{o}$C is higher than the ultimate strength at ambient temperature for low strength steels. The same chemical reactions may occur in high strength steel too. However, the strength acquired from cold working drops due to increasing temperature for high strength steel parallel with these chemical reactions. Therefore significant differences cannot be seen in high

strength steel as they were in the low strength steel although the chemical reactions occur in high strength steel.

Table 3.8   Ultimate Strength Reduction Factors

Temperature (°C)	0.60 mm		0.80 mm		0.95 mm	
	G550	G250	G550	G250	G550	G250
20	1.000	1.000	1.000	1.000	1.000	1.000
100	1.000	0.985	0.978	0.974	0.975	0.968
200	1.000	1.152	0.967	1.132	0.962	1.238
350	0.899	1.005	0.881	0.963	0.932	0.983
500	0.473	0.432	0.461	0.433	0.535	0.460
650	0.114	0.164	0.121	0.171	0.118	0.177
800	0.030	0.040	0.050	0.070	0.040	0.060
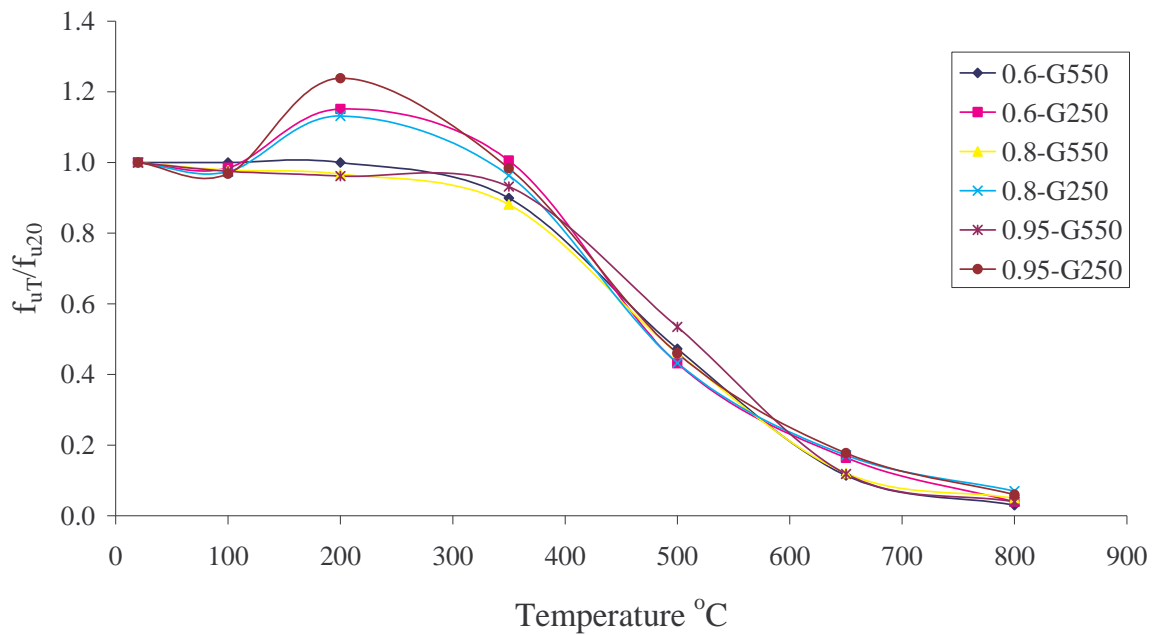
Figure 3.28   Ultimate Strength Reduction Factors versus Temperature for Different Steel Grades and Thicknesses

Table 3.9   Typical Chemical Composition of Tested Steels (G250 and G550) (BlueScope Steel, 2005)

C	P	Mn	S	Si	Ti	N
0.035-0.070	0.00-0.02	0.2-0.3	0.00-0.02	0.00-0.02	0.02-0.07	0.000-0.008
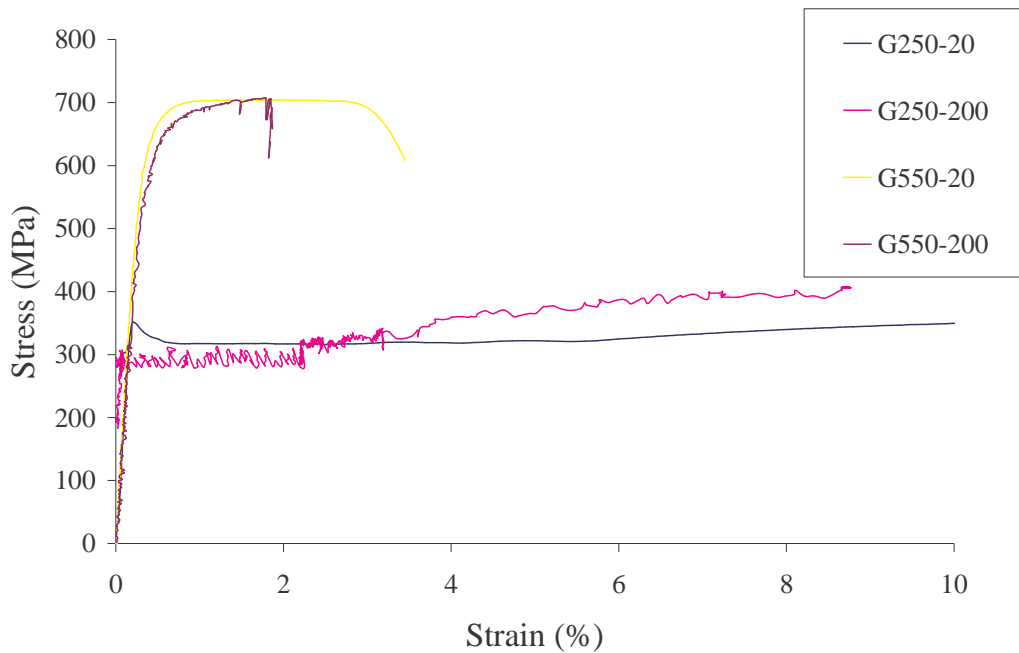
Figure 3.29   Stress-strain Curves for 0.6 mm Steel at Selected Temperatures

3.2.4   Ductility of Low and High Strength Steels at Elevated Temperatures

The ductility is one of the most important factors in the design of steel structures. A shortcoming of using high strength steel is its low ductility. Low strength steel shows much higher ductility than high strength steel. High strength steel loses its ductility as a result of cold-working used to achieve higher strength. However, both low and high strength steels can withstand significant deformations without fracture when compared with other building materials.

Yu (2000) defines ductility as "an extent to which a material can sustain plastic deformation without rupture". The ductility can be measured as the percentage of elongation or strain at failure of a tensile test specimen. In this study tensile strains were measured until specimen fracture. The strain values at fracture were compared with respect to the temperature and steel grade.
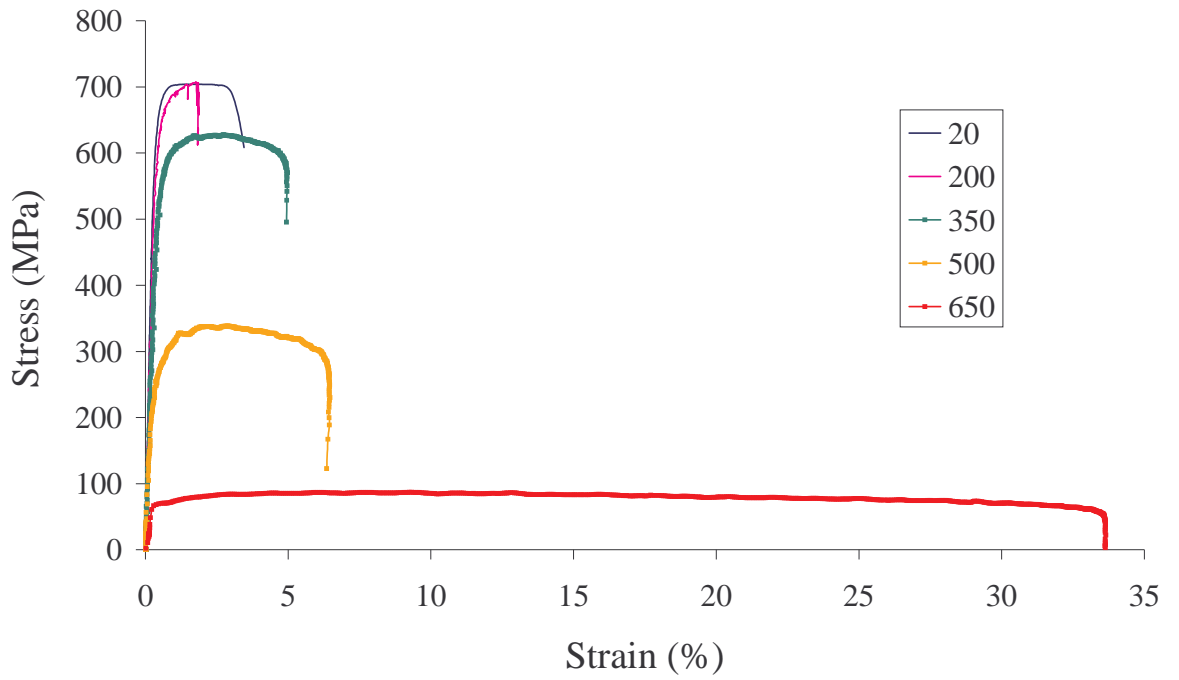
(a) 0.6 mm G550 steel
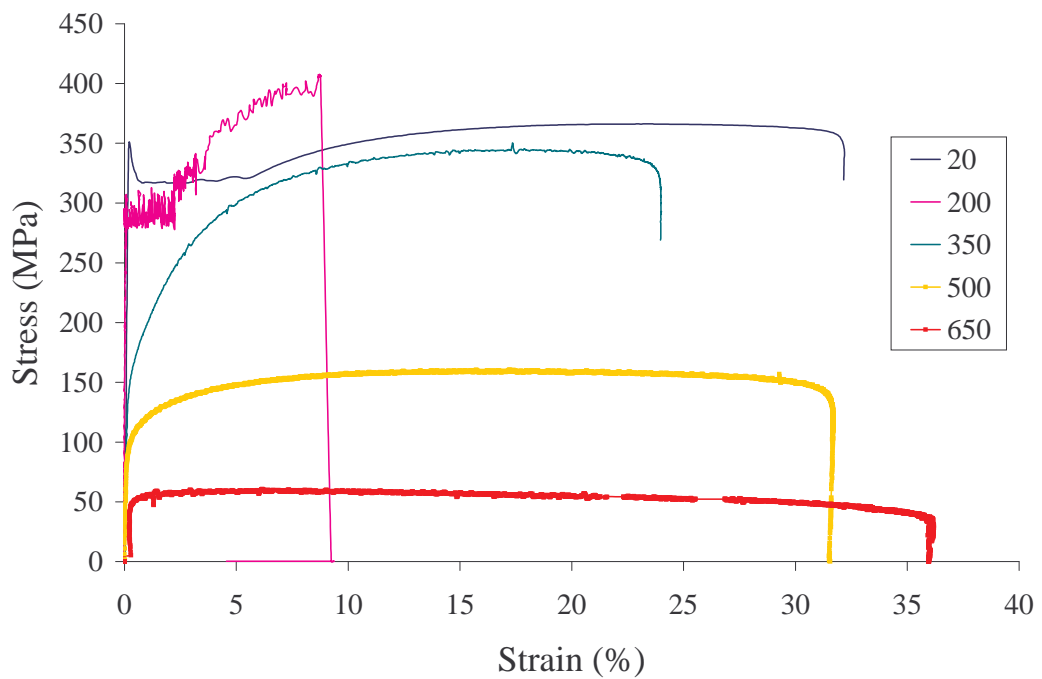
(b) 0.6 mm G250 steel

Figure 3.30   Stress-strain Curves of 0.6 mm Steels at Varying Temperatures

The results obtained in this research show interesting results for both low and high strength steels at various temperatures. Figures 3.30 (a) and (b) show the stress-strain curves for 0.6 mm steels at different temperature levels. The low strength steel shows higher ductility than the high strength steel at ambient temperature. Both low and high strength steels lose their ductility when the temperature is increased to 200°C. However, the ductility of low strength steels drops significantly than high strength steel when the temperature is increased to 200°C. As shown in Figure 3.30 (b), 0.6 mm G250 steel's ductility drops by about 75% while it is around 50% for G550 steel when the temperature is increased from ambient temperature to 200°C. However, high strength steel improves its ductility when the temperature reaches 350°C while low strength steel shows lower ductility at 350°C than ambient temperature, but higher ductility than at 200°C. This strange behaviour of ductility at various temperatures can be explained with the help of chemical composition of steel. As shown in Table 3.9 cold-formed steels have a small amount of Nitrogen. When the specimen temperature is increased, Nitrogen starts chemical reactions which lead to lower ductility. However the chemical composition is the same for both low and high strength steels. But the reduction of ductility at 200°C was higher for low strength steel than high strength steel. The ductility of high strength steel is decreased due to the chemical reactions while it is increased with temperature. Although the same phenomenon occurs for low strength steel, the ductility increase at 200°C due to temperature increase is lower than that of high strength steel. Therefore low strength steel shows a considerable difference when compared to high strength steel.

When the specimen temperature is increased to 650°C, both low and high strength steels show the same level of ductility. In other words, at 650°C, there is no difference between low and high strength steels as the latter has lost its cold-working characteristics at ambient temperature. Therefore the lack of ductility cannot be considered as a disadvantage for cold-formed high strength steel members at elevated temperatures and thus fire safety.
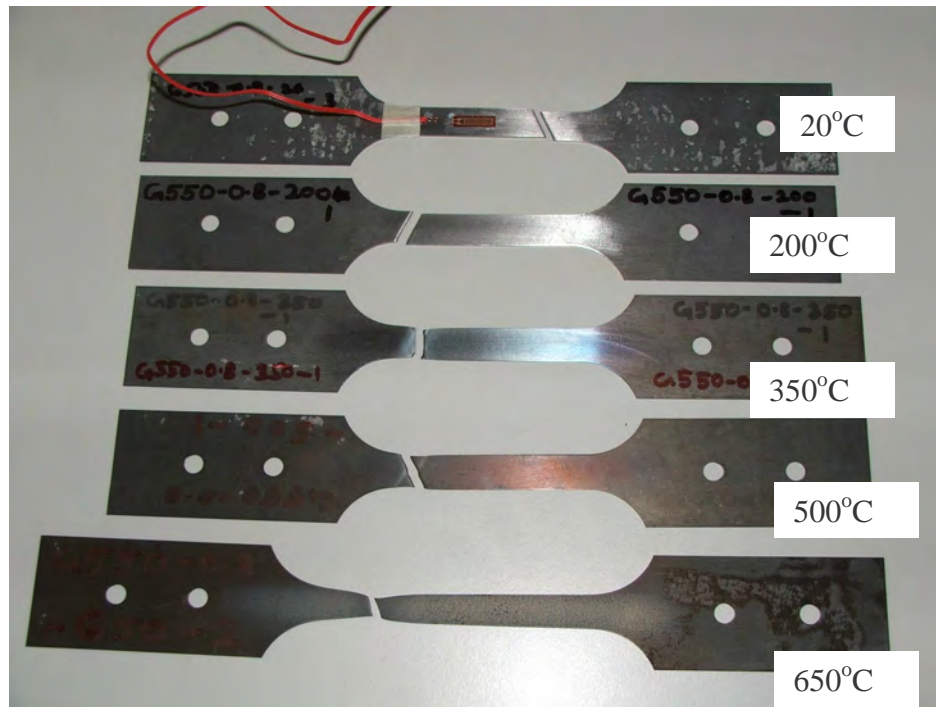
(a) 0.8 mm G550 Steel
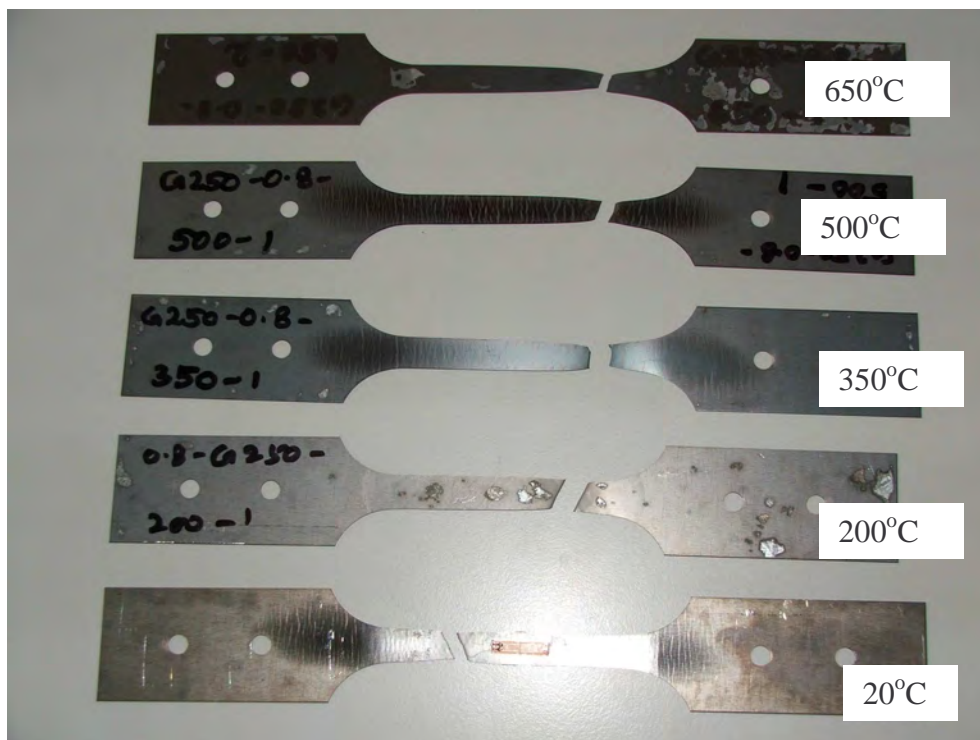
(b) 0.8 mm G250 Steel

Figure 3.31   Failure Modes of Tensile Specimens at Temperatures

of 20 to 650 ℃

Figures 3.31 (a) and (b) show the typical failure modes of tensile test specimens from 20°C to 650°C for 0.8 mm low and high strength steels. Failure modes for other thicknesses are given in Appendix A. They clearly show that when the temperatures are 20°C and 200°C, high strength steel's failure modes are brittle, but when the temperature increases beyond 200°C it becomes more ductile. A brittle failure mode can be seen in the low strength steel when the temperature is 200°C than at ambient temperature.   When the temperature is 650°C high strength steel specimens elongated much more than at other temperatures. From this investigation, it can be concluded that ductility of high strength steels improved significantly at elevated temperatures.

3.2.5   Discussion of Results

3.2.5.1   Comparison of yield strength and elasticity modulus results with current cold-formed steel design standards

The yield strength and elasticity modulus reduction factors at elevated temperatures were compared with those in relevant cold-formed steel design standards. BS 5950-8 (BSI, 1990) and Eurocode 3 Part 1.2 (ECS, 1993) were considered for this purpose. The British Standards BS 5950-8 provides reduction factors for three different total strain levels: 0.5%, 1.5% and 2.0%. Among them only 0.5% strain values were considered since the yield strengths based on 0.5% strain and the 0.2% proof stress method are close to each other. However, BS 5950 does not provide reduction factors for the elasticity modulus.

Figure 3.32 (a) shows the yield strength reduction factors for both low and high strength steels from this research, Eurocode (ECS, 1993) and BS 5950-8 (BSI, 1990). As shown in the figure there is a significant difference between the reduction factors obtained from this research and the current steel design standards. However, there is good agreement between the reduction factors obtained from this research and the design standards at low temperatures (up to 200°C) and very high temperatures (800°C). The difference varies from 0 to 30% depending on the

temperature. On the other hand the reduction factors presented in Eurocode and BS 5950 are also not the same. Most of the yield strength reduction factors presented in both Eurocode and BS 5950 are unconservative. There is a considerable difference in the reduction factors for the different steel grades at some temperatures. However, none of the design standards have discussed this. Therefore the yield strength reduction factors obtained in this research should be used in the analysis and design.
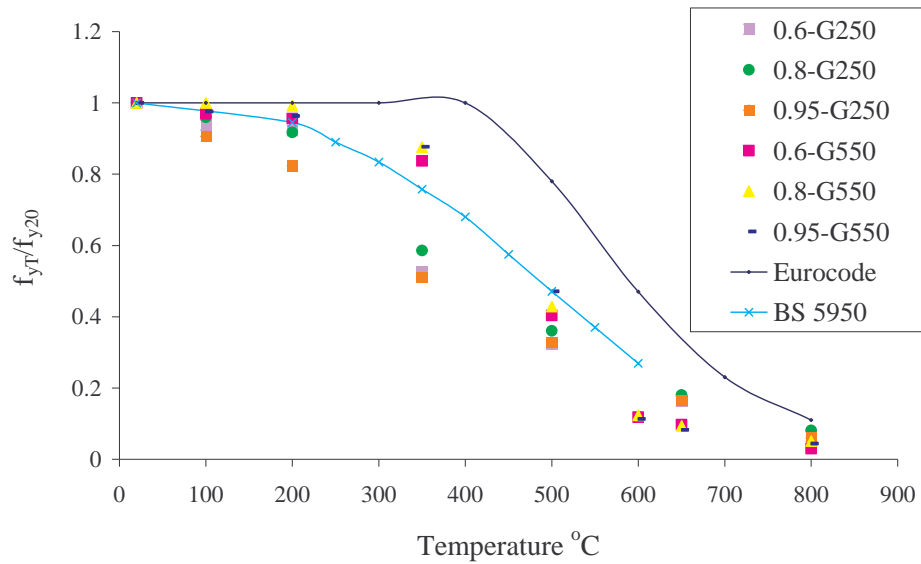
(a) Yield strength reduction factors
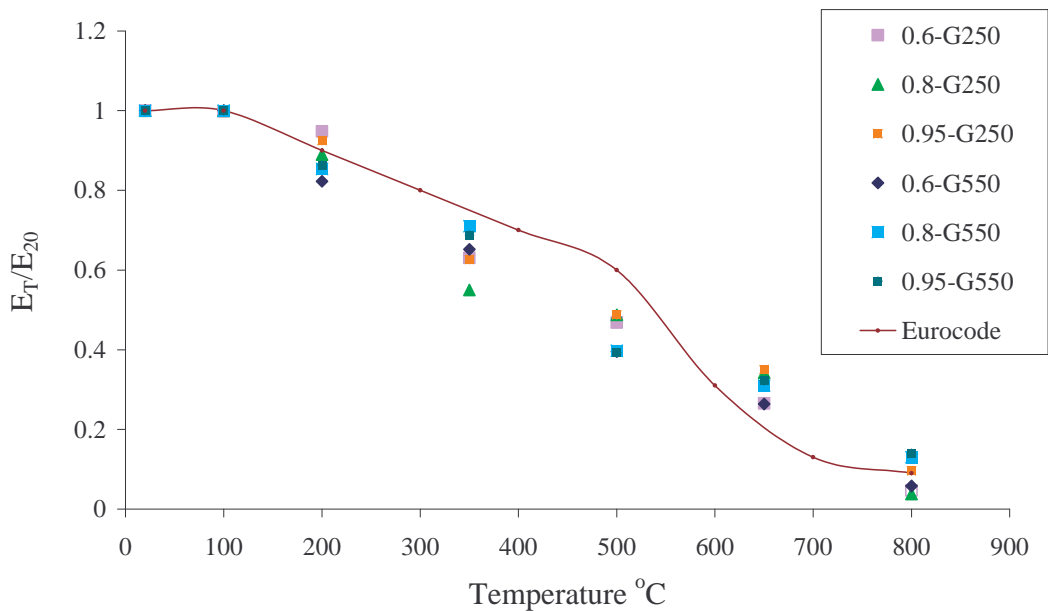
(b) Elasticity modulus reduction factors

Figure 3.32   Comparison of the Variation of Reduction Factors at Elevated Temperatures with Current Steel Design Rules

Figure 3.32 (b) shows the comparison of elasticity modulus reduction factors from this research and Eurocode. The elasticity modulus reduction factors obtained from Eurocode overestimate the values for both low and high strength steels in the temperature range of 300°C to 500°C. The values obtained from Eurocode are close to test results at lower temperatures (up to 200°C) and very high temperature (800°C). As shown in Figure 3.32 (b), Eurocode 3 slightly overestimates the reduction factors for high strength steel even at lower temperatures. The maximum difference of test results and Eurocode factors is about 30%. Therefore the elasticity modulus reduction factors obtained in this research should be used in the analysis and design.

3.2.5.2   Comparison of yield strength and elasticity modulus results with available research results

Outinen (1999) provided reduction factors for both yield strength and elasticity modulus by undertaking tests on 2 mm S350GD+Z (minimum yield strength of 350 MPa) steel specimens. Chen and Young (2004) also carried out high temperature tests to obtain the mechanical properties of 1 mm G550 steel and provided reduction factors for both yield strength and elasticity modulus. Both Outinen's (1999) and Chen and Young's (2004) values were compared with the reduction factors obtained from this research. Chen and Young (2004) provided equations to determine the yield strength reduction factors, but not for the elasticity modulus reduction factors. Therefore their test values were used to compare the elasticity modulus reduction factors.

Figure 3.33 (a) compares the yield strength reduction factors obtained from this research and others' research results. The reduction factors presented by Chen and Young (2004) for yield strength of 1 mm G550 steel agree well up to 400°C, but are too conservative beyond 400°C. There is a 30% difference at 500°C between Chen and Young's results and the reduction factor of 0.95 mm G550 steel in this research. However, when the temperature reaches 650°C the reduction factors obtained in this research agree with their results. The reduction factors presented by Outinen (1999) also disagree in the temperature range of 300 to 600°C, but agree reasonably well at

lower and very high temperatures. The maximum difference of Outinen's results and those from this research is about 35% at 350°C for 0.95 mm G250 steel. Therefore the available strength reduction factors cannot be used and the reduction factors obtained from this research should be used in the analyses.
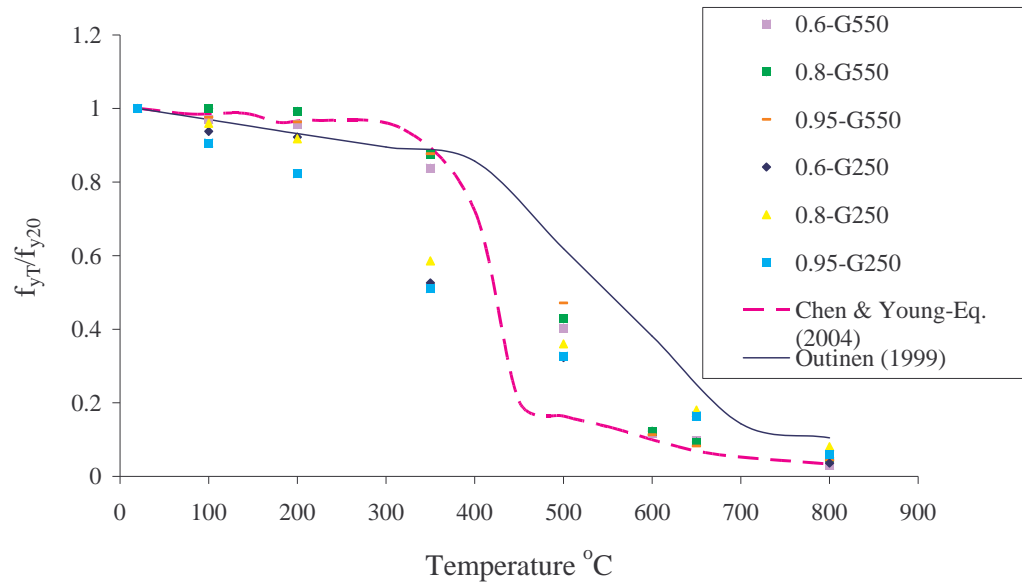
(a) Yield strength reduction factors
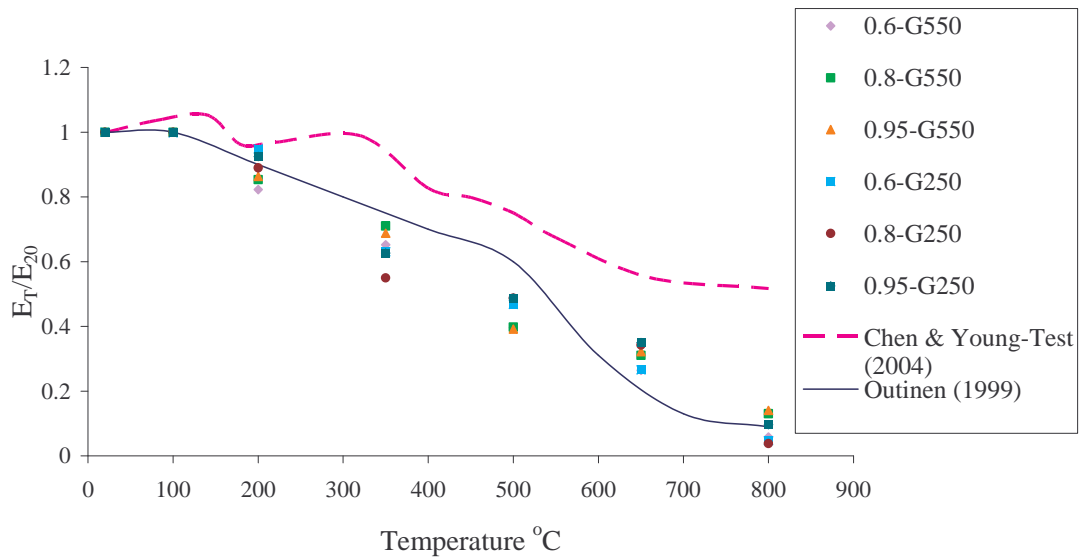
(b) Elasticity modulus reduction factors

Figure 3.33   Comparison of the Variation of Reduction Factors at Elevated Temperatures with Other Researchers' Results

As shown in Figure 3.33 (b) the elasticity modulus reduction factors were compared with other researchers' results. The results presented by Chen and Young (2004) considerably overestimate the reduction factors. Outinen's reduction factors agree reasonably well at some temperatures but disagree at other temperatures by up to 25%. Therefore the reduction factors from Chen and Young (2004) and Outinen (1999) cannot be used.

In summary, the reduction factors presented in the current Australian and International Standards confirm that the yield strength and the elasticity modulus do not deteriorate much at lower temperatures (up to 200°C). On the other hand most of the available results and results obtained from this research show that when the temperature is very high (650°C) more than 90% reduction occurs in yield strength. However, there are considerable differences at other temperatures. Most of the reduction factors overestimate the tested values while some of them are conservative. However, the overestimated values are not safe and the conservative values are not economical. Therefore the currently available reduction factors for both yield strength and elasticity modulus cannot be used in the design of light gauge cold-formed steel structures at elevated temperatures. In addition, the reduction factors presented by other researchers are also not safe nor economical. The reduction factors obtained in this research and available values are further investigated in Chapter 5 using finite element analyses to compare the experimental column test results at various temperatures. Such an investigation will determine the effects of reduction factors on the distortional buckling strength at elevated temperatures.

3.2.5.3   Comparison of cold-formed steel with hot-rolled steel

As stated in the SCI Publication (1993), the performance of hot-rolled steel structures in fire does not vary significantly with steel grade. In other words the yield strength and elasticity modulus reduction factors are almost the same for both low and high strength steels. Further it stated that the reduction of strength of cold-formed steels at elevated temperatures is more than that of hot-rolled steels and is about 10 to 20%. The reduction factors stated in BS 5950-8 (BSI, 1990) also confirmed it. Figure 3.34 presented here is from SCI Publication (1993) and is based

on the data obtained from tests performed by British Steel. In addition, SCI (1993) states that the elasticity modulus is also broadly reduced at the same rate as strength.

In order to obtain the difference between the reduction factors of hot-rolled steels and cold-formed steels, the available design standards were considered. For this purpose, the reduction factors given in AS 4100 (SA, 1998) and BS 5950-8 (BSI, 1990) were considered. BS 5950-8 does not discuss the elasticity modulus reduction factors of hot-rolled steels. In addition it presents the strength reduction factors only at 0.5, 1.5 and 2.0% strain levels. Therefore the reduction factors based on 0.5% strain level were used to compare the yield strength reduction factors of cold-formed steel in this research.
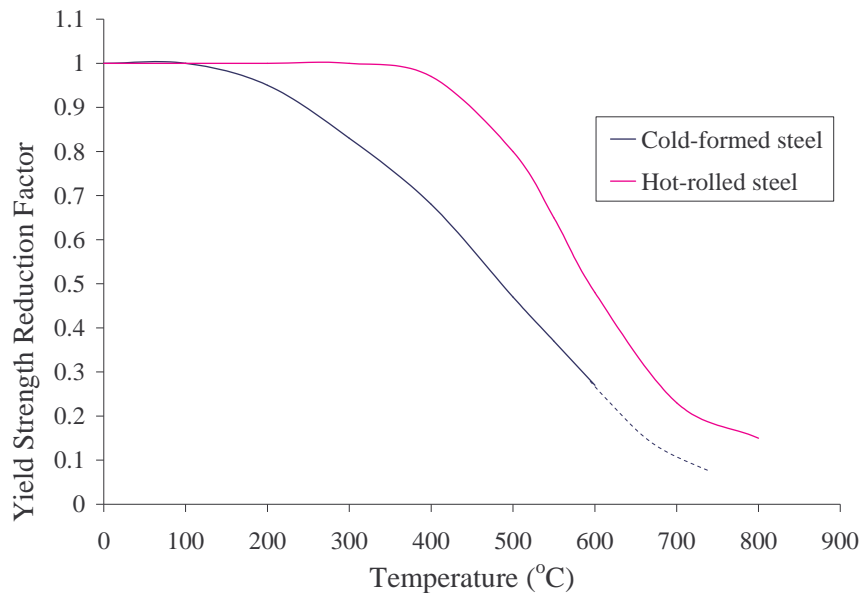
Figure 3.34   Yield Strength Reduction Factors for Cold-formed

and Hot-rolled Steels

As shown in Figures 3.35 (a) and (b) the reduction factors presented in AS 4100 and BS 5950-8 for hot-rolled steel overestimate the reduction factors of cold-formed seel most of the times for both yield strength and elasticity modulus. These results agree well with the SCI publication (1993). However, the difference between the reduction factors of these two steel types varies from 0 to 30%. Therefore it is clear that the

reduction factors obtained for hot-rolled steels cannot be used in the design of cold-formed steel structures under fire conditions.
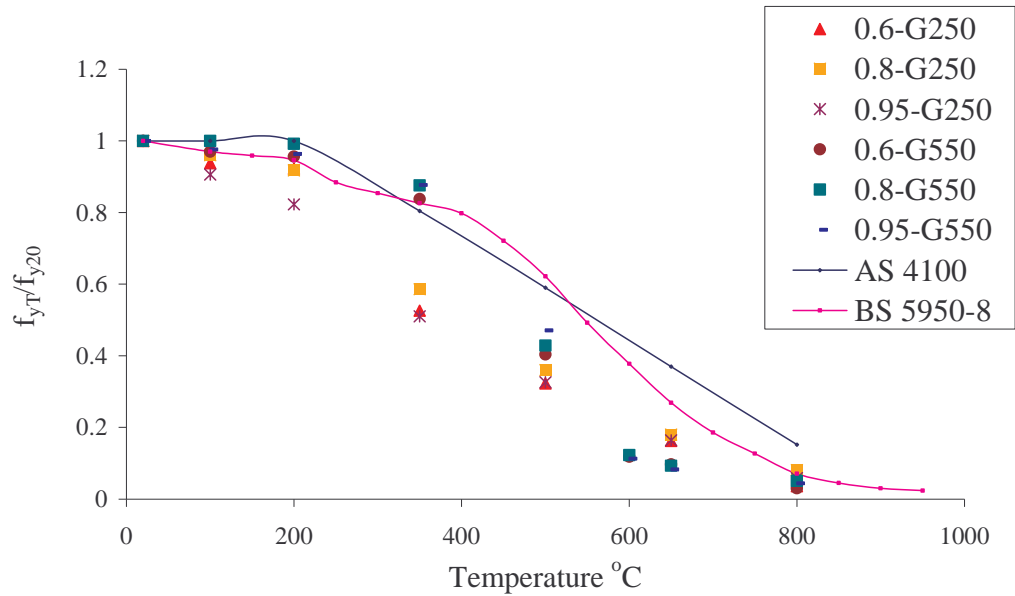
(a) Yield strength reduction factors
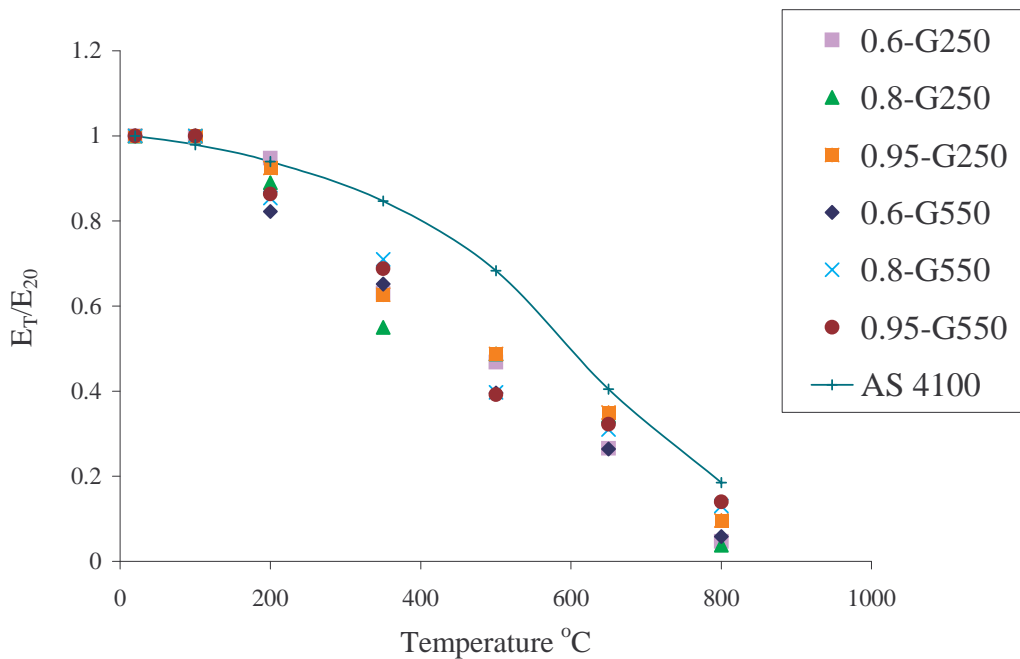
(b) Elasticity modulus reduction factors

Figure 3. 35   Comparison of Reduction Factors for Cold-formed

and Hot-rolled Steels

3.2.6 Predictive Equations for Mechanical Properties

3.2.6.1 Yield strength

Based on the yield strength results obtained from the tensile coupon tests at various temperatures, empirical equations were developed to determine the reduction factors for light gauge cold-formed steels. Since the temperature is the main factor causing the degradation of yield strength of steel, they were developed as a function of temperature. Other researchers (Olawale and Plank, 1988; Outinen et al., 1999 and SA, 1998) also determined the yield strength reduction factors as a function of temperature.

Although various strain levels (0.2%, 0.5%, 1.5% and 2%) were considered to determine the (yield) strength of steel, only the reduction factors obtained from the 0.2% proof stress method were used in deriving the empirical equations at elevated temperatures. The main reason for selecting this strain level is that the other strain levels have not been accepted widely and not defined well. On the other hand the strength values obtained at 1.5 and 2% strain levels are close to the ultimate strength than the 0.2% proof strength.

As shown in Section 3.2.2.2 and Figure 3.23, considerable differences were observed in the reduction factors of low and high strength steels. Therefore separate equations were developed for low and high strength steels. The reduction factors of high strength steels show three main regions while low strength steels show two main regions. The high strength steel shows a linear reduction in strength up to 200$^{\mathrm{o}}$C due to increasing temperatures. It then has a non-linear reduction due to the meteorological behaviour and the loss of strength gained due to cold-working. However, the latter effect is minimal up to about 500$^{\mathrm{o}}$C. Therefore the reduction factors of high strength steel are higher than that of low strength steel. However, the strength gain due to cold-working is lost when the temperature is above 500$^{\mathrm{o}}$C as seen by the sudden loss of strength (see Figure 3.23). Hence there is hardly any difference between low and high strength steels beyond 500$^{\mathrm{o}}$C. Three different equations were developed for high strength steels considering the three main regions.

Since low strength steels do not have any strength gain due to cold-working it has only two regions. Therefore two equations were developed for them.

Equations 3.2 (a) to (c) present the reduction factors (f_{yT}/f_{y20}) for high strength steels while Equations 3.3 (a) and (b) present the reduction factors for low strength steels based on various temperatures, where f_{yT} and f_{y20} are the 0.2% proof stress at elevated and ambient temperatures, respectively and T is the temperature. Figures 3.36 (a) and (b) show the comparison of experimental results and the predictions of Equations 3.2 and 3.3, respectively. As shown in Figure 3.36 there is very good agreement between the test results and predicted values from Equations 3.2 and 3.3. Therefore Equations 3.2 and 3.3 are recommended for use in future analyses to determine the yield strength reduction factors at any given temperature.

For G550 steels

$$\frac{f_{yT}}{f_{y20}} = -0.00016T + 1.0003 \qquad\qquad 20^o C \leq T \leq 200^o C \qquad\qquad (3.2a)$$

$$\frac{f_{yT}}{f_{y20}} = 0.97 - \frac{(T-200)^{1.81}}{58500} \qquad\qquad 200^o C < T < 600^o C \qquad\qquad (3.2b)$$

$$\frac{f_{yT}}{f_{y20}} = -0.00037T + 0.3363 \qquad\qquad 600^o C \leq T \leq 800^o C \qquad\qquad (3.2c)$$

For G250 steels

$$\frac{f_{yT}}{f_{y20}} = -0.0007T + 1.014 \qquad\qquad 20^o C \leq T \leq 200^o C \qquad\qquad (3.3a)$$

$$\frac{f_{yT}}{f_{y20}} = 3.7 - \frac{(T-74)^{0.15}}{0.736} \qquad\qquad 200^o C < T \leq 800^o C \qquad\qquad (3.3b)$$
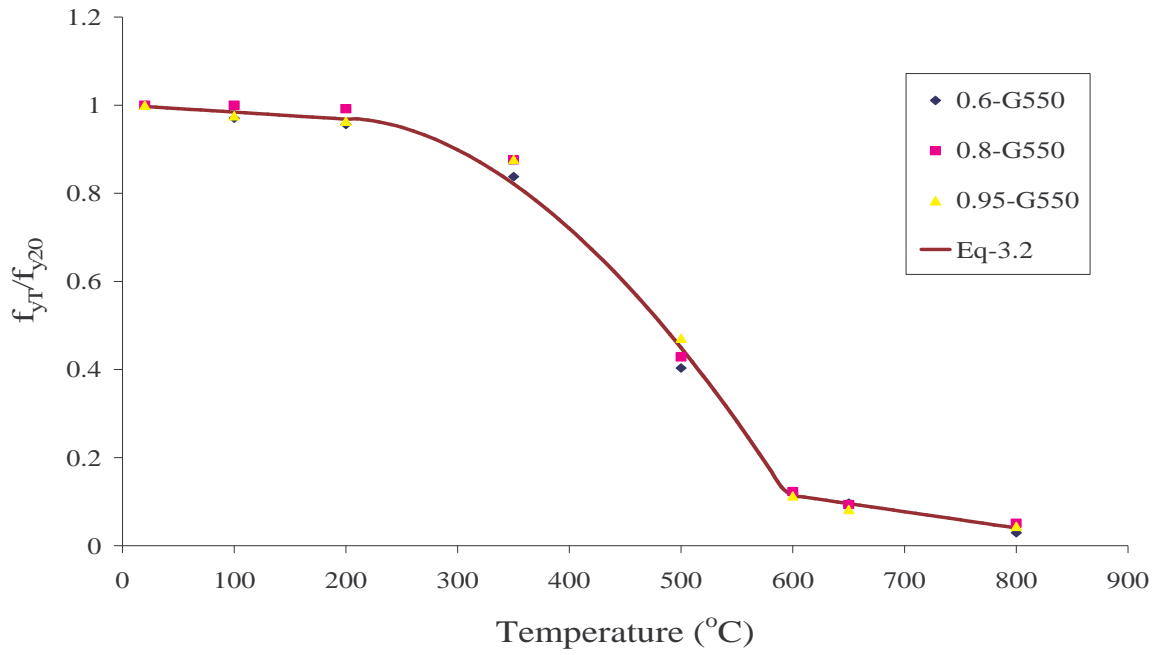
(a) G550 steel
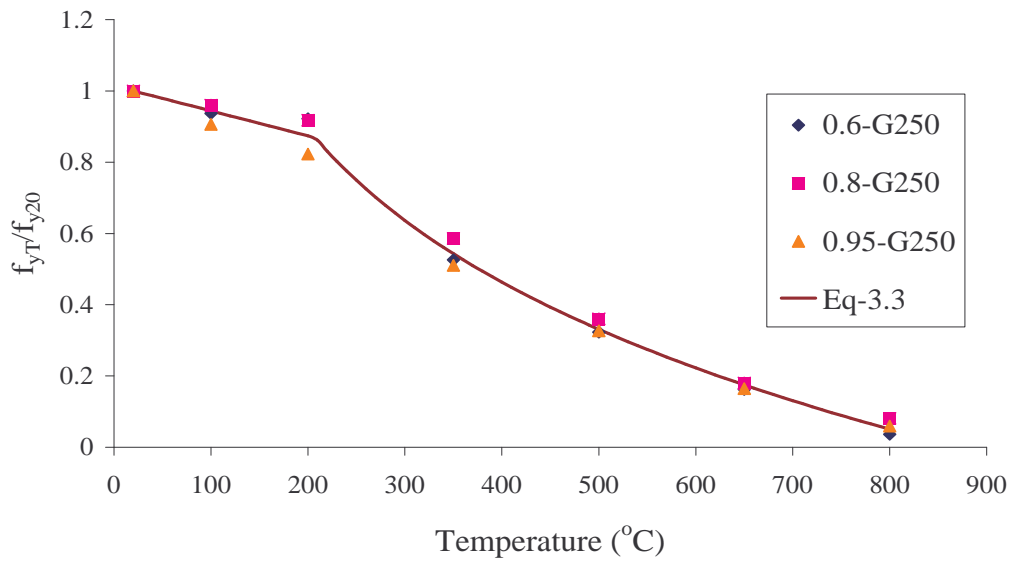
(b) G250 steel

Figure 3.36   Comparison of Predicted Yield Strength Reduction

Factors with Test Results

Alternatively Equations 3.4 and 3.5 can be used to predict the reduction factors at any given temperatures (up to 800°C). Figure 3.37 shows the comparison of the predictions from Equations 3.4 and 3.5 and the experimental results. Since there is a considerable difference between low and high strength steels, separate equations were developed. However, the influence of steel thickness is not a major factor affecting the deterioration of yield strength with elevated temperatures. Therefore it was not considered in developing these equations. Figure 3.37 shows a good agreement between predicted values and test results.

For G550 steel

$$\frac{f_{yT}}{f_{y20}} = 1.8476X10^{-11}T^{3.98} - 1.91X10^{-8}T^{3} + 3.625X10^{-6}T^{1.997} - 10^{-4}T + 0.99 \tag{3.4}$$

$$20^{o}C \leq T \leq 800^{o}C$$

For G250 steel

$$\frac{f_{yT}}{f_{y20}} = -1.26X10^{-11}T^{3.99} + 2.5675X10^{-8}T^{2.99} - 1.58766X10^{-5}T^{1.996} + 2X10^{-3}T + 0.89$$

$$\tag{3.5}$$

$$100^{o}C \leq T \leq 800^{o}C$$

Note: $\frac{f_{yT}}{f_{y20}} = 1$ at 20°C and linear interpolation can be used in between 20 and 100°C.
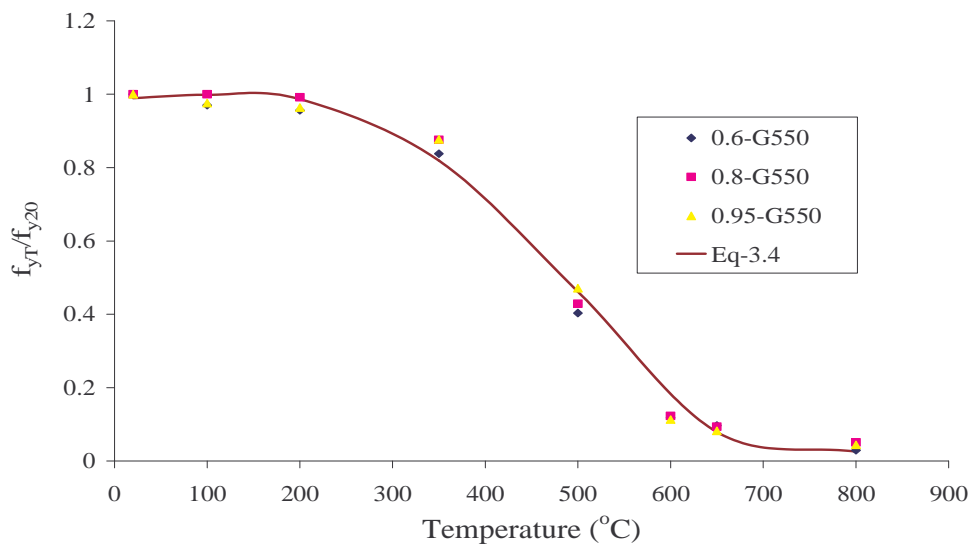
(a) G550 steel

Figure 3.37   Comparison of Predicted Yield Strength Reduction Factors with Test Results
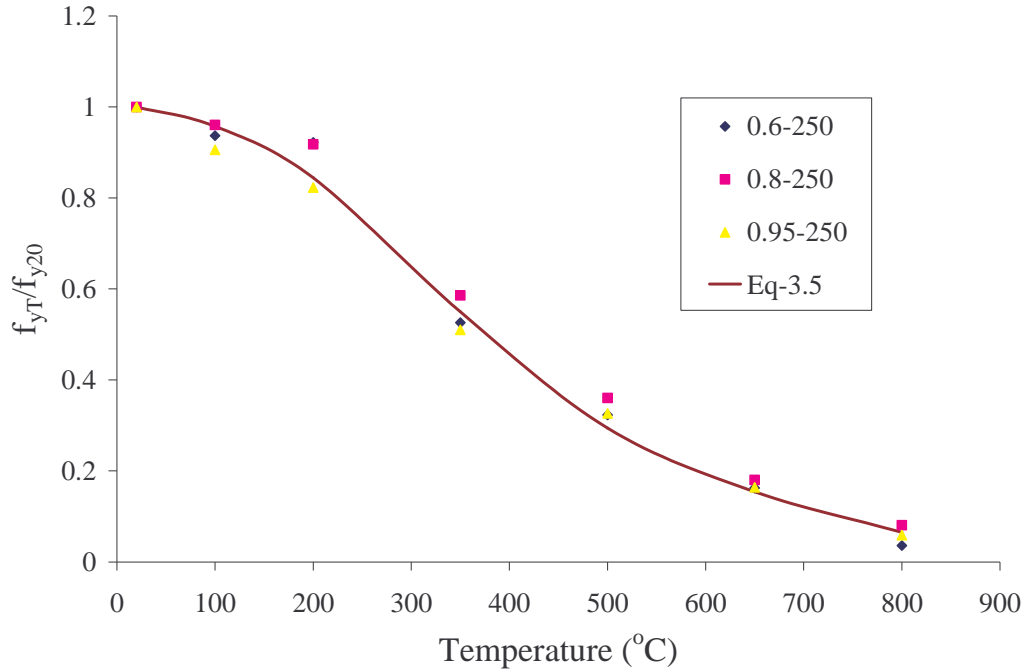
(b) G250 Steel

Figure 3.37   Comparison of Predicted Yield Strength Reduction

Factors with Test Results

3.2.6.2   Elasticity modulus

Elasticity modulus also deteriorates with the temperature as yield strength and is one of the important factors determining the buckling behaviour of light gauge steel members. Therefore empirical equations were developed for elasticity modulus with respect to temperature. As shown in Section 3.2.2.3 and Figure 3.27 there is a difference in the reduction factors for low and high strength steels. However, it is negligible. The influence of steel thickness is also negligible. Therefore the steel grade and thickness were not considered in developing the predictive equations.

Experimental results show that the elasticity modulus remains the same up to about 100°C. Beyond this there is a linear reduction. Therefore a linear equation was generated to predict the elasticity modulus reduction factors at elevated temperatures (see Equation 3.6). The calculated values from the equations and the tested values were then compared in Figure 3.38. It is clear that the predicted values agree well with the test results.

$$\frac{E_T}{E_{20}} = 1 \qquad\qquad 20^o\,C \le T \le 100^o\,C \qquad (3.6a)$$

$$\frac{E_T}{E_{20}} = -0.0013T + 1.1297 \qquad\qquad 100^o\,C < T \le 800^o\,C \qquad (3.6b)$$
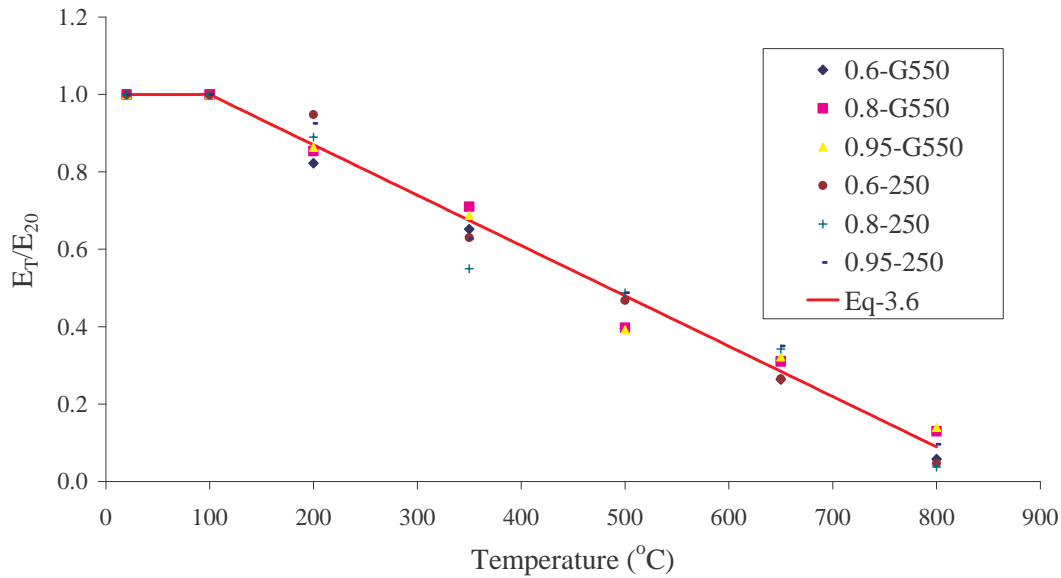
Figure 3.38   Comparison of Predicted Elasticity Modulus Reduction Factors with Test Results

3.2.6.3   Stress-strain model

Stress-strain models mainly depend on three parameters, yield strength, elasticity modulus and temperature, which were considered to develop a suitable stress-strain model. Ramberg and Osgood (1943) first developed the stress-strain model but it has been modified by various authors. The stress-strain model is usually given as shown in Equation 3.7 where ε_T is the strain corresponding to a given stress f_T at temperature T, E_T and f_{yT} are elasticity modulus and yield strength, respectively. β and η_T are parameters.

$$\varepsilon_T = \frac{f_T}{E_T} + \beta\left(\frac{f_{y,T}}{E_T}\right)\left(\frac{f_T}{f_{y,T}}\right)^{\eta_T} \qquad (3.7)$$

Various authors have modified the values of   and η_T depending on the steel types they have used. The parameter   in Equation 3.7 was considered as a constant value of 3/7 and 6/7 by Olawale and Plank (1988) and Outinen et al. (1999), respectively. The other parameter η_T decides the slope of the inelastic zone and the plastic stress in the stress-strain curve. Therefore the parameter η_T was determined as a function of temperature by both researchers.

Lee et al. (2003) used a different method to determine the stress-strain model. Although there are some shortcomings in their test results, Lee et al.'s model was also considered in this investigation. They considered $\eta_T = 15$ instead of using it as a function of T. However, their   value varies with temperature and is given in Table 3.10.

Table 3.10   Coefficients β from Lee et al. (2003)

Temperature (^{o}C)	20-300	400	500	600	700	800
	3.5	0.8	0.45	0.1	0.02	0.001

However, Lee et al.'s (2003) method was unable to predict the stress-strain model of light gauge cold-formed steel at elevated temperatures accurately. Therefore a new set of equations was generated from the simple curve fitting method with the consideration of all the above methods. The same equation was modified with different   and η_T parameters in this research. The parameter   was determined as 0.86 while the parameter η_T varied with temperature. The proposed values of η_T are given separately by Equations 3.8 (a) and (b) for both low and high strength steels. Equation 3.8 (a) is valid for the temperature range of 20°C to 800°C while Equation 3.8 (b) is valid for 350°C to 800°C. The stress-strain curves for low strength steels at temperatures below 350°C show a yield plateau and hence cannot be predicted using Equation 3.8 (b) that was developed only for gradually changing stress-strain behaviour.

For G550 steel

$$\eta_T = -3.05 X 10^{-7} T^3 + 0.0005 T^2 - 0.2615 T + 62.653 \qquad 20^o C \le T \le 800^o C \qquad (3.8a)$$

For G250 steel

$$\eta_T = 0.000138 T^2 - 0.085468 T + 19.212 \qquad 350^o C \le T \le 800^o C \qquad (3.8b)$$
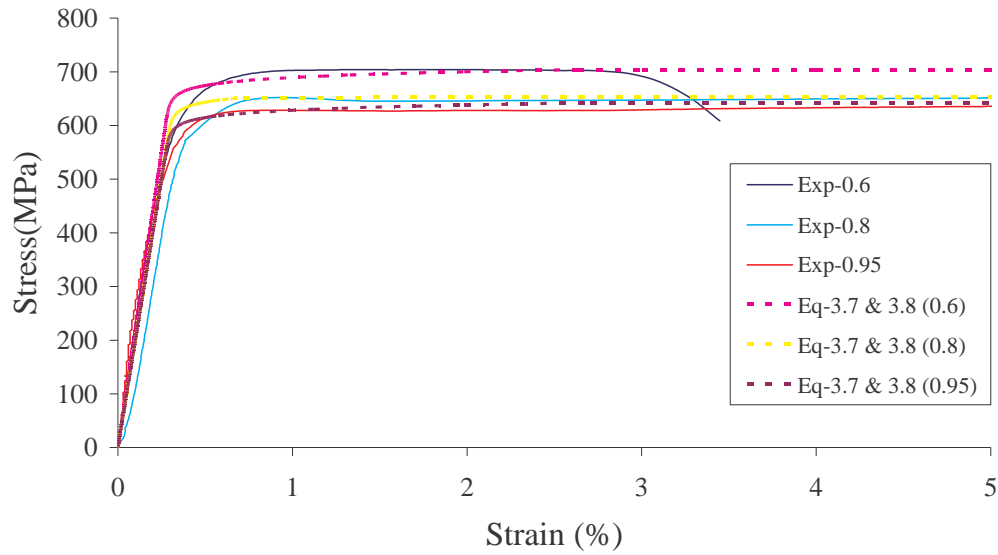
(a) At ambient temperature
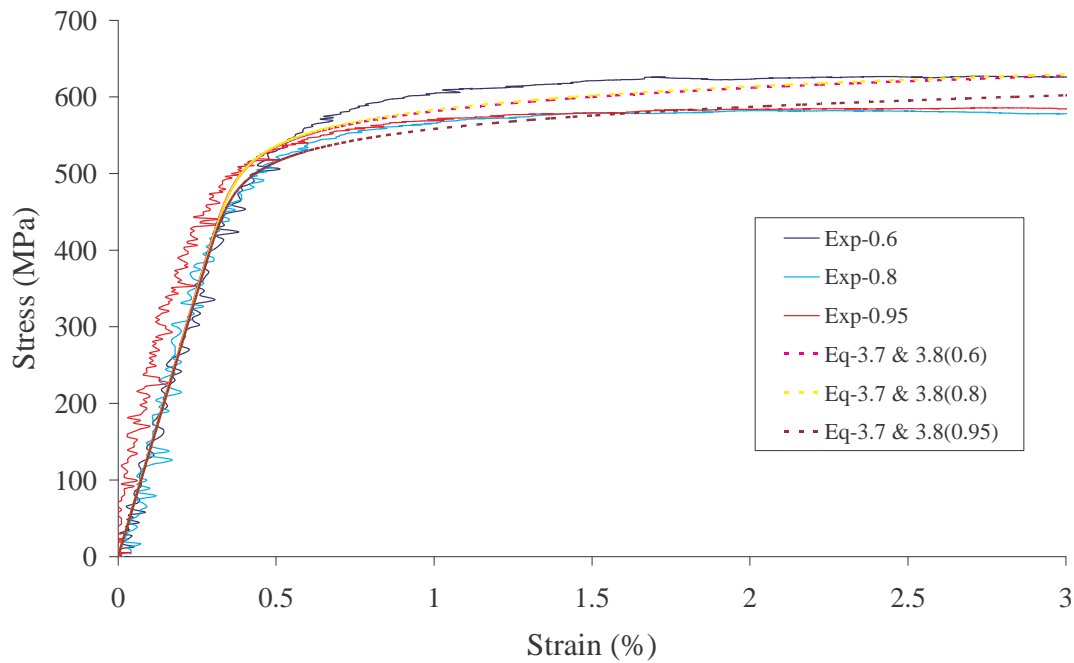
(b) At 350°C

Figure 3.39   Stress-strain Curves from Equations 3.7 and 3.8 and

Tests for G550 Steel
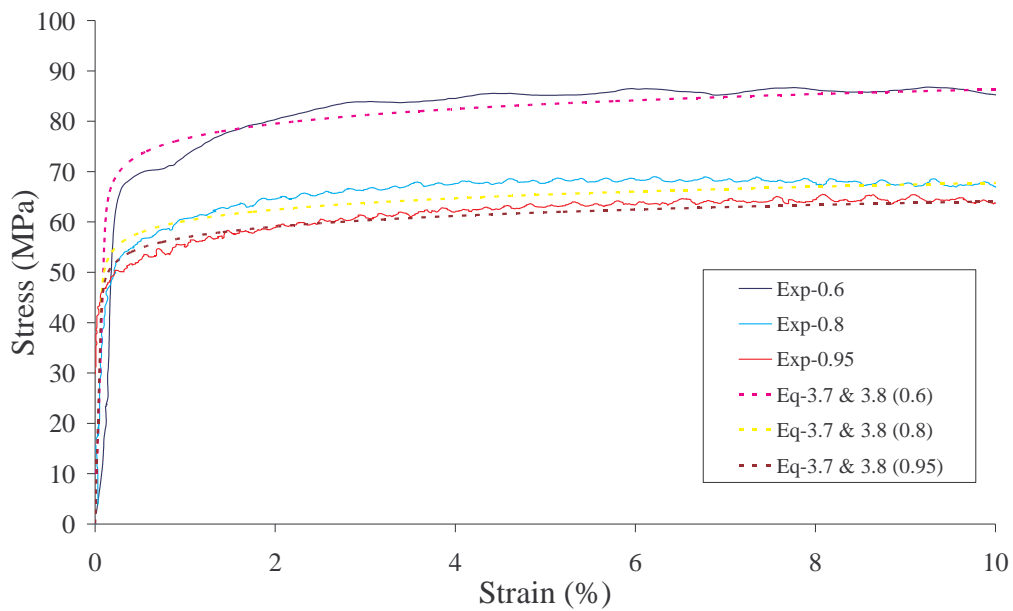
(c) At 650°C

Figure 3.39   Stress-strain Curves from Equations 3.7 and 3.8 and

Tests for G550 Steel

Figures 3.38 (a) and (b) compare the predicted stress-strain curves from Equations 3.7 and 3.8 with experimental results at ambient temperature and at 650°C for high strength steel. The comparison of predicted stress-strain curves with experimental results at other temperatures and both steel grades are shown in Appendix A. The results clearly show that there is a very good agreement between the predicted stress-strain curves from Equations 3.7 and 3.8 and test results. Therefore Equations 3.7 and 3.8 (a) and (b) are recommended for the determination of the stress-strain curves of 0.6, 0.8 and 0.95 mm G250 and G550 steels at any given temperature for further analyses.

3.2.7   Conclusions

This research was based on a detailed experimental study into the mechanical properties of light gauge cold-formed steels at elevated temperatures. The tests were undertaken by using three different thicknesses and two different steel grades at

seven different temperature levels to determine the yield strength, ultimate strength, the elasticity modulus and the stress-strain curve. The results showed that the steel grade has an influence on the yield strength of steel. However, it can be seen that there is no clear relationship between the elasticity modulus and the steel grade or the thickness of steel. Unusual behaviour was observed at 200°C, mainly for low strength steel. The main reason for this behaviour is considered to be the chemical reactions that take place at that temperature. Current literatures including various design standards do not present accurate reduction factors for both yield strength and elasticity modulus of light gauge cold-formed steels at elevated temperatures. Further, the available stress-strain models also do not predict the accurate stress-strain curves for light gauge cold-formed steels.

By considering all the results from this research, a new set of predictive equations was generated for both yield strength and elasticity modulus at elevated temperatures. Further, a new stress-strain model was also developed based on the available stress-strain models. The use of such accurate mechanical properties developed from this research will lead to safe design of light gauge cold-formed steel structures under fire conditions.

4 Experimental Investigation of Cold-formed Steel Compression Members

Light gauge cold-formed steel sections are more economical than traditional heavy hot-rolled steel sections. They have a high strength to weight ratio compared to the thicker hot-rolled members. The use of very thin (0.42 to 1.2 mm) cold-formed steels has increased rapidly around the world due to the development of advanced manufacturing technologies. However, the knowledge and understanding of the structural behaviour of cold-formed steel members is limited. Local and distortional buckling are the most common failure modes of short light gauge cold-formed steel compression members. Therefore in order to determine the capacity of steel compression members, both local and distortional buckling modes should be considered. However, local buckling mode has been thoroughly investigated at both ambient and elevated temperatures and there is a wealth of knowledge on this topic (Lee, 2004 and Ranby, 1999). On the other hand, there is limited research on the distortional buckling behaviour of cold-formed steel compression members at ambient and elevated temperatures. For these reasons a series of laboratory experiments was carried out to determine the distortional buckling failure behaviour of light gauge cold-formed steel compression members at various temperatures. The main focus was on two different types of cross-sections with two different steel grades and three different thicknesses.

> ➤ Ambient temperature tests: Experiments were carried out at room temperature (20°C)
> ➤ Elevated temperature tests: Experiments were carried out at steady state conditions. First the temperature was increased up to the required pre-set level and then the load was increased until failure while maintaining the pre-set temperature.

4.1 Distortional Buckling of Cold-formed Steel Compression Members at Ambient Temperature

An experimental study was carried out first to investigate the structural behaviour of light gauge cold-formed steel compression members, which were subjected to distortional buckling failure mode at ambient temperature. Suitable light gauge cold-formed steel cross sections were determined based on the available literature review (see Chapter 2), elastic buckling analyses (from the Thin-wall program and finite element model) and the constructability of the sections in the QUT Civil Engineering Workshop. Commonly available sections as shown in Figure 1.2 and some other constructable sections were considered in this process. This led to the choice of two sections, lipped C-sections with and without additional lips (see Figure 4.1). The dimensions of the designed sections were verified for fixed-end conditions using the validated finite element model. Both low and high strength steels were considered since they are commonly used in Australia. High strength steel G550 with a nominal yield strength of 550 MPa and low strength steel G250 with a nominal yield strength of 250 MPa were used. The thicknesses of cold-formed steels varied from 0.6 mm to 0.95 mm. i.e. 0.6, 0.8, and 0.95 mm.
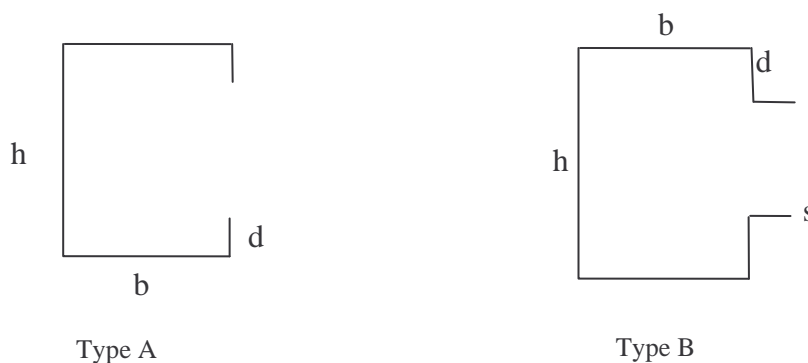
Figure 4.1   Designed Sections for Experiments

4.1.1   Preliminary Investigation

A series of preliminary experiments was carried out first in order to obtain the best method of undertaking experimental investigations on light gauge cold-formed steel compression members at ambient temperature. Further, the effect of end boundary

conditions was observed during this preliminary testing. It allowed a decision to be made on suitable boundary conditions and test procedures.

4.1.1.1 Test specimen

The required column length and the cross-sectional dimensions were obtained based on the buckling stress plots of the compression members from Thin-wall program (see Figure 4.2). However, the Thin-wall program (Papangelis and Hancock, 1998) is based on finite strip analyses and only simply supported conditions are considered. Therefore, the suitability of selected sections was verified using the finite element program ABAQUS (HKS, 2004) for fixed-end conditions. Figure 4.3 shows the results of finite strip analyses using Thin-wall program and finite element analyses using ABAQUS. These plots clearly show that the end conditions and column length have a significant effect on the elastic distortional buckling strength.
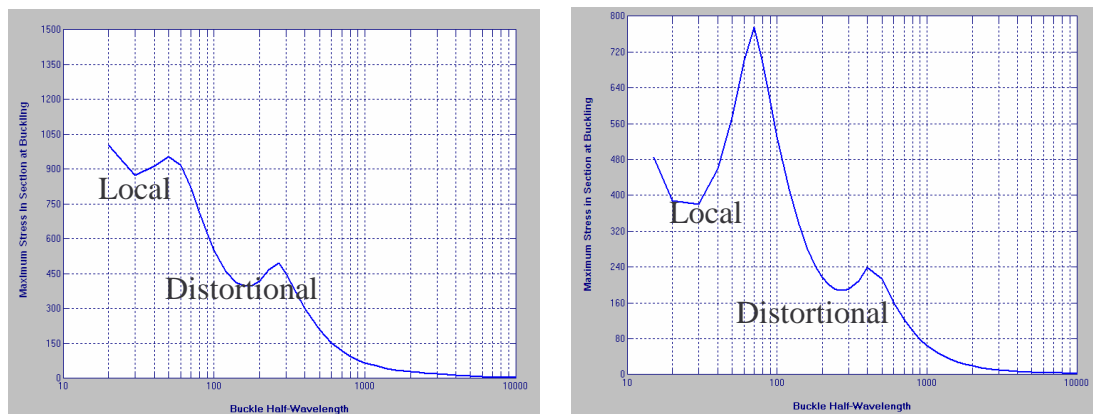
(a) Type A   (a) Type B

Figure 4.2   Buckling Stress Plots (Maximum Stress in Section at Buckling versus Buckling Half-Wavelength) for 0.6 mm Thick Specimen at 20°C from Thin-wall Program
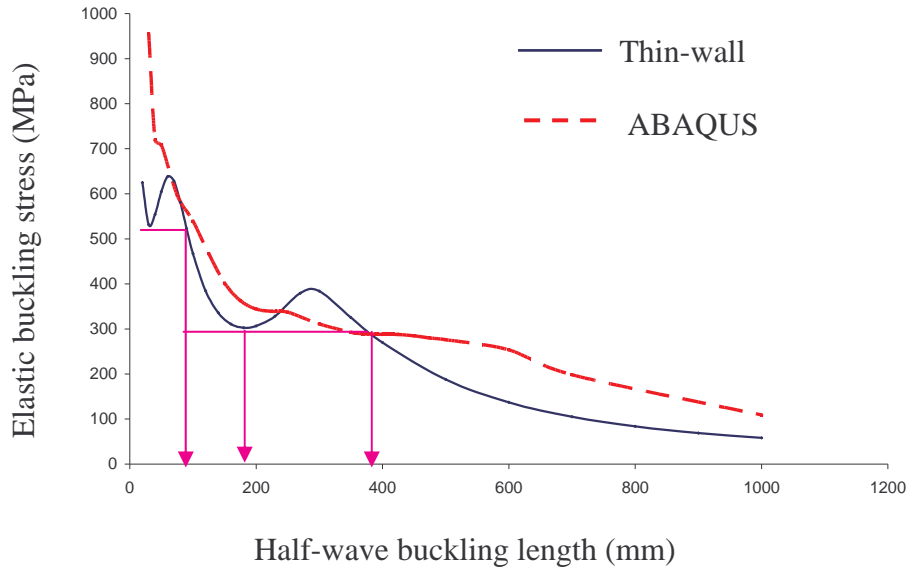
Figure 4.3 **Buckling Stress Plots for 0.8 mm Lipped Channel Type A Sections at 20°C from Thin-wall and ABAQUS**

As shown in Figure 4.3 the Thin-wall program results show that the pure local buckling occurs up to a half wave length of 100 mm and pure distortional buckling from 140 mm to 300 mm. The minimum elastic distortional buckling stress occurs when the half wave length equals 180 mm. The behaviour changes to a pure global buckling mode when the half wave length is about 400 mm. According to the finite element model, pure local buckling occurs up to 125 mm, but from 150 mm to 250 mm, this shows pure distortional buckling with one wave. However, when the column length is more than 300 mm it shows pure distortional buckling failure mode with more than one wave. When it is close to 600 mm the failure occurs due to the interaction of global and distortional buckling modes while pure global buckling occurs for the lengths greater than 700 mm. However, according to the results from Thin-wall and finite element analyses, both showed that pure distortional buckling with one half wave occurs when the column length is between 150 mm to 250 mm. Therefore, the column length was selected as 180 mm for the high strength cold-formed lipped C-section of 0.8 mm thickness so that pure distortional buckling would occur. However, the elastic distortional buckling stress for fixed-end conditions based on finite element analyses (FEA) is higher than that for pin-end conditions based on Thin-wall program (see Figure 4.3). Therefore, all the columns

were first designed based on Thin-wall program results. It was then validated using the finite element analyses.

Table 4.1   Selected Dimensions of Type A and Type B Columns

Section Type	Nominal Thickness (mm)	h	b	d	s	Length (mm)
A	0.60	30	30	5	-	200
	0.80	30	30	5	-	180
	0.95	30	35	5	-	180
B	0.60	40	30	5	10	280
	0.80	40	30	5	10	240
	0.95	40	30	5	10	220

Using the buckling analysis results, suitable shapes and dimensions were selected so that the chosen sections buckle by pure distortional mode. Mainly two types of cross sections as shown in Figure 4.1 and Table 4.1 were selected for pure distortional buckling behaviour at ambient temperature.

4.1.1.2   Test set-up and procedure

Past research reveals that the effect of end boundary conditions is not well understood. Kwon and Hancock (1992a) and Kesti and Davies (1999) stated that the end boundary conditions have a significant influence on the distortional buckling behaviour whereas Young and Rasmussen (1995) stated that end boundary conditions have only a small effect on the distortional buckling failure. Therefore the effect of the following end conditions was investigated in this research.

- Fixed-fixed condition, (both ends fixed, see Figure 4.4 (a))
- Pin-pin condition, (both ends pinned, see Figure 4.4 (b))
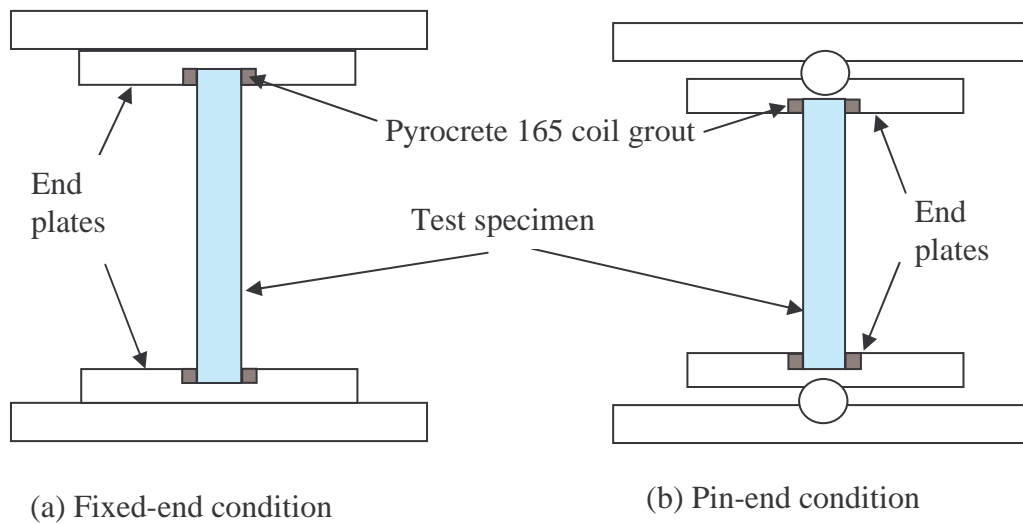
Figure 4.4   End Boundary Conditions

Figure 4.5   End Plate with 5 mm Depth Groove
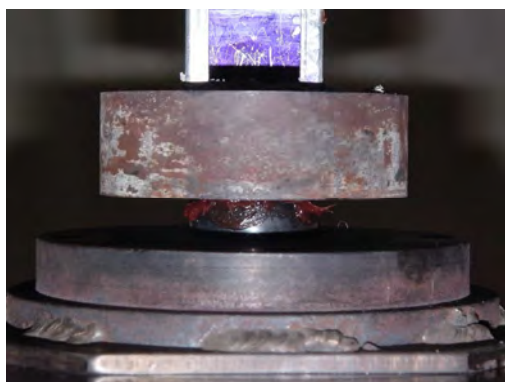
(a) Pin-end   (b) Fixed-end

Figure 4.6   Experimental Set-Up for End Conditions

Specially designed end plates with a groove (see Figure 4.5) were used to provide the required fixed-end and pin-end conditions (see Figure 4.6). The groove depth was 5 mm as it was adequate to fix the specimen to the end plates accurately. The groove should be filled with a material that can properly fix the specimen to the end plate. The filling material should have higher strength to prevent any failure reducing the degree of fixity at the specimen ends. This will allow the presence of required fixed-end conditions until the specimen failed. On the other hand the filling material should also resist elevated temperatures and therefore should have a higher strength at elevated temperatures too. Therefore three types of fire resisting filling materials were considered. A series of compression cube tests was conducted for all of them. Table 4.2 shows the different filling materials used and their compressive strengths.

Table 4.2   Compression Test Results of Different Types of Filling Materials

Material	Failure Load (kN)	Strength (MPa)
Furnace patch 125	17.7	30.1
Pyroplas 85 PB plastic	1.1	1.7
Pyrocrete 165 coil grout	23.9	37.3

As seen in Table 4.2, Pyrocrete 165 coil grout had the highest compression strength and was therefore selected as the filling material. It also has a higher strength at elevated temperatures and is easy to handle with no shrinkage after setting. Despite this, it was considered necessary to verify its suitability using trial tests. In these tests, epoxy which has a higher strength than Pyrocrete 165 was also used for comparison purposes. It must be noted that epoxy cannot be used at elevated temperatures.

Two trial tests were carried out to compare the strength of Pyrocrete 165 coil grout with epoxy. Cold-formed steel lipped channel sections made of 0.8 mm G250 steel were used for these trial tests. The tests were carried out at ambient temperature with pin-end conditions. They showed the same results for both types of materials (see Table 4.3). Based on these results it was decided to use Pyrocrete 165 coil grout in the column tests, mainly because it has a higher strength even at elevated

temperatures. By filling the specially designed end plates with Pyrocrete 165 coil grout the required fixed-end conditions were simulated in the column tests (see Figure 4.6 (b)).

Table 4.3   Trial Test Results

Material used	Failure Load (kN)
Epoxy	22.5
Pyrocrete 165 coil grout	22.1

Experiments were undertaken to compare the effect of pin-end and fixed-end conditions (see Figure 4.7) on the distortional buckling behaviour of light gauge cold-formed steel compression members. Both low and high strength brake-pressed Aluminium/Zinc coated light gauge cold-formed steel specimens were considered in this investigation. A 0.8 mm thick Type A cross section was used in these tests. All the dimensions were kept constant for both methods in order to compare the distortional buckling behaviour with respect to the end boundary conditions. Three specimens were used for each type and all the tests were carried out at ambient temperature. The compression tests were carried out using the Tinius Olsen testing machine in the QUT Structural Testing Laboratory. A displacement control method was used to apply a uniformly distributed compression load at a rate of 0.3 mm/min. Three LVDTs (Linear Variable Displacement Transducers) were used to measure the deformations of specimens during testing. A 5 mm LVDT was used to measure the out-of-plane deformation at the centre of the web while 20 mm LVDTs were used to measure the out-of-plane deformation of flanges at a location of 5 mm away from the lips. Axial shortening of the specimens was also recorded during the tests.

The centroid axis of the end plates and the specimen cross section were kept the same to simulate a uniformly distributed load for pin-end and fixed-end conditions. Further, the two end plates were kept parallel to each other and their horizontal level was maintained to ensure a uniformly distributed load. In this way, the compression load was applied to the centroid of the column without any moments.

(a) Fixed-end condition   (b) Pin-end condition

Figure 4.7   Preliminary Distortional Buckling Test

4.1.1.3   Effect of End Boundary Conditions

The recorded data was used to plot the axial compression load versus axial shortening and out-of-plane deflection curves and to compare the effects of pin-end and fixed-end conditions. The results in Figures 4.8 (a) and (b) show that the ultimate loads of pin-end specimens were less than that of the fixed-end specimens. However, the difference between them was small. On the other hand, the failure mode of the specimens was the same. All the specimens failed with flanges moving towards the inside of the column (see Figure 4.9). However, the pin-end specimens showed early deformation of web and flanges than in the case of fixed-end conditions. There were small variations in the deflection of flanges and web with respect to the pin-end and fixed-end conditions. However, it is difficult to say that there are no effects from the end boundary conditions to the distortional buckling behaviour of compression members.
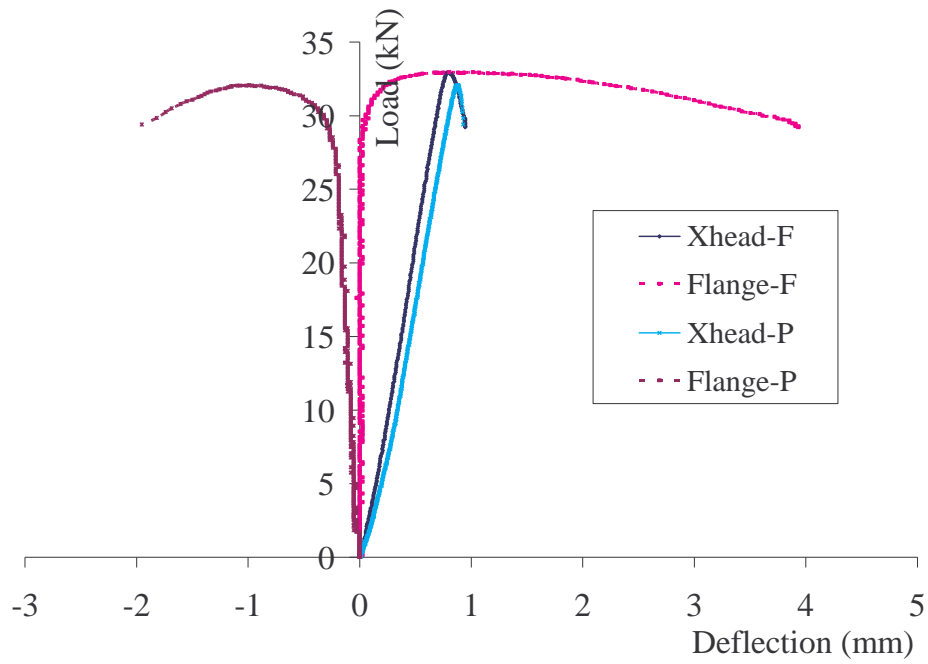
(a)   Comparison of fixed-end and pin-end conditions for G550 steel specimens
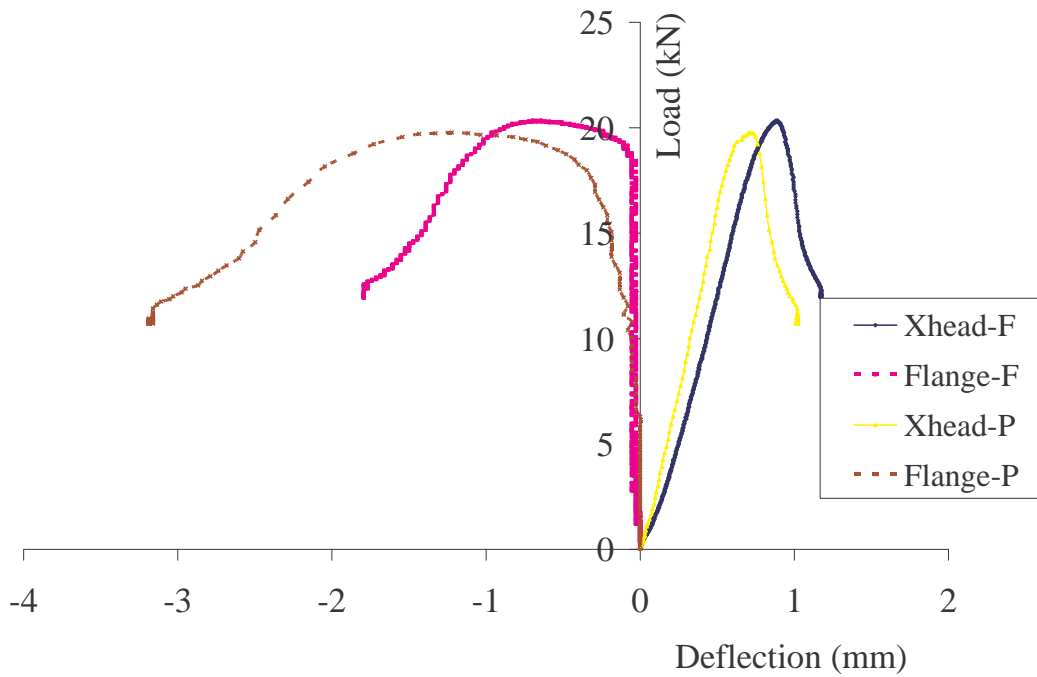
(b)   Comparison of fixed-end and pin-end conditions for G250 steel specimens

Note: Xhead-F and Xhead-P are Axial shortening of the fixed-end and pin-end columns, respectively.

Flange-F and Flange-P are out-of-plane deflection of the fixed-end and pin-end columns, respectively.

Figure 4.8   Load-Deflection Curves of 0.8 mm Type A Specimen

The experimental methods adopted in this study for pin-end conditions should be further improved to compare the effect of end boundary conditions on the distortional buckling behaviour. The fixed-end condition was used in the remaining experiments since the test set-up is simpler than that of pin-end conditions. Further, in the case of pin-end specimens, an additional moment is created due to the shift in the line of axial compression force after the elastic local buckling failure. This may complicate the problem. This was another reason for using the fixed-end condition in the remaining experiments.

Figure 4.9   Distortional Buckling Failure Mode Observed During Preliminary Tests

4.1.2   Distortional Buckling Tests under Fixed End Conditions

The aim of this experimental study was to investigate the distortional buckling behaviour of the chosen light gauge cold-formed steel lipped C-sections with and without additional lips (see Figure 4.1) subjected to axial compression loads. A series of tests was undertaken at ambient temperature for both low and high strength steel specimens with three different thicknesses as explained earlier. Both low and high strength steel columns were selected to examine the effects of steel grade on the distortional buckling behaviour of compression members. Three different

thicknesses were also used to determine the effect of steel thickness. As mentioned earlier all the test specimens were designed to fail by pure distortional buckling under axial compression.

4.1.2.1 Test specimens

Eighteen steel columns from each grade (G250 and G550) were tested. The specimen dimensions were measured using a vernier calliper and the specimens were marked prior to testing. The total coated and base metal thicknesses of each specimen were measured using a micrometer screw gauge and a special coating thickness gauge, respectively. In addition the base metal thickness was obtained by removing the coating by using 1:1 diluted hydrochloric acid for greater accuracy. The base metal thicknesses were then used to determine the distortional buckling stresses at ambient temperature. The ends of each specimen were grinded flat and parallel to each other to ensure full contact between the specimen and the end plates. The test specimen length (L) was varied from 190 mm to 290 mm with respect to the thickness and the section type as shown in Tables 4.4 and 4.5. The cross section dimensions of the specimens shown in these tables are average measured values. All the test specimens were labelled in order to identify the grade and thickness of specimen, test temperature, type of specimen and specimen number as shown below.

G250-0.6-20-A1

- Specimen number
- Specimen type
- Test temperature
- Specimen thickness
- Specimen grade
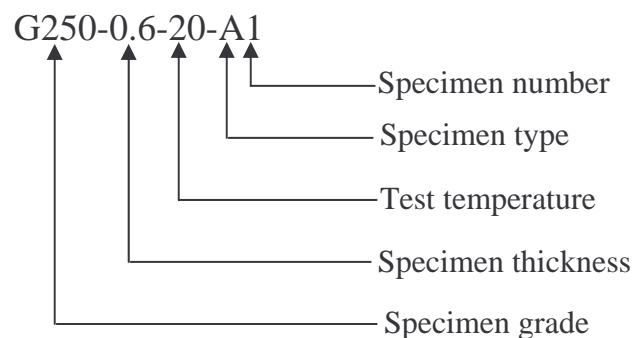
The measured dimensions were used to obtain the elastic buckling and ultimate strengths based on finite element analyses. Further, the initial geometric imperfections of all the specimens were measured using a special laser beam device (see Figure 4.10). The measured imperfections were found to be close to the

thickness of the high strength steel specimens, but less for low strength steel specimens.

Table 4.4 Measured Dimensions of Type A Specimens

Specimen	t (mm)		h (mm)	b (mm)	d (mm)	L (mm)
	TCT	BMT				
G250-0.6-20-A1	0.59	0.54	30.71	30.82	5.22	210
G250-0.6-20-A2	0.60	0.55	30.74	30.86	5.18	210
G250-0.6-20-A3	0.59	0.54	30.72	30.80	5.23	210
G250-0.8-20-A1	0.81	0.76	30.84	30.92	5.45	190
G250-0.8-20-A2	0.80	0.75	30.92	30.88	5.55	190
G250-0.8-20-A3	0.80	0.75	30.82	30.88	5.50	190
G250-0.95-20-A1	1.00	0.94	30.95	31.12	5.78	190
G250-0.95-20-A2	0.99	0.93	31.00	31.15	5.75	190
G250-0.95-20-A3	1.00	0.94	30.94	31.18	5.82	190
G550-0.6-20-A1	0.67	0.60	30.88	30.88	5.20	210
G550-0.6-20-A2	0.66	0.59	30.76	30.84	5.22	210
G550-0.6-20-A3	0.67	0.60	30.82	30.86	5.19	210
G550-0.8-20-A1	0.85	0.80	30.92	31.20	5.52	190
G550-0.8-20-A2	0.86	0.80	31.00	31.28	5.54	190
G550-0.8-20-A3	0.85	0.80	30.89	31.26	5.45	190
G550-0.95-20-A1	1.00	0.94	31.22	31.60	5.80	190
G550-0.95-20-A2	1.01	0.95	31.45	31.58	5.78	190
G550-0.95-20-A3	1.00	0.95	31.50	31.65	5.81	190

❖ BMT and TCT refer to base metal thickness and total coated thickness, respectively while L is specimen length.

Type A   Type B
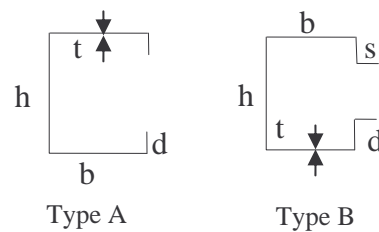
Table 4.5   Measured Dimensions of Type B Specimens

Specimen	t (mm)		h	b	d	s	L
	TCT	BMT	(mm)	(mm)	(mm)	(mm)	(mm)
G250-0.6-20-B1	0.60	0.54	40.60	30.47	5.55	10.10	290
G250-0.6-20-B2	0.60	0.55	40.58	30.46	5.56	10.12	290
G250-0.6-20-B3	0.59	0.54	40.61	30.48	5.54	10.11	290
G250-0.8-20-B1	0.80	0.75	41.82	30.82	5.65	9.05	250
G250-0.8-20-B2	0.81	0.76	41.80	30.85	5.67	9.04	250
G250-0.8-20-B3	0.81	0.75	41.83	30.86	5.66	9.08	250
G250-0.95-20-B1	0.99	0.93	38.54	30.03	6.04	9.29	230
G250-0.95-20-B2	1.00	0.94	38.52	30.05	6.05	9.28	230
G250-0.95-20-B3	1.00	0.94	38.53	30.05	6.18	9.27	230
G550-0.6-20-B1	0.66	0.60	40.68	30.45	5.58	9.68	290
G550-0.6-20-B2	0.66	0.59	40.64	30.48	5.55	9.72	290
G550-0.6-20-B3	0.67	0.60	40.69	30.47	5.59	9.69	290
G550-0.8-20-B1	0.85	0.80	41.94	30.85	6.07	9.42	250
G550-0.8-20-B2	0.86	0.80	41.88	30.91	6.05	9.43	250
G550-0.8-20-B3	0.85	0.80	41.92	30.89	6.05	9.40	250
G550-0.95-20-B1	1.01	0.95	38.55	30.02	6.15	9.72	230
G550-0.95-20-B2	1.01	0.95	38.56	30.04	6.14	9.78	230
G550-0.95-20-B3	1.00	0.95	38.55	30.05	6.16	9.75	230

❖   BMT and TCT refer to base metal thickness and total coated thickness, respectively while L is specimen length.
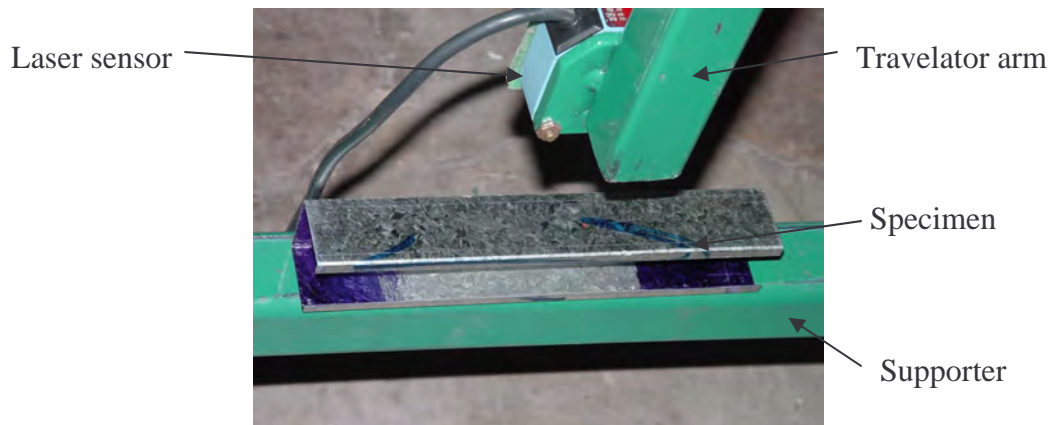
Figure 4.10   Imperfection Measurements

4.1.2.2 Test set-up and procedure

Fixed-end support conditions were selected for the reasons indicated in the earlier sections. The length of the test specimens was decided based on the buckling half-wave length obtained from the Thin-wall program and ABAQUS. Additional lengths of 5 mm were provided for each top and bottom end to allow for the fixing of specimens to the end plates (see Figure 4.11). The specimens were then properly fixed to the end plates by using Pyrocrete 165 coil grout as described in Section 4.1.1.2. The test specimens with the fixed-end plates were then placed between the large cross heads of a universal testing machine (Tinius Olsen) and loaded in axial compression until the specimens failed. In this test set-up there was no eccentric loading or additional moments.

Figure 4.11   Test Specimens with End Plates

Figure 4.12 shows the overall test set-up while Figure 4.13 shows the details of deflection measurements. The out-of-plane deflections of both flanges were measured using 20 mm LVDTs at mid-height and 5 mm away from the flange-lip junction for Type A specimen. The out-of-plane deflections of one flange and one lip were measured for Type B specimens. An additional 5 mm displacement transducer was located on the web to monitor any deformation of web. The LVDT positions are shown in Figure 4.13 (c) for Type A and Type B specimens. The shortening of the specimen was also recorded during the tests by the Tinius Olsen testing machine.
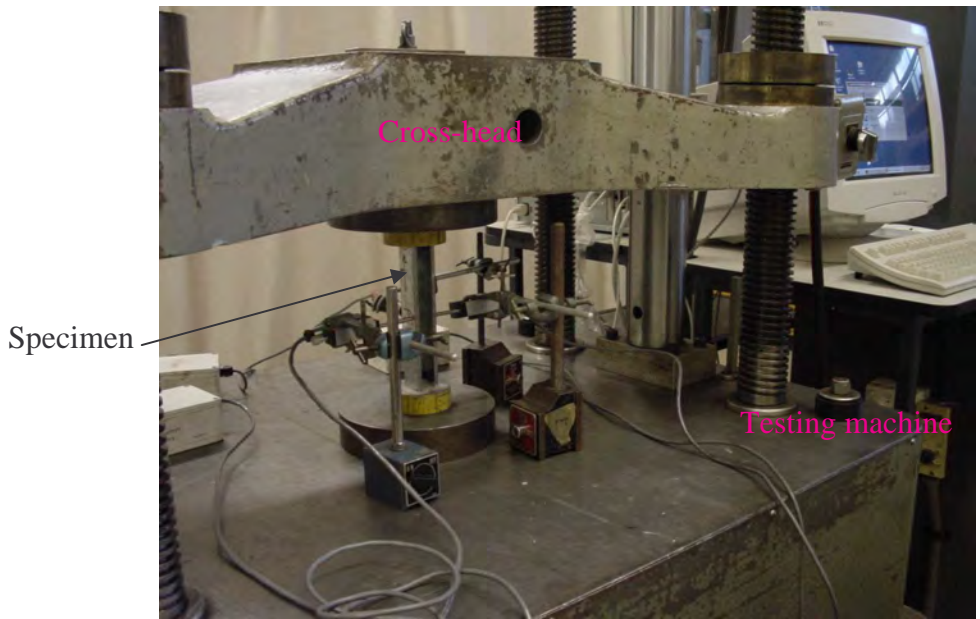
Figure 4.12   Overall Test Set-Up
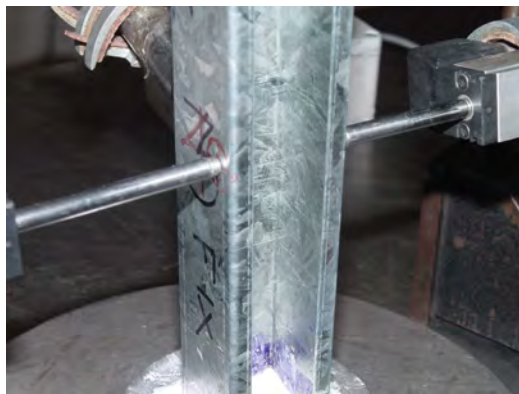
(a) Out-of-plane deflection measurement

(b) Axial shortening measurement

Type A

Type B
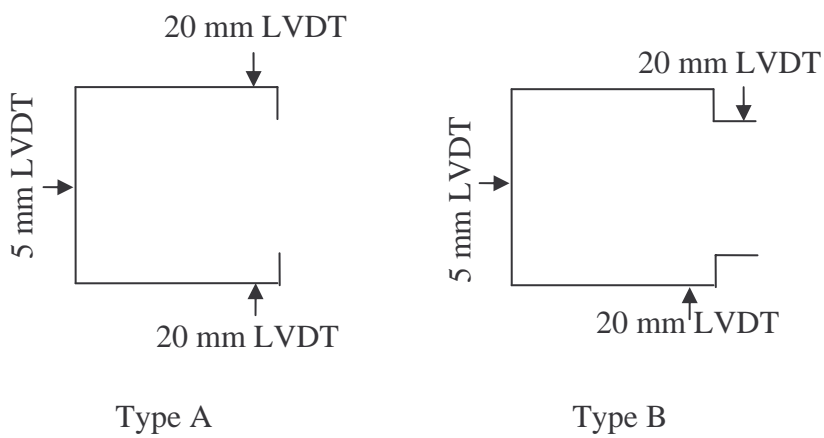
(c) LVDT positions

Figure 4.13   Deflection Measurements

4.1.2.3 Test results

The elastic buckling and ultimate loads were recorded during the tests. The distortional buckling failure modes are shown in Figure 4.14. The elastic buckling failure load was taken as the load at which the flanges were seen to move out-of-plane. However, it is difficult to determine the exact elastic buckling failure load through visual observations. It will depend on the observer's judgment and experience. Figures 4.15 and 4.16 show the axial compression load versus out-of-plane deflection and the axial compression load versus axial shortening graphs for 0.95 mm Type A and Type B specimens, respectively. Appendix B presents all the load versus axial shortening and load versus out-of-plane deflection graphs.

(a) Distortional buckling failure of
Type A specimen

(b) Distortional buckling failure of
Type B specimen

Figure 4.14   Distortional Buckling Failure Modes
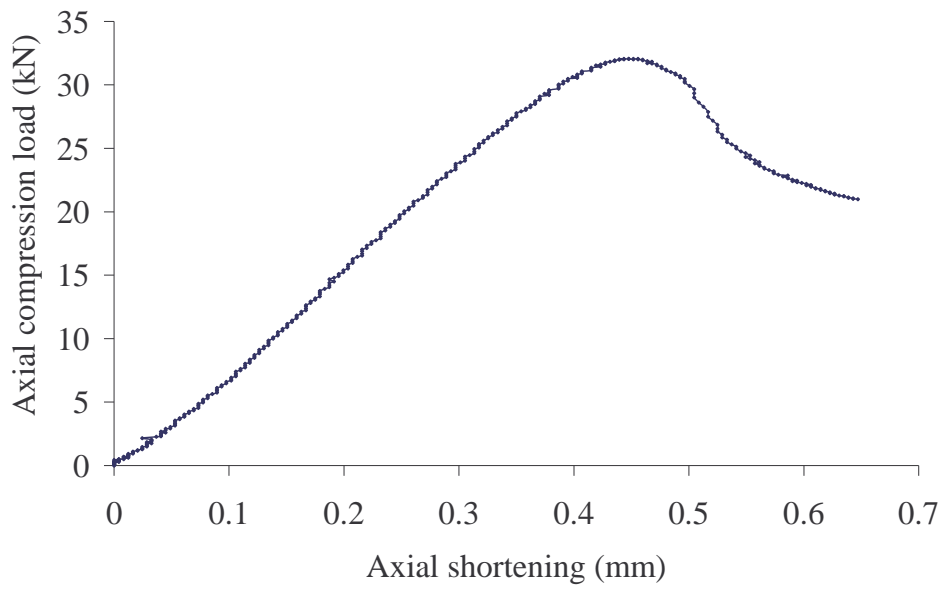
Axial compression load versus axial shortening
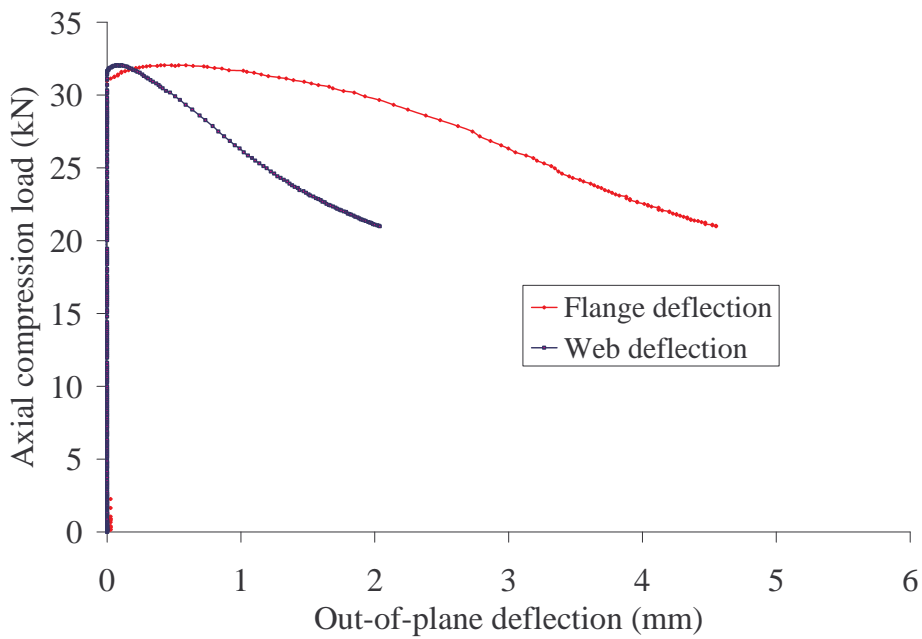
Axial compression load versus out-of-plane deflection

(a) G250 steel

Figure 4.15   Load-Deformation Curves for 0.95 mm Type A Specimen

Axial compression load versus axial shortening
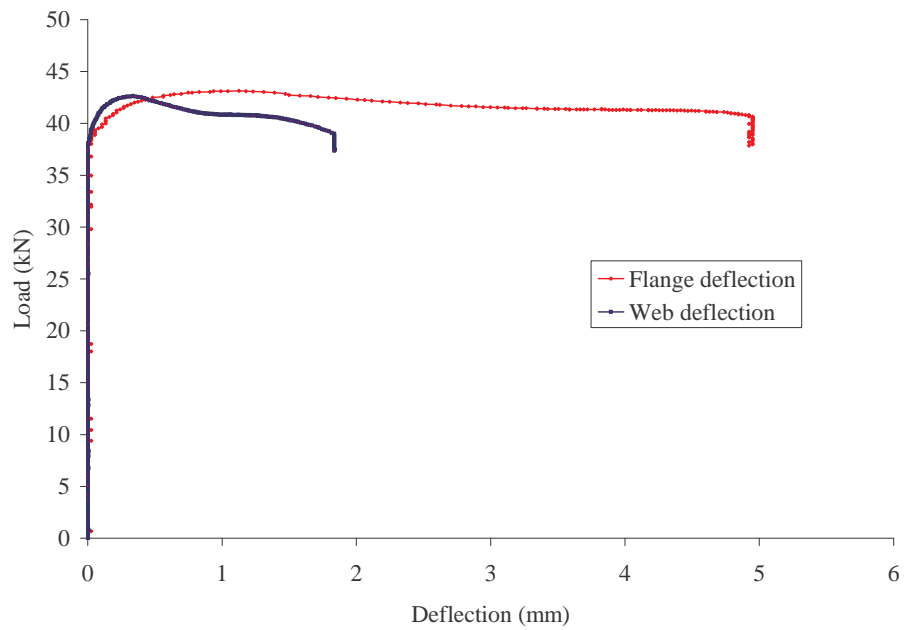
Axial compression load versus out-of-plane deflection

(b) G550 steel

Figure 4.15   Load-Deformation Curves for 0.95 mm Type A Specimen
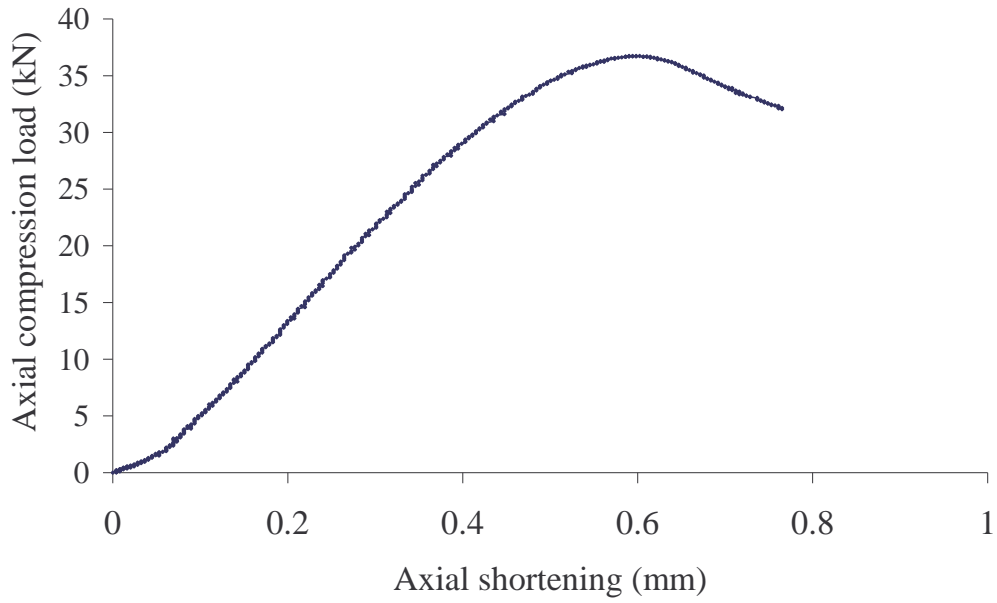
Axial compression load versus axial shortening

Axial compression load versus out-of-plane deflection

(a) G250 steel

Figure 4.16   Load-Deformation Curves for 0.95 mm Type B Specimen

Axial compression load versus axial shortening
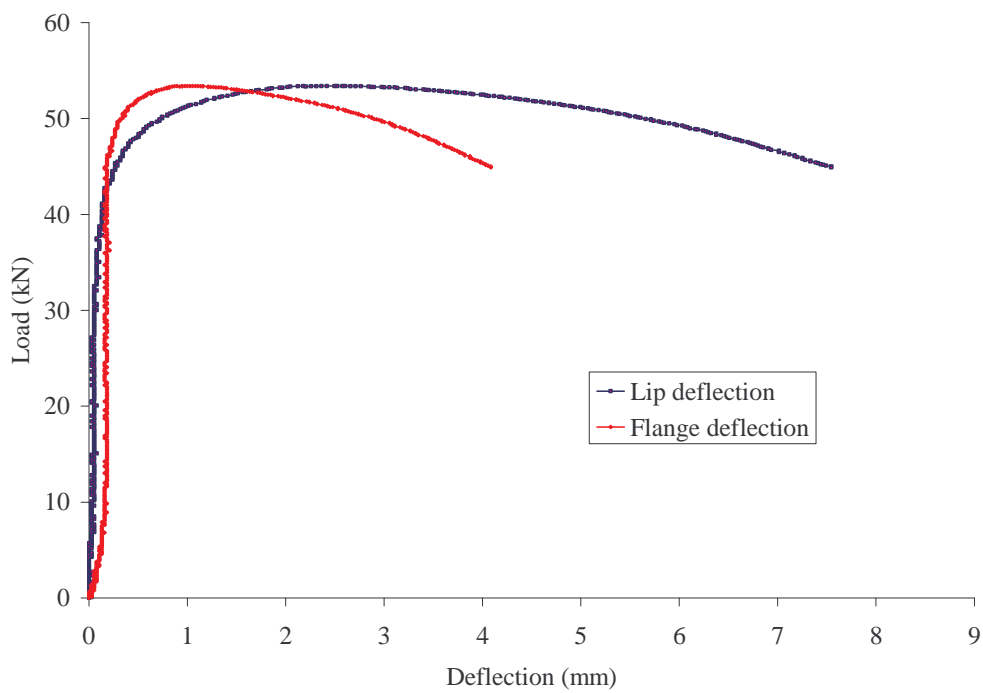
Axial compression load versus out-of-plane deflection

(b) G550 steel

Figure 4.16   Load-Deformation Curves for 0.95 mm Type B Specimen

Unlike in a perfect plate, the deflection begins with the application of the loads for an imperfect plate. Therefore the determination of the elastic buckling load for imperfect plates is not straightforward. Venkataramaiah and Roorda (1982) presented a method as an alternative method (P-δ^2 method) to the Southwell method to determine the elastic local buckling load. According to their method the elastic local buckling load can be determined from the compression load versus out-of-plane deflection[2] curve. As shown in Figure 4.17 the initial post-buckling curve is a parabolic shape for perfect plate and it becomes a straight line when the graph is plotted as load versus deflection[2]. The elastic buckling load is the intersection point of the load axis and the post-buckling curve. The results of the imperfect plate also appear to be similar and hence the tangent line can be drawn towards the load axis as shown in Figure 4.17 and the elastic buckling load can be obtained for the imperfect plate.
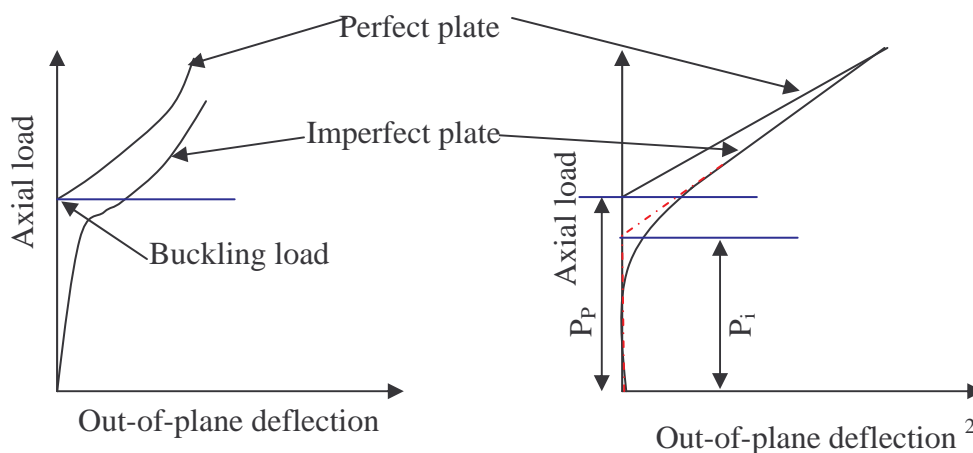
Note: P_P and P_i are the buckling loads of perfect and imperfect plates, respectively

Figure 4.17   Axial Load versus Out-of-Plane Deflection[2] Method from Venkataramaiah and Roorda (1982)

However, Venkataramaiah and Roorda's (1982) method does not refer to the elastic distortional buckling load. Despite this their method was also used to determine the elastic distortional buckling load in this study, so that its accuracy for elastic distortional buckling load can be determined. The elastic distortional buckling load was taken as the intersection point of the two straight lines of the curve as shown in

Figure 4.17. Figure 4.18 shows the compression load versus out-of-plane deflection^2 curves from the test results of this research. The observed and calculated elastic distortional buckling loads are presented in Table 4.6.
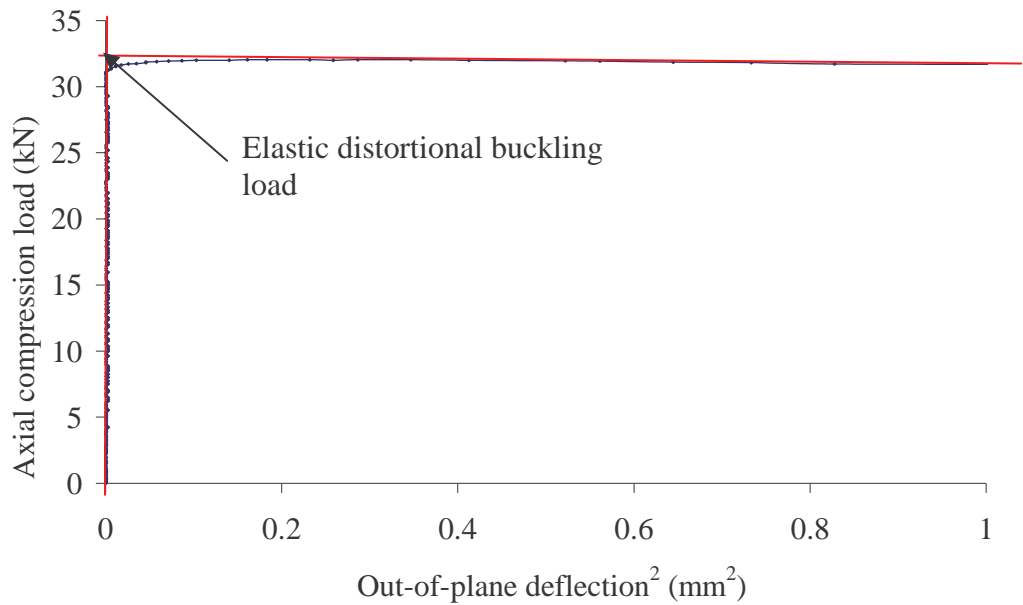
(a) G250 Type A
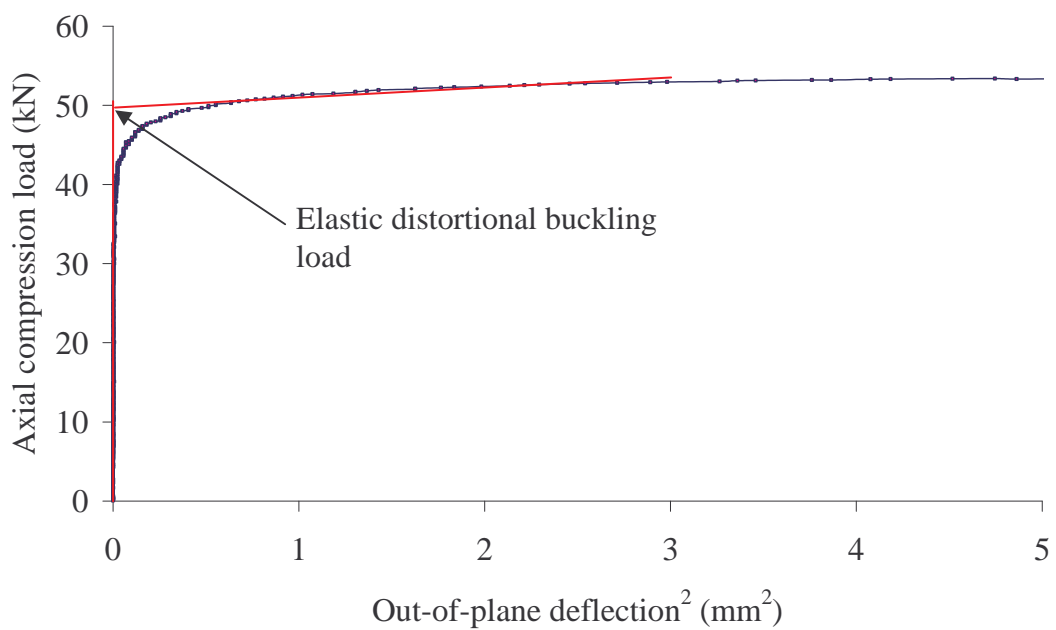
(b) G550 Type B

Figure 4.18   Compression Load versus Out-of-Plane Deflection^2

for 0.95 mm Specimens

Table 4.6   Elastic Buckling and Ultimate Loads at Ambient Temperature

Specimen	P_{E1} (kN)	P_{E2} (kN)	Ultimate Load P_U (kN)				$\dfrac{P_{Uave.}}{P_{E1}}$ (%)	$\dfrac{P_U}{P_{E2}}$ (%)
			P_{U1}	P_{U2}	P_{U3}	$P_{Uave.}$		
G250-0.6-20-A	12.5	13.2	13.2	12.3	13.1	12.8	1.02	0.97
G250-0.8-20-A	18.8	20.0	20.3	19.9	20.8	20.4	1.08	1.02
G250-0.95-20-A	29.9	32.0	32.0	31.4	30.8	31.4	1.05	0.98
G250-0.6-20-B	15.3	15.4	15.1*	16.2		15.7	1.03	1.02
G250-0.8-20-B	23.9	26.5	25.3	26.6		26.0	1.09	0.98
G250-0.95-20-B	31.5	35.0	36.7	38.2		37.5	1.19	1.07
G550-0.6-20-A	18.2	19.0	19.7	19.6		19.7	1.09	1.04
G550-0.8-20-A	30.4	31.0	33.0	29.2		31.1	1.02	1.00
G550-0.95-20-A	41.9	42.0	42.2	42.6	43.8	42.9	1.02	1.02
G550-0.6-20-B	22.7	23.0	23.9*	24.3		24.1	1.06	1.05
G550-0.8-20-B	36.4	38.0	39.1	40.1		39.6	1.09	1.04
G550-0.95-20-B	51.5	50.0	53.8	53.4		53.6	1.04	1.07

Note : P_{E1}- Observed elastic buckling load, P_{E2}- Calculated elastic buckling load from P-δ^2 method, P_{U1}, P_{U2}, P_{U3} and $P_{U,ave}$- Ultimate loads for Test 1, Test 2, Test 3 and the average ultimate load based on repeated tests, respectively. The sign * indicates the columns which showed some local buckling effects.

The post-buckling capacities of these members were determined as the ratio of ultimate load to elastic buckling load for both observed and calculated elastic buckling loads. The elastic distortional buckling load determined using Venkataramaiah and Roorda's (1982) method is higher than the observed elastic buckling load. On the other hand it is much closer to the ultimate load of most of the specimens and higher than the ultimate load of some specimens. There are four reasons for this:

1. The observed elastic buckling load from the test is not accurate since it depends on the observer's judgment

2. The Venkataramaiah and Roorda's method cannot be used to determine the elastic distortional buckling load since it was developed for elastic local buckling

3. Unlike elastic local buckling, the elastic distortional buckling load is higher than the ultimate load or very close to the ultimate load in some cases

4. The calculated elastic distortional buckling load from Venkataramaiah and Roorda's method also depends on the observer's judgement

According to Table 4.6 post-buckling capacity is negligible for distortional buckling failure modes. These results agree with Lau and Hancock's (1988) and Schafer and Pekoz's (1998) observations. But only the C-section and the C-section with additional lips were considered in this experimental investigation. The post-buckling capacity can depend upon the section type, thickness, steel grade and imperfections of the sections. The influence of imperfections on the post-buckling capacity will be discussed using finite element analysis in Chapter 5.

4.1.2.4   Specimen behaviour and failure mode

In the tests the flanges began to buckle by deflecting out-of-plane first at column mid-height when the load reached around 90% of ultimate strength. This was soon followed by rapid flange deformations until the specimen reached the ultimate load (see Figure 4.14). But 0.6 mm lipped channel sections with additional lips showed some local buckling effects in addition to distortional buckling. However, all the specimens failed by distortional buckling mode. All of them only had one half wave buckling. Figures 4.15 and 4.16 (b) clearly show that only flange deformation occurred initially whereas web deformation occured only after the specimen reached its ultimate load. For Type B section both flanges and lips deflected simultaneously.

Generally two different distortional buckling modes occurred at ambient temperature: both flanges moved inward or outward (see Figure 4.19). The different modes were observed with respect to the steel grade, thickness and the cross section of the specimens. However, it was found that the failure mode depended upon the initial geometric imperfections of the cross section rather than the steel grade,

thickness or cross section of the specimen. Further it was observed that the two types of failure modes occurred in the same cross section with the same steel grade and thickness when the tests were repeated. Further investigations of these failure modes are presented in Chapter 5.

(a) Both flanges moving outwards

(b) Both flanges moving inwards

Figure 4.19   Distortional Failure Modes at Ambient Temperature

4.2   Distortional Buckling of Cold-formed Steel Compression Members at Elevated Temperatures

Structural behaviour under fire conditions is an important area of research. Considerable research and development have been undertaken all around the world since fire safety is a major issue in the construction industry. However, the relatively new distortional buckling behaviour of cold-formed steel members at elevated temperatures is not well understood even though the significance of fire safety design is increasingly being recognised due to large losses of life and property. Therefore, experimental studies on the distortional buckling behaviour of light gauge

cold-formed steel members subject to uniform axial compression at elevated temperatures were undertaken in this research project.

A series of experiments was undertaken to investigate the distortional buckling behaviour at elevated temperatures by considering two different sections. Both low and high strength steel members were used to study the effect of steel grade at higher temperatures. It is well known that the mechanical properties of steel have a significant influence on the ultimate load. On the other hand mechanical properties deteriorate at elevated temperatures. Therefore mechanical properties of light gauge cold-formed steel were determined for both low and high strength grade steels at various temperatures as described in Chapter 3.

4.2.1   Experimental Study

The experimental study was carried out to determine the behaviour of light gauge cold-formed steel compression members which were subjected to distortional buckling effects at elevated temperatures. Suitable light gauge cold-formed steel cross sections were determined based on the finite strip analysis program Thin-wall and finite element analysis program ABAQUS as for the ambient temperature test design. The reduced mechanical properties were used to determine suitable cross sections from the above mentioned analysis methods.   As for the ambient temperature tests, both low and high strength grade steels with two different cross sections and three different thicknesses were also used here.

4.2.1.1   Test specimen

The required cross sections were obtained based on the buckling stress plots from Thin-wall program as shown in Figure 4.20. Two minimum points were observed for all the cross sections as presented in Figure 4.20. The first minimum point is for local buckling while the second minimum point is for distortional buckling. Significant differences were maintained at all times between these two minimum points to design the sections for pure distortional buckling. The elastic distortional

buckling strength was kept much less than the elastic local buckling strength so that the specimen failed only in the distortional buckling mode. The chosen section types and their nominal dimensions were the same as for ambient temperature and are shown in Figure 4.21 and Table 4.1.
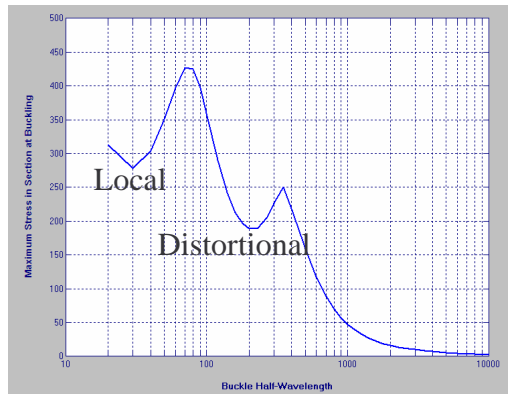
(a) 0.6 mm thickness Type A at 200°C
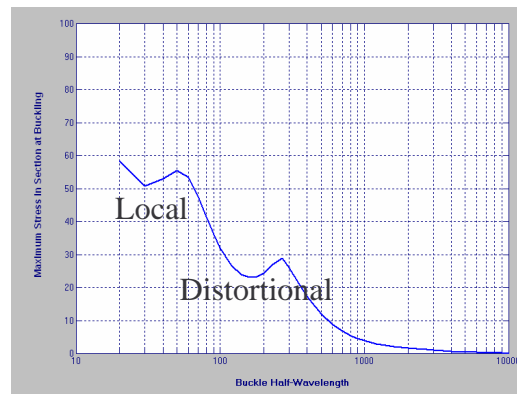
(b) 0.6 mm thickness Type A at 800°C
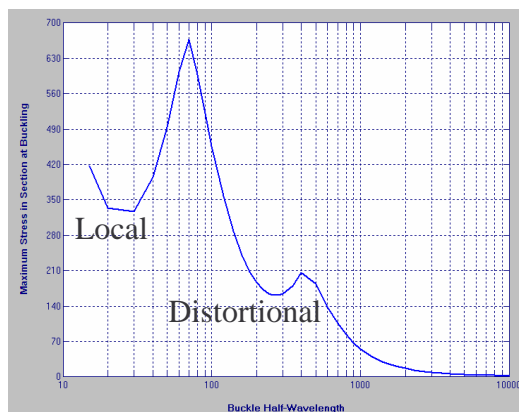
(c) 0.6 mm thickness Type B at 200°C
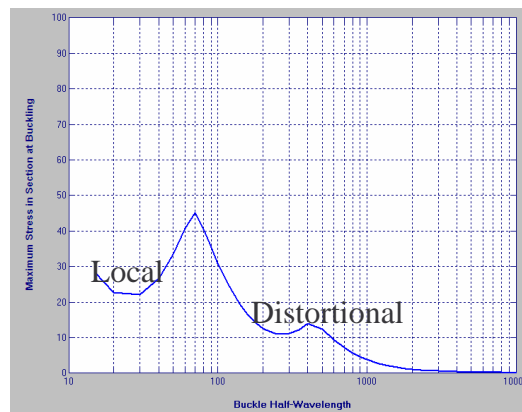
(c) 0.6 mm thickness Type B at 800°C

Figure 4.20   Buckling Plots from Thin-wall Program

All the column lengths were decided based on the buckling half wave length. If the column lengths were decided as multiples of the half wave length, the columns may buckle because of global buckling or an interaction of global and distortional buckling modes rather than pure distortional buckling mode. The aim of this study was to investigate the pure distortional buckling behaviour at elevated temperatures. On the other hand column length had to be restricted to below 600 mm since the available furnace height is around 600 mm. However, 5 mm additional length was

provided for both ends of the specimen to fix it properly to the end plates as described in the ambient temperature test design. The specimens were C-sections with and without additional lips made of G550 and G250 steels with the same cross sectional dimensions and thicknesses as used for ambient temperature tests (see Figure 4.21). More than 120 tests were carried out including the tests at five different temperatures. Some tests were repeated two times while some of them were repeated three times depending on the similarity of the results.

Type A   Type B

Figure 4.21   Designed Sections for Experiments at Elevated Temperatures

4.2.1.2   Test set-up and method

A specially designed electrical furnace which is now available in the QUT structural laboratory was used to simulate fire conditions in the experiments (see Figure 4.22). Temperature in the furnace was controlled by a microcomputer based temperature indicating system, and the rate of temperature increase was adjustable. Four glow bars were used to heat the furnace electrically at a rate of 10 to 20°C/min. The glow bars were placed in the furnace to ensure evenly distributed heat throughout the furnace. A small hole on the front door of the furnace was used to observe the buckling behaviour of the specimen during testing. However, the behaviour of the columns was difficult to observe during the tests due to the darkness inside the furnace. The air temperature inside the furnace was measured by two thermo couples located inside the furnace. An additional portable thermometer was used externally and attached to the specimen to measure the specimen temperature so that the accuracy can be increased. Two shafts were used to fix the specimen and to apply the uniformly distributed load to the specimens. The bottom shaft was fixed and the top shaft can be extended. The maximum temperature of the furnace is 1200°C.
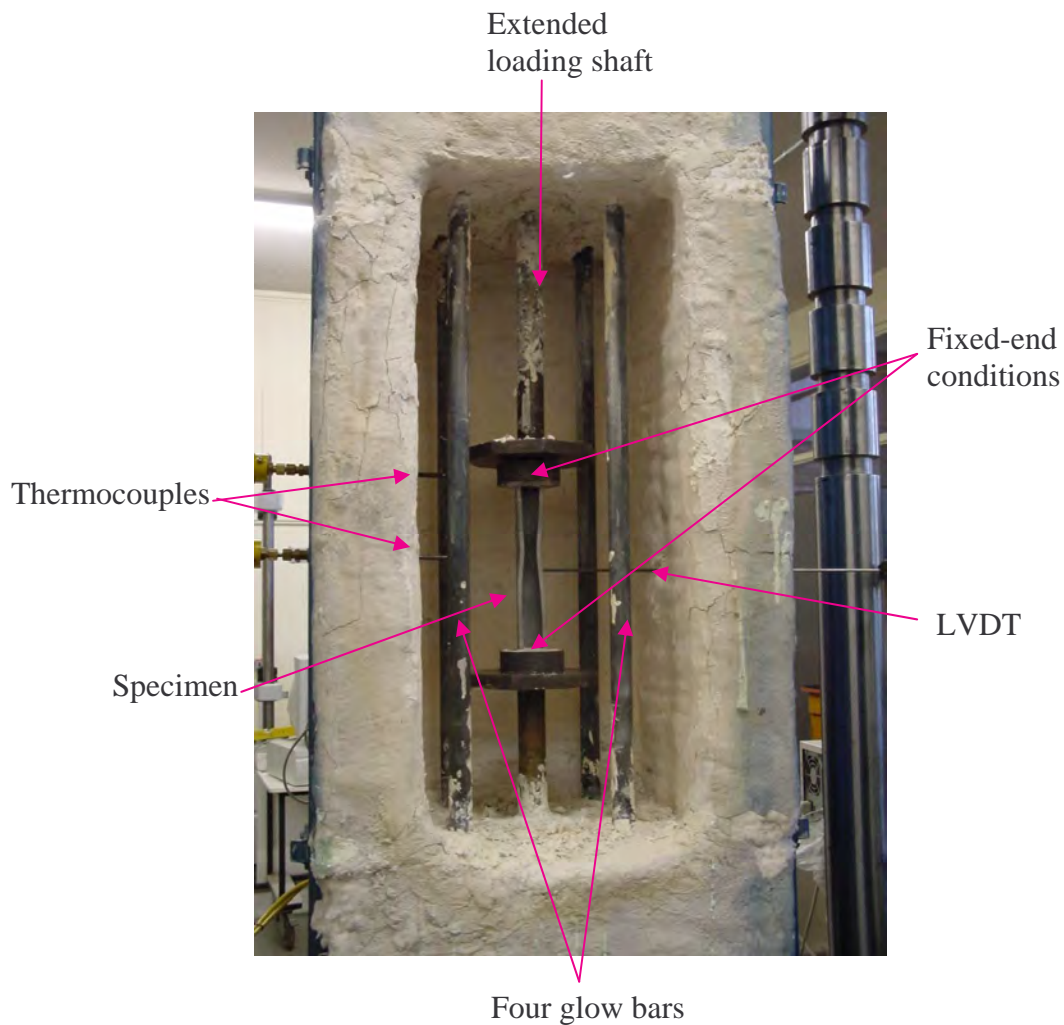
Figure 4.22   Details of the Furnace

All the experiments were undertaken in the steady state condition. The different levels of temperatures were decided prior to testing based on the literature review and the observed mechanical properties at various temperatures. These temperatures were selected to include all the regions of the strength changing with respect to the temperature. The furnace was first heated up to the required temperature. It was then maintained for about 20 minutes so that the specimen also reached the required temperature. The applied load on the specimens due to thermal expansion was carefully observed during the heating process and the specimen was allowed to freely expand when the temperature was increased. An automatic temperature controller was used to ensure the upper limit of the temperature and to control the increasing rate of temperature.

Although the steady state test method was used in the experiments, it is not the same as the real fire. The creep effect is one of the major issues in real fire conditions. In a real fire the temperature is increased while maintaining the same applied load. The transient state test method is generally considered to be close to the real fire condition. Therefore the difference between steady state and transient state tests was studied first. It was observed that the steady state condition also gives the same results as transient state test method based on the available literatures (Lee, 2004).

The following factors show that the steady state test method is suitable for investigating column failure behaviour under fire conditions which are the same as in the transient state test method.

Lee (2004) conducted compression tests using both steady state and transient state test methods. They used different types of cross sections in their tests. Two test series were carried out and the results showed that the difference between the transient sate and steady state test methods is negligible. In addition the difference between the ultimate strengths obtained from these two methods was quite small. Further they mentioned that the accurate ultimate strength was difficult to determine from the transient state test method due to limited loading rates in the test procedure since the initial loading rates and the final loading rates are not the same. This problem occurred due to the thermal expansion of the specimen at high temperatures. As mentioned in Chapter 3, Outinen's (1999) tensile test results showed that the difference between the steady state and transient state test methods was very small.

According to Callister (2000) a typical creep test is conducted at elevated temperatures under constant temperature and constant load conditions since creep is time dependent. A steady state test is carried out by keeping temperature constant while a transient state test is carried out by keeping load constant. However, it is not known whether temperature or applied load is more critical. Therefore it is not possible to specify which method best simulates the creep behaviour.

The duration of the experiment for both the steady state and the transient state test methods was approximately one hour long. Therefore the duration of steel members

exposed to fire may only have a negligible effect on creep. Although there are some effects of creep for both these test methods, that effect can be considered to be negligible.

On the other hand, fire started in one position in buildings or any other structures and moves to other rooms and floors. In this situation one side of the structure is affected by fire first and then the heat is transferred to the other side. As an example, one side of the column and wall will be first affected by the fire and then the heat will be transferred to the other side. When it happens, the heated side expands rapidly than the other side of the column while increasing the applied load. When one side of the column is expanding, an additional bending moment will be induced on the column. Hence the column will fail due to the combination of compression load and bending moment. But in this research only pure compression action was considered. Therefore any bending action should be avoided while conducting tests and hence the inside of the furnace was heated uniformly. All sides of the specimens were heated uniformly and hence all the columns failed due to the application of a pure compression load.

The temperature range chosen in this study was from ambient temperature to 800ºC at intervals of 150ºC, i.e., 200, 350, 500, 650 and 800ºC. The heating rate was varied from 10 to 20ºC/min. When the temperature reached the pre-selected value, it usually exceeded the pre-selected value by a small margin, but the difference was less than 1% at the higher temperatures of 650 and 800ºC and 5% at lower temperatures of 200 and 350ºC. However, the furnace temperature reached its required temperature quickly. The specimen temperature measured by thermometer and the air temperature measured by thermocouples were observed during the test period. It was noticed that the air temperature measured by the thermocouples and the specimen temperature measured by the thermometer were the same.

The specimens were loaded until they failed while maintaining the pre-selected temperatures after the furnace reached a steady state condition. A 300 kN capacity Tinius Olsen universal testing machine (UTM) was used to apply the axial compression load to the test specimens with fixed-ends. Horizontal displacement was measured at the mid height of Type A specimen to observe the flange

deformation during the test. However, the placing of the LVDT depended upon the column height and available top and bottom rods. Therefore out-of-plane deflection of Type B specimen was measured near the middle of the columns and positions were marked and measured from the bottom of the column. Axial shortening of the specimen was also measured. They were recorded at a rate of twice a second so that accurate load-shortening graphs could be plotted. Load was applied by using displacement control method at a rate of 0.3 mm/min to avoid sudden failures. The overall test set-up is shown in Figure 4.23 while Figure 4.24 shows both types of specimens.
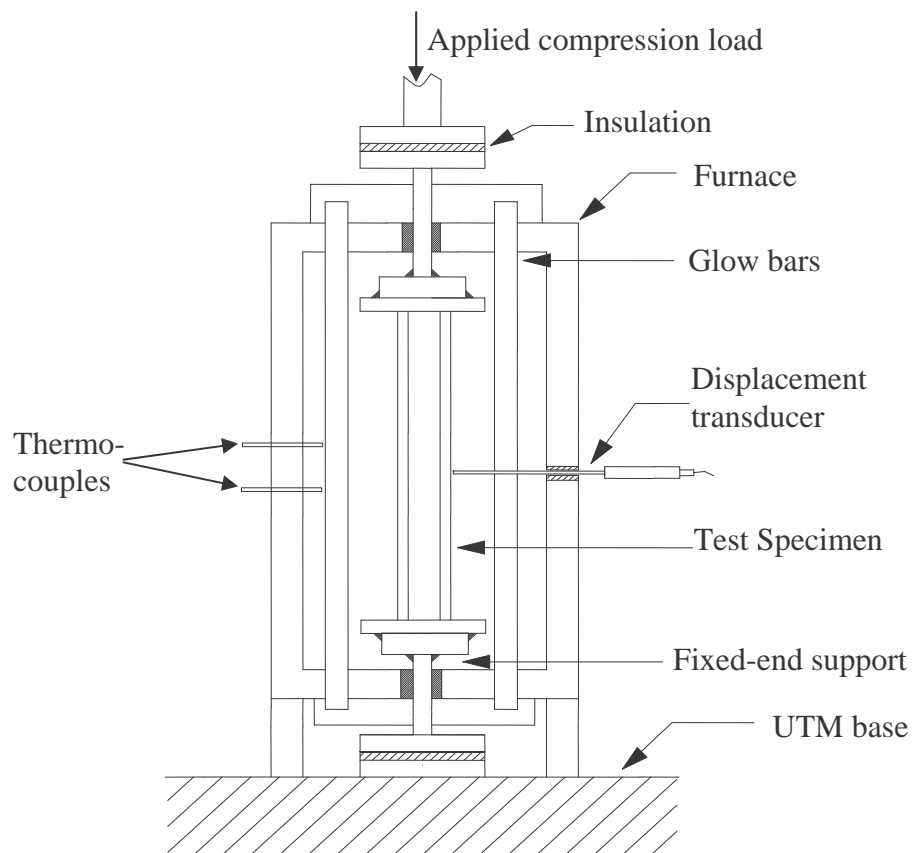
Figure 4.23   Overall Test Set-up for Elevated Temperatures

The overall dimensions of all the specimens were measured prior to the experiments. The total thicknesses and the base metal thicknesses were measured using a micrometer screw gauge and a special coating thickness gauge, respectively. The other dimensions were measured using a vernier calliper. In addition, the corner radii were measured and it was noticed that the measured values were less than the

thickness of the steel. The measured specimen sizes were then used in all the strength calculations. The error bands in the measurements of the independent variables of specimen sizes, applied load and specimen deflections are very small. For example, the error band for load measurement was 0.02% while for specimen deflections and sizes was 0.1%. Therefore the maximum error band for the reported load-deflection data in this chapter can be considered as less than 1 %.

Test set-up   Failure mode

(a) Type A specimen

Test set-up   Failure mode
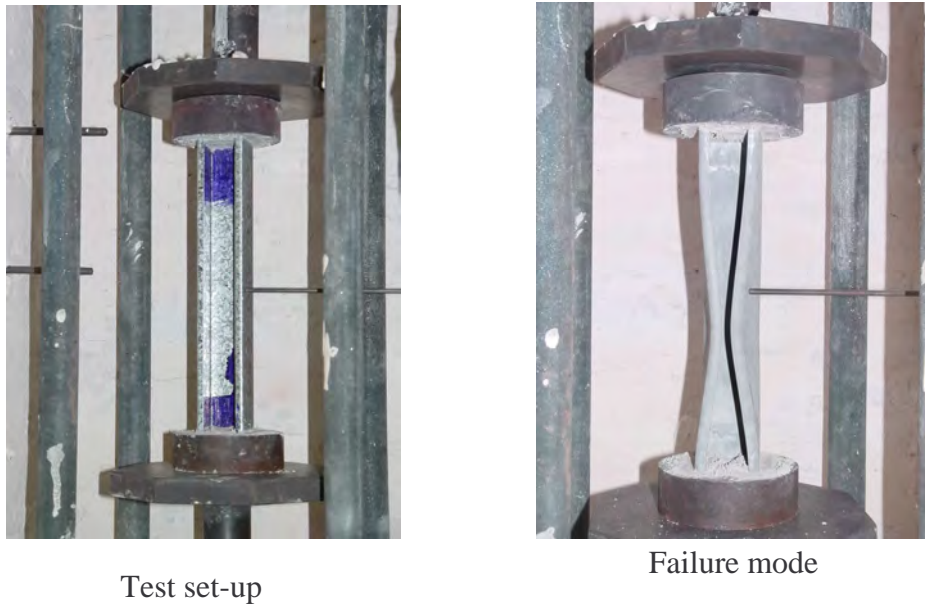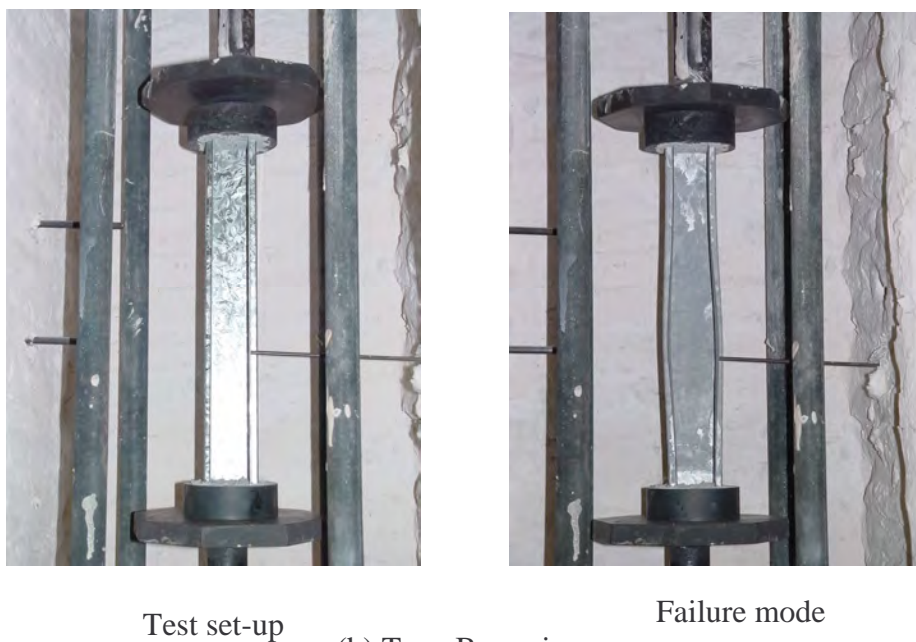
(b) Type B specimen

Figure 4.24   Distortional Buckling Tests at Elevated Temperatures

Table 4.7   Measured Dimensions of Type A Specimens

| Specimen | t (mm) | | h | b (mm) | d (mm) | L |
	TCT	BMT	(mm)			(mm)
G250-0.6-200-A	0.59	0.54	30.71	30.82	5.22	210
G250-0.6-350-A	0.60	0.55	30.74	30.86	5.18	210
G250-0.6-500-A	0.59	0.54	30.72	30.80	5.23	210
G250-0.6-650-A	0.59	0.54	30.69	30.22	5.25	210
G250-0.6-800-A	0.60	0.55	30.72	30.88	5.25	210
G250-0.8-200-A	0.82	0.80	30.96	31.40	5.50	190
G250-0.8-350-A	0.81	0.79	30.92	31.40	5.45	190
G250-0.8-500-A	0.82	0.79	30.84	31.10	5.53	190
G250-0.8-650-A	0.81	0.79	30.82	31.10	5.41	190
G250-0.8-800-A	0.81	0.79	30.91	30.60	5.47	190
G250-0.95-200-A	1.00	0.94	30.95	31.12	5.78	190
G250-0.95-350-A	1.00	0.94	31.00	31.15	5.75	190
G250-0.95-500-A	0.99	0.93	30.94	31.18	5.82	190
G250-0.95-650-A	1.00	0.94	31.00	31.18	5.84	190
G250-0.95-800-A	0.99	0.93	30.99	31.16	5.85	190
G550-0.6-200-A	0.67	0.61	30.88	30.89	5.20	210
G550-0.6-350-A	0.66	0.60	30.86	30.84	5.19	210
G550-0.6-500-A	0.67	0.61	30.81	30.87	5.19	210
G550-0.6-650-A	0.66	0.60	30.85	30.89	5.22	210
G550-0.6-800-A	0.66	0.60	30.78	30.87	5.21	210
G550-0.8-200-A	0.86	0.81	30.86	31.10	5.46	190
G550-0.8-350-A	0.85	0.80	30.92	30.95	5.53	189
G550-0.8-500-A	0.84	0.80	30.86	31.70	5.70	190
G550-0.8-650-A	0.85	0.80	30.80	31.70	5.48	190
G550-0.8-800-A	0.86	0.81	30.87	31.40	5.43	190
G550-0.95-200-A	1.00	0.94	31.42	31.60	5.82	190
G550-0.95-350-A	1.01	0.95	31.45	31.59	5.78	190
G550-0.95-500-A	1.01	0.95	31.40	31.63	5.79	190
G550-0.95-650-A	1.01	0.95	31.45	31.64	5.83	190
G550-0.95-800-A	1.00	0.95	31.55	31.58	5.80	190

Table 4.8   Measured Dimensions of Type B Specimens

Specimen	t (mm)		h (mm)	b (mm)	d (mm)	s (mm)	L (mm)
	TCT	BMT					
G250-0.6-200-B	0.60	0.55	40.61	30.45	5.53	10.10	290
G250-0.6 -350-B	0.60	0.55	40.60	30.46	5.52	10.12	290
G250-0.6-500-B	0.59	0.54	40.59	30.44	5.58	10.11	290
G250-0.6-650-B	0.60	0.55	40.57	30.50	5.55	10.10	290
G250-0.6-800-B	0.59	0.54	40.62	30.48	5.57	10.13	290
G250-0.8-200-B	0.82	0.80	41.80	30.83	5.64	9.03	250
G250-0.8-350-B	0.82	0.79	41.83	30.87	5.65	9.08	250
G250-0.8-500-B	0.82	0.79	41.81	30.86	5.68	9.06	250
G250-0.8-650-B	0.81	0.79	41.82	30.81	5.65	9.04	250
G250-0.8-800-B	0.82	0.79	41.81	30.85	5.67	9.07	250
G250-0.95-200-B	0.99	0.93	38.55	30.05	6.09	9.31	230
G250-0.95-350-B	1.00	0.94	38.54	30.04	6.05	9.29	230
G250-0.95-500-B	0.99	0.93	38.55	30.02	6.08	9.25	230
G250-0.95-650-B	0.99	0.93	38.56	30.03	6.08	9.27	230
G250-0.95-800-B	1.00	0.94	38.51	30.05	6.04	9.30	230
G550-0.6-200-B	0.67	0.61	40.69	30.49	5.61	9.64	290
G550-0.6-350-B	0.66	0.60	40.63	30.48	5.59	9.69	290
G550-0.6-500-B	0.66	0.60	40.67	30.46	5.60	9.67	290
G550-0.6-650-B	0.67	0.61	40.68	30.42	5.62	9.69	290
G550-0.6-800-B	0.66	0.60	40.65	30.46	5.63	9.70	290
G550-0.8-200-B	0.85	0.80	41.90	30.87	6.07	9.43	250
G550-0.8-350-B	0.84	0.80	41.89	30.89	6.03	9.43	250
G550-0.8-500-B	0.84	0.80	41.94	30.91	6.05	9.40	250
G550-0.8-650-B	0.86	0.81	41.93	30.85	6.07	9.40	250
G550-0.8-800-B	0.85	0.81	41.88	30.91	6.05	9.41	250
G550-0.95-200-B	1.01	0.95	38.55	30.04	6.16	9.78	230
G550-0.95-350-B	1.00	0.94	38.57	30.04	6.14	9.78	230
G550-0.95-500-B	1.00	0.95	38.55	30.02	6.15	9.73	230
G550-0.95-650-B	1.01	0.95	38.54	30.02	6.15	9.72	230
G550-0.95-800-B	1.00	0.94	38.56	30.05	6.14	9.78	230

BMT and TCT refer to base metal thickness and total coating thickness, respectively.

Geometric imperfections of the specimens were measured before the test since they are required for finite element analyses to verify their accuracy. Major variables in this study were temperature T, steel thickness t and the steel grade. The average measured values from three test specimens are shown in Tables 4.7 and 4.8. The specimens were labelled prior to tests as shown in these tables (see also Section 4.1.2.1 for more details of the labelling method used).

4.2.2   Test Results

Unlike for the ambient temperature tests, the specimen behaviour cannot be observed during the elevated temperature tests since all the experiments were carried out inside the furnace. Therefore the elastic buckling failure load was not noticeable and only the ultimate failure mode and load were observed in the elevated temperature tests.

The ultimate load of compression members at elevated temperatures was directly obtained from the data recorded by the universal testing machine. However, the elastic distortional buckling load could not be observed while the test was progressing and it was difficult to determine this load from the universal testing machine records. The axial compression load versus axial shortening and out-of-plane deflections plots were used to determine the elastic distortional buckling load. If the test columns were perfect, the elastic distortional buckling load could be read from the load versus out-of-plane deflection graphs directly. However, the test columns had some imperfections and also some residual stresses. Therefore the elastic distortional buckling load could not be observed from the above mentioned graph and instead the load versus out-of-plane deflection^2 graph was used as in Section 4.1.

Typical axial compression load versus axial shortening and out-of-plane deflection graphs were plotted for both Type A and B sections as shown in Figures 4.25 and 4.26, respectively. Other curves are given in Appendix B. In addition the load versus out-of-plane deflection^2 graphs were plotted as shown in Figures 4.27 and 4.28 using Venkataramaiah and Roorda's (1982) method to calculate the elastic distortional

buckling load for Type A and B specimens, respectively. However, their method was developed only at ambient temperature and for local buckling failure mode. But in this research their method was used to calculate the elastic distortional buckling load at an elevated temperature. However, the accuracy of Venkataramaiah and Roorda's (1982) method was not known at elevated temperatures under distortional buckling failure modes. Therefore it was further investigated using finite element analyses as presented in Chapter 5.
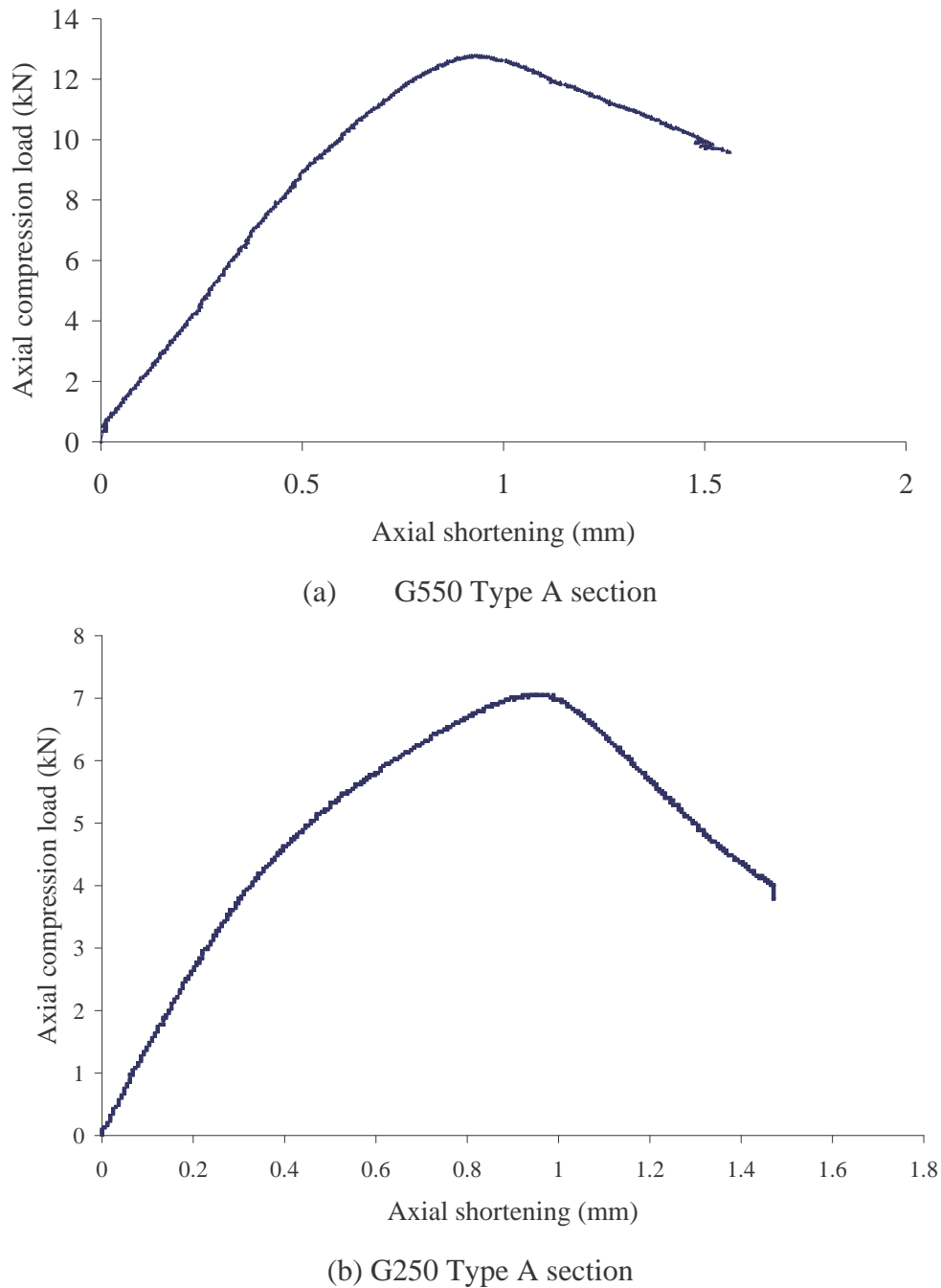
(a) G550 Type A section

(b) G250 Type A section

Figure 4.25 Typical Axial Compression Load versus Axial Shortening Curves of 0.8 mm Specimen at 500ºC
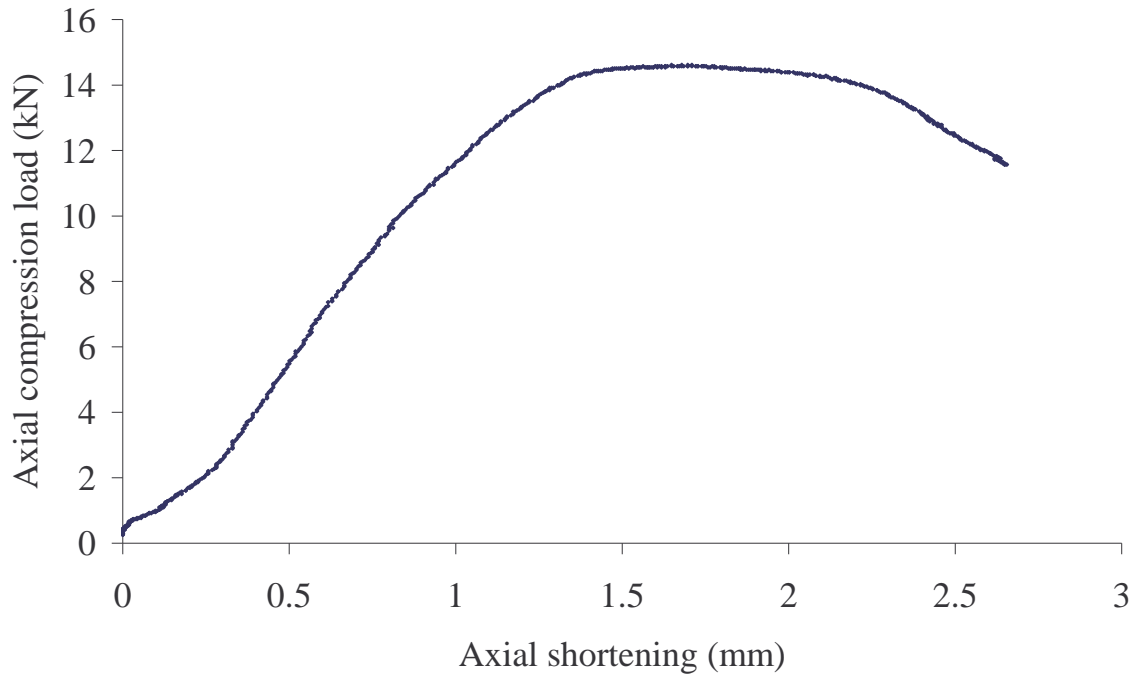
(c)   G550 Type B section

(d) G250 Type B section

Figure 4.25   Typical Axial Compression Load versus Axial Shortening Curves of 0.8 mm Specimen at 500°C

(a)   G550 Type A section
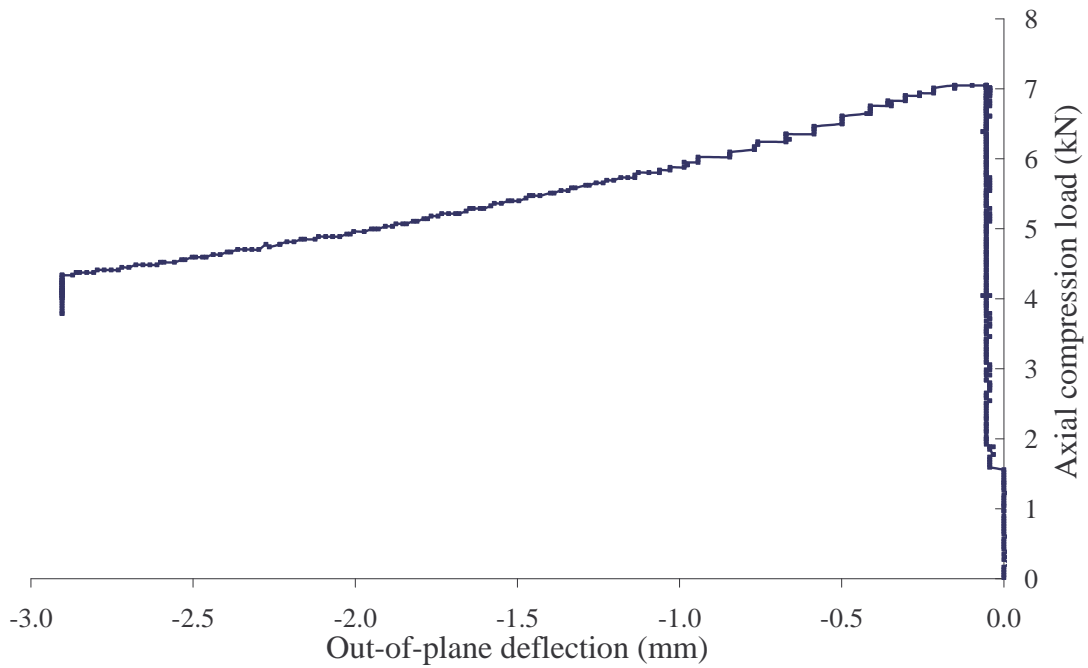
(b)   G250 Type A section

Figure 4.26   Typical Axial Compression Load versus Out-of-Plane Deflection Curves of 0.8 mm Specimen at 500°C
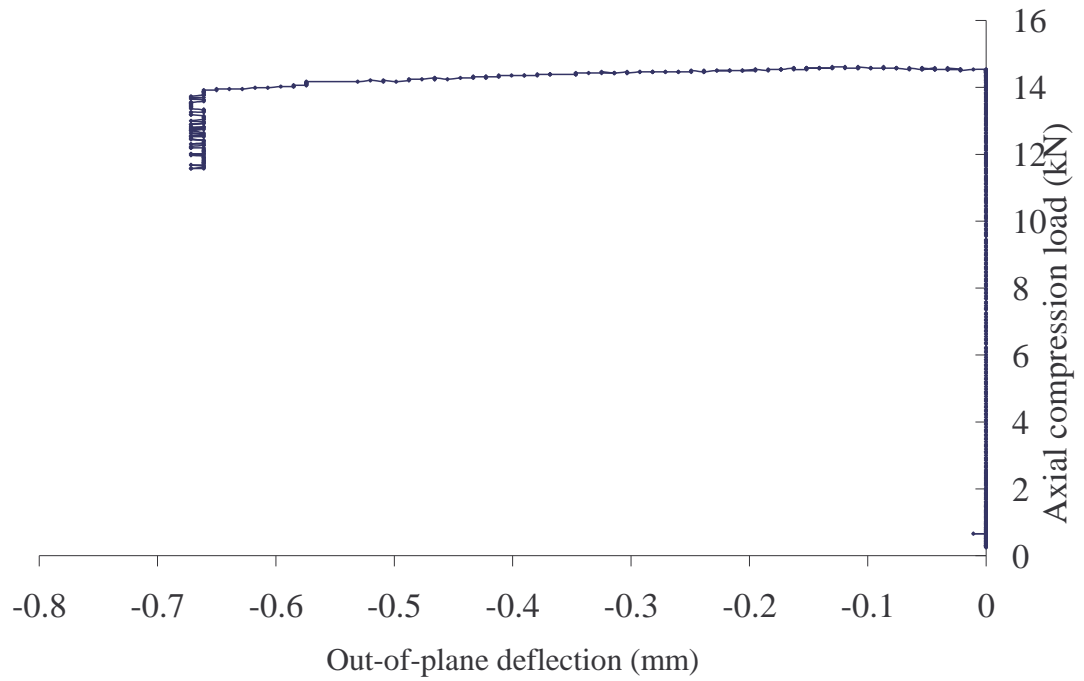
(c)   G550 Type B section
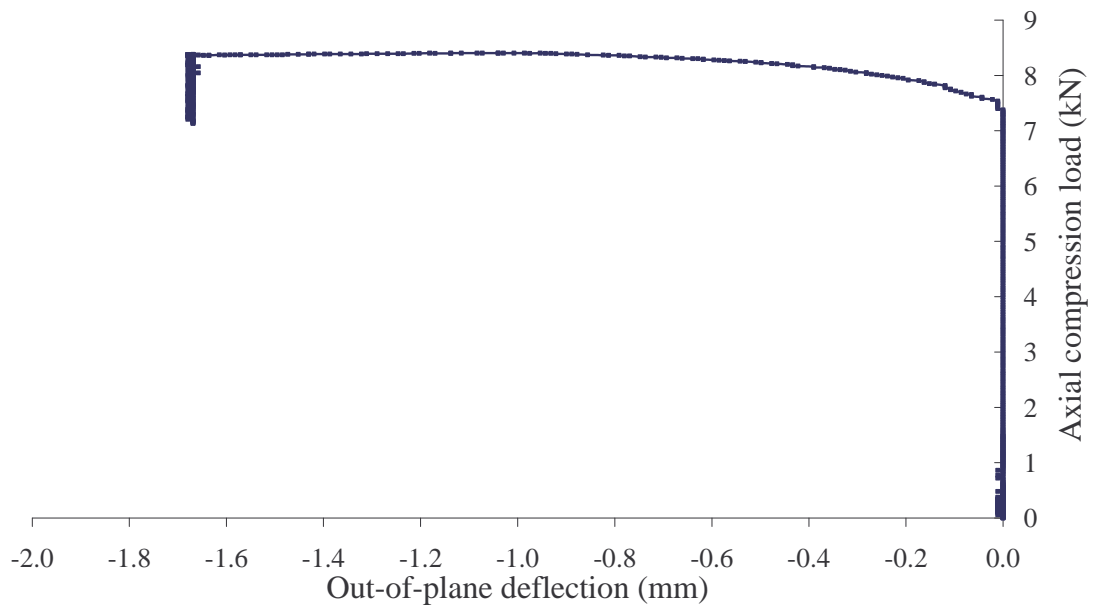
(d)   G250 Type B section

Figure 4.26   Typical Axial Compression Load versus Out-of-Plane Deflection Curves of 0.8 mm Specimen at 500ºC
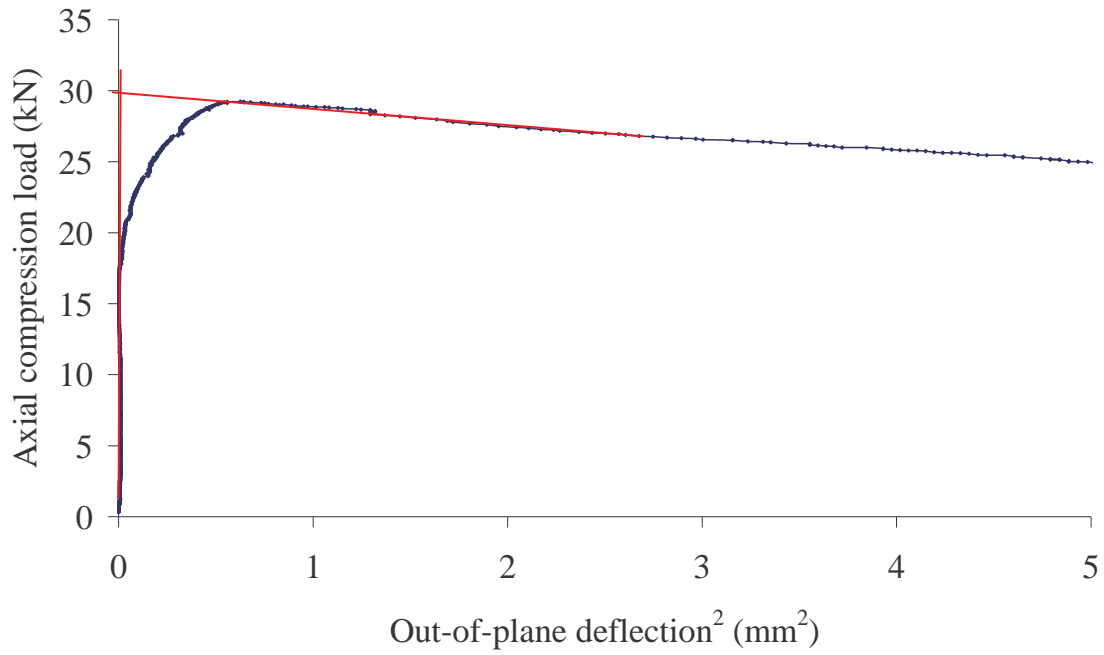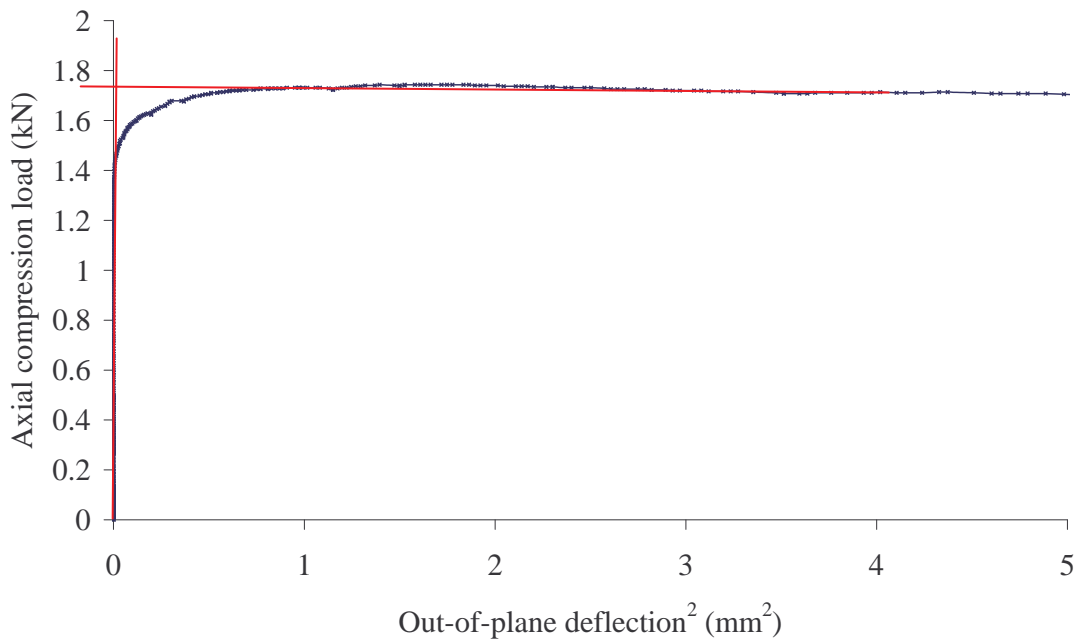
(a)   G550-0.8-200-A

(b)   G550-0.8-800-A

Figure 4. 27   Typical Axial Compression Load versus Out-of-Plane Deflection^2 Curves of Type A G550 Specimens at Different Temperatures
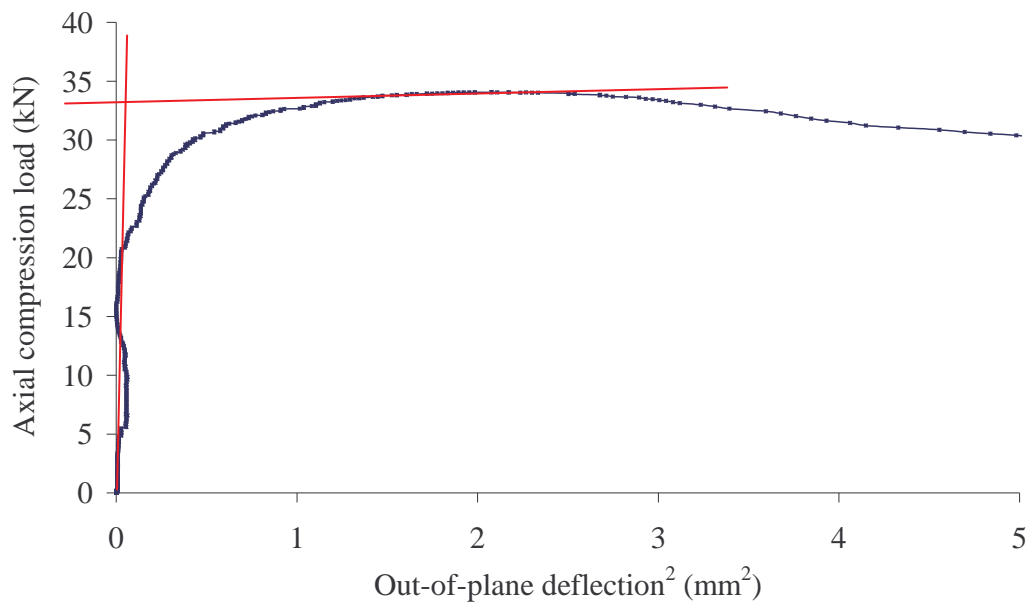
(a)   G550-0.8-200-B
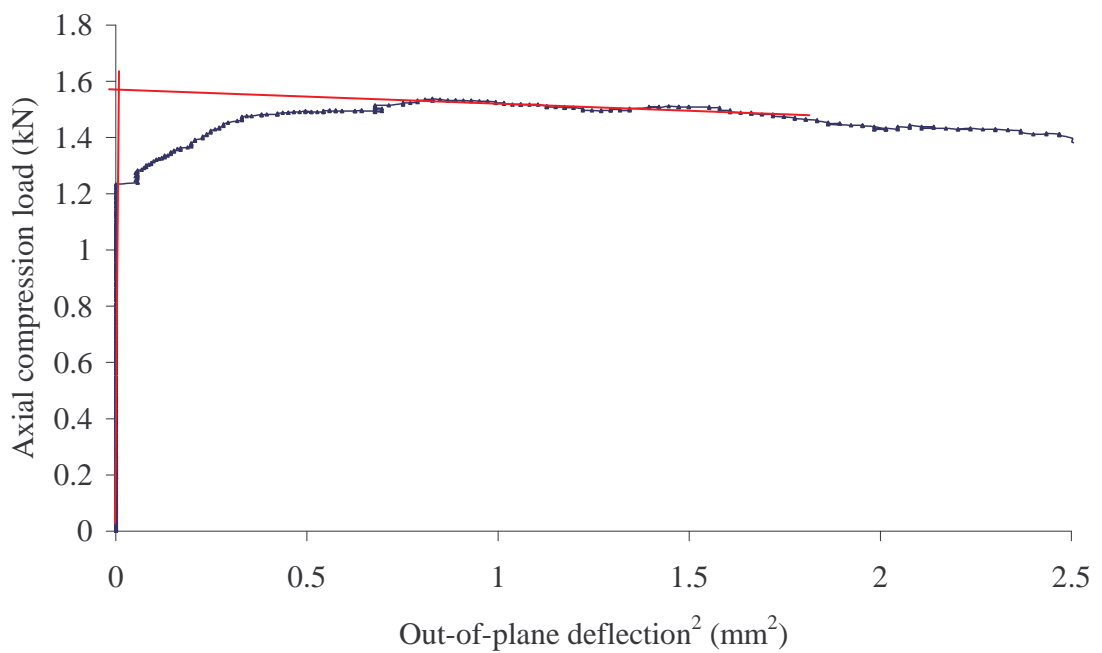
(b)   G550-0.8-800-B

Figure 4.28   Typical Axial Compression Load versus Out-of-Plane Deflection^2 Curves of Type B G550 Specimens at Different Temperatures

Table 4.9   Elastic Buckling and Ultimate Loads of Type A Specimens at Elevated Temperatures

Specimen	P_{E2} (kN)	Ultimate Load (kN)				$\dfrac{P_{E2}}{P_U}$
		P_{U1}	P_{U2}	P_{U3}	$P_{Uave.}$	
G250-0.6-200-A	9.25	9.70	8.83	9.38	9.30	0.99
G250-0.6-350-A	5.85	5.60	6.17		5.89	0.99
G250-0.6-500-A	3.75	3.84	3.81		3.83	0.98
G250-0.6-650-A	1.85	1.88	1.94		1.91	0.97
G250-0.6-800-A	0.62	0.62	0.61		0.61	1.02
G250-0.8-200-A	17.50	17.72	16.92	17.20	17.28	1.01
G250-0.8-350-A	10.25	10.64	10.53	9.54	10.23	1.00
G250-0.8-500-A	7.05	7.04	7.26	7.05	7.12	0.99
G250-0.8-650-A	3.28	3.20	3.17		3.18	1.03
G250-0.8-800-A	1.36	1.32	1.40		1.36	1.00
G250-0.95-200-A	25.04	24.65	25.63	25.23	25.17	0.99
G250-0.95-350-A	17.98	16.90	17.90		17.40	1.03
G250-0.95-500-A	10.32	10.36	10.40	10.39	10.38	0.99
G250-0.95-650-A	4.94	4.91	5.04	5.02	4.99	0.99
G250-0.95-800-A	1.47	1.47	1.46		1.47	1.00
G550-0.6-200-A	14.75	15.05	15.34		15.20	0.97
G550-0.6-350-A	13.65	13.26	13.88		13.57	1.01
G550-0.6-500-A	6.91	7.16	6.73		6.95	0.99
G550-0.6-650-A	2.27	2.54	2.19	2.28	2.34	0.97
G550-0.6-800-A	0.65	0.55	0.72	0.77	0.68	0.96
G550-0.8-200-A	27.73	27.87	26.51		27.19	1.02
G550-0.8-350-A	23.50	24.61	23.55	23.07	23.74	0.99
G550-0.8-500-A	12.95	13.22	12.71	12.78	12.90	1.00
G550-0.8-650-A	4.32	4.24	4.25		4.24	1.02
G550-0.8-800-A	1.72	1.71	1.74		1.73	0.99
G550-0.95-200-A	37.67	35.27	38.42	38.96	37.55	1.00
G550-0.95-350-A	31.20	32.52	29.30	31.59	31.14	1.00
G550-0.95-500-A	18.50	19.41	19.63		19.52	0.95
G550-0.95-650-A	4.50	4.42	4.41	4.72	4.52	1.00
G550-0.95-800-A	1.78	1.84	1.77		1.80	0.99

Table 4.10   Elastic Buckling and Ultimate Loads of Type B Specimens at Elevated Temperatures

Specimen	P_{E2} (kN)	Ultimate Load (kN)				$\dfrac{P_{E2}}{P_U}$
		P_{U1}	P_{U2}	P_{U3}	$P_{Uave.}$	
G250-0.6-200-B	14.75	14.54	14.72	15.04	14.77	1.00
G250-0.6-350-B	8.75	9.30	8.94		9.12	0.96
G250-0.6-500-B	5.85	5.63	6.11		5.87	1.00
G250-0.6-650-B	2.40	2.51	2.44		2.48	0.96
G250-0.6-800-B	0.84	0.89	0.83		0.86	0.98
G250-0.8-200-B	22.96	22.12	24.02		23.07	1.00
G250-0.8-350-B	14.40	14.21	14.79		14.50	1.00
G250-0.8-500-B	8.40	8.51	8.40		8.46	1.00
G250-0.8-650-B	3.85	4.08	4.08		4.08	0.95
G250-0.8-800-B	1.43	1.46	1.41		1.43	1.00
G250-0.95-200-B	28.31	29.15	27.65		28.40	1.00
G250-0.95-350-B	19.02	19.52	19.81		19.67	0.97
G250-0.95-500-B	11.38	12.12	11.35		11.74	0.97
G250-0.95-650-B	5.10	5.40	5.33		5.36	0.96
G250-0.95-800-B	1.90	1.97	1.92		1.94	0.98
G550-0.6-200-B	20.10	19.41	21.17	22.05	20.87	0.97
G550-0.6-350-B	18.50	18.20	19.23		18.71	0.99
G550-0.6-500-B	10.60	10.37	9.73		10.05	1.01
G550-0.6-650-B	3.17	3.25	3.13		3.19	1.00
G550-0.6-800-B	1.00	1.08	1.00		1.04	0.96
G550-0.8-200-B	32.75	34.09	31.75	31.85	32.53	1.01
G550-0.8-350-B	31.00	29.11	27.68		28.40	1.04
G550-0.8-500-B	14.62	14.61	14.76		14.69	1.00
G550-0.8-650-B	4.25	4.28	4.49		4.38	0.97
G550-0.8-800-B	1.50	1.53	1.50		1.51	0.99
G550-0.95-200-B	46.34	46.25	46.95		46.6	1.00
G550-0.95-350-B	38.82	38.34	39.73		39.04	1.00
G550-0.95-500-B	21.50	21.72	22.08		21.90	0.99
G550-0.95-650-B	4.95	4.97	5.06		5.02	0.99
G550-0.95-800-B	1.85	1.93	1.96		1.95	0.95

Note : P_{E2}- Elastic buckling load from P-δ^2 method, P_{U1}, P_{U2}, P_{U3} and P_{Uave}- Ultimate loads from Test 1, Test 2, Test 3 and average ultimate load, respectively.

The ultimate loads obtained directly from tests and the elastic distortional buckling loads obtained based on Venkataramaiah and Roorda's (1982) method are presented in Tables 4.9 and 4.10, respectively. The elastic distortional buckling loads were found to be very close to the ultimate loads. These results are the same as ambient temperature test results. In the ambient temperature tests, the elastic distortional buckling loads were much close to the observed elastic buckling load and ultimate load. Therefore this method seems to be accurate at elevated temperatures. If Venkataramaiah and Roorda's (1982) method can be used at ambient temperature to determine the elastic distortional buckling load, it can also be used at elevated temperatures.

After

Before

Figure 4.29   Test Specimen Before and After Failure

Figure 4.29 shows the specimen before and after failure. Figure 4.29 shows the three different failure modes that were observed: both flanges moving inward, both flanges moving outward and one flange moving inward while the other one moving outward. It was observed that temperature, thickness, steel grade, section types and imperfection can affect the failure modes. Therefore the failure modes were further investigated considering different directions and values of the imperfections and other relevant parameters in Chapter 5. According to the results obtained, the post-buckling capacity in the case of distortional buckling is insignificant.
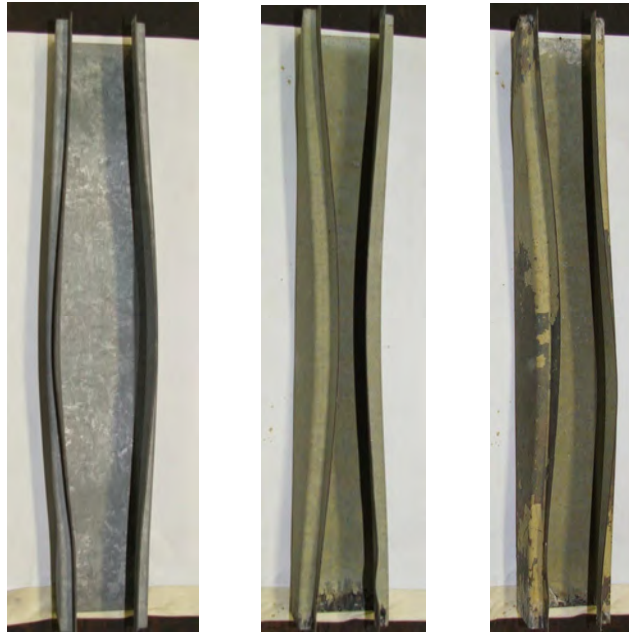
Figure 4.30   Main Buckling Shapes at Elevated Temperatures

4.3   Discussion of Results

4.3.1   Buckling Modes

Two main types of distortional buckling failure modes were observed at ambient temperature while three different types were observed at elevated temperatures. Ambient temperature test results showed that column fails by both flanges moving inwards or outwards. In addition to these two modes, many test columns failed due to one flange moving outward while the other flange moving inward at elevated temperatures (see Figure 4.29). However, the cross sectional dimensions and length of test specimens used at elevated temperatures were the same as those at ambient temperature. The end conditions were fixed for all the specimens. The only difference was the temperature. Therefore it is clear that temperature can affect the failure modes. On the other hand the imperfections can also influence the failure modes of the specimens.

However, the different types of buckling occur mainly because of the thickness, steel grade, section types, temperature and imperfection. The experimental results suggest that imperfections and temperatures have governed the failure mode rather than other parameters. They showed that the failure modes of the three nominally identical columns were different even though the failure loads were about the same. The study of all these parameters is discussed in Chapter 6 under parametric study.

4.3.2   Ductility

It is well known that ductility of the low strength cold-formed steel is higher than that of high strength steel. Tensile coupon test results also prove that the low strength steel shows higher ductility than high strength steel. In this research, ductility of the sections was measured with respect to the distortional buckling behaviour, temperature and the steel grade. Ductility of Type A specimens was measured from the load versus shortening plots as shown in Figure 4.31 for both low and high strength steel sections. It was measured as δ_U/δ_Y (δ_U is the displacement at 85% of the ultimate load on the descending curve while δ_Y is at specimen yield). The yield load was observed as the load at the point where the axial compression versus axial shortening graph changes from its original straightness. This point can vary depending upon the observer's judgement since the curves do not show clear straight lines at the beginning for very high temperatures. To eliminate this shortcoming, an alternative definition of $\delta U^+/ \delta U^-$ can be used, where δU^- is the displacement corresponding to 85% of the ultimate load in the ascending curve while δU^+ is the displacement for the descending curve. Since this approach also gave similar results, the original definition of δ_U/δ_Y was used in this chapter.

Table 4.11 presents the ductility (δ_U/δ_Y) of the sections. According to the results, high strength steel specimens show higher ductility capacity than the low strength specimens although tensile coupon test results show just the opposite. Main reason for this behaviour is that the ductility defined by the tensile coupon test is only the behaviour at material level. But it can change when considering the cross section of a member. The reason is that the low strength steel specimen fails after it passes its

yield capacity although it shows higher ductility. This may be due to the physical opening of the sections since it does not have the same strength as high strength steel. Mistakidis (1999) stated that the ductility obtained from the tensile coupon test gives completely different results when compared with the ductility measured based on actual cross-sections. However, the ductility of the specimens has increased with respect to the temperatures. At 800°C the ductility of the specimens has increased more than three times that at the ambient temperature. However these are approximate values and depend to some extent upon the observer's own judgement.
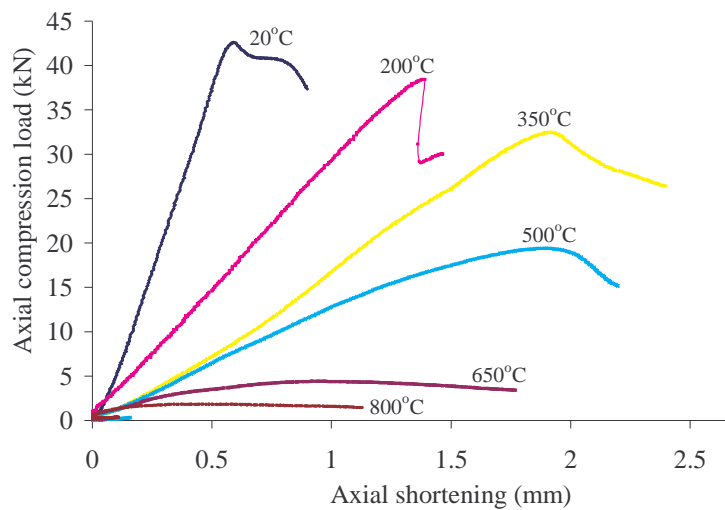
(a) G550 steel
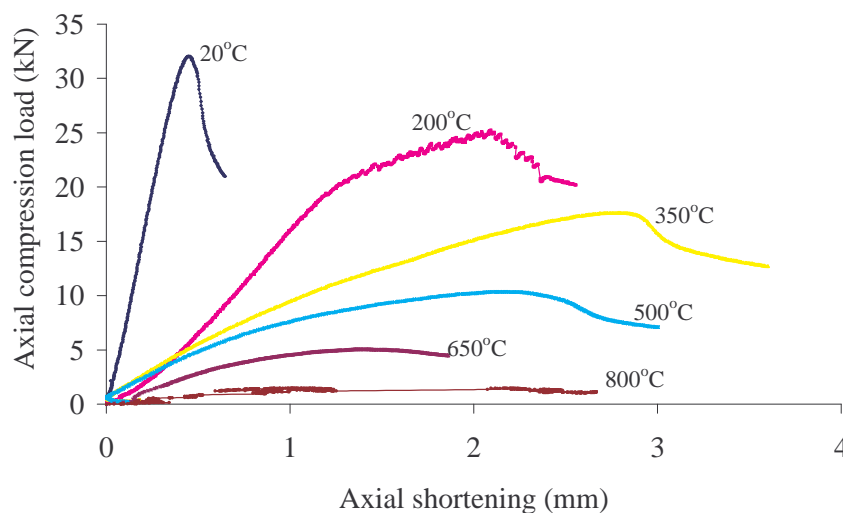
(b) G250 steel

Figure 4.31   Comparison of Buckling Behaviour and Ductility with Respect to the Temperature and the Steel Grade for 0.95 mm Steels

Table 4.11   Ductility of Compression Members Subject to Distortional Buckling Failures at Various Temperatures (δ_U/δ_Y Factor)

Steel grade	Temperature (^{o}C)	Nominal column thickness (mm)		
		0.6	0.8	0.95
G250	20	1.23	1.30	1.34
	200	1.29	1.49	1.69
	350	2.61	2.45	1.90
	500	2.76	3.01	2.71
	650	3.01	3.65	2.80
	800	2.82	4.09	4.78
G550	20	1.64	1.62	1.64
	200	2.52	1.65	1.82
	350	2.99	2.23	1.65
	500	3.06	3.02	1.77
	650	3.19	4.54	3.60
	800	5.40	7.35	6.80

4.3.3   Post-buckling Capacity

Based on Figure 4.32 (AISI, 2004), post-buckling capacity in the case of distortional buckling of compression members mainly depends upon the slenderness of the section. When the slenderness of the section is small, post-buckling capacity does not exist. However, when the slenderness is less than 1 or slightly higher than 1, the specimen fails by distortional buckling mode with higher elastic buckling capacity. In this region elastic buckling curve is higher than the ultimate capacity curve. However when the column slenderness is in the post-buckling regime, the elastic buckling curve is below the ultimate capacity curve. In this region the elastic buckling load is less than the ultimate load. However, when the slenderness of the section is around 1 and 1.5 both elastic buckling load and ultimate load are much close to each other.

Inelastic Regime | Post-Buckling Regime

$\dfrac{P_n}{P_y}$

Distortional buckling
curve (Ultimate capacity)

Elastic buckling curve

$Slendedrness = \sqrt{P_y \Big/ P_{od}}$
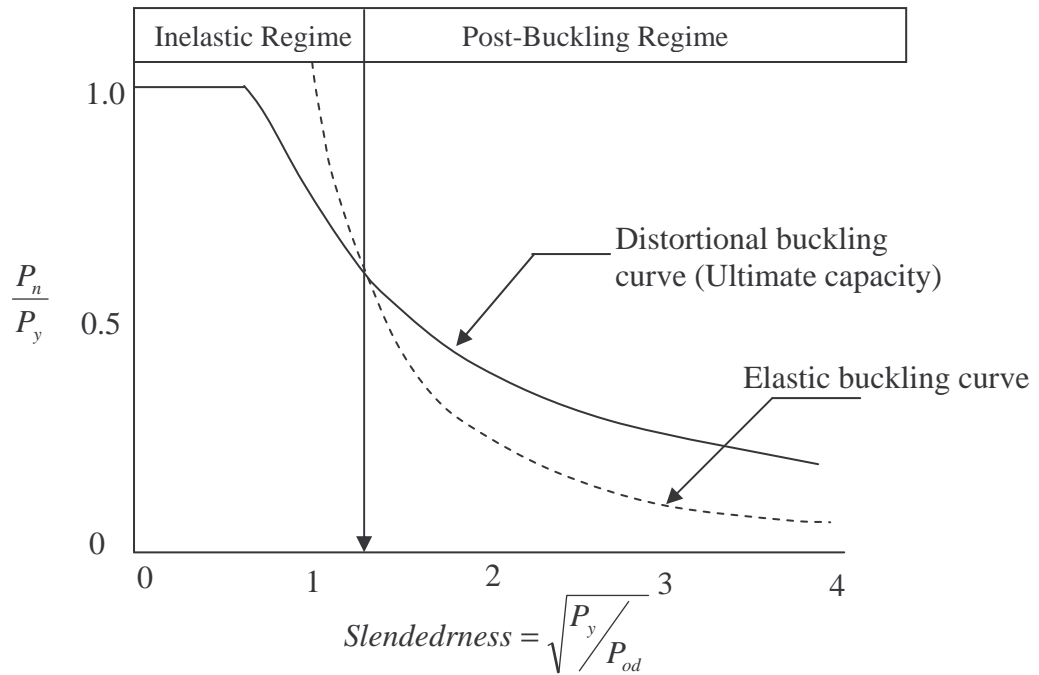
Figure 4.32   Distortional Buckling Behaviour (AISI, 2004)

Sections 4.1 shows that the observed elastic buckling loads, and those determined using Venkataramaiah and Roorda's (1982) method at ambient temperature tests are much closer to the ultimate test load. Further, Section 4.2 shows the calculated elastic buckling load from Venkataramaiah and Roorda's (1982) method at elevated temperature test is also the same as the ultimate test load. According to the above results the sections selected in this research seem to have a slenderness between 1 and 1.5 or in the inelastic regime. However, it is difficult to say about the slenderness of the sections without knowing the theoretical buckling load. As explained earlier in this section, the experimental elastic buckling load depends upon the initial geometric imperfections. However, in both cases the theoretical elastic buckling load can be higher than the experimental elastic buckling load. Further investigation of theoretical and experimental elastic buckling loads will be presented in Chapter 5 under finite element analyses.

4.3.4 Distortional Buckling Behaviour of Low and High Strength Steel Specimens with Respect to Temperature

The ultimate loads of the low and high strength steel specimens were compared under temperatures ranging from ambient temperature to elevated temperatures. As can be seen in Figure 4.33, the ultimate loads decrease with increasing temperatures. However, the strength reduction is not uniform. It was reduced at a lower rate at low temperatures (up to 350°C), but increased at high temperatures (350°C to 650°C). The ultimate load was very small at 800°C. However, it is clear that the steel specimens cannot resist a considerable load after 800°C.
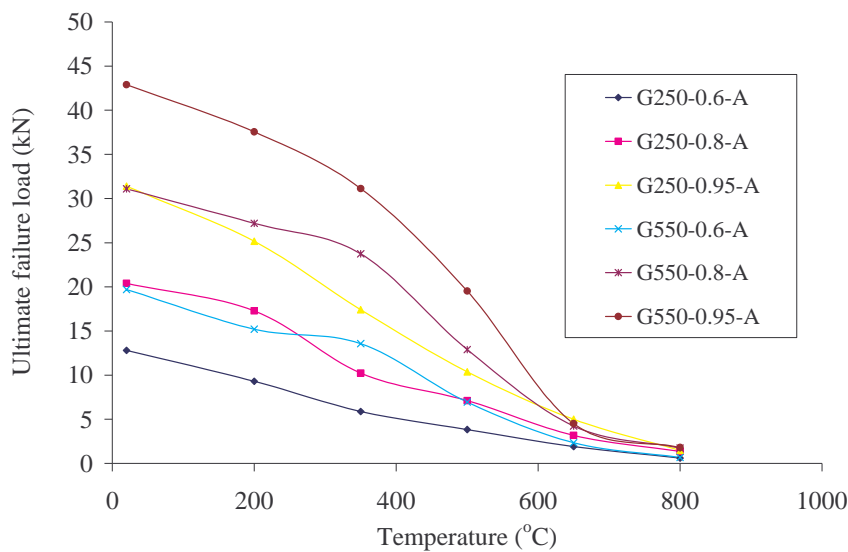
(a) Type A specimens
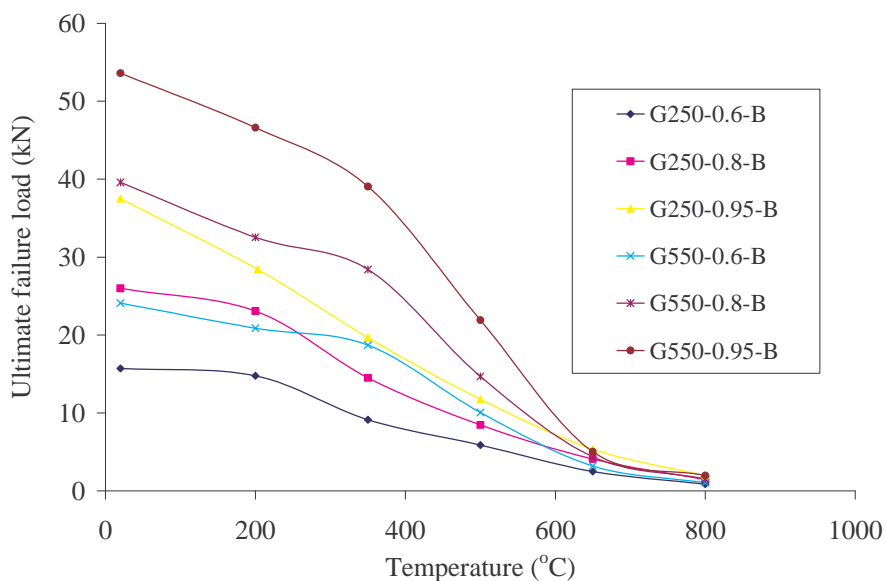
(b) Type B specimens

Figure 4.33   Ultimate Load versus Temperature Curves

The ultimate loads were also compared with respect to the steel grade and the temperature. According to Table 4.12 low and high strength steel columns show a considerable difference in the ultimate load between them at low temperatures. However, when the temperature was increased, the difference of ultimate load between these two steel grades decreased and in some occasions low strength steel columns show higher ultimate load than that of high strength steel columns at very high temperatures. However, this difference is not significant. This may happen due to the softening of both steels. The softening of high strength steel was more than that of low strength steel at very high temperatures and hence the difference between the ultimate loads of low and high strength steel columns is small at very high temperatures. Therefore the use of high strength steel structures at very high temperatures is not economical.

Table 4.12   Comparison of Ultimate Loads of Low and High Strength

Steel Columns

Section Type	Temperature (^{o}C)	P_{u550}/P_{u250}		
		0.6 mm	0.8 mm	0.95 mm
A	20	1.54	1.52	1.37
	200	1.63	1.57	1.49
	350	2.30	2.32	1.79
	500	1.81	1.81	1.88
	650	1.23	1.33	0.91
	800	1.11	1.27	1.22
B	20	1.54	1.52	1.43
	200	1.41	1.41	1.64
	350	2.05	1.96	1.98
	500	1.71	1.74	1.87
	650	1.29	1.07	0.94
	800	1.21	1.06	1.01

4.4 Comparison of Test Results with Predictions from Current Design Equations

4.4.1 Ambient Temperature

4.4.1.1 AS/NZS 4600

The ultimate loads obtained from the tests were compared with the available design equations in the Australian/New Zealand Standard, AS/NZS 4600 (SA, 1996) for cold-formed steel structures. Only AS/NZS 4600 presents the distortional buckling equations among the various design standards. This provides the design equations for distortional buckling of singly-symmetric sections such as lipped channels with additional rear flanges. When singly symmetric sections are subjected to distortional buckling effects, the ultimate load P_n is obtained as follows.

- For $f_{od} > f_y/2$:
$$P_n = Af_n = Af_y \left(1 - \frac{f_y}{4 f_{od}} \right) \qquad (4.1(a))$$

- For $f_y/13 \leq f_{od} \leq f_y/2$:
$$P_n = Af_n = Af_y \left[0.055 \left(\sqrt{\frac{f_y}{f_{od}}} - 3.6 \right)^2 + 0.237 \right] \qquad (4.1(b))$$

where A = Area of the gross cross-section, f_y = Yield strength of steel as discussed in Chapter 3, f_n = Ultimate strength of the specimen. f_{od} = Elastic distortional buckling strength which can be calculated using a finite strip analysis program such as Thin-wall for pin-end conditions and a finite element program ABAQUS for both pinned and fixed end conditions or Appendix D of AS/NZS 4600 for standard sections. In this research f_{od} was obtained from the finite element analysis (ABAQUS) since all the tests were undertaken with fixed-end conditions.

According to AS/NZS 4600 (Clause 1.5.1.5), the yield strengths of 0.6 and 0.8 mm G550 steels should be taken as 90% of the corresponding values or 495 MPa whichever is the lesser when steels do not satisfy Clause 1.5.1.5(a) requirements. The ratio of tensile strength to yield strength should not be less than 1.08 and the

total elongation based on a 50 mm gauge length should not be less than 10% as given in Clause 1.5.1.5(a). The calculated values show that the ratios of tensile strength to yield strength are less than 1.08 and total elongations are less than 10% for 0.6 and 0.8 mm specimens (see Chapter 3). Therefore reduced yield strengths were used in Equation 4.1 to calculate the ultimate load of the 0.6 and 0.8 mm thick G550 steel specimens. Table 4.13 provides the predicted ultimate loads and the average ultimate load from experiments (see Appendix C for an example calculation).

Table 4.13   Comparison of Predicted Ultimate Loads from Equation 4.1 with Test Results at Ambient Temperature

Specimen	Ultimate Load (kN)		Exp. /Predicted	
	Experiment (Average)	Predicted	Actual	Mean/COV
G250-0.6-20-A	12.8	12.37	1.03	1.07/ 0.042
G250-0.8-20-A	20.4	19.08	1.07	
G250-0.95-20-A	31.4	28.11	1.12	
G250-0.6-20-B	15.7	12.76	1.23	1.18/ 0.039
G250-0.8-20-B	26.0	22.57	1.15	
G250-0.95-20-B	37.5	32.60	1.15	
G550-0.6-20-A	19.7	19.02	1.04	1.00/ 0.040
G550-0.8-20-A	31.1	30.70	1.01	
G550-0.95-20-A	42.9	44.55	0.96	
G550-0.6-20-B	24.1	18.89	1.28	1.14/ 0.127
G550-0.8-20-B	39.6	34.15	1.16	
G550-0.95-20-B	53.6	54.09	0.99	

Table 4.13 presents the experimental ultimate load and the predicted ultimate loads from Equations 4.1 (a) and (b) of AS/NZS 4600. The mean values of the ratio between the two loads are 1.07 and 1 for low and high strength steels, respectively while the COV is about 0.04 for Type A specimens. The mean values of Type B specimens are 1.18 and 1.14 for low and high strength steels, respectively while the

COV of low strength steel is 0.127. Therefore it can be concluded that although AS/NZS 4600 predictions are for both types of sections, Type A specimens show a very good agreement while Type B specimen values are more conservative. Therefore the accuracy of AS/NZS 4600 design rules for distortional buckling should be further investigated by considering other types of light gauge steel sections.

On the other hand AS/NZS 4600 predictions are only for pure distortional buckling. The interaction of local and distortional buckling was also considered in this study. During the ambient temperature tests it was noticed that very thin members (0.6 mm) had both distortional and local buckling failure modes at the commencement of failure. However, the ultimate collapse of the specimen was based on distortional buckling. In these cases, the effective area was used instead of gross area in Equations 4.1 (a) and (b) and the modified equations are shown next.

- For $f_{od} > f_y/2$:
$$P_n = A_e f_n = A_e f_y \left(1 - \frac{f_y}{4f_{od}}\right) \qquad (4.2(a))$$

- For $f_y/13 \leq f_{od} \leq f_y/2$:
$$P_n = A_e f_n = A_e f_y \left[0.055\left(\sqrt{\frac{f_y}{f_{od}}} - 3.6\right)^2 + 0.237\right] \qquad (4.2(b))$$

where A_e is the effective area while others are the same as defined earlier for Equations (4.1 (a) and (b)). A_e is calculated as specified in AS/NZS 4600 Clause 2.2 for stiffened elements and Clause 2.3 for unstiffened elements.

$A_e = \sum b_e * t$

For $\lambda \leq 0.673$: $\quad b_e = b$
$$ \qquad (4.2(c))$$
For $\lambda > 0.673$: $\quad b_e = \rho b$

$$\rho = \frac{\left(1 - \frac{0.22}{\lambda}\right)}{\lambda} \leq 1.0 \qquad (4.2(d))$$

$$\lambda = \left(\frac{1.052}{\sqrt{k}}\right)\left(\frac{b}{t}\right)\left(\sqrt{\frac{f^*}{E}}\right) \qquad (4.2(e))$$

where, b = flat width of elements excluding radii, t = thickness, ρ = effective width factor, λ = slenderness ratio, E = Young's modulus of elasticity and k = 4 and 0.43 for stiffened and unstiffend elements, respectively. f* = design stress in the compression element calculated in Equation 4.1 equal to f_n in this study.

The predicted failure loads of 0.6 mm specimens are shown in Table 4.14. Table 4.14 clearly shows that the predicted values considering effective areas are too conservative. Therefore it can be concluded that although there was a local buckling mode at the beginning, the failure load was governed by the distortional buckling mode. However, this phenomenon should be further studied by considering other specimens. Chapter 6 presents more details of the interaction of local and distortional buckling modes.

Table 4.14   Comparison of Equation 4.2 Predictions with Test Results

Specimen	Ultimate Load (kN)		Exp. /Predicted
	Exp. (Ave.)	Predicted	
G250-0.6-20-A	12.8	10.16	1.26
G550-0.6-20-A	19.7	15.82	1.25
G250-0.6-20-B	15.7	10.92	1.44
G550-0.6-20-B	24.1	16.02	1.50

In addition the comparison of predicted ultimate loads from Equations 4.1 (a) and (b) with test results is shown in Figure 4.34. Lau and Hancock (1987) developed Equation 4.1 (a) whereas Kwon and Hancock (1992b) developed Equation 4.1 (b) to extend Lau and Hancock's curve for slender sections which may buckle in the distortional mode in the post-buckling range.

The total cross sectional area is considered here rather than the effective area since local buckling failure mode is not significant. The measured yield strength values from the tensile coupon test results were used to non-dimensionalise the test results as given in Hancock (1998). f_{od} was determined from finite element analyses for the tested specimens. Figure 4.34 shows a good agreement between test results and

Equation 4.1. Therefore based on Table 4.13 and Figure 4.34 it can be concluded that the design equations in AS/NZS 4600 are reasonably accurate for the commonly used light gauge cold-formed steel compression members (C-section and C-section with additional lips) at ambient temperature. Further studies investigating the accuracy of these equations are presented in Chapter 6.
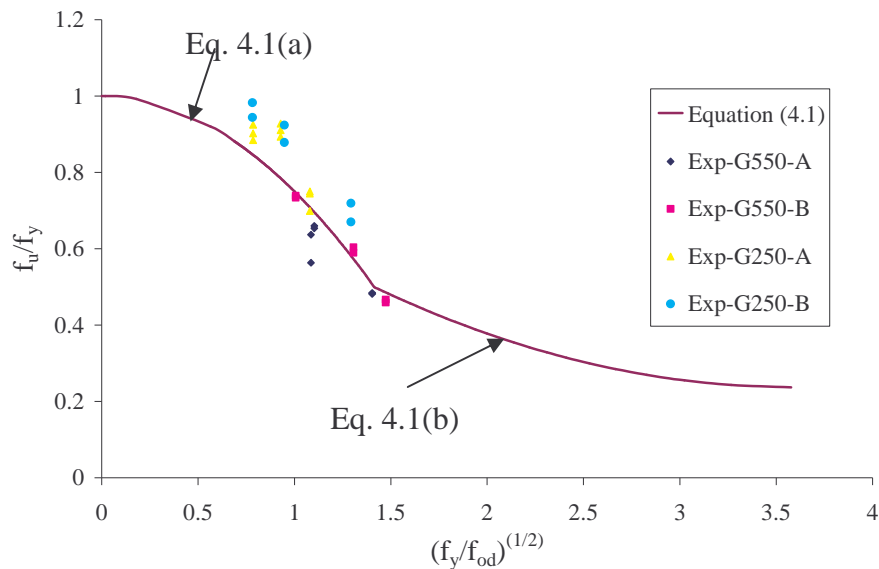
Figure 4.34   Comparison of Equation 4.1 predictions with Test Results at Ambient Temperature

4.4.1.2   Direct strength method

The direct strength method proposed by Schafer and Pekoz (1998b) is one of the alternative methods to determine the strength of cold-formed steel members. The direct strength method includes the distortional buckling of cold-formed steel compression members. Therefore the predictions of the direct strength method were compared with the test results in this research. However, it must be noted that the direct strength method was calibrated by using the available test data for pin-end concentrically loaded compression members (AISI, 2004). Equations 4.3 (a) and (b) give the ultimate load of the compression members which fail by distortional buckling mode.

$$\lambda \leq 0.561 \qquad\qquad P_n = Af_n = Af_y \qquad\qquad\qquad\qquad (4.3(a))$$

and

$$\lambda > 0.561 \qquad\qquad P_n = Af_n = Af_y \left[1 - 0.25 \left(\frac{f_{od}}{f_y} \right)^{0.6} \right] \left[\frac{f_{od}}{f_y} \right]^{0.6} \qquad (4.3(b))$$

where,

$$\lambda = \sqrt{\frac{f_y}{f_{od}}}$$

Note: All the symbols are the same as in Equations 4.1 and 4.2
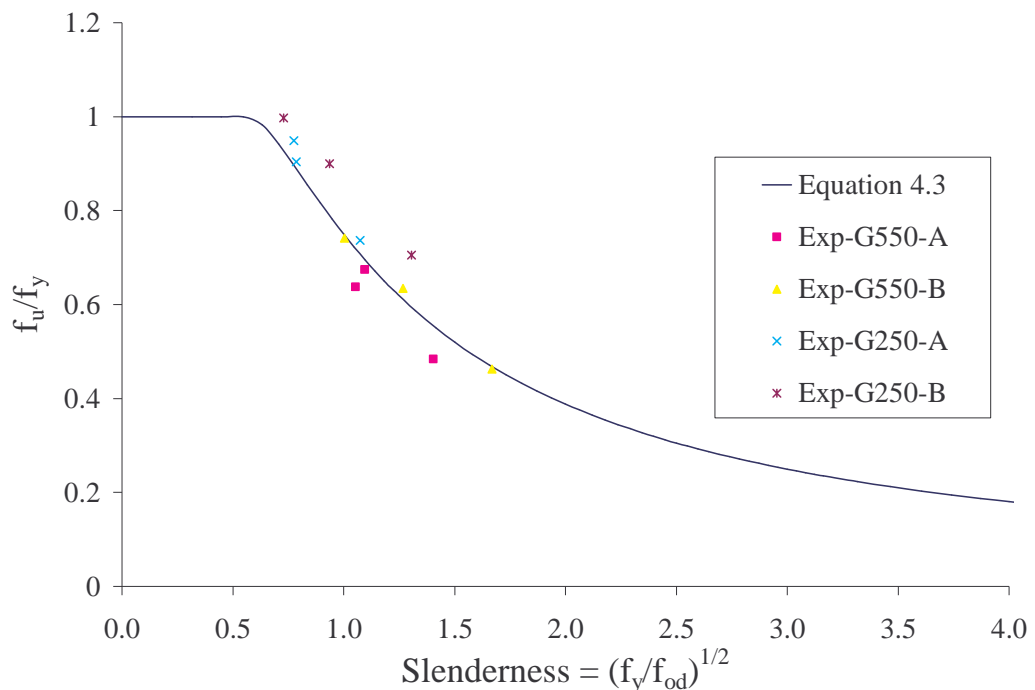
Figure 4.35   Comparison of Predictions from Equation 4.3 with Test Results at Ambient Temperature

As given in AS/NZS 4600 (Clause 1.5.1.5), the yield strength reduction factor for 0.6 and 0.8 mm G550 steels was also used in the direct strength method. The yield strength should be taken as 90% of the corresponding values or 495 MPa whichever is the lesser when steels do not satisfy Clause 1.5.1.5(a) requirements. Table 4.15 and Figure 4.35 show the comparison of test results with Equation 4.3 predictions. The yield strengths were measured values from the experiments and f_{od} was determined from finite element analyses based on the measured test specimen sizes.

As shown in Table 4.15 and Figure 4.35 the direct strength method predicts the ultimate strength of compression members reasonably well which failed from distortional buckling at ambient temperature. As stated earlier although the direct strength method was developed based on the results of pin-end compression members, the results show that it can also be used for fixed-end conditions. However, the experimental to predicted ultimate load ratios are 1.002 and 1.039 for Type A specimens and 1.105 and 1.134 for Type B specimens with lower COV values. Therefore it can be concluded that the direct strength method is also accurate for Type A specimens while being conservative for Type B specimens.

Table 4.15   Comparison of Predictions from Equation 4.3 with Test Results at Ambient Temperature

| | Ultimate Load (kN) | | Exp/Predicted | |
Specimen	Predicted	Experiment (Ave.)	Actual	Mean/COV
G550-0.6-20-A	19.08	19.7	1.032	1.002/
G550-0.8-20-A	30.96	31.1	1.005	0.032
G550-0.95-20-A	44.27	42.9	0.969	
G550-0.6-20-B	20.78	24.1	1.160	1.105/
G550-0.8-20-B	34.00	39.6	1.165	0.089
G550-0.95-20-B	54.07	53.6	0.991	
G250-0.6-20-A	12.30	12.8	1.041	1.039/
G250-0.8-20-A	20.07	20.4	1.016	0.021
G250-0.95-20-A	29.66	31.4	1.059	
G250-0.6-20-B	13.21	15.7	1.188	1.134/
G250-0.8-20-B	22.82	26.0	1.139	0.050
G250-0.95-20-B	34.86	37.5	1.076	

4.4.2   Elevated Temperatures

4.4.2.1   AS/NZS 4600

Although AS/NZS 4600 design rules are available for the prediction of distortional buckling failure loads of compression members, they are limited to ambient

temperature conditions. Therefore they were modified to predict the ultimate loads at elevated temperatures by substituting the appropriate reduction factors for yield strengths at relevant temperatures in the original equations (Equation 4.1). The modified equations are presented here as Equations 4.4 (a) and (b).

For $f_{od} > f_y/2$: $\qquad P_n = A f_n = A k_{yT} f_y \left(1 - \dfrac{k_{yT} f_y}{4 f_{od}} \right)$ $\hfill$ (4.4(a))

For $f_y/13 \leq f_{od} \leq f_y/2$: $\quad P_n = A f_n = A k_{yT} f_y \left[0.055 \left(\sqrt{\dfrac{k_{yT} f_y}{f_{od}}} - 3.6 \right)^2 + 0.237 \right]$ $\hfill$ (4.4(b))

where k_{yT} = measured yield strength reduction factor at a given temperature while the other parameters are the same as in Equations 4.1 to 4.3.

As specified in AS/NZS 4600, a reduction factor of 0.9 was used for 0.6 and 0.8 mm G550 steels. However, AS/NZS 4600 defines this reduction factor only at ambient temperature. Therefore two different cases were considered. In the first case measured yield strength at any given temperature was used without the reduction factor of 0.9 while in the second case this factor was used for all. All the parameters were based on experimentally measured values. The elastic buckling strength (f_{od}) was calculated from finite element analyses (ABAQUS) based on the measured specimen dimensions as for the ambient temperature case, and the measured elasticity modulus at any given temperature.

Table 4.16 and Figure 4.36 show the comparison of predictions from Equations 4.4 (a) and (b) and the test results. A reasonable agreement between the predictions and test results can be seen. However, some of them are too conservative while others are unsafe. The mean values of the ultimate load ratio of experimental results to predictions vary from 0.806 to 1.248. Therefore these equations should be further modified by considering additional results. Hence a parametric study was undertaken considering various specimen geometries and temperatures (see Chapter 6).

Table 4.16   Comparison of Predictions from Equation 4.4 with Test Results at Elevated Temperatures

Specimen	AS 4600 –P_n (kN)		Exp. Ave (kN)	Exp/Pred.1	Exp/Pred.2
	Pred.1	Pred.2			
G550-0.6-200-A	18.274	17.084	15.198	0.832	0.890
G550-0.6-350-A	15.370	14.397	13.568	0.883	0.942
G550-0.6-500-A	8.407	7.839	6.946	0.826	0.886
G550-0.6-650-A	3.310	3.054	2.367	0.715	0.775
G550-0.6-800-A	0.880	0.820	0.680	0.773	0.829
			Mean	*0.806*	*0.865*
			COV	*0.079*	*0.074*
G250-0.6-200-A	10.635		9.302	0.875	
G250-0.6-350-A	6.798		5.886	0.866	
G250-0.6-500-A	4.485		3.829	0.854	
G250-0.6-650-A	2.254		1.906	0.845	
G250-0.6-800-A	0.470		0.610	1.298	
			Mean	*0.948*	
			COV	*0.207*	
G550-0.6-200-B	20.418	17.430	20.874	1.022	1.198
G550-0.6-350-B	17.245	16.000	18.713	1.085	1.170
G550-0.6-500-B	9.477	8.894	10.046	1.060	1.130
G550-0.6-650-B	3.809	3.562	3.189	0.837	0.895
G550-0.6-800-B	0.960	0.910	1.040	1.083	1.143
			Mean	*1.018*	*1.107*
			COV	*0.102*	*0.109*
G250-0.6-200-B	10.858		14.630	1.347	
G250-0.6-350-B	7.521		9.119	1.212	
G250-0.6-500-B	5.129		5.871	1.145	
G250-0.6-650-B	2.627		2.477	0.943	
G250-0.6-800-B	0.540		0.860	1.593	
			Mean	*1.248*	
			COV	*0.194*	
G550-0.8-200-A	32.369	30.539	27.191	0.840	0.890
G550-0.8-350-A	27.041	25.748	23.743	0.878	0.922
G550-0.8-500-A	14.670	13.769	12.903	0.880	0.937
G550-0.8-650-A	4.224	3.832	4.242	1.004	1.107
G550-0.8-800-A	2.200	2.000	1.730	0.786	0.865
			Mean	*0.878*	*0.944*
			COV	*0.091*	*0.101*

Table 4.16   Comparison of Predictions from Equation 4.4 with Test Results at Elevated Temperatures (Continued)

Specimen	AS 4600 –P_n (kN)		Exp. Ave (kN)	Exp/Pred.1	Exp/Pred.2
	Pred.1	Pred.2			
G250-0.8-200-A	17.937		17.280	0.963	
G250-0.8-350-A	11.094		10.234	0.923	
G250-0.8-500-A	7.348		7.118	0.969	
G250-0.8-650-A	3.708		3.184	0.859	
G250-0.8-800-A	1.240		1.360	1.097	
			Mean	*0.962*	
			COV	*0.091*	
G550-0.8-200-B	31.949	31.408	32.922	1.030	1.048
G550-0.8-350-B	26.713	24.925	28.397	1.063	1.139
G550-0.8-500-B	14.957	14.530	14.685	0.982	1.011
G550-0.8-650-B	5.171	4.714	4.383	0.848	0.930
G550-0.8-800-B	2.650	2.430	1.510	0.570	0.621
			Mean	*0.899*	*0.950*
			COV	*0.224*	*0.209*
G250-0.8-200-B	20.521		23.071	1.124	
G250-0.8-350-B	12.976		14.500	1.117	
G250-0.8-500-B	8.715		8.455	0.970	
G250-0.8-650-B	4.563		4.078	0.894	
G250-0.8-800-B	1.250		1.430	1.144	
			Mean	*1.050*	
			COV	*0.106*	
G550-0.95-200-A	42.156		37.549	0.891	
G550-0.95-350-A	36.266		30.908	0.852	
G550-0.95-500-A	21.963		19.519	0.889	
G550-0.95-650-A	4.773		4.516	0.946	
G550-0.95-800-A	2.540		1.800	0.709	
			Mean	*0.857*	
			COV	*0.105*	
G250-0.95-200-A	23.560		25.171	1.068	
G250-0.95-350-A	15.120		18.091	1.196	
G250-0.95-500-A	9.752		10.382	1.065	
G250-0.95-650-A	5.046		4.978	0.986	
G250-0.95-800-A	1.690		1.470	0.870	
			Mean	*1.037*	
			COV	*0.116*	

Table 4.16   Comparison of Predictions from Equation 4.4 with Test Results at Elevated Temperatures (Continued)

Specimen	AS 4600 –P_n (kN)		Exp. Ave (kN)	Exp/Pred.1	Exp/Pred.2
	Pred.1	Pred.2			
G550-0.95-200-B	50.347		44.629	0.886	
G550-0.95-350-B	43.660		39.038	0.894	
G550-0.95-500-B	24.379		21.899	0.898	
G550-0.95-650-B	5.475		5.019	0.917	
G550-0.95-800-B	2.920		1.950	0.668	
			Mean	*0.853*	
			COV	*0.122*	
G250-0.95-200-B	27.249		28.400	1.042	
G250-0.95-350-B	17.449		19.666	1.127	
G250-0.95-500-B	11.413		11.737	1.028	
G250-0.95-650-B	5.784		5.361	0.927	
G250-0.95-800-B	1.940		1.940	1.000	
			Mean	*1.025*	
			COV	*0.071*	

where Pred.1 = Ultimate load obtained based on the measured yield strength while Pred.2 = Ultimate load obtained by using the reduced yield strength as specified in AS/NZS 4600.
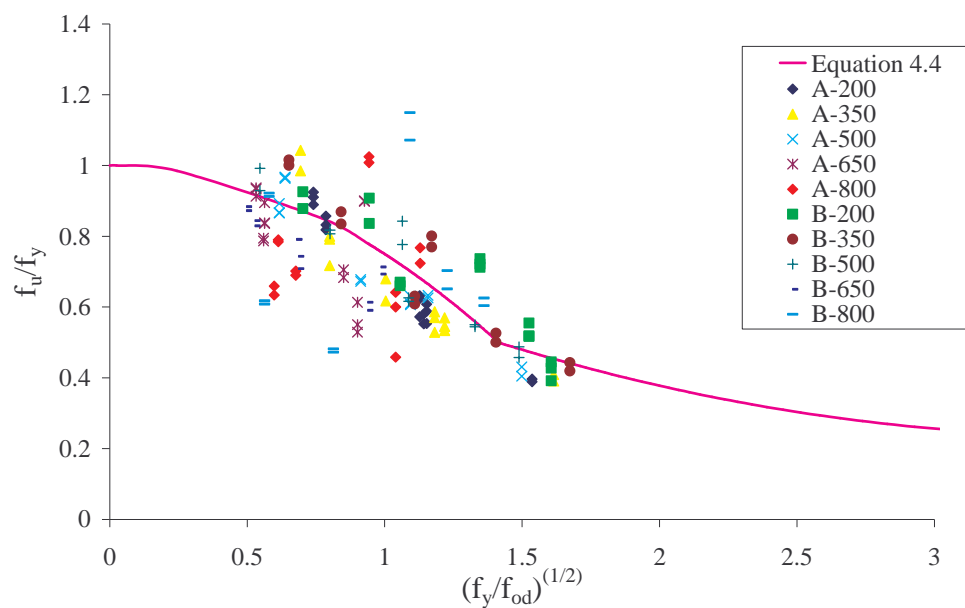
Figure 4.36   Comparison of Equation 4.4 Predictions with Test Results at Elevated Temperatures

4.4.2.2 Direct strength method

As discussed earlier the direct strength method is an alternative method to predict the failure load when columns fail by distortional buckling. However, the direct strength method was developed for ambient temperature conditions. In addition, the direct strength method was developed based on the pin-end column test results. Therefore the above equations were modified by including the yield strength reduction factors obtained in this research to determine the distortional buckling failure loads so that the accuracy of this method can be investigated at elevated temperatures with fixed-end conditions. As specified in AS/NZS 4600 the yield strength reduction factor for 0.6 and 0.8 mm high strength steels were also included in the direct strength method (see Section 4.4.2.1 for more details). Equations 4.5 (a) and (b) show the modified direct strength method used in this research to predict the ultimate loads at elevated temperatures. Table 4.17 and Figure 4.37 compare the ultimate loads predicted by the direct strength method and test results. The measured values were used in calculating the ultimate loads from Equations 4.5 (a) and (b).

$$\lambda \leq 0.561 \qquad P_n = Af_n = Ak_{yT}f_y$$

And
(4.5 (a))

$$\lambda > 0.561 \qquad P_n = Af_n = Ak_{yT}f_y\left[1 - 0.25\left(\frac{f_{od}}{k_{yT}f_y}\right)^{0.6}\right]\left[\frac{f_{od}}{k_{yT}f_y}\right]^{0.6} \qquad (4.5 (b))$$

where,
$$\lambda = \sqrt{\frac{k_{yT}f_y}{f_{od}}}$$

Note: All the symbols are the same as in Equations 4.3 and 4.4
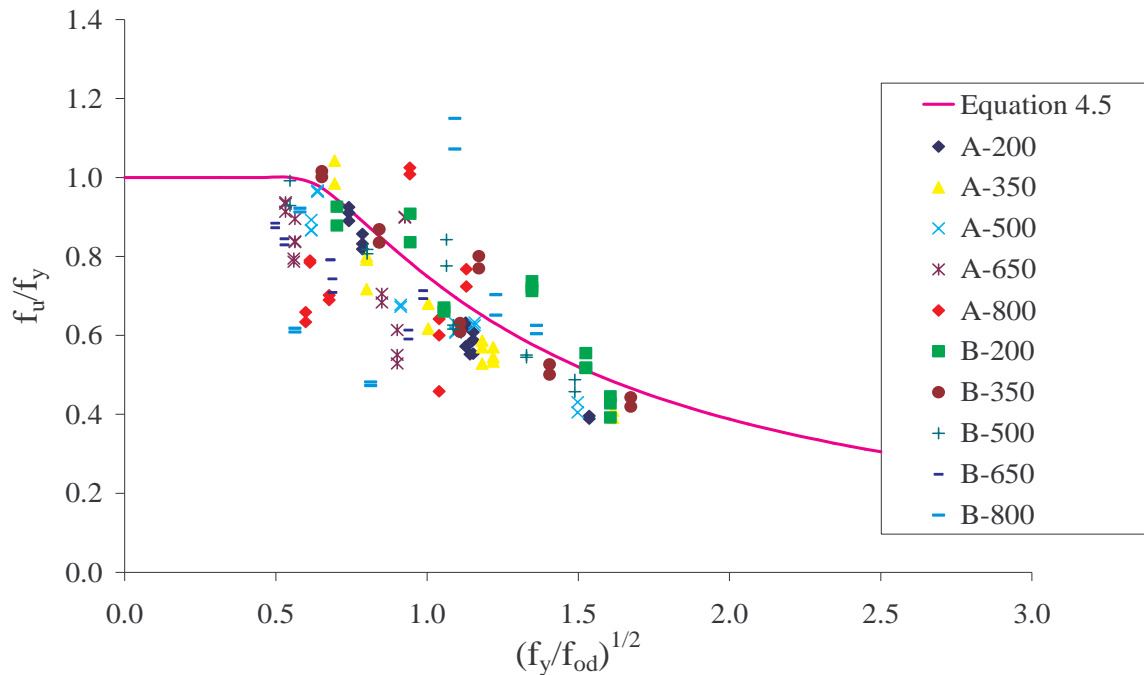
Figure 4.37   Comparison of Equation 4.5 with Test Results at Elevated Temperatures

As shown in Table 4.17 and Figure 4.37, the direct strength method does not accurately predict the ultimate strength of compression members at elevated temperatures which failed by distortional buckling. The direct strength method over-predicts the ultimate load in many specimens and conservative for some specimens. The mean values of the ultimate load ratio of experimental results to predictions vary from 0.771 to 1.229. As stated earlier the direct strength method was developed using the results of compression members with pin-ends. But the tests undertaken in this research were for fixed-end conditions so the results can be different. On the other hand the direct strength method is developed for ambient temperature conditions. Therefore it is unable to predict the ultimate load results at elevated temperatures.

Table 4.17   Comparison of Predictions from Equation 4.5 with Test Results at Elevated Temperatures

Specimen	Direct strength method P_n (kN)		Exp. Ave (kN)	Exp/ Pred. 1	Exp/ Pred. 2
	Pred.1	Pred. 2			
G550-0.6-200-A	19.70	17.16	15.20	0.772	0.886
G550-0.6-350-A	16.37	15.32	13.57	0.829	0.886
G550-0.6-500-A	9.23	8.74	6.95	0.753	0.795
G550-0.6-650-A	3.38	3.15	2.34	0.692	0.742
G550-0.6-800-A	0.84	0.79	0.68	0.810	0.859
			Mean	*0.771*	*0.834*
			COV	*0.069*	*0.076*
G250-0.6-200-A	10.60		9.30	0.877	
G250-0.6-350-A	6.80		5.89	0.866	
G250-0.6-500-A	4.56		3.83	0.840	
G250-0.6-650-A	2.33		1.91	0.820	
G250-0.6-800-A	0.47		0.61	1.298	
			Mean	*0.940*	
			COV	*0.214*	
G550-0.8-200-A	32.22	28.85	27.01	0.838	0.936
G550-0.8-350-A	27.19	25.65	23.74	0.873	0.926
G550-0.8-500-A	14.58	13.71	12.90	0.885	0.941
G550-0.8-650-A	4.56	4.10	4.24	0.930	1.033
G550-0.8-800-A	2.48	2.23	1.73	0.698	0.775
			Mean	*0.845*	*0.922*
			COV	*0.105*	*0.101*
G250-0.8-200-A	19.17		17.28	0.901	
G250-0.8-350-A	11.61		10.23	0.881	
G250-0.8-500-A	8.03		7.12	0.887	
G250-0.8-650-A	4.03		3.18	0.789	
G250-0.8-800-A	1.17		1.36	1.162	
			Mean	*0.924*	
			COV	*0.152*	
G550-0.95-200-A	41.90		37.55	0.896	
G550-0.95-350-A	36.24		31.14	0.859	
G550-0.95-500-A	21.88		19.52	0.892	
G550-0.95-650-A	5.17		4.52	0.874	
G550-0.95-800-A	2.79		1.8	0.645	
			Mean	*0.833*	
			COV	*0.128*	

Table 4.17   Comparison of Predictions from Equation 4.5 with Test Results at Elevated Temperatures (Continued)

| Specimen	Direct strength method Pₙ (kN)		Exp. Ave (kN)	Exp/ Pred. 1	Exp/ Pred. 2
	Pred.1	Pred. 2			
G250-0.95-200-A	25.18		25.17	1.000	
G250-0.95-350-A	16.34		17.40	1.065	
G250-0.95-500-A	10.64		10.38	0.976	
G250-0.95-650-A	5.43		4.99	0.919	
G250-0.95-800-A	1.86		1.47	0.790	
			Mean	*0.950*	
			COV	*0.109*	
G550-0.6-200-B	21.25	18.63	20.87	0.982	1.120
G550-0.6-350-B	17.84	16.74	18.71	1.049	1.118
G550-0.6-500-B	9.99	9.48	10.05	1.006	1.060
G550-0.6-650-B	3.79	3.56	3.19	0.842	0.896
G550-0.6-800-B	1.00	0.95	1.04	1.040	1.099
			Mean	*0.984*	*1.059*
			COV	*0.085*	*0.089*
G250-0.6-200-B	11.61		14.77	1.272	
G250-0.6-350-B	7.53		9.12	1.211	
G250-0.6-500-B	5.10		5.87	1.151	
G250-0.6-650-B	2.62		2.48	0.947	
G250-0.6-800-B	0.55		0.86	1.564	
			Mean	*1.229*	
			COV	*0.182*	
G550-0.8-200-B	34.52	31.17	32.53	0.942	1.044
G550-0.8-350-B	29.18	27.63	28.40	0.973	1.028
G550-0.8-500-B	15.67	14.81	14.69	0.937	0.992
G550-0.8-650-B	5.61	5.25	4.38	0.781	0.834
G550-0.8-800-B	2.87	2.66	1.51	0.526	0.569
			Mean	*0.832*	*0.893*
			COV	*0.224*	*0.223*
G250-0.8-200-B	20.69		23.07	1.115	
G250-0.8-350-B	13.04		14.50	1.112	
G250-0.8-500-B	9.11		8.46	0.929	
G250-0.8-650-B	4.94		4.08	0.826	
G250-0.8-800-B	1.42		1.43	1.007	
			Mean	*0.998*	
			COV	*0.124*	

Table 4.17   Comparison of Predictions from Equation 4.5 with Test Results at Elevated Temperatures (Continued)

Specimen	Direct strength method P_n (kN)		Exp. Ave (kN)	Exp/ Pred. 1	Exp/ Pred. 2
	Pred.1	Pred. 2			
G550-0.95-200-B	50.09		46.60	0.930	
G550-0.95-350-B	43.39		39.04	0.900	
G550-0.95-500-B	24.24		21.90	0.903	
G550-0.95-650-B	5.88		5.02	0.854	
G550-0.95-800-B	3.17		1.95	0.615	
			Mean	*0.840*	
			COV	*0.153*	
G250-0.95-200-B	29.46		28.40	0.964	
G250-0.95-350-B	19.00		19.67	1.035	
G250-0.95-500-B	12.34		11.74	0.951	
G250-0.95-650-B	6.17		5.36	0.869	
G250-0.95-800-B	2.12		1.94	0.915	
			Mean	*0.947*	
			COV	*0.065*	

Accordingly, the direct strength method appears to be more unsafe than the AS/NZS 4600 predictions at elevated temperatures and it seems that the direct strength method cannot be simply modified by including the yield strength reduction factors at elevated temperatures. However, more results are required for the modification of the direct strength method. Therefore further investigation in to the use of direct strength method was undertaken in finite element analyses and the results are presented in Chapter 6. On the other hand it can be concluded that the both AS/NZS 4600 and direct strength methods are reasonably accurate at ambient temperature while some modifications are required at elevated temperatures as their predictions are either conservative or unsafe as the temperature increases.

5 Numerical Model Development and Validation

5.1 General

Numerous finite element analysis programs are available for research purposes that can eliminate the excessive resource and time requirements in experimental investigations. Once a finite element model is developed and verified it can be further used to analyse the behaviour and determine the failure loads of structures. These finite element programs increase the efficiency of research projects. In this research, ABAQUS standard version 6.3 (HKS, 2002) was used as a finite element tool. QUT's high performance computing centre provided the facilities required for all the finite element analyses. ABAQUS has been developed as a flexible tool for multi-purpose finite element analyses. Both elastic and nonlinear analyses can be undertaken using this finite element program.

In this research the well known finite strip program Thin-wall was used for elastic buckling analyses of the chosen light gauge cold-formed steel sections, while the finite element program ABAQUS was used for both elastic buckling and nonlinear analyses of the same sections. Elastic buckling analyses were undertaken using ABAQUS for both pinned and fixed end conditions and varying temperatures. This was carried out to compare the elastic buckling loads from experiments and numerical models of Thin-wall and ABAQUS, and thus the first stage of validation of numerical models. Distortional buckling behaviour of the selected sections at ambient and elevated temperatures was carefully studied in this process. Numerical analysis was also used to study the effect of end support conditions on the distortional buckling behaviour.

Following the elastic buckling analyses, nonlinear analyses were undertaken using the finite element models of the same sections at varying temperatures and end support conditions. For this purpose, appropriate material properties, initial

geometric imperfections and residual stresses were used. Nonlinear analysis results including the ultimate load and load-deflection curves were compared with the corresponding experimental results obtained from Chapter 4. Comparisons of the results from buckling and nonlinear analyses thus enabled a complete validation of the numerical models, in particular, the finite element model based on ABAQUS. This chapter presents the details of the numerical models developed in this research and their validation.

5.2 Finite Strip Analyses

Finite strip analyses using Thin-wall were undertaken prior to experimental investigation and finite element analyses. The theoretical buckling failure mode and the suitable section sizes were first obtained from the finite strip analysis program Thin-wall. In addition, a half-wave buckling length range during which distortional buckling occurs was obtained. This range was then used in the finite element analyses to select the appropriate member length for distortional buckling failure. The details of the finite strip analyses have been presented in Chapter 4.

5.3 Finite Element Analyses

In the numerical analyses finite element models were developed first using ABAQUS (HKS, 2002). A total of 12 models was developed to study the distortional buckling behaviour of compression members at ambient temperature. They were then modified at elevated temperatures by including the appropriately reduced mechanical properties. This led to a total of 72 models in this process. Two types of sections as discussed earlier were modelled with three thicknesses and two steel grades.

5.3.1 Elements

ABAQUS and MSC/PATRAN (HKS, 2002) were used as finite element analysis tools to analyse the cold-formed steel compression members. Element types should be defined correctly to simulate the true member behaviour. Various shell element types are available in ABAQUS. Among the variety of shell element types, the S4 element type was selected to analyse the light gauge cold-formed steel compression members to ensure sufficient degrees of freedom for buckling deformation. Element types S4 and S4R5 were studied prior to selecting the suitable element type. Element type S4 is a fully integrated, general purpose, finite membrane strain shell element that allows for transverse shear. The S4R5 element has one integration location per element while the S4 element type has four integration locations per element. Although the disk usage and memory required are greater for the S4 element type than the other elements, the S4 element type was selected for further studies since it provides better results than the S4R5 elements. On the other hand, the difference between the disk usage and the time was negligible when S4 and S4R5 elements were used for the small specimens used in this research.
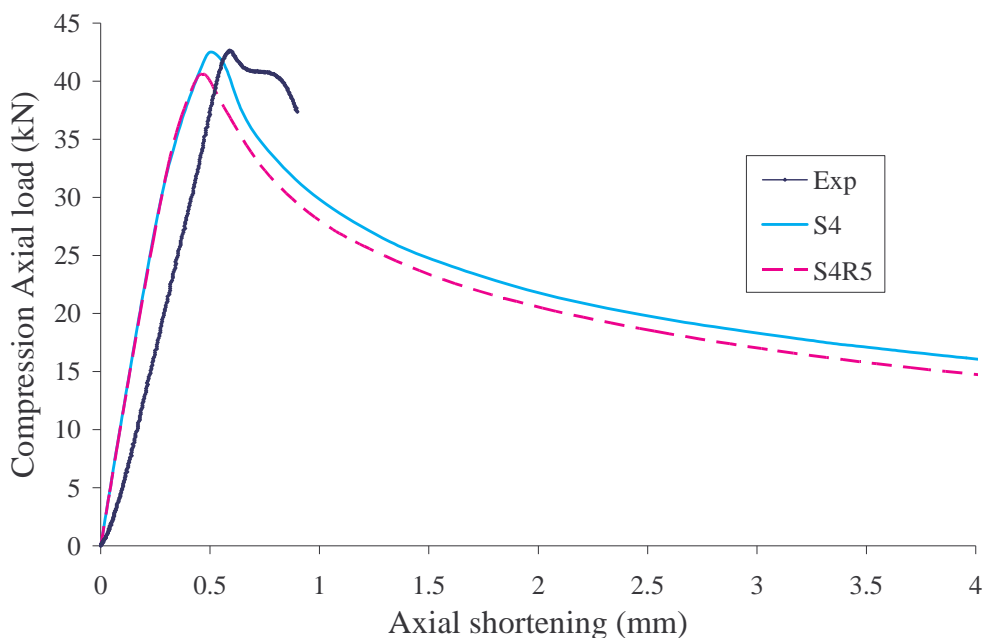
Figure 5.1 **Comparison of Load-Shortening Curves obtained from FEA using S4 and S4R5 Elements**

The ultimate failure load and the axial compression load versus axial shortening graphs obtained from FEA using S4 and S4R5 element types show considerable difference to each other. In some cases the difference of elastic distortional buckling load was more than five percent. The axial compression load versus axial shortening curve for 0.95 mm G550 steel Type A specimen at ambient temperature is shown in Figure 5.1. It shows that the ultimate load obtained from the S4 element type is similar to the experimental results rather than the S4R5 element type. Therefore the element type S4 was selected for the finite element analyses in this research. In addition, Camotim et al. (2005) investigated the difference when S4 and S4R elements were used. They argued that the critical stresses obtained from S4 and S4R elements are similar in the case of local and global buckling failures whereas there is a considerable difference for the distortional buckling failure. They proved that the S4 element is more suitable than the S4R element.

5.3.2   Finite Element Mesh

One of the most important factors in finite element analyses is the mesh size. The accuracy of the results is governed by the mesh size and therefore it is desirable to use as many elements as possible in the finite element analyses. The finite element mesh should be fine enough to analyse the compression members subject to distortional buckling. However, excessively finer mesh is not economical in terms of processor time and disk usage. Therefore preliminary analyses were undertaken to decide the most suitable finite element mesh.

The studies were undertaken with various mesh sizes from 1 mm to 10 mm. The results obtained from the FEA showed that the 5 mm mesh size is adequate to analyse the distortional buckling and nonlinear ultimate strength behaviour of both the C-section and C-section with additional lips (Types A and B specimens). Therefore 5 mm x 5 mm mesh size was selected for all the sections.
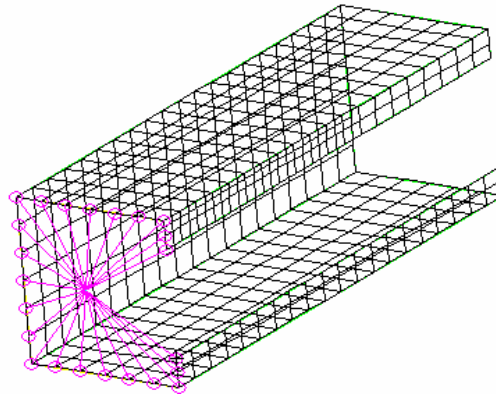
(a) 0.6 mm G550 Type A specimen
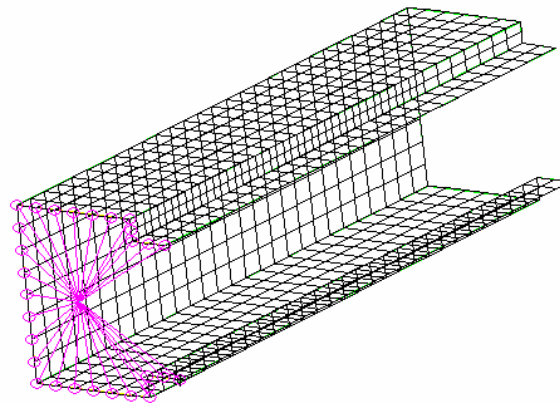
(b) 0.6 mm G550 Type B specimen

Figure 5.2   Finite Element Models using 5 mm x 5 mm Mesh Size

Except Lips

Figures 5.2 (a) and (b) show the finite element mesh for 0.6 mm G550 Type A and Type B sections, respectively. There are 20 elements along the specimen length for Type A section (100 mm is the half column length). Two elements were provided for the lip height as 2.5 mm x 5 mm since the lip height is 5 mm. Six elements were used in both flange and web (30 mm width). The maximum aspect ratio used in the mesh was 2, and is considered good.

5.3.3   Geometric Imperfections

Unlike in hot-rolled steels, light gauge cold-formed steel sections can deform easily during handling and thus can have larger initial geometric imperfections. These geometric imperfections cause the creation of additional moments in the compression members and hence can show a large influence on the ultimate failure load. The larger the initial imperfections, the smaller the ultimate failure load. Therefore the effect of initial geometric imperfections on the distortional buckling behaviour should be studied. Thus initial geometric imperfections were included in the nonlinear analyses.

Many researchers have used the measured geometric imperfections to study the effect of geometric imperfections on the ultimate strength of cold-formed steel members (Sivakumaran and Abdel-Rahman, 1998; Schafer and Pekoz, 1998; Young and Yan, 2000; Dubina and Ungureanu, 2002). Walker (1975) has derived theoretical specified values for plate initial imperfections based on Roberston's (1925) deflection analyses. He proposed an equation for initial geometric imperfection, as shown next.

$$\Delta = \beta\, t\, \sqrt{P_y/P_{cr}} \tag{5.1}$$

where Δ is the magnitude of initial imperfection;

$\quad$ β is a constant that can be adjusted to fit experimental results;

$\quad$ P_y is the yield or crushing load;

$\quad$ P_{cr} is the elastic buckling load.

Walker (1975) recommended a value of 0.3 for β due to the variations of edge restraint for various geometries and different imperfections. Because of the many variables involved in the buckling and crushing loads, Equation 5.1 needs to be revised in order to specify major functions affecting the initial imperfections. Substituting the theoretical distortional buckling stress obtained from the elastic distortional buckling analyses into Equation 5.1 leads to Equation 5.2, as follows:

$$\Delta = 0.3t \sqrt{\frac{f_y}{f_{od}}} \tag{5.2}$$

where, f_y = yield strength and f_{od} = elastic distortional buckling stress

As seen in Equation 5.2, the steel thickness plays an important role in the magnitude of initial imperfections. On the other hand, thickness (t) should show a significant influence on the light gauge cold-formed steel due to the cold-forming processes used. Therefore there is a need to consider initial imperfections in cold-formed steel sections.

Ala-Outinen and Myllymaki's (1995) studies of 900 mm long rectangular hollow sections at ambient temperature have shown that the maximum initial imperfection is about h/200 (h = width) for local and L/500 (L = length) for global buckling failures. Feng et al. (2004) carried out similar studies by considering different column lengths at various temperatures. They stated that initial geometric imperfection shows a large influence on the ultimate load. However, their study was limited to local and global buckling behaviour of rectangular hollow sections.

(a) Type 1   (b) Type 2
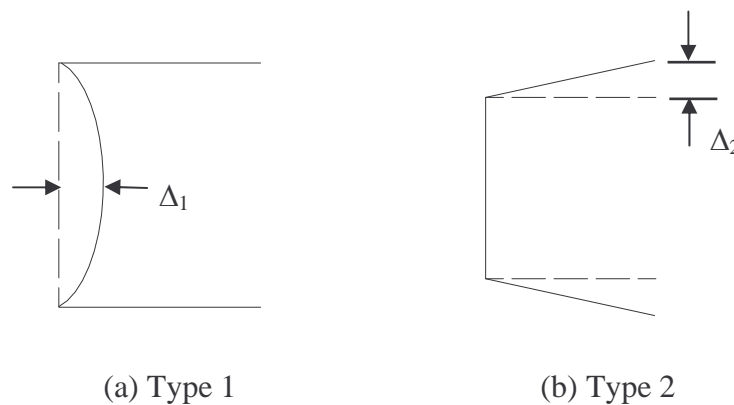
Figure 5.3 Geometric Imperfections in Cold-formed Channel Sections

Schafer and Pekoz (1998) observed two types of initial imperfections as shown in Figure 5.3. They collected the data on measured geometric imperfections of cold-formed channel sections from existing experimental data and recommended realistic magnitudes of geometric imperfections using statistical and probabilistic analyses.

Maximum magnitudes for these types (Types 1 and 2) of imperfections are given by the following equations:

$$\Delta_1 = 6te^{-2t} \text{ or } 0.006 \times \text{plate width} \qquad (5.3)$$

$$\Delta_2 = t \qquad (5.4)$$

where Δ_1, Δ_2, t and plate width are in mm.

Among these two types of imperfections, Type 1 governs the local buckling failure whereas Type 2 governs the distortional buckling failure. However, for the prediction of Type 1 imperfections, either a plate width or thickness is taken into account based on certain trends in experimental data as shown in Equation 5.3. The predicted values for Type 2 imperfection are given by a function of thickness only as seen in Equation 5.4. As seen above, different equations have been proposed for geometric imperfections. Therefore their predictions are compared in Table 5.1 for a 0.8 mm high strength cold-formed steel specimen Type A.

Table 5.1   Comparison of Initial Geometric Imperfections

of Type A Specimen

Researcher	Predicted geometric imperfection (mm)
Walker (1975)	0.26
Ala-Outinen and Myllymaki (1995)	0.15
Schafer and Pekoz (1998) for distortional buckling	0.80

As seen in Table 5.1, the predicted initial geometric imperfections are not the same. Therefore the initial geometric imperfections were measured in this study as shown in Figure 5.4 to obtain more accurate values. Geometric imperfections were measured in both flanges and web along parallel lines at 5 to 10 mm intervals along the specimen length. The measurements were recorded along three lines in the longitudinal direction of the specimen: two lines close to corners and one along the centre line of the specimen. In addition, imperfections were also measured along the centre line of stiffeners of Type B specimens. The values were recorded at every 10

mm along the parallel lines. The geometric imperfection measurement positions are shown in Figures 5.4 (a) and (b) for Type A and B specimens, respectively. The measured values were then used to obtain the ultimate load from finite element analyses (FEA).

(a) Type A   (b) Type B

(c) Measuring instrument
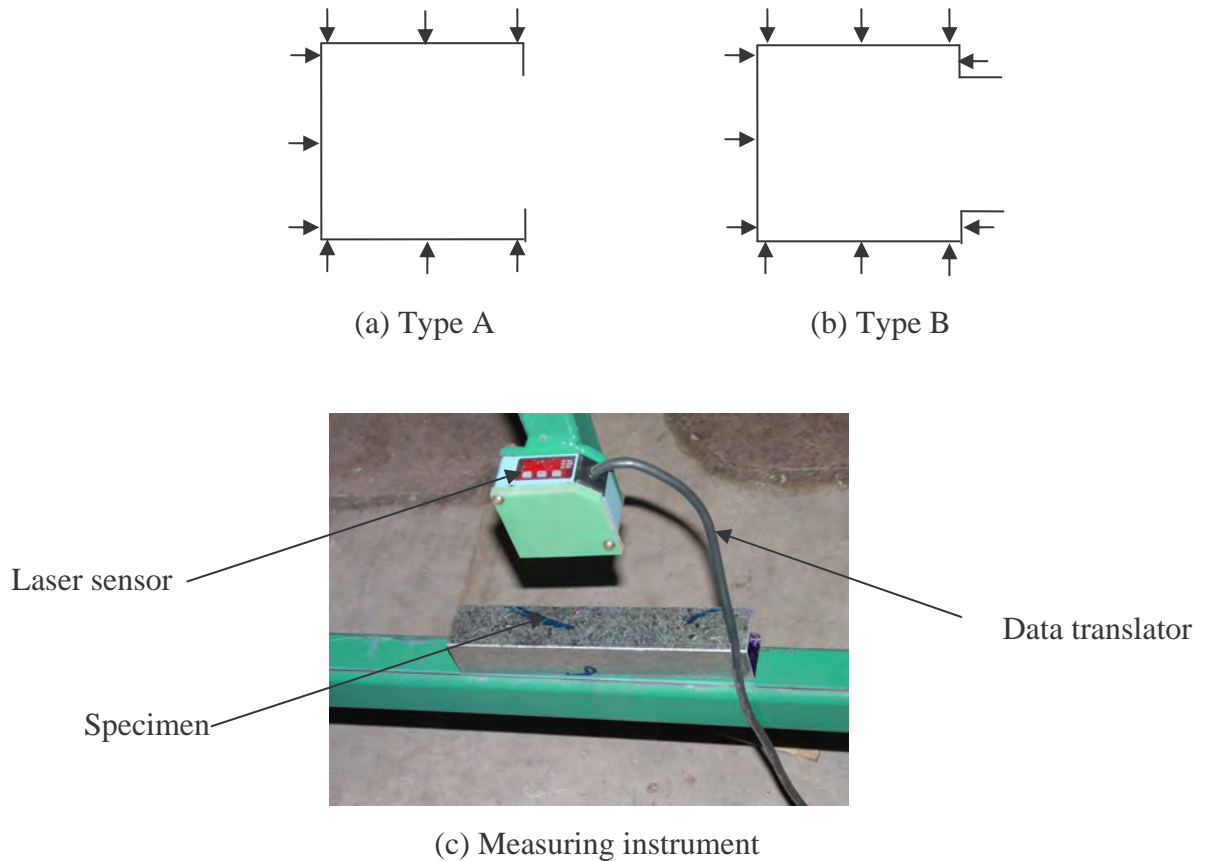
Figure 5.4   Geometric Imperfection Measurements

The measured values showed that steel grade and thickness had an influence on the initial geometric imperfection. They were higher for the higher steel grades and further increased when the thickness was increased. However, only Walker's (1975) equation presented the relationship between yield strength and initial imperfections. But Walker's calculated values were not equivalent to the measured values. On the other hand, his geometric imperfection values depend on the buckling load of the specimen. However, the buckling load depends on the used experimental methods when the column buckles distortionally. The elastic buckling load is higher when the column is tested under fixed-end conditions than under pin-end conditions. But

initial geometric imperfections does not depend upon the experimental methods. It depends on the manufacturing method.

Ala-Outinen and Myllymaki's (1995) methods depend on the width and length of the specimen for local buckling behaviour and global buckling behaviour, respectively. They recommended that geometric imperfections with respect to the width show an effect on the local buckling failure and imperfections with respect to length show an effect on the global buckling failure. But they did not consider the influence of geometric imperfections on the distortional buckling failure. Therefore in this research, the average values of the measured initial geometric imperfections were included in the finite element model before using it for nonlinear analyses. The average measured geometric imperfections are given in Table 5.2.

Table 5.2 Average Measured Geometric Imperfections of

Types A and B Specimens

Specimen	Ave. measured imperfection based on Type 2 (mm)
G550-0.6	0.65
G550-0.8	0.80
G550-0.95	1.00
G250-0.6	0.40
G250-0.8	0.45
G250-0.95	0.55

5.3.4   Residual Stresses

Unlike in hot-rolled and welded members, light gauge cold-formed steel members have a different kind of residual stresses due to their cold-forming process. Residual stresses occur with varying magnitudes due to the cold-forming process and may cause members to fail prematurely. Therefore appropriate residual stresses should be

included in the finite element analyses to get accurate results. Schafer and Pekoz (1998) gives the details of flexural residual stress distributions in cold-formed steel sections based on their measurements on lipped channels as shown in Figure 5.5.

According to their proposal the maximum residual stress occurs at the corners of the section. There is a considerable difference between the residual stresses in press-braked and roll-formed specimens. In this study all the specimens were made using the press-braking method and hence the values for press-braked specimens were used in FEA. Schafer and Pekoz's (1998) figures show the residual stresses of C-section, but not for lips. On the other hand there is a considerable difference between the residual stresses of web and flange although they were affected by the same cold-working.
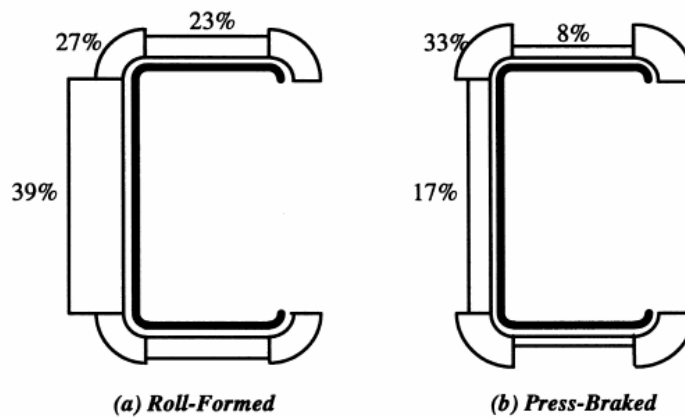
Figure 5.5   Residual Stresses in C-Sections (Schafer and Pekoz, 1998)

According to Schafer and Pekoz (1998) and Young and Rasmussen (1999), membrane residual stresses generated during the cold-working process were considered reasonably small and can be ignored. Therefore, only the flexural residual stresses in press-braked sections were considered as shown in Figure 5.5 (b) based on Schafer and Pekoz (1998).

In this research two types of cold-formed steel sections: C-sections with and without additional lips were considered as discussed in Chapter 4. A new set of residual stresses was proposed for these sections as shown in Figures 5.6 and 5.7 based on private communication with Schafer (2004) and based on preliminary investigation

of FEA. According to Schafer and Pekoz's (1998) model, higher residual stresses occur at the corners of the specimens. In this research corner radii were measured and the small measured radii were included in the FEA with the residual stresses. However, the difference between the two values obtained from the FEA with corner radius and without corner radius was negligible. Therefore, higher residual stresses were not used at the corners of the sections. On the other hand the proposed residual stress of web and flanges are the same for Type A specimen while they are the same for web, flanges and lips of Type B specimen since they were affected by the same level of cold-working in the manufacturing process.
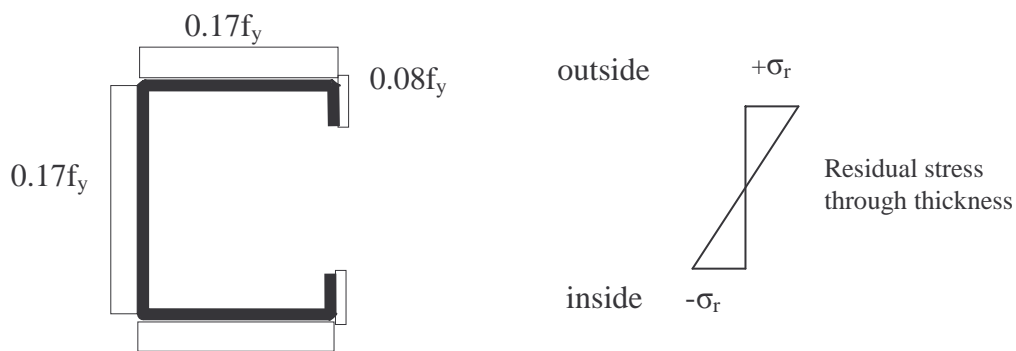
(a) Assumed flexural residual stress distribution
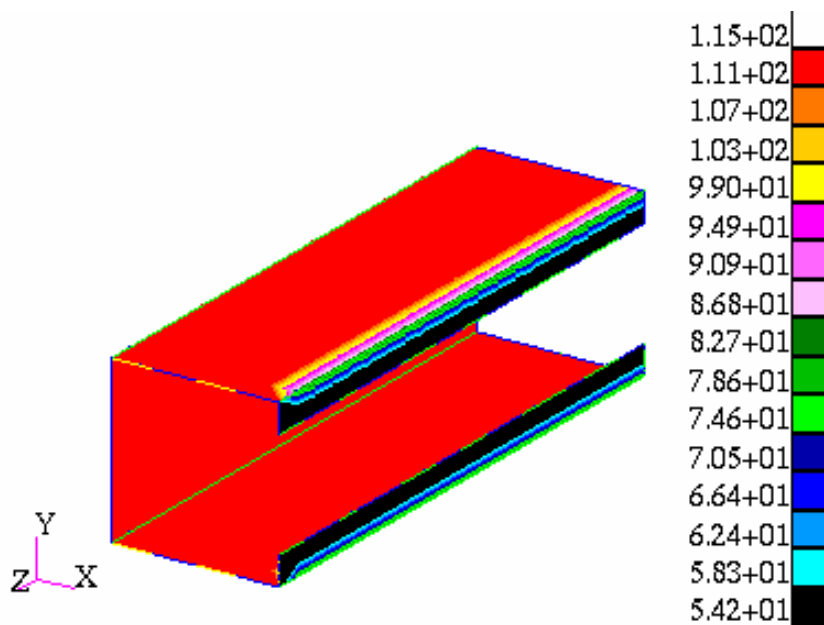
(b) FEA output

Figure 5.6   Residual Stress Distribution of Type A Specimen

0.17f$_y$

0.08f$_y$

0.17f$_y$

0.17f$_y$

outside

inside

$+\sigma_r$

$-\sigma_r$

Residual stress
through thickness
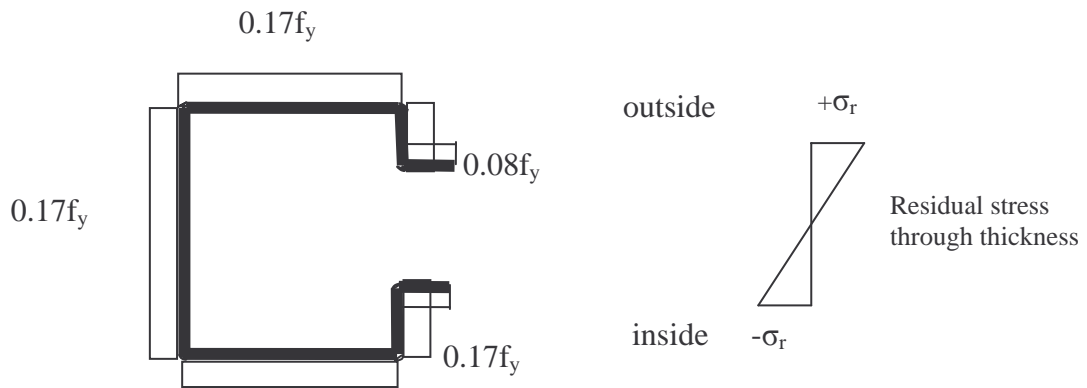
(a) Assumed flexural residual stress distribution
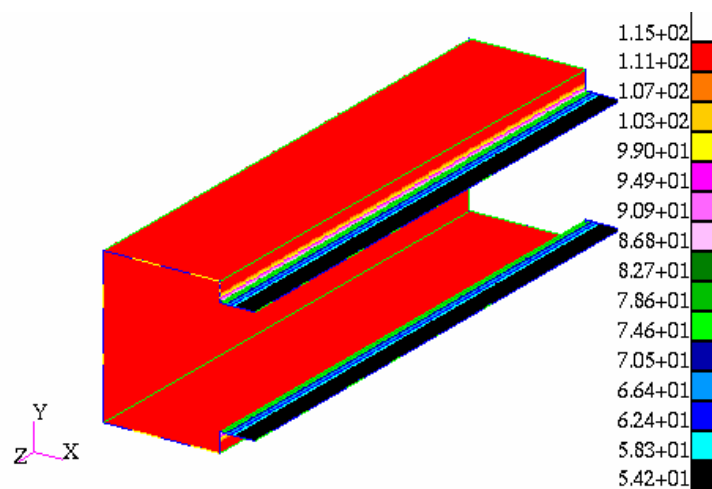
(b)   FEA output

Figure 5.7   Residual Stress Distribution of Type B Specimen

In addition, the residual stresses diminish when the specimens are exposed to high temperatures. Therefore, suitable reduction factors should be included in the finite element analyses at elevated temperatures. Lee, (2004) presented a linear equation to determine the reduction factors of residual stresses at elevated temperatures. They assumed that the residual stresses are totally diminished when the temperature is 800°C. Equation 5.5 presents the reduction factors of residual stresses while Table 5.3 gives the relevant reduction factors at different temperature levels.

$$a = 1.0181\text{-}0.00128{\cdot}T \qquad\qquad\qquad (5.5)$$

where a is the residual stress reduction factor and T is the temperature in °C in the range of $20 \leq T \leq 800°C$.

Table 5.3   Residual Stress Reduction Factor

Temp.(°C)	20	200	350	500	650	800
a	1.00	0.76	0.57	0.38	0.19	0.00

The residual stresses were modelled using the ABAQUS*INITIAL CONDITIONS option with TYPE=STRESS, USER. The user defined initial stresses were created using the SIGINI, FORTRAN user subroutine. It was necessary to ensure that the coordinate system for stress components was correctly defined to produce the residual stresses on the required axis. This was achieved by defining the variables of SIGNI for each axis. For this purpose, the global coordinate system was used defining the stress values on each element. This subroutine defines the variation of the residual stress through the thickness. Five interpolation points were used to vary the residual stress through the thickness. It was ensured that tension residual stress on the outside of the fold and compression on the inside were correctly defined as shown in Figures 5.6 (a) and 5.7 (a). The subroutine including the user defined residual stress distribution is given in Appendix D.

The specimens were then analysed only with the residual stresses by considering the same boundary conditions as used in the experimental model. The details of the contours of residual stresses are presented in Figures 5.6 (b) and 5.7 (b) for Types A and B sections, respectively. The ultimate failure load was determined with and without residual stresses and the residual stresses were found to show a small (about 0.2%) influence on the ultimate failure load when the column failed by distortional buckling.

5.3.5 Material Properties

The material properties are one of the most important factors in the finite element analyses. The material properties required for elastic and nonlinear analyses are Young's modulus of elasticity, yield strength and Poisson's ratio. They should be the same as the material properties of experimental specimens to verify the finite element model. Therefore all the material properties were measured and, the measured elasticity modulus and yield strength values were used in the analyses. In addition, they were also determined based on both compression and tension coupon tests (see Chapter 3). The yield strengths obtained from these two methods showed that the compression coupon test results are lower than that of tension coupon test results. Therefore both values obtained from compression and tension coupon tests were included separately in the finite element analyses to determine their effects on the behaviour of compression members.
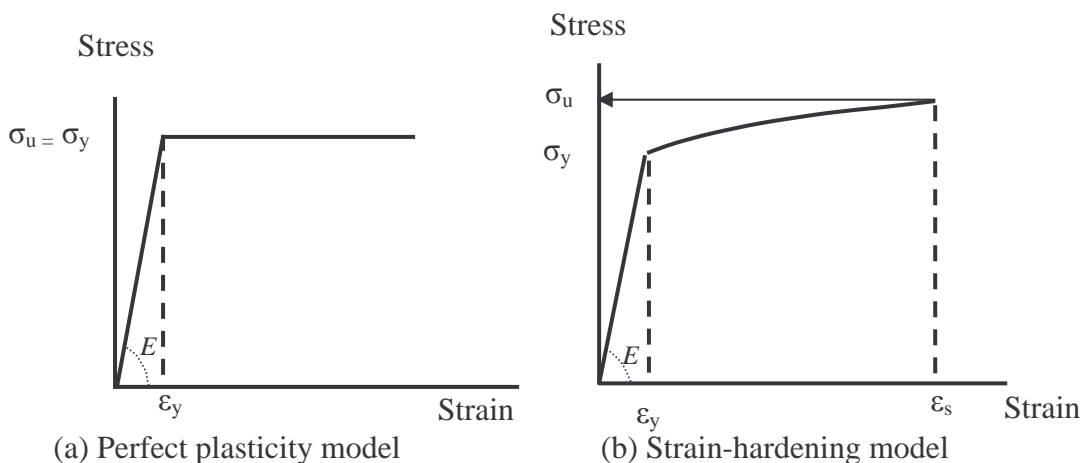
Figure 5.8   Stress-strain Relationship

All the specimens were modelled based on isotropic strain-hardening behaviour. The isotropic strain-hardening behaviour is more accurate than the perfect plasticity behaviour since it can simulate the actual mechanical properties behaviour as shown in Figure 5.8. Perfect plasticity behaviour assumes no strain hardening and no change of yield strength with increasing plastic strain. True stress and logarithmic strain are given to imply the relevant stress and strain values for all these finite

element models. The nominal stress-strain data were converted to true stress and logarithmic plastic strain from the following equations.

$$\sigma_{true} = \sigma_{nom}\left(1 + \varepsilon_{nom}\right)$$ 5.6(a)

$$\varepsilon_{ln}{}^{pl} = \ln\left(1 + \varepsilon_{nom}\right) - \frac{\sigma_{true}}{E}$$ 5.6(b)

where E = Young's modulus, σ_{nom} = nominal stress, σ_{true} = true stress, ε_{nom} = nominal strain, $\varepsilon_{ln}{}^{pl}$ = logarithmic plastic strain

.
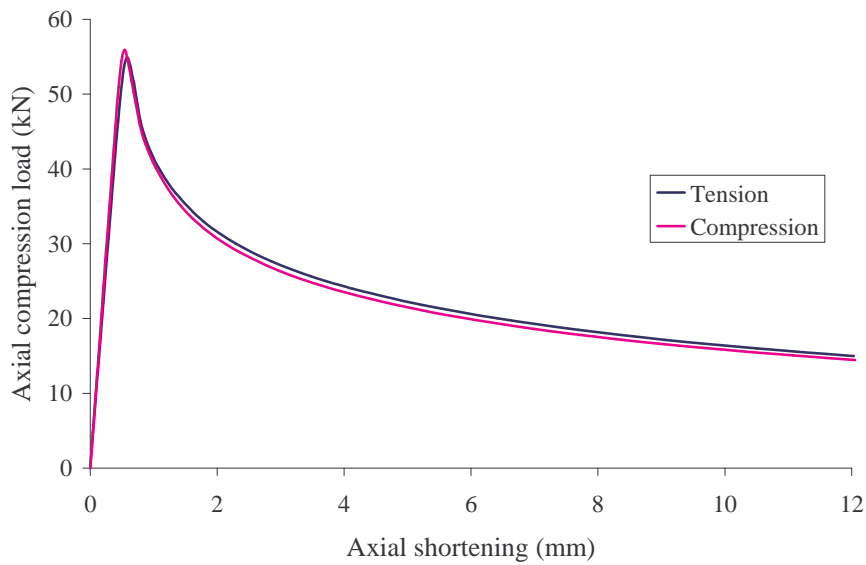
Figure 5.9   Comparison of FEA Load-Shortening Curves for 0.95 mm G550 Type B   Specimen with Mechanical Properties based on Tension and Compression Coupon Tests

The ultimate failure loads based on the stress-strain curves from tension and compression coupon tests showed negligible differences, ie. less than 1% (see Figure 5.9). Therefore stress-strain curves from tensile coupon tests were used in the finite element analysis since only the tensile coupon test results are available for elevated temperatures.

The reduction of mechanical properties at elevated temperatures significantly influences the elastic distortional buckling and the ultimate strength behaviour. Therefore the mechanical properties should be explicitly considered in the finite

element analyses for elevated temperatures. As stated in Chapter 3, the mechanical properties are reduced with increasing temperature. Therefore the measured mechanical properties were used in the finite element analyses. However, it was assumed that the Poisson's ratio remains unchanged with the temperature as stated in Ranby, (1999). Effect of mechanical properties on the distortional buckling behaviour was further studied at ambient and elevated temperatures in this research.

5.3.6 Loading and Boundary Conditions

Appropriate boundary conditions must be included in the finite element model in order to simulate the test specimens as close as possible. Fixed-end condition was used in the experimental investigation since it was easier to build than the pin-end condition (see Chapter 4). The end plate was used with a groove to fix the ends of the specimen properly so that no rotations were allowed in the ends. The geometric centroids of the specimen and the end plates were kept the same so that no additional moments were created.
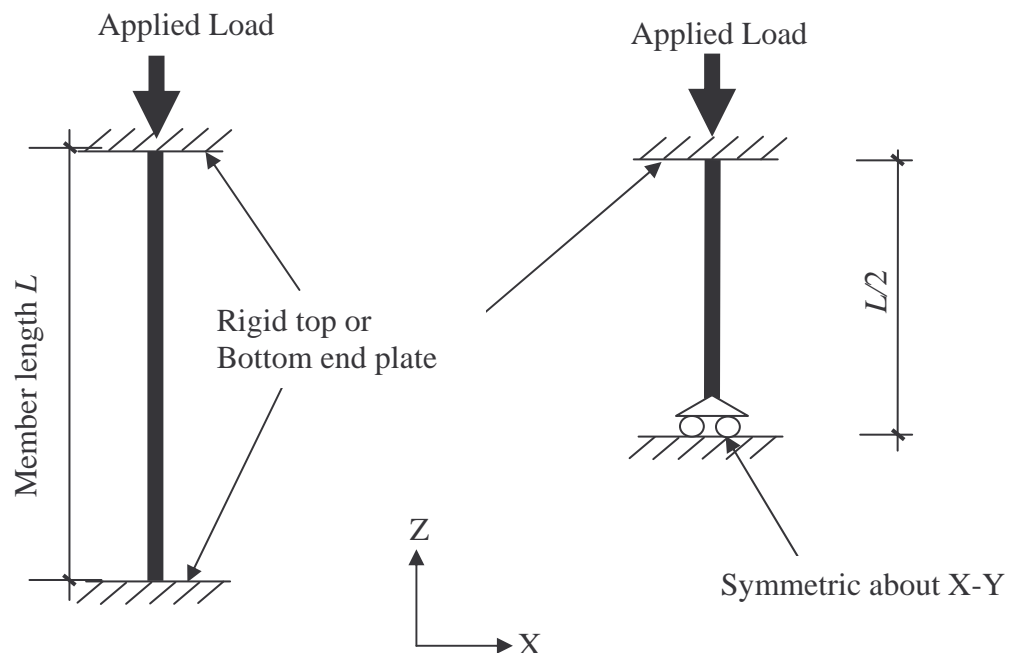
Figure 5.10   Boundary Conditions

In the finite element model, the loading direction was given by the Z-axis (compression load was given as a negative value). The X-axis was parallel with the flanges by pointing to the right side of the paper while the Y-axis was perpendicular to the paper. Three different models: full-wave length, half-wave length and quarter-wave length can be considered to simulate the symmetric buckling waveform. However if the full distortional buckling wave length is considered it becomes the half-wave length of the global buckling mode. Therefore the column length was selected as half-wave length of the distortional buckling failure mode even in the experimental investigation. Half of the column length was selected for all the models in this study (see Figure 5.10). This half column length was adequate to simulate the experimental conditions and to investigate the experimental behaviour of the distortional buckling failure mode due to the symmetric nature of the distortional buckling waveform. On the other hand, the half length model is more economical than the full column length model since time consumption and disk usage are less.

The displacement boundary condition for the fixed-end condition of the top was simulated as 12456, so that no rotations were allowed in any directions and no translations were allowed in horizontal directions. This means displacements were restrained in X and Y directions and only rotations were restrained in all three directions at the top. The upper boundary conditions introduced to the centroid node and they were distributed to the other nodes through the MPC as shown in Figures 5.11 (a) and (b) for Type A and B specimens, respectively. The boundary conditions at the mid length was given as 345 to the edge nodes, so that translations were restrained in Z direction and rotations were restrained in both X and Y directions. Figures 5.11 (a) and (b) show the provided boundary conditions in the upper and mid nodes for both types of sections with comparison of experimental conditions.

Axial compression load was defined as a concentrated nodal force at the top. It was then distributed to the ends of the specimen through the MPC. A node was created in the geometric centroid of the section and it was then connected to the edge of the section through the edge nodes to create the MPC. Each node on the edge of the sections is considered a dependent node. These dependent nodes were then connected to the independent node which was created at the geometric centroid of the sections. They were connected by using rigid beams and hence they were

controlled by the independent node. Hence the applied concentrated force can be equally distributed along the edges of the section.
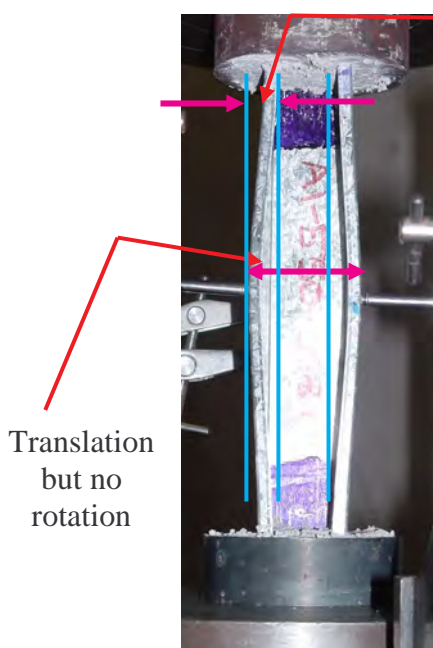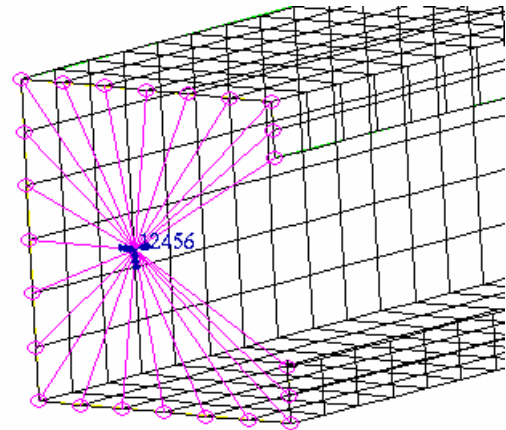
No translation or rotation
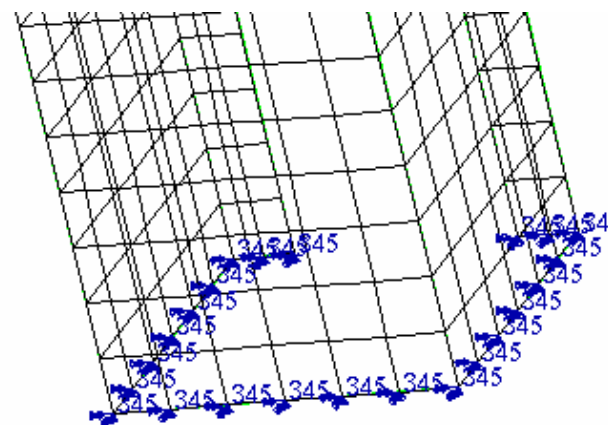
Translation but no rotation

(a) Type A section

Figure 5.11   Applied Boundary Conditions

No translation or rotation

Translation but no rotation
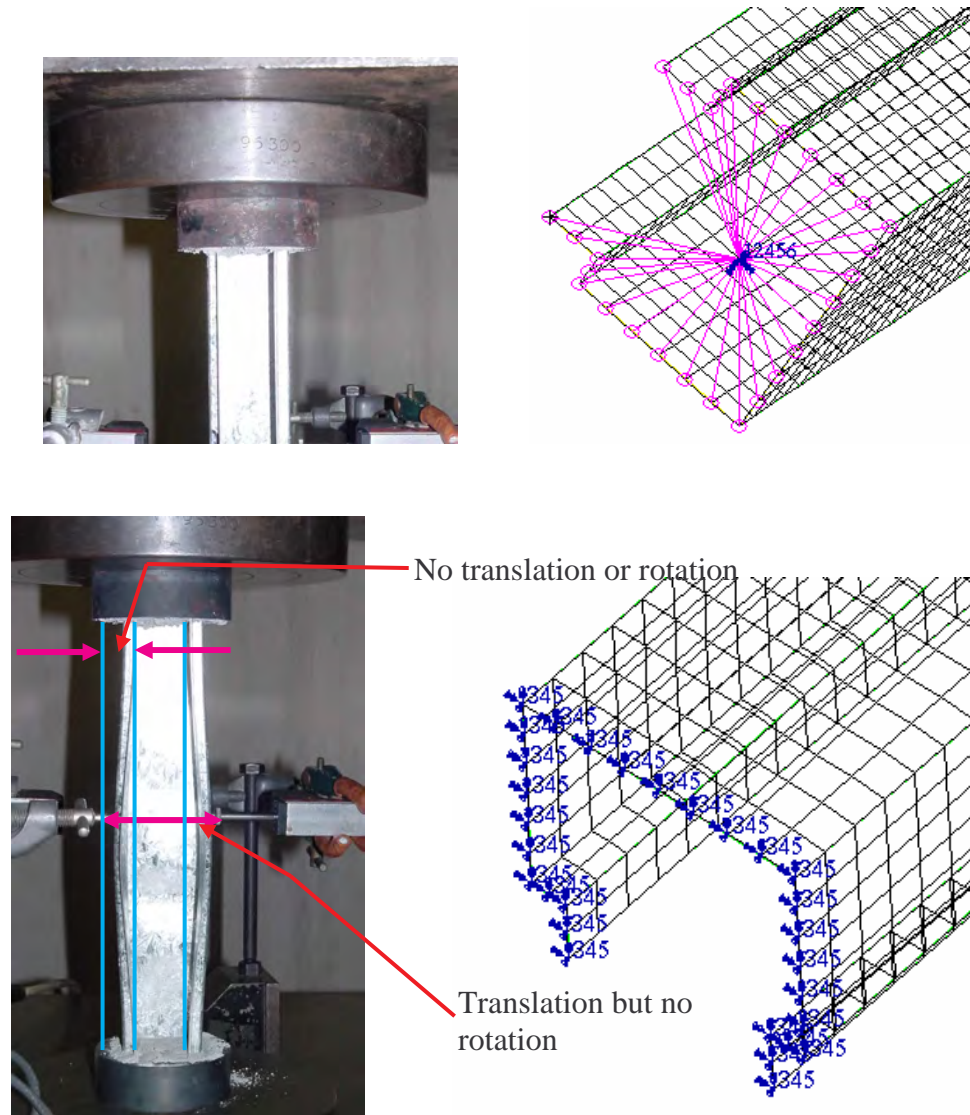
(b) Type B section

Figure 5.11   Applied Boundary Conditions

Figure 5.12 shows the methods of generating boundary conditions from multi-purpose constraints (MPC). Measured specimen sizes were used in the finite element model. The coating thickness was measured by using a special coating thickness gauge. Since the strength of the coating is very small compared to the strength of steel, the base metal thickness was used in all the models.
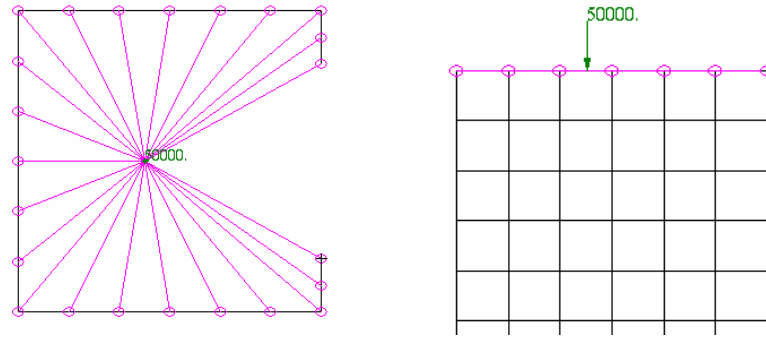
(a) Type A section
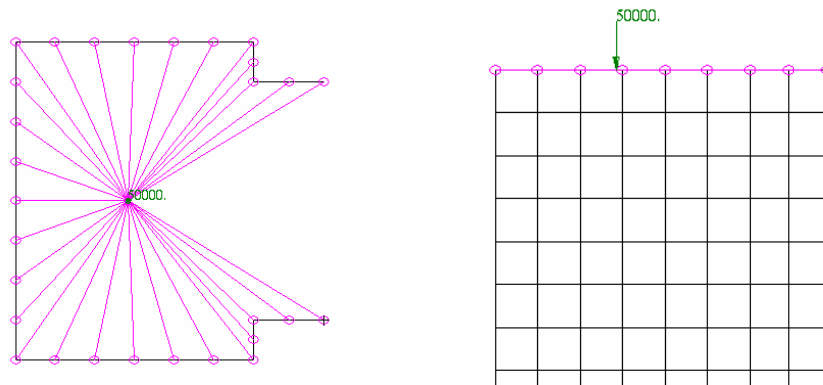
(b) Type B section

Figure 5.12   Load Application through MPC

5.3.7   Analysis Methods

Finite element analyses were undertaken by using half length models. Six different sections were modelled for two types (Types A and B) and three thicknesses. The buckling half-wave lengths and the section dimensions were first determined using the results of Thin-wall program and then checked from ABAQUS for fixed-end conditions (see Chapter 4). The finite element modelling was undertaken using the MSC/PATRAN pre-processing program. The model was created in the MSC/PATRAN environment and submitted to ABAQUS. The modelled sections were analysed and the results compared with experimental results. The loads and deformations were also read from the MSC/PATRAN post-processing facilities. Two types of analyses were undertaken, that is, the bifurcation buckling analysis to determine the elastic distortional buckling loads and modes, and the nonlinear

analysis to determine the ultimate loads and deformations. The half length models were then validated using experimental results.

5.4 Validation of the Finite Element Model

Finite element analyses (FEA) are increasingly used for research purposes since they show many advantages when compared with experimental studies. Valuable time and physical resources can be saved by using finite element analyses rather than experiments. However, the validity of FEA must be established before undertaking detailed parametric studies. As discussed in Chapter 4, experiments were undertaken for both low and high strength steels by considering two different sections and three different thicknesses with six different temperatures. Same specimens were used in FEA, that is, Types A and B specimens made of G250 and G550 steels and thicknesses of 0.6, 0.8 and 0.95 mm. The selected temperatures were 20, 200, 350, 500, 650 and 800°C.

Both the experimental elastic buckling and ultimate loads were compared with the corresponding FEA results. Although the ultimate load could be observed accurately in the experiments at all the temperatures, the elastic buckling load was only obtained based on visual observations for ambient temperature, while it could not be obtained at elevated temperatures. Therefore, as discussed in Chapter 4, Venkataramaiah and Roordar's (1982) method was used to obtain the elastic buckling load at elevated temperatures.

5.4.1 Elastic Buckling Analysis

Elastic buckling analyses were conducted to determine the critical buckling load and the associated buckling modes. The relevant elastic buckling modes were then used to include the geometric imperfections in the nonlinear analyses. The critical distortional buckling loads were used to predict the ultimate load of the compression members by using the direct strength method and the AS/NZS 4600 design rules. The predictions from the direct strength method and the AS/NZS 4600 design rules

were compared with experimental results in Chapter 4. Tables 5.4 and 5.5 show the comparison of elastic buckling loads from FEA and experiments.

It was noticed that the first buckling mode was critical in many cases, but was different in some cases. Therefore it was considered useful to apply a combination of two or three buckling modes due to the complexity of the distribution of initial geometric imperfections. On the other hand, the initial geometric imperfections can be applied in the opposite direction to determine the ultimate failure mode. Figure 5.13 shows the elastic buckling mode and the ultimate failure mode from FEA and experimental results for 0.95 mm G550 steel specimens at ambient temperature. Elastic buckling mode from FEA shows both flanges moving inwards while experimental results show both flanges moving outwards. This is considered to be mainly due to the imperfection direction and hence the imperfection direction was changed in the nonlinear analyses. Therefore further studies were undertaken to observe the effect of initial geometric imperfection on failure modes.

As shown in Tables 5.4 and 5.5 the elastic distortional buckling loads determined from FEA were compared with the experimental elastic buckling loads determined using Venkataramaiah and Roorda's (1982) method. This method gives the experimental buckling loads while FEA gives the theoretical buckling loads. The results obtained from these two methods do not compare well. At very high temperatures the elastic buckling loads obtained from FEA are four or five times higher than the buckling loads obtained from Venkataramaiah and Roorda's method. The FEA results are higher than the experimental results in many cases (around 80%). The main reason for this may be due to the effects of geometric imperfections and residual stresses. Therefore it can be stated that the effect of geometric imperfections and residual stresses show a high influence on the elastic distortional buckling load. However, as discussed in Chapter 4, the method suggested by Venkataramaiah and Roorda is for local buckling at ambient temperature and may not be valid for distortional buckling at elevated temperatures or even at ambient temperature. Therefore the elastic distortional buckling loads obtained from FEA were used in further studies.

Table 5.4   Comparison of Elastic Distortional Buckling Loads obtained from FEA and Experiments for Type A specimens

Specimen	Elastic Distortional Buckling Load (kN)		Exp/FEA
	FEA	Exp	
G550-0.6-20-A	20.65	19.00	0.920
G550-0.6-200-A	16.40	14.75	0.899
G550-0.6-350-A	12.97	13.65	1.052
G550-0.6-500-A	8.26	6.91	0.837
G550-0.6-650-A	5.16	2.27	0.440
G550-0.6-800-A	1.11	0.72	0.649
G250-0.6-20-A	15.08	13.20	0.875
G250-0.6-200-A	11.97	9.25	0.773
G250-0.6-350-A	9.04	5.85	0.647
G250-0.6-500-A	6.80	3.75	0.552
G250-0.6-650-A	3.81	1.85	0.486
G250-0.6-800-A	0.68	0.60	0.882
G550-0.8-20-A	44.04	31.00	0.704
G550-0.8-200-A	36.85	27.73	0.753
G550-0.8-350-A	29.10	23.50	0.808
G550-0.8-500-A	17.46	12.95	0.742
G550-0.8-650-A	15.46	4.32	0.279
G550-0.8-800-A	5.42	1.75	0.323
G250-0.8-20-A	36.51	20.00	0.548
G250-0.8-200-A	38.67	17.50	0.453
G250-0.8-350-A	20.53	10.25	0.499
G250-0.8-500-A	21.08	7.05	0.334
G250-0.8-650-A	12.67	3.28	0.259
G250-0.8-800-A	1.43	1.33	0.930
G550-0.95-20-A	53.10	42.00	0.791
G550-0.95-200-A	49.11	37.67	0.767
G550-0.95-350-A	40.09	31.20	0.778
G550-0.95-500-A	28.02	18.50	0.660
G550-0.95-650-A	16.84	4.50	0.267
G550-0.95-800-A	7.80	1.78	0.228
G250-0.95-20-A	55.01	32.00	0.582
G250-0.95-200-A	50.89	25.04	0.492
G250-0.95-350-A	36.03	17.98	0.499
G250-0.95-500-A	26.68	10.32	0.387
G250-0.95-650-A	19.25	4.94	0.257
G250-0.95-800-A	4.95	1.50	0.303

Table 5.5   **Comparison of Elastic Distortional Buckling Loads obtained from FEA and Experiments for Type B specimens**

Specimen	Elastic DistortionalBuckling Load (kN)		Exp/FEA
	FEA	Exp	
G550-0.6-20-B	18.69	23.00	1.230
G550-0.6-200-B	14.97	20.10	1.343
G550-0.6-350-B	12.12	18.50	1.526
G550-0.6-500-B	7.54	10.60	1.406
G550-0.6-650-B	4.71	3.17	0.673
G550-0.6-800-B	1.02	1.00	0.980
G250-0.6-20-B	13.04	15.40	1.181
G250-0.6-200-B	10.90	14.75	1.353
G250-0.6-350-B	8.24	8.75	1.062
G250-0.6-500-B	6.19	5.85	0.944
G250-0.6-650-B	3.47	2.40	0.692
G250-0.6-800-B	0.65	0.85	1.308
G550-0.8-20-B	38.85	38.00	0.978
G550-0.8-200-B	32.00	32.75	1.023
G550-0.8-350-B	25.60	31.00	1.211
G550-0.8-500-B	15.16	14.62	0.965
G550-0.8-650-B	12.80	4.25	0.332
G550-0.8-800-B	4.80	1.55	0.323
G250-0.8-20-B	33.00	26.50	0.803
G250-0.8-200-B	29.34	22.96	0.783
G250-0.8-350-B	18.13	14.40	0.794
G250-0.8-500-B	15.99	8.40	0.525
G250-0.8-650-B	11.21	3.85	0.343
G250-0.8-800-B	1.26	1.40	1.111
G550-0.95-20-B	71.86	50.00	0.696
G550-0.95-200-B	62.88	46.34	0.737
G550-0.95-350-B	51.33	38.82	0.756
G550-0.95-500-B	29.94	21.50	0.718
G550-0.95-650-B	21.55	4.95	0.230
G550-0.95-800-B	10.00	1.91	0.191
G250-0.95-20-B	70.64	35.00	0.495
G250-0.95-200-B	65.34	28.31	0.433
G250-0.95-350-B	46.27	19.02	0.411
G250-0.95-500-B	41.15	11.38	0.277
G250-0.95-650-B	24.72	5.10	0.206
G250-0.95-800-B	6.29	1.90	0.302
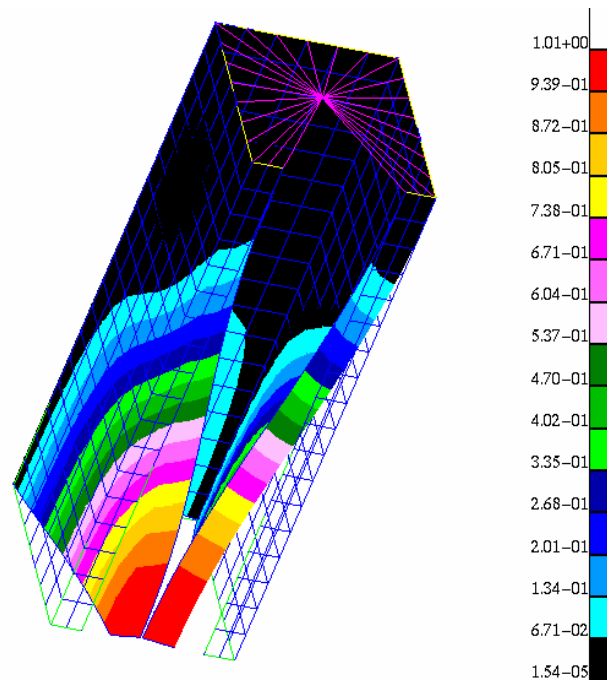
(a) Elastic buckling mode

FEA

Experiment
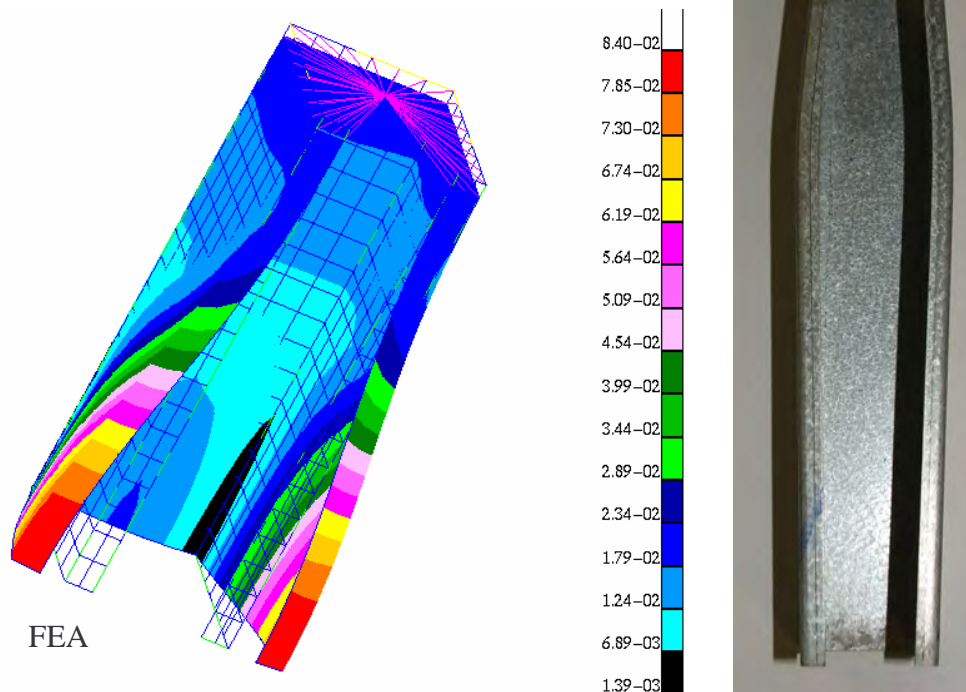
(b) Ultimate failure mode

Figure 5.13   Elastic Buckling and Ultimate Failure Modes

5.4.2 Nonlinear Analysis

Nonlinear analyses were undertaken by using the appropriate geometric imperfection values (see Section 5.3.3) with the critical elastic buckling modes. The geometric imperfections were mainly included as the distortional buckling of the sections i.e. both flanges moving outward, both flanges moving inward and one flange moving outward while other flange moving inward depending upon the elastic buckling mode. The residual stresses were also applied to the model. As discussed earlier the residual stresses decrease with increasing temperatures. Therefore appropriate reduction factors (see Section 5.3.4) were included with increasing temperatures.
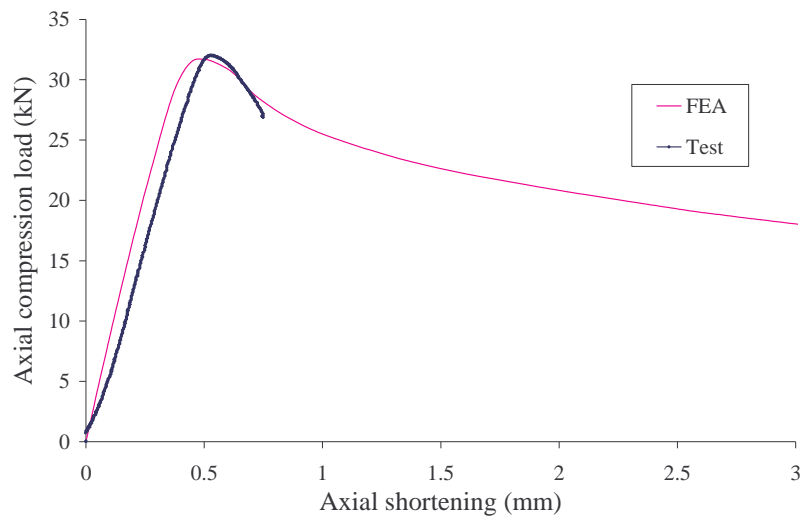
(a) Axial shortening curves
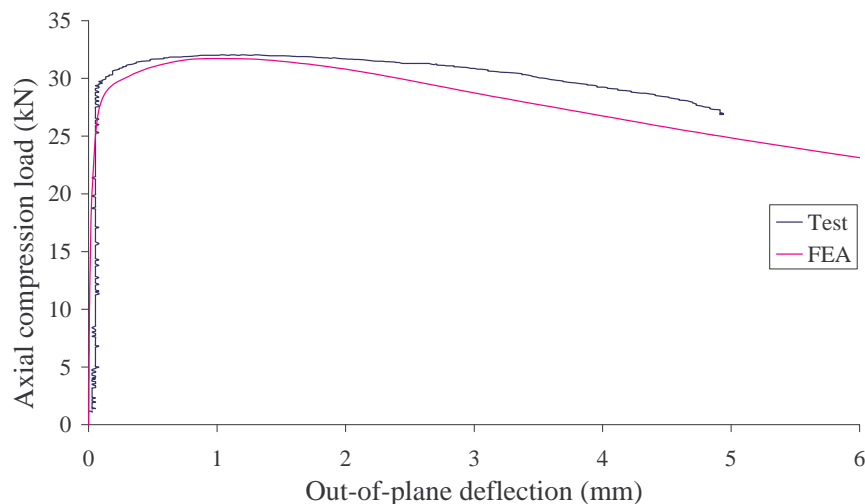
(b) Out-of-plane deflection curves

Figure 5.14   Comparison of Experimental and FEA Load-Deformation Curves for 0.8 mm G550 Type A Specimen at 20°C
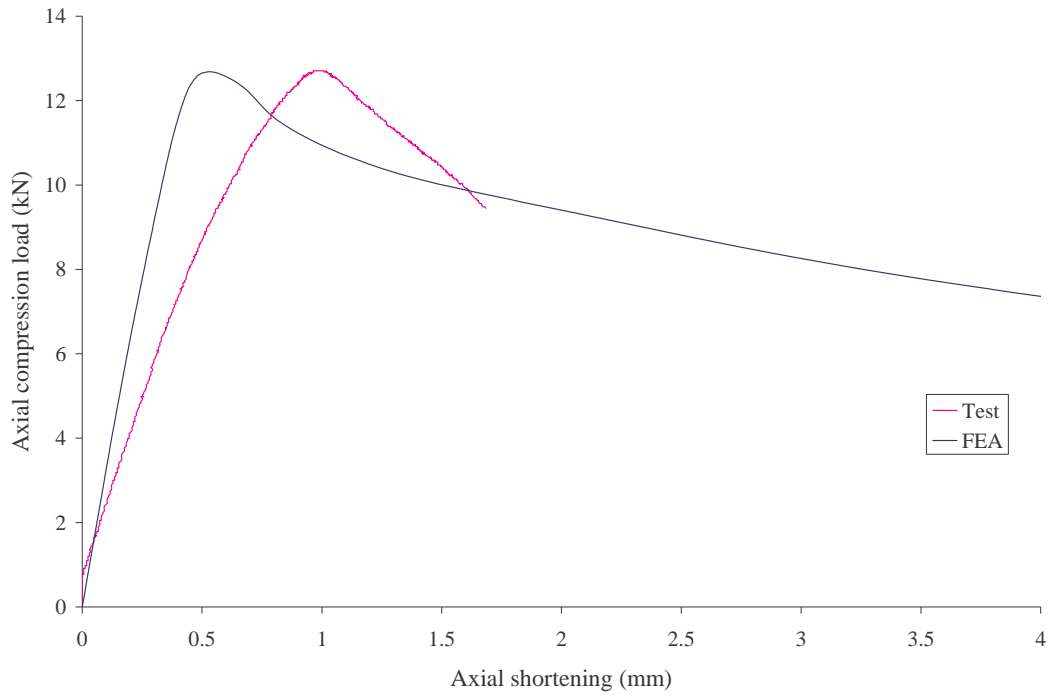
(a) Axial shortening curves
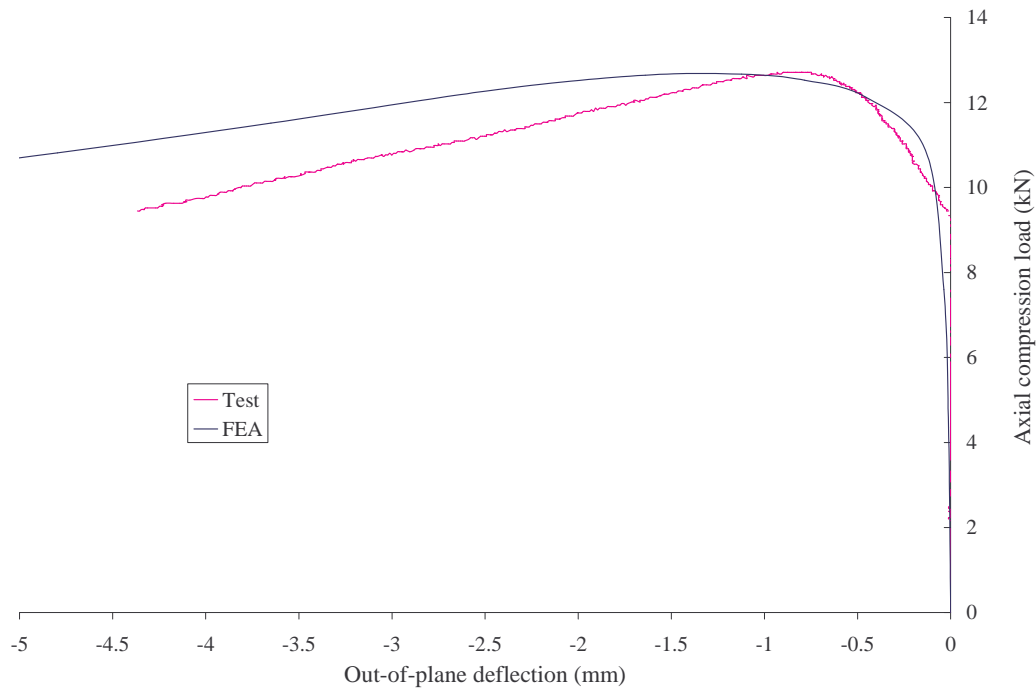
(b) Out-of-plane deflection curves

Figure 5.15   Comparison of Experimental and FEA Load-Deformation Curves for 0.8 mm G550 Type A Specimen at 500°C
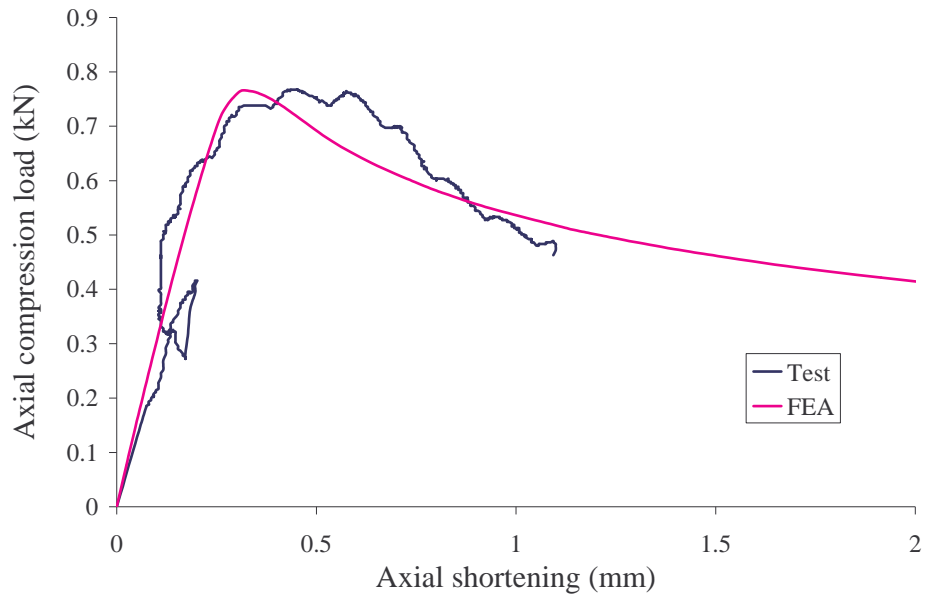
(a) Axial shortening curves

(b) Out-of-plane deflection curves

Figure 5.16   Comparison of Experimental and FEA Load-Deformation Curves for 0.6 mm G550 Type A Specimen at 800°C
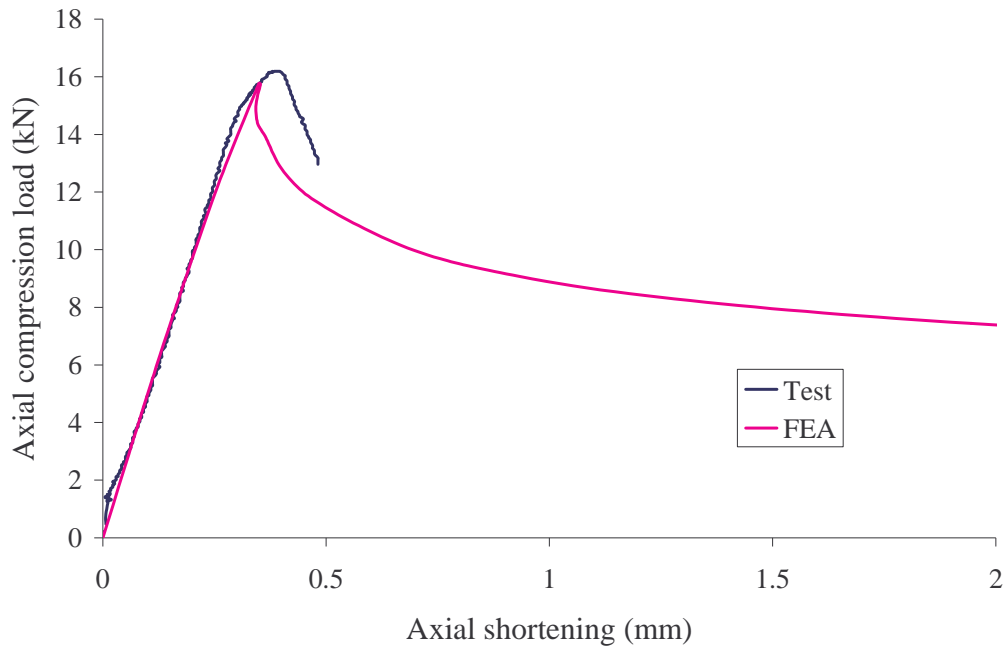
(a) Axial shortening curves
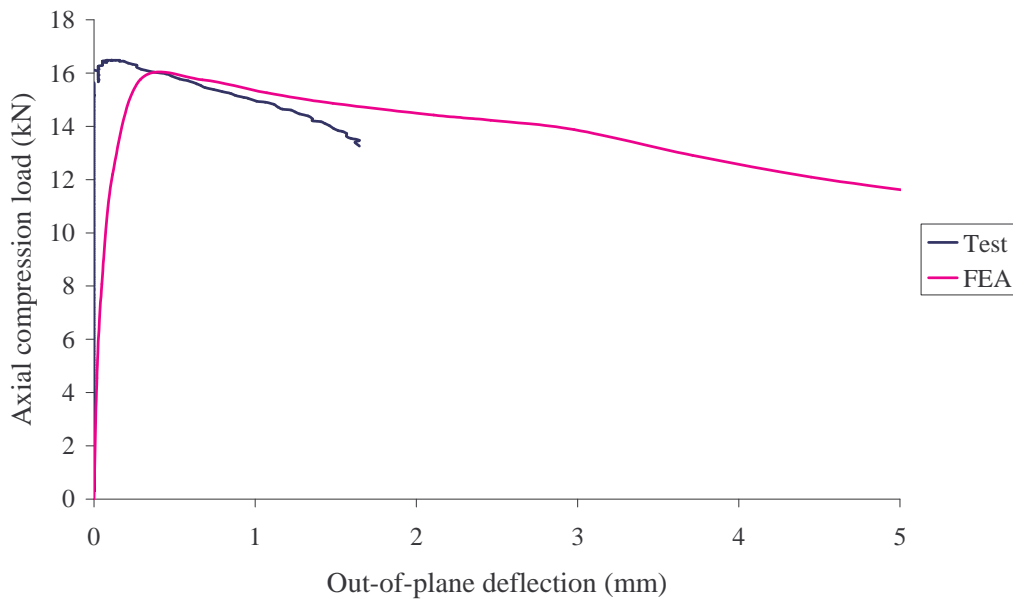
(b) Out-of-plane deflection curves

**Figure 5.17   Comparison of Experimental and FEA Load-Deformation Curves
for 0.6 mm G250 Type B Specimen at 20°C**
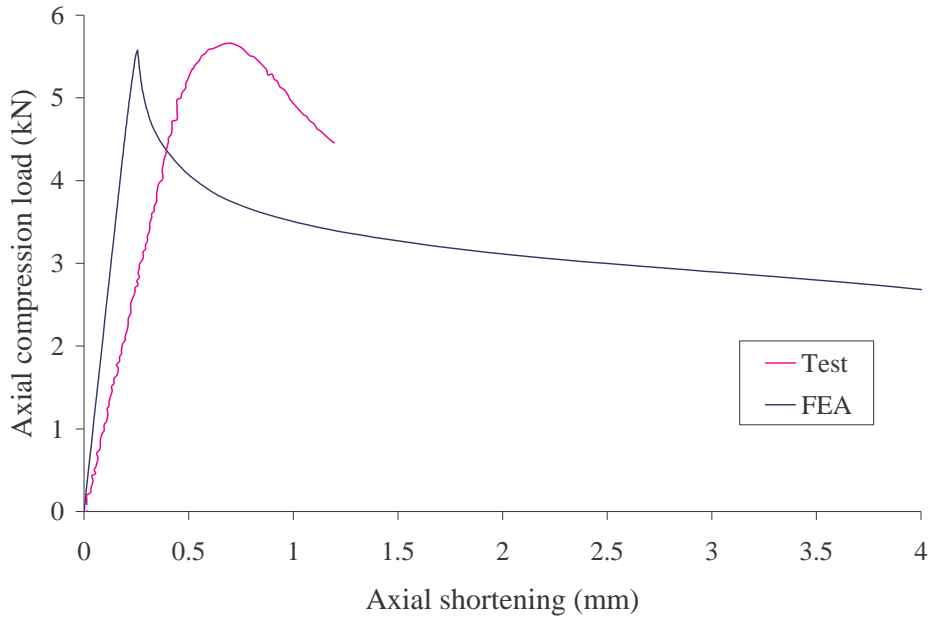
(a) Axial shortening curves
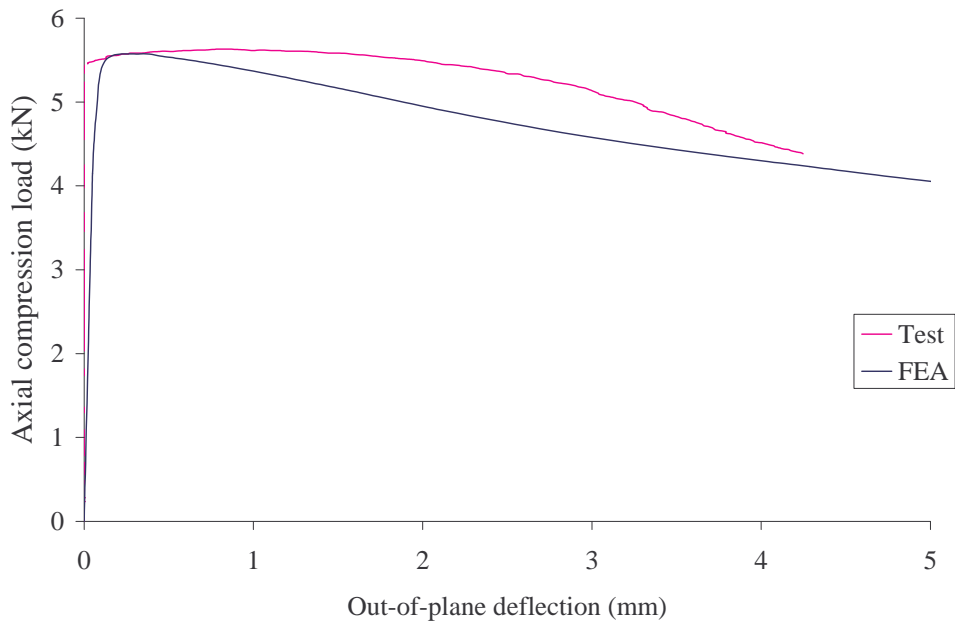
(b) Out-of-plane deflection curves

Figure 5.18   Comparison of Experimental and FEA Load-Deformation Curves for 0.6 mm G250 Type B Specimen at 500°C
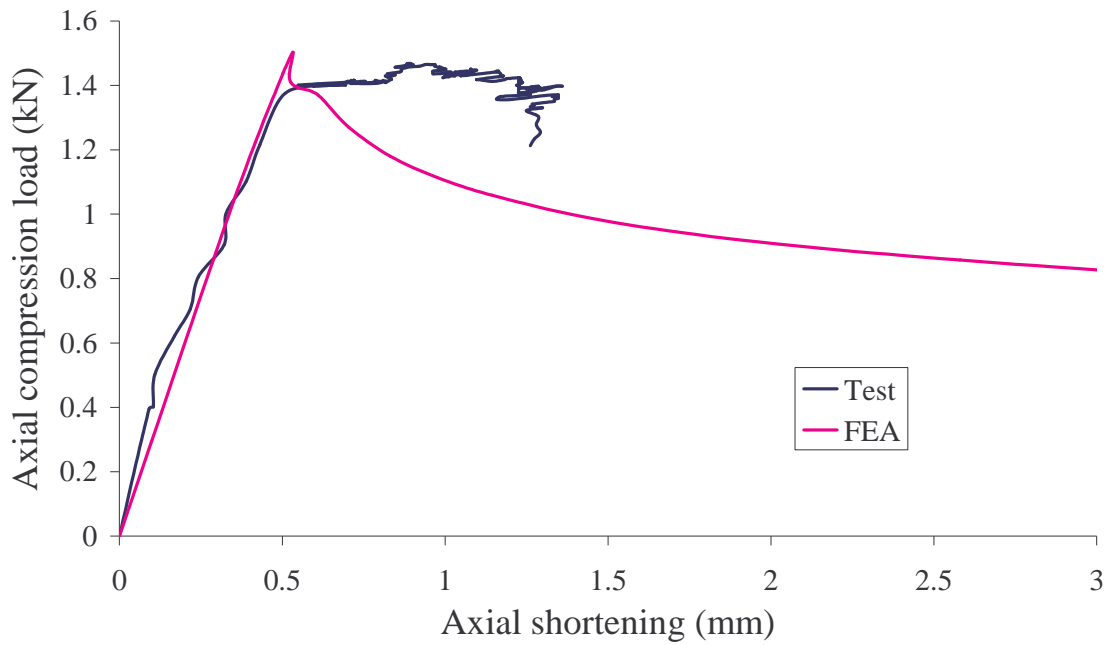
(a) Axial shortening curves
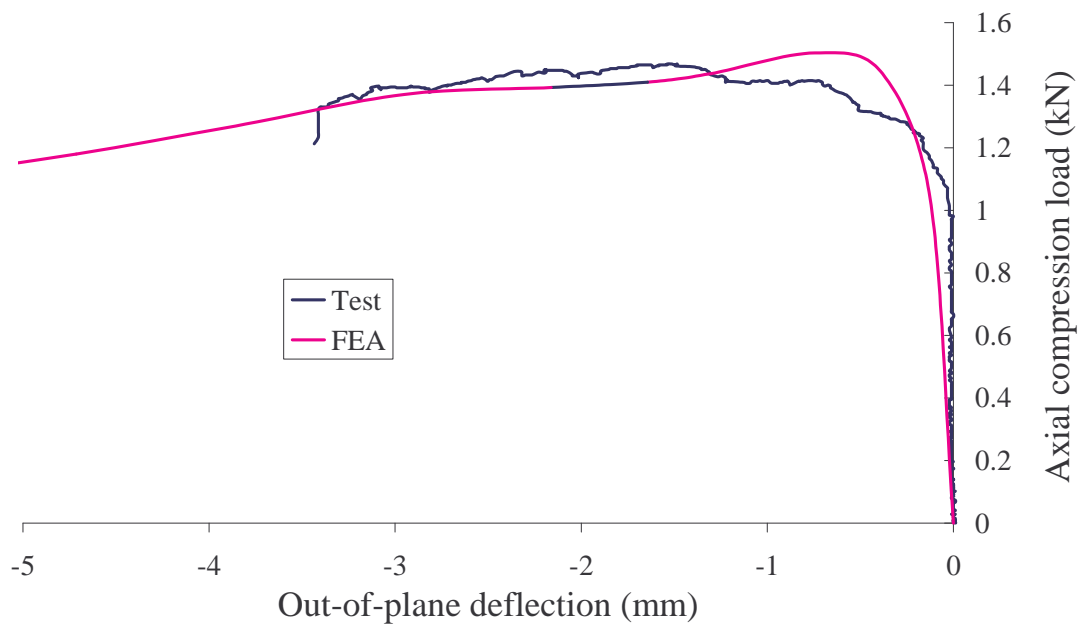
(b) Out-of-plane deflection curves

Figure 5.19   Comparison of Experimental and FEA Load-Deformation Curves
for 0.8 mm G250 Type B Specimen at 800°C

Axial compression load versus axial shortening curves and the axial compression load versus out-of-plane deflection curves were determined for all the tested specimens. The FEA curves were obtained using the RIKs method which enabled the unloading function in the nonlinear analysis. Figures 5.14 to 5.19 show the axial compression load versus axial shortening curves and axial compression load versus out-of-plane deflection for Type A and B specimens. Figures 5.14 and 5.17 show the results at ambient temperature, Figures 5.15 and 5.18show the results at 500°C and Figures 5.16 and 5.19 show the results at 800°C. All the other load-deformation curves are presented in Appendix B.

The out-of-plane deflections were measured at the middle of the flanges in Type A specimen and slightly below the middle of the flanges in Type B specimens. All the measured dimensions were included in the FEA to obtain the out-of-plane deflection at the same point as in the experiment. The load-deformation curves show that the experimental and FEA results are in good agreement. However, there is a small difference between experimental and FEA curves in some cases. This is because the available axial shortening measuring instrument and the LVDT used did not have a very high accuracy. Since the difference is about 0.5 to 1 mm it can be considered negligible.

Tables 5.6 and 5.7 and Figures 5.20 (a) and (b) present the comparison of ultimate loads obtained from experiments and the FEA. It proves that all the FEA models show very good agreement with the experimental results. Since all the load-deformation curves and ultimate loads agree well with the experimental results the finite element model was used in further investigations into the distortional buckling behaviour of light gauge cold-formed steel members. The same model was used in the parametric studies by varying the relevant parameters including section geometry.

Table 5.6   Comparison of Ultimate Loads from Experiments and FEA for Type A Specimens

Specimen	Ultimate Loads (kN)					Exp/ FEA
	Exp 1	Exp 2	Exp 3	Exp-Ave	FEA	
G550-0.6-20-A	19.74	19.63		19.68	19.75	0.999
G550-0.6-200-A	15.05	15.34		15.20	16.05	0.956
G550-0.6-350-A	13.26	13.88		13.57	14.60	0.951
G550-0.6-500-A	7.16	6.73		6.95	7.20	0.994
G550-0.6-650-A	2.54	2.19		2.37	2.57	0.991
G550-0.6-800-A	0.55	0.72	0.77	0.68	0.76	0.895
G250-0.6-20-A	13.15	12.30	13.07	12.84	12.45	1.031
G250-0.6-200-A	9.70	8.83	9.38	9.30	9.45	0.984
G250-0.6-350-A	5.60	6.17		5.89	5.55	1.009
G250-0.6-500-A	3.84	3.81		3.83	3.61	1.057
G250-0.6-650-A	1.88	1.94		1.91	1.88	1.014
G250-0.6-800-A	0.62	0.61		0.61	0.64	0.953
G550-0.8-20-A	32.96	29.22		31.09	31.70	0.981
G550-0.8-200-A	27.87	26.51		27.19	26.95	1.009
G550-0.8-350-A	24.61	23.55	23.07	23.74	23.60	1.006
G550-0.8-500-A	13.22	12.71	12.78	12.90	12.65	1.020
G550-0.8-650-A	4.24	4.25		4.24	4.16	1.020
G550-0.8-800-A	1.71	1.74		1.73	1.78	0.972
G250-0.8-20-A	20.32	19.95	20.80	20.36	20.25	1.005
G250-0.8-200-A	17.72	16.92	17.20	17.28	17.65	0.979
G250-0.8-350-A	10.64	10.53	9.54	10.23	9.75	1.050
G250-0.8-500-A	7.04	7.26	7.05	7.12	7.10	1.003
G250-0.8-650-A	3.20	3.17		3.18	3.11	1.025
G250-0.8-800-A	1.32	1.40		1.36	1.32	1.030
G550-0.95-20-A	42.22	42.62	43.80	42.88	42.50	1.009
G550-0.95-200-A	35.27	38.42	38.96	37.55	37.00	1.015
G550-0.95-350-A	32.52	29.30		30.91	30.35	1.018
G550-0.95-500-A	19.41	19.63		19.52	19.80	0.986
G550-0.95-650-A	4.42	4.41	4.72	4.52	4.33	1.044
G550-0.95-800-A	1.84	1.77		1.80	1.89	0.952
G250-0.95-20-A	32.04	31.42	30.84	31.43	31.65	0.993
G250-0.95-200-A	24.65	25.63	25.23	25.17	25.20	0.999
G250-0.95-350-A	16.90	17.90		17.40	15.50	1.090
G250-0.95-500-A	10.36	10.40		10.38	9.75	1.063
G250-0.95-650-A	4.91	5.04		4.98	4.70	1.045
G250-0.95-800-A	1.47	1.46		1.47	1.56	0.942
Mean						1.002
COV						0.038

Table 5.7   Comparison of Ultimate Loads from Experiments and FEA for Type B Specimens

| Specimen | Ultimate Loads (kN) | | | | | Exp/ FEA |
	Exp 1	Exp 2	Exp 3	Exp-Ave	FEA	
G550-0.6-20-B	23.88	24.32		24.10	24.80	0.972
G550-0.6-200-B	19.41	21.17	22.05	20.87	20.55	1.016
G550-0.6-350-B	18.20	19.23		18.71	18.85	0.993
G550-0.6-500-B	10.37	9.73		10.05	10.05	1.000
G550-0.6-650-B	3.25	3.13		3.19	3.54	0.918
G550-0.6-800-B	1.08	1.00		1.04	1.11	0.937
G250-0.6-20-B	15.12	16.19		15.66	15.75	0.994
G250-0.6-200-B	14.54	14.72		14.63	14.05	1.041
G250-0.6-350-B	9.30	8.94		9.12	8.30	1.077
G250-0.6-500-B	5.63	6.11		5.87	5.60	1.006
G250-0.6-650-B	2.51	2.44		2.48	2.42	1.024
G250-0.6-800-B	0.89	0.83		0.86	0.88	0.977
G550-0.8-20-B	39.11	40.06		39.59	39.65	0.998
G550-0.8-200-B	34.09	31.75		32.92	32.60	1.010
G550-0.8-350-B	29.11	27.68		28.40	28.25	1.005
G550-0.8-500-B	14.61	14.76		14.69	14.95	0.982
G550-0.8-650-B	4.28	4.49		4.38	4.73	0.950
G550-0.8-800-B	1.53	1.50		1.51	1.56	0.968
G250-0.8-20-B	25.31	26.59		25.95	24.70	1.025
G250-0.8-200-B	22.12	24.02		23.07	21.50	1.029
G250-0.8-350-B	14.21	14.79		14.50	14.45	0.983
G250-0.8-500-B	8.51	8.40		8.46	8.40	1.007
G250-0.8-650-B	4.08	4.08		4.08	4.25	0.960
G250-0.8-800-B	1.46	1.41		1.43	1.50	0.953
G550-0.95-20-B	53.76	53.39		53.58	55.00	0.974
G550-0.95-200-B	40.69	46.25	46.95	44.63	47.60	0.986
G550-0.95-350-B	38.34	39.73		39.04	38.35	1.018
G550-0.95-500-B	21.72	22.08		21.90	22.50	0.973
G550-0.95-650-B	4.97	5.06		5.02	5.00	1.004
G550-0.95-800-B	1.93	1.96		1.95	2.05	0.951
G250-0.95-20-B	36.73	38.16		37.45	35.95	1.042
G250-0.95-200-B	29.15	27.65		28.40	29.10	0.976
G250-0.95-350-B	19.52	19.81		19.67	18.35	1.064
G250-0.95-500-B	12.12	11.35		11.74	11.45	1.025
G250-0.95-650-B	5.40	5.33		5.36	5.40	0.993
G250-0.95-800-B	1.97	1.92		1.94	1.93	1.01
Mean						1.018
COV						0.034

(a) Type A specimens

(b) Type B specimens

Figure 5.20   Comparison of Experimental and FEA Ultimate Loads

5.5 Finite Element Analyses Investigating a Number of Important Parameters

This section presents the details and results of a series of finite element analyses to investigate the number of important parameters and their effects on distortional buckling cold-formed steel compression members.

5.5.1 Distortional Buckling Modes

The distortional buckling modes obtained from experiments and FEA are also compared. As discussed in Chapter 4, three main failure modes were observed in both experiments and FEA as seen in Figure 5.21. The first and second modes involved both flanges moving outwards and both flanges moving inwards and were common for many specimens while the third mode involved one flange moving outward while the other flange moving inward, which occurred only in some specimens. The FEA also shows similar behaviour for half length models. Therefore the half length finite element model was used in the parametric studies.

It should be noted that the failure mode of the column was affected by the geometric imperfections. As discussed in Chapter 4, some identical columns showed all three buckling modes when tests were repeated. The only reason for this was the presence of geometric imperfections. Therefore the influence of geometric imperfections was studied by changing their direction and magnitude. As an example, the 0.95 mm G550 Type A specimen showed three types of buckling mode at 500°C when tests were repeated. However, the difference in the ultimate load was negligible. The failure mode of the same column was then obtained from FEA. Table 5.8 shows the experimental and FEA results obtained for this specimen. Since the difference between the ultimate loads corresponding to these three modes was negligible, it can be stated that geometric imperfections of the specimen govern the failure mode and hence the first elastic buckling mode is not critical in all the cases. Therefore it is useful to investigate the effect of initial geometric imperfections on the distortional buckling of light gauge steel compression members.
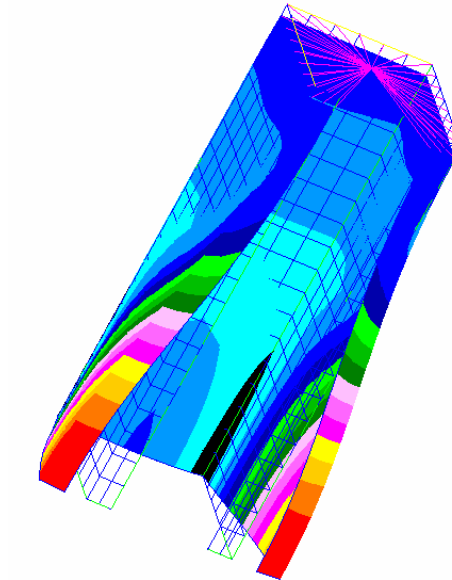
Experiments   FEA

(a) Both flanges moving outward

FEA
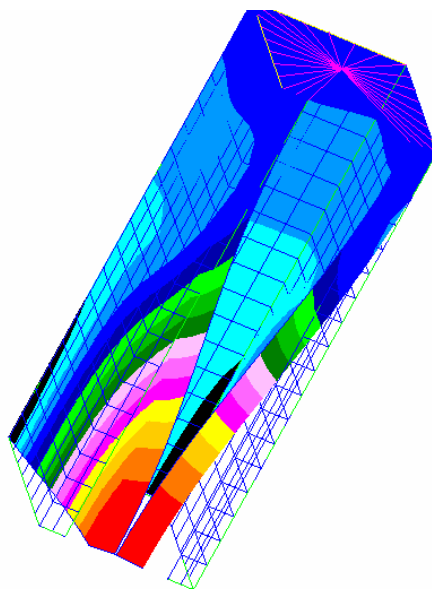
Experiments

(b) Both flanges moving inward

Figure 5.21   **Comparison of Experimental and FEA Failure Modes**

FEA
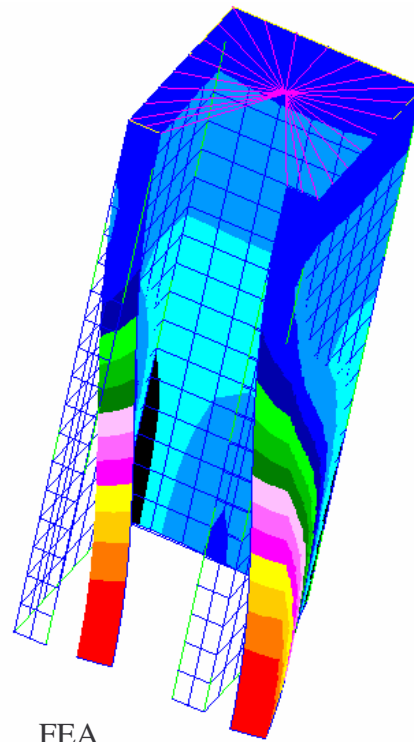
Experiments

(c) One flange moving outward while other one moving inward

Figure 5.21   Comparison of Experimental and FEA Failure Modes

Table 5.8   Experimental and FEA Results of 0.95 mm G550 Type A Specimens

Failure Mode	Ultimate Load (kN)	
	Experiments	FEA
Both flanges moving in	20.40	18.85
Both flanges moving out	19.41	19.35
Flanges moving in and out	19.63	19.80

5.5.2 Effect of Geometric Imperfection

The same test specimen considered in the last section, 0.95 mm G550 Type A specimen at 20 and 500°C, was considered here to study the effect of geometric imperfections. Elastic buckling analysis of this specimen gave the first mode as both flanges moving inwards and the third mode as one flange moving outward while other flange moving inward. When the geometric imperfection was included as a positive value in the first mode the ultimate failure mode was due to both flanges moving inward. In addition, when geometric imperfections are not present the ultimate mode is the same as the elastic buckling mode (both flanges moving inward). However, when it was included as a negative value, the ultimate failure mode was due to both flanges moving outward. This demonstrates that the direction of geometric imperfection can affect the failure mode.

The magnitude of the geometric imperfections was also varied in the same specimen with the same conditions as above. The imperfection magnitudes were changed from -1.9 to 1.9 mm ie. -2t to +2t at 0.25t intervals. The residual stresses were not applied in this case since the only variable considered was the geometric imperfections. This study was undertaken at two different temperatures of 20°C and 500°C so that the influence of geometric imperfections can be observed with varying temperatures. Only the first elastic buckling mode (both flanges moving inwards) was considered in this study.

As shown in Table 5.9 and Figure 5.22 it is clear that there is a considerable influence of initial geometric imperfections on the ultimate load. The difference between the maximum and minimum ultimate loads is about 20 and 30% at ambient and elevated temperatures, respectively. Further, it shows a considerable difference in the ultimate load for the cases of with and without geometric imperfections. The ultimate load decreases rapidly when small geometric imperfections are introduced, but does not decrease rapidly with increasing large imperfections (see Figure 5.22). On the other hand, as discussed earlier, the direction of the imperfections governs the failure behaviour of the specimen. Therefore appropriate initial geometric imperfections should be included in the parametric studies. Schafer and Pekoz

(1998) presented various equations for initial geometric imperfections based on extensive measured data. Therefore their equations were used to determine the initial geometric imperfections for use in the parametric studies.

Table 5.9   Effect of Geometric Imperfections on the Ultimate Load

Imperfection	FEA Results			
	20°C		500°C	
	Ult. Load (kN)	mode	Ult. Load (kN)	mode
-1.9	41.00	Out	18.53	Out
-1.66	41.30	Out	18.72	Out
-1.425	42.10	Out	19.02	Out
-1.1875	42.35	Out	19.33	Out
-0.95	43.35	Out	19.70	Out
-0.7125	43.75	Out	20.07	Out
-0.475	44.90	Out	20.62	Out
-0.2375	45.90	Out	21.23	Out
-0.05	48.45	Out	22.21	Out
-0.01	54.00	Out	24.40	Out
0	56	In	27.13	In
0.01	54.00	In	24.43	In
0.05	50.00	In	22.78	In
0.2375	46.2	In	21.75	In
0.475	44.2	In	20.16	In
0.7125	42.45	In	19.73	In
0.95	41.25	In	19.00	In
1.1875	41	In	18.33	In
1.425	40.05	In	18.21	In
1.66	39.9	In	17.90	In
1.9	39.3	In	17.53	In

Note: In = both flanges moving inwards and Out = both flanges moving outwards
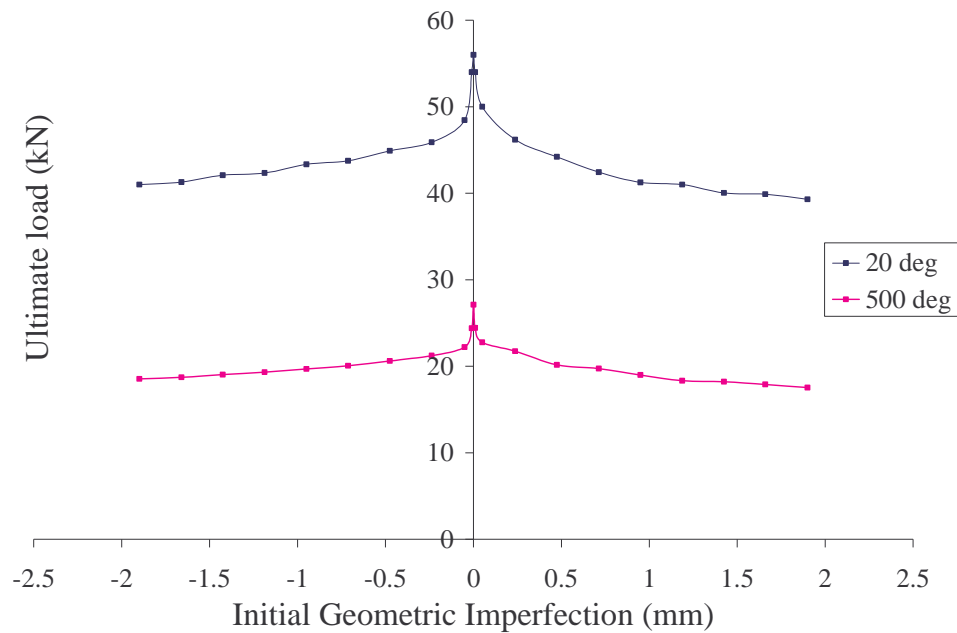
Figure 5.22   Effect of Initial Geometric Imperfections on Failure Loads

5.5.3   Effect of Residual Stresses

In addition to the geometric imperfections, the residual stresses can also affect the failure load. Therefore the effect of residual stresses was investigated by considering 0.95 mm G550 Type A specimen at ambient temperature. Both the residual stresses and initial geometric imperfections were included in this investigation. Elevated temperatures were not considered in this investigation since the residual stresses decreased with increasing temperatures. The initial geometric imperfection value was not varied, but the residual stress was varied from 0 to 100% at 10% intervals. The ultimate loads obtained demonstrated that the influence of residual stress is negligible (the variation is about 0.2%).

5.5.4   Effect of Mechanical Properties

Mechanical properties are one of the governing factors determining failure behaviour and the ultimate load of steel specimens. Therefore accurate mechanical properties were obtained as discussed in Chapter 3 at ambient and elevated temperatures. As

shown in Chapter 3, the obtained mechanical properties in this research and the available mechanical properties from other researchers' results show considerable difference. Therefore it is useful to investigate the effect of mechanical properties on the distortional buckling behaviour of cold-formed steel columns at elevated temperatures.

Although accurate stress-strain curves were obtained and included in the finite element analyses of this research, the available mechanical properties from other research do not include the stress-strain curves. Therefore the modulus of elasticity and the yield strength were used with an elastic-perfect-plastic assumption when other researchers' data were used. Outinen's (1999) and Chen and Young's (2004) results were considered in the analyses of 0.95 mm G250 and G550 steel specimens since their results were based on low strength and high strength steel specimens, respectively.
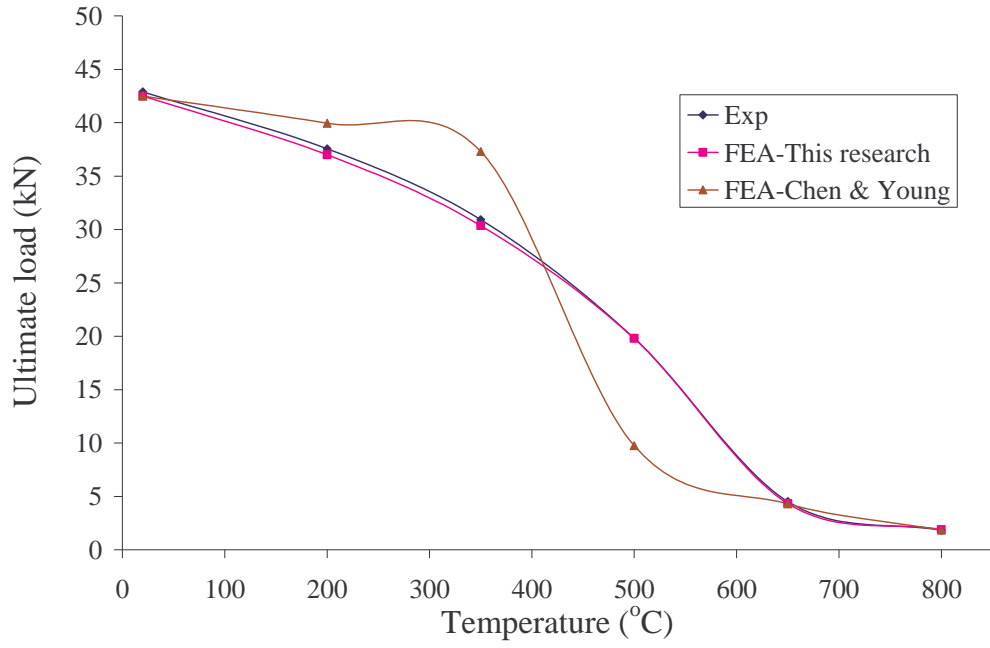
Table 5.10   Effect of Mechanical Properties on the Ultimate Load of 0.95 mm G550 Steel Specimen

| Temp (^{o}C)	Type A & B Specimens	Ultimate Load (kN)			Exp./FEA	Exp./FEA$_{Chen}$
		Exp.	FEA	FEA$_{Chen}$		
20	G550-0.95-20-A	42.88	42.50	42.50	1.009	1.009
200	G550-0.95-200-A	37.55	37.00	39.95	1.015	0.940
350	G550-0.95-350-A	30.91	30.35	37.30	1.018	0.829
500	G550-0.95-500-A	19.81	19.80	9.75	1.001	2.032
650	G550-0.95-650-A	4.52	4.33	4.30	1.044	1.051
800	G550-0.95-800-A	1.80	1.89	1.84	0.952	0.978
20	G550-0.95-20-B	53.58	55.00	55.00	0.974	0.974
200	G550-0.95-200-B	46.95	47.60	53.00	0.986	0.886
350	G550-0.95-350-B	39.04	38.35	48.45	1.018	0.806
500	G550-0.95-500-B	21.90	22.50	11.25	0.973	1.947
650	G550-0.95-650-B	5.02	5.00	4.98	1.004	1.008
800	G550-0.95-800-B	1.95	2.05	2.13	0.951	0.915
				Mean	0.996	1.115
				COV	0.029	0.373

Table 5.11   Effect of Mechanical Properties on the Ultimate Load of

0.95 mm G250 Steel Specimen

Temp (^{o}C)	Type A & B	Ultimate Load (kN)			Exp./FEA	Exp./FEA$_{Outinen}$
	Specimens	Exp.	FEA	FEA$_{Outinen}$		
20	G250-0.95-20-A	31.43	31.65	31.65	0.993	0.993
200	G250-0.95-200-A	25.17	25.20	26.10	0.999	0.964
350	G250-0.95-350-A	17.40	15.50	23.20	1.123	0.750
500	G250-0.95-500-A	10.38	9.75	17.35	1.065	0.598
650	G250-0.95-650-A	4.98	4.70	6.90	1.060	0.722
800	G250-0.95-800-A	1.47	1.56	2.73	0.942	0.538
20	G250-0.95-20-B	37.45	35.95	35.95	1.042	1.042
200	G250-0.95-200-B	28.40	29.10	29.65	0.976	0.958
350	G250-0.95-350-B	19.67	18.35	27.55	1.072	0.714
500	G250-0.95-500-B	11.74	11.45	19.80	1.025	0.593
650	G250-0.95-650-B	5.36	5.40	7.95	0.993	0.674
800	G250-0.95-800-B	1.94	1.93	3.33	1.005	0.583
				Mean	1.024	0.761
				COV	0.049	0.238

Tables 5.10 and 5.11 and Figures 5.23 (a) to (d) compare the experimental results with FEA results based on the mechanical properties obtained from this research, Chen and Young (2004), and Outinen (1999). According to these tables and figures, it is clear that the influence of mechanical properties at elevated temperatures on the distortional buckling failure load is significant. According to the mean and COV values obtained, the results obtained from Chen and Young's and Outinen's mechanical properties show a considerable variation from the experimental results obtained in this research. However, the ultimate loads obtained based on the mechanical properties determined in this research (Chapter 3) show a very good agreement with the experimental results as discussed earlier. Therefore, accurate mechanical properties must be used in FEA to determine the failure loads accurately and hence to develop new design rules for distortional buckling. In addition, it can be stated that the currently available mechanical properties are inaccurate for light gauge cold-formed steels.
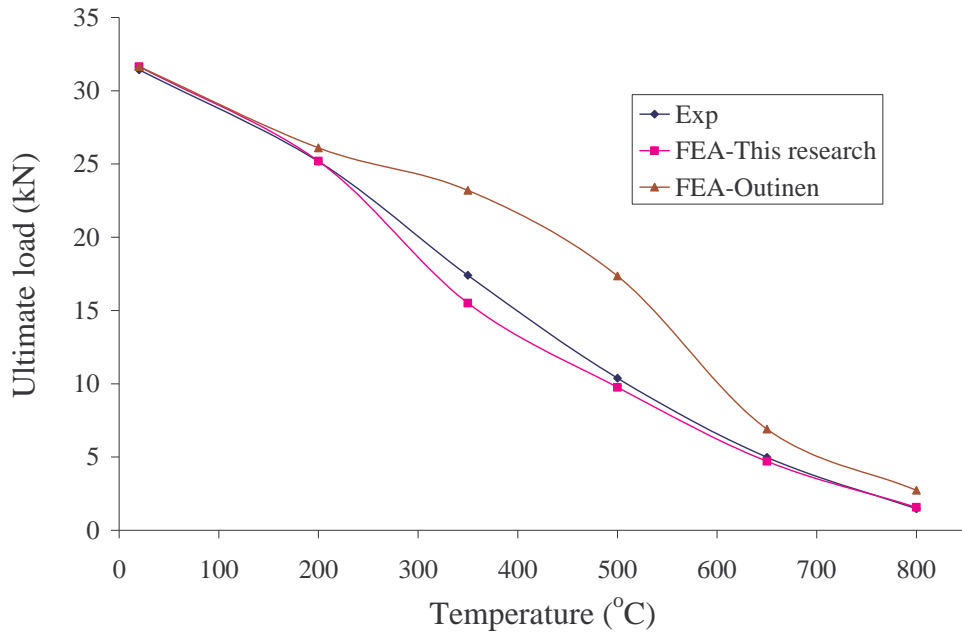
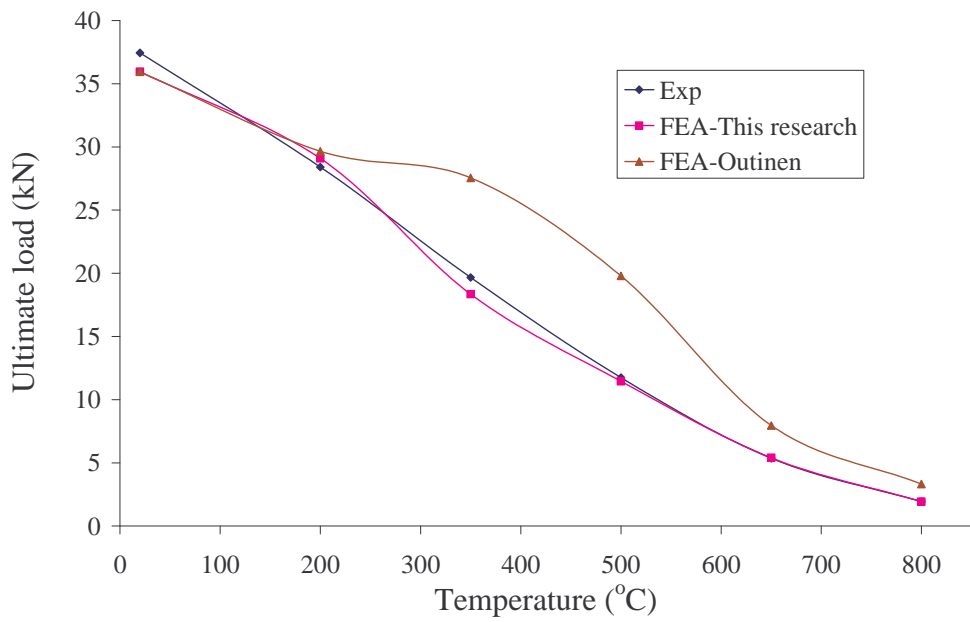(a) 0.95 mm G550 Type A specimen
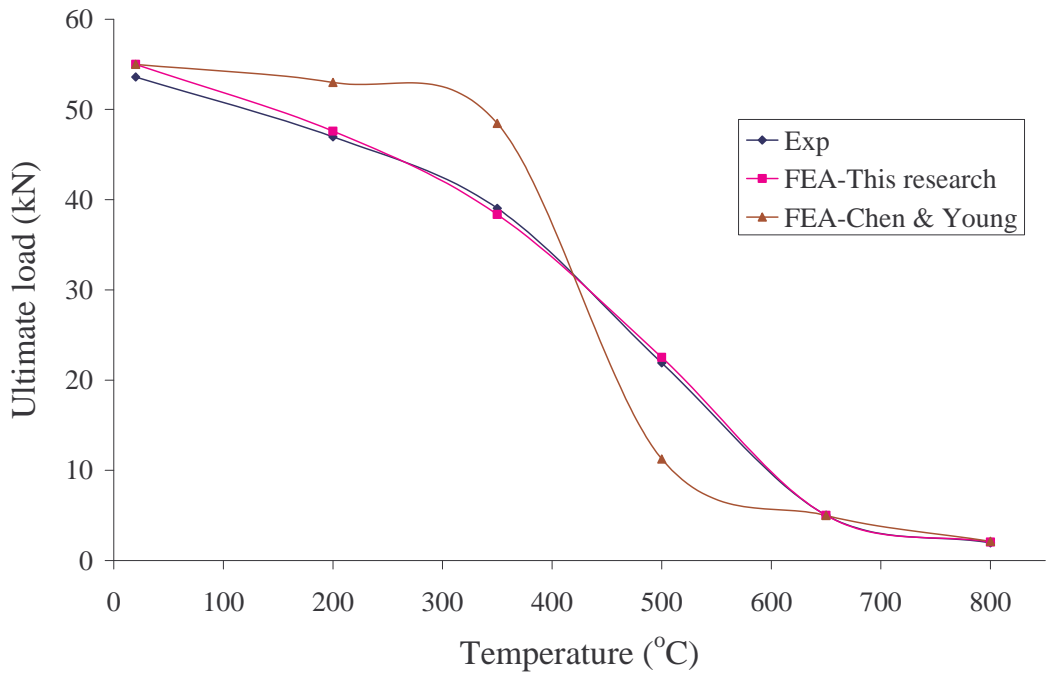
(b) 0.95 mm G550 Type B specimen

Figure 5.23   Effect of Mechanical Properties on the Ultimate Load

(c) 0.95 mm G250 Type A specimen

(d)   0.95 mm G250 Type B specimen

Figure 5.23   Effect of Mechanical Properties on the Ultimate Load

5.5.5 Comparison of Elastic Buckling and Ultimate Loads obtained from FEA

Tables 5.12 and 5.13 compare the elastic buckling and ultimate loads from FEA. The ratio between these two loads for Type A specimens varied from 0.88 to 4.1 while it was 0.64 to 4.57 for Type B specimens. However, the maximum elastic buckling load can be seen when the temperature was very high. The obtained results were then compared with appropriate curves in AISI (2004). According to Figure 5.24 the elastic buckling load can be higher or lower than the ultimate load depending on the slenderness of specimens. The selected specimens show considerable variation between the maximum and minimum values of the ratio of elastic buckling load to ultimate load. The parametric study was also carried out by considering both regimes as in Figure 5.24 and the results are presented in Chapter 6.
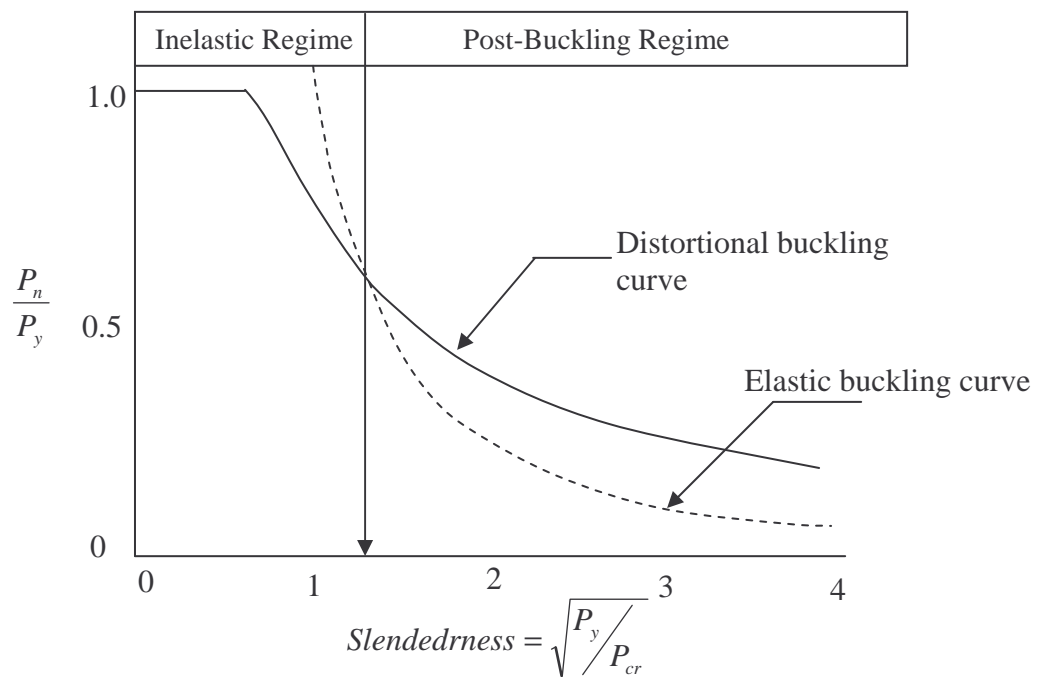
Figure 5.24   Distortional Buckling Behaviour (AISI, 2004)

Table 5.12   Comparison of Elastic Buckling and Ultimate Loads obtained

from FEA for Type A Specimens

Specimen	P_{od} (kN)	P_u (kN)	P_{od}/P_u
G550-0.6-20-A	20.65	19.75	1.046
G550-0.6-200-A	16.40	16.05	1.022
G550-0.6-350-A	12.97	14.60	0.889
G550-0.6-500-A	8.26	7.20	1.147
G550-0.6-650-A	5.16	2.57	2.009
G550-0.6-800-A	1.11	0.76	1.461
G250-0.6-20-A	15.08	12.45	1.211
G250-0.6-200-A	11.97	9.45	1.266
G250-0.6-350-A	9.04	5.55	1.629
G250-0.6-500-A	6.80	3.61	1.883
G250-0.6-650-A	3.81	1.88	2.027
G250-0.6-800-A	0.68	0.64	1.063
G550-0.8-20-A	44.04	31.70	1.389
G550-0.8-200-A	36.85	26.95	1.367
G550-0.8-350-A	29.10	23.60	1.233
G550-0.8-500-A	17.46	12.65	1.380
G550-0.8-650-A	15.46	4.16	3.716
G550-0.8-800-A	5.42	1.78	3.045
G250-0.8-20-A	36.51	20.25	1.803
G250-0.8-200-A	38.67	17.65	2.191
G250-0.8-350-A	20.53	9.75	2.105
G250-0.8-500-A	21.08	7.10	2.969
G250-0.8-650-A	12.67	3.11	4.074
G250-0.8-800-A	1.43	1.32	1.083
G550-0.95-20-A	53.10	42.50	1.249
G550-0.95-200-A	49.11	37.00	1.327
G550-0.95-350-A	40.09	30.35	1.321
G550-0.95-500-A	28.02	19.80	1.415
G550-0.95-650-A	16.84	4.33	3.888
G550-0.95-800-A	7.80	1.89	4.127
G250-0.95-20-A	55.01	31.65	1.738
G250-0.95-200-A	50.89	25.20	2.019
G250-0.95-350-A	36.03	15.50	2.325
G250-0.95-500-A	26.68	9.75	2.736
G250-0.95-650-A	19.25	4.70	4.096
G250-0.95-800-A	4.95	1.56	3.173

Table 5.13   Comparison of Elastic Buckling and Ultimate Loads obtained from FEA for Type B Specimens

Specimen	P_{od} (kN)	P_u (kN)	P_{od}/P_u
G550-0.6-20-B	18.69	24.80	0.754
G550-0.6-200-B	14.97	20.55	0.729
G550-0.6-350-B	12.12	18.85	0.643
G550-0.6-500-B	7.54	10.05	0.750
G550-0.6-650-B	4.71	3.54	1.331
G550-0.6-800-B	1.02	1.11	0.919
G250-0.6-20-B	13.04	15.75	0.828
G250-0.6-200-B	10.90	14.05	0.776
G250-0.6-350-B	8.24	8.30	0.993
G250-0.6-500-B	6.19	5.60	1.106
G250-0.6-650-B	3.47	2.42	1.433
G250-0.6-800-B	0.65	0.88	0.739
G550-0.8-20-B	38.85	39.65	0.980
G550-0.8-200-B	32.00	32.60	0.982
G550-0.8-350-B	25.60	28.25	0.906
G550-0.8-500-B	15.16	14.95	1.014
G550-0.8-650-B	12.80	4.73	2.706
G550-0.8-800-B	4.80	1.56	3.077
G250-0.8-20-B	33.00	24.70	1.336
G250-0.8-200-B	29.34	21.50	1.365
G250-0.8-350-B	18.13	14.45	1.255
G250-0.8-500-B	15.99	8.40	1.903
G250-0.8-650-B	11.21	4.25	2.637
G250-0.8-800-B	1.26	1.50	0.840
G550-0.95-20-B	71.86	55.00	1.306
G550-0.95-200-B	62.88	47.60	1.321
G550-0.95-350-B	51.33	38.35	1.338
G550-0.95-500-B	29.94	22.50	1.331
G550-0.95-650-B	21.55	5.00	4.310
G550-0.95-800-B	10.00	2.05	4.878
G250-0.95-20-B	70.64	35.95	1.965
G250-0.95-200-B	65.34	29.10	2.245
G250-0.95-350-B	46.27	18.35	2.521
G250-0.95-500-B	41.15	11.45	3.594
G250-0.95-650-B	24.72	5.40	4.578
G250-0.95-800-B	6.29	1.93	3.259

where, P_{od} and P_u are elastic and ultimate loads obtained from FEA, respectively.

6 Parametric Studies and Development of Design Rules

6.1 General

As described in Chapters 4 and 5 both the experimental and finite element studies were undertaken for ambient and elevated temperatures. The finite element models in Chapter 5 covered all the tested temperatures (20, 200, 350, 500, 650 and 800 $^{\circ}$C) with two different cross sections (Type A and Type B). In addition to this, different steel thicknesses (nominal thicknesses are 0.60, 0.80 and 0.95 mm) and both low (G250) and high (G550) strength steels with nominal yield strengths of 250 and 550 MPa, respectively, were included. As described in Chapters 4 and 5 the initial geometric imperfections were measured and the measured imperfections were included in all the finite element models. Since the mechanical properties govern the failure mode and load at different temperatures, the mechanical properties were measured at these temperatures and included in the finite element models. Residual stresses also show some influence on the distortional buckling behaviour and hence they were included in the finite element models based on varying temperatures. Therefore the half-length finite element model used in Chapter 5 included the effects of accurate mechanical properties, initial geometric imperfections, residual stresses, thickness of the steel, cross-section and the steel grade in the analyses. The results of the comparison between experimental and numerical studies described in Chapter 5 have shown that the half-length experimental finite element models accurately simulated the distortional buckling behaviour of light gauge cold-formed steel compression members. Therefore this finite element model with ideal conditions were used in a detailed parametric study to determined the ultimate loads of compression members subjected to distortional buckling at ambient and elevated temperatures.

The accuracy of the current design rules (AS/NZS 4600 and the direct strength method) was determined first based on the parametric study results at ambient

temperature. New design rules were developed at ambient temperature since the current design rules are not accurate for light gauge cold-formed steel compression members. The developed design rules were simply modified using relevant mechanical properties at various temperatures to determine the applicability of ambient temperature equations at elevated temperatures. However, it was noticed that the new ambient temperature equations are reasonable but not highly accurate at elevated temperatures. Therefore more accurate design equations were developed to predict the ultimate loads of cold-formed steel compression members at elevated temperatures subjected to distortional buckling. This chapter presents the results of the parametric study into the distortional buckling behaviour of light gauge cold-formed steel compression members at ambient and elevated temperatures and the results including a number of new design rules.

6.2   Details of Finite Element Model used in the Parametric Study

Extensive finite element analyses (FEA) are required to fully understand the distortional buckling behaviour of cold-formed steels compression members in this parametric study. Therefore, a large number of ABAQUS input files were created in MSC PATRAN environment. They were analysed using the bifurcation buckling solution sequence to obtain the elastic distortional buckling loads and associated eigenvectors. The initial geometric imperfections were then incorporated into the nonlinear analysis model based on the critical buckling mode shown by the eigenvectors. Finally, the analyses were continued using the nonlinear static solution sequence to obtain the ultimate loads. Elastic distortional buckling and ultimate stresses were obtained by dividing the relevant loads by the gross area of section.

The half-length finite element model described in Chapter 5 was capable of predicting the distortional buckling behaviour accurately. Therefore the same model with fixed ends was used in the parametric study by changing numerous parameters such as section geometry, mechanical properties, steel thickness and grade and temperature. Isotropic strain-hardening behaviour was used since it is more accurate than the elastic perfect plasticity behaviour. The stress-strain curves were obtained based on the developed equations in Chapter 3 for yield strength, elasticity modulus

and the stress-strain behaviour of cold-formed steels at various temperatures. The yield strength was varied to study the effect of yield strength on distortional buckling and also to see the validity of current design rules for varying yield strengths. Table 6.1 presents the mechanical properties used at ambient temperature while Equations 6.1 to 6.4 present the reduction factors for mechanical properties, and the stress-strain curves used for all the temperatures. The measured mechanical properties were used for G250 steel up to 200°C as given in Chapter 3. The lack of ductility in G550 steel was not modelled in this study. The initial geometric imperfections were included based on Schafer and Pekoz (1998) (Equation 5.4) as given in Chapter 5 instead of measured imperfections. The residual stresses were also included as described in Chapter 5. The thickness of steel was varied from 0.55 to 0.94 mm (0.55, 0.60, 0.75, 0.80 and 0.94 mm) to match the values used in earlier chapters. The slenderness of the sections also varied from 0.5 to 3.2 to observe the applicability of design equations at various slender sections.

Table 6.1   Mechanical Properties used in Parametric Study at Ambient Temperature

Steel	f_y (MPa)	E (MPa)
0.55-G250	320	200000
0.75-G250	300	200000
0.94-G250	300	200000
0.60-G550	678	220000
0.80-G550	648	202000
0.94-G550	618	200000

Reduction factors for yield strength

For G550 steels

$$\frac{f_{yT}}{f_{y20}} = -0.00016T + 1.0003 \qquad 20^o\,C \leq T \leq 200^o\,C \qquad (6.1a)$$

$$\frac{f_{yT}}{f_{y20}} = 0.97 - \frac{(T-200)^{1.81}}{58500} \qquad 200^o\,C < T < 600^o\,C \qquad (6.1b)$$

$$\frac{f_{yT}}{f_{y20}} = -0.00037T + 0.3363 \qquad\qquad 600^{o}C \leq T \leq 800^{o}C \tag{6.1c}$$

For G250 steels

$$\frac{f_{yT}}{f_{y20}} = -0.0007T + 1.014 \qquad\qquad 20^{o}C \leq T \leq 200^{o}C \tag{6.2a}$$

$$\frac{f_{yT}}{f_{y20}} = 3.7 - \frac{(T-74)^{0.15}}{0.736} \qquad\qquad 200^{o}C < T \leq 800^{o}C \tag{6.2b}$$

Reduction factors for elasticity modulus

$$\frac{E_{T}}{E_{20}} = 1 \qquad\qquad 20^{o}C \leq T \leq 100^{o}C \tag{6.3a}$$

$$\frac{E_{T}}{E_{20}} = -0.0013T + 1.1297 \qquad\qquad 100^{o}C < T \leq 800^{o}C \tag{6.3b}$$

Equation for stress-strain curve

$$\varepsilon_{T} = \frac{f_{T}}{E_{T}} + \beta \left(\frac{f_{yT}}{E_{T}}\right)\left(\frac{f_{T}}{f_{y,T}}\right)^{\eta_{T}} \tag{6.4}$$

where β = 0.86 and

$$\eta_{T} = -3.05 X 10^{-7} T^{3} + 0.0005T^{2} - 0.2615T + 62.653 \qquad 20^{o}C \leq T \leq 800^{o}C \quad \text{for}$$

G550 steel

$$\eta_{T} = 0.000138T^{2} - 0.085468T + 19.212 \qquad 350^{o}C \leq T \leq 800^{o}C \quad \text{for}$$

G250 steel

6.3   Distortional Buckling Behaviour at Ambient Temperature

6.3.1   Parametric Study of Type A Sections

Unlike in other buckling modes (local and global), distortional buckling of light gauge cold-formed steel compression members is complicated. The type A section was first considered by varying the thickness and the yield strength of the steel. Further, the flange width and web height were also changed to observe the effect of

them on distortional buckling failure mode and load. Figure 6.1 shows the nomenclature of Type A section used in this study. The obtained results from the parametric analyses were first compared with the current design rules to determine their accuracy at ambient temperatures for various thicknesses and steel grades. As described in Chapter 4, both AS/NZS 4600 and Direct Strength Methods were considered in this investigation. A total of 100 analyses was undertaken for both low and high strength steels but only 79 of them failed by distortional buckling. The following diagram shows the section and the nomenclature used.

G550-0.8-25-25-5

Lip length (d)
Flange width (b)
Web height (h)
Thickness (t)
Grade
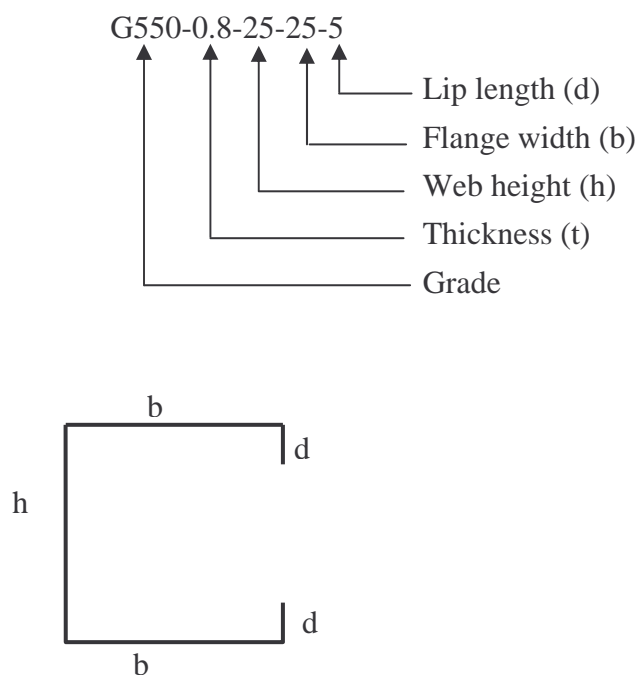
Figure 6.1   Nomenclature of Type A section

6.3.1.1 AS/NZS 4600 design method

The ultimate loads obtained from the parametric study were compared with the design equations in the Australian/New Zealand Standard, AS/NZS 4600 (SA, 1996) for cold-formed steel structures. This provides the design equations for distortional buckling of singly-symmetric sections such as lipped channels with additional rear flanges. When singly symmetric sections are subjected to distortional buckling effects, the ultimate load P_n is obtained as follows (Equation 6.5)

- For $f_{od} > f_y/2$:
$$P_n = Af_n = Af_y\left(1 - \frac{f_y}{4f_{od}}\right)$$
(6.5(a))

- For $f_y/13 \leq f_{od} \leq f_y/2$:
$$P_n = Af_n = Af_y\left[0.055\left(\sqrt{\frac{f_y}{f_{od}}} - 3.6\right)^2 + 0.237\right]$$
(6.5(b))

where A = Area of the gross cross-section, f_y = Yield strength of steel as discussed in Chapter 3, f_n = Ultimate strength of the section. f_{od} = Elastic distortional buckling strength which was determined from ABAQUS.

Table 6.2   Comparison of FEA Results with AS/NZS 4600 Predictions for Type A High Strength Steel Sections

(a)   0.6 mm G550 steel

Specimen	P_{od} (kN)	Ultimate load (kN)		FEA/Pred.
		FEA	Pred.	
G550-0.6-25-25-5	31.0	22.9	24.9	0.918
G550-0.6-20-20-5	34.3	23.0	22.6	1.019
G550-0.6-25-20-5	33.7	23.1	23.6	0.979
G550-0.6-30-30-5	27.1	22.6	25.4	0.889
G550-0.6-40-40-5	17.5	20.6	22.6	0.911
			Mean	0.943
			COV	0.057

(b)   0.8 mm G550 steel

Specimen	P_{od} (kN)	Ultimate load (kN)		FEA/Pred.
		FEA	Pred.	
G550-0.8-25-25-5	47.0	32.2	33.7	0.954
G550-0.8-25-30-5	42.1	33.5	34.8	0.961
G550-0.8-25-35-5	37.4	31.9	34.6	0.921
G550-0.8-25-40-5	33.5	32.1	33.1	0.970
G550-0.8-25-45-5	29.5	30.7	31.3	0.979
G550-0.8-25-50-5	26.8	30.9	31.7	0.974
G550-0.8-20-20-5	55.1	29.9	30.3	0.986
G550-0.8-25-20-5	54.0	31.5	31.9	0.988
G550-0.8-30-20-5	51.8	33.0	33.2	0.995
G550-0.8-30-30-5	42.4	35.1	36.0	0.975
G550-0.8-40-40-5	27.4	33.7	31.3	1.078
G550-0.8-40-50-5	22.9	32.8	31.6	1.037
G550-0.8-40-60-5	19.6	31.9	31.5	1.013
G550-0.8-50-40-5	27.0	33.4	32.5	1.026
G550-0.8-50-50-5	23.1	30.2	32.9	0.917
G550-0.8-50-60-5	19.9	30.2	32.7	0.924
G550-0.8-60-40-5	38.3	32.1	38.7	0.830
			Mean	0.972
			COV	0.057

Table 6.2   Comparison of FEA Results with AS/NZS 4600 Predictions for Type A High Strength Steel Sections

(c)   0.94 mm G550 steel

Specimen	P_{od} (kN)	Ultimate load (kN)		FEA/Pred.
		FEA	Pred.	
G550-0.94-25-25-5	63.3	38.8	39.7	0.976
G550-0.94-25-30-5	56.0	40.0	41.6	0.962
G550-0.94-25-35-5	50.3	40.5	42.5	0.953
G550-0.94-25-40-5	45.9	40.0	42.5	0.941
G550-0.94-25-45-5	41.7	39.3	41.0	0.958
G550-0.94-25-50-5	37.5	38.7	38.6	1.003
G550-0.94-25-70-5	22.7	36.7	36.4	1.008
G550-0.94-25-90-5	17.9	38.8	35.9	1.080
G550-0.94-25-110-5	15.1	39.7	36.9	1.076
G550-0.94-20-20-5	76.1	34.8	35.2	0.988
G550-0.94-25-20-5	74.7	36.9	37.2	0.992
G550-0.94-30-20-5	72.4	40.0	39.0	1.025
G550-0.94-30-30-5	56.4	41.9	43.1	0.971
G550-0.94-40-40-5	37.4	39.6	37.6	1.053
G550-0.94-40-50-5	30.9	43.0	38.3	1.122
G550-0.94-40-60-5	26.7	42.4	38.7	1.096
G550-0.94-50-40-5	37.1	43.5	39.4	1.105
G550-0.94-50-50-5	31.3	39.1	40.0	0.977
G550-0.94-50-60-5	27.2	39.3	40.2	0.977
G550-0.94-60-40-5	35.6	38.8	40.5	0.958
			Mean	1.011
			COV	0.056

P_{od} = Elastic distortional buckling load in kN

Tables 6.2 (a) to (c) present the results obtained from the parametric study and the AS/NZS 4600 design equations for 0.60, 0.80 and 0.94 mm G550 steels. It should be stated that the yield strength reduction factors for thinner (< 0.9 mm) G550 steels were not included in AS/NZS 4600 design equations as the finite element analysis results did not include the effects of reduced ductility in thinner G550 steels. It was observed that many sections of 0.80 and 0.94 mm thicknesses failed by distortional buckling while only limited sections of 0.60 mm steel failed by distortional buckling mode. Many 0.60 mm sections showed local buckling and interaction of local and distortional buckling failure modes rather than pure distortional buckling mode.

Theses results were not included and only the results for pure distortional buckling mode were considered in this study. It is obvious that the thickness of steel influences the failure mode.

As shown in Tables 6.2 (a) to (c) the mean values of the ratio of FEA to predicted results from AS/NZS 4600 vary from 0.943 to 1.011. So it can be stated that AS/NZS 4600 design rules are slightly unsafe for very thin members (0.60 and 0.80 mm thick steel) but conservative for 0.94 mm thick steel. These equations were originally developed based on the test results for the thicknesses above 1 mm and hence may not be appropriate for very thin steels (Kwon and Hancock, 1992a).

Moreover, Figure 6.2 gives a comparison of FEA results with AS/NZS 4600 design curves. Figure 6.2 also confirms that the AS/NZS 4600 predictions are appropriate for 0.94 mm steel while for other thicknesses they are rather unsafe. However, as a conclusion it can be stated that all the predicted values are in an acceptable region. Therefore AS/NZS 4600 equations can be used to accurately predict the distortional buckling failure loads of 0.60, 0.80 and 0.94 mm thick high strength steel Type A sections.
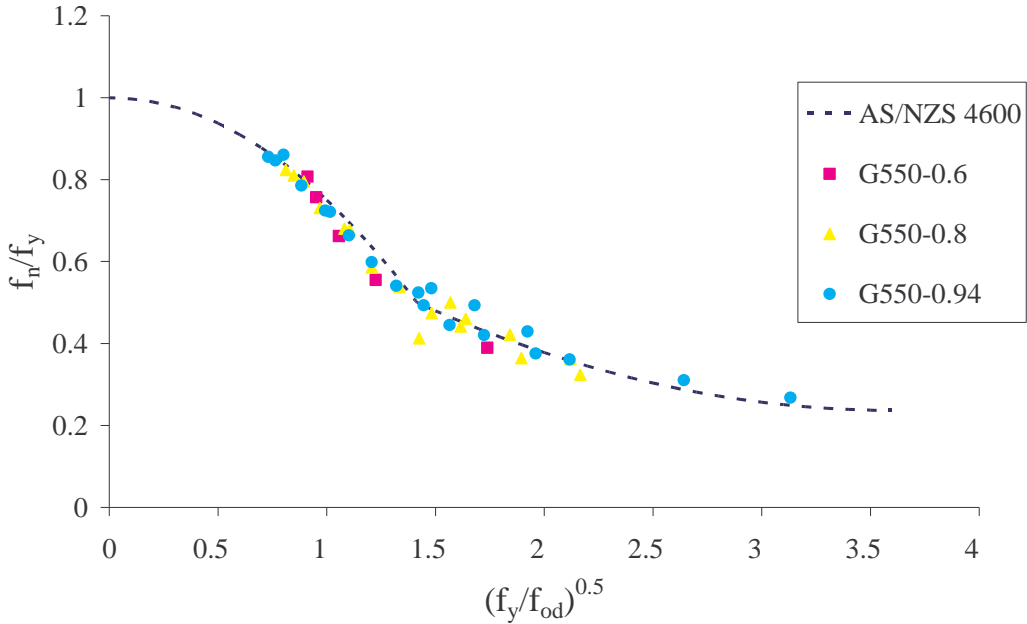
Figure 6.2   Comparison of AS/NZS 4600 Predictions with FEA Results for Type A G550 Steel Sections

Table 6.3   Comparison of FEA Results with AS/NZS 4600 Predictions for Type A Low Strength Steel Sections

(a)   0.55 mm G250 steel

Specimen	P_{od} (kN)	Ultimate load (kN)		FEA/Pred.
		FEA	Pred.	
G250-0.55-25-25-5	22.0	12.4	12.4	0.999
G250-0.55-20-20-5	26.7	11.1	10.9	1.018
G250-0.55-25-20-5	26.0	11.5	11.5	0.998
			Mean	1.005
			COV	0.012

(b)   0.75 mm G250 steel

Specimen	P_{od} (kN)	Ultimate load (kN)		FEA/Pred.
		FEA	Pred.	
G250-0.75-25-25-5	41.4	16.9	16.9	0.999
G250-0.75-25-30-5	37.2	17.8	18.3	0.972
G250-0.75-25-35-5	33.2	16.6	19.4	0.855
G250-0.75-25-40-5	28.7	17.2	20.0	0.858
G250-0.75-25-45-5	24.9	16.7	20.2	0.827
G250-0.75-20-20-5	47.9	14.6	14.5	1.010
G250-0.75-25-20-5	47.2	15.5	15.4	1.009
G250-0.75-30-20-5	46.0	15.9	16.2	0.979
G250-0.75-30-30-5	37.0	18.0	19.1	0.943
G250-0.75-40-40-5	24.0	19.8	20.3	0.974
G250-0.75-40-50-5	20.0	19.3	19.5	0.989
G250-0.75-40-60-5	17.0	18.9	16.7	1.129
G250-0.75-50-40-5	23.8	19.5	21.1	0.925
G250-0.75-50-50-5	20.5	17.2	20.2	0.852
G250-0.75-60-40-5	33.3	22.6	25.2	0.897
			Mean	0.948
			COV	0.085

P_{od} = Elastic distortional buckling load in kN

Table 6.3   Comparison of FEA Results with AS/NZS 4600 Predictions for Type A Low Strength Steel Sections

(c)   0.94 mm G250 steel

Specimen	P_{od} (kN)	Ultimate load (kN)		FEA/Pred.
		FEA	Pred.	
G250-0.94-25-25-5	63.3	21.7	21.7	1.000
G250-0.94-25-30-5	56.0	23.2	23.6	0.984
G250-0.94-25-35-5	50.3	24.0	25.3	0.950
G250-0.94-25-40-5	45.9	24.3	26.7	0.910
G250-0.94-25-45-5	41.7	23.8	27.8	0.856
G250-0.94-25-110-5	15.1	24.5	25.0	0.980
G250-0.94-25-90-5	17.9	23.9	24.7	0.968
G250-0.94-25-70-5	22.7	23.6	24.0	0.985
G250-0.94-20-20-5	76.1	18.5	18.5	1.002
G250-0.94-25-20-5	74.7	19.8	19.7	1.007
G250-0.94-30-20-5	72.4	21.3	20.8	1.024
G250-0.94-30-30-5	56.4	24.3	24.7	0.985
G250-0.94-40-40-5	37.4	29.2	27.7	1.055
G250-0.94-40-50-5	30.9	27.4	27.8	0.985
G250-0.94-40-60-5	26.7	27.4	26.4	1.037
G250-0.94-50-40-5	37.1	28.7	29.0	0.990
G250-0.94-50-50-5	31.3	27.8	28.9	0.963
G250-0.94-50-60-5	27.2	27.2	27.1	1.004
G250-0.94-60-40-5	35.6	28.1	29.7	0.945
			Mean	0.981
			COV	0.046

Tables 6.3 (a) to (c) present the distortional buckling failure loads of G250 0.55, 0.75 and 0.94 mm thick steel sections. A low number of sections showed distortional buckling mode when the thickness of steel was small. The mean values of the ratio of FEA to predicted values are 1.005, 0.948 and 0.981 for 0.55, 0.75 and 0.94 mm, respectively with COV values of 0.012, 0.085 and 0.046, respectively. From these results it can be concluded that the AS/NZS 4600 predictions are appropriate for low strength steel sections. Figure 6.3 shows the comparison of FEA results with AS/NZS 4600 design curves. According to Tables 6.3 (a) to (c) and Figure 6.3 it can be stated that the AS/NZS 4600 predictions are acceptable for low strength steel sections in general, but unsafe for some sections. Appendix E shows example calculations of AS/NZS 4600 predicted loads shown in Tables 6.2 and 6.3 and the non-dimensional stress and slenderness values required for Figures 6.2 and 6.3.
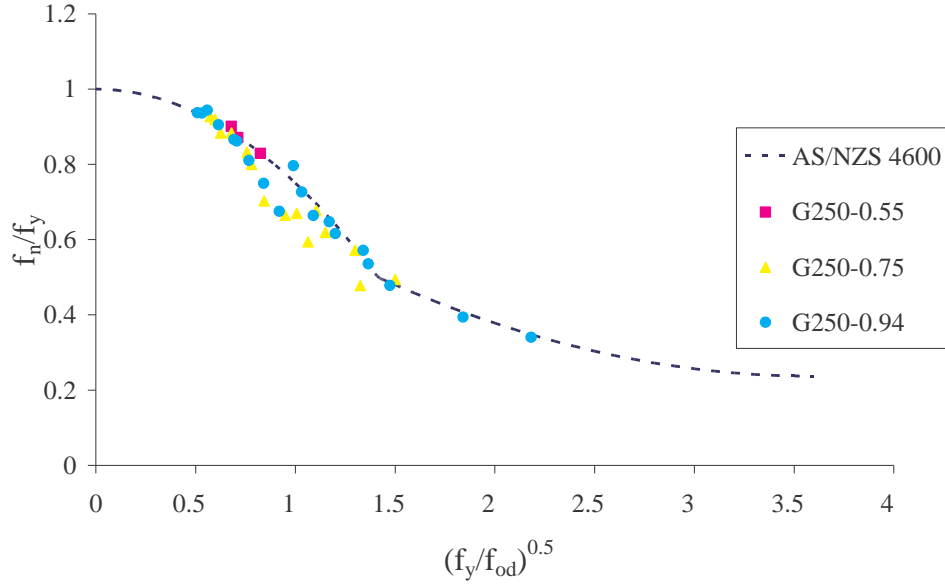
Figure 6.3   Comparison of AS/NZS 4600 Predictions with FEA Results for Type A G250 Steel Sections

6.3.1.2 Direct strength method

The FEA results were then compared with the well known direct strength method proposed by Schafer and Pekoz (1998). It is one of the alternative methods to determine the distortional buckling failure loads of cold-formed steel compression members. Equation 6.6 presents the determination of distortional buckling failure loads of compression members from the direct strength method.

$\lambda \leq 0.561$ $P_n = Af_n = Af_y$

and

$\lambda > 0.561$ $P_n = Af_n = Af_y \left[1 - 0.25 \left(\dfrac{f_{od}}{f_y} \right)^{0.6} \right] \left[\dfrac{f_{od}}{f_y} \right]^{0.6}$ (6.6)

where, $\lambda = \sqrt{\dfrac{f_y}{f_{od}}}$

Note: All the symbols are the same as in Equation 6.5.

Table 6.4   Comparison of FEA Results with Direct Strength Method Predictions for Type A High Strength Steel Sections

(a)   0.6 mm G550 steel

Specimen	P_{od} (kN)	Ultimate load (kN)		FEA/Pred.
		FEA	Pred.	
G550-0.6-25-25-5	31.0	22.9	24.8	0.923
G550-0.6-20-20-5	34.3	23.0	22.9	1.003
G550-0.6-25-20-5	33.7	23.1	23.8	0.971
G550-0.6-30-30-5	27.1	22.6	25.6	0.882
G550-0.6-40-40-5	17.5	20.6	23.7	0.868
			Mean	0.929
			COV	0.062

(b)   0.8 mm G550 steel

Specimen	P_{od} (kN)	Ultimate load (kN)		FEA/Pred.
		FEA	Pred.	
G550-0.8-25-25-5	47.0	32.2	33.9	0.950
G550-0.8-25-30-5	42.1	33.5	34.6	0.967
G550-0.8-25-35-5	37.4	31.9	34.8	0.917
G550-0.8-25-40-5	33.5	32.1	34.7	0.924
G550-0.8-25-45-5	29.5	30.7	34.1	0.900
G550-0.8-25-50-5	26.8	30.9	33.8	0.914
G550-0.8-20-20-5	55.1	29.9	31.6	0.945
G550-0.8-25-20-5	54.0	31.5	32.9	0.956
G550-0.8-30-20-5	51.8	33.0	33.9	0.975
G550-0.8-30-30-5	42.4	35.1	35.8	0.981
G550-0.8-40-40-5	27.4	33.7	33.6	1.004
G550-0.8-40-50-5	22.9	32.8	32.9	0.998
G550-0.8-40-60-5	19.6	31.9	32.1	0.993
G550-0.8-50-40-5	27.0	33.4	34.6	0.966
G550-0.8-50-50-5	23.1	30.2	34.0	0.887
G550-0.8-50-60-5	19.9	30.2	33.3	0.908
G550-0.8-60-40-5	38.3	32.1	42.5	0.755
			Mean	0.938
			COV	0.063

Table 6.4   **Comparison of FEA Results with Direct Strength Method Predictions for Type A High Strength Steel Sections**

(c)   0.94 mm G550 steel

Specimen	P_{od} (kN)	Ultimate load (kN)		FEA/Pred.
		FEA	Pred.	
G550-0.94-25-25-5	63.3	38.8	40.7	0.954
G550-0.94-25-30-5	56.0	40.0	41.6	0.961
G550-0.94-25-35-5	50.3	40.5	42.2	0.959
G550-0.94-25-40-5	45.9	40.0	42.7	0.937
G550-0.94-25-45-5	41.7	39.3	42.7	0.920
G550-0.94-25-50-5	37.5	38.7	42.3	0.915
G550-0.94-25-70-5	22.7	36.7	37.1	0.988
G550-0.94-25-90-5	17.9	38.8	35.9	1.081
G550-0.94-25-110-5	15.1	39.7	35.2	1.126
G550-0.94-20-20-5	76.1	34.8	37.7	0.924
G550-0.94-25-20-5	74.7	36.9	39.4	0.936
G550-0.94-30-20-5	72.4	40.0	40.9	0.979
G550-0.94-30-30-5	56.4	41.9	43.1	0.973
G550-0.94-40-40-5	37.4	39.6	41.4	0.956
G550-0.94-40-50-5	30.9	43.0	40.5	1.062
G550-0.94-40-60-5	26.7	42.4	39.9	1.062
G550-0.94-50-40-5	37.1	43.5	42.9	1.015
G550-0.94-50-50-5	31.3	39.1	42.1	0.929
G550-0.94-50-60-5	27.2	39.3	41.4	0.949
G550-0.94-60-40-5	35.6	38.8	43.5	0.892
			Mean	0.976
			COV	0.064

Tables 6.4 (a) to (c) present a comparison of FEA results and direct strength method predictions for high strength steel sections. The predictions from the direct strength method also show the same phenomenon as AS/NZS 4600 predictions. The mean values of the ratio of FEA to predicted values from the direct strength method vary from 0.929 to 0.976. The predictions are more unsafe for very thin members (0.60 and 0.80 mm) but appropriate for 0.94 mm steel sections. However, it can be concluded that all the ultimate load predictions obtained from the direct strength method are reasonably accurate but not as accurate as the AS/NZS 4600 predictions for high strength steel sections. Figure 6.4 shows the non-dimensional results from the direct strength method and FEA.
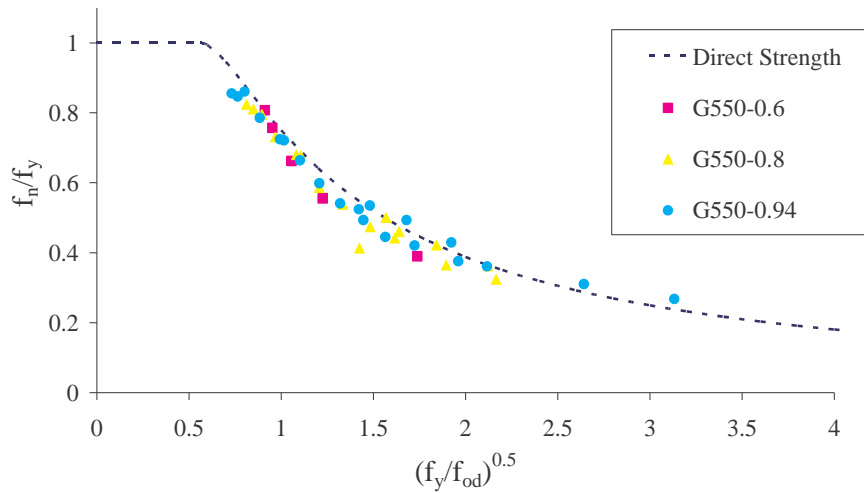
Figure 6.4   Comparison of Direct Strength Method Predictions with FEA Results for Type A G550 Steel Sections

Table 6.5   Comparison of FEA Results with Direct Strength Method Predictions for Type A Low Strength Steel Sections

(a)   0.55 mm G250 steel

Specimen	P_{od} (kN)	Ultimate load (kN)		FEA/Pred.
		FEA	Pred.	
G250-0.55-25-25-5	22.0	12.4	12.9	0.960
G250-0.55-20-20-5	26.7	11.1	11.8	0.940
G250-0.55-25-20-5	26.0	11.5	12.4	0.929
			Mean	0.943
			COV	0.017

(b)   0.75 mm G250 steel

Specimen	P_{od} (kN)	Ultimate load (kN)		FEA/Pred.
		FEA	Pred.	
G250-0.75-25-25-5	41.4	16.9	18.3	0.923
G250-0.75-25-30-5	37.2	17.8	19.4	0.917
G250-0.75-25-35-5	33.2	16.6	20.1	0.826
G250-0.75-25-40-5	28.7	17.2	20.2	0.851
G250-0.75-25-45-5	24.9	16.7	20.1	0.832
G250-0.75-20-20-5	47.9	14.6	15.7	0.928
G250-0.75-25-20-5	47.2	15.5	16.8	0.923
G250-0.75-30-20-5	46.0	15.9	17.7	0.897
G250-0.75-30-30-5	37.0	18.0	20.1	0.895
G250-0.75-40-40-5	24.0	19.8	20.2	0.980
G250-0.75-40-50-5	20.0	19.3	20.2	0.958
G250-0.75-40-60-5	17.0	18.9	19.9	0.950
G250-0.75-50-40-5	23.8	19.5	21.0	0.929
G250-0.75-50-50-5	20.5	17.2	21.1	0.815
G250-0.75-60-40-5	33.3	22.6	25.2	0.898
			Mean	0.901
			COV	0.055

Table 6.5   Comparison of FEA Results with Direct Strength Method Predictions for Type A Low Strength Steel Sections

(c)   0.94 mm G250 steel

Specimen	P_{od} (kN)	Ultimate load (kN)		FEA/Pred.
		FEA	Pred.	
G250-0.94-25-25-5	63.3	21.7	23.7	0.915
G250-0.94-25-30-5	56.0	23.2	25.5	0.911
G250-0.94-25-35-5	50.3	24.0	26.7	0.898
G250-0.94-25-40-5	45.9	24.3	27.6	0.879
G250-0.94-25-45-5	41.7	23.8	28.2	0.844
G250-0.94-25-110-5	15.1	24.5	25.4	0.964
G250-0.94-25-90-5	17.9	23.9	25.7	0.932
G250-0.94-25-70-5	22.7	23.6	26.1	0.904
G250-0.94-20-20-5	76.1	18.5	19.7	0.937
G250-0.94-25-20-5	74.7	19.8	21.2	0.936
G250-0.94-30-20-5	72.4	21.3	22.6	0.944
G250-0.94-30-30-5	56.4	24.3	26.5	0.915
G250-0.94-40-40-5	37.4	29.2	27.7	1.054
G250-0.94-40-50-5	30.9	27.4	27.8	0.986
G250-0.94-40-60-5	26.7	27.4	27.8	0.985
G250-0.94-50-40-5	37.1	28.7	28.9	0.994
G250-0.94-50-50-5	31.3	27.8	29.0	0.960
G250-0.94-50-60-5	27.2	27.2	28.9	0.941
G250-0.94-60-40-5	35.6	28.1	29.5	0.951
			Mean	0.940
			COV	0.050
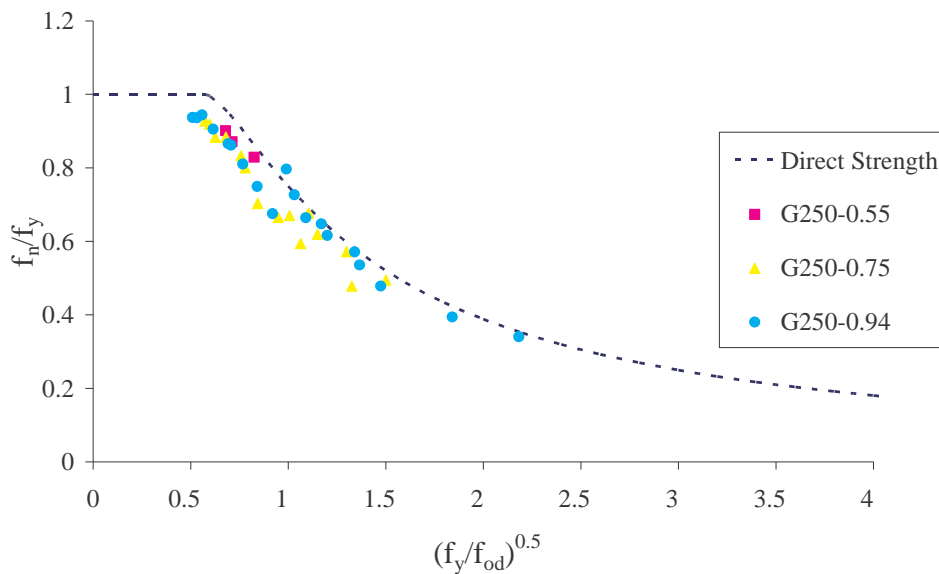
Figure 6.5   Comparison of Direct Strength Method Predictions with FEA Results for Type A G250 Steel Sections

Figure 6.5 and Tables 6.5 (a) to (c) show the predictions from the direct strength method and the FEA for low strength (G250) steel sections. The predictions for low strength steel sections are also unsafe when they fail in the distortional buckling mode. The mean values of the ratio of FEA to predictions are 0.943, 0.901 and 0.940 for 0.55, 0.75 and 0.94 mm thickness steel sections, respectively. Appendix E shows example calculations of direct strength method predicted loads shown in Tables 6.4 and 6.5 and the non-dimensional stress and slenderness values required for Figures 6.4 and 6.5.

6.3.2 Parametric Study of Type B Sections

The behaviour of Type B section (see Figure 6.6) subjected to distortional buckling failure mode under axial compression was also investigated. As discussed in Section 6.2.1 for Type A sections the varying thicknesses (0.60, 0.80 and 0.95 mm nominal thicknesses) with both low (G250) and high (G550) strength steels were considered in this investigation. The web height, flange width and the lip length (s) were all varied to study their effect on distortional buckling. The other lip length (d) was kept constant (5 mm).

G550-0.8-25-25-5

- Lip length (s)
- Flange width (b)
- Web height (h)
- Thickness (t)
- Grade
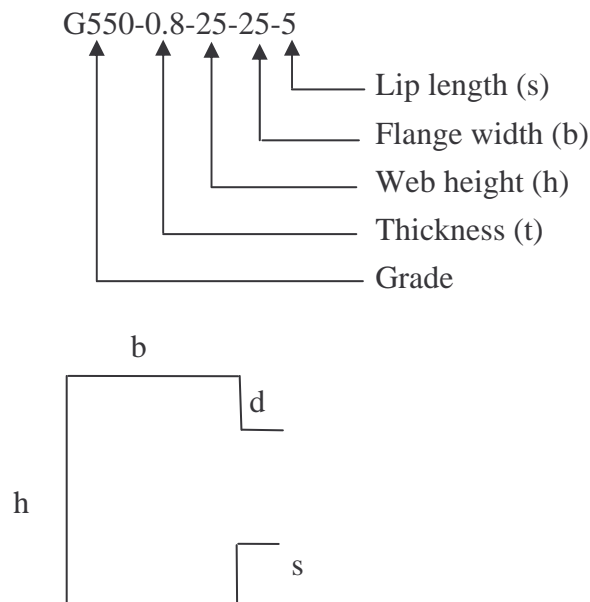
Figure 6.6   Nomenclature of Type B section

A total of 100 FEA analyses was conducted for Type B sections but only 80 sections failed by distortional buckling. The ultimate loads obtained from the parametric study were then compared with predictions from the AS/NZS 4600 design equations and the direct strength method. The analysed sections were named as follows for easy identification in the parametric studies (see Figure 6.6).

6.3.2.1 AS/NZS 4600 design method

Equation 6.5 gives the design equations for AS/NZS 4600 predictions. As discussed in Section 6.2.1, the same design methods were considered in predicting the ultimate loads of Type B sections. Tables 6.6 (a) to (c) give the FEA and predicted loads of G550 Type B sections for 0.60, 0.80 and 0.94 mm, respectively. The mean value of FEA to predicted ultimate loads are 0.922, 0.914 and 0.954 for 0.60, 0.80 and 0.94 mm thick Type B sections, respectively. Therefore, it is clear that the current AS/NZS 4600 design equations are unsafe for Type B sections. However it is within 10% and hence it can be stated that the predicted values are in an acceptable region. Figure 6.7 shows the non-dimensional results from AS/NZS 4600 and FEA. It is clear that the predictions are unsafe for some sections.
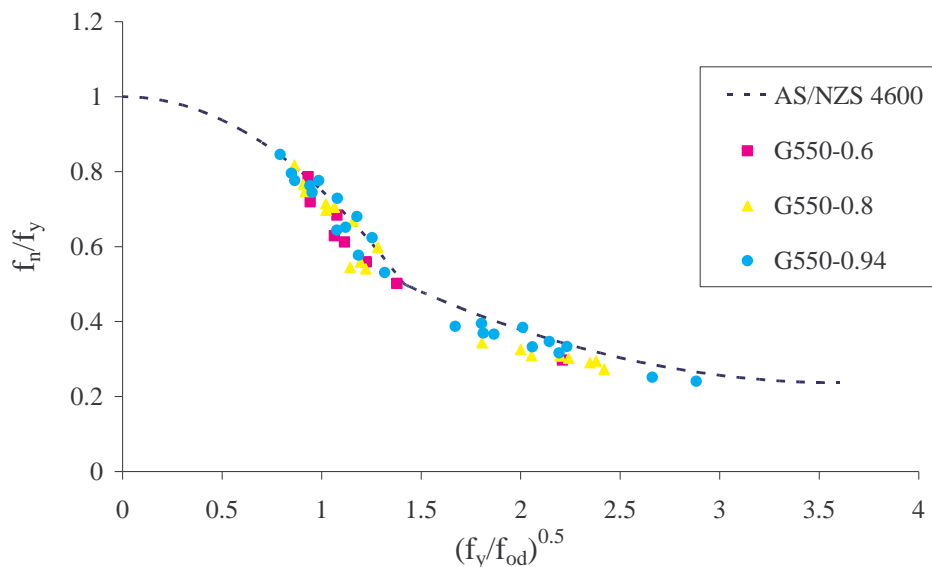
Figure 6.7   Comparison of AS/NZS 4600 Predictions with FEA Results for Type B G550 Steel Sections

Table 6.6   Comparison of FEA Results with AS/NZS 4600 Predictions for Type B High Strength Steel Sections

(a)   0.6 mm G550 steel

Specimen	P_{od} (kN)	Ultimate load (kN)		FEA/Pred.
		FEA	Pred.	
G550-0.6-30-30-5	36.0	27.4	30.8	0.888
G550-0.6-30-30-8	31.5	26.4	29.5	0.894
G550-0.6-40-30-8	27.0	25.7	26.9	0.954
G550-0.6-40-60-8	15.5	22.5	26.0	0.866
G550-0.6-20-20-5	37.4	25.6	25.5	1.005
G550-0.6-25-25-5	43.5	27.8	30.1	0.925
G550-0.6-25-25-8	35.4	28.1	29.2	0.963
G550-0.6-25-30-8	39.9	28.4	32.4	0.877
			Mean	0.922
			COV	0.053

(b)   0.8 mm G550 steel

Specimen	P_{od} (kN)	Ultimate load (kN)		FEA/Pred.
		FEA	Pred.	
G550-0.8-30-40-5	51.6	36.7	45.4	0.809
G550-0.8-30-30-5	50.4	40.2	40.9	0.983
G550-0.8-30-30-8	44.8	40.2	40.0	1.006
G550-0.8-30-40-8	49.4	39.4	45.3	0.869
G550-0.8-40-30-8	39.7	39.1	38.5	1.017
G550-0.8-40-40-8	50.7	40.9	47.4	0.862
G550-0.8-30-60-8	28.0	31.3	37.8	0.828
G550-0.8-30-80-8	20.3	32.5	36.2	0.898
G550-0.8-40-60-8	24.1	31.4	36.4	0.862
G550-0.8-40-70-8	22.1	32.9	36.9	0.893
G550-0.8-40-80-8	20.7	34.5	37.4	0.923
G550-0.8-50-60-8	24.1	31.4	37.4	0.839
G550-0.8-50-70-8	22.3	33.8	37.9	0.891
G550-0.8-50-80-8	20.9	33.3	38.4	0.868
G550-0.8-20-20-5	55.7	33.9	33.8	1.004
G550-0.8-20-30-5	61.6	38.7	40.9	0.946
G550-0.8-25-25-5	59.8	37.7	39.1	0.964
G550-0.8-25-25-8	50.2	37.4	38.7	0.966
G550-0.8-25-25-8	55.1	40.1	42.5	0.943
			Mean	0.914
			COV	0.070

Table 6.6   Comparison of FEA Results with AS/NZS 4600 Predictions for Type B High Strength Steel Sections

(c)   0.94 mm G550 steel

Specimen	P_{od} (kN)	Ultimate load (kN)		FEA/Pred.
		FEA	Pred.	
G550-0.94-30-40-5	65.2	48.60	53.7	0.906
G550-0.94-30-30-5	65.8	49.60	48.4	1.025
G550-0.94-30-30-8	58.0	49.30	47.9	1.029
G550-0.94-30-40-8	63.0	51.50	54.2	0.950
G550-0.94-30-50-8	64.5	52.30	58.8	0.890
G550-0.94-40-30-8	52.8	49.80	47.8	1.041
G550-0.94-40-40-8	54.0	52.90	51.5	1.027
G550-0.94-40-50-8	55.6	51.20	54.6	0.937
G550-0.94-30-60-8	36.6	39.60	45.1	0.877
G550-0.94-30-70-8	35.0	45.00	47.2	0.954
G550-0.94-30-80-8	27.3	43.50	44.4	0.980
G550-0.94-40-60-8	32.9	39.90	44.6	0.895
G550-0.94-40-70-8	29.6	46.00	45.0	1.023
G550-0.94-40-80-8	27.3	41.50	45.4	0.914
G550-0.94-50-60-8	32.7	41.70	45.8	0.910
G550-0.94-50-70-8	29.6	41.70	46.1	0.904
G550-0.94-50-80-8	27.5	45.70	46.6	0.981
G550-0.94-30-110-8	19.3	38.60	42.5	0.907
G550-0.94-30-100-8	21.0	37.40	42.4	0.881
G550-0.94-20-20-5	74.3	39.30	39.2	1.002
G550-0.94-20-30-5	77.7	45.10	47.2	0.955
G550-0.94-25-25-5	76.7	43.90	45.3	0.970
G550-0.94-25-25-8	64.7	43.70	45.4	0.963
G550-0.94-25-30-8	69.7	47.10	48.1	0.980
			Mean	0.954
			COV	0.055

Table 6.7   Comparison of FEA Results with AS/NZS 4600 Predictions for Type B Low Strength Steel Sections

(a)   0.75 mm G250 steel

Specimen	P_{od} (kN)	Ultimate load (kN)		FEA/Pred.
		FEA	Pred.	
G250-0.75-30-40-5	45.9	22.8	24.6	0.927
G250-0.75-30-30-5	45.3	21.1	21.4	0.987
G250-0.75-30-30-8	40.1	21.6	21.9	0.988
G250-0.75-30-40-8	45.1	23.5	25.4	0.925
G250-0.75-40-30-8	35.2	22.7	22.6	1.003
G250-0.75-30-60-8	25.1	21.9	24.0	0.913
G250-0.75-40-60-8	21.1	22.5	21.0	1.073
G250-0.75-40-70-8	19.6	20.9	21.8	0.958
G250-0.75-50-60-8	21.1	22.9	21.7	1.055
G250-0.75-50-70-8	19.6	22.6	22.5	1.005
			Mean	0.983
			COV	0.055

(b)   0.94 mm G250 steel

Specimen	P_{od} (kN)	Ultimate load (kN)		
		FEA	Pred.	FEA/Pred.
G250-0.94-30-40-5	65.2	31.3	31.5	0.993
G250-0.94-30-30-5	65.8	28.0	27.4	1.023
G250-0.94-30-30-8	58.0	28.6	28.1	1.018
G250-0.94-30-40-8	63.0	32.5	32.5	1.000
G250-0.94-30-50-8	64.5	32.8	36.5	0.899
G250-0.94-40-30-8	52.8	29.8	29.6	1.008
G250-0.94-40-40-8	54.0	33.0	33.3	0.990
G250-0.94-40-50-8	55.6	36.6	37.0	0.990
G250-0.94-30-60-8	36.6	32.9	28.0	1.177
G250-0.94-30-70-8	35.0	31.5	29.8	1.057
G250-0.94-30-80-8	27.3	29.4	29.3	1.003
G250-0.94-40-60-8	32.9	33.2	28.2	1.178
G250-0.94-40-70-8	29.6	32.1	29.2	1.099
G250-0.94-40-80-8	27.3	27.8	30.2	0.922
G250-0.94-50-60-8	32.7	34.4	29.2	1.179
G250-0.94-50-70-8	29.6	30.5	30.1	1.012
G250-0.94-50-80-8	27.5	32.9	31.1	1.059
G250-0.94-30-110-8	19.3	26.6	29.3	0.908
			Mean	1.029
			COV	0.083

Tables 6.7 (a) and (b) show the FEA and predicted results from AS/NZS 4600 for low strength steel sections. Unlike in high strength steel, only one section of 0.55 mm G250 steel failed by distortional buckling and the ratio of FEA to predicted load from AS/NZS 4600 is 0.950. The mean values of the ratio of FEA to predicted results for 0.75 and 0.94 mm thick steel sections are 0.983 and 1.029, respectively. Therefore it can be stated that the AS/NZS 4600 design equations are accurate for G250 steel sections. Further Figure 6.8 shows the comparison of FEA results and the predictions from AS/NZS 4600 in a non-dimensionalised format.
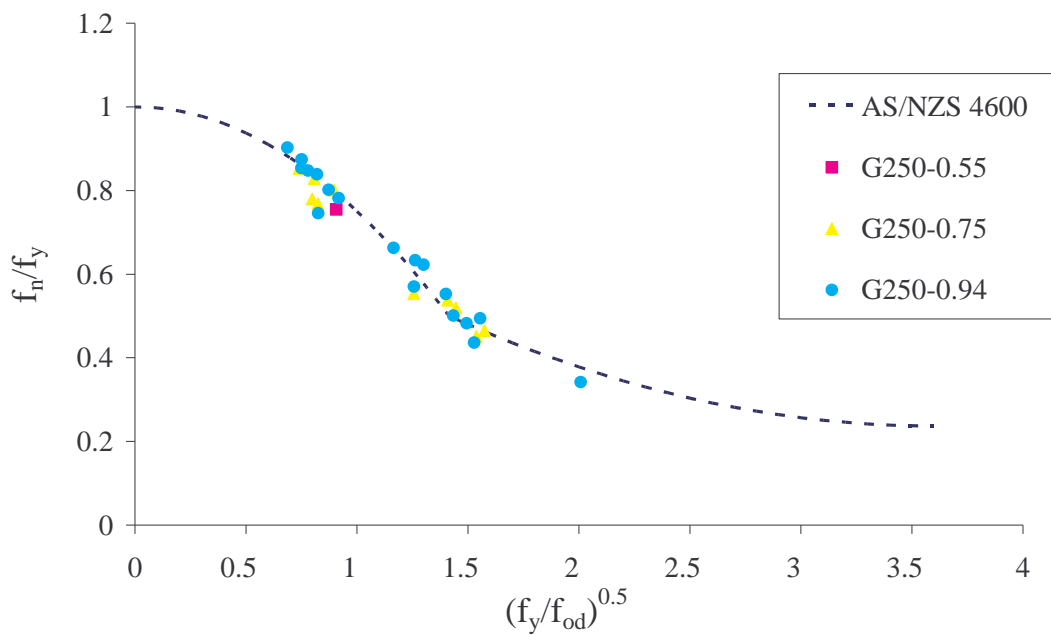
Figure 6.8   Comparison of AS/NZS 4600 Predictions with FEA Results for Type B G250 Steel Sections

6.3.2.2 Direct strength method

As given in Section 6.2.1, the direct strength method was used to predict the distortional buckling failure loads of Type B sections (see Equation 6.6). Tables 6.8 (a) to (c) compare the predictions from the direct strength method and the FEA results of 0.60, 0.80 and 0.94 mm G550 steel Type B sections. The mean values of the ratio of FEA to predicted values from the direct strength method are 0.910, 0.903 and 0.938 for 0.60, 0.80 and 0.94 mm thick Type B sections, respectively. Therefore it can be stated that the direct strength method is unsafe for thin members of high

strength steel Type B sections. Figure 6.9 also shows that the direct strength method is unsafe for some sections.

Table 6.8 Comparison of FEA Results with Direct Strength Method Predictions for Type B High Strength Steel Sections

(a)   0.6 mm G550 steel

Specimen	P_{od} (kN)	Ultimate load (kN)		FEA/Pred.
		FEA	Pred.	
G550-0.6-30-30-5	36.0	27.4	30.7	0.894
G550-0.6-30-30-8	31.5	26.4	29.8	0.887
G550-0.6-40-30-8	27.0	25.7	29.0	0.888
G550-0.6-40-60-8	15.5	22.5	26.4	0.852
G550-0.6-20-20-5	37.4	25.6	25.8	0.994
G550-0.6-25-25-5	43.5	27.8	30.4	0.916
G550-0.6-25-25-8	35.4	28.1	29.0	0.970
G550-0.6-25-30-8	39.9	28.4	32.2	0.882
			Mean	0.910
			COV	0.053

(b)   0.8 mm G550 steel

Specimen	P_{od} (kN)	Ultimate load (kN)		FEA/Pred.
		FEA	Pred.	
G550-0.8-30-40-5	51.6	36.7	45.2	0.812
G550-0.8-30-30-5	50.4	40.2	40.7	0.989
G550-0.8-30-30-8	44.8	40.2	39.8	1.009
G550-0.8-30-40-8	49.4	39.4	45.5	0.867
G550-0.8-40-30-8	39.7	39.1	39.5	0.991
G550-0.8-40-40-8	50.7	40.9	47.8	0.855
G550-0.8-30-60-8	28.0	31.3	39.4	0.795
G550-0.8-30-80-8	20.3	32.5	36.6	0.888
G550-0.8-40-60-8	24.1	31.4	37.4	0.840
G550-0.8-40-70-8	22.1	32.9	37.5	0.878
G550-0.8-40-80-8	20.7	34.5	37.7	0.914
G550-0.8-50-60-8	24.1	31.4	38.3	0.819
G550-0.8-50-70-8	22.3	33.8	38.5	0.878
G550-0.8-50-80-8	20.9	33.3	38.7	0.860
G550-0.8-20-20-5	55.7	33.9	34.7	0.976
G550-0.8-20-30-5	61.6	38.7	41.5	0.931
G550-0.8-25-25-5	59.8	37.7	39.8	0.947
G550-0.8-25-25-8	50.2	37.4	38.6	0.969
G550-0.8-25-25-8	55.1	40.1	42.4	0.946
			Mean	0.903
			COV	0.073

Table 6.8   Comparison of FEA Results with Direct Strength Method

Predictions for Type B High Strength Steel Sections

(c)   0.94 mm G550 steel

Specimen	P_{od} (kN)	Ultimate load (kN)		FEA/Pred.
		FEA	Pred.	
G550-0.94-30-40-5	65.2	48.6	53.3	0.911
G550-0.94-30-30-5	65.8	49.6	48.5	1.023
G550-0.94-30-30-8	58.0	49.3	47.6	1.035
G550-0.94-30-40-8	63.0	51.5	53.9	0.955
G550-0.94-30-50-8	64.5	52.3	58.8	0.889
G550-0.94-40-30-8	52.8	49.8	47.8	1.042
G550-0.94-40-40-8	54.0	52.9	52.4	1.010
G550-0.94-40-50-8	55.6	51.2	56.8	0.901
G550-0.94-30-60-8	36.6	39.6	47.7	0.829
G550-0.94-30-70-8	35.0	45.0	49.2	0.915
G550-0.94-30-80-8	27.3	43.5	45.2	0.962
G550-0.94-40-60-8	32.9	39.9	46.5	0.859
G550-0.94-40-70-8	29.6	46.0	46.2	0.997
G550-0.94-40-80-8	27.3	41.5	46.2	0.899
G550-0.94-50-60-8	32.7	41.7	47.5	0.878
G550-0.94-50-70-8	29.6	41.7	47.2	0.883
G550-0.94-50-80-8	27.5	45.7	47.3	0.966
G550-0.94-30-110-8	19.3	38.6	41.9	0.922
G550-0.94-30-100-8	21.0	37.4	42.4	0.882
G550-0.94-20-20-5	74.3	39.3	41.2	0.954
G550-0.94-20-30-5	77.7	45.1	48.6	0.928
G550-0.94-25-25-5	76.7	43.9	46.8	0.939
G550-0.94-25-25-8	64.7	43.7	45.7	0.956
G550-0.94-25-30-8	69.7	47.1	48.5	0.970
			Mean	0.938
			COV	0.061
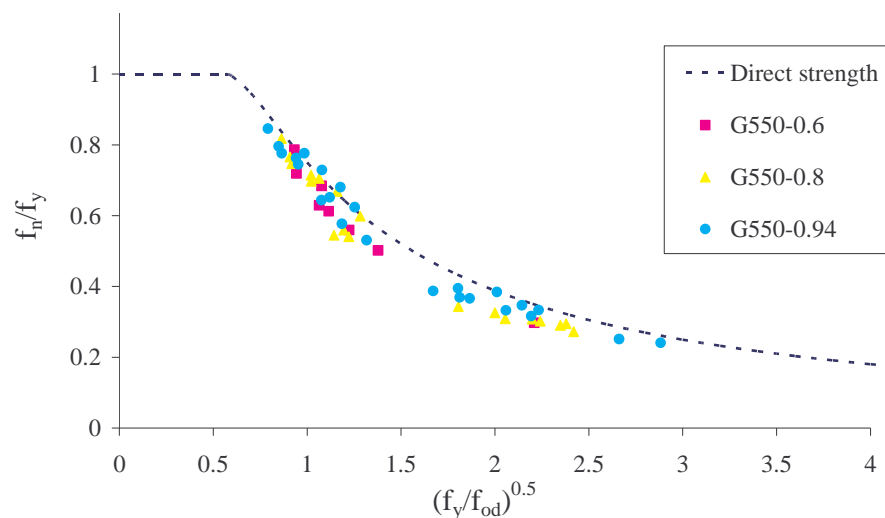
Figure 6.9   Comparison of Direct Strength Method Predictions with FEA

Results for Type B G550 Steel Sections

Table 6.9   Comparison of FEA Results with Direct Strength Method Predictions for Type B Low Strength Steel Sections

(a)   0.75 mm G250 steel

Specimen	P_{od} (kN)	Ultimate load (kN)		FEA/Pred.
		FEA	Pred.	
G250-0.75-30-40-5	45.9	22.8	25.8	0.885
G250-0.75-30-30-5	45.3	21.1	22.8	0.926
G250-0.75-30-30-8	40.1	21.6	22.8	0.945
G250-0.75-30-40-8	45.1	23.5	26.4	0.889
G250-0.75-40-30-8	35.2	22.7	23.1	0.983
G250-0.75-30-60-8	25.1	21.9	24.4	0.898
G250-0.75-40-60-8	21.1	22.5	23.1	0.972
G250-0.75-40-70-8	19.6	20.9	23.5	0.888
G250-0.75-50-60-8	21.1	22.9	23.8	0.963
G250-0.75-50-70-8	19.6	22.6	24.1	0.938
			Mean	0.929
			COV	0.040

(b)   0.94 mm G250 steel

Specimen	Pod (kN)	Ultimate load (kN)		FEA/Pred.
		FEA	Pred.	
G250-0.94-30-40-5	65.2	31.3	33.5	0.934
G250-0.94-30-30-5	65.8	28.0	29.6	0.946
G250-0.94-30-30-8	58.0	28.6	29.9	0.957
G250-0.94-30-40-8	63.0	32.5	34.3	0.949
G250-0.94-30-50-8	64.5	32.8	37.9	0.865
G250-0.94-40-30-8	52.8	29.8	30.8	0.968
G250-0.94-40-40-8	54.0	33.0	34.2	0.965
G250-0.94-40-50-8	55.6	36.6	37.5	0.976
G250-0.94-30-60-8	36.6	32.9	32.7	1.005
G250-0.94-30-70-8	35.0	31.5	34.0	0.926
G250-0.94-30-80-8	27.3	29.4	31.8	0.924
G250-0.94-40-60-8	32.9	33.2	32.2	1.032
G250-0.94-40-70-8	29.6	32.1	32.3	0.994
G250-0.94-40-80-8	27.3	27.8	32.6	0.854
G250-0.94-50-60-8	32.7	34.4	33.0	1.043
G250-0.94-50-70-8	29.6	30.5	33.1	0.921
G250-0.94-50-80-8	27.5	32.9	33.4	0.985
G250-0.94-30-110-8	19.3	26.6	30.1	0.885
			Mean	0.952
			COV	0.055

Tables 6.9 (a) and (b) show the FEA and predicted loads from the direct strength method for 0.75 and 0.94 mm G250 steel Type B sections. Only one section of 0.55 mm G250 steel failed by distortional buckling and the ratio between FEA to predicted value is 0.933. The mean of the ratios of FEA to predicted values are 0.929 and 0.952 for 0.75 and 0.94 mm thick steel sections, respectively. As shown in Tables 6.9 (a) and (b) and Figure 6.10 the predicted values obtained from the direct strength method are unsafe. However, they are in an acceptable region.
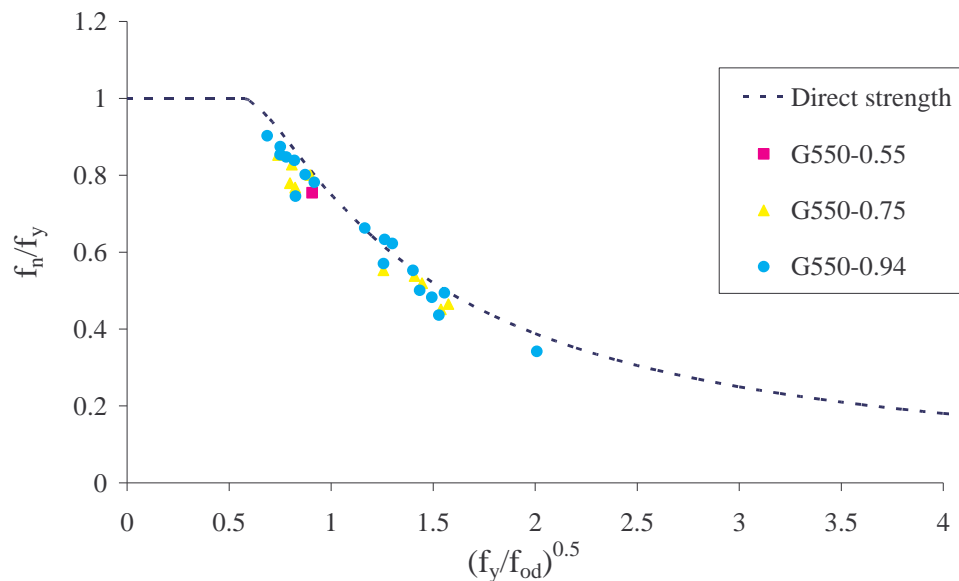
Figure 6.10   **Comparison of Direct Strength Method Predictions with FEA Results for Type B G250 Steel Sections**

6.3.3   Results

Table 6.10 gives a summary of results from Tables 6.2 to 6.9. It clearly shows that AS/NZS 4600 predictions are better than the predictions of the direct strength method. This summary table of results helps to investigate the effect of steel grade, thickness and geometry of the sections. However, based on the mean and the COV values given in Table 6.10 it is difficult to state that the AS/NZS 4600 predictions improve with increasing thickness. It can be observed that the AS/NZS 4600 predictions are better for 0.94 mm thick steel than other thicknesses. The results clearly show that the accuracy of AS/NZS 4600 predictions do not depend on the steel grade. However, in general the predictions for high strength Type B sections are less accurate than other sections. Finally it can be concluded that the AS/NZS 4600

predictions are reasonably accurate for light gauge cold-formed steel compression members subjected to distortional buckling, but improvements can be made to the current design equations to improve their accuracy further.

The overall mean and COV values for Type A and Type B sections made of G550 and G250 steels are shown in Table 6.11 while Figure 6.11 shows the comparison of FEA results with the design curves based on AS/NZS 4600 and direct strength method. This allows the comparison of the two design methods in different ways. Figure 6.11 shows that the AS/NZS 4600 design curves compare well with the FEA results than the direct strength method. The overall mean and the COV of the ratio of FEA to predicted values are 0.970 and 0.071 for the AS/NZS 4600 predictions while they are 0.935 and 0.062 and for the direct strength method predictions. This also confirms that the AS/NZS 4600 design equations are more accurate than the direct strength method for the cold-formed steel sections considered in this study.

Table 6.10   Summary of Tables 6.2 to 6.9

| Sections | FEA/Pred. Ultimate Load | | | | | |
| | AS/NZS 4600 | | | Direct Strength Method | | |
	Mean	COV	Φ	Mean	COV	Φ
G550-0.60-A	0.943	0.057	0.825	0.929	0.062	0.808
G550-0.80-A	0.972	0.057	0.867	0.938	0.063	0.833
G550-0.94-A	1.011	0.056	0.903	0.976	0.064	0.867
G250-0.55-A	1.005	0.012	-	0.943	0.017	-
G250-0.75-A	0.948	0.085	0.825	0.901	0.055	0.805
G250-0.94-A	0.981	0.046	0.881	0.940	0.050	0.842
G550-0.60-B	0.922	0.053	0.820	0.910	0.053	0.810
G550-0.80-B	0.914	0.070	0.808	0.903	0.073	0.796
G550-0.94-B	0.954	0.055	0.853	0.938	0.061	0.835
G250-0.55-B	0.950	-	-	0.933	-	-
G250-0.75-B	0.983	0.055	0.876	0.929	0.040	0.835
G250-0.94-B	1.029	0.083	0.898	0.952	0.055	0.850

Table 6.11 Overall Mean and COV for all the Considered Sections

	Mean / COV of FEA/Pred. Ultimate Load			
	Section	G550	G250	Overall
AS/NZS 4600	Type A	0.987 / 0.061	0.969 / 0.064	0.979 / 0.063
	Type B	0.934 / 0.063	1.010 / 0.076	0.962 / 0.078
	Overall	*0.958 / 0.067*	*0.987 / 0.072*	***0.970 / 0.071***
Direct Strength Method	Type A	0.955 / 0.066	0.924 / 0.053	0.941 / 0.062
	Type B	0.921 / 0.066	0.943 / 0.050	0.929 / 0.061
	Overall	*0.936 / 0.067*	*0.933 / 0.052*	***0.935 / 0.062***

However, the mean and COV values were calculated based on the nominal predicted values. But the actual ultimate load of the compression members may be less than that due to the expected variations of materials, fabrication and loading conditions. Therefore, in addition to the mean and COV values, the capacity reduction factor (Φ), which is commonly used in design codes, was calculated for each case.
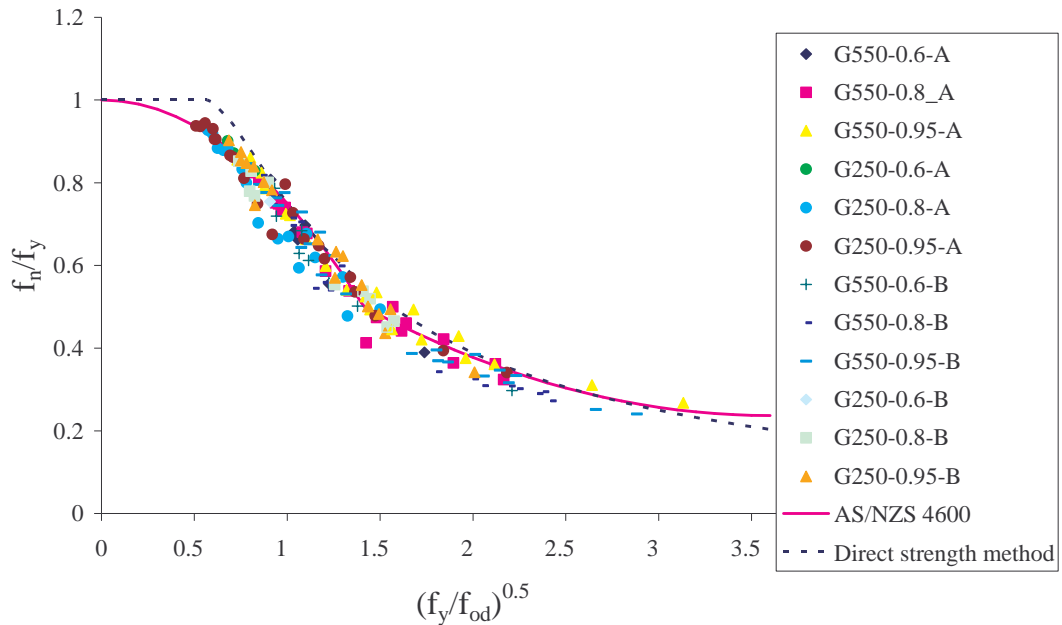
Figure 6.11 Comparison of FEA Results with the AS/NZS 4600 and Direct Strength Method Predictions

6.3.4   Capacity Reduction Factor

The American cold-formed steel structures code (AISI, 1996) recommends a statistical model to determine the capacity reduction factors. This model accounts for the variations in material, fabrication and the loading effects. The capacity reduction factor Φ is given by Equation 6.7.

$$\phi = 1.5 M_m F_m P_m e^{-\beta_0 \sqrt{V_m{}^2 + V_f{}^2 + C_p V_p{}^2 + V_q{}^2}} \tag{6.7}$$

where, M_m, V_m = Mean and coefficient of variation of the material factor = 1.1, 0.1

F_m, V_f = Mean and coefficient of variation of the fabrication factor = 1, 0.05

V_q = coefficient of variation of load effect = 0.21

β_0 = Target reliability index = 2.5

C_p = Correction factor depending on the number of tests = $\left(1 + \dfrac{1}{n}\right)\left(\dfrac{m}{m-2}\right)$

P_m = mean value of the tested to predicted load ratio

V_p = Coefficient of variation of the tested to predicted load ratio

n = Number of tests

m = Degree of freedom = n-1

V_p and P_m values have to be determined from experiments or analyses. In this investigation FEA ultimate loads were considered. Hence V_p and P_m are the mean and coefficient of variation of the ratio of ultimate load from FEA to ultimate load predicted by design equations. The substitution of all the above values leads to the following equation.

$$\phi = 1.65 P_m e^{-2.5\sqrt{0.0566 + C_p V_p{}^2}} \tag{6.8}$$

Equation 6.8 was used to determine the capacity reduction factors for the values obtained from the AS/NZS 4600 design equations and the direct strength method. The capacity reduction factors obtained for different grades of steels and thicknesses are shown in Table 6.10. It is clear that the geometry of the section, steel thickness or grade does not have a significant influence on the capacity reduction factor. From the list of capacity reduction factors in Table 6.10 also it can be concluded that the

AS/NZS 4600 predictions are more accurate than the direct strength method predictions. However, the obtained capacity reduction factors based on the AS/NZS 4600 and direct strength method predictions are less than the currently used factor of 0.9. It appears that the AS/NZS 4600 predictions are more accurate for 0.94 mm low and high strength steel Type A sections and Type B low strength steel sections than the other sections.

In conclusion, AS/NZS 4600 predictions are reasonably accurate for the cold-formed steel sections considered in this study, but not accurate in some cases while the direct strength method is more unsafe than the AS/NZS 4600 predictions. Therefore a new design equation was developed in this study to improve the accuracy of design load predictions.

6.3.5   Development of a New Design Equation

As shown in the last section the current design rules can be improved further to predict the ultimate loads of compression members subject to distortional buckling failures. In this section a new design equation is proposed based on the FEA results obtained. As stated earlier, two different section geometries with five thicknesses and two steel grades were considered in this process. The new equation was developed from simple curve fitting methods.

The approaches used to develop the AS/NZS 4600 and the direct strength method design equations are not the same although the same test results were used in developing these equations (Schafer and Pekoz, 1998). Therefore these distortional buckling equations were compared with the equations of other buckling modes (local and global/flexural) prior to the development of new equations. Figure 6.12 shows the comparison of available distortional buckling equations, the local buckling and the flexural buckling equations. The flexural buckling design curve drops from the beginning while the first part of the local buckling design curve gives a constant squash load up to a certain slenderness (λ) before dropping off. Distortional buckling has characteristics that are between those of local and flexural buckling. Therefore the distortional buckling design curve may be between the local and flexural

buckling curves. Figure 6.12 shows that both distortional buckling curves (AS/NZS 4600 and direct strength method) are between the local and global buckling curves. But their characteristics are different. The AS/NZS 4600 design curve (Distortional 1 in Figure 6.12) drops from the beginning while the direct strength method design curve (Distortional 2 in Figure 6.12) is horizontal at the beginning and then drops.
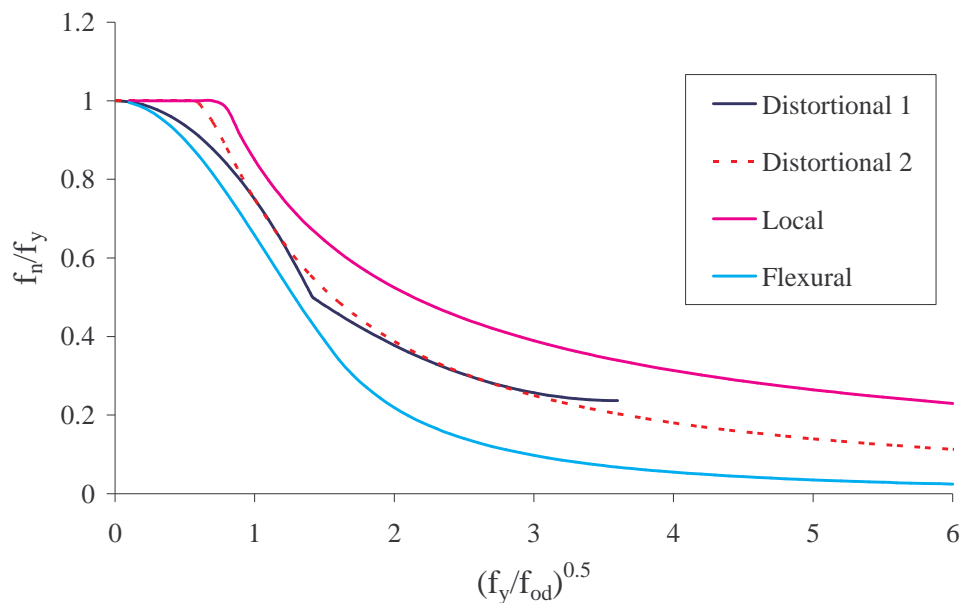
Figure 6.12   Comparison of Available Design Curves for Various Buckling Modes

As shown in Figure 6.11 the results obtained in this research show mainly two different patterns. When the slenderness is greater than about 0.7 it shows one pattern and below that, it shows a different pattern. Therefore the available distortional buckling equation cannot be simply modified and hence three options were considered first.

Option 1:

$\lambda \leq 0.4$ (about), $f_n/f_y = 1$ (considering no distortional buckling in this region, only simple yeilding)

$0.4 < \lambda < 0.7$ $f_n/f_y =$ Equation (a) (considering distortional buckling)

$\lambda \geq 0.7$ $f_n/f_y =$ Equation (b)   (considering distortional buckling)

Option 2:

$\lambda \leq 0.5$ (about), $f_n/f_y = 1$ (considering no distortional buckling in this region, only simple yielding)

$\lambda > 0.5$ $f_n/f_y =$ Equation (a) (considering distortional buckling)

Option 3:

$0 < \lambda \leq 0.7$ $f_n/f_y =$ Equation (a) (considering both distortional buckling and simple yielding)

$\lambda > 0.7$ $f_n/f_y =$ Equation (b) (considering distortional buckling)

Among these three options, Option 1 is based on simple curve fitting but seems to be more complex than the available design curves while Option 2 is similar to the design curve based on the direct strength method and Option 3 is similar to the AS/NZS 4600 design curve. Option 3 assumes that column strength decreases from the beginning, ie. $\lambda = 0$. Theoretically it is not possible to have column strength reducing from $\lambda = 0$.

In addition, the AS/NZS 4600 design equation is limited to $\lambda = 3.6$ while the equation based on the direct strength method has no limits. On the other hand the characteristics of the AS/NZS 4600 distortional buckling design curve is not the same as local and global buckling design curves. Therefore Option 3 or any modification of AS/NZS 4600 equation was not considered although the AS/NZS 4600 equation agrees reasonably well with FEA predictions. Further, since Option 1 is more complicated, Option 2 was considered at the beginning. The characteristics of the direct strength method were thus considered since Option 2 is similar to the direct strength method.

As shown in Figure 6.11 and in the above results, the direct strength method is somewhat unsafe for sections with low slenderness. Therefore the shape of the design curve should be changed for low slenderness. But it is not known whether the distortional buckling design curve will have a plateau for low slenderness values as for local buckling or whether it should drop from the beginning as for global buckling. However, Schafer (2006) stated that the distortional buckling strength curve does not drop off immediately as is the case for global buckling. Therefore

additional finite element analyses were conducted for the same sections (Type A) but with very low slenderness values. For this purpose, a range of half-wave lengths were chosen from 6 to 100 mm for FEA. A Type A section was chosen with 20 mm web height, 20 mm flange width and 5 mm lip length. Both low and high strength steels were considered with different thicknesses. Moreover, these sections were investigated with and without residual stresses. A total of 14 analyses were conducted and the results are presented in Figure 6.13 as short columns.

Figure with y-axis labeled f_n/f_y ranging from 0 to 1.2, and x-axis labeled $(f_y/f_{od})^{0.5}$ ranging from 0 to 4. Legend: G550-0.6-A, G550-0.8_A, G550-0.95-A, G250-0.6-A, G250-0.8-A, G250-0.95-A, G550-0.6-B, G550-0.8-B, G550-0.95-B, G250-0.6-B, G250-0.8-B, G250-0.95-B, short columns, Half-im.
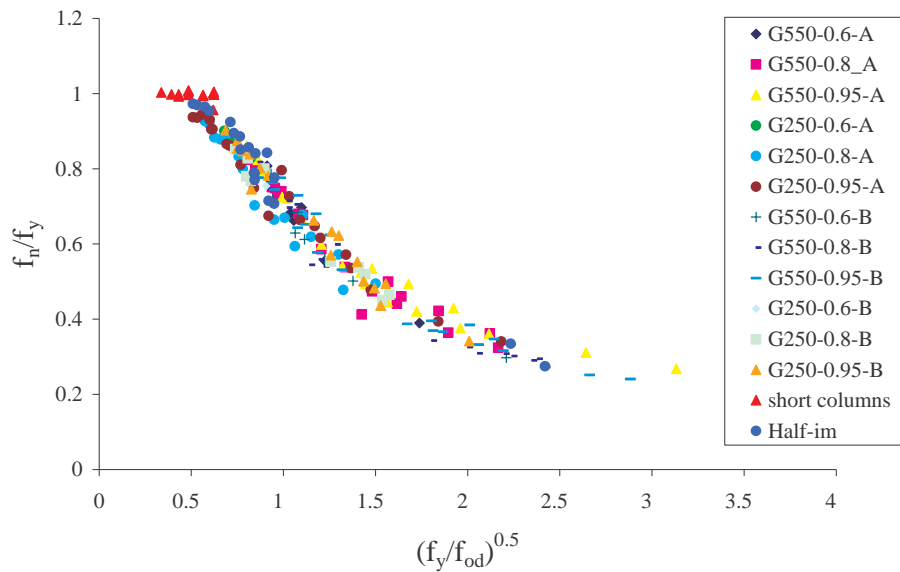
**Figure 6.13   Distortional Buckling Results for Various Sections
at Ambient Temperature**

Some of these sections were further analysed by using only half the initial geometric imperfections (defined as Half-im in Figure 6.13) used in the earlier analyses. This was undertaken to investigate the effect of the likely variation of imperfections in cold-formed steel specimens. The sections were arbitrarily selected from previously analysed sections. A total of 19 analyses was conducted. Type A sections were selected for both low and high strength steels with different thicknesses. As shown in Figure 6.13 the ultimate loads of the sections with low slenderness were equal to the squash load as for local buckling. Schafer (2006) also presented this phenomenon. The analyses of sections with half imperfections gave more data points to confidently develop the new design equation. These data points did not deviate significantly from those obtained with maximum imperfection values. All of these results gave confidence in the choice of the shape of the new design curves and the associated equations.

By considering all the above factors and the information in Figure 6.13 a new equation is proposed based on the equation used in the direct strength method (Option 2) and is given as Equation 6.9. The mean and COV values of the ratio between FEA to predictions from AS/NZS 4600 and the new equation (Equation 6.9) were determined and are shown in Table 6.12. The capacity reduction factor was also determined. Table 6.12 compares the predictions from AS/NZS 4600 and the new design equation. It clearly shows that the new equation predictions are better than the AS/NZS 4600 predictions for light gauge cold-formed steel compression members. Therefore this new equation (Equation 6.9) was used for further studies to examine the distortional buckling behaviour of compression members at elevated temperatures. In this way the effects of elevated temperatures on the distortional buckling behaviour of Type A and Type B sections chosen in this study were investigated.

$$\lambda < 0.55 \qquad P_n = Af_n = Af_y$$

$$\lambda \ge 0.55 \qquad P_n = Af_n = Af_y\left(1 - 0.31\left(\frac{f_{od}}{f_y}\right)^{0.4}\right)\left(\frac{f_{od}}{f_y}\right)^{0.58} \qquad (6.9)$$

$$\text{where,} \quad \lambda = \sqrt{\frac{f_y}{f_{od}}}$$

Additionally, Figure 6.14 gives a comparison of ultimate load predictions from AS/NZS 4600, the direct strength method and Equation 6.9. It clearly shows that the new design equation compares well with finite element analysis results. Further the overall mean and COV were determined from Equation 6.9 as 1.002 and 0.0641. They are better than AS/NZS 4600 predictions of 0.970 and 0.071. It should be stated that although the half geometric imperfections analyses were considered for some sections in the development of the new design equation, the values given for the mean and the COV are without considering them. The overall mean and COV based on all the analysis results are 1.005 and 0.0614 which is close to the mean and COV values for the case without considering the half geometric imperfections. It must be noted that the Φ factors for Equation 6.9 are closer to the currently used factor of 0.9 with the overall Φ factor of 0.893. Finally it can be concluded that Equation 6.9 accurately predicts the ultimate loads of light gauge cold-formed steel compression members subjected to distortional buckling failure at ambient temperature.

Table 6.12   Comparison of Predictions from AS/NZS 4600 and Equation 6.9

| Section | FEA/Pred. Ultimate Load | | | | | |
| | AS/NZS 4600 | | | Equation 6.9 | | |
	Mean	COV	Φ	Mean	COV	Φ
G550-0.60-A	0.943	0.057	0.825	1.019	0.063	0.896
G550-0.80-A	0.972	0.057	0.867	1.013	0.061	0.901
G550-0.94-A	1.011	0.056	0.903	1.043	0.051	0.935
G250-0.55-A	1.005	0.012	-	1.008	0.026	-
G250-0.75-A	0.948	0.085	0.825	0.963	0.051	0.862
G250-0.94-A	0.981	0.046	0.881	0.994	0.059	0.887
G550-0.60-B	0.922	0.053	0.820	0.983	0.060	0.869
G550-0.80-B	0.914	0.070	0.808	0.967	0.084	0.844
G550-0.94-B	0.954	0.055	0.853	1.003	0.069	0.889
G250-0.55-B	0.950	-	-	1.013	-	-
G250-0.75-B	0.983	0.055	0.876	1.000	0.041	0.900
G250-0.94-B	1.029	0.083	0.898	1.024	0.058	0.914
Overall	**0.970**	**0.071**	**0.860**	**1.002**	**0.064**	**0.893**
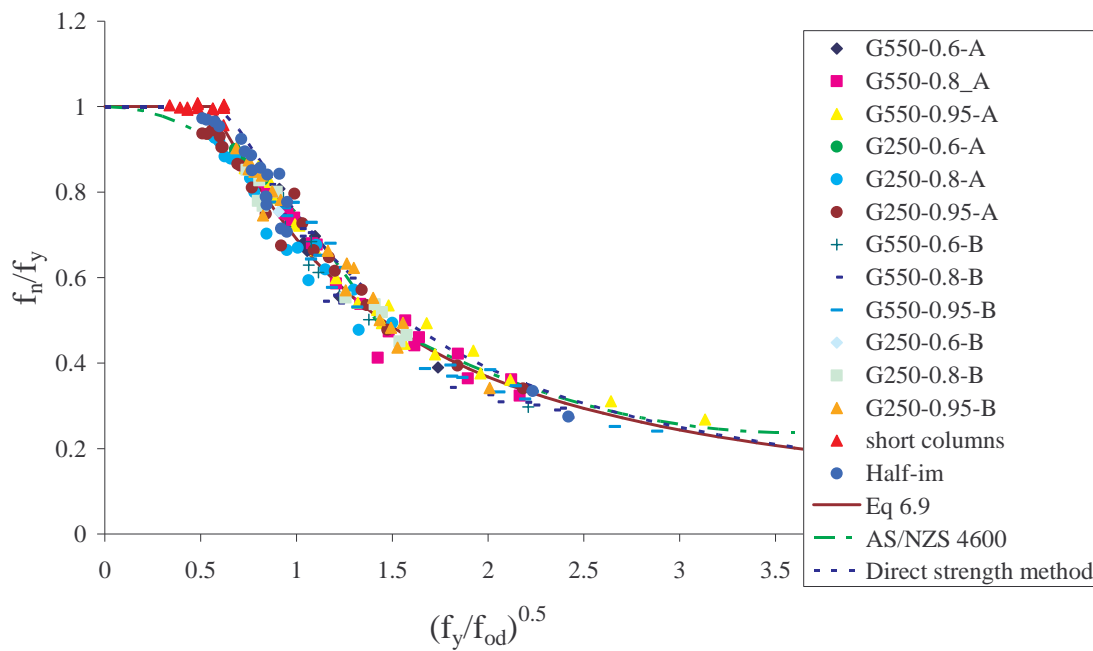
**Figure 6.14   Comparison of Equation 6.9 with FEA Results and
Other Design Equations**

6.4 Distortional Buckling Behaviour at Elevated Temperatures

The behaviour of cold-formed steel compression members which failed in the distortional buckling mode at elevated temperatures was investigated and the results were compared with the predictions from the developed equations in the last section. More than 700 analyses were undertaken in this investigation. The analysed sections were arbitrarily selected from the previous section (Section 6.3). Temperatures ranging from 100 to 800°C were considered: 100, 200, 350, 500, 650 and 800°C for the same cross-sections (Types A and B) used at ambient temperature. Both low (G250) and high (G550) strength steels were considered with the nominal thicknesses of 0.60, 0.80 and 0.95 mm. The imperfections were determined according to Schafer and Pekoz's (1998) equations given in Chapter 5 as Equation 5.4. The residual stresses were included based on Lee (2004) given in Chapter 5 as Equation 5.5. Mechanical properties were introduced in FEA as stated in Section 6.2. The isotropic strain-hardening behaviour was used since it is more accurate than the elastic perfect plasticity method. The stress-strain curves, yield strengths and elasticity modulus values used are given in Section 6.2. The obtained FEA results are given in Tables 6.13 to 6.18. The results presented in these tables are only for pure distortional buckling mode. In the first phase of this investigation the effect of temperature on different factors was studied.

The buckling mode is one of the most important factors of compression members subjected to distortional buckling. Therefore the effects of temperature on buckling modes were studied. Three main buckling modes were observed in the experimental study as discussed in Chapter 4: both flanges move inwards, both flanges move outwards and one flange move inwards while other moves outwards. As discussed in Chapter 4, some specimens show all three modes when the same tests were repeated and when the temperature was changed. However the results obtained from FEA showed that the buckling mode does not change with increasing temperatures. Those which failed when both flanges moved inwards or outwards at ambient temperature showed the same behaviour at elevated temperatures. Therefore, it can be concluded that the temperature does not affect the failure mode, but initial imperfections and thickness may affect it. The influence of imperfections on failure mode has already been discussed in Chapter 5 and it is clear that the direction of initial imperfection governs the type of distortional buckling failure mode of cold-formed steel sections.

Table 6.13   Ultimate Load (P_{nT}) and Elastic Buckling Load (P_{odT}) Obtained from FEA at 100°C

(a)   Type A sections

(b) Type B sections

Section	P_{odT} (kN)	P_{nT} (kN)	Section	P_{odT} (kN)	P_{nT}
G550-0.6-25-25-5	31.0	22.5	G250-0.55-25-25-5	22.0	12.0
G550-0.6-20-20-5	34.3	22.7	G250-0.55-20-20-5	26.7	10.0
G550-0.6-25-20-5	33.7	22.8	G250-0.55-25-20-5	26.0	11.0
G550-0.6-30-30-5	27.1	22.4	G250-0.75-25-25-5	41.4	16.1
G550-0.6-40-40-5	17.5	20.5	G250-0.75-25-30-5	37.2	17.0
G550-0.8-25-25-5	47.0	32.1	G250-0.75-25-35-5	33.2	15.9
G550-0.8-25-25-5	45.1	32.2	G250-0.75-25-40-5	28.7	16.4
G550-0.8-25-30-5	42.1	33.0	G250-0.75-25-45-5	24.9	16.4
G550-0.8-25-35-5	37.4	31.5	G250-0.75-20-20-5	47.9	13.9
G550-0.8-25-40-5	33.5	31.6	G250-0.75-25-20-5	47.2	14.8
G550-0.8-25-45-5	29.5	30.5	G250-0.75-30-20-5	46.0	15.3
G550-0.8-25-50-5	26.8	30.5	G250-0.75-30-30-5	37.0	17.3
G550-0.8-20-20-5	55.1	29.4	G250-0.75-40-40-5	24.0	19.8
G550-0.8-25-20-5	54.0	31.1	G250-0.94-25-25-5	63.3	20.7
G550-0.8-30-20-5	51.8	32.5	G250-0.94-25-30-5	56.0	22.2
G550-0.8-30-30-5	42.4	34.3	G250-0.94-25-35-5	50.3	23.1
G550-0.8-40-40-5	27.4	29.7	G250-0.94-25-40-5	45.9	23.5
G550-0.94-25-25-5	63.3	38.3	G250-0.94-25-45-5	41.7	23.0
G550-0.94-25-30-5	56.0	39.5	G250-0.94-25-110-5	15.1	23.5
G550-0.94-25-35-5	50.3	39.8	G250-0.94-25-90-5	17.9	23.1
G550-0.94-25-40-5	45.9	39.5	G250-0.94-25-70-5	22.7	22.9
G550-0.94-25-45-5	41.7	38.8	G250-0.94-20-20-5	76.1	17.7
G550-0.94-25-50-5	37.5	38.2	G250-0.94-25-20-5	74.7	18.8
G550-0.94-25-70-5	22.7	36.3	G250-0.94-30-20-5	72.4	20.3
G550-0.94-25-90-5	17.9	38.4	G250-0.94-30-30-5	56.4	23.3
G550-0.94-25-110-5	15.1	39.2	G250-0.94-40-40-5	37.4	28.4
G550-0.94-20-20-5	76.1	34.3			
G550-0.94-25-20-5	74.7	36.4			
G550-0.94-30-20-5	72.4	39.3			
G550-0.94-30-30-5	56.4	41.4			
G550-0.94-40-40-5	37.4	38.8			

Section	P_{odT} (kN)	P_{nT} (kN)	Section	P_{odT} (kN)	P_{nT}
G550-0.6-30-30-5	36.0	25.9	G250-0.55-30-30-8	24.8	14.9
G550-0.6-30-30-8	31.5	26.3	G250-0.75-30-40-5	45.9	22.2
G550-0.6-40-30-8	27.0	25.0	G250-0.75-30-30-5	45.3	20.1
G550-0.6-20-20-5	37.4	25.2	G250-0.75-30-30-8	40.1	20.6
G550-0.6-25-25-5	43.5	27.4	G250-0.75-30-40-8	45.1	22.6
G550-0.8-30-40-5	51.6	36.5	G250-0.75-40-30-8	35.2	21.8
G550-0.8-30-30-5	50.4	39.7	G250-0.75-30-60-8	25.1	21.3
G550-0.8-30-30-8	44.8	39.7	G250-0.94-30-40-5	65.2	30.0
G550-0.8-30-40-8	49.4	39.1	G250-0.94-30-30-5	65.8	26.8
G550-0.8-40-30-8	39.7	38.8	G250-0.94-30-30-8	58.0	27.4
G550-0.8-40-40-8	50.7	40.7	G250-0.94-30-40-8	63.0	31.2
G550-0.8-40-50-8	44.2	37.6	G250-0.94-30-50-8	64.5	31.4
G550-0.8-30-60-8	28.0	31.0	G250-0.94-40-30-8	52.8	28.7
G550-0.8-20-20-5	55.7	33.4	G250-0.94-40-40-8	54.0	31.8
G550-0.8-20-30-5	61.6	38.2	G250-0.94-40-50-8	55.6	35.7
G550-0.8-25-25-5	59.8	37.2	G250-0.94-30-60-8	36.6	32.9
G550-0.94-30-40-5	65.2	48.1			
G550-0.94-30-30-5	65.8	48.8			
G550-0.94-30-30-8	58.0	48.6			
G550-0.94-30-40-8	63.0	51.1			
G550-0.94-30-50-8	64.5	51.4			
G550-0.94-40-30-8	52.8	48.9			
G550-0.94-40-40-8	54.0	52.2			
G550-0.94-40-50-8	55.6	50.8			
G550-0.94-30-60-8	36.6	39.2			
G550-0.94-20-20-5	74.3	38.7			
G550-0.94-20-30-5	77.7	44.5			
G550-0.94-25-25-5	76.7	43.3			

**Table 6.14   Ultimate Load (P_{nT}) and Elastic Buckling Load (P_{odT}) Obtained from FEA at 200°C**

(a) Type A sections

Section	P_{odT} (kN)	P_{nT} (kN)	Section	P_{odT} (kN)	P_{nT}
G550-0.6-25-25-5	27.0	20.5	G250-0.55-25-25-5	19.1	11.3
G550-0.6-20-20-5	29.9	21.1	G250-0.55-20-20-5	23.2	9.9
G550-0.6-25-20-5	29.3	21.5	G250-0.55-25-20-5	22.6	10.3
G550-0.6-30-30-5	23.6	20.7	G250-0.75-25-25-5	36.0	15.5
G550-0.6-40-40-5	15.2	18.8	G250-0.75-25-30-5	32.3	16.3
G550-0.8-25-25-5	40.9	30.5	G250-0.75-25-35-5	28.9	15.1
G550-0.8-25-30-5	36.6	31.2	G250-0.75-25-40-5	24.9	15.4
G550-0.8-25-35-5	32.5	28.8	G250-0.75-25-45-5	21.6	15.4
G550-0.8-25-40-5	29.1	29.7	G250-0.75-20-20-5	41.7	13.5
G550-0.8-25-45-5	25.7	28.8	G250-0.75-25-20-5	41.0	14.3
G550-0.8-25-50-5	23.3	28.5	G250-0.75-30-20-5	40.0	14.8
G550-0.8-20-20-5	47.9	27.9	G250-0.75-30-30-5	32.2	16.4
G550-0.8-25-20-5	47.1	29.5	G250-0.75-40-40-5	20.8	18.1
G550-0.8-30-20-5	45.5	30.6	G250-0.94-25-25-5	55.1	19.7
G550-0.8-30-30-5	36.9	32.3	G250-0.94-25-30-5	48.7	21.0
G550-0.8-40-40-5	23.8	26.9	G250-0.94-25-35-5	43.7	21.7
G550-0.94-25-25-5	55.1	36.4	G250-0.94-25-40-5	39.9	21.8
G550-0.94-25-30-5	48.7	37.5	G250-0.94-25-45-5	36.2	21.5
G550-0.94-25-35-5	43.7	37.6	G250-0.94-25-110-5	13.1	22.1
G550-0.94-25-40-5	39.9	37.2	G250-0.94-25-90-5	15.6	21.3
G550-0.94-25-45-5	36.2	36.4	G250-0.94-25-70-5	19.8	21.4
G550-0.94-25-50-5	32.6	35.6	G250-0.94-20-20-5	66.2	16.9
G550-0.94-25-70-5	19.8	34.0	G250-0.94-25-20-5	65.0	18.0
G550-0.94-25-90-5	15.6	35.9	G250-0.94-30-20-5	63.0	19.4
G550-0.94-25-110-5	13.1	36.6	G250-0.94-30-30-5	49.0	22.4
G550-0.94-20-20-5	66.2	32.7	G250-0.94-40-40-5	32.5	26.1
G550-0.94-25-20-5	65.0	34.7			
G550-0.94-30-20-5	63.0	37.2			
G550-0.94-30-30-5	49.0	40.5			
G550-0.94-40-40-5	32.5	35.8			

(b) Type B sections

Section	P_{odT} (kN)	P_{nT} (kN)	Section	P_{odT} (kN)	P_{nT}
G550-0.6-30-30-5	31.3	22.6	G250-0.55-30-30-8	21.6	13.6
G550-0.6-30-30-8	27.4	23.4	G250-0.75-30-40-5	39.9	20.9
G550-0.6-40-30-8	23.5	22.3	G250-0.75-30-30-5	39.4	19.3
G550-0.6-20-20-5	32.6	23.6	G250-0.75-30-30-8	34.9	19.8
G550-0.6-25-25-6	37.8	24.9	G250-0.75-30-40-8	39.0	21.3
G550-0.8-30-40-5	44.9	33.2	G250-0.75-40-30-8	30.6	20.7
G550-0.8-30-30-5	44.3	36.7	G250-0.75-30-60-8	21.9	19.7
G550-0.8-30-30-8	39.0	36.9	G250-0.94-30-40-5	56.7	28.2
G550-0.8-30-40-8	43.0	35.9	G250-0.94-30-30-5	57.2	25.4
G550-0.8-40-30-8	34.5	35.6	G250-0.94-30-30-8	50.5	25.9
G550-0.8-40-40-8	44.1	36.8	G250-0.94-30-40-8	54.8	29.5
G550-0.8-40-50-8	38.4	32.9	G250-0.94-30-50-8	56.1	29.4
G550-0.8-30-60-8	24.4	27.9	G250-0.94-40-30-8	45.9	27.1
G550-0.8-20-20-5	48.4	31.5	G250-0.94-40-40-8	46.9	29.7
G550-0.8-20-30-5	53.6	35.6	G250-0.94-40-50-8	48.3	33.4
G550-0.8-25-25-5	52.0	35.1	G250-0.94-30-60-8	31.9	28.9
G550-0.94-30-40-5	56.7	43.4			
G550-0.94-30-30-5	57.2	45.6			
G550-0.94-30-30-8	50.5	44.9			
G550-0.94-30-40-8	54.8	45.8			
G550-0.94-30-50-8	56.1	47.2			
G550-0.94-40-30-8	45.9	46.2			
G550-0.94-40-40-8	46.9	47.2			
G550-0.94-40-50-8	48.3	45.9			
G550-0.94-30-60-8	31.9	36.5			
G550-0.94-20-20-5	64.6	36.7			
G550-0.94-20-30-5	67.6	42.0			
G550-0.94-25-25-5	66.7	41.0			

Table 6.15   Ultimate Load (P_{nT}) and Elastic Buckling Load (P_{odT}) Obtained from FEA at 350°C

(a) Type A sections

Section	P_{odT} (kN)	P_{nT} (kN)	Section	P_{odT} (kN)	P_{nT}
G550-0.6-25-25-5	20.9	16.2	G250-0.55-25-25-5	14.8	6.7
G550-0.6-20-20-5	23.2	17.0	G250-0.55-20-20-5	18.0	6.2
G550-0.6-25-20-5	22.8	17.3	G250-0.55-25-20-5	17.5	6.3
G550-0.6-30-30-5	18.3	16.6	G250-0.75-25-25-5	27.9	9.7
G550-0.6-40-40-5	11.8	15.0	G250-0.75-25-30-5	25.1	9.9
G550-0.8-25-25-5	31.7	25.2	G250-0.75-25-35-5	22.4	9.4
G550-0.8-25-30-5	28.4	25.8	G250-0.75-25-40-5	19.4	9.6
G550-0.8-25-35-5	25.2	23.9	G250-0.75-25-45-5	16.9	9.5
G550-0.8-25-40-5	22.6	24.1	G250-0.75-30-20-5	31.1	9.4
G550-0.8-25-45-5	19.9	23.2	G250-0.75-30-30-5	25.0	9.9
G550-0.8-25-50-5	18.1	22.9	G250-0.75-40-40-5	16.2	10.9
G550-0.8-20-20-5	37.1	23.0	G250-0.94-25-25-5	44.9	12.8
G550-0.8-25-20-5	36.5	24.2	G250-0.94-25-30-5	37.8	13.5
G550-0.8-30-20-5	35.3	25.1	G250-0.94-25-35-5	33.9	13.5
G550-0.8-30-30-5	28.6	26.0	G250-0.94-25-40-5	31.0	13.6
G550-0.8-40-40-5	18.5	21.5	G250-0.94-25-45-5	28.1	13.5
G550-0.94-25-25-5	42.7	30.1	G250-0.94-25-110-5	10.2	14.0
G550-0.94-25-30-5	37.8	30.9	G250-0.94-25-90-5	12.1	13.6
G550-0.94-25-35-5	33.9	30.8	G250-0.94-25-70-5	15.3	13.5
G550-0.94-25-40-5	31.0	29.3	G250-0.94-30-30-5	38.0	14.0
G550-0.94-25-45-5	28.1	30.1	G250-0.94-40-40-5	25.2	15.1
G550-0.94-25-50-5	25.3	29.8			
G550-0.94-25-70-5	15.3	27.8			
G550-0.94-25-90-5	12.1	29.2			
G550-0.94-25-110-5	10.2	29.8			
G550-0.94-20-20-5	51.4	27.1			
G550-0.94-25-20-5	50.4	28.7			
G550-0.94-30-20-5	48.9	30.4			
G550-0.94-30-30-5	38.0	32.3			
G550-0.94-40-40-5	25.2	28.7			

(b) Type B sections

Section	P_{odT} (kN)	P_{nT} (kN)	Section	P_{odT} (kN)	P_{nT}
G550-0.6-30-30-5	24.3	18.5	G250-0.55-30-30-8	16.7	8.1
G550-0.6-30-30-8	21.3	18.7	G250-0.75-30-40-5	30.9	12.2
G550-0.6-40-30-8	18.2	17.7	G250-0.75-30-30-5	30.6	11.5
G550-0.6-20-20-5	25.3	19.2	G250-0.75-30-30-8	27.1	11.9
G550-0.6-25-25-6	29.3	19.8	G250-0.75-30-40-8	30.5	12.4
G550-0.8-30-40-5	34.8	26.4	G250-0.75-40-30-8	23.7	12.2
G550-0.8-30-30-5	34.3	29.7	G250-0.75-30-60-8	17.0	12.5
G550-0.8-30-30-8	30.3	29.5	G250-0.94-30-40-5	44.0	16.7
G550-0.8-30-40-8	33.3	28.7	G250-0.94-30-30-5	44.4	15.6
G550-0.8-40-30-8	26.8	28.6	G250-0.94-30-30-8	39.2	16.1
G550-0.8-40-40-8	34.2	29.1	G250-0.94-30-40-8	42.5	17.7
G550-0.8-40-50-8	29.8	28.2	G250-0.94-30-50-8	43.6	18.2
G550-0.8-30-60-8	18.9	23.3	G250-0.94-40-30-8	35.6	16.7
G550-0.8-20-20-5	37.6	25.6	G250-0.94-40-40-8	36.4	18.2
G550-0.8-20-30-5	41.5	28.9	G250-0.94-40-50-8	37.5	19.5
G550-0.8-25-25-5	40.4	28.6	G250-0.94-30-60-8	24.7	17.8
G550-0.94-30-40-5	44.0	34.3			
G550-0.94-30-30-5	44.4	36.8			
G550-0.94-30-30-8	39.2	36.5			
G550-0.94-30-40-8	42.5	35.8			
G550-0.94-30-50-8	43.6	37.7			
G550-0.94-40-30-8	35.6	37.7			
G550-0.94-40-40-8	36.4	38.3			
G550-0.94-40-50-8	37.5	36.4			
G550-0.94-30-60-8	24.7	29.8			
G550-0.94-20-20-5	50.1	30.0			
G550-0.94-20-30-5	52.4	34.5			
G550-0.94-25-25-5	51.7	33.7			

Table 6.16   Ultimate Load (P$_{nT}$) and Elastic Buckling Load (P$_{odT}$) Obtained from FEA at 500°C

(a) Type A sections

Section	P$_{odT}$ (kN)	P$_{nT}$ (kN)	Section	P$_{odT}$ (kN)	P$_{nT}$
G550-0.6-25-25-5	14.9	10.2	G250-0.55-25-25-5	10.6	4.3
G550-0.6-20-20-5	16.5	10.1	G250-0.55-20-20-5	12.8	3.7
G550-0.6-25-20-5	16.2	10.4	G250-0.55-25-20-5	12.5	3.9
G550-0.6-30-30-5	13.0	10.4	G250-0.75-25-25-5	19.8	5.8
G550-0.6-40-40-5	8.4	9.5	G250-0.75-25-30-5	17.8	6.2
G550-0.8-25-25-5	22.5	14.8	G250-0.75-25-35-5	15.9	6.1
G550-0.8-25-30-5	20.2	15.1	G250-0.75-25-40-5	13.8	6.1
G550-0.8-25-35-5	17.9	14.5	G250-0.75-25-45-5	11.9	6.0
G550-0.8-25-40-5	16.1	14.4	G250-0.75-20-20-5	23.0	5.0
G550-0.8-25-45-5	14.2	13.8	G250-0.75-25-20-5	22.7	5.3
G550-0.8-25-50-5	12.9	13.7	G250-0.75-30-20-5	22.1	5.6
G550-0.8-20-20-5	26.4	13.3	G250-0.75-30-30-5	17.7	6.2
G550-0.8-25-20-5	26.0	14.0	G250-0.75-40-40-5	11.5	7.4
G550-0.8-30-20-5	25.1	14.7	G250-0.94-25-25-5	30.4	7.5
G550-0.8-30-30-5	20.3	15.8	G250-0.94-25-30-5	26.8	8.0
G550-0.8-40-40-5	13.1	13.8	G250-0.94-25-35-5	24.1	8.3
G550-0.94-25-25-5	30.4	17.5	G250-0.94-25-40-5	22.1	8.5
G550-0.94-25-30-5	26.8	18.0	G250-0.94-25-45-5	20.0	8.6
G550-0.94-25-35-5	24.1	18.2	G250-0.94-25-110-5	7.2	8.8
G550-0.94-25-40-5	22.1	18.0	G250-0.94-25-90-5	8.6	8.7
G550-0.94-25-45-5	20.0	17.8	G250-0.94-25-70-5	10.9	8.6
G550-0.94-25-50-5	19.8	17.6	G250-0.94-20-20-5	36.5	6.5
G550-0.94-25-70-5	10.9	16.6	G250-0.94-25-20-5	35.8	6.9
G550-0.94-25-90-5	8.6	17.5	G250-0.94-30-20-5	34.8	7.4
G550-0.94-25-110-5	7.2	17.9	G250-0.94-30-30-5	27.0	8.4
G550-0.94-20-20-5	36.5	15.5	G250-0.94-40-40-5	17.9	9.8
G550-0.94-25-20-5	35.8	16.4			
G550-0.94-30-20-5	34.8	17.5			
G550-0.94-30-30-5	27.0	18.8			
G550-0.94-40-40-5	17.9	17.8			

(b) Type B sections

Section	P$_{odT}$ (kN)	P$_{nT}$ (kN)	Section	P$_{odT}$ (kN)	P$_{nT}$
G550-0.6-30-30-5	17.3	11.6	G250-0.55-30-30-8	11.9	5.3
G550-0.6-30-30-8	15.1	12.3	G250-0.75-30-40-5	22.0	7.9
G550-0.6-40-30-8	13.0	11.6	G250-0.75-30-30-5	21.7	7.1
G550-0.6-20-20-5	18.0	11.3	G250-0.75-30-30-8	19.2	7.3
G550-0.6-25-25-6	20.8	12.2	G250-0.75-30-40-8	21.7	8.1
G550-0.8-30-40-5	24.8	16.8	G250-0.75-40-30-8	16.9	7.7
G550-0.8-30-30-5	24.4	17.9	G250-0.75-30-60-8	12.1	8.6
G550-0.8-30-30-8	21.5	18.0	G250-0.94-30-40-5	31.3	10.5
G550-0.8-30-40-8	23.7	17.9	G250-0.94-30-30-5	31.5	9.4
G550-0.8-40-30-8	19.0	17.9	G250-0.94-30-30-8	27.8	9.4
G550-0.8-40-40-8	24.3	18.8	G250-0.94-30-40-8	30.2	10.9
G550-0.8-40-50-8	21.2	17.8	G250-0.94-30-50-8	31.0	11.4
G550-0.8-30-60-8	13.4	14.4	G250-0.94-40-30-8	25.3	10.1
G550-0.8-20-20-5	26.7	14.9	G250-0.94-40-40-8	25.9	11.3
G550-0.8-20-30-5	29.5	17.3	G250-0.94-40-50-8	26.7	12.6
G550-0.8-25-25-5	28.7	16.8	G250-0.94-30-60-8	17.6	12.1
G550-0.94-30-40-5	31.3	21.9			
G550-0.94-30-30-5	31.5	21.8			
G550-0.94-30-30-8	27.8	21.3			
G550-0.94-30-40-8	30.2	23.2			
G550-0.94-30-50-8	31.0	23.5			
G550-0.94-40-30-8	25.3	22.2			
G550-0.94-40-40-8	25.9	24.0			
G550-0.94-40-50-8	26.7	23.2			
G550-0.94-30-60-8	17.6	18.2			
G550-0.94-20-20-5	35.7	17.3			
G550-0.94-20-30-5	37.3	20.1			
G550-0.94-25-25-5	36.8	19.5			

Table 6.17   Ultimate Load (P_{nT}) and Elastic Buckling Load (P_{odT}) Obtained from FEA at 650°C

(a) Type A sections

Section	P_{odT} (kN)	P_{nT} (kN)	Section	P_{odT} (kN)	P_{nT}
G550-0.6-25-25-5	8.8	2.9	G250-0.55-25-25-5	6.3	2.3
G550-0.6-20-20-5	9.8	2.6	G250-0.55-20-20-5	7.6	2.0
G550-0.6-25-20-5	9.6	2.7	G250-0.55-25-20-5	7.4	2.1
G550-0.6-30-30-5	7.7	3.1	G250-0.75-25-25-5	11.8	3.1
G550-0.6-40-40-5	5.0	3.4	G250-0.75-25-30-5	10.6	3.3
G550-0.8-25-25-5	13.4	3.8	G250-0.75-25-35-5	9.4	3.4
G550-0.8-25-30-5	12.0	4.0	G250-0.75-25-40-5	8.2	3.4
G550-0.8-25-35-5	10.7	4.2	G250-0.75-25-45-5	7.1	3.3
G550-0.8-25-40-5	9.5	4.2	G250-0.75-20-20-5	13.6	2.6
G550-0.8-25-45-5	8.4	4.1	G250-0.75-25-20-5	13.4	2.8
G550-0.8-25-50-5	7.6	4.0	G250-0.75-30-20-5	13.1	2.9
G550-0.8-20-20-5	15.7	3.2	G250-0.75-30-30-5	10.5	3.3
G550-0.8-25-20-5	15.4	3.5	G250-0.75-40-40-5	6.8	4.2
G550-0.8-30-20-5	14.9	3.6	G250-0.94-25-25-5	18.0	3.9
G550-0.8-30-30-5	12.1	4.2	G250-0.94-25-30-5	15.9	4.2
G550-0.8-40-40-5	7.8	5.0	G250-0.94-25-35-5	14.3	4.5
G550-0.94-25-25-5	18.0	4.3	G250-0.94-25-40-5	13.1	4.7
G550-0.94-25-30-5	15.9	4.7	G250-0.94-25-45-5	11.9	4.7
G550-0.94-25-35-5	14.3	4.9	G250-0.94-25-110-5	4.3	4.9
G550-0.94-25-40-5	13.1	5.1	G250-0.94-25-90-5	5.1	4.8
G550-0.94-25-45-5	11.9	5.1	G250-0.94-25-70-5	6.5	4.8
G550-0.94-25-50-5	10.7	5.0	G250-0.94-20-20-5	21.7	3.3
G550-0.94-25-70-5	6.5	5.1	G250-0.94-25-20-5	21.3	3.5
G550-0.94-25-90-5	5.1	5.1	G250-0.94-30-20-5	20.6	3.8
G550-0.94-25-110-5	4.3	5.3	G250-0.94-30-30-5	16.0	4.4
G550-0.94-20-20-5	21.7	3.7	G250-0.94-40-40-5	10.6	5.5
G550-0.94-25-20-5	21.3	3.9			
G550-0.94-30-20-5	20.6	4.2			
G550-0.94-30-30-5	16.0	4.9			
G550-0.94-40-40-5	10.6	6.0			

(b) Type B sections

Section	P_{odT} (kN)	P_{nT} (kN)	Section	P_{odT} (kN)	P_{nT}
G550-0.6-30-30-5	10.3	3.4	G250-0.55-30-30-8	7.1	3.0
G550-0.6-30-30-8	9.0	3.7	G250-0.75-30-40-5	13.1	4.4
G550-0.6-40-30-8	7.7	3.9	G250-0.75-30-30-5	12.9	3.8
G550-0.6-20-20-5	10.7	2.9	G250-0.75-30-30-8	11.4	4.0
G550-0.6-25-25-6	12.4	3.3	G250-0.75-30-40-8	12.8	4.5
G550-0.8-30-40-5	14.7	5.3	G250-0.75-40-30-8	10.0	4.3
G550-0.8-30-30-5	14.5	4.7	G250-0.75-30-60-8	7.2	4.9
G550-0.8-30-30-8	12.8	4.8	G250-0.94-30-40-5	18.6	5.7
G550-0.8-30-40-8	14.1	5.4	G250-0.94-30-30-5	18.7	5.0
G550-0.8-40-30-8	11.3	5.2	G250-0.94-30-30-8	16.5	5.1
G550-0.8-40-40-8	14.4	6.0	G250-0.94-30-40-8	17.9	5.9
G550-0.8-40-50-8	12.6	6.3	G250-0.94-30-50-8	18.4	6.2
G550-0.8-30-60-8	8.0	5.3	G250-0.94-40-30-8	15.0	5.5
G550-0.8-20-20-5	15.9	3.7	G250-0.94-40-40-8	15.4	6.1
G550-0.8-20-30-5	17.5	4.4	G250-0.94-40-50-8	15.8	6.9
G550-0.8-25-25-5	17.0	4.2	G250-0.94-30-60-8	10.4	6.9
G550-0.94-30-40-5	18.6	6.2			
G550-0.94-30-30-5	18.7	5.5			
G550-0.94-30-30-8	16.5	5.6			
G550-0.94-30-40-8	17.9	6.5			
G550-0.94-30-50-8	18.4	6.8			
G550-0.94-40-30-8	15.0	6.0			
G550-0.94-40-40-8	15.4	6.7			
G550-0.94-40-50-8	15.8	7.5			
G550-0.94-30-60-8	10.4	7.3			
G550-0.94-20-20-5	21.1	4.2			
G550-0.94-20-30-5	22.1	5.0			
G550-0.94-25-25-5	21.8	4.8			

Table 6.18   Ultimate Load (P_{nT}) and Elastic Buckling Load (P_{odT}) Obtained from FEA at 800°C

(a) Type A sections

Section	P_{odT} (kN)	P_{nT} (kN)	Section	P_{odT} (kN)	P_{nT}
G550-0.6-25-25-5	2.8	1.2	G250-0.75-25-25-5	3.7	0.9
G550-0.6-20-20-5	3.1	1.0	G250-0.75-25-30-5	3.3	1.0
G550-0.6-25-20-5	3.0	1.1	G250-0.75-25-35-5	3.0	1.0
G550-0.6-30-30-5	2.4	1.2	G250-0.75-25-40-5	2.6	1.0
G550-0.6-40-40-5	1.6	1.3	G250-0.75-25-45-5	2.2	1.0
G550-0.8-25-25-5	4.2	1.6	G250-0.75-20-20-5	4.3	0.8
G550-0.8-25-30-5	3.8	1.7	G250-0.75-25-20-5	4.2	0.8
G550-0.8-25-35-5	3.4	1.7	G250-0.75-30-20-5	4.1	0.9
G550-0.8-25-40-5	3.0	1.7	G250-0.75-30-30-5	3.3	1.0
G550-0.8-25-45-5	2.6	1.6	G250-0.75-40-40-5	2.1	1.3
G550-0.8-25-50-5	2.4	1.6	G250-0.94-25-25-5	5.7	1.1
G550-0.8-20-20-5	4.9	1.3	G250-0.94-25-30-5	5.0	1.2
G550-0.8-25-20-5	4.8	1.4	G250-0.94-25-35-5	4.5	1.3
G550-0.8-30-20-5	4.7	1.5	G250-0.94-25-40-5	4.1	1.4
G550-0.8-30-30-5	3.8	1.7	G250-0.94-25-45-5	3.7	1.4
G550-0.8-40-40-5	2.5	2.0	G250-0.94-25-110-5	1.4	1.5
G550-0.94-25-25-5	5.7	1.8	G250-0.94-25-90-5	1.6	1.4
G550-0.94-25-30-5	5.0	1.9	G250-0.94-25-70-5	2.0	1.4
G550-0.94-25-35-5	4.5	2.0	G250-0.94-20-20-5	6.8	1.0
G550-0.94-25-40-5	4.1	2.0	G250-0.94-25-20-5	6.7	1.0
G550-0.94-25-45-5	3.7	2.0	G250-0.94-30-20-5	6.5	1.1
G550-0.94-25-50-5	3.4	2.0	G250-0.94-30-30-5	5.1	1.3
G550-0.94-25-70-5	2.0	2.0	G250-0.94-40-40-5	3.4	1.7
G550-0.94-25-90-5	1.6	2.0			
G550-0.94-25-110-5	1.4	2.0			
G550-0.94-20-20-5	6.8	1.5			
G550-0.94-25-20-5	6.7	1.6			
G550-0.94-30-20-5	6.5	1.8			
G550-0.94-30-30-5	5.1	2.0			
G550-0.94-40-40-5	3.4	1.7			

(b) Type B sections

Section	P_{odT} (kN)	P_{nT} (kN)	Section	P_{odT} (kN)	P_{nT}
G550-0.6-30-30-5	3.2	1.4	G250-0.75-30-40-5	4.1	1.3
G550-0.6-30-30-8	2.8	1.5	G250-0.75-30-30-5	4.1	1.1
G550-0.6-40-30-8	2.4	1.6	G250-0.75-30-30-8	3.6	1.2
G550-0.6-20-20-5	3.4	1.2	G250-0.75-30-40-8	4.0	1.3
G550-0.6-25-25-6	3.9	1.3	G250-0.75-40-30-8	3.2	1.3
G550-0.8-30-40-5	4.6	2.2	G250-0.75-30-60-8	2.3	1.5
G550-0.8-30-30-5	4.6	2.0	G250-0.94-30-40-5	5.9	1.7
G550-0.8-30-30-8	4.0	2.0	G250-0.94-30-30-5	5.9	1.5
G550-0.8-30-40-8	4.4	2.2	G250-0.94-30-30-8	5.2	1.5
G550-0.8-40-30-8	3.6	2.1	G250-0.94-30-40-8	5.6	1.8
G550-0.8-40-40-8	4.6	2.4	G250-0.94-30-50-8	5.8	1.8
G550-0.8-40-50-8	4.0	2.5	G250-0.94-40-30-8	4.7	1.6
G550-0.8-30-60-8	2.5	2.0	G250-0.94-40-40-8	4.8	1.8
G550-0.8-20-20-5	5.0	1.5	G250-0.94-40-50-8	5.0	2.1
G550-0.8-20-30-5	5.5	1.8	G250-0.94-30-60-8	3.3	2.1
G550-0.8-25-25-5	5.4	1.7			
G550-0.94-30-40-5	5.9	2.5			
G550-0.94-30-30-5	5.9	2.3			
G550-0.94-30-30-8	5.2	2.3			
G550-0.94-30-40-8	5.6	2.7			
G550-0.94-30-50-8	5.8	2.7			
G550-0.94-40-30-8	4.7	2.4			
G550-0.94-40-40-8	4.8	2.7			
G550-0.94-40-50-8	5.0	3.0			
G550-0.94-30-60-8	3.3	2.7			
G550-0.94-20-20-5	6.7	1.7			
G550-0.94-20-30-5	7.0	2.1			
G550-0.94-25-25-5	6.9	2.0			

The post-buckling capacity is an important factor for compression members subjected to distortional buckling. As given in Chapter 2 some authors argued that distortional buckling mode shows low post-buckling capacity while some others say distortional buckling mode shows higher post-buckling capacity (see Chapter 2 for more details). Figure 6.15 shows the elastic and distortional buckling curve as stated in AISI (2004). As given in Figure 6.15 compression members subjected to distortional buckling show higher post buckling capacity for high slender sections while no post-buckling capacity for low slender sections.

$$Slendedrness = \sqrt{P_y/P_{od}}$$
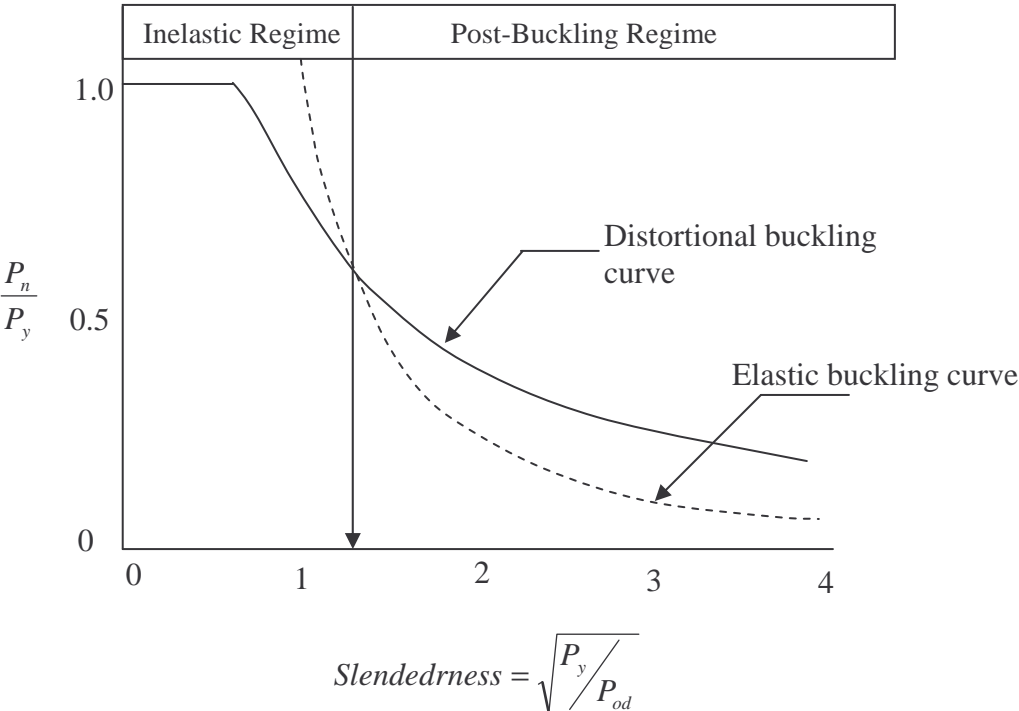
Figure 6.15   Distortional Buckling Behaviour (AISI, 2004)

The results obtained from FEA were further studied to see the variation of post-buckling capacity with slenderness. Table 6.19 shows the variation of post buckling capacity with slenderness. Type A G550 steel sections at 100°C were randomly selected for this investigation. Figure 6.16 shows the ratio of ultimate load to elastic buckling load versus slenderness. As given in Table 6.19 and Figure 6.16 it is clear that the cold-formed steel compression members show high post-buckling capacity for high slender sections.

Table 6.19   Post-buckling Capacity of Type A G550 Steel Sections at 100°C

Section	P_{odT} (kN)	P_{nT} (kN)	$\lambda = (P_{yT}/P_{odT})^{0.5}$	P_{nT}/P_{odT}
G550-0.94-20-20-5	76.1	34.3	0.725	0.451
G550-0.94-25-20-5	74.7	36.4	0.758	0.487
G550-0.94-30-20-5	72.4	39.3	0.795	0.543
G550-0.8-20-20-5	55.1	29.4	0.805	0.534
G550-0.8-25-20-5	54.0	31.1	0.842	0.576
G550-0.94-25-25-5	63.3	38.3	0.876	0.605
G550-0.8-30-20-5	51.8	32.5	0.888	0.627
G550-0.6-20-20-5	34.3	22.7	0.904	0.662
G550-0.6-25-20-5	33.7	22.8	0.944	0.677
G550-0.8-25-25-5	47.0	32.1	0.961	0.683
G550-0.94-25-30-5	56.0	39.5	0.985	0.705
G550-0.94-30-30-5	56.4	41.4	1.007	0.734
G550-0.6-25-25-5	31.0	22.5	1.048	0.726
G550-0.8-25-30-5	42.1	33.0	1.073	0.784
G550-0.94-25-35-5	50.3	39.8	1.092	0.791
G550-0.8-30-30-5	42.4	34.3	1.097	0.809
G550-0.94-25-40-5	45.9	39.5	1.197	0.861
G550-0.8-25-35-5	37.4	31.5	1.197	0.842
G550-0.6-30-30-5	27.1	22.4	1.215	0.827
G550-0.94-25-45-5	41.7	38.8	1.309	0.930
G550-0.8-25-40-5	33.5	31.6	1.324	0.943
G550-0.94-40-40-5	37.4	38.8	1.409	1.037
G550-0.94-25-50-5	37.5	38.2	1.434	1.019
G550-0.8-25-45-5	29.5	30.5	1.471	1.034
G550-0.8-40-40-5	27.4	29.7	1.556	1.084
G550-0.8-25-50-5	26.8	30.5	1.603	1.138
G550-0.6-40-40-5	17.5	20.5	1.724	1.171
G550-0.94-25-70-5	22.7	36.3	2.099	1.599
G550-0.94-25-90-5	17.9	38.4	2.620	2.145
G550-0.94-25-110-5	15.1	39.2	3.107	2.596
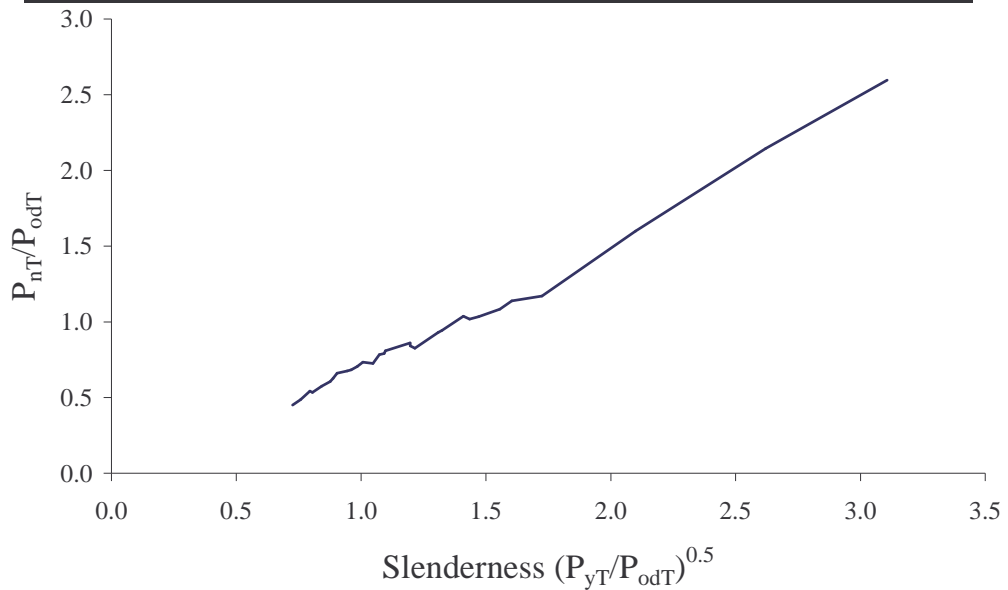
Figure 6.16   Post-buckling Capacity of Type A G550 Steel Sections at 100°C

Table 6.20   Average Slenderness (λ) of Sections used in This Study with respect to Temperature

Section	G550		G250	
Temp. (^{o}C)	A	B	A	B
20	1.220	1.126	0.845	0.862
100	1.210	1.230	0.821	0.837
200	1.286	1.310	0.847	0.864
350	1.346	1.370	0.833	0.774
500	1.178	1.202	0.701	0.715
650	0.706	0.719	0.660	0.673
800	0.817	0.832	0.641	0.641
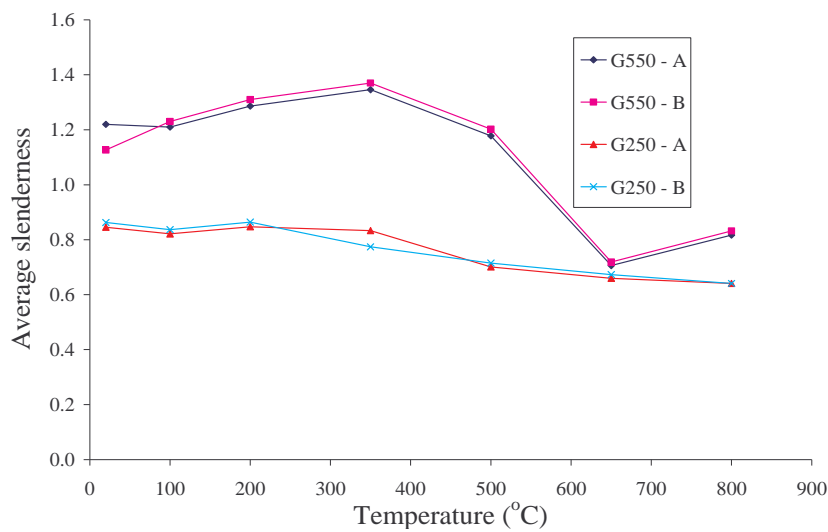
Figure 6.17   Average Slenderness with respect to the Temperatures

A parametric study was carried out to investigate the effect of temperature on the slenderness ($\lambda = (P_{yT}/P_{odT})^{0.5}$) of the sections so that the variation of post-buckling capacity at elevated temperatures can be determined. The mean values of the slenderness of each analysed section are presented in Table 6.20 based on various temperatures. Figure 6.17 shows the comparison of slenderness for various temperatures, types of section and steel grades. It shows that the type of section does not affect the variation of slenderness with temperature. Both Type A and Type B sections behave the same way. However, high strength steel sections had a higher slenderness than low strength steel sections. Both steel grades show higher slenderness at lower temperatures but lower slenderness at higher temperatures. However, the reduction of slenderness of high strength steel sections is higher than the low strength steel sections at higher temperatures greater than 500°C. This may

be due to that the reduction of yield strength of high strength steel is higher than that of low strength steel. As given in Table 6.20 and Figure 6.17 it is clear that the high post-buckling capacity can be obtained for temperatures around 300°C while low or no post-buckling capacity can be obtained at very high temperatures for high strength steel sections.

The ultimate load is the most important factor in structural design. Therefore the variation of ultimate load with temperature was thoroughly investigated. Equation 6.9 was considered since it is more accurate at ambient temperature than the current design equations (AS/NZS 4600 and direct strength method). Equation 6.9 was developed for ambient temperature and hence it should be modified for elevated temperatures since the mechanical properties are not the same as at ambient temperature. However, for uniformly heated sections, the steels at elevated temperatures can be considered as equivalent to different grades of steel at ambient temperature. Based on this phenomenon, the actual mechanical properties relevant to that temperature can be used rather than the mechanical properties at ambient temperature.

Additionally, some authors used the ambient temperature design equations by simply modifying them at elevated temperatures by introducing the relevant reduced mechanical properties. Feng et al. (2003b) studied the design equations of BS5950 Part 5 (BSI, 1990), Eurocode3 Part 1.3 (ECS, 1993)   and AISI (1996) and concluded that these design equations can be simply modified by introducing the reduced mechanical properties at elevated temperatures. Further, Ranby (1999) studied the phenomena of local, flexural and flexural torsional buckling of light gauge steel compression members at elevated temperatures. He investigated the design equations in Eurocode3 Part 1.3 (ECS, 1993) and concluded that these equations can be simply modified by introducing reduced mechanical properties at elevated temperatures.

6.4.1   Development of Design Equations for Elevated Temperatures

As the first phase of this study aimed at developing suitable design equations for elevated temperatures, the design equation at ambient temperature (Equation 6.9) was therefore simply modified by introducing the reduced mechanical properties at elevated temperatures. The yield strength reduction factors were included in this

investigation based on the developed equations as given in Section 6.2. The elastic buckling stress (f_{od}) was determined by considering the elasticity modulus reduction factors and described here as f_{odT} at elevated temperatures. Equation 6.10 shows the modified equation to predict the ultimate load at elevated temperatures. The reduced yield strength at elevated temperatures was presented in Equation 6.10 as f_{yT}.

$$\lambda < 0.55 \qquad P_{nT} = Af_{nT} = Af_{yT}$$

$$\lambda \geq 0.55 \qquad P_{nT} = Af_{nT} = Af_{yT}\left(1 - 0.31\left(\frac{f_{odT}}{f_{yT}}\right)^{0.4}\right)\left(\frac{f_{odT}}{f_{yT}}\right)^{0.58} \qquad (6.10)$$

$$\text{Where,} \qquad \lambda = \sqrt{\frac{f_{yT}}{f_{odT}}}$$

Table 6.21   The Mean and COV of the Ratio of Ultimate Loads from FEA and Equation 6.10 Predictions

(a) Type A section

Temp. (°C)	Mean/COV of FEA/Pred. Ultimate Load					
	G550			G250		
	0.60 mm	0.80 mm	0.94 mm	0.55 mm	0.75 mm	0.94mm
20	1.019/ 0.063	1.013/ 0.061	1.043/ 0.051	1.008/ 0.026	0.963/ 0.051	0.994/ 0.059
100	1.017/ 0.061	1.017/ 0.034	1.036/ 0.043	0.989/ 0.055	0.957/ 0.054	0.973/ 0.055
200	1.004/ 0.061	1.023/ 0.041	1.047/ 0.046	1.040/ 0.037	1.004/ 0.047	1.008 /0.051
350	0.982/ 0.061	1.022/ 0.046	1.049/ 0.046	0.956/ 0.017	0.932/ 0.050	0.948/ 0.039
500	0.992/ 0.049	0.996/ 0.037	1.008/ 0.045	0.932/ 0.022	0.917/ 0.050	0.927/ 0.035
650	0.931/ 0.030	0.906/ 0.053	0.918/ 0.048	0.934/ 0.025	0.924/ 0.060	0.933/ 0.043
800	0.955/ 0.036	0.945/ 0.055	0.918/ 0.050	- -	0.926/ 0.070	0.925/ 0.048

Table 6.21   The Mean and COV of the Ratio of Ultimate Loads from FEA and Equation 6.10 Predictions

(b) Type B section

Temp. (°C)	Mean/COV of FEA/Pred. Ultimate Load					
	G550			G250		
	0.60 mm	0.80 mm	0.94 mm	0.55 mm	0.75 mm	0.94 mm
20	0.983/ 0.060	0.967/ 0.084	1.003/ 0.069	1.013	1.000/ 0.041	1.024/ 0.058
100	0.978/ 0.060	0.979/ 0.095	1.030/ 0.071	1.017	0.993/ 0.039	1.030/ 0.053
200	0.943/ 0.084	0.964/ 0.109	1.020/ 0.075	1.025	1.039/ 0.046	1.061/ 0.042
350	0.929/ 0.086	0.957/ 0.099	1.000/ 0.081	0.903	0.924/ 0.048	0.964/ 0.040
500	0.953/ 0.055	0.960/ 0.084	0.996/ 0.063	0.918	0.927/ 0.041	0.942/ 0.049
650	0.910/ 0.053	0.914/ 0.032	0.929/ 0.054	0.952	0.944/ 0.048	0.945/ 0.061
800	0.952/ 0.064	0.953/ 0.045	0.959/ 0.051	-	0.957/ 0.052	0.954/ 0.066

The ultimate loads were determined from Equation 6.10 for all the sections and temperatures listed in Tables 6.13 to 6.18. The ratios of FEA results in Tables 6.13 to 6.18 to predicted ultimate loads from Equation 6.10 were then calculated to determine the accuracy of Equation 6.10. Appendix E shows a sample calculation of predicted ultimate loads from Equation 6.10.

Table 6.21 (a) gives the mean and COV values of the ratio of FEA to predicted values from Equation 6.10 for low and high strength steel Type A sections while Table 6.21 (b) gives the same for Type B sections. It should be noted that most of the 0.55 mm thick steel sections did not show pure distortional buckling and hence were not included here. Therefore the mean and COV values could not be determined for

them. As given in Table 6.21 (a) (for Type A sections) the maximum and minimum mean values obtained are 1.049 and 0.906 for G550 steel while they are 1.040 and 0.917 for G250 steel. The maximum mean value obtained for Type B G550 steel sections is 1.03 while the minimum mean value is 0.910. The maximum and minimum mean values obtained for Type B G250 steels are 1.061 and 0.903.
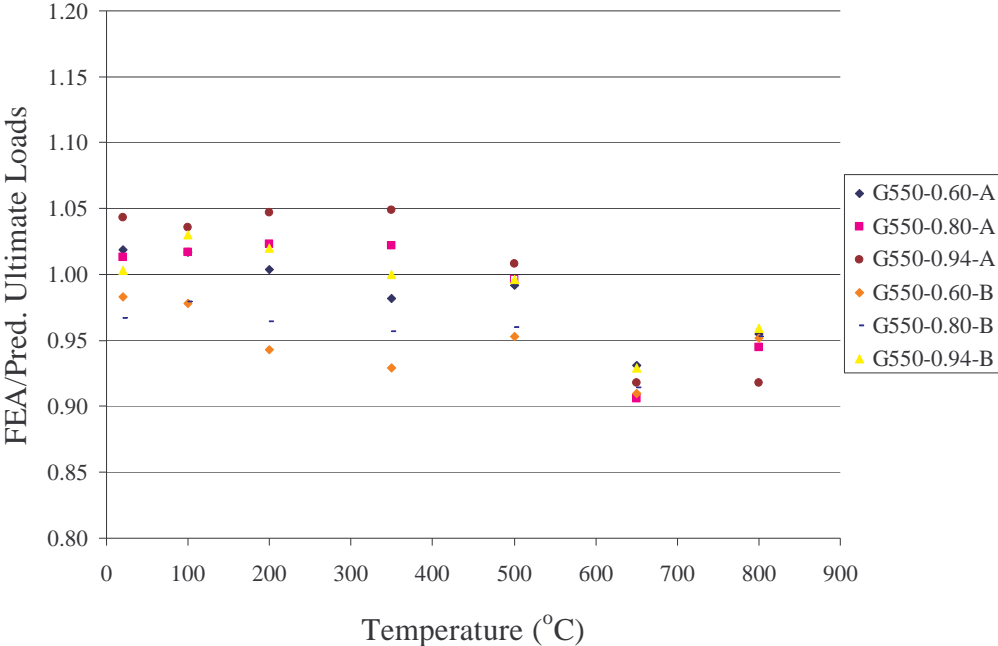
(a) G550 steel
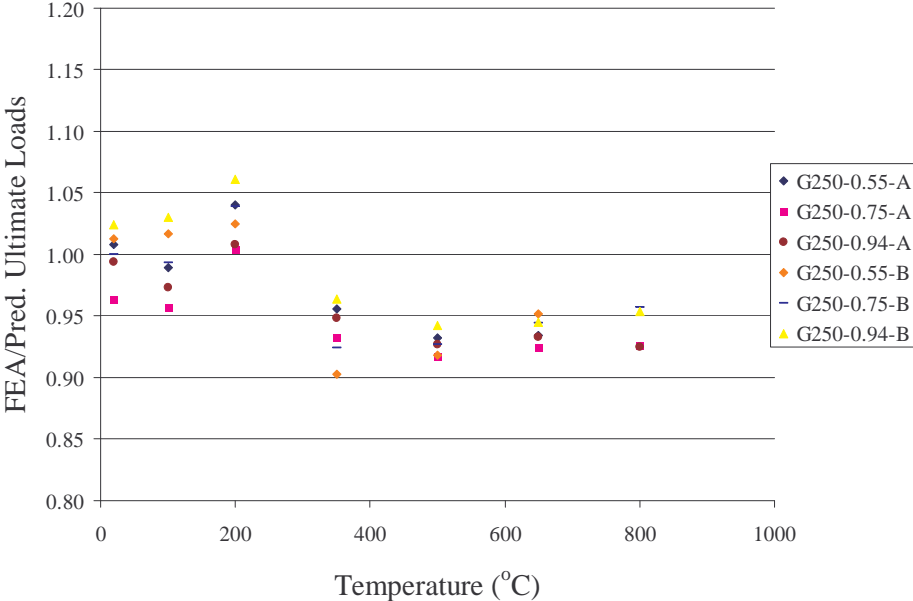
(b) G250 steel

Figure 6.18   Applicability of Equation 6.10 at Different Temperatures
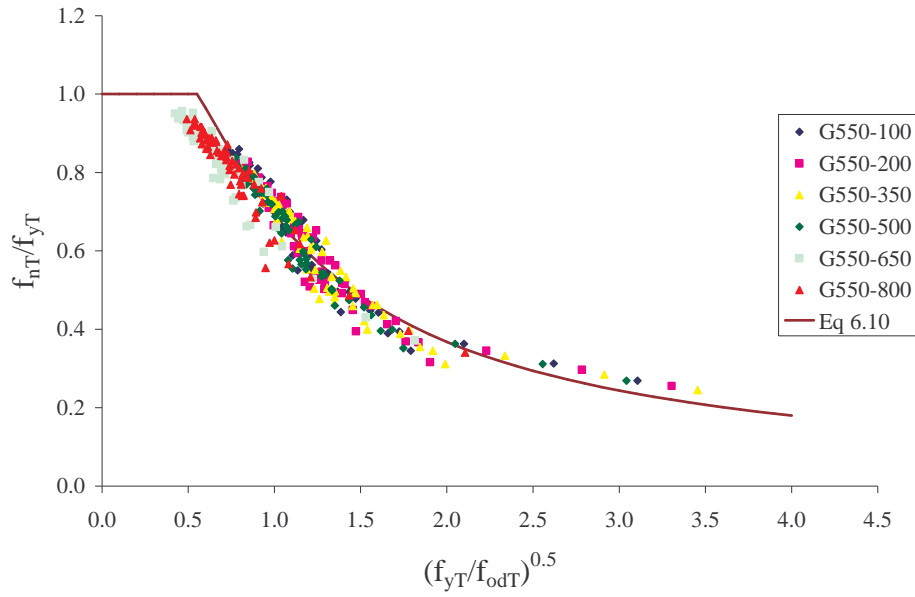
(a) G550 steel
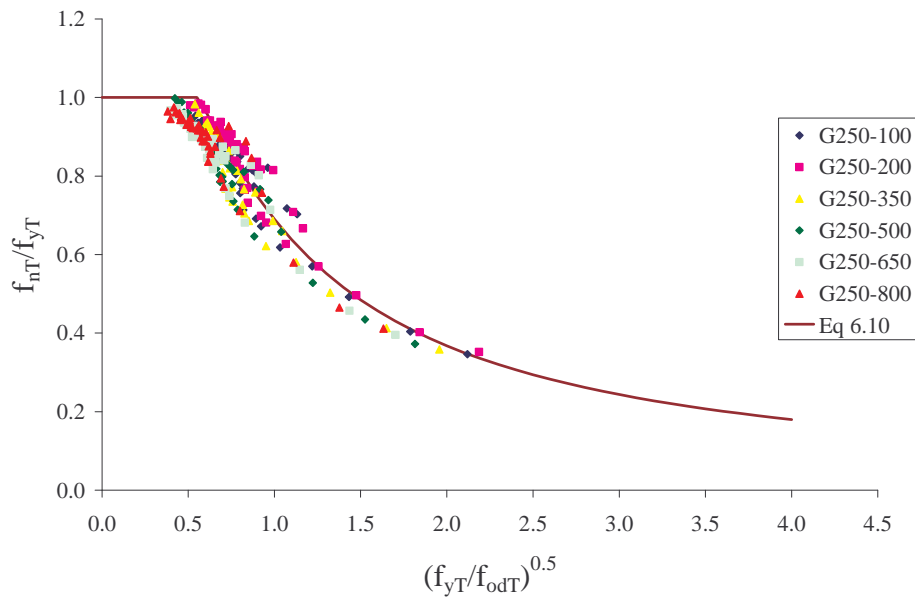
(b) G250 steel

Figure 6.19   Comparison of FEA Results with Equation 6.10 Predictions

Figure 6.18 presents the obtained mean values with temperatures so that the applicability of Equation 6.10 with increasing temperature can be further observed. Figure 6.18 (a) shows the applicability based on high strength steel sections while Figure 6.18 (b) shows the applicability based on low strength steel sections. According to Tables 6.21 (a) and (b) and Figure 6.18 it is clear that the equation

developed for ambient temperature can reasonably predict the ultimate loads of cold-formed steel compression members at elevated temperatures by using the relevant reduced yield strength and elasticity modulus values. However, the modified equation shows very good agreement for high strength steel sections up to 500°C while it was accurate for low strength steel sections in the limited range of 200 to 350°C. The accuracy is not good enough for other temperatures. Therefore it is clear that elevated temperature has an influence on the ultimate loads of cold-formed steel compression members subjected to distortional buckling failure.

Furthermore, Figures 6.19 (a) and (b) show the non-dimensional stress versus slenderness curves for both low and high strength steel sections. Based on Table 6.21 and Figures 6.18 and 6.19 it can be concluded that the modified equation (Equation 6.10) is reasonable as some other researchers (Feng et al., 2003b and Ranby, 1999) stated but unsafe for some temperatures. In addition to that, the slenderness of section has decreased at very high temperatures. This is because the yield strength decreases at a faster rate than the elasticity modulus at higher temperatures.

Finally it can be concluded that the simply modified ambient temperature equation is not suitable to predict the ultimate load at elevated temperatures when the sections fail by distortional buckling mode. Therefore the equation should be further modified by considering various factors hence the accuracy of ultimate load predictions can be improved. Mainly there are three different factors to be considered.

➢ Although the ambient temperature equation was developed based on the isotropic strain hardening behaviour the stress-strain curves at ambient temperature are nearly equal to the elastic perfect plastic curve. But the stress-strain curves become more non-linear with increasing temperature. Therefore the non-linearity should be considered.

➢ The ambient temperature equation was developed when the ratio of yield strength reduction factor to elasticity modulus reduction factor was one ($k_{yT}/k_{ET} = 1$). However, the ratio between yield strength reduction factor to elasticity modulus reduction factor is different at higher temperatures.

➢ Residual stresses decrease with increasing temperatures.

The above factors should be considered for the modification of the equation at elevated temperatures. In addition to the above main factors, there are some other parameters such as section geometry, flange width and web height which can influence the ultimate load of compression members when they fail by distortional buckling. Therefore all the corresponding factors were considered before developing a new design equation at elevated temperatures.

6.4.1.1 Effect of non-linear stress-strain curves

As discussed above, the ambient temperature equation was developed based on the ultimate loads obtained from FEA. The FEA results were determined from actual stress-strain curves rather than the idealised elastic perfectly-plastic material behaviour at ambient temperature. Although the full stress-strain curve was considered in the finite element analyses the stress-strain curve considered at ambient temperature is close to elastic-perfect plastic behaviour (see Figure 6.20). Many of the currently available design equations were developed based on the elastic-perfect plastic behaviour. However the stress-strain curves become non-linear (rounded shape) with increasing temperatures as shown in Figure 6.20. However, the influence of non-linearity of material behaviour has not been well understood. Recently, Gardner and Nethercot (2006) discussed the effect of non-linearity based on stainless steel members and presented a new design approach different from carbon steel design equations. However, the effect of non-linearity on light gauge cold-formed steel compression members which failed by distortional buckling mode is not known. Therefore the effect of non-linear stress-strain curve was studied in this research.
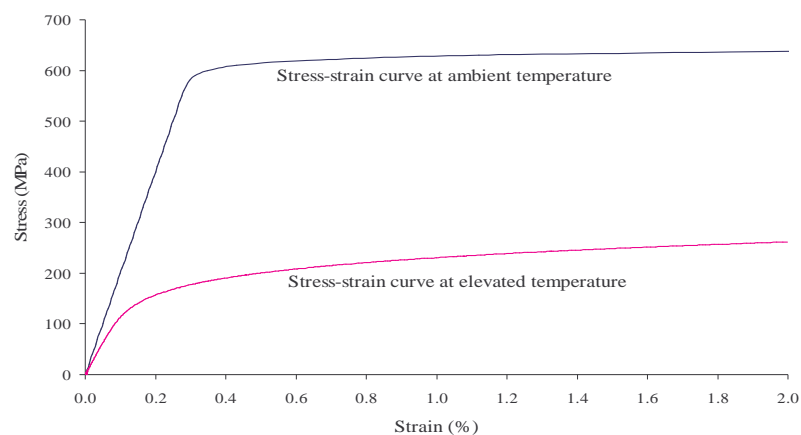
Figure 6.20   Variation of Stress-Strain Curve with Temperature

Finite element analyses were first undertaken to study the effect of non-linear material behaviour on the ultimate load. The non-linear stress-strain curve was included in FEA for varying temperatures from 20 to 800°C. So a less non-liner stress-strain curve was included at 20°C while a higher non-linear stress-strain curve was included at 800°C. All the other parameters were kept constant for this investigation. The ratio between yield strength reduction factor to elasticity modulus reduction factor was kept constant ($k_{yT}/k_{ET} = 1$) for all the analyses. The ultimate loads were obtained for 0.94 mm thick G550 Type A section with 25 mm web height, 50 mm flange width and 5 mm lip length from FEA. The ultimate load predictions were then determined for the same section from Equation 6.10 by including the relevant yield strength and elasticity modulus values.

The influence of non-linear stress-strain curve on the ultimate loads of the light gauge cold-formed steel compression members subjected to distortional buckling failure was then observed by determining the ratio of ultimate loads obtained from FEA and Equation 6.10. Table 6.22 shows the comparison of FEA results and Equation 6.10 predictions. The ratio at ambient temperature is 0.982 and it is 0.964 at 800°C (which gives the highest non-linear stress-strain curve). This compares the effect of using the most non-linear stress-strain curve to that of the least non-linear stress-strain curve. As shown in Table 6.22 the effect of non-linear stress-strain curve is not significant. The maximum variation is below 2%.

Table 6.22   Effect of Non-linear Stress-strain Curve on the Ultimate Loads of 0.94 mm Type A G550 Sections

Temp. (°C)	P_{od} (kN)	Ultimate Load (kN)		FEA/Pred.
		FEA	Pred.	
20	37.5	38.6	39.3	0.982
100	36.9	38.0	38.7	0.983
200	36.3	37.3	38.0	0.981
350	30.8	31.6	32.3	0.978
500	16.8	17.3	17.7	0.980
650	3.6	3.7	3.8	0.977
800	1.5	1.5	1.6	0.964

Additionally the effect of non-linear stress-strain curve was invetigated for more sections. The sections were selected based on different geometry (Type A and B), steel grades (G550 and G250), thicknesses (0.6 and 0.94 mm) and different slenderness limits (λ). Only the critical temperatures were considered for this, ie, 20 and 800°C as 20°C gives the stress-strain curve closer to the elastic perfect plastic curve while 800°C gives the most non-liner stress-strain curve. Table 6.23 shows the ultimate loads obtained from FEA and Equation 6.10. The ratio of FEA results to Equation 6.10 predictions show the effect of non-linear stress-strain curve on the ultimate load. The ratios of ultimate load obtained from FEA to Equation 6.10 predictions vary from 1.043 to 0.998 for 0.6 mm G550 Type A steel section with the slenderness of 0.94, 1.011 to 0.986 for 0.94 mm G550 Type A steel section with the slenderness of 2.23 and 1.055 to 1.033 for 0.94 mm G250 Type B steel section with the slenderness of 1.56. Based on these analyses it is clear that the effect of elastic perfect-plastic to non-linear behaviour is less than 5%. This investigation led to the conclusion that the non-linearity of stress-strain curve has an influence on the ultimate load but is not significant.

Table 6.23   Effect of Non-linear Stress-strain Curve on the Ultimate Loads of Selected Types A and B Sections

Section	P_{od}	Slenderness	Ultimate Load (kN)		FEA/Pred.
	(kN)	λ	FEA	Pred.	
G550-0.6-20-A	34.30	0.94	23.0	22.0	1.043
G550-0.6-800-A	1.37	0.94	0.9	0.9	0.998
G550-0.94-20-B	27.50	2.23	45.7	45.2	1.011
G550-0.94-800-B	1.11	2.24	1.8	1.8	0.986
G250-0.94-20-B	27.50	1.56	32.9	31.2	1.055
G250-0.94-800-B	1.38	1.56	1.6	1.6	1.033

Note: P_{od} and Pred. are based on relevant elasticity modulus and yield strength at temperatures considered in this study (20 and 800°C).

6.4.1.2   Effect of k_{yT}/k_{ET} factor

As discussed earlier, Equation 6.10 was simply modified by including the reduced mechanical properties at elevated temperatures. Equation 6.9 was developed based on the ultimate loads obtained at ambient temperature. However, both yield strength and the elasticity modulus decrease with temperature and the decreasing rate is not the same. Therefore the ratio of yield strength reduction factor ($k_{yT} = f_{yT}/f_y$) to the elasticity modulus reduction factor $k_{ET} = E_T/E$ is different at various temperatures. As the first phase of this investigation, the variation of k_{yT}/k_{ET} was studied at different temperatures. Interestingly, although some design standards and other researchers focussed on the variation of mechanical properties at different temperatures, the influence of the reduction of yield strength and the elasticity modulus on the ultimate load was not thoroughly investigated. Therefore the k_{yT}/k_{ET} factor in this research was compared with others' results for cold-formed steel and other steel types. Further details of mechanical properties are presented in Chapter 3.
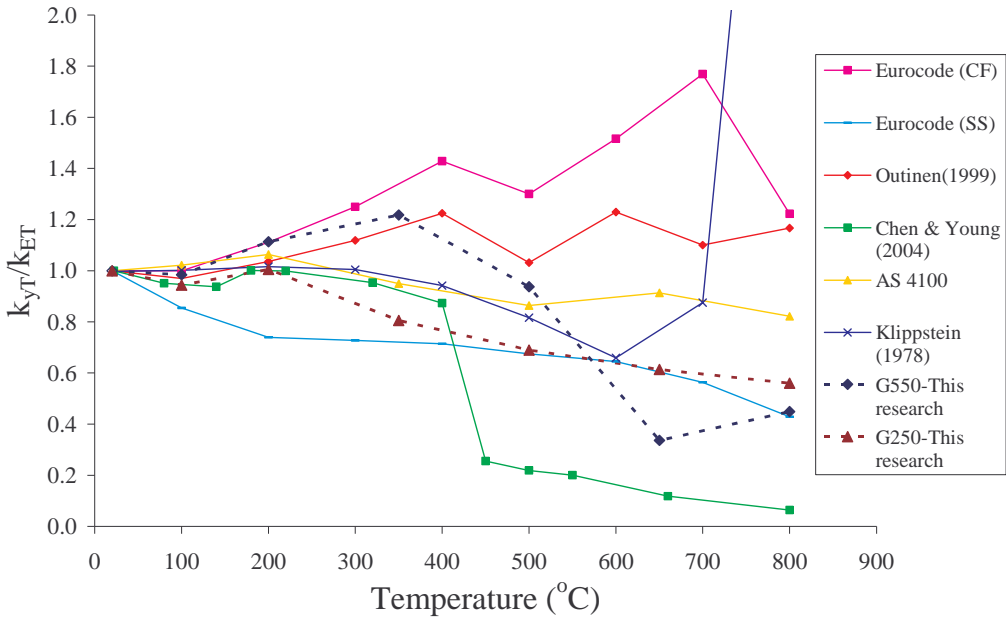
where CF = Cold-formed steel and SS = stainless steel

Figure 6.21   Comparison of k_{yT}/k_{ET} Factor with Available Results

According to Figure 6.21 the ratio between k_{yT} and k_{ET} provided by Design Standards and researchers are dissimilar to each other. However, the most recent

results provided by Chen and Young (2004) and this research look similar. Both results agree that the yield strength reduced at a faster rate than the elasticity modulus at very high temperatures. Further the results presented by Klippstein (1978) show the same phenomenon up to 700°C but his values increased to unbelievably high values at high temperatures. However, the results proposed by Outinen (1999) and Eurocode 3 Part 1.2 (ECS, 1993) disagree with this phenomenon. According to Outinen's (1999) and Eurocode values, elasticity modulus reduces faster than the yield strength with increasing temperatures.

The influence of k_{yT}/k_{ET} factors obtained from this research was studied based on the ultimate loads predicted by Equation 6.10. Figure 6.21 shows that the minimum k_{yT}/k_{ET} was observed at 650°C and it increases again at 800°C for G550 steels. Figure 6.18 shows the ratio of FEA ultimate loads to Equation 6.10 predictions for high strength steel sections (G550). It clearly shows that the applicability of Equation 6.10 at 650°C is not as good compared with other temperatures. The ratio of FEA ultimate loads to Equation 6.10 predictions is lower at 650°C but increases again at 800°C as k_{yT}/k_{ET} increases (compare Figure 6.18 and 6.21). Therefore it is clear that the k_{yT}/k_{ET} factor has an influence on the distortional buckling behaviour and ultimate loads of cold-formed steel sections. Therefore the effect of the k_{yT}/k_{ET} factor on the ultimate load was investigated thoroughly when the light gauge cold-formed steel compression members failed by distortional buckling modes. Table 6.24 shows the variation of results for different k_{yT}/k_{ET} factors. The range of k_{yT}/k_{ET} factor was selected from 1.5 to 0.2 to give a wide range that also includes others' results as shown in Figure 6.21. The ultimate loads were obtained for 0.94 mm thick G550 Type A section with 25 mm web height, 50 mm flange width and 5 mm lip length from FEA. The elastic perfect plastic stress-strain curve was used in this investigation.

The ratios of FEA ultimate loads to those predicted by Equation 6.10 show that there is a considerable influence from the k_{yT}/k_{ET} factor. Table 6.24 clearly shows that when the ratio of k_{yT}/k_{ET} is increased, the results obtained from Equation 6.10 are conservative while they become unsafe when k_{yT}/k_{ET} factor is decreased. The difference of the ratio of FEA to predicted ultimate loads is around 30% when the k_{yT}/k_{ET} factor is varied from 1.5 to 0.2. In this study, the k_{yT}/k_{ET} ratio varied from 0.3

to 1.2 and the corresponding ratios of FEA to predicted ultimate loads varied by about 20%. Therefore the influence of k_{yT}/k_{ET} factor should be considered when developing new design equations at elevated temperatures.

Table 6.24   Effect of k_{yT}/k_{ET} Factor on the Ultimate Loads of 0.94 mm Type A G550 Sections

k_{yT}/k_{ET}	Ultimate Load (kN)		FEA/Pred.
	FEA	Pred.	
1.50	51.9	48.7	1.066
1.25	45.6	44.3	1.030
1.00	38.7	39.3	0.985
0.90	36.3	37.1	0.978
0.80	33.4	34.8	0.960
0.70	30.3	32.3	0.939
0.60	27.0	29.6	0.914
0.50	23.7	26.6	0.892
0.40	20.3	23.2	0.875
0.30	16.4	19.3	0.849
0.20	11.9	14.6	0.816

Further, as shown in Table 6.24 it is clear that the equation developed at ambient temperature can be simply modified by including the reduced mechanical properties at elevated temperatures for higher k_{yT}/k_{ET} factors in the range of 0.90 to 1.50. As shown in Figure 6.21 the k_{yT}/k_{ET} factor obtained from Eurocode 3 Part 1.2 (ECS, 1993) and Outinen's (1999) are always higher than 1. Therefore the design equations developed at ambient temperature can be simply modified at elevated temperatures by using the mechanical properties proposed by Eurocode and Outinen (1999) and hence some other researchers' (Ranby, 1999 and Feng et al., 2003) suggestions are accurate at elevated temperatures. This is why these researchers were able to recommended that the ambient temperature design equation can be simply modified by including the relevant reduction factors of mechanical properties at elevated temperatures. However, the mechanical properties proposed by other researchers are not accurate for light gauge cold-formed steels. Therefore their mechanical properties cannot be used to determine the ultimate loads of light gauge cold-formed steel compression members at elevated temperatures and hence new design equation should be proposed for elevated temperatures.

6.4.1.3   Effect of residual stresses

The residual stresses should also be considered at elevated temperatures since the residual stresses at ambient temperature decline with increasing temperatures (see Chapter 5). Chapter 5 described the effect of residual stresses on the ultimate load of compression members. It clearly shows that the effect of residual stresses on distortional buckling mode is not significant ($< 0.2\%$). Therefore the residual stresses were not further studied at elevated temperatures.

6.4.1.4   Effect of other parameters

Further, the variation of predicted values obtained from Equation 6.10 and FEA was studied by considering other parameters. The section geometry, steel thickness, the web height and the flange width were considered.

Effect of section geometry

The effect of section geometry was also studied at various temperatures. Tables 6.21 (a) and (b) show the effect of Type A and B sections separately at various temperatures and for both steel grades. As shown in Tables 6.21 (a) and (b) both Type A and Type B steel sections display the same behaviour at elevated temperatures. Therefore the section geometry does not show any significant effect on the variation of predictions from the proposed design equation and FEA.

Effect of steel thickness

The effect of steel thickness was studied by considering the FEA results for different thicknesses: 0.55, 0.60, 0.75, 0.80 and 0.94 mm. Various temperatures and two steel grades were also considered in this study to investigate the effect of thickness at different temperatures. Table 6.25 shows the mean and COV values of the ratio of ultimate loads obtained from FEA and Equation 6.10. There is no clear variation of mean or COV values when steel thickness increases and hence Table 6.25 led to the conclusion that the effect of steel thickness is not considerable when sections fail by distortional buckling. However, it should be noted that when steel thickness decreases considerable, the steel sections buckle locally rather than distortionally.

Table 6.25   Effect of Steel Thickness

Temp (°C) Section	20 Mean/ COV	100 Mean/ COV	200 Mean/ COV	350 Mean/ COV	500 Mean/ COV	650 Mean/ COV	800 Mean/ COV
G550-0.60	1.000/ 0.062	1.001/ 0.061	0.978/ 0.074	0.960/ 0.074	0.976/ 0.053	0.922/ 0.041	0.956/ 0.047
G550-0.80	0.990/ 0.075	1.000/ 0.068	0.997/ 0.081	0.994/ 0.078	0.980/ 0.063	0.910/ 0.044	0.949/ 0.050
G550-0.94	1.022/ 0.063	1.032/ 0.055	1.033/ 0.060	1.030/ 0.065	1.003/ 0.053	0.923/ 0.051	0.936/ 0.054
G250-0.55	1.010/ 0.021	0.996/ 0.046	1.035/ 0.031	0.943/ 0.031	0.929/ 0.020	0.939/ 0.023	-
G250-0.75	0.977/ 0.050	0.969/ 0.052	1.016/ 0.048	0.929/ 0.048	0.921/ 0.046	0.931/ 0.056	0.936/ 0.065
G250-0.94	1.008/ 0.060	0.994/ 0.060	1.028/ 0.053	0.955/ 0.039	0.933/ 0.041	0.937/ 0.049	0.936/ 0.047

Effect of web height

The effect of web height was studied at different temperatures by considering different web dimensions. The web height was changed from 20 to 40 mm. However, it should be noted that when web height was smaller than 20 mm, the sections tend to yield rather than buckling distortionally. Table 6.26 shows the mean value of the ratio of FEA ultimate loads to those predicted by Equation 6.10. Based on this table it can be concluded that there is no effect from web height.

Table 6.26   Effect of Web Height

Temp (°C) Web height (mm)	20 Mean/ COV	100 Mean/ COV	200 Mean/ COV	350 Mean/ COV	500 Mean/ COV	650 Mean/ COV	800 Mean/ COV
20	1.014/ 0.048	1.007/ 0.051	1.023/ 0.031	1.022/ 0.030	0.980/ 0.038	0.926/ 0.031	0.918/ 0.020
25	1.005/ 0.051	0.999/ 0.051	1.019/ 0.043	0.994/ 0.067	0.963/ 0.059	0.906/ 0.032	0.922/ 0.030
30	0.990/ 0.064	0.995/ 0.068	1.005/ 0.075	0.956/ 0.077	0.953/ 0.066	0.925/ 0.051	0.947/ 0.047
≥ 40	1.006/ 0.077	1.022/ 0.082	1.022/ 0.106	0.967/ 0.078	0.978/ 0.064	0.982/ 0.043	1.001/ 0.078

Effect of Flange width

The effect of flange width is shown in Table 6.27. The effect of flange width was observed by increasing it from 20 to 110 mm. It is clear that when flange width is very small, the section fails by yielding and when it is too large the section fails by local buckling. These results were not considered here. The effect was observed for each temperature by using Equation 6.10 as same as above and it was observed that the flange width did not show any effect.

Table 6.27   Effect of Flange Width

Temp (°C) Flange width (mm)	20 Mean/ COV	100 Mean/ COV	200 Mean/ COV	350 Mean/ COV	500 Mean/ COV	650 Mean/ COV	800 Mean/ COV
20 to 30	1.013/ 0.045	1.006/ 0.046	1.025/ 0.031	1.014/ 0.043	0.977/ 0.044	0.925/ 0.028	0.925/ 0.024
30 to 40	1.019/ 0.055	1.015/ 0.056	1.031/ 0.064	0.991/ 0.073	0.973/ 0.062	0.918/ 0.032	0.947/ 0.040
40 to 50	0.992/ 0.071	0.987/ 0.066	0.995/ 0.071	0.937/ 0.061	0.942/ 0.061	0.929/ 0.066	0.947/ 0.081
50 to 70	0.996/ 0.081	0.960/ 0.090	0.957/ 0.102	0.924/ 0.060	0.926/ 0.065	0.942/ 0.091	0.965/ 0.081
≥70	0.985/ 0.064	1.041/ 0.070	1.066/ 0.059	1.028/ 0.103	0.992/ 0.094	0.910/ 0.007	0.936/ 0.036

6.4.2   Development of a More Accurate Design Equation

The investigation of the effects of all the above parameters led to the conclusion that the ratio of k_{yT} and k_{ET} factor has a more significant influence than other parameters. Even though the non-linear stress-strain behaviour showed some influence it is not significant as k_{yT}/k_{ET} factor. All the other parameters showed little or no influence on the ultimate load. Therefore the effect of k_{yT}/k_{ET} factor was first considered in the development of a more accurate distortional buckling equation for cold-formed steel compression members at elevated temperatures based on the simply modified equation as shown in Equation 6.10.

Table 6.24 shows the effect of k_{yT}/k_{ET} factor for randomly selected sections from all the analysed sections in this study. However to develop a more accurate design equation all the analysed sections should be considered. Table 6.28 shows the results of these further studies on the effect of k_{yT}/k_{ET} factor based on Equation 6.10. Table 6.28 shows the mean values of the ratio of FEA ultimate load to those predicted by Equation 6.10 for all the studied sections. Table 6.28 clearly shows the variation of mean values with respect to the k_{yT}/k_{ET} factors. As shown in Table 6.28, Equation 6.10 predictions agree well with the FEA results when the k_{yT}/k_{ET} factor is higher than 0.9. On the other hand it can be noticed that the variation of predicted values from Equation 6.10 and FEA show different behaviour at the same temperature if k_{yT}/k_{ET} factors are different in the case of both low and high strength steels. Therefore it is recommended that the simply modified equation (Equation 6.10) can be used when k_{yT}/k_{ET} factor is higher than 0.9. However, it should be further modified when the k_{yT}/k_{ET} factor was less than 0.9.

Table 6.28   Variation of Mean of the Ratio of Ultimate Loads from FEA and Equation 6.10 with k_{yT}/k_{ET} Factor

Steel	G550		G250	
Temperature (°C)	k_{yT}/k_{ET}	Mean	k_{yT}/k_{ET}	Mean
20	1.000	1.006	1.000	0.996
100	0.984	1.014	0.944	0.984
200	1.113	1.010	1.005	1.024
350	1.218	1.003	0.805	0.943
500	0.937	0.989	0.689	0.928
650	0.336	0.917	0.614	0.935
800	0.449	0.944	0.560	0.936

A new equation was therefore developed based on a simple curve fitting method. The developed equation at elevated temperature based on k_{yT}/k_{ET} factor is shown as Equation 6.11. Table 6.29 shows the mean and COV values of the ratio of ultimate loads obtained from FEA to those predicted by Equation 6.10 when k_{yT}/k_{ET} factor is higher than 0.9 and from Equation 6.11 when k_{yT}/k_{ET} factor is less or equal to 0.9. The maximum mean value obtained from Equation 6.10 is 1.035 with 0.031 COV

and the minimum mean value is 0.960 with COV of 0.074. The maximum and minimum mean values obtained from Equation 6.11 are 1.041 and 0.982, respectively with the corresponding COV value of 0.049. The overall maximum and minimum mean values by using Equation 6.10 and 6.11 in this way are thus 1.041 and 0.960, compared to the values of 1.061 and 0.903 obtained without using Equation 6.11 (See Table 6.21). It is therefore proposed that Equation 6.11 is used when the k_{yT}/k_{ET} factor is less or equal to 0.9. Moreover, Table 6.30 shows the overall summary, while Figures 6.22 and 6.23 show the non-dimensional stress versus slenderness curves based on Equations 6.10 and 6.11 and a comparison with FEA results. Tables 6.29 and 6.30 and Figures 6.22 and 6.23 clearly show that the predictions from Equations 6.10 and 6.11 agree well with the FEA results.

$$\lambda < 0.43 \qquad P_{nT} = Af_{nT} = Af_{yT}$$

$$\lambda \geq 0.43 \qquad P_{nT} = Af_{nT} = Af_{yT}\left(1 - 0.37\left(\frac{f_{odT}}{f_{yT}}\right)^{0.31}\right)\left(\frac{f_{odT}}{f_{yT}}\right)^{0.58} \qquad (6.11)$$

$$\text{Where,} \quad \lambda = \sqrt{\frac{f_{yT}}{f_{odT}}}$$

Table 6.29   The Mean and COV of the Ratio of Ultimate Loads from FEA and Equations 6.10 and 6.11 Predictions

Temp (°C) Section	20 Mean/ COV	100 Mean/ COV	200 Mean/ COV	350 Mean/ COV	500 Mean/ COV	650 Mean/ COV	800 Mean/ COV
G550-0.60	1.000/ 0.062	1.001/ 0.061	0.978/ 0.074	0.960/ 0.074	0.976/ 0.053	1.000/ 0.043	1.041/ 0.049
G550-0.80	0.990/ 0.075	1.000/ 0.068	0.997/ 0.081	0.994/ 0.078	0.980/ 0.063	0.982/ 0.049	1.034/ 0.052
G550-0.94	1.022/ 0.063	1.032/ 0.055	1.033/ 0.060	1.030/ 0.065	1.003/ 0.053	0.989/ 0.057	1.018/ 0.057
G250-0.55	1.010/ 0.021	0.996/ 0.046	1.035/ 0.031	1.028/ 0.029	1.010/ 0.022	1.014/ 0.032	-
G250-0.75	0.977/ 0.050	0.969/ 0.052	1.016/ 0.048	1.013/ 0.046	0.999/ 0.048	0.997/ 0.062	1.009/ 0.072
G250-0.94	1.008/ 0.060	0.994/ 0.060	1.028/ 0.053	1.041/ 0.039	1.009/ 0.043	1.000/ 0.056	1.004/ 0.065

Table 6.30   Overall Summary of Design Equations 6.10 and 6.11

Temp (°C) Steel Grade	100	200	350	500	650	800
	Mean/ COV	Mean/ COV	Mean/ COV	Mean/ COV	Mean/ COV	Mean/ COV
G550	1.004/ 0.062	1.010/ 0.073	1.003/ 0.075	0.989/ 0.057	0.988/ 0.051	1.028/ 0.054
G250	0.984/ 0.056	1.024/ 0.049	1.028/ 0.042	1.005/ 0.043	1.000/ 0.056	1.006/ 0.067

The capacity reduction factor which is commonly used in the design codes is then calculated for Equations 6.10 and 6.11. Table 6.31 presents the capacity reduction factor for each temperature and steel grade. The average capacity reduction factor obtained for Equation 6.10 is 0.900 while for Equation 6.11 it is 0.903. Table 6.31 capacity reduction factors are close to 0.9, which is commonly used in the cold-formed steel design codes. Based on Table 6.31, the capacity reduction factor Φ can be recommended as 0.9 for Equations 6.10 and 6.11. Finally, it is recommended that Equation 6.9 is used to determine the ultimate load of light gauge cold-formed steel compression members subjected to distortional buckling at ambient temperature, but for elevated temperatures Equation 6.10 is recommended when the k_{yT}/k_{ET} factor is higher than 0.9 and Equation 6.11 when the k_{yT}/k_{ET} factor is less or equal to 0.9.
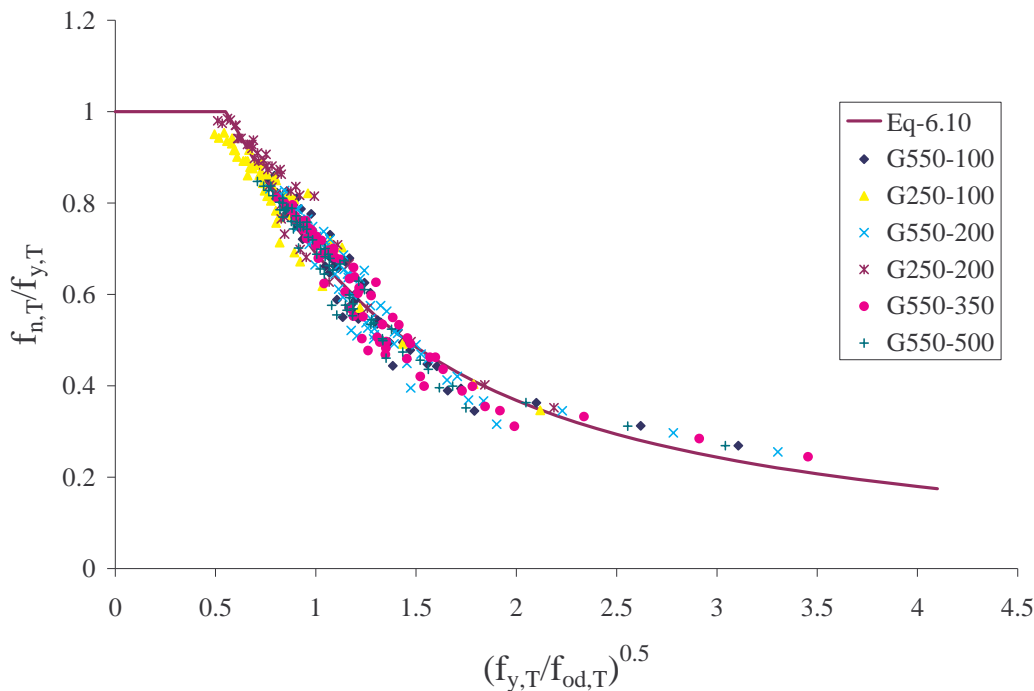
Figure 6.22   Comparison of FEA Results with Equation 6.10 ($k_{yT}/k_{ET} > 0.9$)
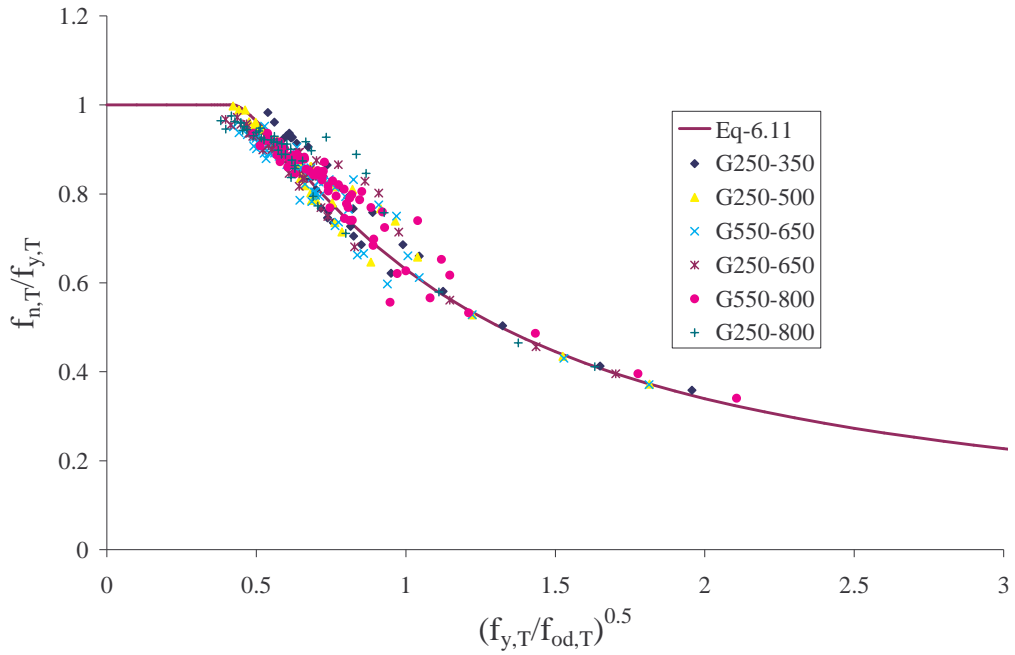
Figure 6.23   Comparison of FEA Results with Equation 6.11 ($k_{yT}/k_{ET} \leq 0.9$)

Table 6.31   Capacity Reduction Factor

Temp. (^{o}C) Section	100	200	350	500	650	800
G550-0.60	0.888	0.858	0.843	0.871	0.899	0.932
G550-0.80	0.886	0.874	0.873	0.872	0.847	0.927
G550-0.94	0.923	0.921	0.915	0.898	0.883	0.909
G250-0.55	0.870	0.925	0.921	0.910	0.905	-
G250-0.75	0.868	0.912	0.910	0.896	0.886	0.890
G250-0.94	0.886	0.920	0.939	0.908	0.893	0.892

6.4.3   Limiting Temperature Method (SCI, 1993)

Limiting temperature method is another important design method in structural design
for fire conditions. This method relies on the existence of a limiting temperature for
steel members as a function of load ratio. The limiting temperature is the temperature
at which the structure fails under fire conditions. The applied load under fire
conditions is not the same as that at ambient temperature. Therefore the partial safety
factors at fire condition are less than that at ambient temperature. The SCI
publication (1993) stated that the applied load under fire can be considered as half of
the applied load at ambient temperature. The partial factors of safety used in

structural design under fire condition and at ambient temperature are presented in Table 6.32 based on the SCI publication (1993).

The SCI publication is based on the limiting temperature method applied for hot-rolled steel structures in BS 5950 Part 8 (BSI, 1990). SCI (1993) derived limiting temperatures for light gauge cold-formed steel members based on the mechanical properties proposed by Sidey and Teague (1988). The load ratio corresponding to the limiting temperature has been defined as the ratio of the load on the member at elevated temperature to its capacity at ambient temperature.

Table 6.32   Partial Factors of Safety used in Structural Design

Load case	Factors of Safety	
	Ambient temperature	Fire
Dead loads	1.4	1.0
Permanent loads	1.6	1.0
Variable loads	1.6	0.8

$$\text{Load ratio (1)} = \frac{\text{Load on member at the fire limit state}}{\text{Load carrying capacity of member under normal loading}}$$

The SCI publication (1993) stated that the typical load ratio is about 0.5 to 0.6 for structural steel members which have been designed for fully stressed conditions at ambient temperature. It proposes appropriate load ratios at relevant temperatures for cold-formed steel members. These load ratios were then studied with the results obtained in this research. In this research load ratios were determined as the ratio of member capacity at elevated temperature to that at ambient temperature and specified as Load ratio (2).

$$\text{Load ratio (2)} = \frac{\text{Capacity of member at the fire limit state}}{\text{Load carrying capacity of member under normal loading}}$$

Load carrying capacity of members (ultimate load) under normal loading is determined from Equation 6.9 for all the sections analysed in this research. The capacity of member (ultimate load) at the fire limit state is determined from Equations 6.10 and 6.11 based on the k_{yT}/k_{ET} factor for the same section considered

at ambient temperature. The relevant load ratios (2) were determined for each section and the mean values were plotted in Figures 6.24 (a) and (b) at each temperature. Tables 6.33 (a) and (b) present the load ratios (Load Ratio (2)) as a function of temperature for all the sections considered in this research. Figures 6.24 (a) and (b) present the comparison of load ratio versus limiting temperatures determined in this research and compares with that given in the SCI publication (1993). The load ratio versus limiting temperature curves determined in this research are presented based on both types of steel sections (Type A and B) and both low and high strength steels (G250 and G550) in Figures 6.24 (a) and (b).
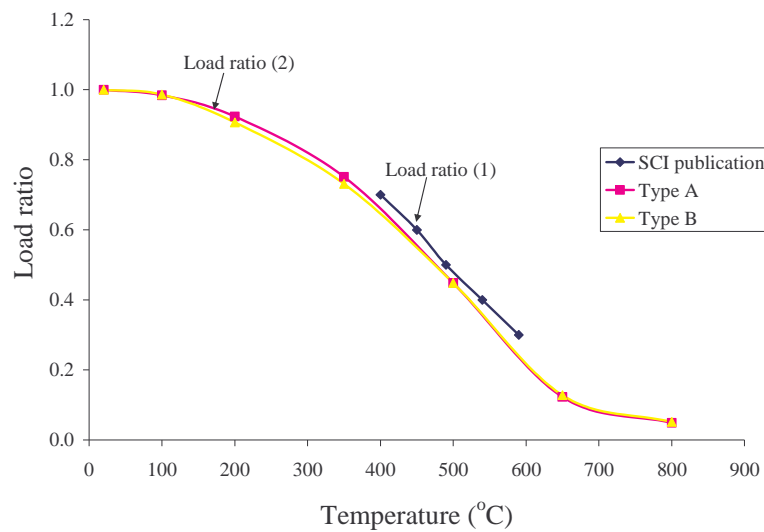
(a) Types A and B G550 steel sections
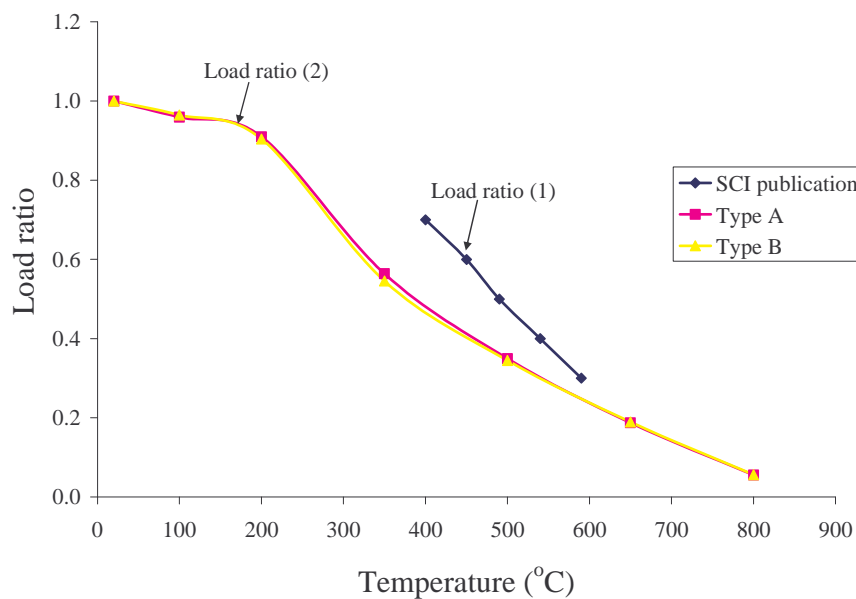
(b) Types A and B G250 steel sections

Figure 6.24   Comparison of Load Ratios

Table 6.33   Load Ratio (2) Values Obtained in This Research

(a) G550 steel sections

Temp (°C) Steel	100	200	350	500	650	800
	0.987	0.915	0.729	0.453	0.122	0.049
	0.983	0.895	0.707	0.445	0.128	0.051
	0.988	0.896	0.710	0.444	0.124	0.050
	0.987	0.917	0.739	0.439	0.113	0.043
	0.987	0.931	0.749	0.450	0.116	0.047
	0.991	0.916	0.735	0.460	0.137	0.053
	0.995	0.913	0.728	0.461	0.163	0.063
	0.985	0.934	0.752	0.450	0.114	0.047
	0.985	0.933	0.761	0.448	0.114	0.047
	0.997	0.947	0.783	0.460	0.117	0.048
	0.988	0.939	0.773	0.451	0.116	0.048
	0.985	0.931	0.770	0.451	0.121	0.050
	0.987	0.903	0.749	0.455	0.131	0.053
	0.984	0.925	0.751	0.449	0.131	0.052
	0.993	0.938	0.756	0.450	0.135	0.053
	0.987	0.922	0.741	0.443	0.129	0.051
G550-A	0.983	0.933	0.769	0.445	0.108	0.045
	0.987	0.937	0.768	0.444	0.110	0.045
	0.985	0.927	0.761	0.445	0.109	0.045
	0.977	0.920	0.741	0.450	0.120	0.048
	0.881	0.798	0.638	0.409	0.148	0.059
	0.985	0.924	0.759	0.442	0.108	0.045
	0.987	0.938	0.776	0.447	0.111	0.046
	0.987	0.938	0.776	0.451	0.111	0.046
	0.988	0.938	0.773	0.450	0.117	0.048
	0.983	0.928	0.760	0.449	0.122	0.049
	0.988	0.930	0.733	0.450	0.127	0.050
	0.987	0.926	0.766	0.453	0.128	0.051
	0.987	0.920	0.770	0.455	0.128	0.051
	0.989	0.926	0.757	0.452	0.140	0.054
	0.990	0.925	0.753	0.451	0.132	0.052
	0.987	0.922	0.751	0.451	0.132	0.051
	0.986	0.940	0.779	0.445	0.106	0.044
	0.986	0.940	0.778	0.444	0.106	0.043
	0.983	0.930	0.760	0.438	0.106	0.044
	0.988	0.967	0.771	0.449	0.117	0.048
	0.980	0.904	0.725	0.449	0.152	0.043
Average	**0.984**	**0.923**	**0.751**	**0.448**	**0.123**	**0.049**
	0.945	0.825	0.675	0.423	0.123	0.050
	0.996	0.886	0.708	0.466	0.142	0.057
	0.973	0.868	0.689	0.451	0.152	0.060
	0.984	0.922	0.750	0.441	0.111	0.045
	0.986	0.896	0.712	0.439	0.119	0.047
	0.995	0.905	0.719	0.458	0.144	0.059
	0.988	0.913	0.739	0.445	0.118	0.049
	0.988	0.918	0.734	0.448	0.120	0.049
	0.992	0.911	0.728	0.454	0.138	0.056
	0.992	0.910	0.731	0.458	0.133	0.054
	0.995	0.900	0.711	0.460	0.147	0.059
	0.990	0.891	0.744	0.460	0.171	0.062
G550-B	0.985	0.929	0.755	0.440	0.108	0.044
	0.987	0.920	0.747	0.447	0.113	0.047
	0.987	0.931	0.759	0.446	0.111	0.045
	0.990	0.893	0.706	0.451	0.128	0.052
	0.984	0.919	0.742	0.440	0.111	0.046
	0.986	0.911	0.740	0.432	0.113	0.047
	0.992	0.889	0.695	0.450	0.126	0.051
	0.983	0.902	0.721	0.449	0.129	0.052
	0.982	0.928	0.757	0.446	0.120	0.048
	0.987	0.892	0.724	0.454	0.127	0.051
	0.992	0.896	0.711	0.453	0.146	0.059
	0.990	0.922	0.753	0.460	0.185	0.068
	0.985	0.934	0.763	0.440	0.107	0.044
	0.987	0.931	0.765	0.446	0.111	0.045
	0.986	0.934	0.768	0.444	0.109	0.045
Average	**0.986**	**0.907**	**0.731**	**0.448**	**0.128**	**0.052**

Table 6.33   Load Ratio (2) Values Obtained in This Research

(b) G250 steel sections

Temp (°C) Steel	100	200	350	500	650	800
	0.968	0.911	0.538	0.344	0.189	0.053
	0.901	0.893	0.562	0.336	0.180	0.053
	0.957	0.896	0.548	0.339	0.183	0.053
	0.958	0.923	0.571	0.345	0.182	0.055
	0.958	0.923	0.576	0.345	0.177	0.061
	0.953	0.917	0.576	0.342	0.180	0.058
	0.955	0.916	0.557	0.346	0.185	0.060
	0.958	0.910	0.569	0.369	0.206	0.052
	0.953	0.895	0.560	0.355	0.195	0.052
	0.982	0.922	0.569	0.359	0.199	0.053
	0.952	0.925	0.591	0.342	0.179	0.056
	0.955	0.923	0.550	0.343	0.181	0.066
	0.962	0.931	0.551	0.352	0.182	0.052
	0.961	0.911	0.574	0.344	0.183	0.052
G250-A	1.000	0.914	0.582	0.374	0.212	0.053
	0.955	0.910	0.563	0.341	0.177	0.053
	0.954	0.908	0.560	0.344	0.179	0.055
	0.954	0.908	0.567	0.344	0.179	0.057
	0.957	0.905	0.571	0.345	0.182	0.059
	0.963	0.904	0.569	0.347	0.187	0.060
	0.967	0.897	0.572	0.351	0.193	0.059
	0.966	0.903	0.576	0.360	0.197	0.061
	0.959	0.902	0.517	0.361	0.201	0.051
	0.967	0.891		0.364	0.201	0.051
	0.970	0.907		0.364	0.203	0.052
	0.957	0.914		0.351	0.179	0.053
	0.949	0.909		0.348	0.177	0.058
	0.953	0.911		0.346	0.178	
	0.959	0.922		0.346	0.181	
	0.973	0.894		0.336	0.188	
Average	**0.959**	**0.910**	**0.564**	**0.349**	**0.187**	**0.056**
	0.968	0.883	0.524	0.342	0.195	0.057
	0.974	0.917	0.535	0.346	0.193	0.054
	0.953	0.915	0.545	0.336	0.182	0.055
	0.954	0.917	0.551	0.338	0.184	0.057
	0.962	0.906	0.528	0.345	0.191	0.057
	0.960	0.912	0.537	0.339	0.189	0.068
G250-B	0.973	0.900	0.571	0.393	0.224	0.054
	0.958	0.901	0.534	0.335	0.181	0.053
	0.957	0.907	0.557	0.336	0.178	0.053
	0.958	0.906	0.563	0.329	0.177	0.054
	0.960	0.908	0.545	0.335	0.181	0.056
	0.957	0.896	0.555	0.348	0.190	0.054
	0.963	0.909	0.560	0.339	0.185	0.055
	0.964	0.900	0.552	0.342	0.185	0.057
	0.975	0.913	0.533	0.344	0.189	0.064
	1.000	0.878	0.541	0.368	0.210	
Average	**0.965**	**0.904**	**0.546**	**0.345**	**0.189**	**0.057**

Figure 6.24 (a) shows that there is a similar load ratio to temperature relationship for Types A and B steel sections for high strength steels (G550) while Figures 6.24 (b) shows the same for low strength steels (G250). The difference between G550 and G250 steels is mainly due to the differences in their mechanical properties and deterioration characteristics with increasing temperatures. Therefore it is recommended that a limiting temperature method as proposed in SCI (1993) can be used but based on the results obtained from this research and as plotted as Load ratio (2) in Figures 6.24 (a) and (b). In fact the results for G550 steel sections agree well with the values given in SCI (1993) (see Load ratio (1) in Figure 6.24 (a). Based on the results in Figures 6.24 (a) and (b), appropriate fire protection can be chosen to limit the temperature in the cold-formed steel members. Based on Figures 6.24 (b), greater fire protection will therefore be needed for low strength steel sections.

Additionally, Eurocode 3 Part 1.2 (ECS, 1993) simply stated that the design capacity equations should not be used if the temperature exceeds $350^{\circ}C$ (see Clause 4.2.3.6 in Eurocode). However, the load ratio-limiting temperature concept is not considered in Eurocode. The results obtained in this research show that the average Load ratio (2) for high strength steel is 0.743 while it is 0.556 for low strength steel at $350^{\circ}C$. These load ratios are reasonably high and in fact even at $500^{\circ}C$, the load ratios are 0.448 and 0.348 for G550 and G250 steel sections. Therefore it appears that simply limiting the temperature to $350^{\circ}C$ for cold-formed steel structures without considering the load ratios is unnecessary. Instead a limiting temperature method as proposed in SCI (1993) based on the results obtained in this research can be used in the fire safety design of cold-formed steel structures to design the required fire protection. It is to be noted that the other steel structures design standards, AS 4100 and BS 5950 use the limiting temperature method for fire safety design.

6.5   Summary

This chapter was based on a detailed parametric study of light gauge cold-formed steel compression members subjected to distortional buckling at both ambient and elevated temperatures. Extensive parametric studies were undertaken using an advanced finite element tool ABAQUS by changing various factors: temperature,

steel grade and thickness, section geometry, flange width and web height. The obtained results from the finite element analyses (FEA) were then compared with available design equations. The design equations based on AS/NZS 4600 (SA, 1996) and the direct strength method were considered at ambient temperature.

The results showed that the AS/NZS 4600 design method is better than the direct strength method. However, both methods are reasonable but unsafe for some sections. Therefore there was a need to develop a new design equation. As a first step of this development, available distortional buckling equations were compared with other buckling mode equations in order to develop the most suitable equation by modifying the available design equations. Current distortional buckling curves showed that the direct strength method has better agreement with other buckling modes than AS/NZS 4600 design curve when non-dimensional stress-slenderness curves were plotted. A new design equation was therefore developed to determine the ultimate load of cold-formed steel compression members subjected to distortional buckling mode at ambient temperature by modifying the direct strength method. The ultimate load predictions from the modified equation agreed well with the ultimate loads obtained from FEA at ambient temperature. The developed equation was then used to predict the ultimate load at elevated temperatures.

The equation was simply modified by including the relevant reduction factors of mechanical properties at various temperatures. There was a reasonable agreement between the ultimate load predicted from simply modified equation and the results obtained from FEA. However the predictions compared well with the FEA results for some temperatures while the predictions were not good at other temperatures. Therefore it was decided that the equation developed for ambient temperature conditions cannot be simply modified by including the reduced mechanical properties at elevated temperatures for light gauge cold-formed steel compression members.

The distortional buckling and ultimate load behaviour of compression members was investigated further with respect to the various influencial parameters at elevated temperatures. The non-linear stress-strain characteristics was first studied since the stress-strain curve of the material becomes nearly elastic perfect plastic to non-linear

with increasing temperatures. The results showed that the non-linear stress-strain curves have an influence on the ultimate load but it is not significant. The k_{yT}/k_{ET} factor was then considered since the k_{yT}/k_{ET} factor changes with temperature. The results showed that there is a considerable influence from k_{yT}/k_{ET} factor on the ultimate load. The effect of residual stresses, section geometry, steel thickness, web height and flange width was also considered. Finally it was shown that mainly the k_{yT}/k_{ET} factor has a significant influence on the distortional buckling behaviour while others show little or no influence. Therefore the initial equation was further modified by considering the effect of k_{yT}/k_{ET} factor. The predictions from the developed equations were then compared with FEA results. The results showed that the ultimate loads predicted from the developed equations for elevated temperature conditions agree well with the FEA results.

The limiting temperature method presented in the SCI publication was also investigated with the results obtained in this research. The results showed that it can be used for cold-formed steel members using the results obtained in this research. Greater fire protection may be required for low strength steel sections than for high strength steel sections. It may not be necessary to restrict the temperature to 350 C for cold-formed steel structures.

Finally, it can be stated that this research has developed accurate strength equations for cold-formed steel compression members that can be used to provide safe structural designs in fire situations. The results can be effectively used to choose the required fire protection and thus to design safe and economical light gauge cold-formed steel structures under fire conditions.

7   Conclusions and Recommendations

This thesis has described a detailed investigation into the structural behaviour of light gauge cold-formed steel compression members subjected to distortional buckling at both ambient and elevated temperatures. Both experimental and finite element analyses were conducted to improve the knowledge and understanding of the behaviour of cold-formed steel compression members subjected to fire effects, and hence this has led to safer structural design methods for fire conditions.

In the first phase of this research, mechanical properties of light gauge cold-formed steels were obtained from more than 115 tension and compression coupon tests at ambient and elevated temperature. In the second phase, extensive experimental investigations were undertaken at both ambient and elevated temperatures for cold-formed steel compression members subjected to distortional buckling. Two different geometries with two steel grades and three thicknesses were considered. In this study, pin and fixed ends were considered initially, however, fixed-end condition was used in the majority of tests. An electrical furnace was used in this study to uniformly heat the test specimens. Static tests were conducted at temperatures ranging from 20 to 800$^{\text{o}}$C. More than 170 compression tests were undertaken at both ambient and elevated temperatures.

Finite element models of tested cold-formed steel compression members were developed using the advanced finite element tool ABAQUS. They were validated by comparing their results with the corresponding experimental results: ultimate loads, load-shortening curves and load-out-of-plane deflection curves. The validated finite element models were then used to undertake an extensive parametric study. More than 900 finite element analyses were conducted for a range of cold-formed steel compression members at both ambient and elevated temperatures. The parametric study results were used to review the current design rules and finally, improved design equations were developed to predict the ultimate loads of light gauge cold-formed steel compression members subjected to distortional buckling.

Chapter 3 of this thesis has presented the detailed investigation of compression and tension coupon tests at ambient and elevated temperatures. It discussed the mechanical properties of ambient and elevated temperatures for both low and high strength steels. Chapter 4 has presented the detailed experimental investigation of light gauge cold-formed steel compression members subjected to distortional buckling while Chapter 5 has presented the details of advanced finite element models developed and their validation. A description of the detailed parametric study and the ultimate load results including the new design equations are presented in Chapter 6.

The most valuable outcomes obtained from this research are as follows

- The development of predictive equations for the important mechanical properties of light gauge cold-formed steels at both ambient and elevated temperatures and hence the yield strength, elasticity modulus and the stress-strain curve at any given temperature up to 800°C can be determined accurately.

- Significantly improved knowledge and understanding of the distortional buckling behaviour of light gauge cold-formed steel compression members at both ambient and elevated temperatures

- Assessment of the currently available design methods for distortional buckling effects at ambient and elevated temperatures

- Development of more accurate design equations to predict the ultimate loads of light gauge cold-formed steel compression members subjected to distortional buckling effects at any temperature up to 800°C.

Following important conclusions and recommendations have been drawn based on this research project.

7.1 Tension and Compression Coupon Tests to Determine Mechanical Properties

- In general tension and compression coupon tests at ambient temperature showed that the mechanical properties obtained from both methods showed

only a small difference. Since the test set-up for compression coupon test was more complicated it could not be used at elevated temperatures.

- Finite element analyses showed that the ultimate load and load-deformation curves of compression members subjected to distortional buckling were similar when the mechanical properties obtained from compression and tension coupon tests were used. Therefore it is recommended that the mechanical properties can be obtained from tension coupon tests at elevated temperatures and used for analysis and design purposes.

- Tensile coupon tests at elevated temperatures were successfully completed with the use of a new non-contact strain measuring device known as Laser Speckle Extensometer. This eliminated the need for conventional strain gauges and extensometers.

- Tensile coupon tests at elevated temperatures produced the mostly needed reduction factors for yield strength and elasticity modulus for light gauge cold-formed steels of three thicknesses and two steel grades. The results showed that the currently available reduction factors for mechanical properties are not accurate for light gauge cold-formed steels. Further, they showed that the reduction factors recommended for hot-rolled steels are considerably higher than those for light gauge cold-formed steel reduction factors and hence cannot be used in the analysis and design of cold-formed steel structures under fire conditions.

- Tensile coupon tests at elevated temperatures showed that the reduction of elasticity modulus was independent of steel grade or steel thickness. However, yield strength reduction factors depend significantly on the steel grade. The reduction factors of high strength steels show three main regions while low strength steels show only two regions. There was a sudden reduction in yield strength in the range of 400°C to 600°C for high strength steels due to the loss of strength gained from cold-working. Hence the yield strengths obtained for both low and high strength steels were about the same

at 800°C. Based on the test results from this research, suitable predictive equations have been developed to determine the mechanical properties of light gauge cold-formed steels at elevated temperatures up to 800°C. These equations are very important in the analysis and design of cold-formed steel structures under fire conditions since the deterioration of mechanical properties are one of the most important factors in fire design.

- A stress-strain model was developed based on the well known Ramberg-Osgood model that can accurately determine the stress-strain behaviour of light-gauge cold-formed steels under fire conditions at any given temperature up to 800°C. The developed stress-strain model was verified using tensile coupon test results.

- Ductility of high strength steels increased considerably with increasing temperatures, particularly after 500°C. However no such improvement was observed for low strength steels.

- Using finite analyses of cold-formed steel compression members, it was shown that the mechanical properties obtained in this research accurately predicted the ultimate loads of compression members subjected to distortional buckling mode at elevated temperatures. The use of the mechanical properties presented in various design standards (Eurocode, BS 5950) and research papers (Outinen, 1999 and Chen and Young, 2004) was unable to accurately determine the ultimate loads. Therefore it is highly recommended that the equations developed in this research are used to determine the yield strength, elasticity modulus and stress-strain curves of light gauge cold-formed steels at any given temperature up to 800°C.

7.2 Experimental Study of Cold-formed Steel Compression Members

- Experimental study of compression members subjected to distortional buckling showed that a test set-up with fixed-end conditions is easier to build

and use than that with pin-end conditions. The test set-up with pin-end conditions is more complicated to build and use at elevated temperatures.

- Specially made end plates with appropriate grooves were able to simulate fixed end conditions in the compression tests. A fire resistant filling material must be used for elevated temperature tests.

- Test specimens at both ambient and elevated temperatures failed by distortional buckling. This therefore confirms that cold-formed steel sections can be designed to fail by distortional buckling by choosing their geometry based on the buckling plots from the simple finite strip analysis programs such as Thin-wall and CUFSM.

- Distortional buckling failure characteristics were similar in tests at ambient and elevated temperatures. However, the ultimate loads of compression members decreased rapidly as temperatures were increased beyond 500°C. It was clear that the cold-formed steel specimens were unable to resist a considerable load after 800°C.

- Experimental study showed the occurrence of three variations of distortional buckling mode even when the same test was repeated: both flanges moved inward, both flanges moved outward and one flange moved inward while the other one moved outward. This observation was thoroughly investigated and it was found that this phenomenon was caused by the type of initial geometric imperfections, and not by increasing temperatures.

- Tests produced useful data for the distortional buckling behaviour of light gauge cold-formed steel compression members in the form of ultimate loads, and load-shortening and load-out-of-plane deflection curves.

- The measured initial geometric imperfections showed that there is a difference between low (G250) and high (G550) strength steels. High strength steel specimens showed higher imperfections than low strength steel

specimens. However the difference is small. The measured imperfection values in this study showed that Schafer and Pekoz's (1998) predictions for initial imperfections are more accurate than other predictions. Therefore it is recommended that Schafer and Pekoz's (1998) equations are used to determine the initial geometric imperfections for use in finite element analyses.

- The high strength steel specimens appeared to show higher ductility capacity based on the usual definition of ductility ratio than the low strength steel specimens although tensile coupon test results show just the opposite. Main reason for this behaviour is that the ductility defined by the tensile coupon test is only the behaviour at material level and it can change when considering the cross section of a member. Further it was observed that the ductility of the specimens increased with increasing temperatures. At 800°C their ductility has increased to more than three times that at the ambient temperature for both low and high strength steel specimens.

- The current design rules based on AS/NZS 4600 (SA, 1996) and direct strength method predicted well the ultimate loads of cold-formed steel compression members subjected to distortional buckling at ambient temperature. However, at elevated temperatures, their predictions were somewhat scattered with some being too conservative while others being unsafe. The AS/NZS 4600 predictions were found to be better than those from the direct strength method.

7.3   Finite Element Analyses

- The elastic distortional buckling and ultimate strength behaviour of compression members at both ambient and elevated temperatures was successfully investigated by using finite element models based on ABAQUS shell elements. The models included accurate mechanical properties, initial imperfections and residual stresses. They predicted the ultimate loads, the

load-shortening and load-out-of-plane deflection curves, and the distortional buckling failure modes of the tested compression members accurately.

- Comparison of finite element analysis results with experimental results showed that the S4 element type is more accurate than the S4R5 element type for compression members subjected to distortional buckling.

- The behaviour of cold-formed steel compression members at elevated temperatures was accurately simulated by the finite element models when the measured mechanical properties were used.

- Comparison of the results obtained from finite element analyses and experiments showed that including the full stress-strain model provided better results than the elastic perfect plastic model. Therefore it is recommended that mechanical properties based on the full stress-strain curve are used in finite element analyses than the elastic perfect plastic method. Further it is recommended that actual initial geometric imperfections and residual stresses are used in finite element modelling.

- Finite element analyses of light gauge cold-formed steel compression members subjected to distortional buckling showed that residual stresses had insignificant influence on their ultimate loads while geometric imperfections had significant influence. Interestingly, the ultimate load decreased significantly with a small imperfection, but did not decrease at the same rate with further increase in imperfections. It was found that the direction of the initial geometric imperfections governed the type of distortional buckling mode, ie. both flanges moved inward, both flanges moved outward and one flange moved inward while the other one moved outward.

- The magnitude of residual stresses was considered to decrease with increasing temperatures in the finite element analyses. The results showed that the influence of residual stresses was negligible even at ambient temperature.

- The results showed that the type of distortional buckling mode did not depend on the temperature.

- It is important to determine the presence of post-buckling capacity for compression members subjected to distortional buckling as there were contradicting results from past research. This research has shown that there was considerable post-buckling capacity for compression members with higher slenderness but there was little or no post-buckling capacity for members with lower slenderness.

7.4   Development of New Design Equations

- The comparison of the ultimate loads predicted by the current design rules (AS/NZS 4600 (SA, 1996) and direct strength method) with the ultimate loads obtained from the detailed parametric study showed that the current design rules are accurate in general, but further improvements can be made. The ultimate load predictions from the Australian cold-formed steel structures code, AS/NZS 4600 (SA, 1996) were found to agree better with finite element analysis results than those from the direct strength method.

- New design equations were developed to accurately predict the ultimate load of compression members subjected to distortional buckling at ambient temperature. The comparison of the ultimate load predictions from the new equations with finite element analyses and the AS/NZS 4600 predictions showed that the new design equation can accurately predict the ultimate loads. The accuracy of the new equations was found to be better than that of the current AS/NZS 4600 design equations. Therefore it is recommended that the new design equations are used to predict the ultimate loads of light gauge cold-formed steel compression members subjected to distortional buckling.

- The developed equations at ambient temperature were then simply modified by including the relevant mechanical properties at various temperatures to

determine the ultimate loads at elevated temperatures. Comparison of the ultimate load predictions from the modified equations and corresponding finite element analysis results showed that the ambient temperature design equation cannot be simply modified by including the relevant mechanical properties for any given temperature as suggested by some fire research papers. However, it showed that the ultimate load predictions based on this simple approach agreed well with the finite element analysis results for some temperatures less than about 650 and 350°C for high and low strength steel, respectively.

- A detailed study on the effects of a number of parameters on the ultimate loads of cold-formed steel compression members subjected to distortional buckling showed that the residual stresses, section geometry, thickness, web height and flange width did not have much influence. However, it showed that the non-linear stress-strain characteristics has a small influence and that the ratio of yield strength and elasticity modulus reduction factors (k_{yT}/k_{ET}) has a significant influence on the ultimate loads.

- Further investigation of the effect of k_{yT}/k_{ET} factor on the ultimate loads of cold-formed steel compression members showed that the simply modified ambient temperature equation can accurately predict the ultimate loads at elevated temperatures when the k_{yT}/k_{ET} factor is higher than 0.9. However, it showed that the equation should be further modified when the k_{yT}/k_{ET} factor is equal or less than 0.9 for more accurate predictions.

- The ultimate load predictions from the modified equation based on k_{yT}/k_{ET} factor compared well with the finite element analysis results.

- The comparisons of ultimate load predictions obtained from the developed equations with finite element analysis results showed that the developed equations in this research accurately predict the ultimate loads of light gauge cold-formed steel compression members subjected to distortional buckling at both ambient and elevated temperatures. Further it showed that the capacity

reduction factor agreed well with the current capacity reduction factor of 0.9 given in design codes. Therefore it is recommended that the developed equations in this research are used to predict the ultimate loads of cold-formed steel compression members subjected to distortional buckling at both ambient and elevated temperatures instead of the current design rules.

- The results from this research showed that the limiting temperature method presented in SCI (1993) can be used for cold-formed steel members. They showed that greater fire protection should be used for low strength steel sections than for high strength steel sections. Further they showed that it may not be necessary to restrict the temperature to 350°C for cold-formed steel structures as given in Eurocode 3 Part 1.2 (ECS, 1993).

7.5   Future Work

Research work has already been undertaken at the Queensland University of Technology to investigate the local buckling behaviour at elevated temperatures for light gauge cold-formed steel compression members. However, the experimental method used was not adequate and therefore further investigation of local buckling behaviour of compression members at elevated temperatures should be undertaken. Further the interaction of local and distortional buckling modes should be investigated at both ambient and elevated temperatures since some cold-formed steel sections may be subjected to an interaction of local and distortional buckling modes.

Cold-formed steel compression members are subject to not only local and distortional buckling effects, but also to flexural/flexural torsional buckling effects. Therefore, further research is required to investigate the flexural and flexural torsional buckling behaviour at elevated temperatures so that a better understanding of the structural behaviour of cold-formed steel compression members subjected to fire conditions can be obtained. Additionally the interaction of local, distortional and flexural buckling is also required to enhance the understanding of the structural behaviour of cold-formed steel members under fire conditions.

Further research work should be undertaken to determine the effect of fire when steel structures are protected by fire proof materials. The limiting temperature method can be investigated properly in this study.

This research was based on uniform heating of cold-formed steel compression members. Further research is recommended to investigate the behaviour of steel members when fire occurs only on one side of the members.

The mechanical properties obtained in this research were only for limited thicknesses and further research is required to determine the mechanical properties of other thicknesses at elevated temperatures.

The new design equations developed in this research were based on two types of section geometry that are commonly used. Other section geometries should be researched to determine the applicability of the new equations for them.

The compression members that fail by distortional or flexural buckling mode at ambient temperature may not fail by the same mode at elevated temperatures due to the degradation of mechanical properties. Hence the influence of temperature on buckling mode should be investigated.

APPENDIX A

A1 Tensile Coupon Test Results
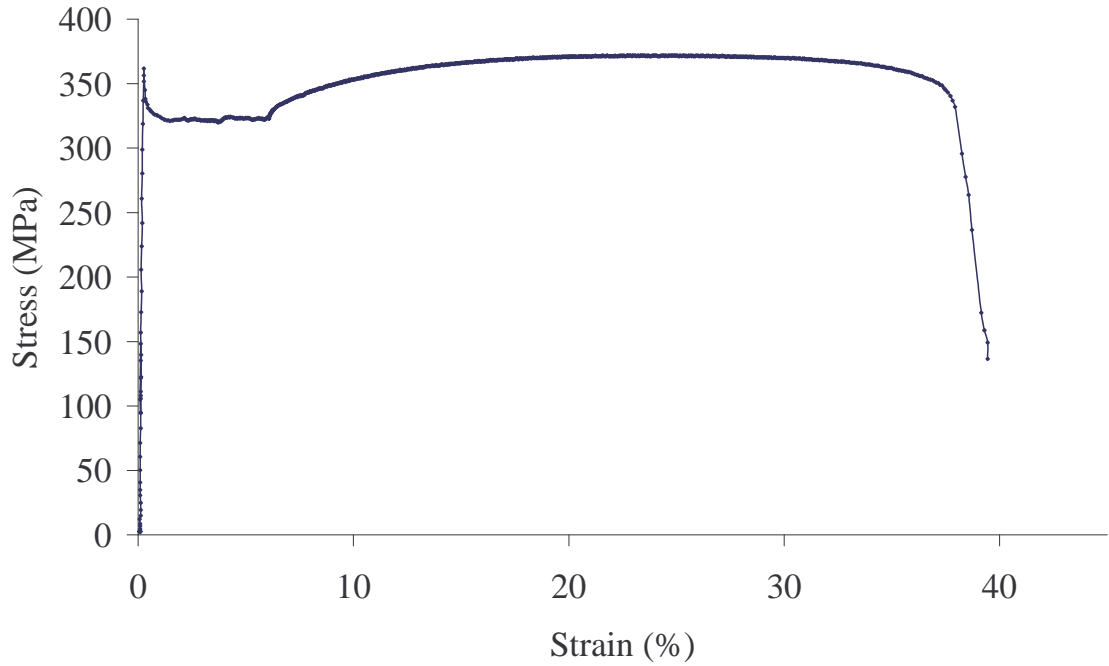
0.6mm G250
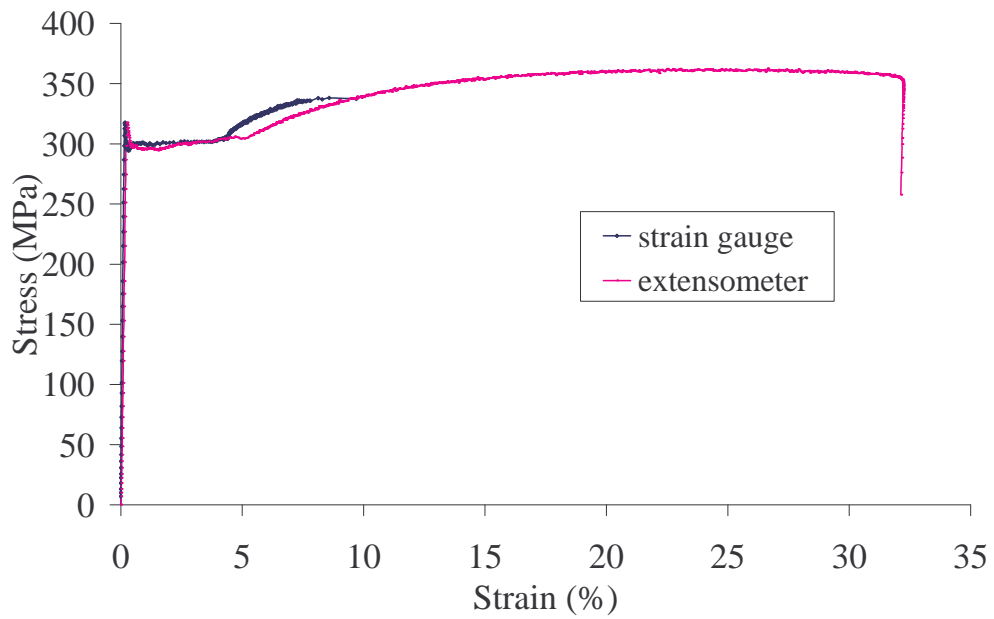
0.8mm G250
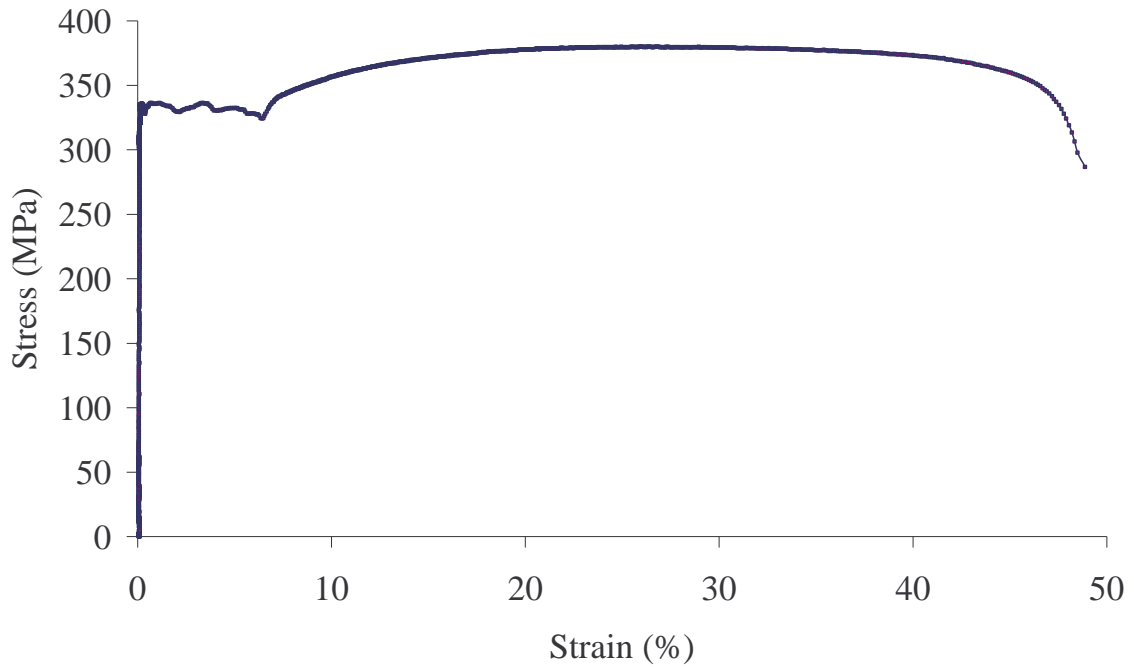
0.95 mm G250
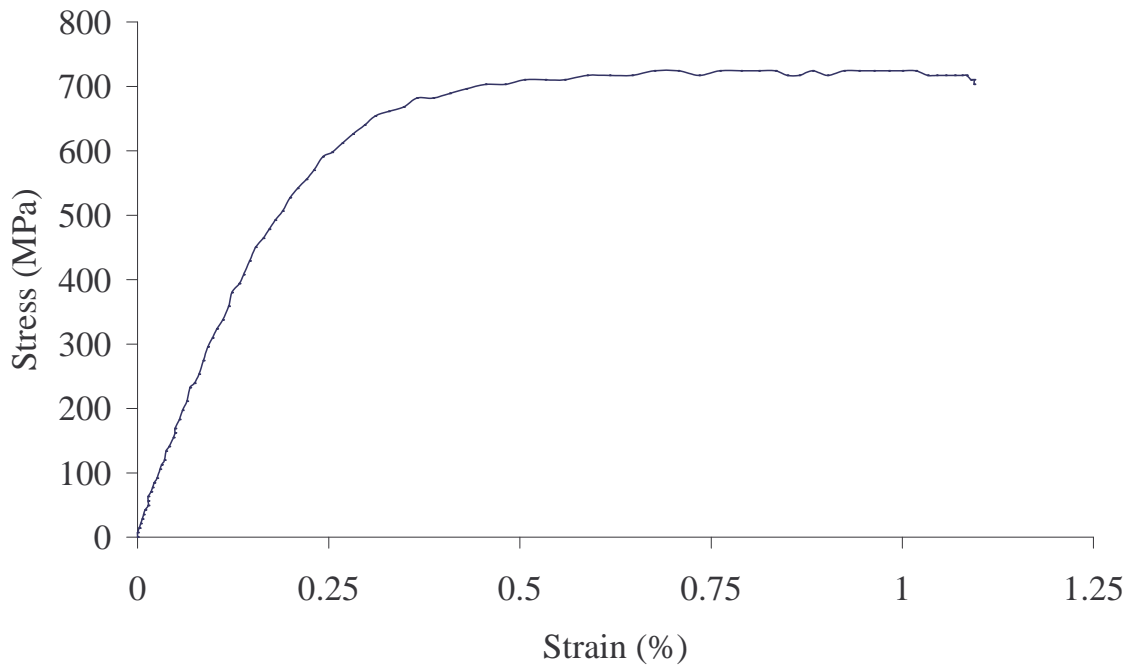
0.42 mm G550
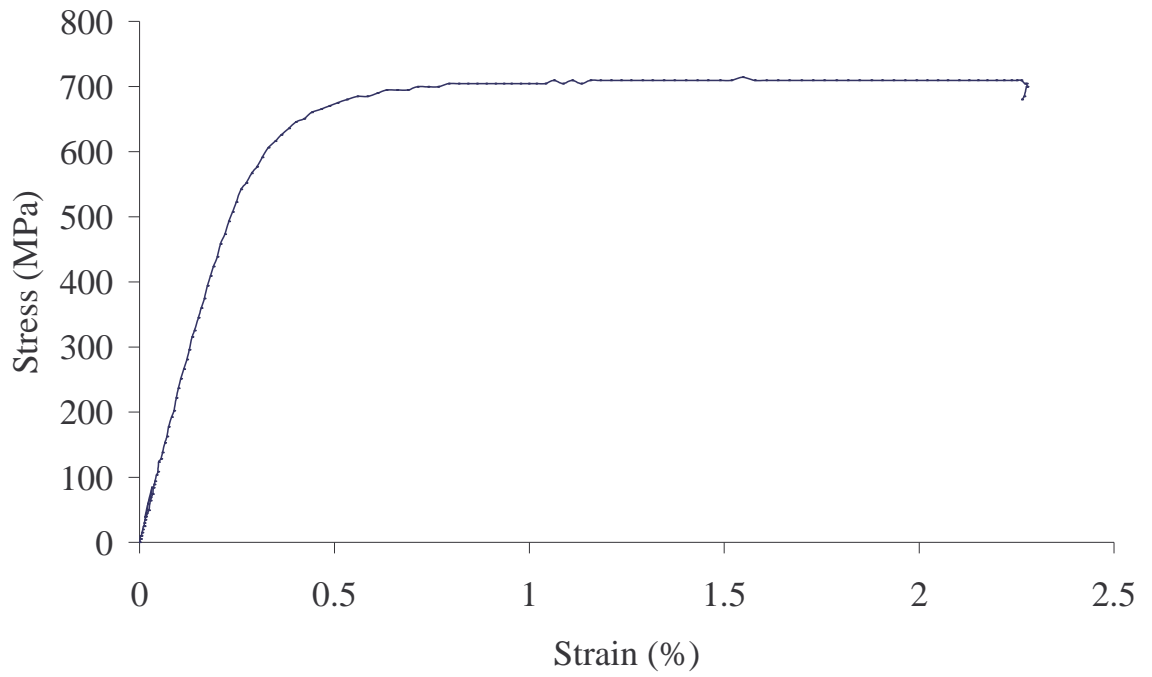
0.6 mm G550
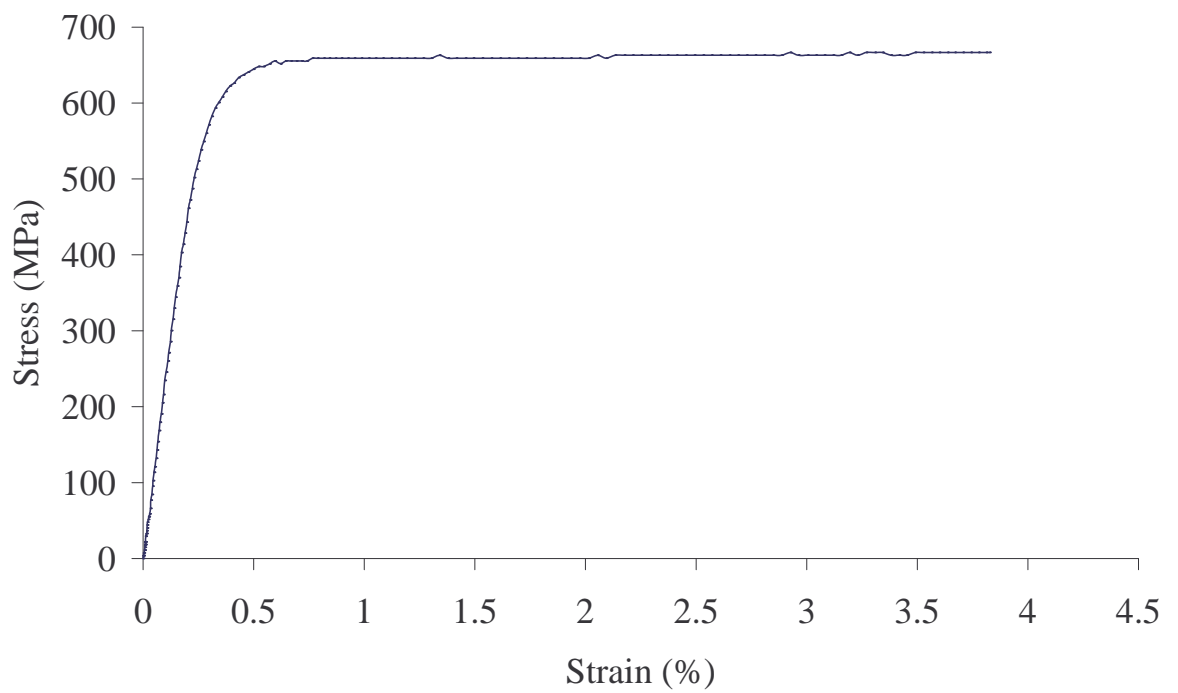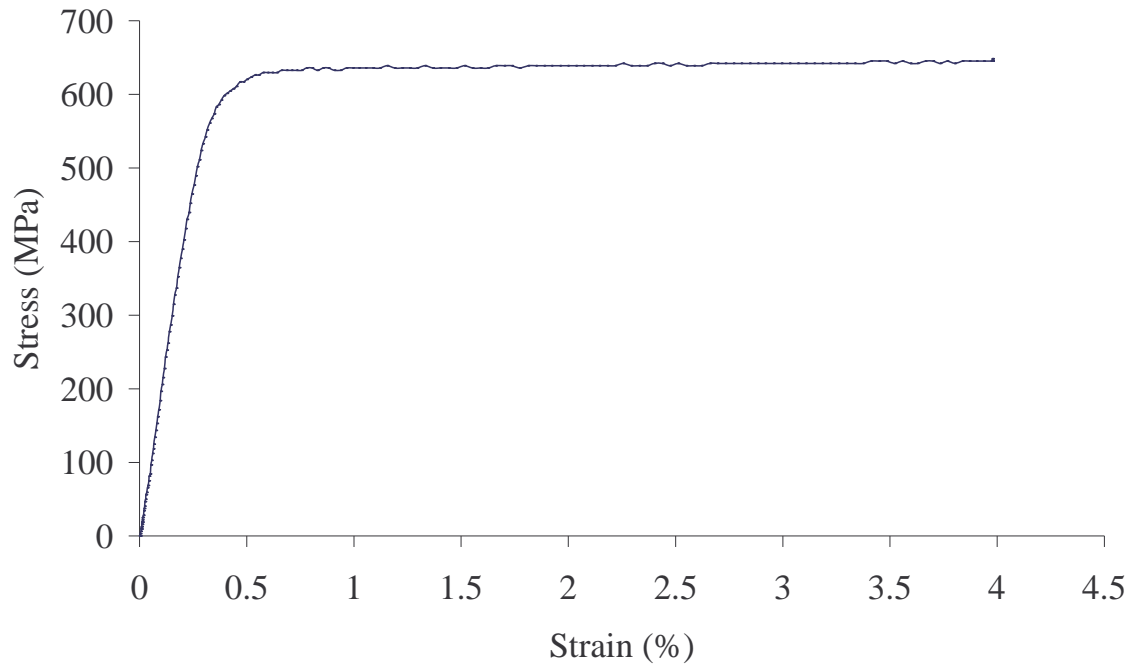
0.8 mm G550

0.95 mm G550

A2 Compression Coupon Test Results
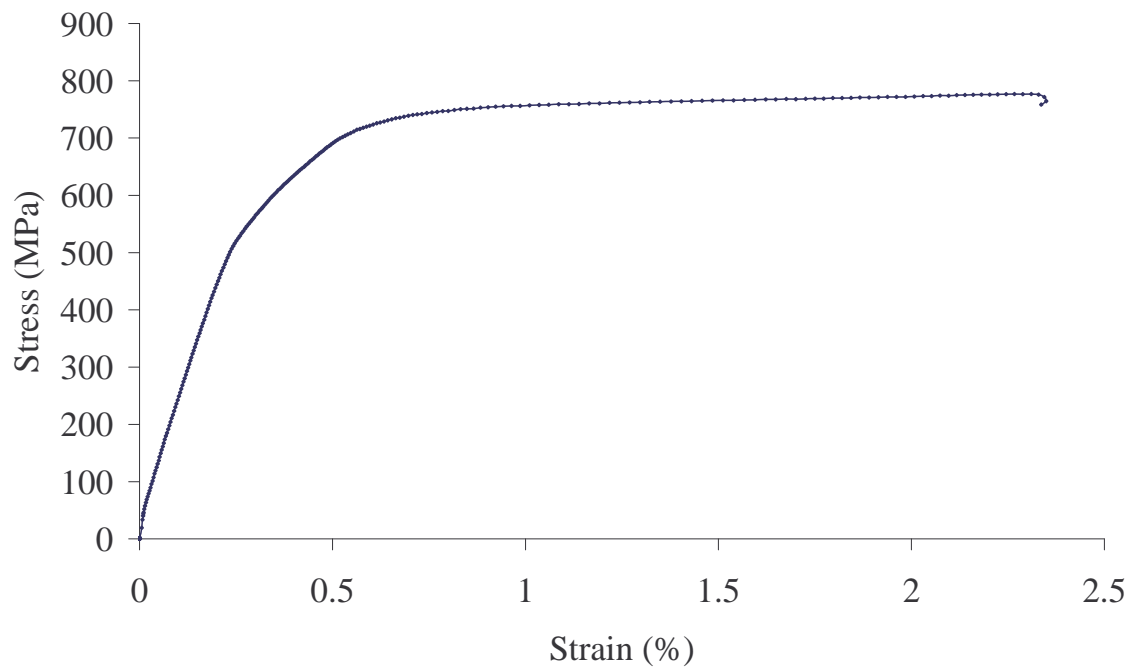
0.42mm G550
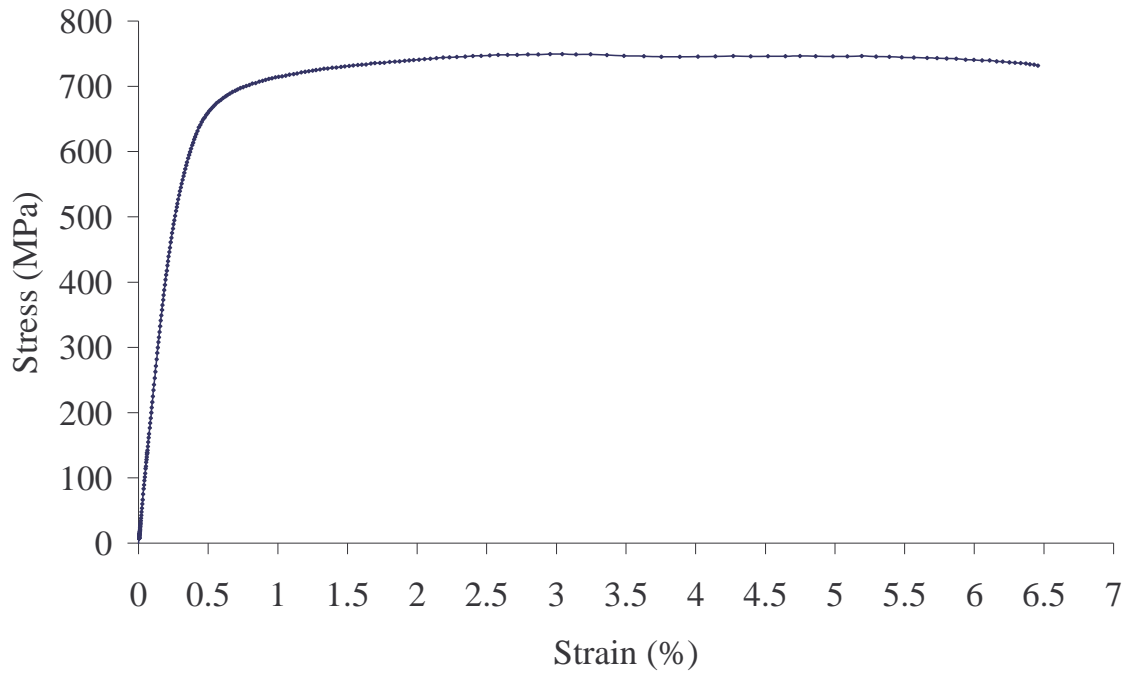
0.6 mm G550
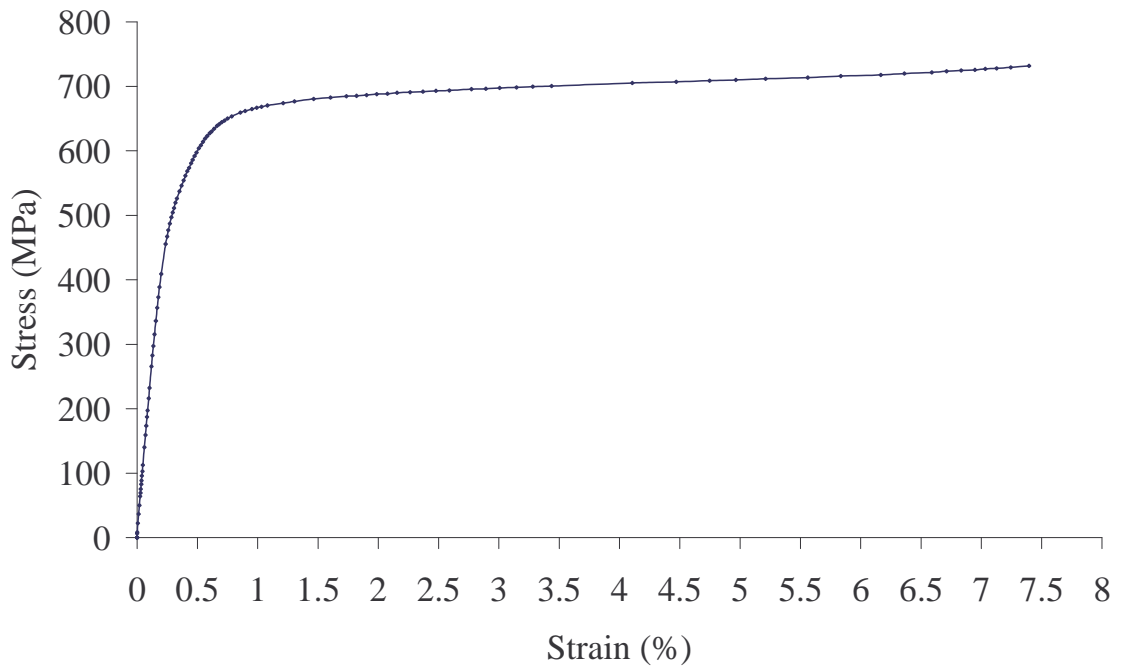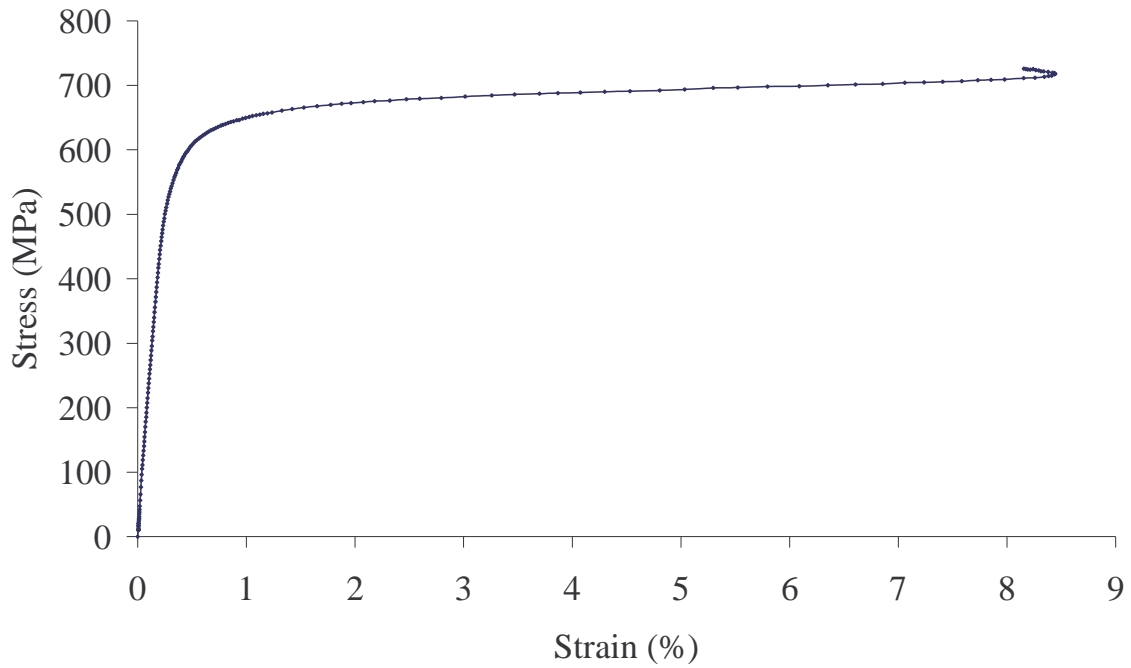
0.8 mm G550

0.95 mm G550

A3 Tensile Coupon Test Results by using Laser Speckle Extensometer at Ambient and Elevated Temperatures
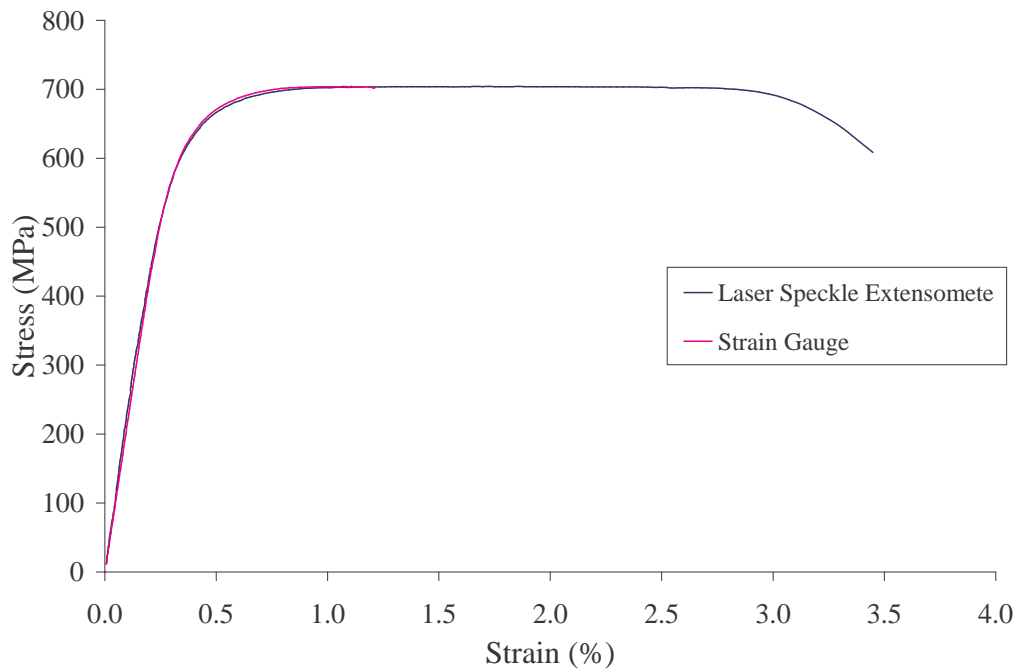
0.6 mm-G550 at 20°C
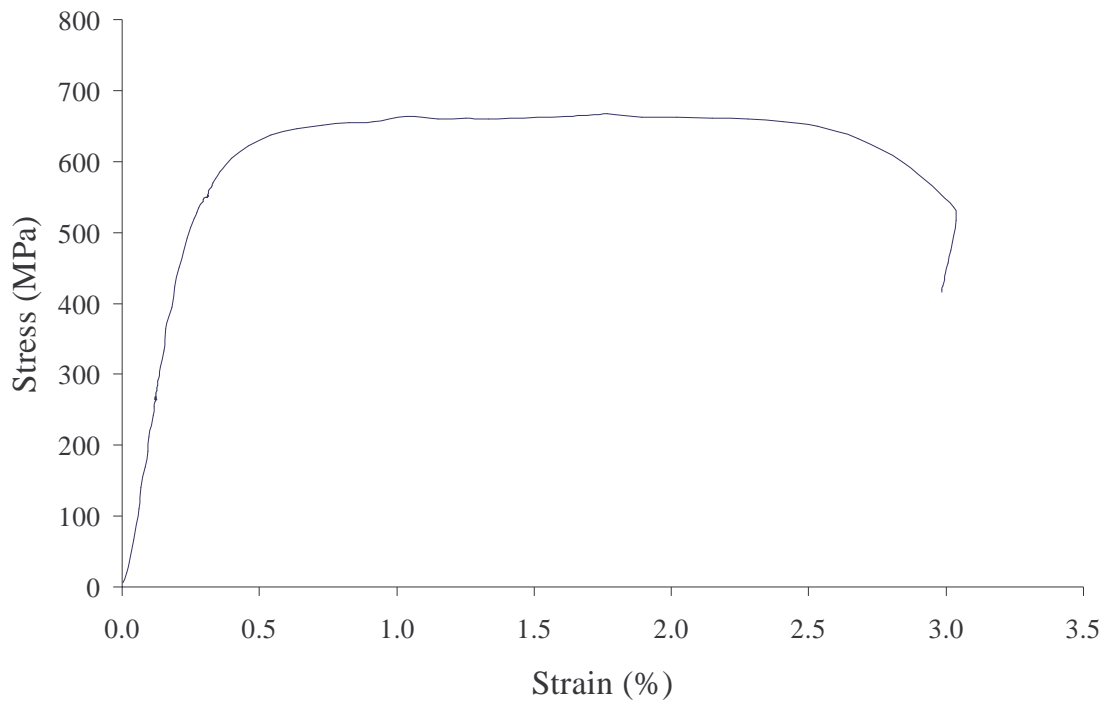
0.6 mm-G550 at 100ºC
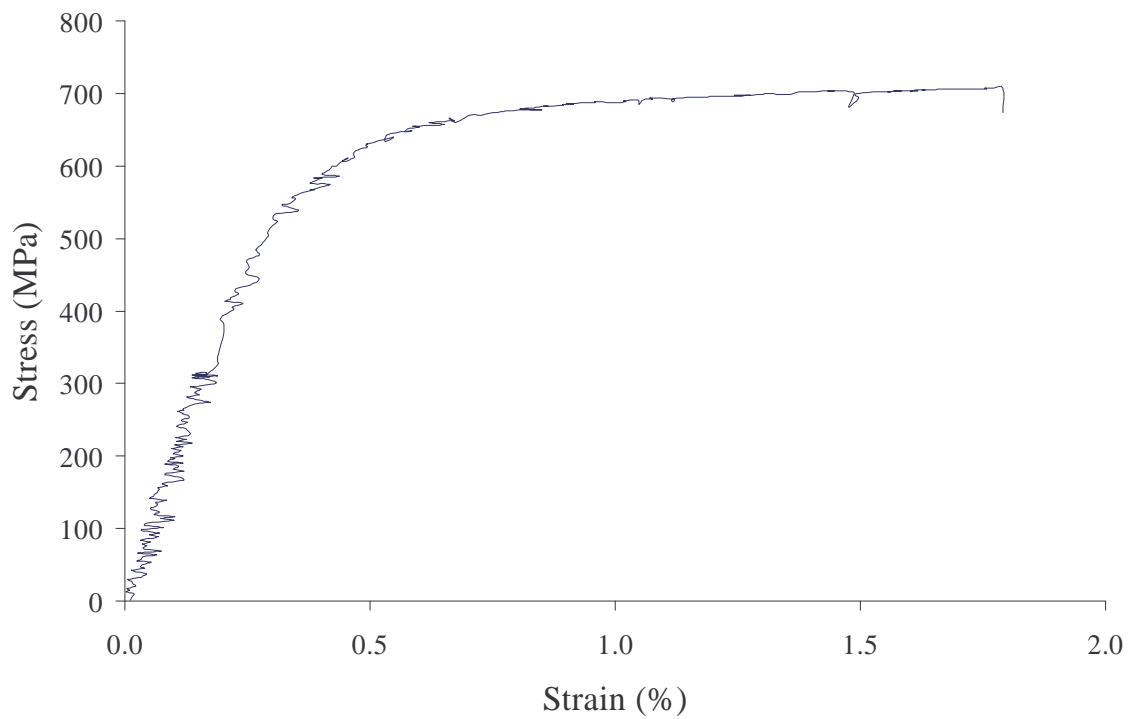
0.6 mm-G550 at 200ºC
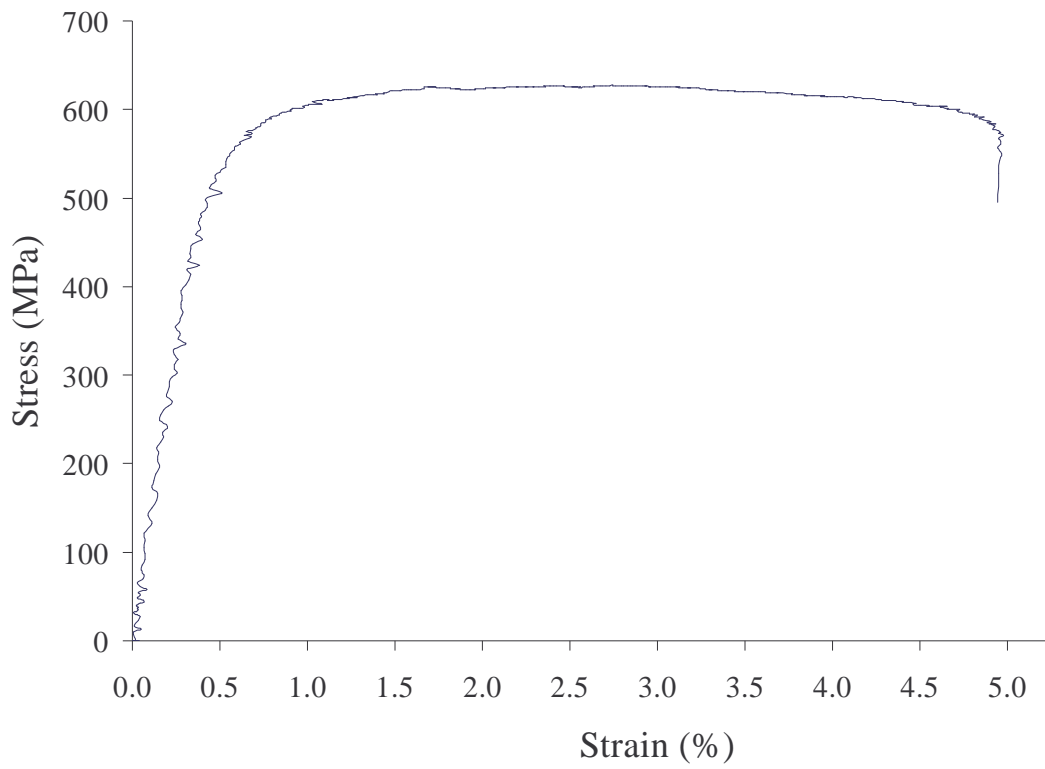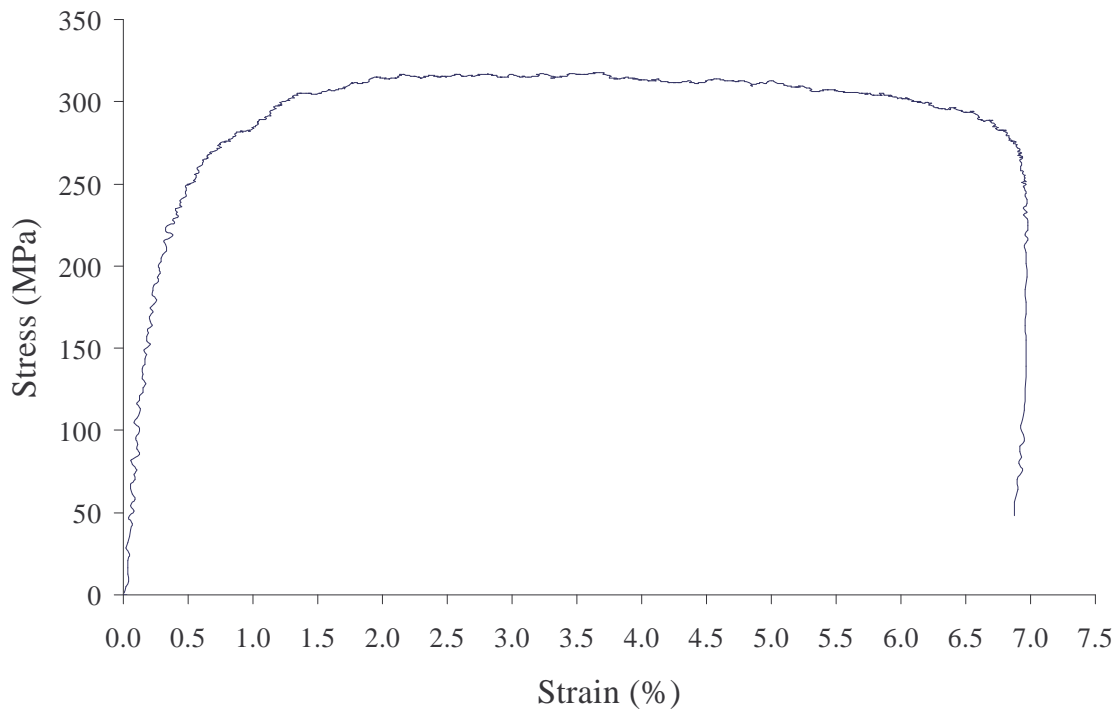
0.6 mm-G550 at 350ºC
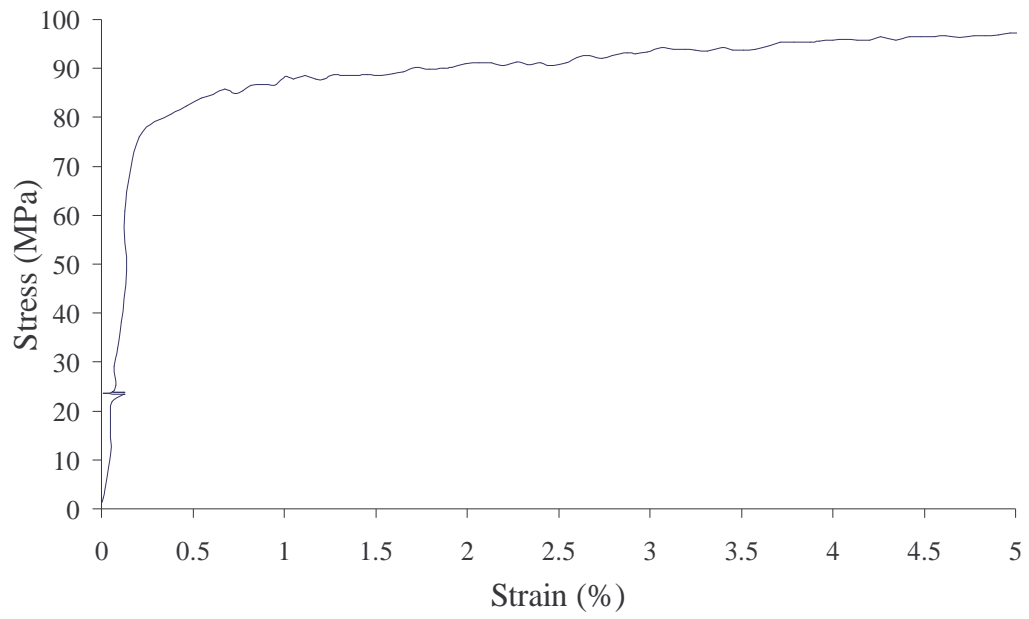
0.6 mm-G550 at 500ºC
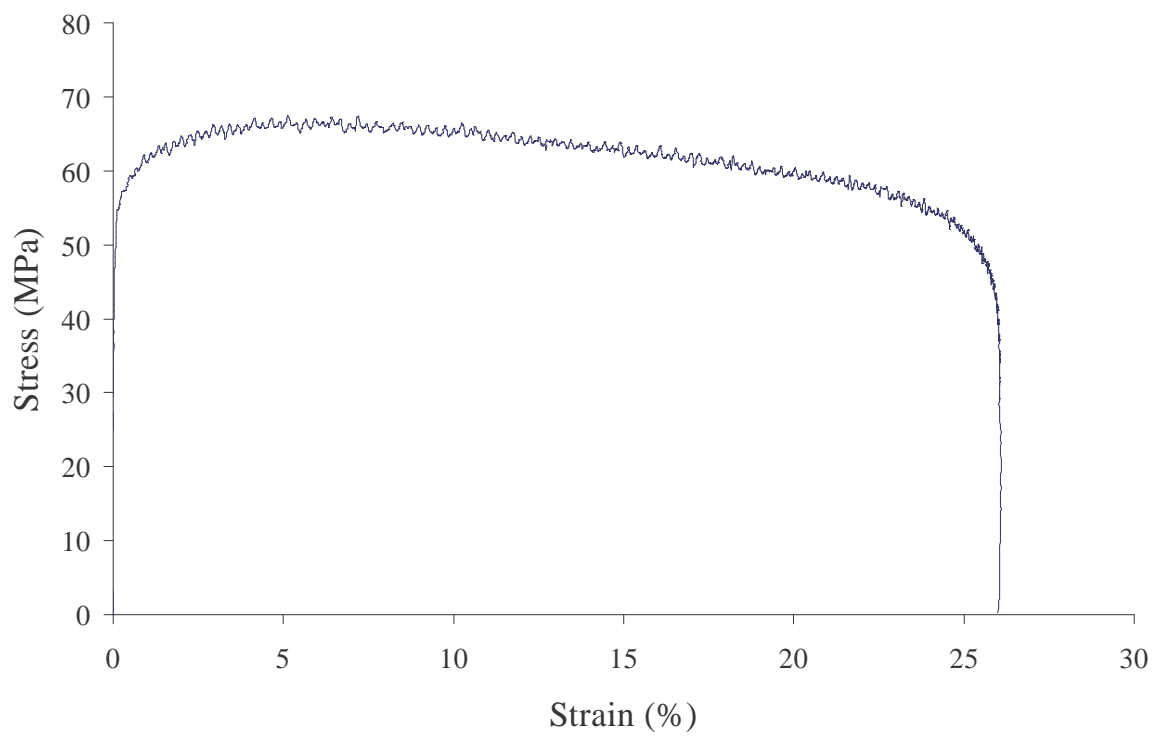
0.6 mm-G550 at 600°C

0.6 mm-G550 at 650°C
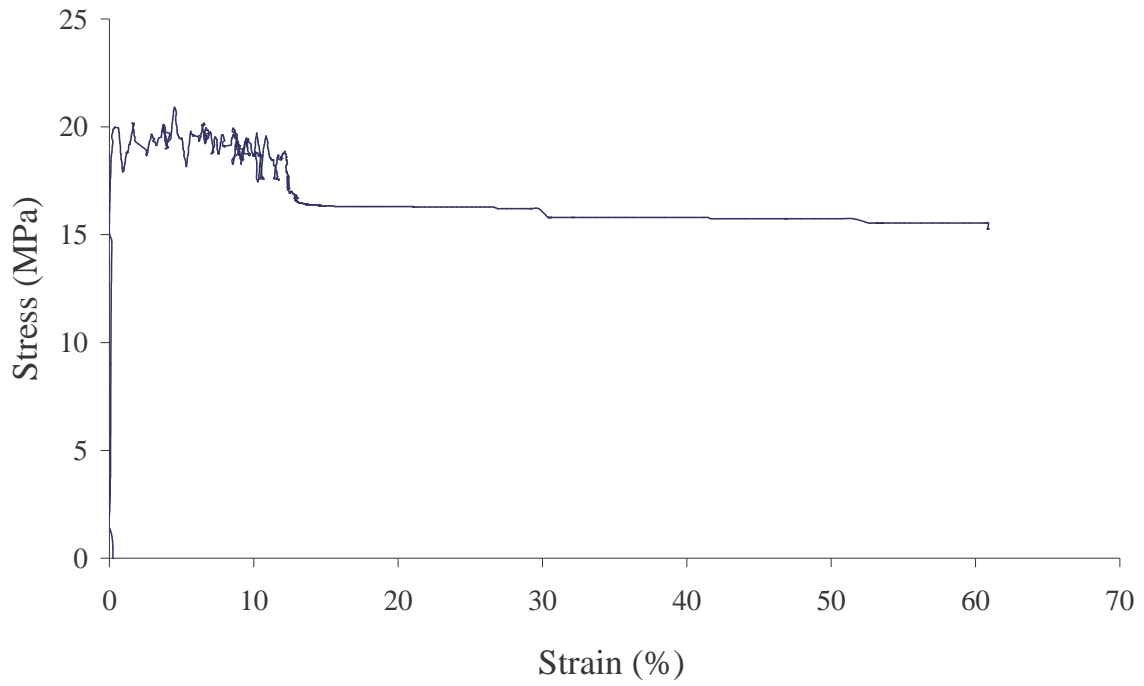
0.6 mm-G550 at 800$^{\mathrm{o}}$C
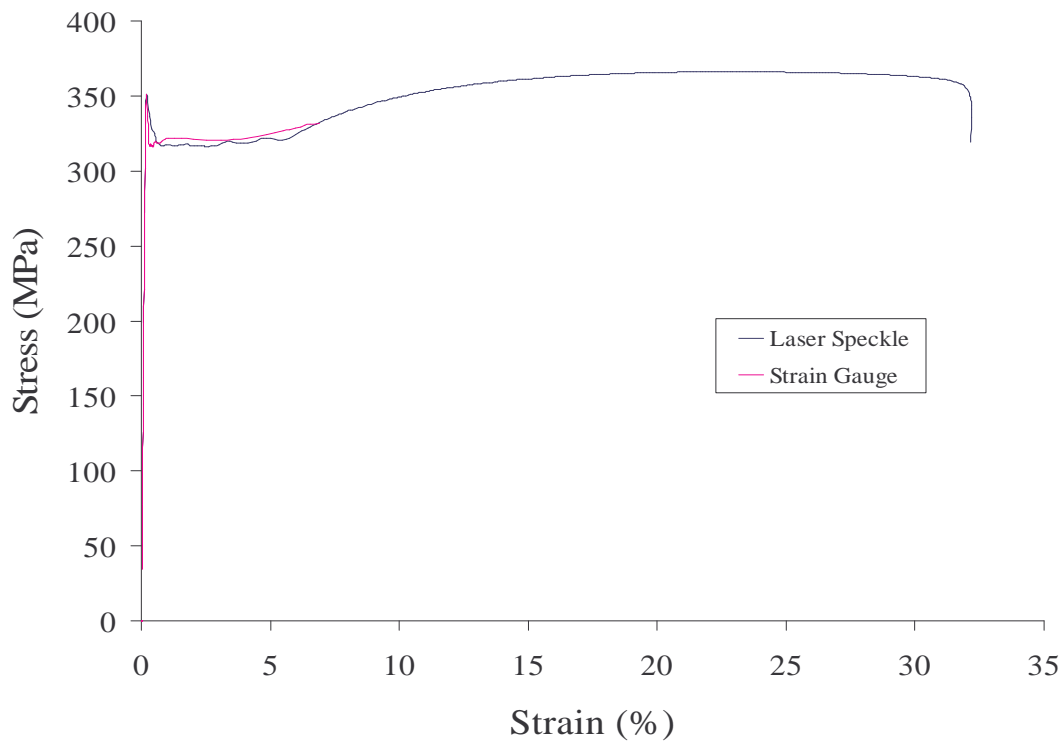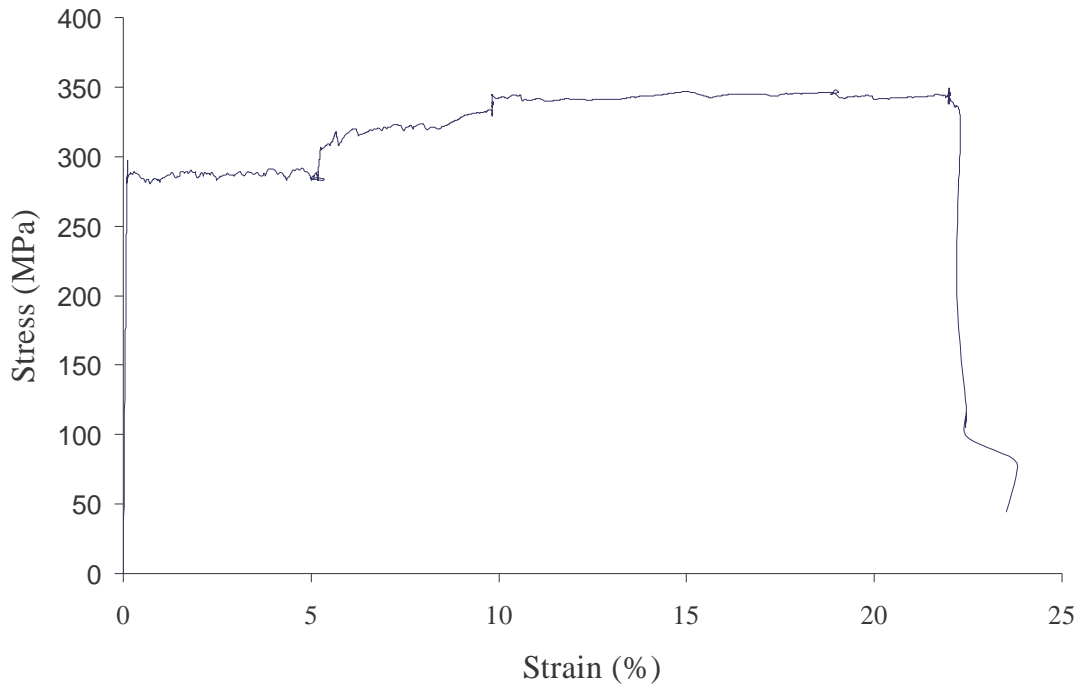
0.6 mm-G250 at 20$^{\mathrm{o}}$C
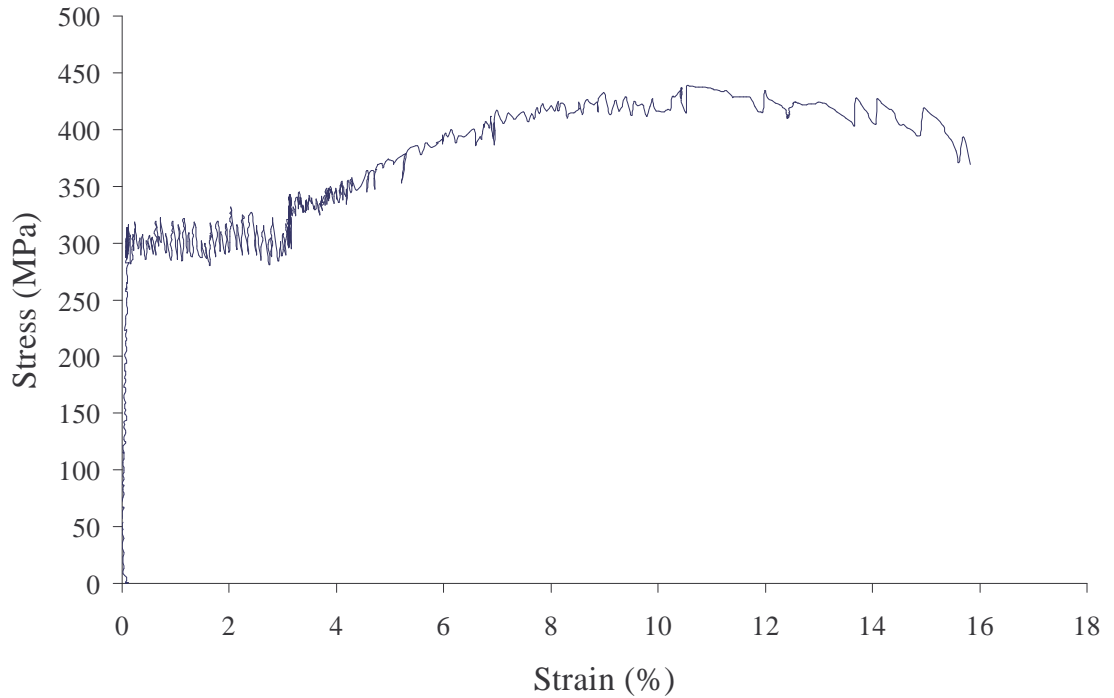
0.6 mm-G250 at 100°C

0.6 mm-G250 at 200°C
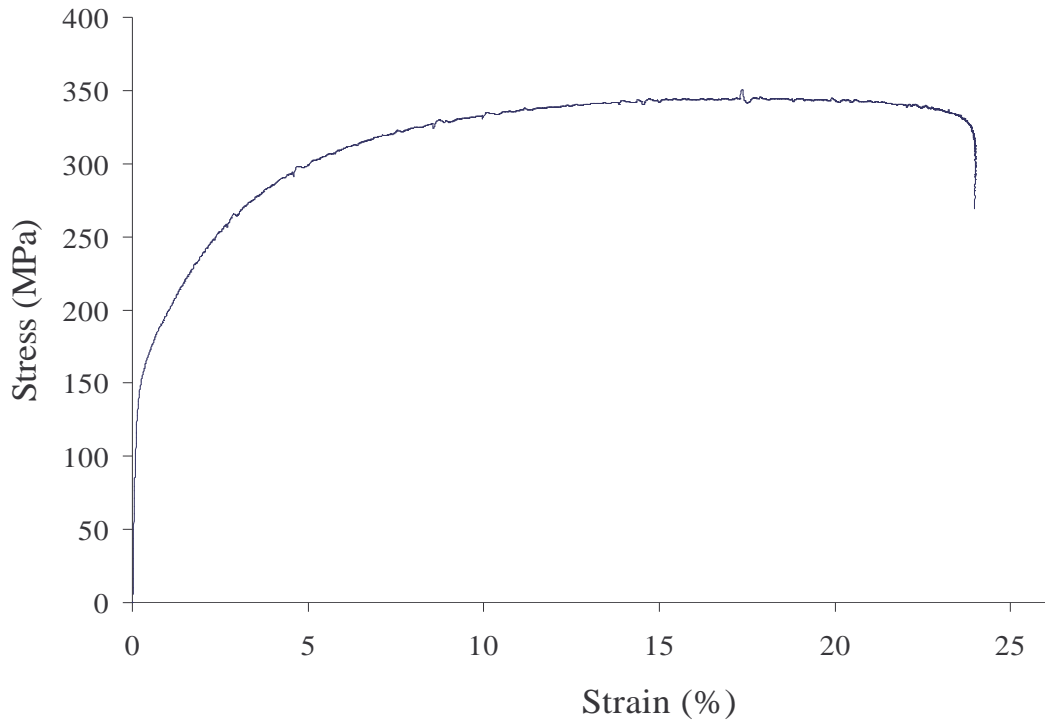
0.6 mm-G250 at 350°C
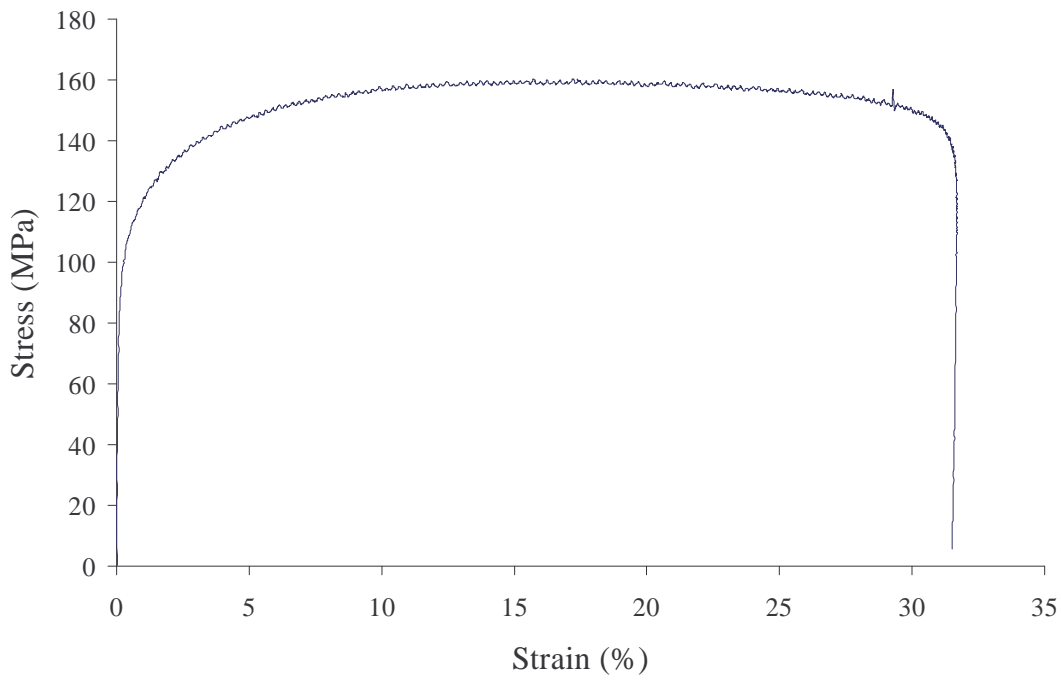
0.6 mm-G250 at 500°C
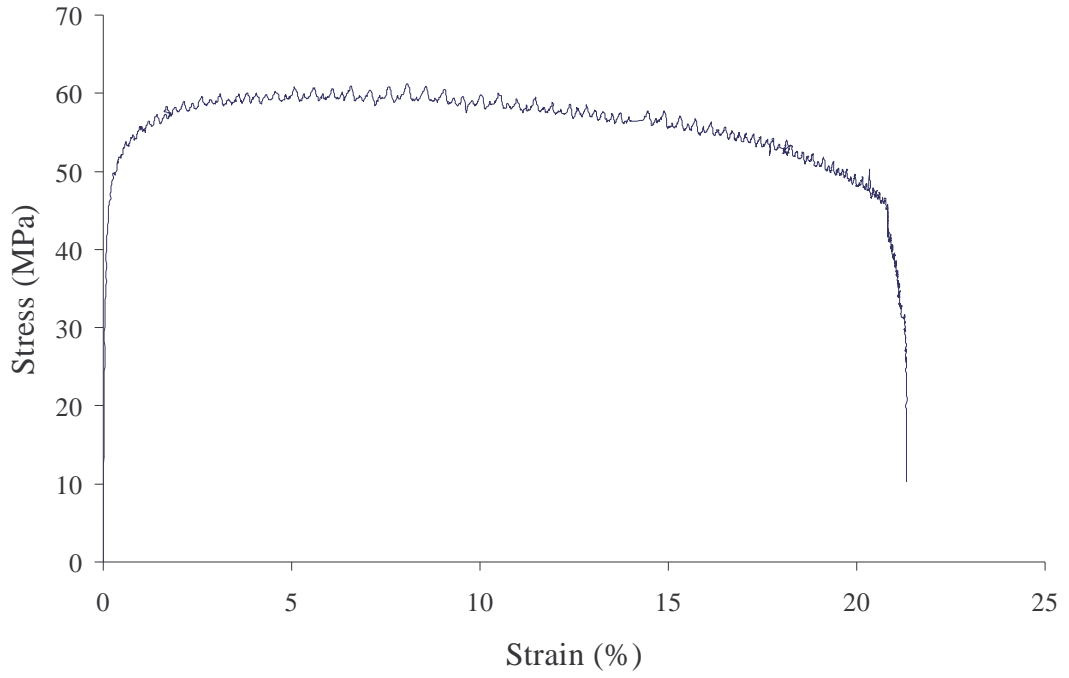
0.6 mm-G250 at 650°C
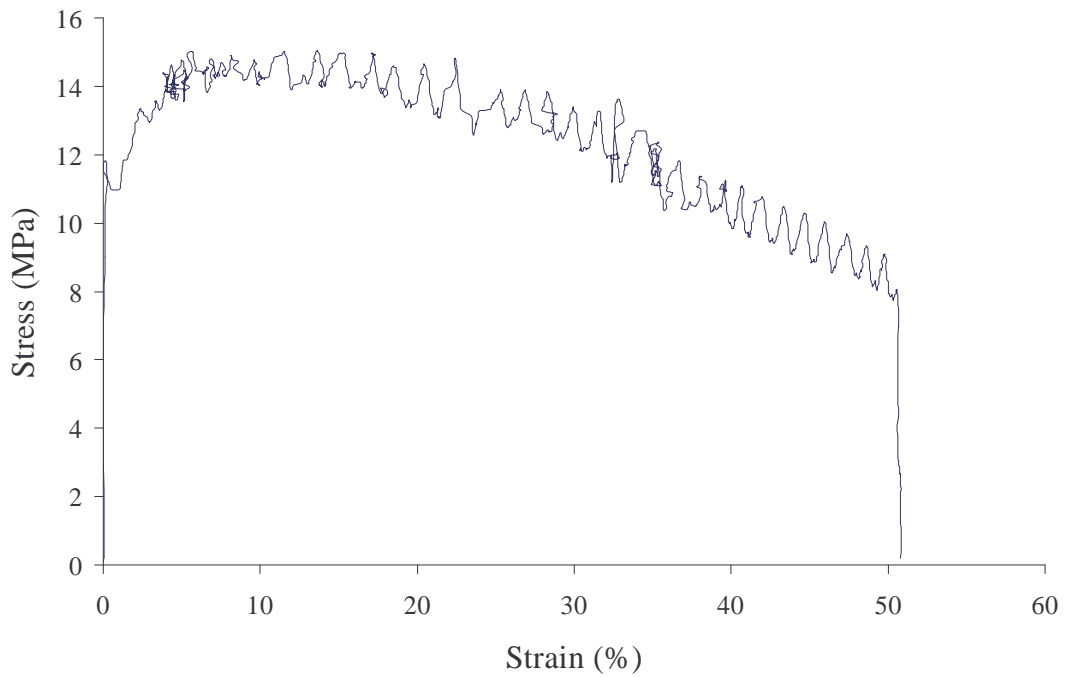
0.6 mm-G250 at 800°C
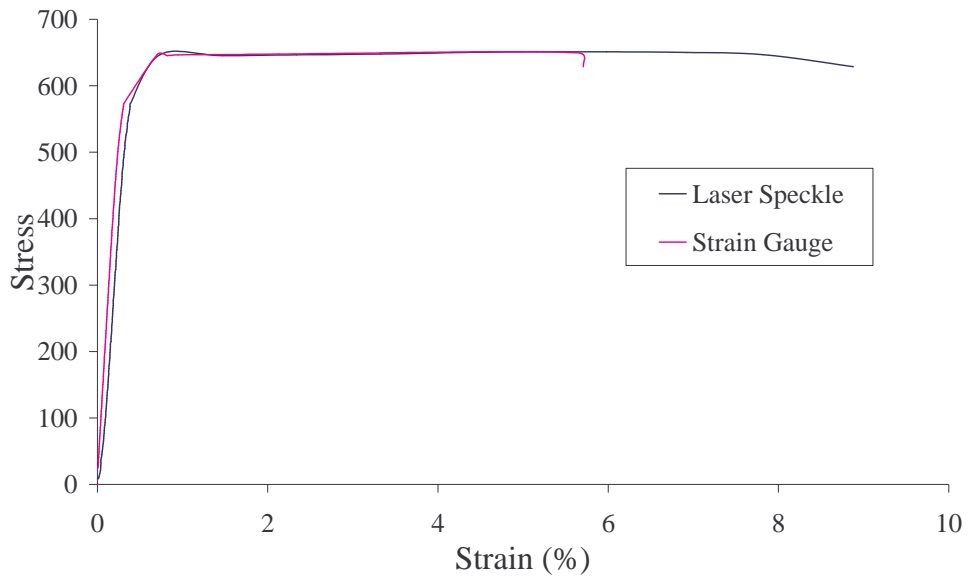
0.8 mm-G550 at 20°C
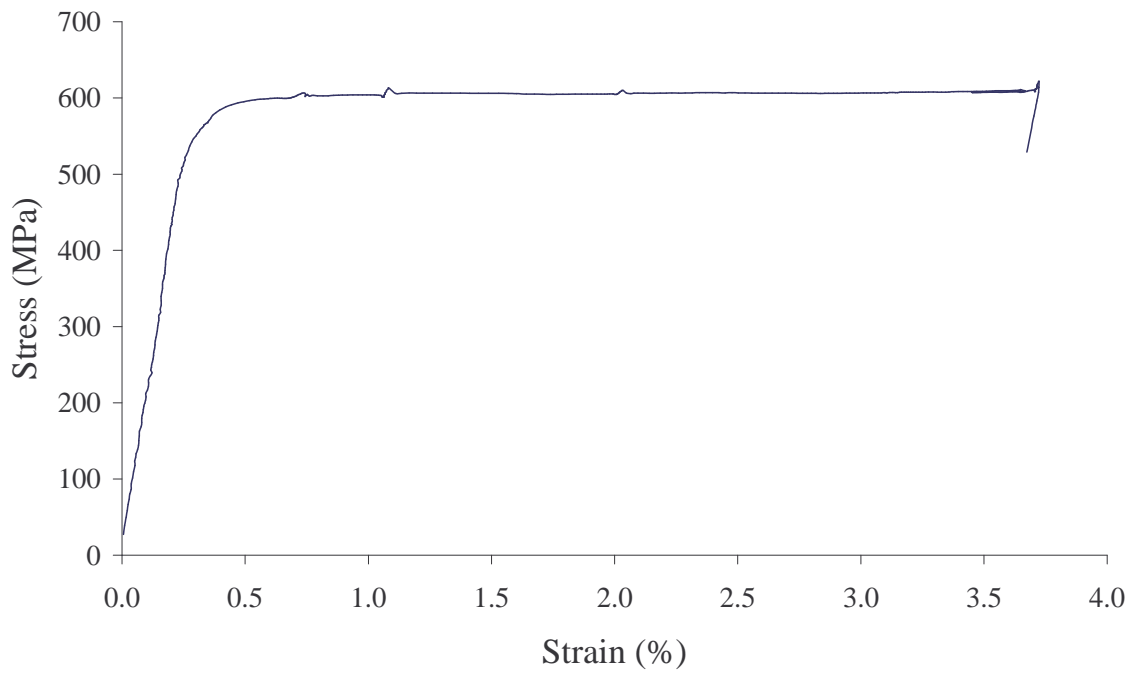
0.8 mm-G550 at 100°C
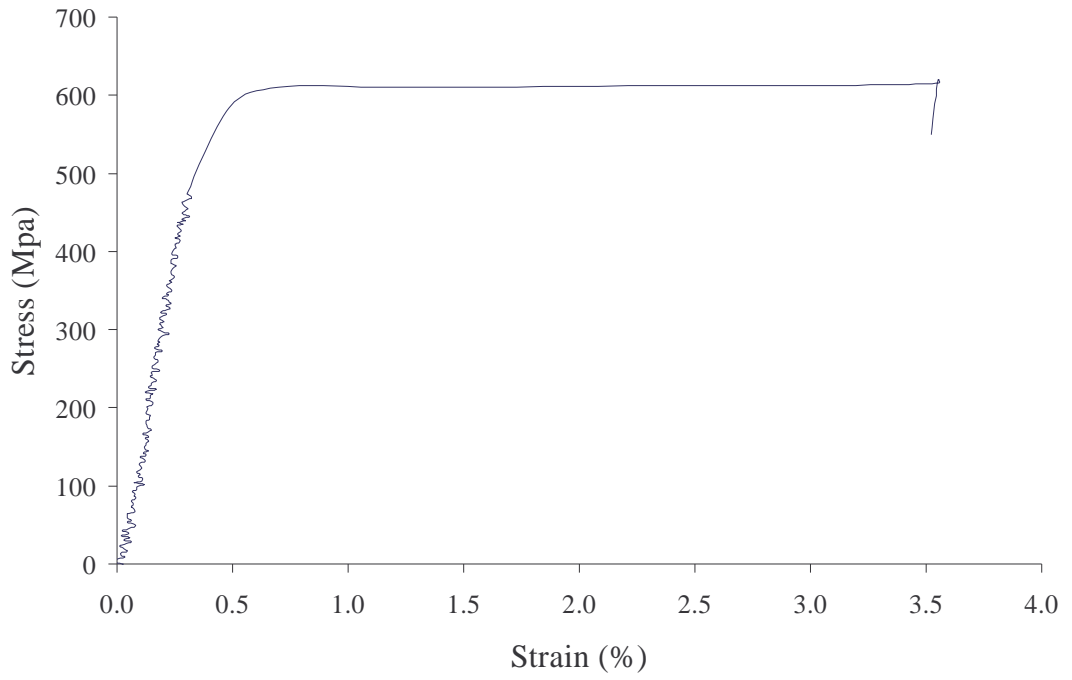
0.8 mm-G550 at 200⁰C
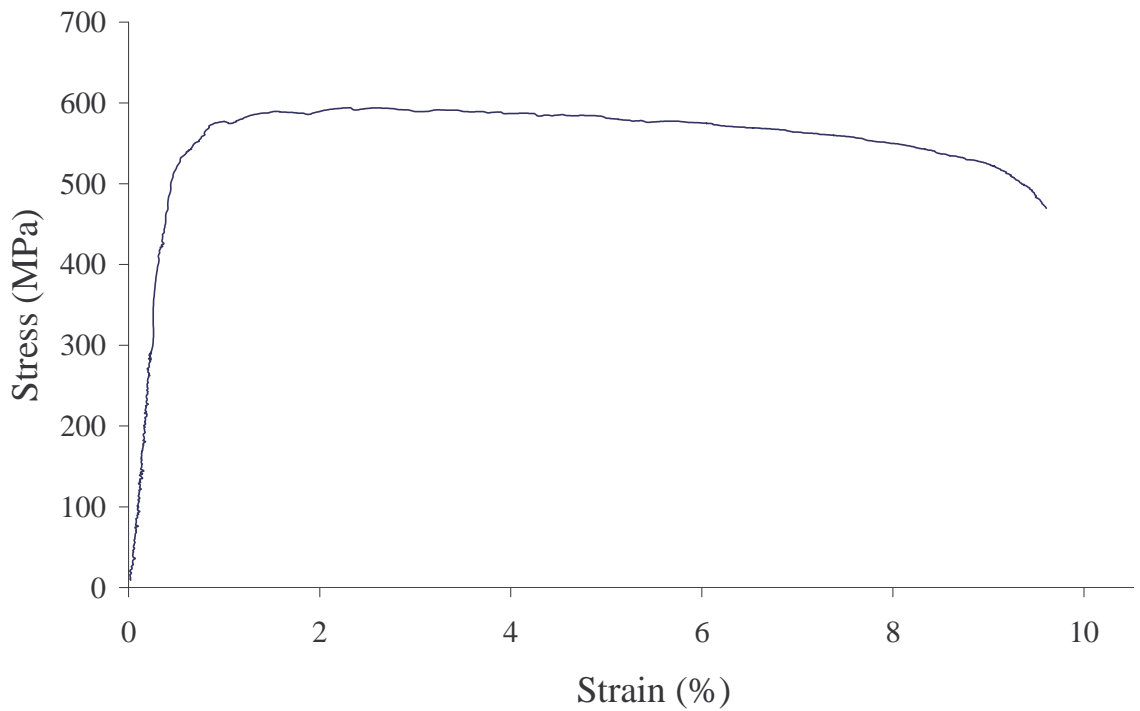
0.8 mm-G550 at 350⁰C
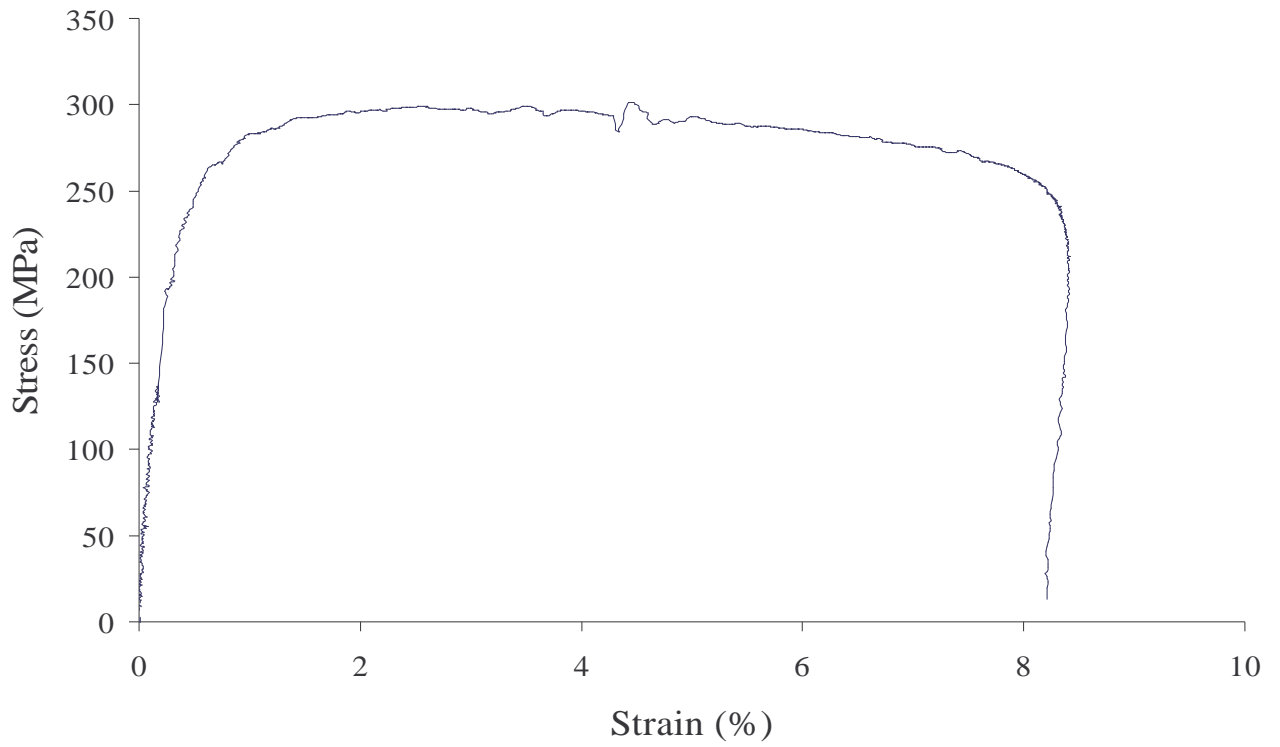
0.8 mm-G550 at 500°C
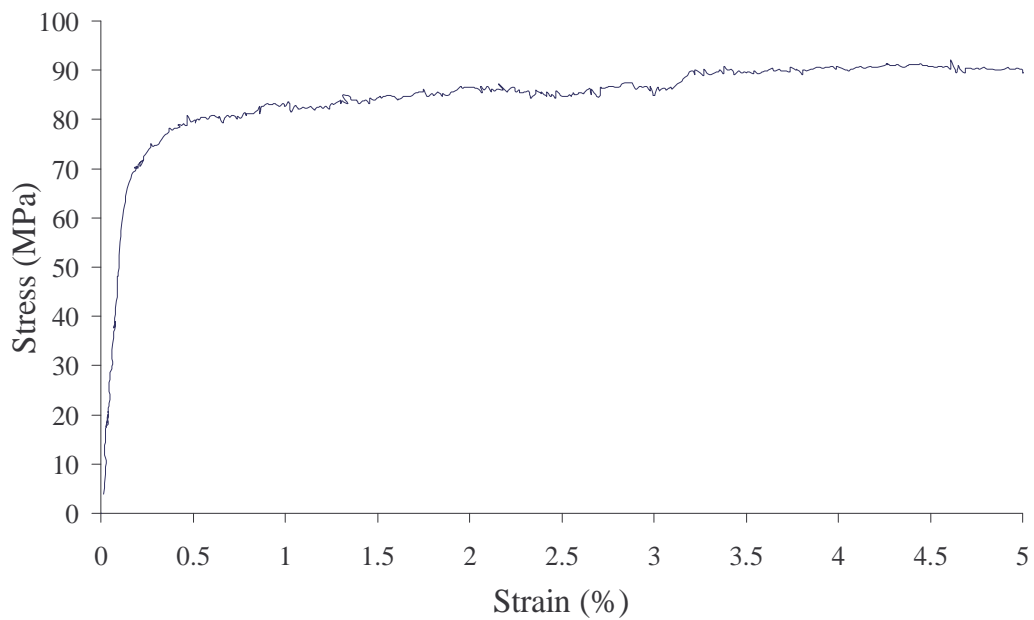
0.8 mm-G550 at 600°C
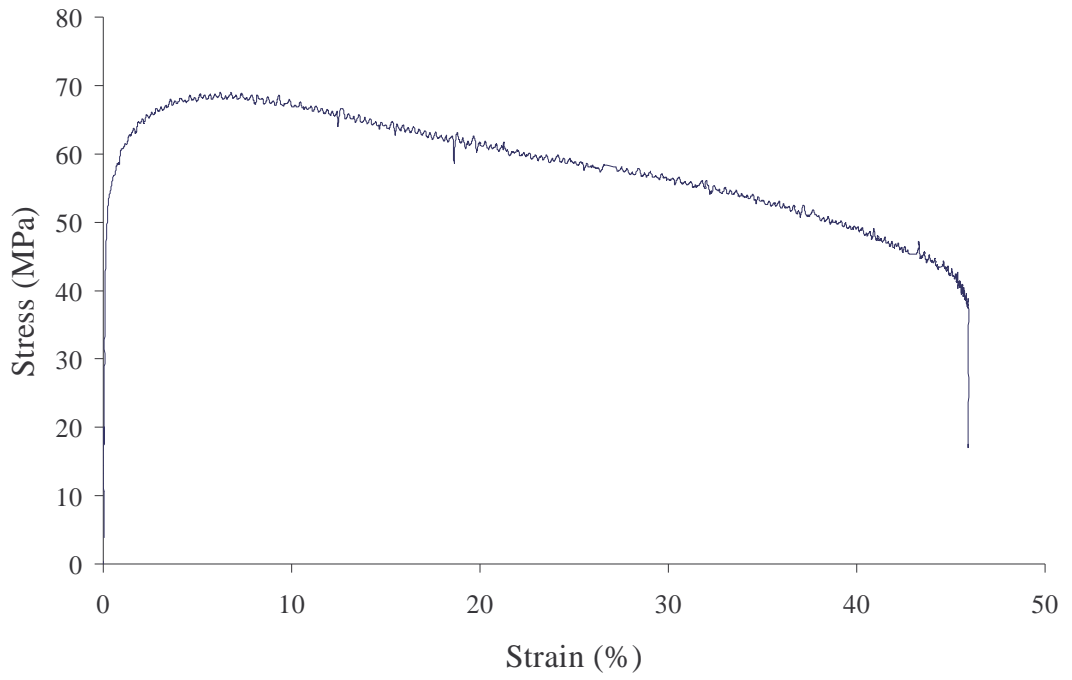
0.8 mm-G550 at 650ºC
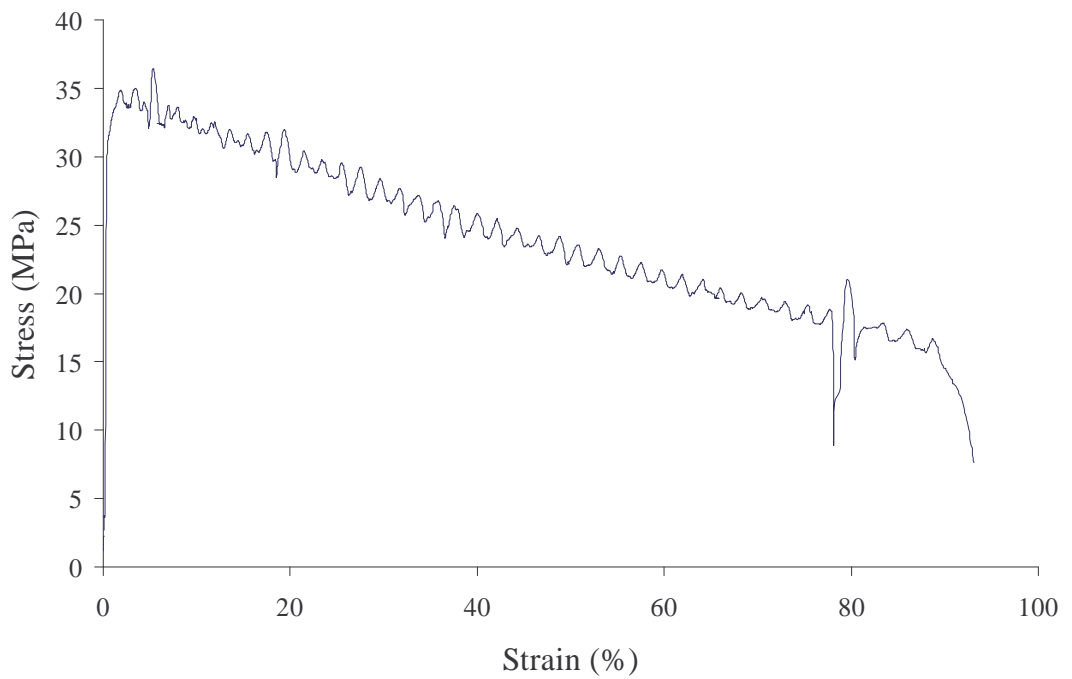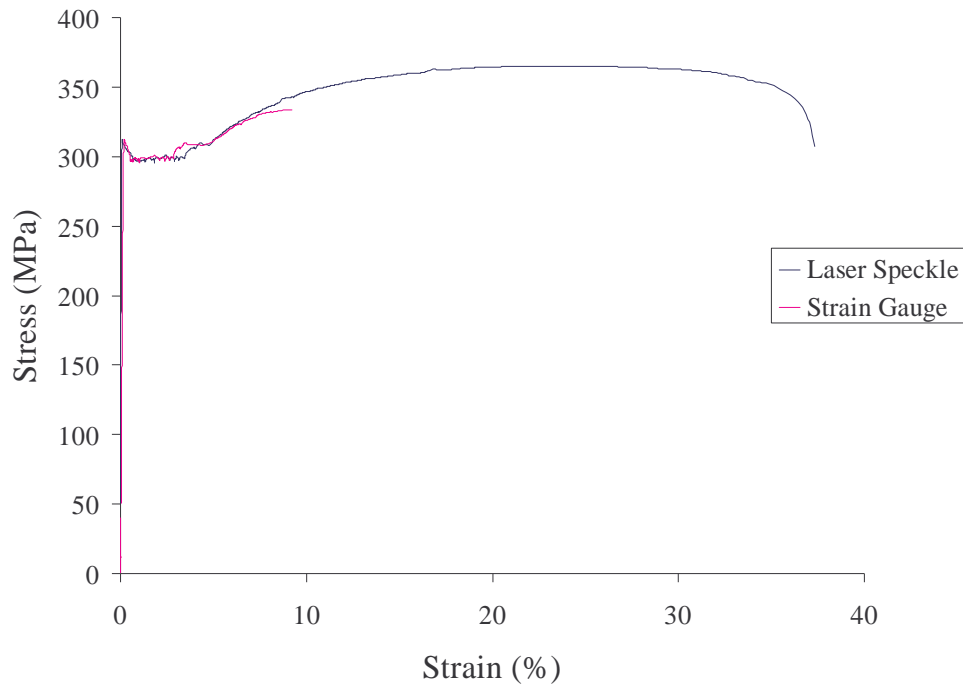
0.8 mm-G550 at 800ºC
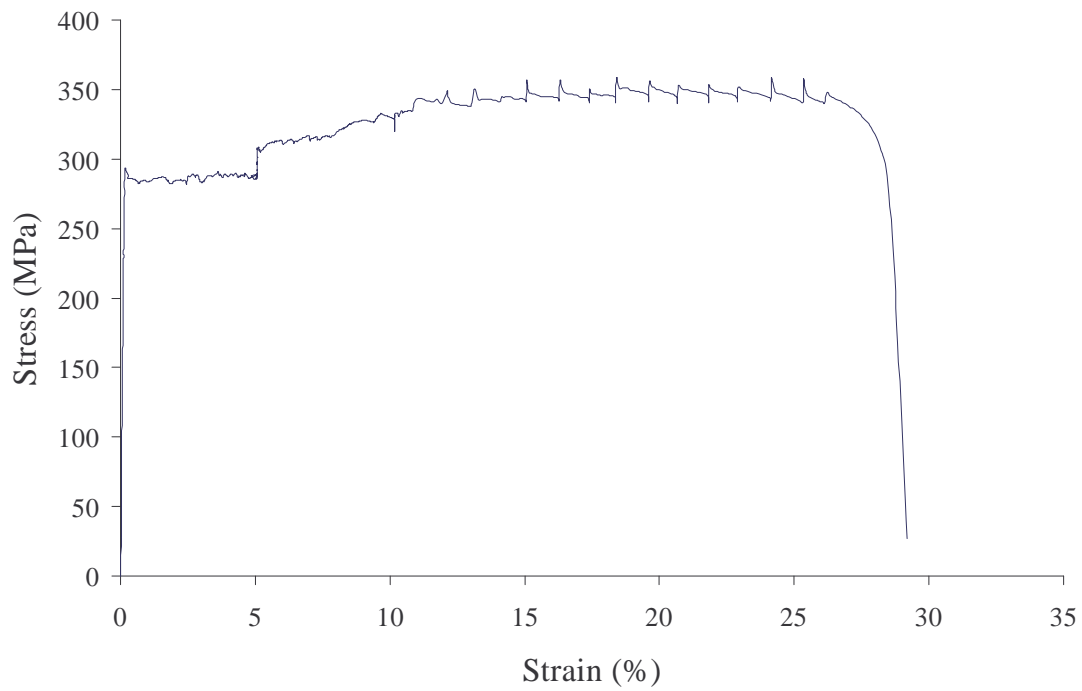
0.8 mm-G250 at 20°C

0.8 mm-G250 at 100°C
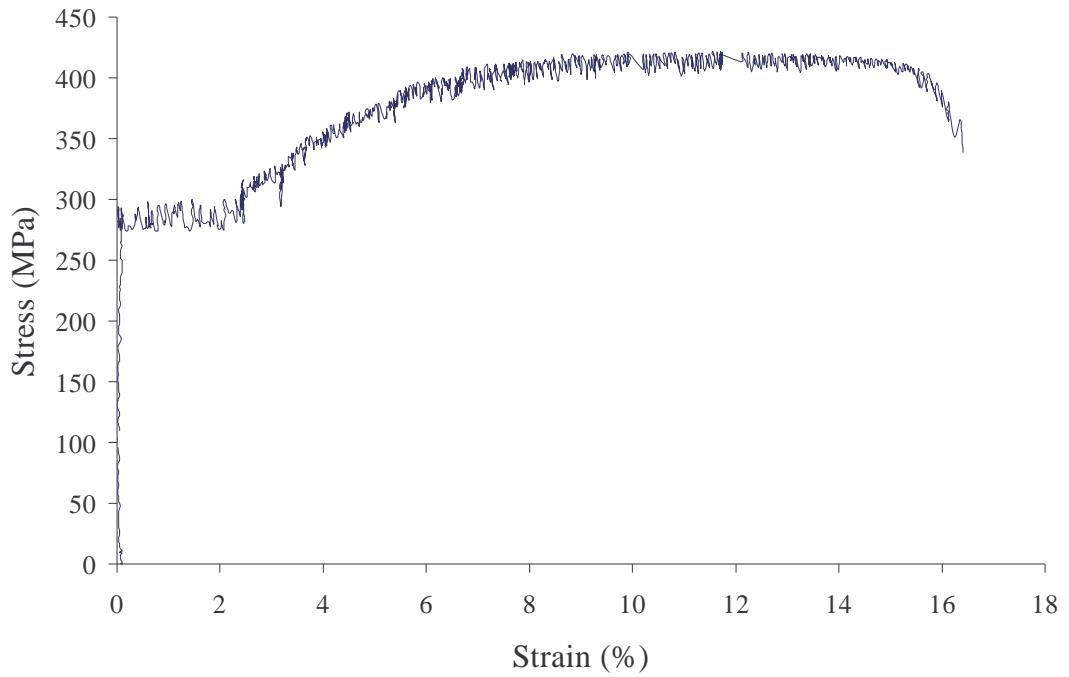
0.8 mm-G250 at 200°C
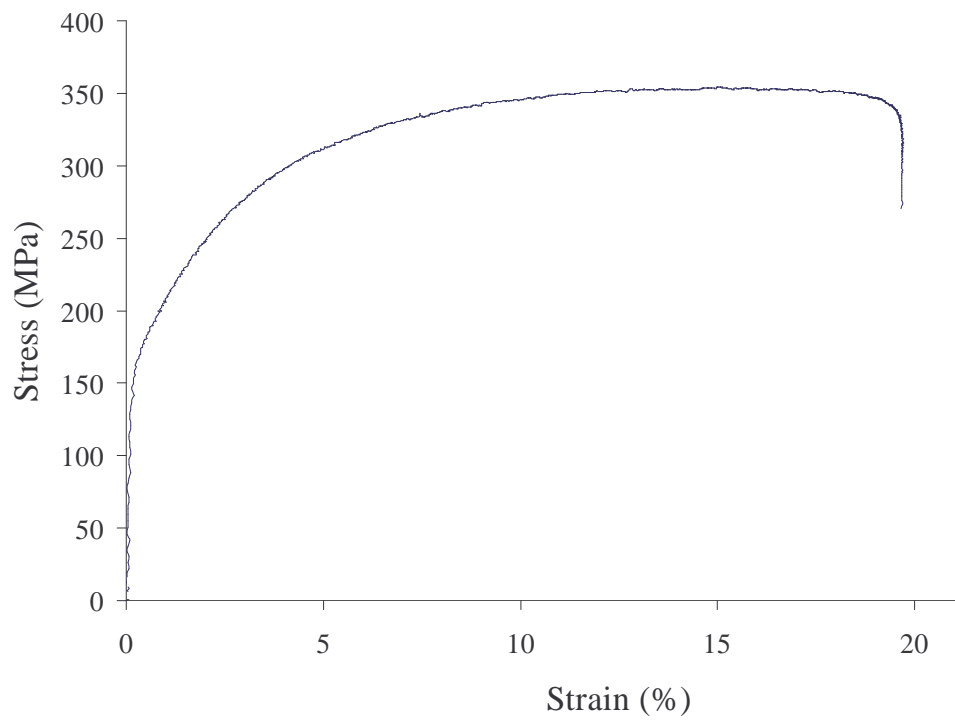
0.8 mm-G250 at 350°C
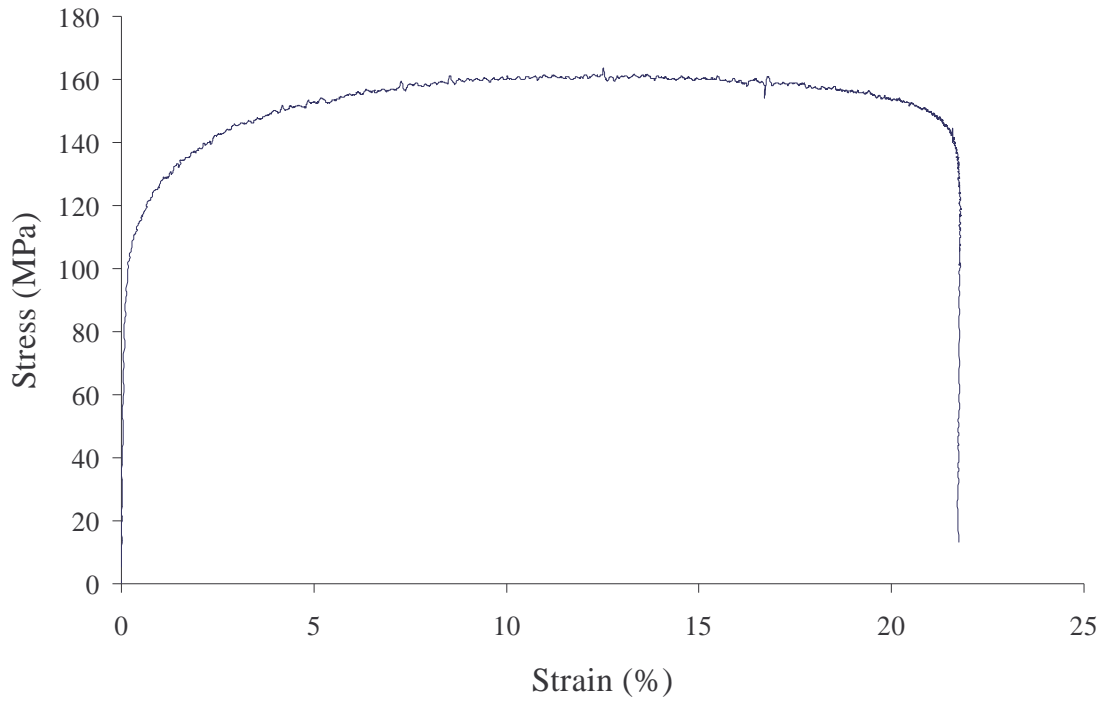
0.8 mm-G250 at 500ºC
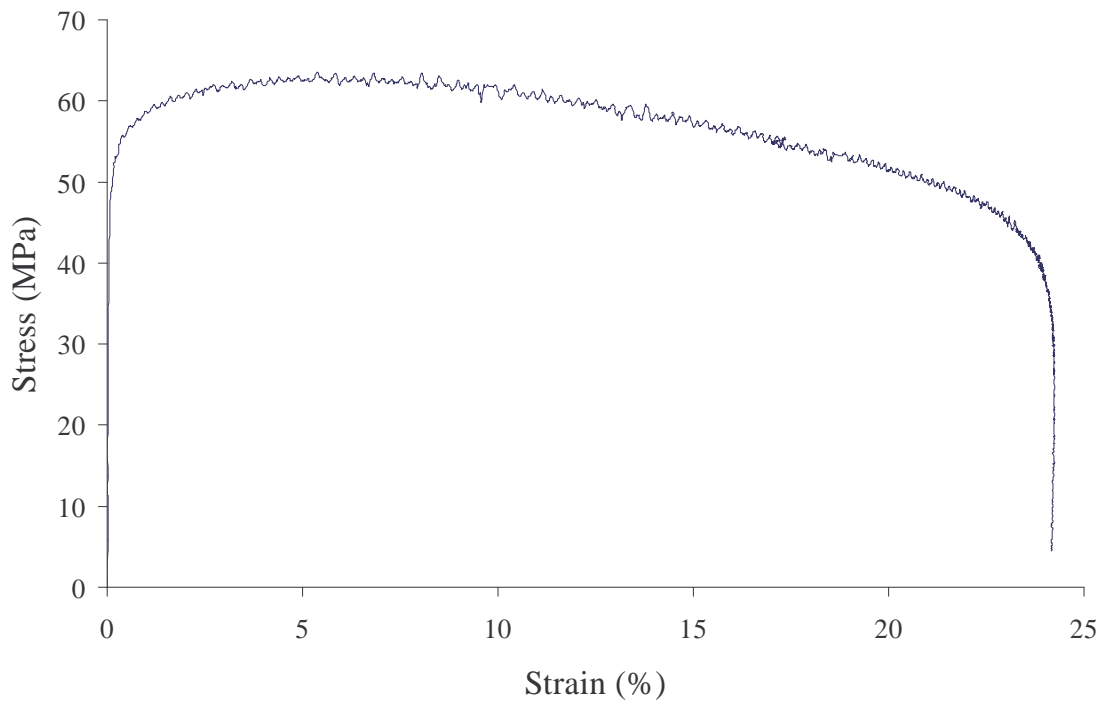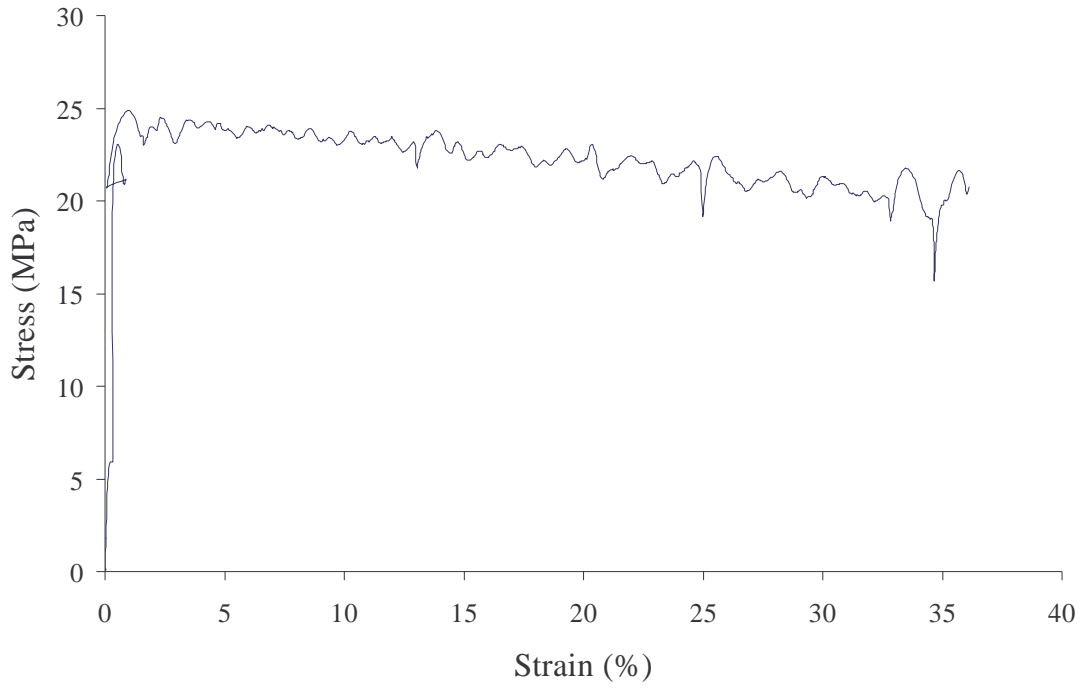
0.8 mm-G250 at 650ºC
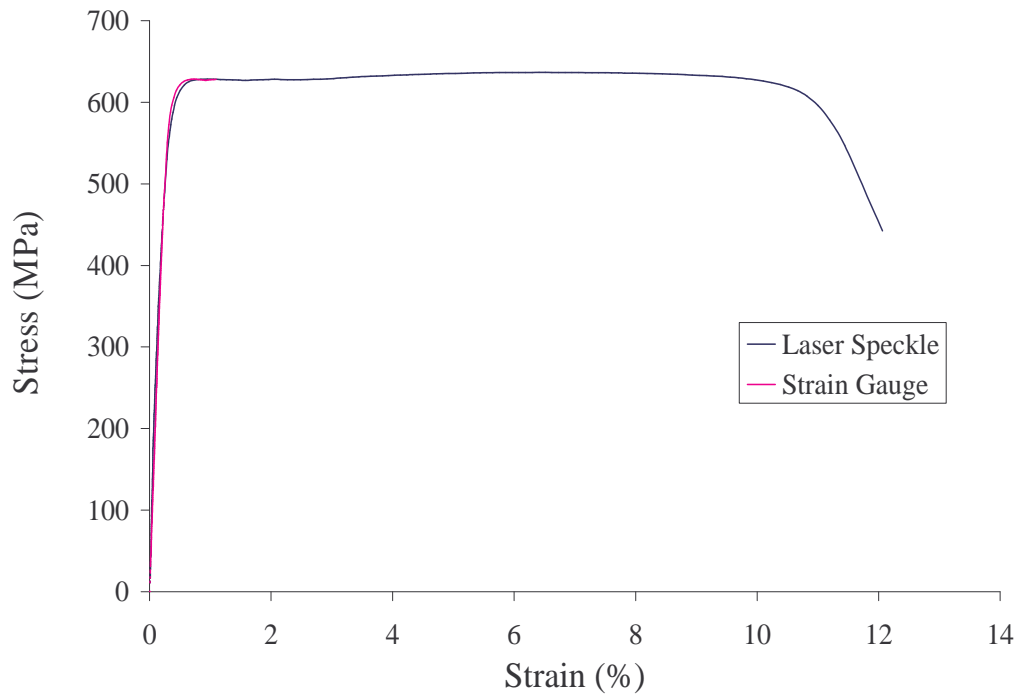
0.8 mm-G250 at 800°C

0.95 mm-G550 at 20°C
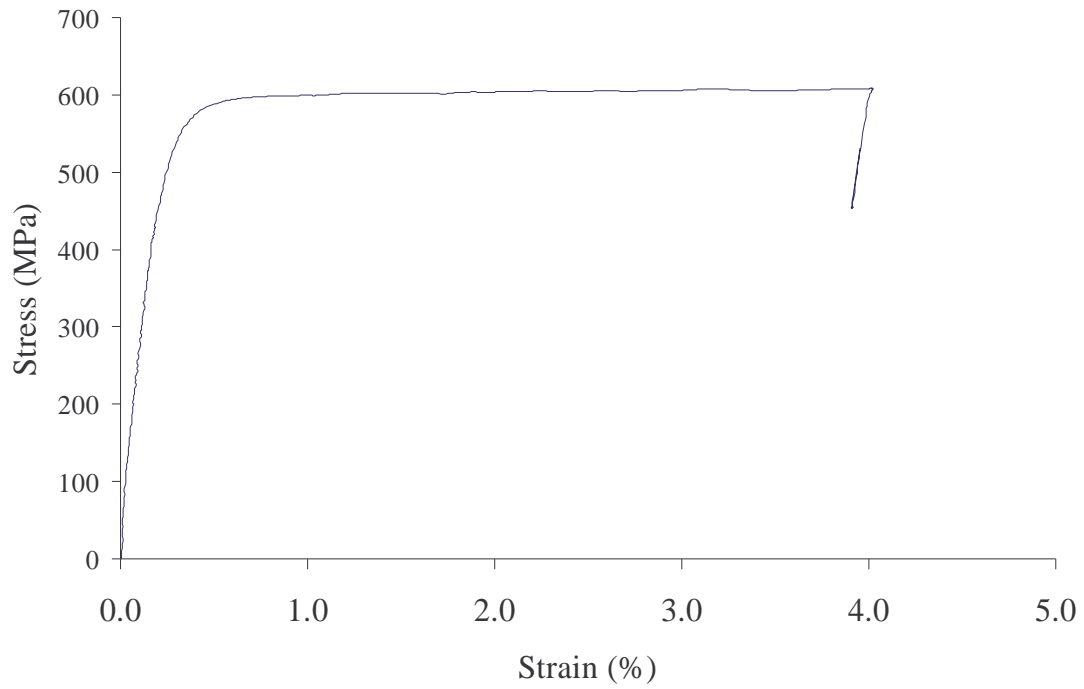
0.95 mm-G550 at 100°C
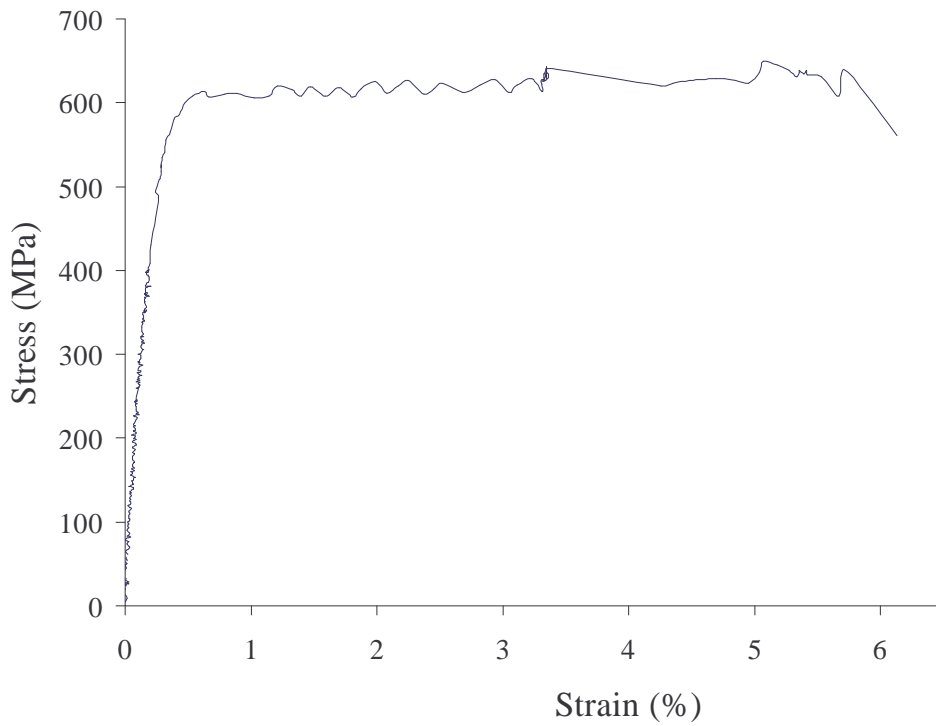
0.95 mm-G550 at 200°C
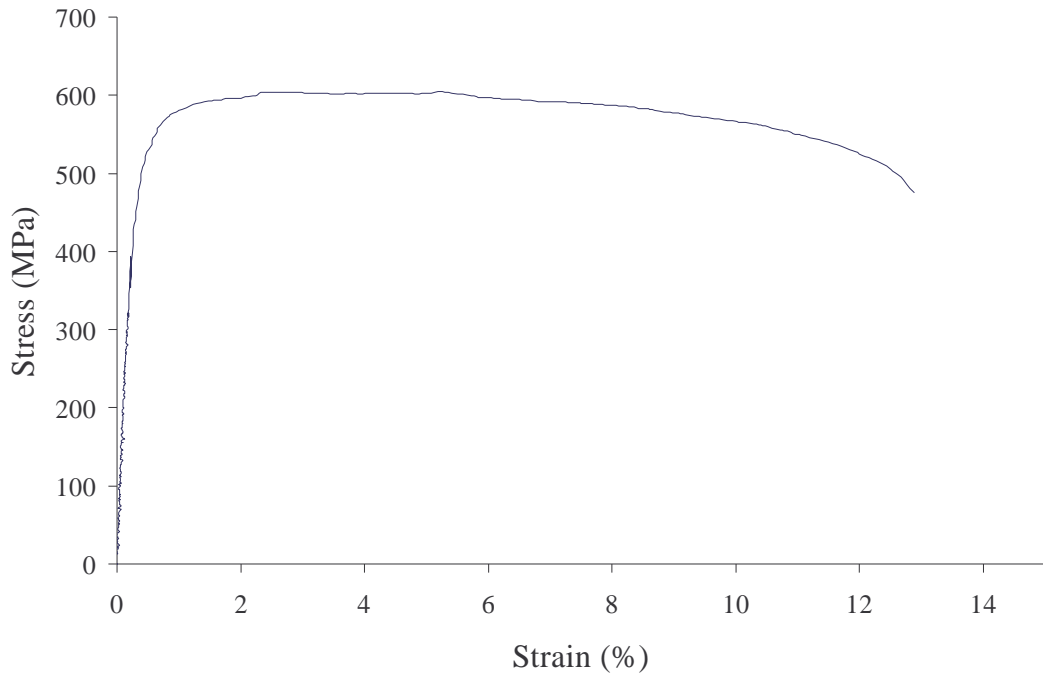
0.95 mm-G550 at 350ºC
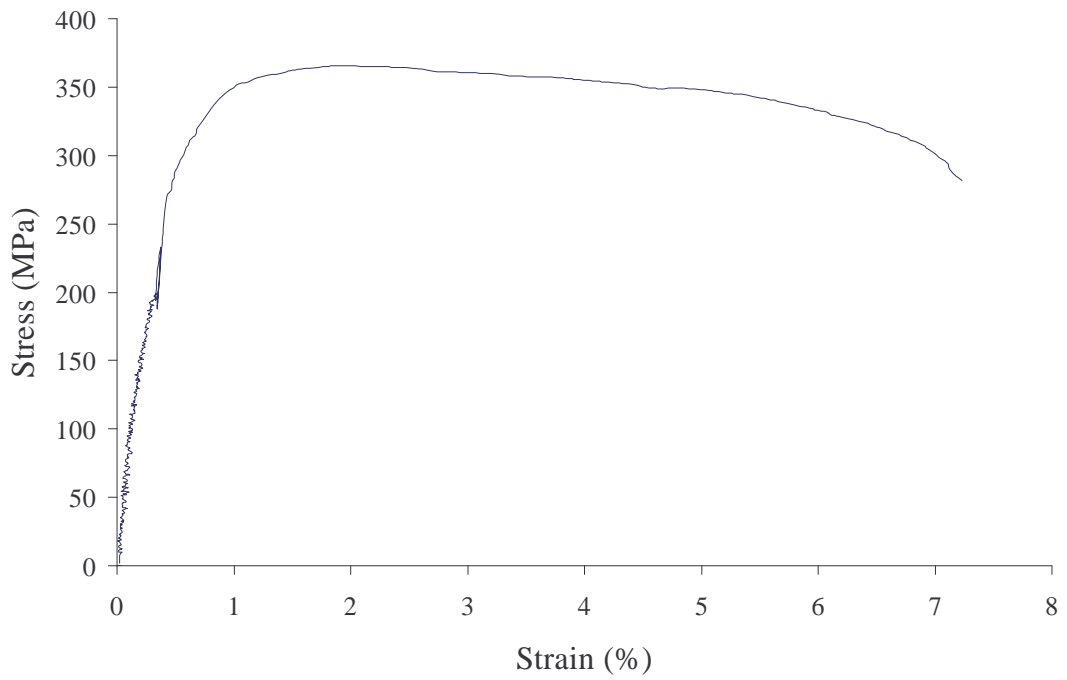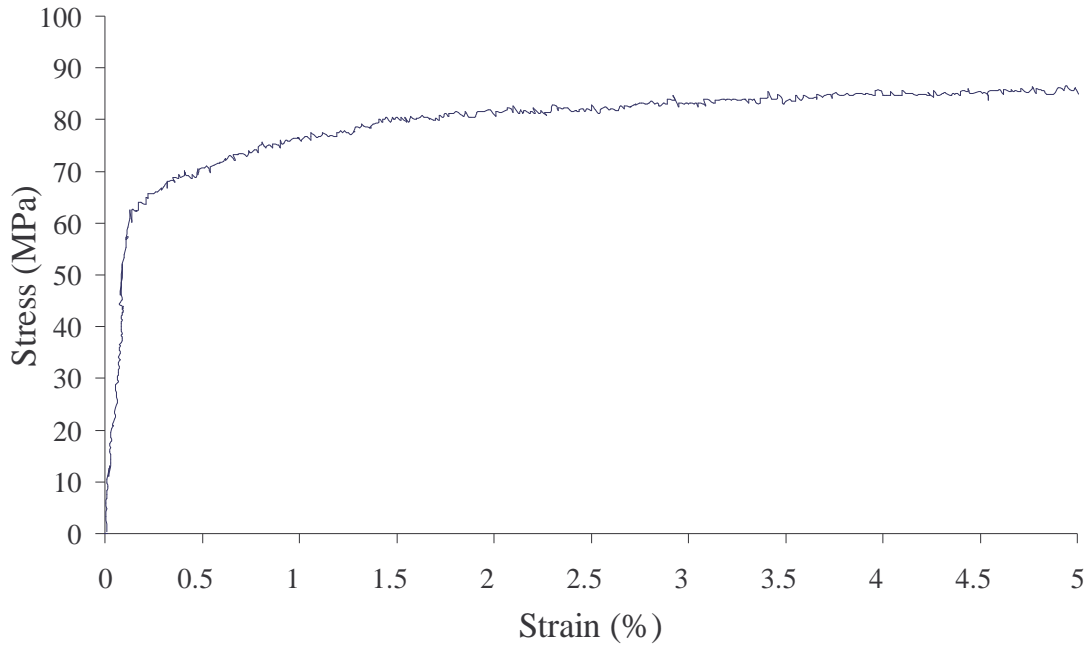
0.95 mm-G550 at 500ºC

0.95 mm-G550 at 600°C
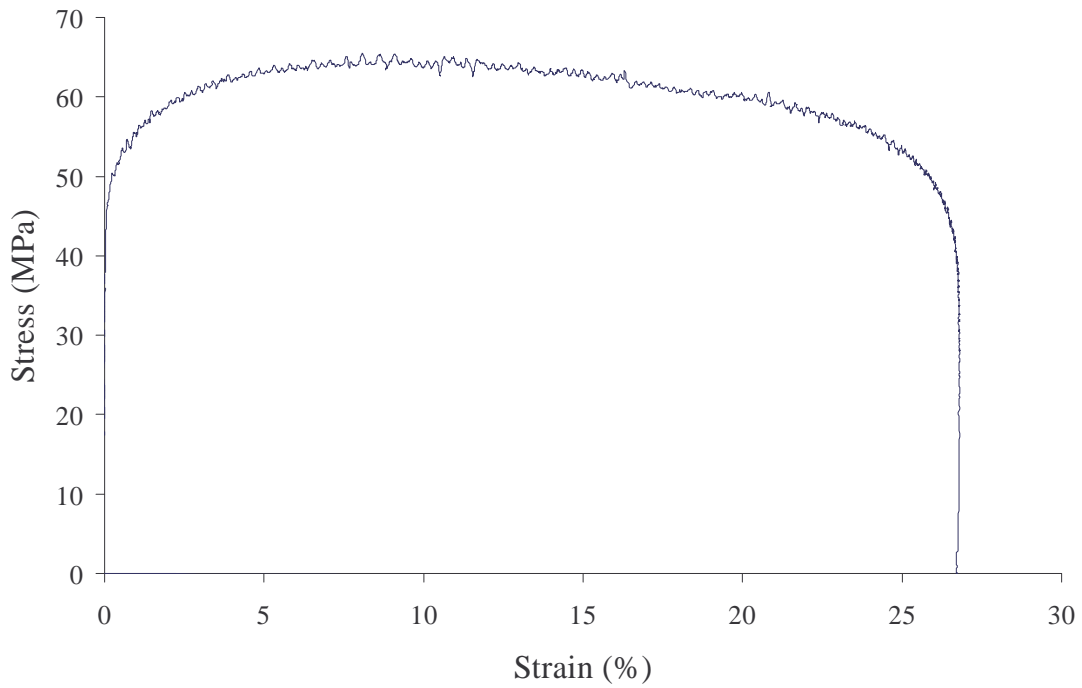
0.95 mm-G550 at 650°C

0.95 mm-G550 at 800°C

- Laser Speckle
- Strain Gauge
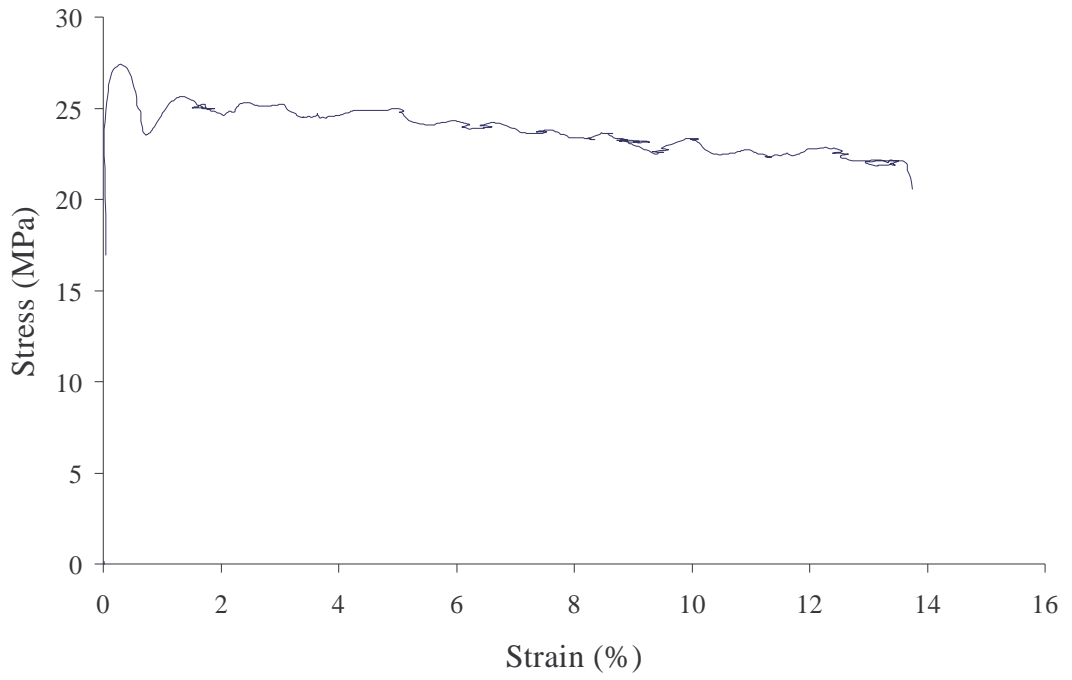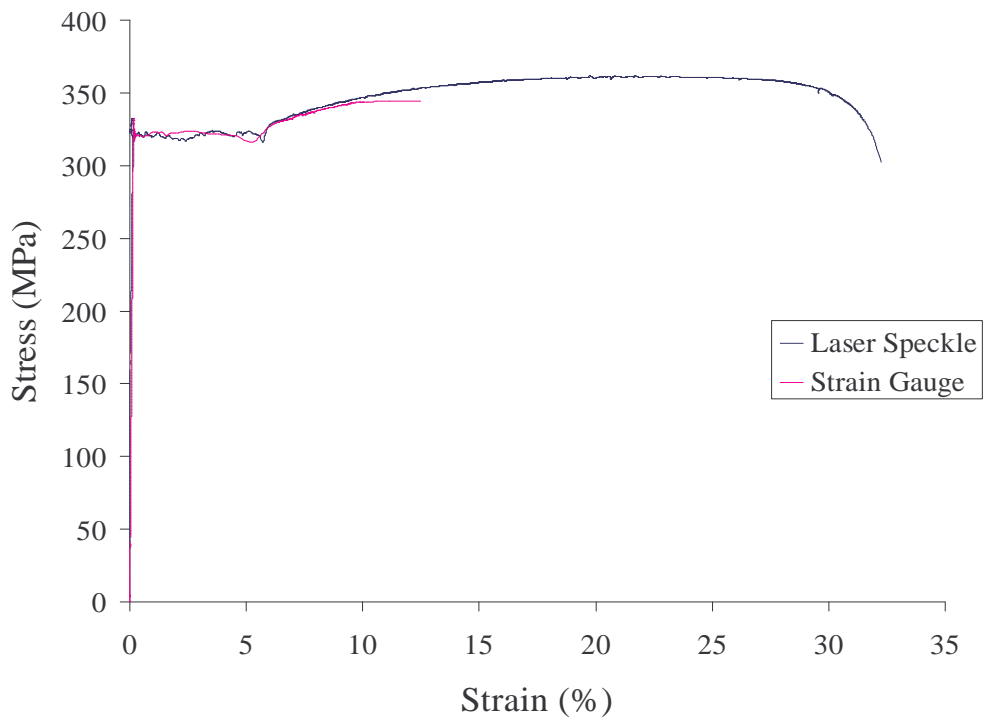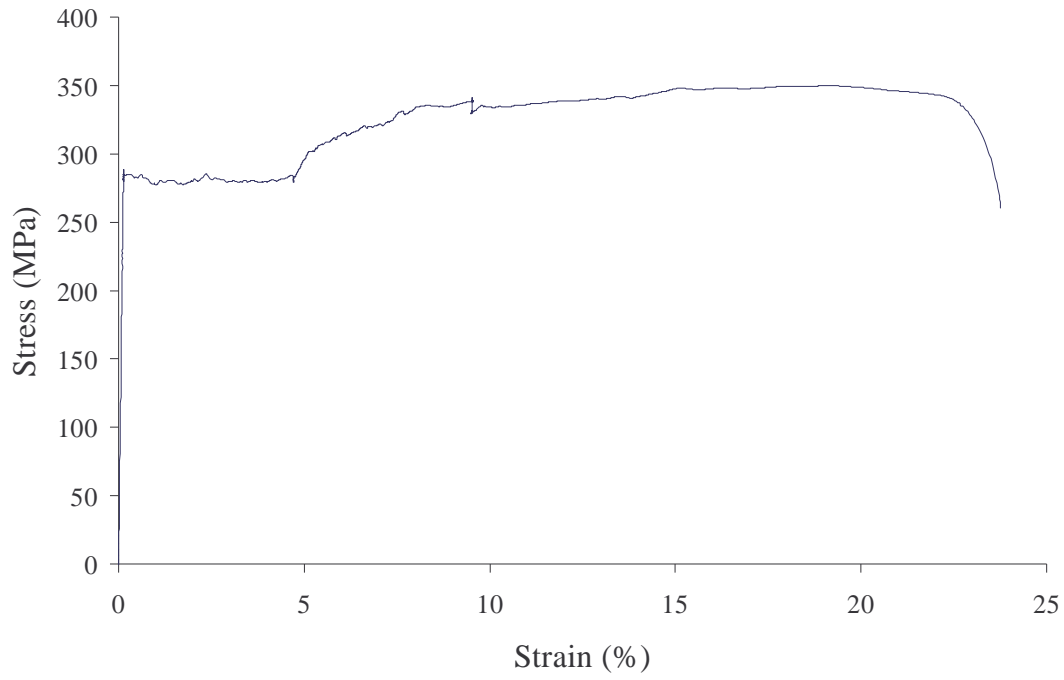
0.95 mm-G250 at 20°C

0.95 mm-G250 at 100°C
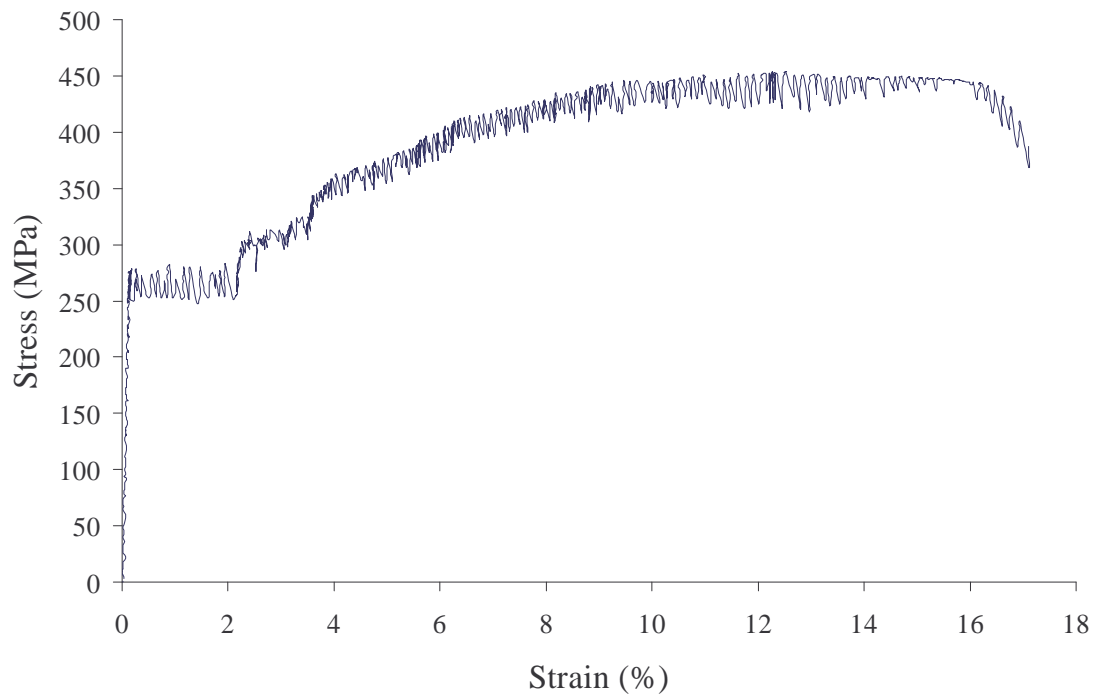
0.95 mm-G250 at 200°C
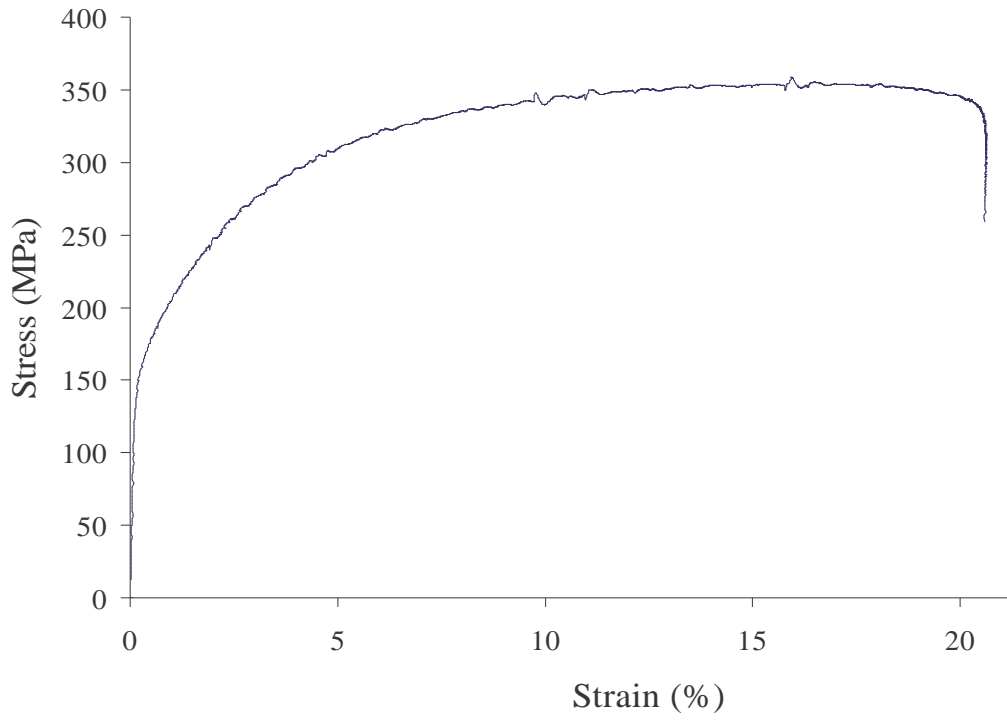
0.95 mm-G250 at 350⁰C
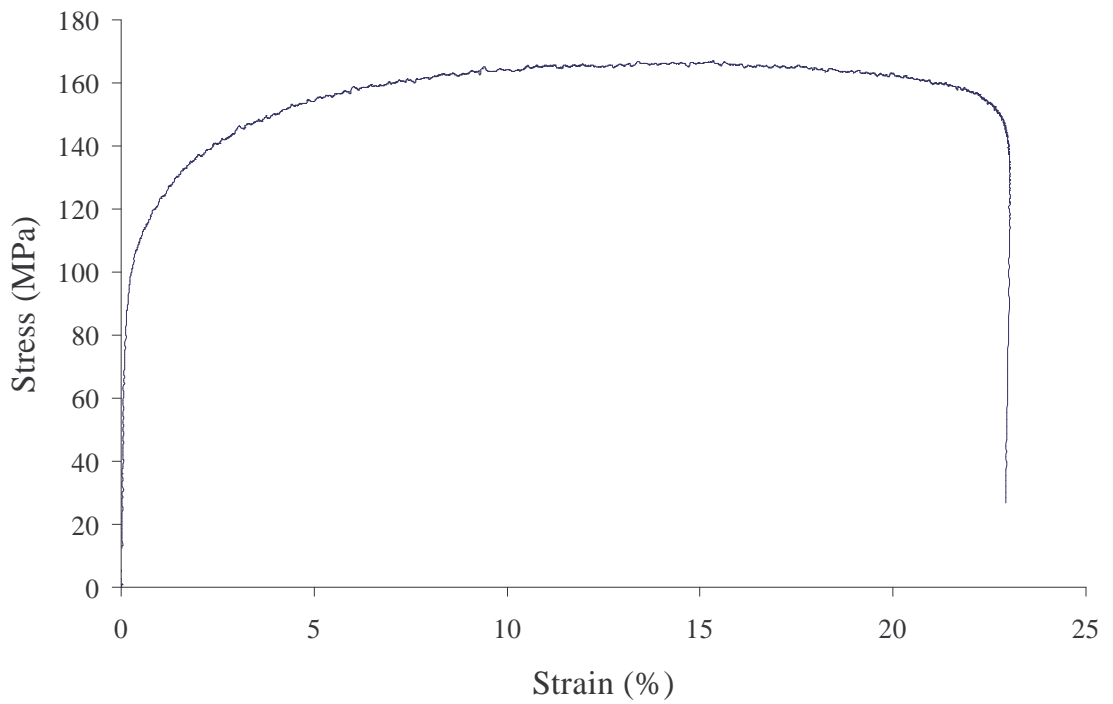
0.95 mm-G250 at 500⁰C
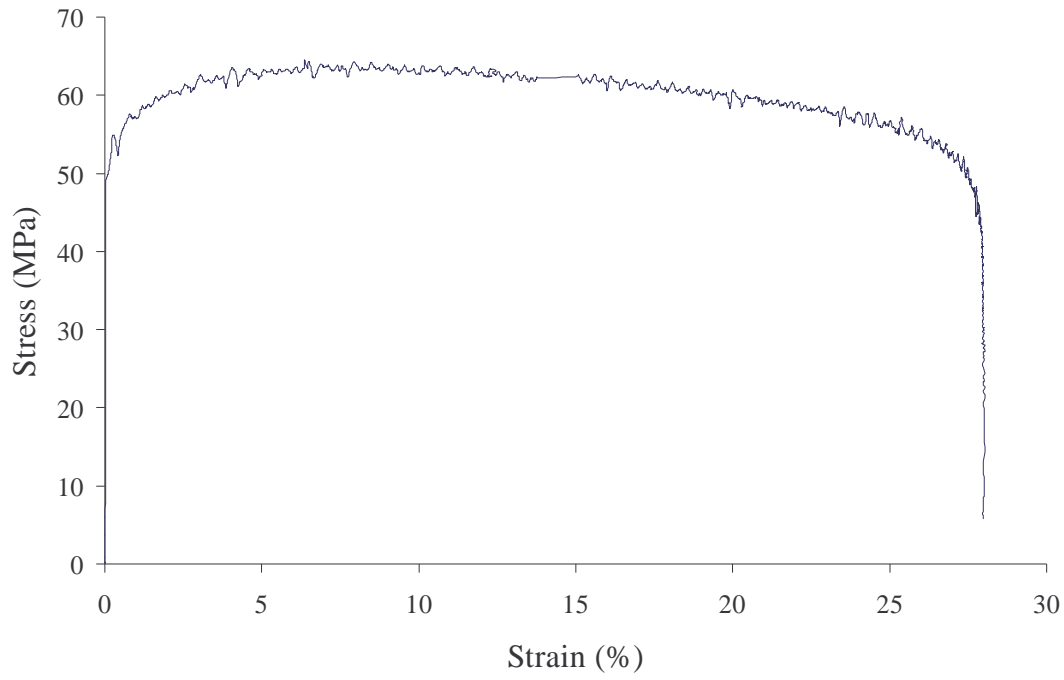
0.95 mm-G250 at 650°C
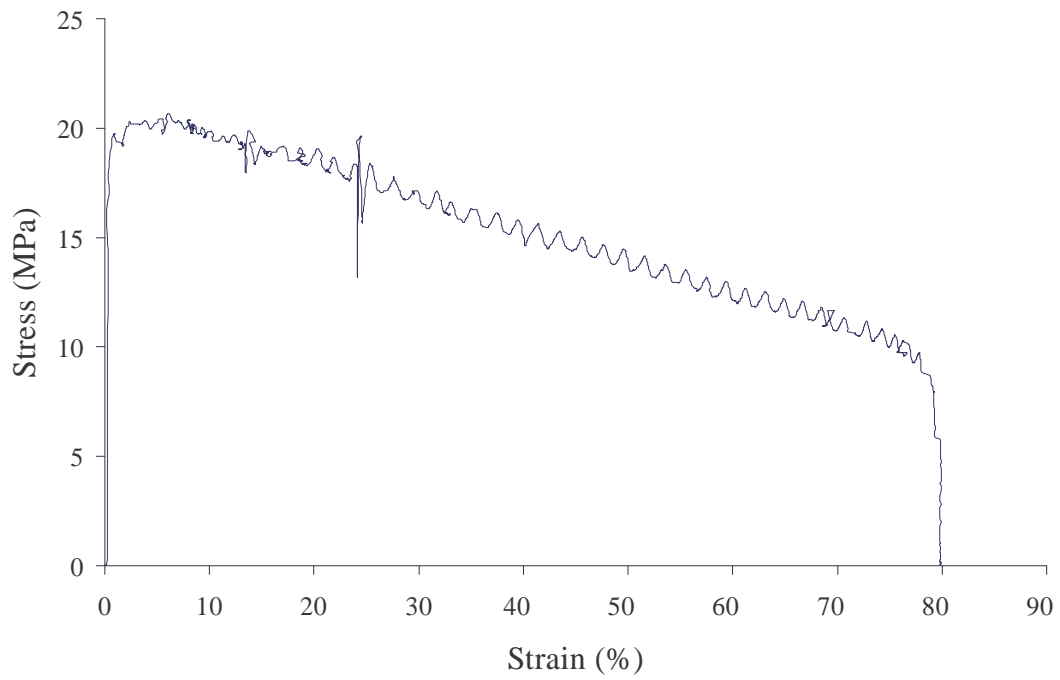
0.95 mm-G250 at 800°C

A4 Typical Failure Modes of Tensile Specimens at Various Temperatures
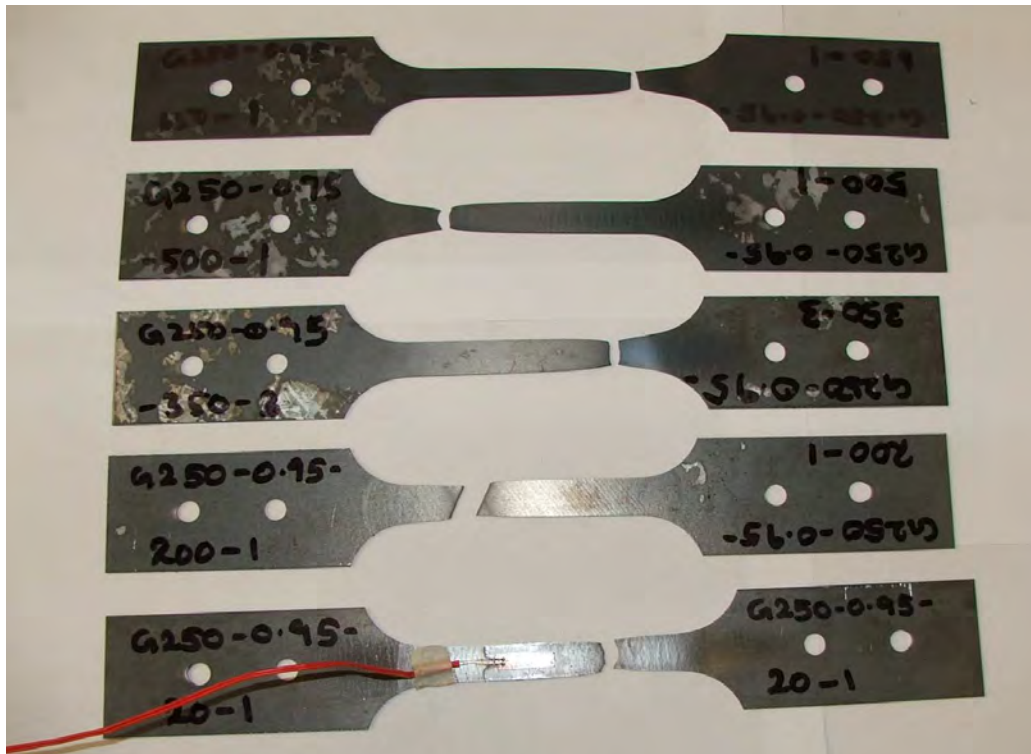
0.95 mm G250 steel
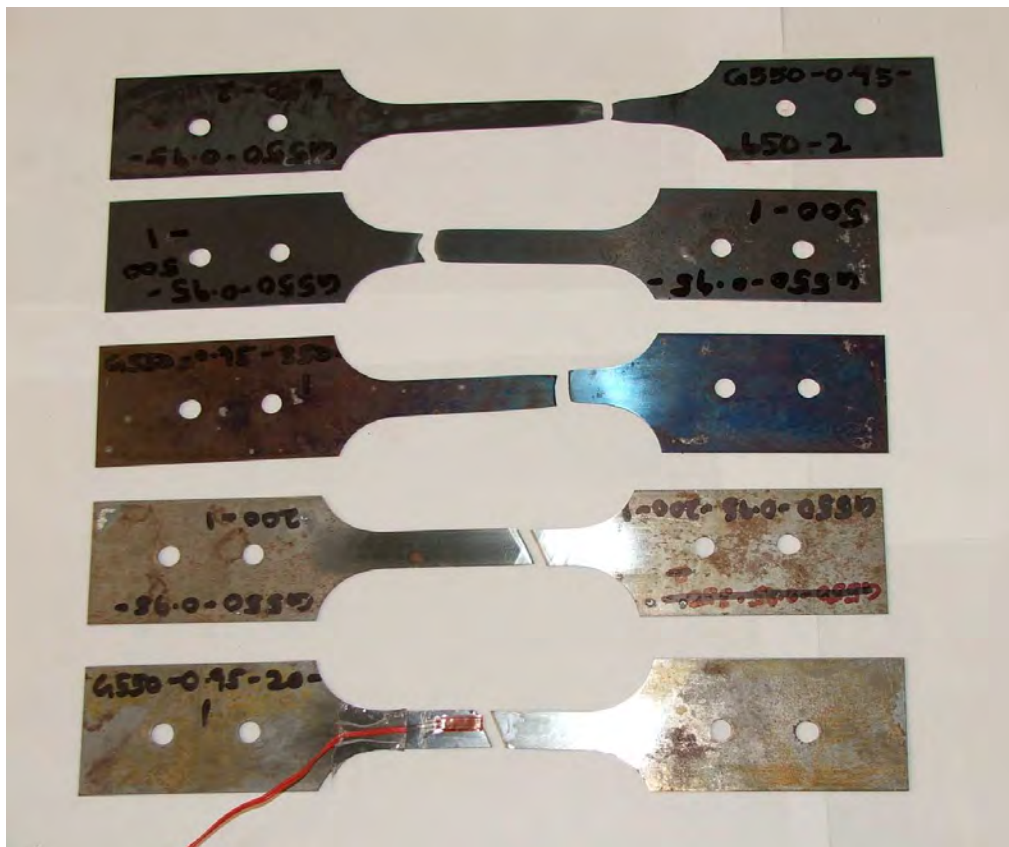
0.95 mm G550 steel
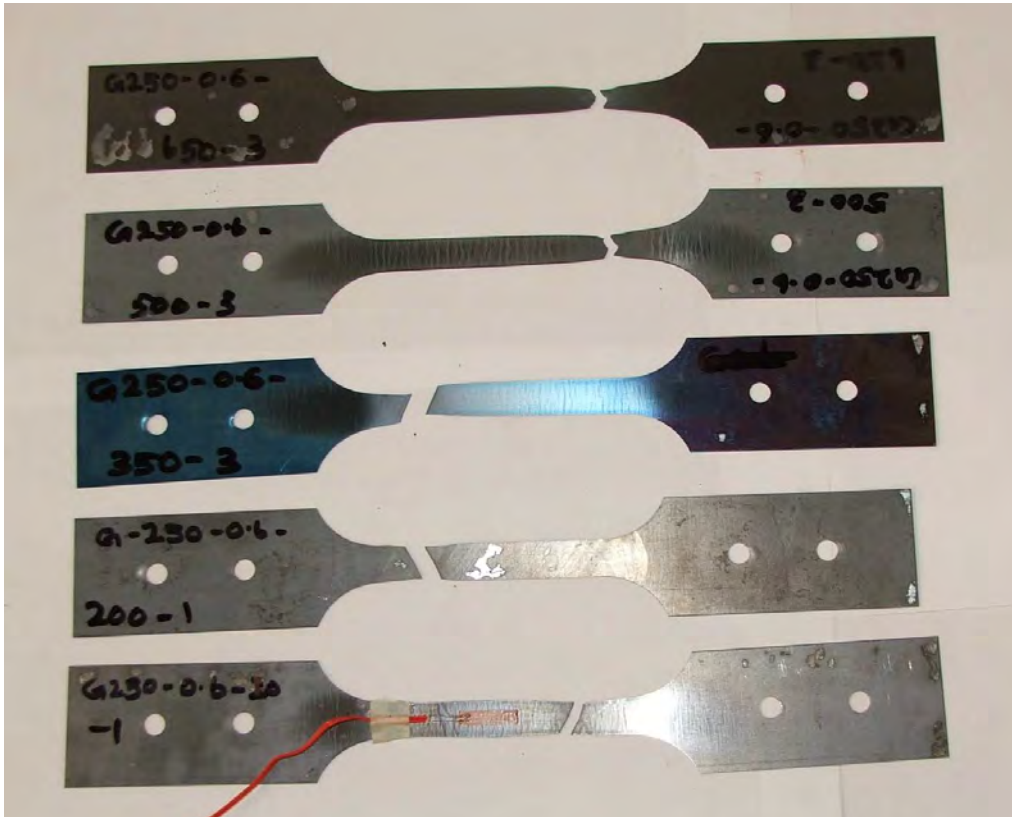
0.6 mm G250 steel
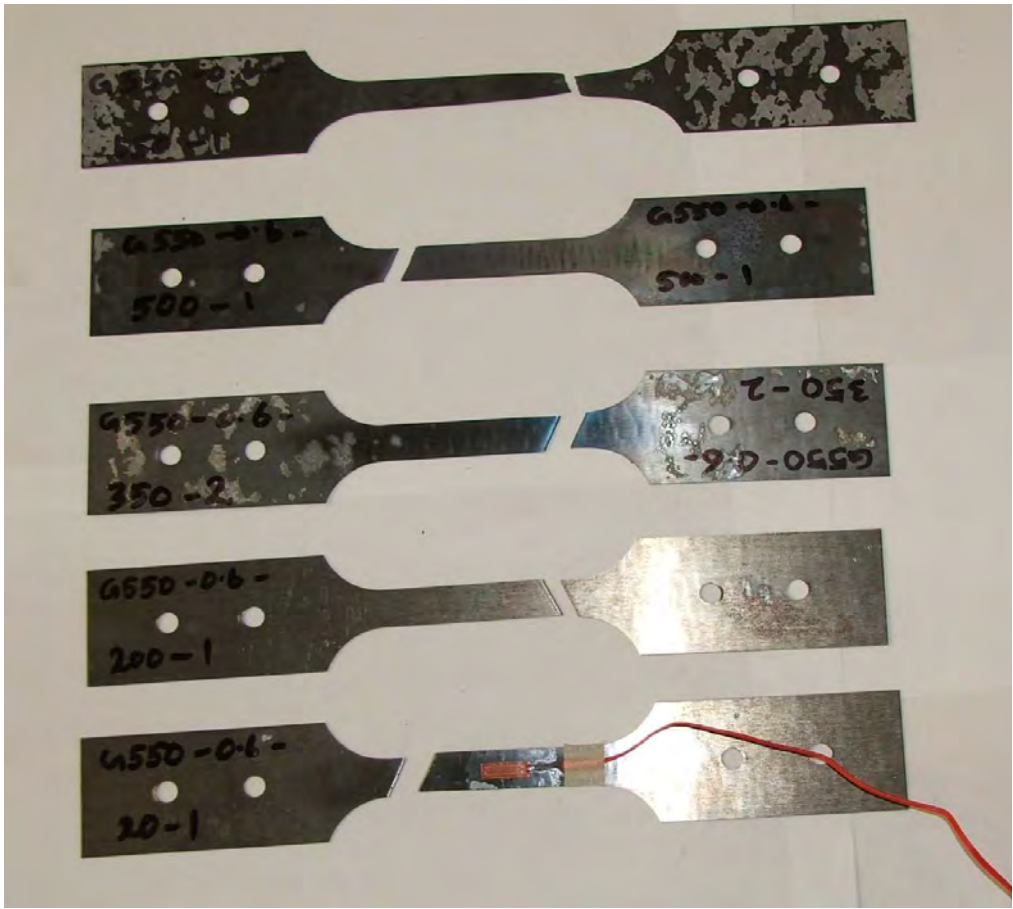
0.6 mm G550 steel

A5 Measured Mechanical Properties and Reduction Factors

Yield Strengths in MPa at Elevated Temperatures for Various Steel Grades and Thicknesses

Temperature (°C)	Spec. no.	0.60 mm				0.80 mm				0.95 mm			
		G250		G550		G250		G550		G250		G550	
		$f_{y,T}$	$f_{y,T}/f_{y,20}$	$f_{y,T}$	$f_{y,T}/f_{y,20}$	$f_{y,T}$	$f_{y,T}/f_{y,20}$	$f_{y,T}$	$f_{y,T}/f_{y,20}$	$f_{y,T}$	$f_{y,T}/f_{y,20}$	$f_{y,T}$	$f_{y,T}/f_{y,20}$
20	1	316	1.000	675	1.000	297	1.000	620	1.000	320	1.000	615	1.000
	2	313						600					
	3												
100	1	295	0.937	654	0.969	284	0.956	615	1.008	292	0.913	600	0.976
	2	296	0.940	656	0.972	287	0.966	605	0.992	288	0.900	601	0.977
	3												
200	1	287	0.911	647	0.959	269	0.906	600	0.984	274	0.856	585	0.951
	2	294	0.933	644	0.954	276	0.929	600	0.984	268	0.838	600	0.976
	3							615	1.008	248	0.775		
350	1	163	0.517	566	0.839	178	0.599	540	0.885	158	0.494	536	0.872
	2	165	0.524	565	0.837	175	0.589	531	0.870	166	0.519	546	0.888
	3	169	0.537			169	0.569	532	0.872	166	0.519	536	0.872
500	1	103	0.327	277	0.410	105	0.354	268	0.439	103	0.322	319	0.519
	2	103	0.327	290	0.430	109	0.367	255	0.418	106	0.331	300	0.488
	3	99	0.315	250	0.370							250	0.407
600	1			80	0.119			75	0.123			69	0.112
650	1	52	0.166	69	0.102	53	0.179	59	0.097	53	0.164	50	0.081
	2	50	0.159	70	0.104	54	0.181	58	0.095	53	0.165	52	0.085
	3			57	0.084			54	0.089			50	0.081
800	1	11	0.035	20	0.030	24	0.081	31	0.051	19	0.059	27	0.044
	2	12	0.038	21	0.031	24	0.081	31	0.051	18	0.056	27	0.044
	3												

Modulus of Elasticity in GPa at Elevated Temperatures for Various Steel Grades and Thicknesses

Temperature (°C)	Spec. no.	0.60 mm				0.80 mm				0.95 mm			
		250	Et/E20	550	Et/E20	250	Et/E20	550	Et/E20	250	Et/E20	550	Et/E20
20	1	200	1.000	214	1.000	200	1.000	200	1.000	200	1.000	205	1.000
	2	222						200					
	3												
100	1	210	0.995	213	0.995	200	1.000	200	1.000	200	1.000	203	0.990
	2	211	1.000	215	1.005	200	1.000	200	1.000	200	1.000	207	1.010
	3												
200	1	200	0.948	176	0.822	178	0.890	167	0.835	182	0.910	175	0.854
	2	200	0.948	176	0.822	178	0.890	167	0.835	188	0.940	179	0.873
	3							178	0.890				
	4							171	0.855				
350	1	95	0.450	143	0.668	114	0.570	133	0.665	114	0.570	142	0.693
	2	88	0.417	136	0.636	108	0.540	147	0.735	133	0.665	133	0.649
	3	133	0.630			108	0.540	146	0.730	129	0.645	148	0.722
	4	133	0.630										
500	1	100	0.474	88	0.411	100	0.500	80	0.400	100	0.500	83	0.405
	2	100	0.474	83	0.388	95	0.475	79	0.395	95	0.475	75	0.366
	3	100	0.474	83	0.388							83	0.405
	4	95	0.450										
650	1	58	0.275	56	0.262	67	0.335	67	0.335	70	0.350	60	0.293
	2	54	0.256	57	0.266	70	0.350	57	0.285	70	0.350	80	0.390
	3											58	0.283
800	1	10	0.047	12	0.056	8	0.040	25	0.125	20	0.100	29	0.141
	2	10	0.047	13	0.061	7	0.035	27	0.135	18	0.090	28	0.137

Ultimate Tensile Strengths at Elevated Temperatures for Various Steel Grades and Thicknesses

Temperature (°C)	spec. no.	0.60 mm				0.80 mm				0.95 mm			
		250	ft/f20	550	ft/f20	250	ft/f20	550	ft/f20	250	ft/f20	550	ft/f20
20	1	366	1.000	704	1.000	365	1.000	670	1.000	361	1.000	637	1.000
	2	366						660					
	3												
100	1	359	0.981	706	1.003	353	0.967	652	0.980	350	0.970	617	0.969
	2	363	0.992	702	0.997	358	0.981	648	0.974	348	0.964	625	0.981
	3	359	0.981										
200	1	406	1.109	705	1.001	408	1.118	620	0.932	445	1.233	600	0.942
	2	437	1.194	703	0.999	418	1.145	645	0.970	444	1.230	625	0.981
	3							664	0.998	452	1.252		
350	1	365	0.997	642	0.912	350	0.959	591	0.889	353	0.978	600	0.942
	2	369	1.008	624	0.886	353	0.967	581	0.874	357	0.989	616	0.967
	3	370	1.011							355	0.983	587	0.922
500	1			338	0.480	156	0.427	312	0.469	165	0.457	365	0.573
	2	157	0.429	344	0.489	160	0.438	301	0.453	167	0.463	343	0.538
	3	159	0.434	316	0.449							314	0.493
650	1			86.6	0.123	62	0.170	86	0.129	65	0.180	80	0.126
	2	59	0.161	87	0.124	63	0.173	86.5	0.130	63	0.175	82	0.129
	3	61	0.167	67	0.095			68	0.102			64	0.100
800	1	15	0.041	21	0.030	25	0.068	34	0.051	21	0.058	26	0.041
	2	14	0.038	22	0.031	26	0.071	33	0.050	22	0.061	25	0.039
	3												

A6 Verification of Stress-strain Model
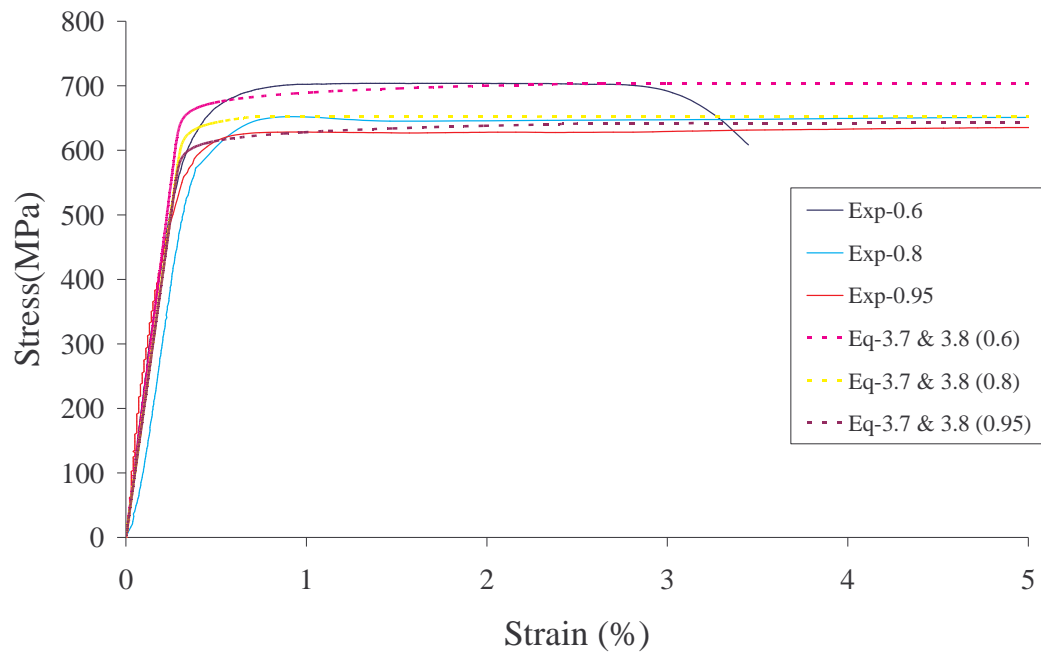
G550 steel at 20ºC
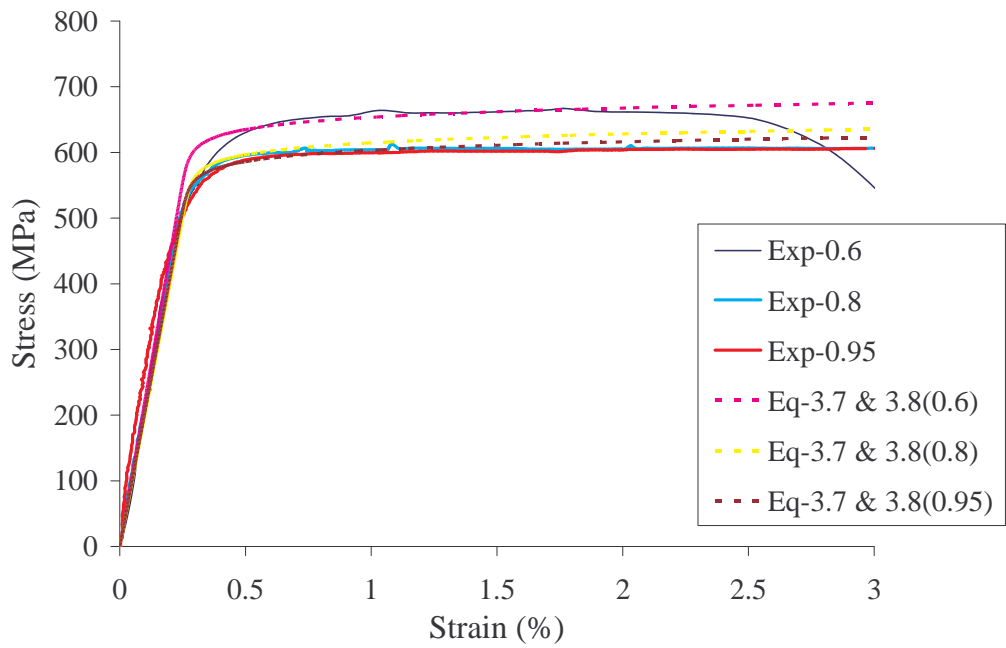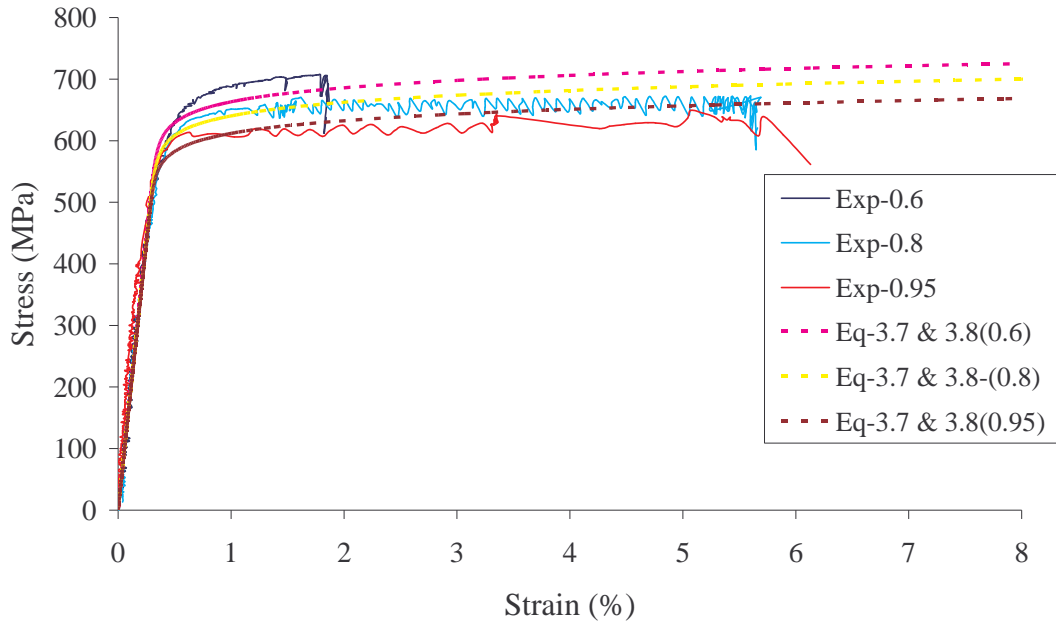
G550 steel at 100ºC

G550 steel at 200°C
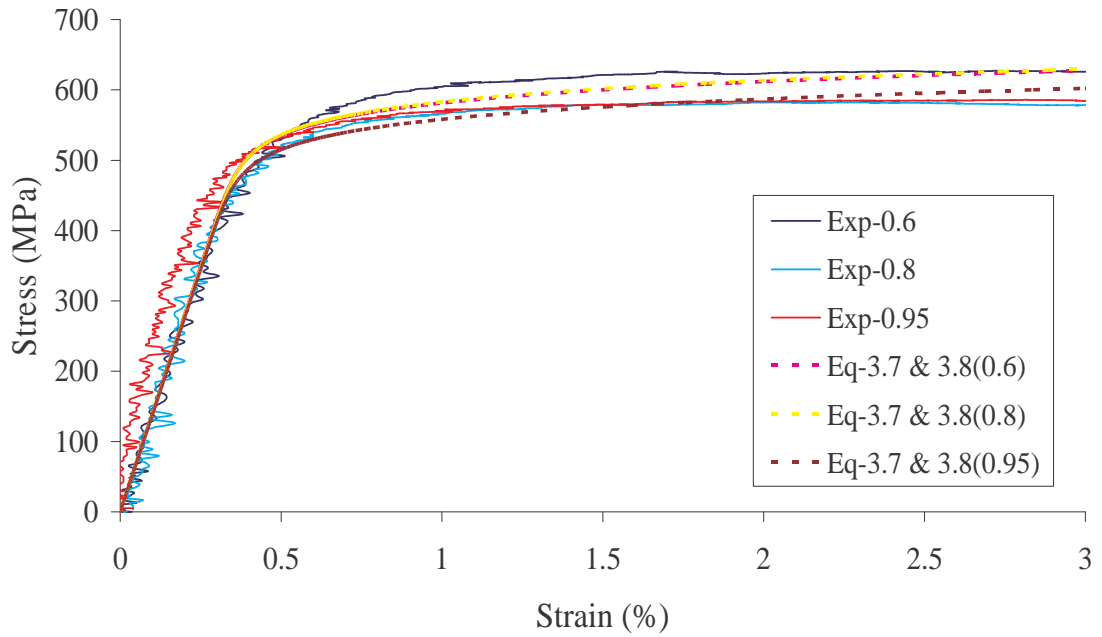
G550 steel at 350°C
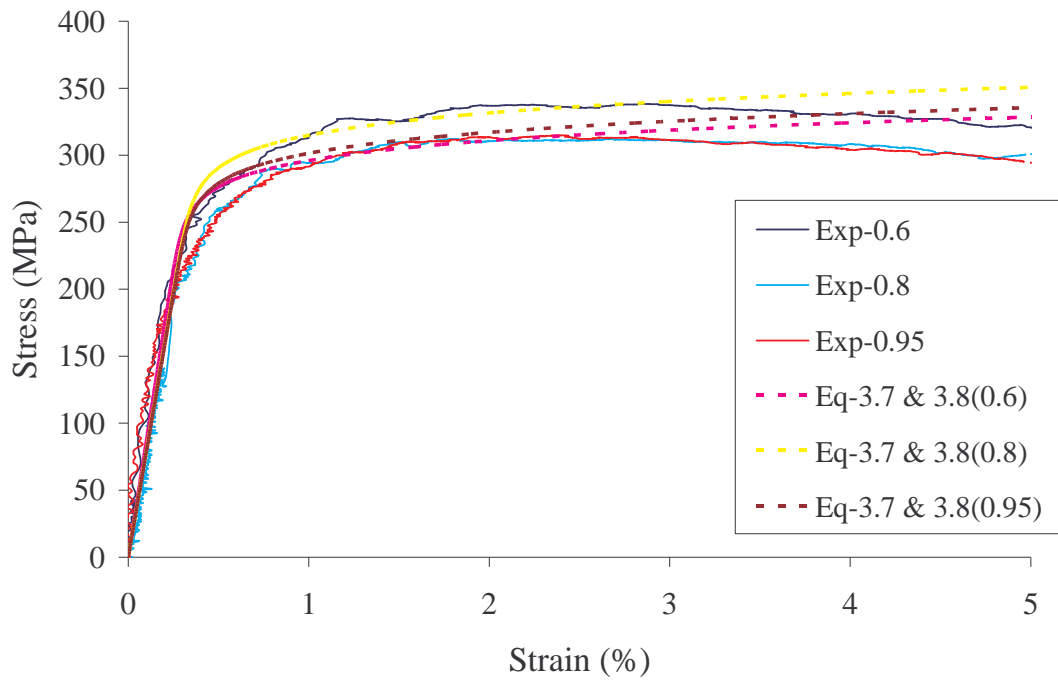
G550 steel at 500°C
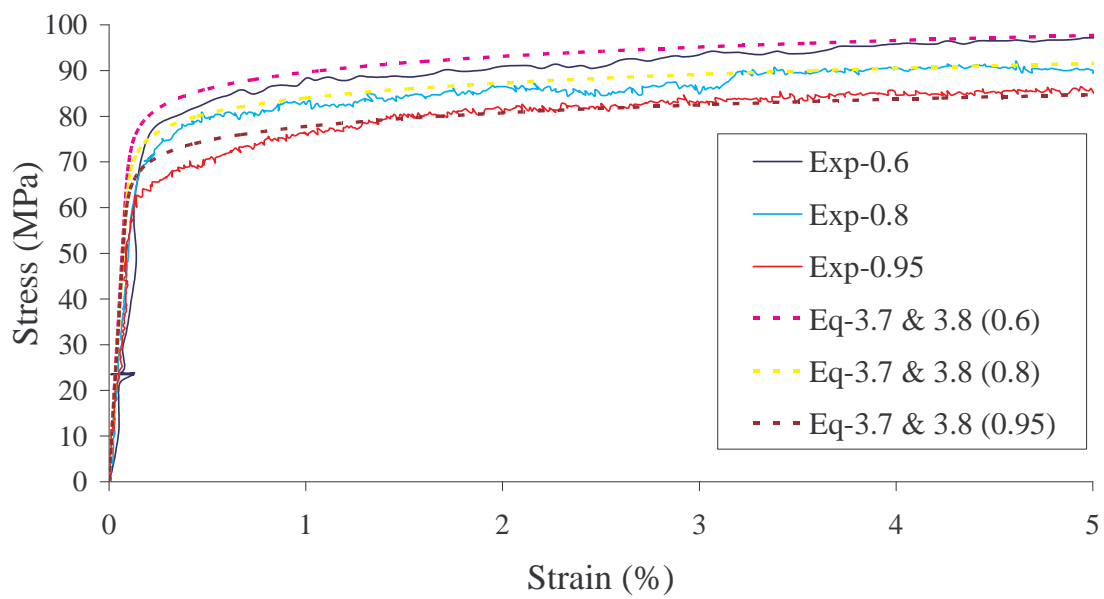
G550 steel at 600°C
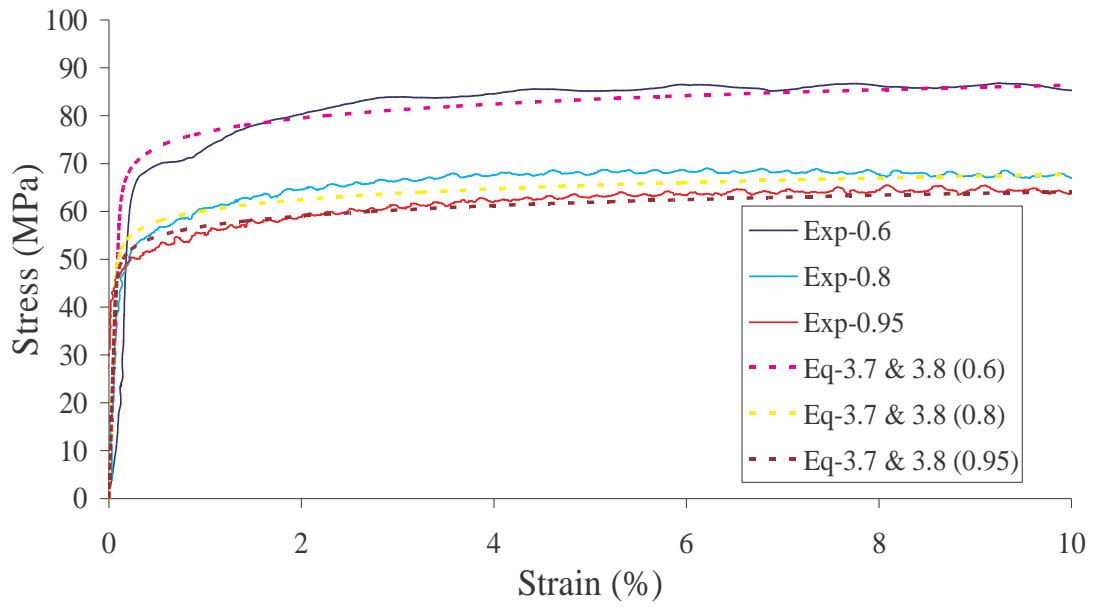
G550 steel at 650°C
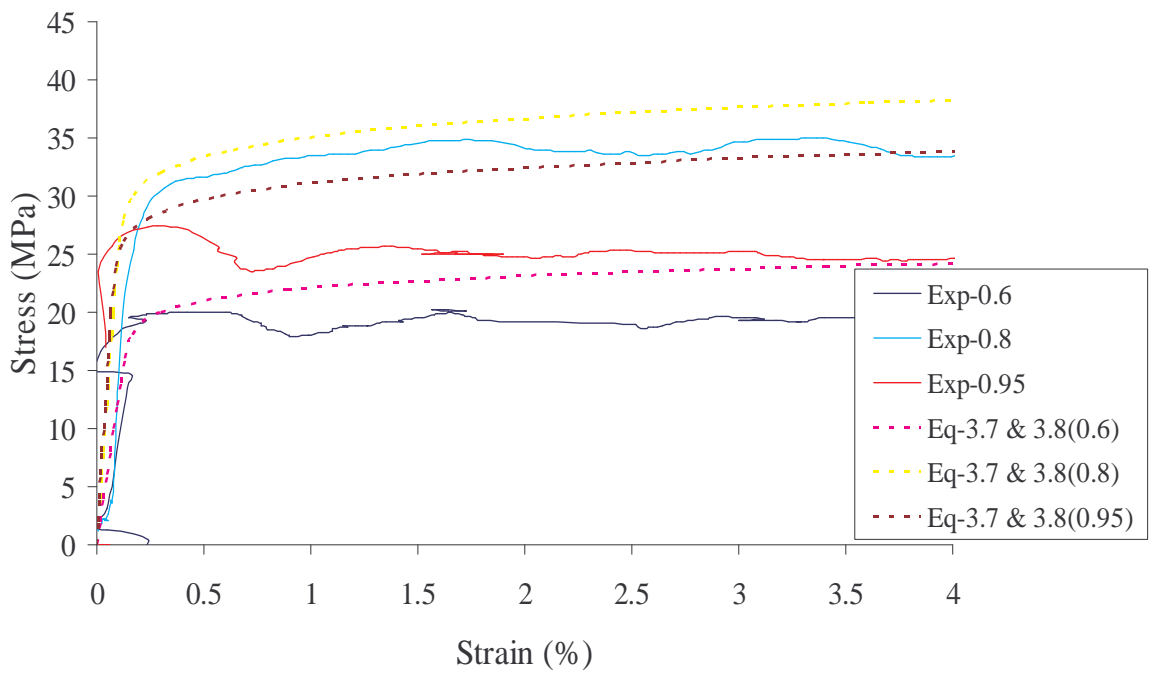
G550 steel at 800°C
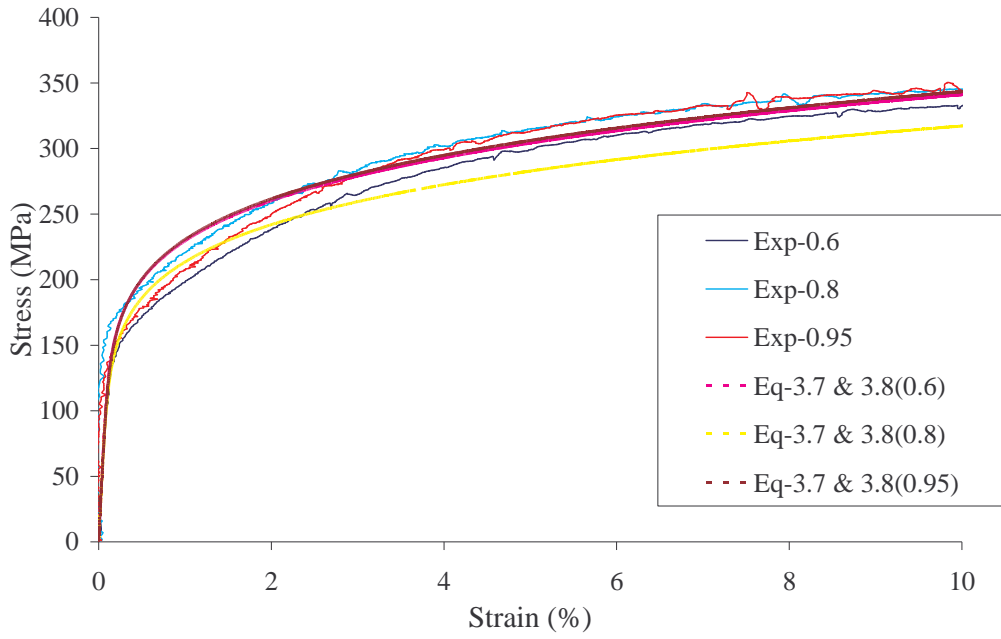
G250 steel at 350⁰C
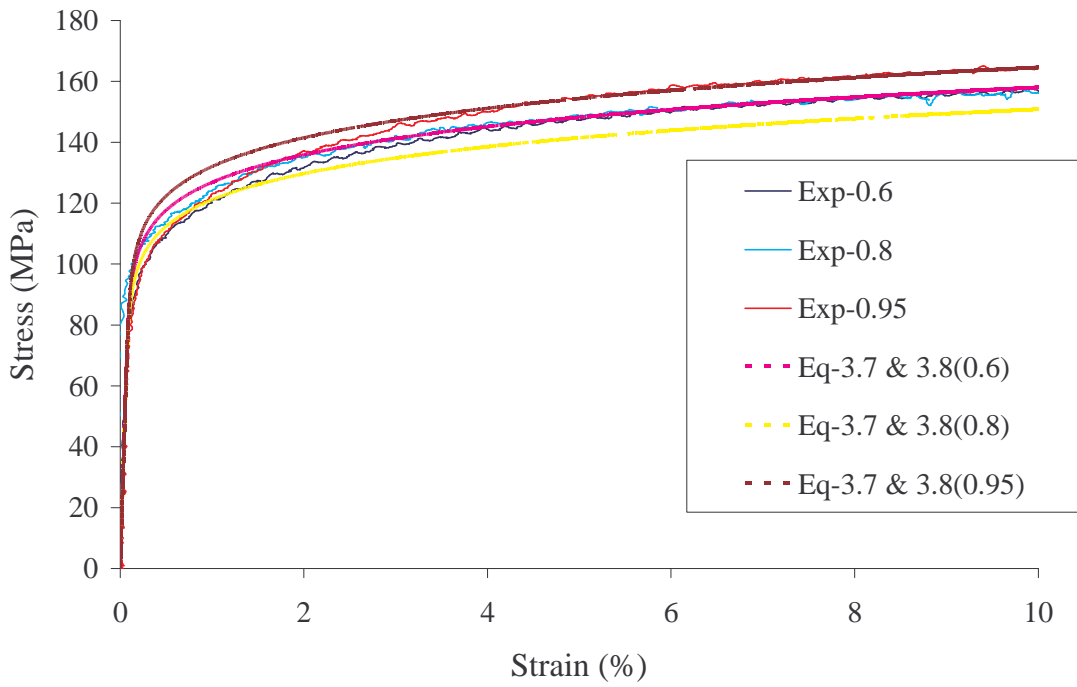
G250 steel at 500⁰C
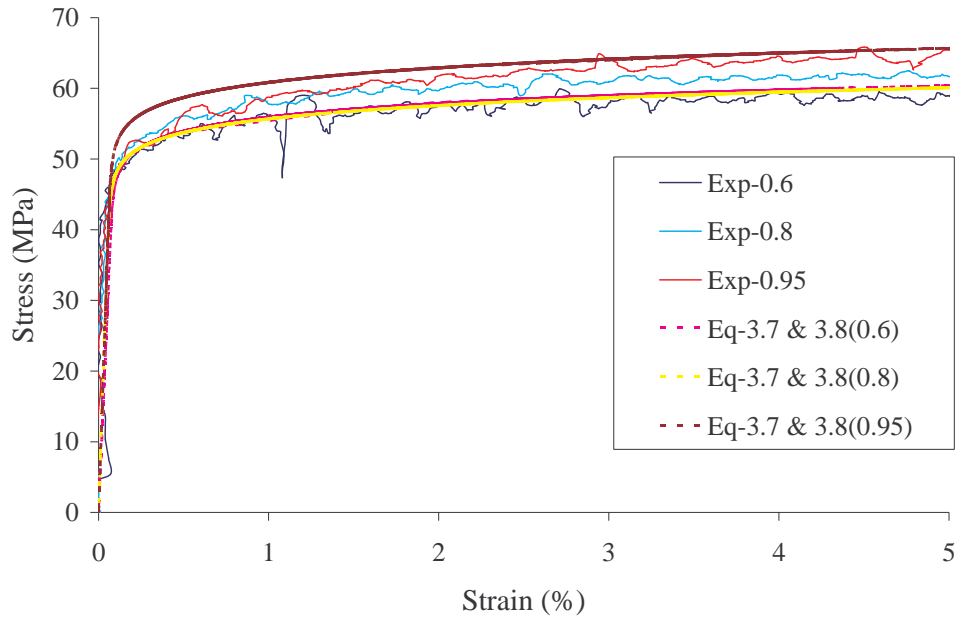
G250 steel at 650°C
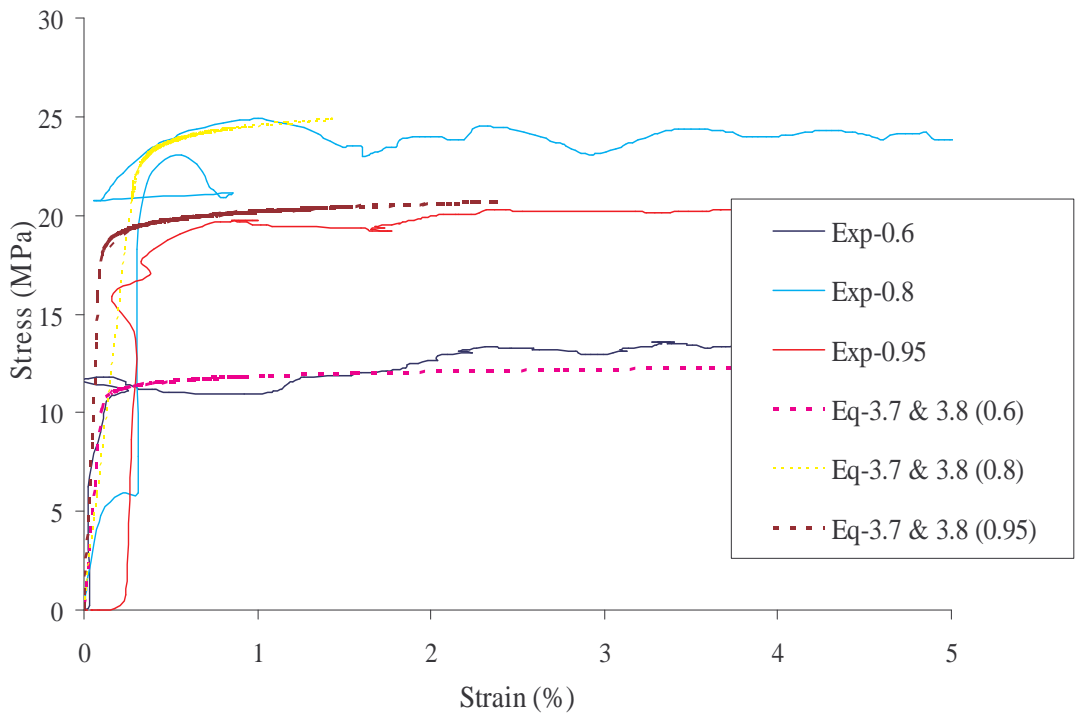
G250 steel at 800°C

Appendix B

Load - Shortening and Load - Deflection Graphs

0.6mm G250 Type A Sections

20°C
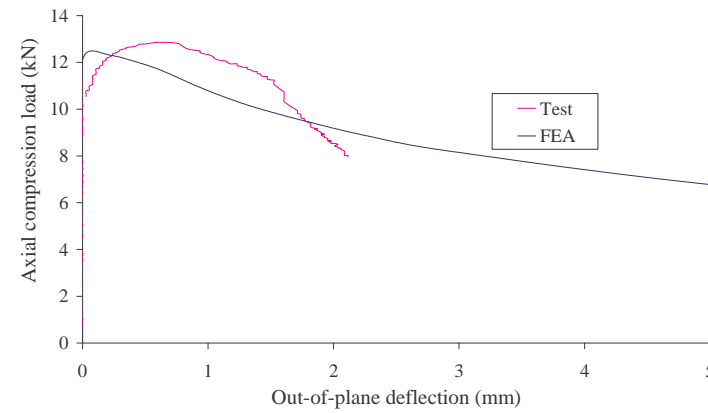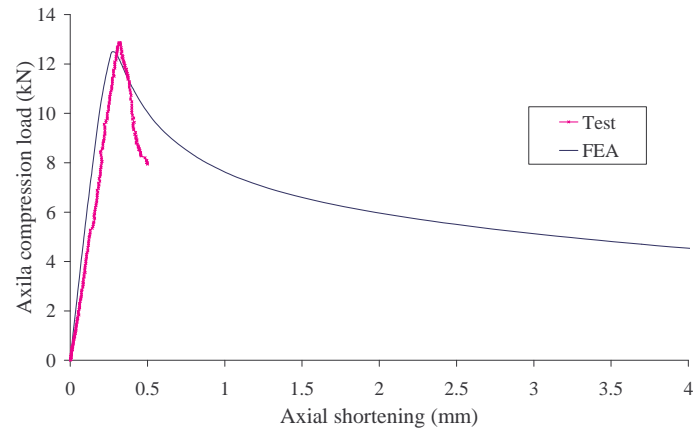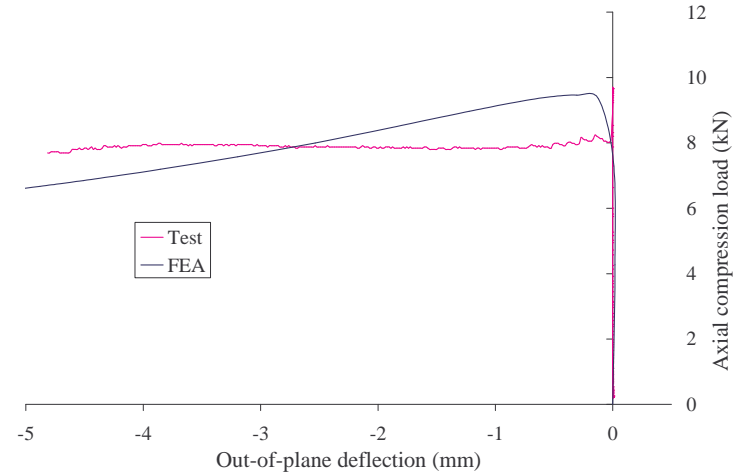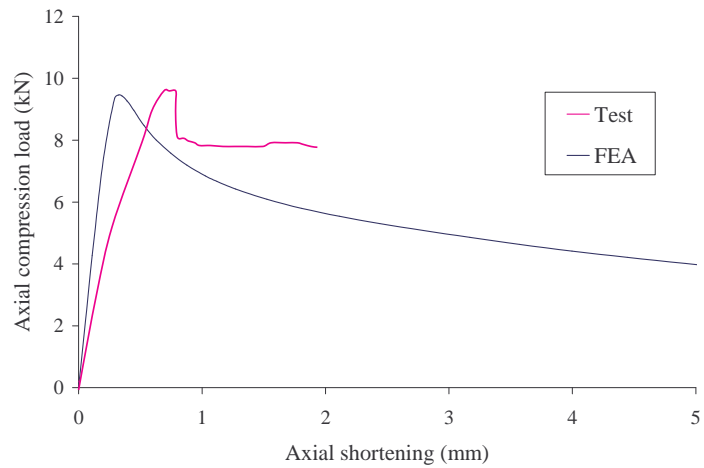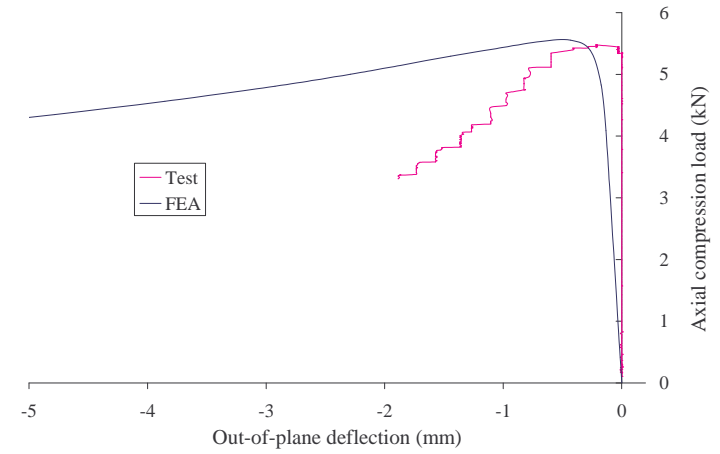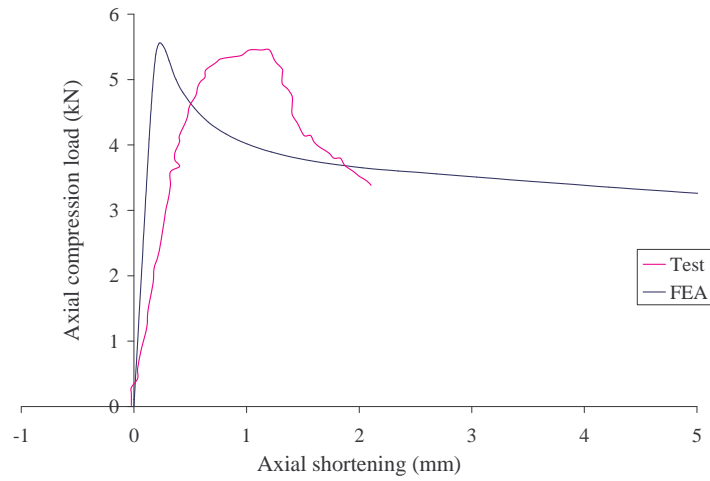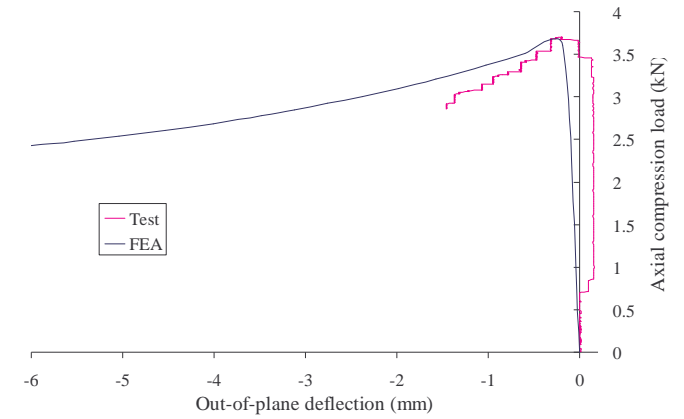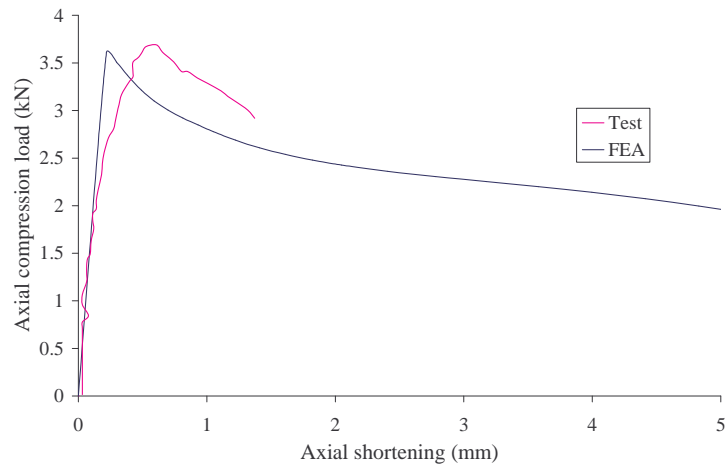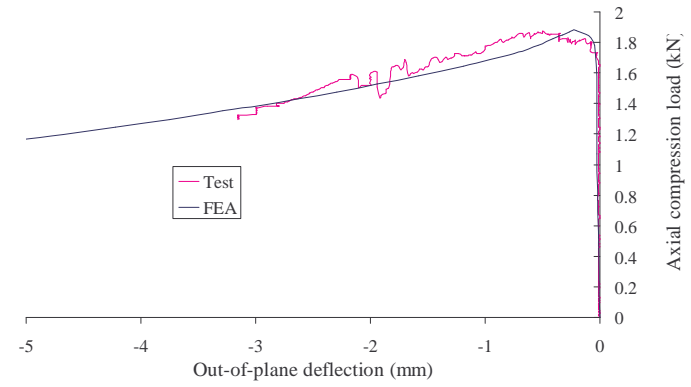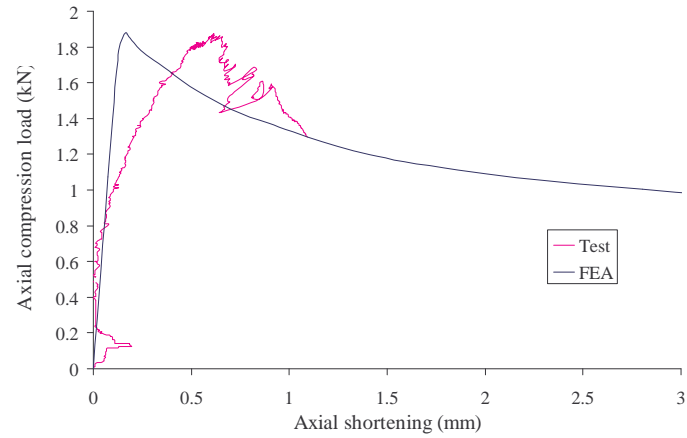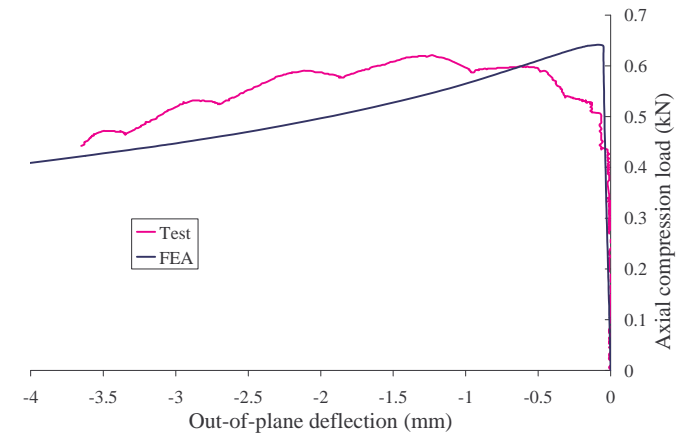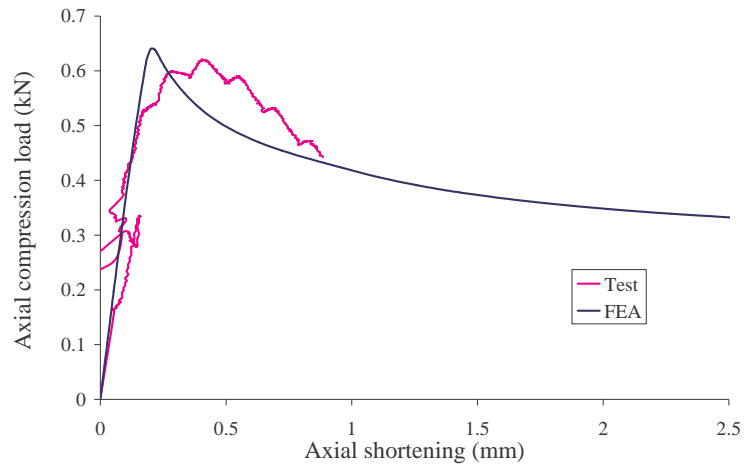
200°C

350°C
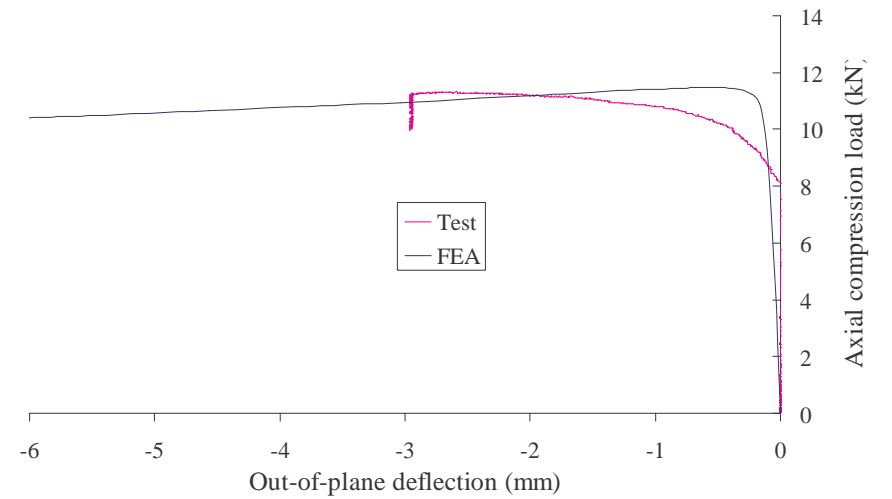
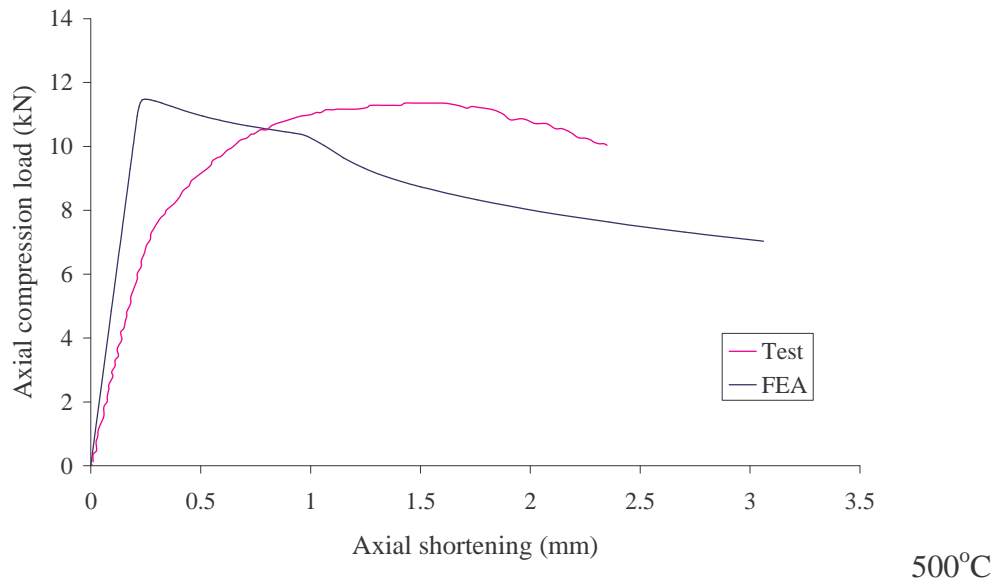

500°C
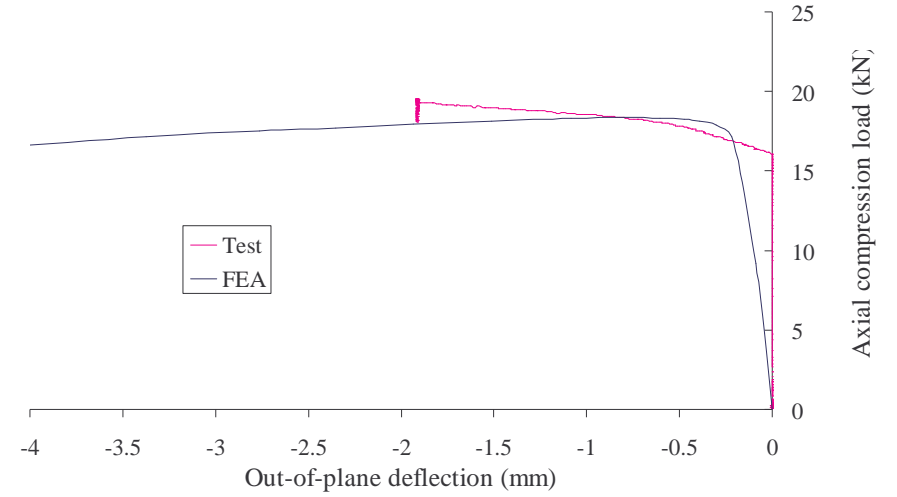
650°C

800°C

0.6mm G550 Type A Sections

20°C
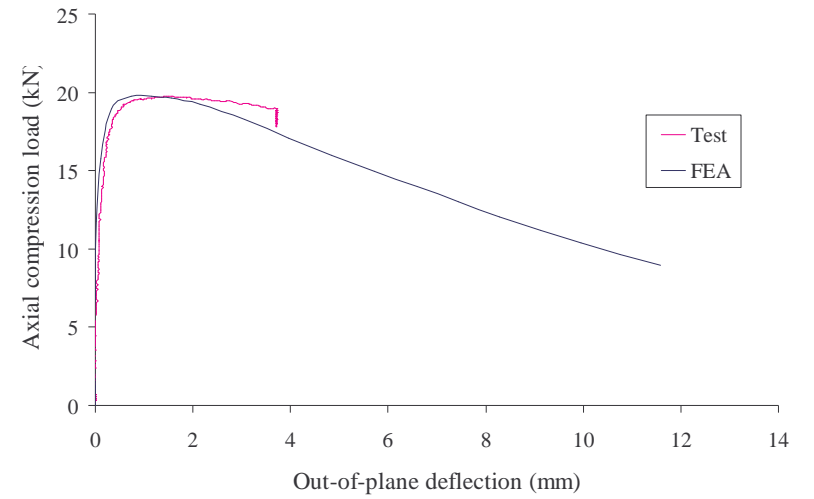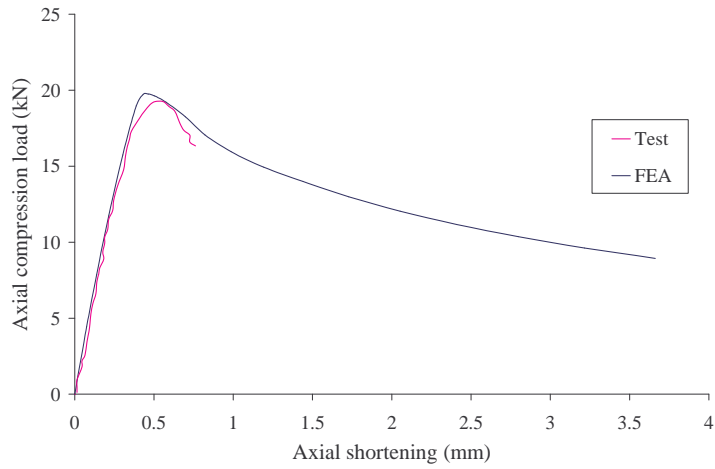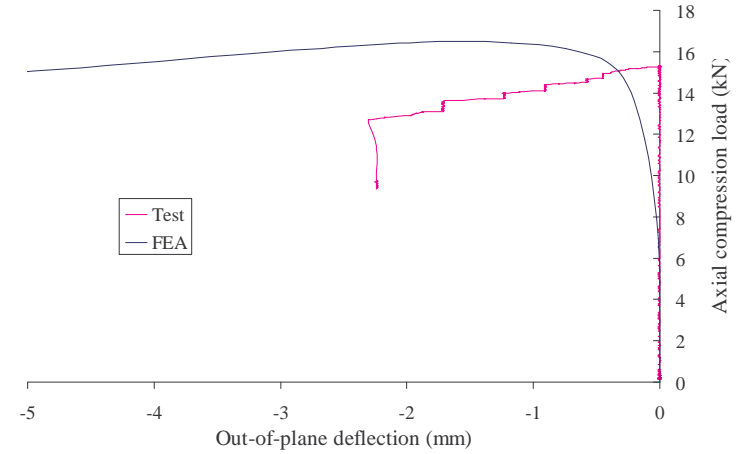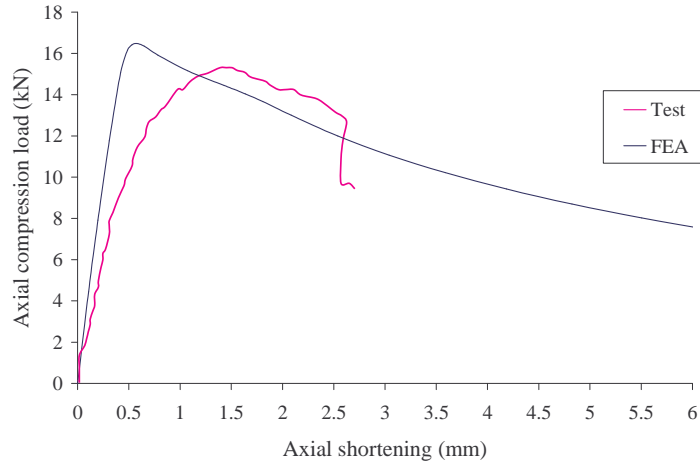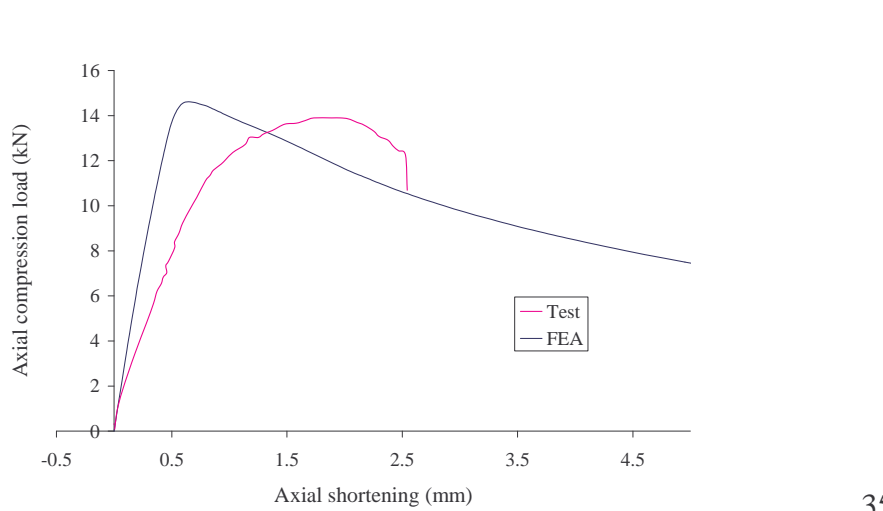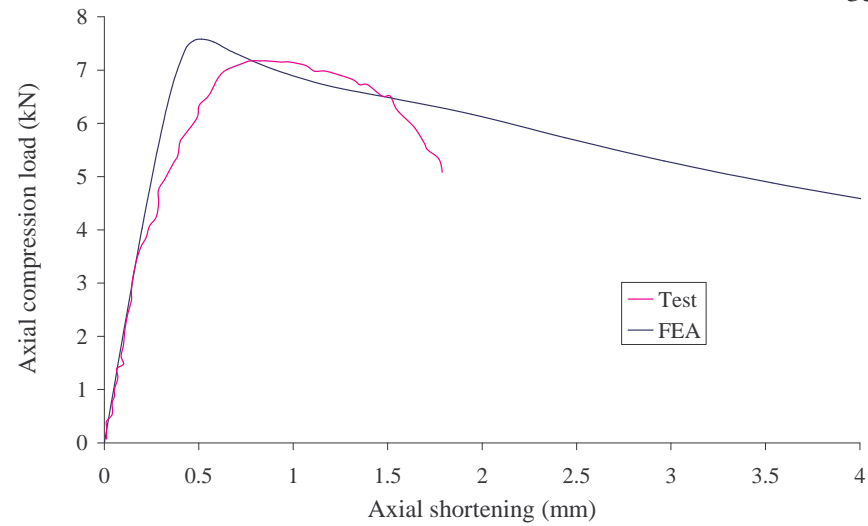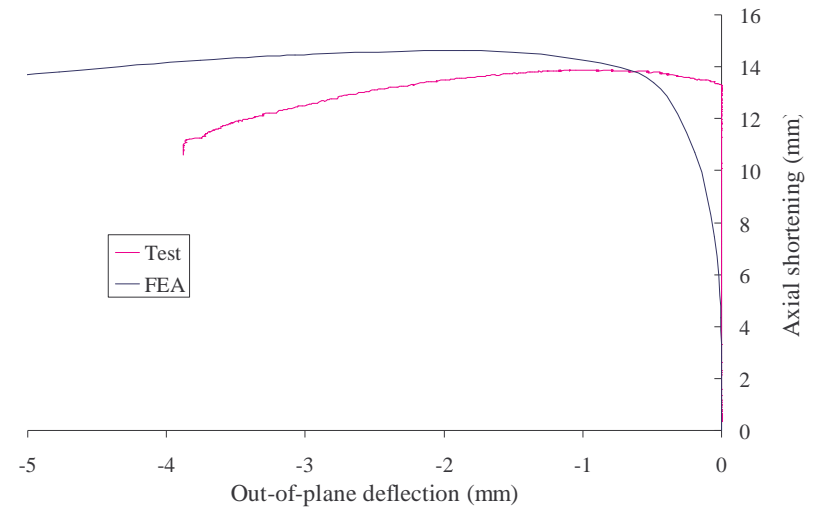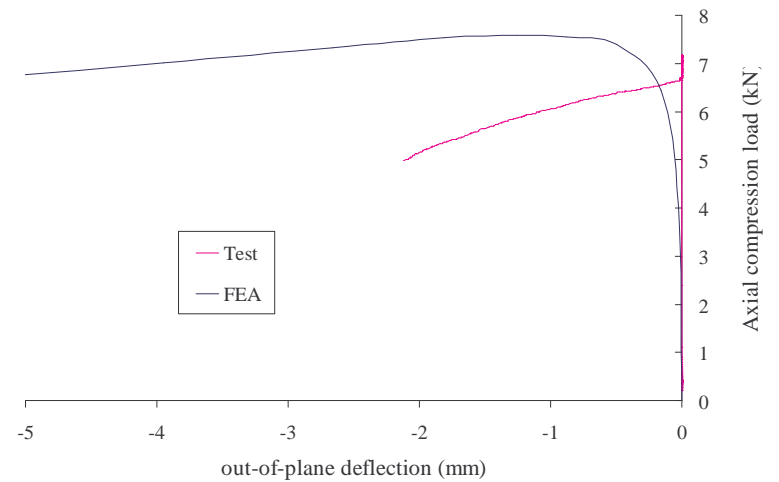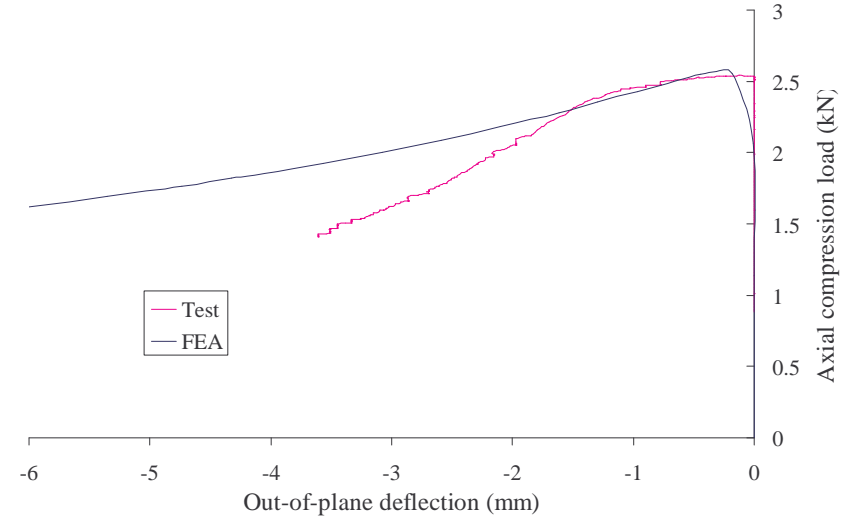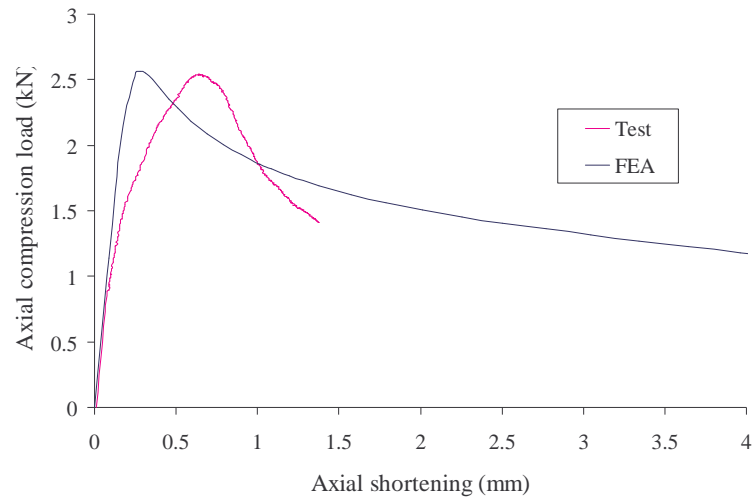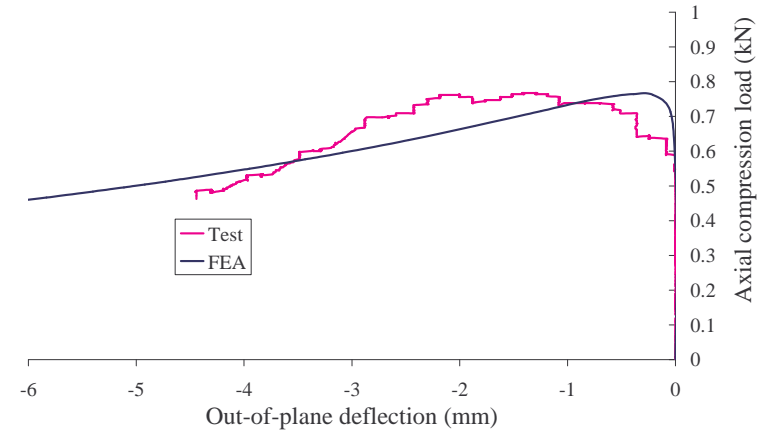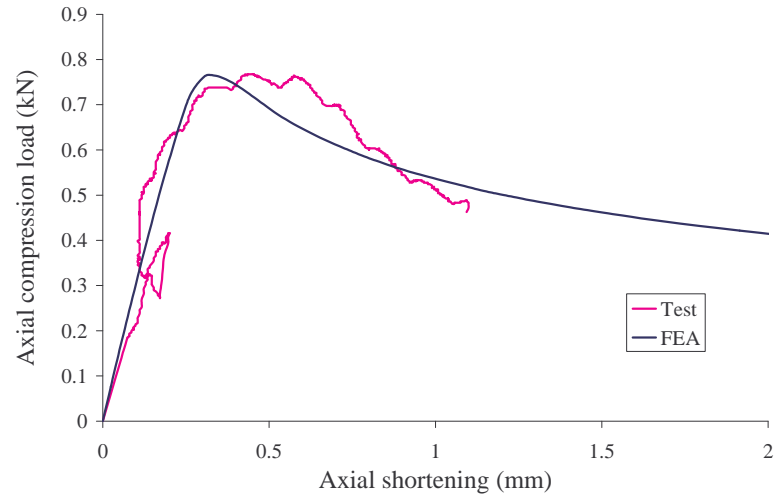
200°C

350°C

500°C

650°C

800°C

0.6mm G250 Type B Sections

20°C
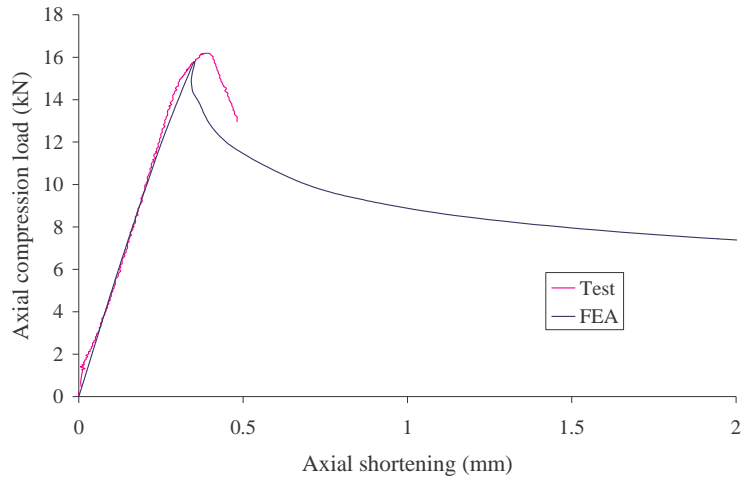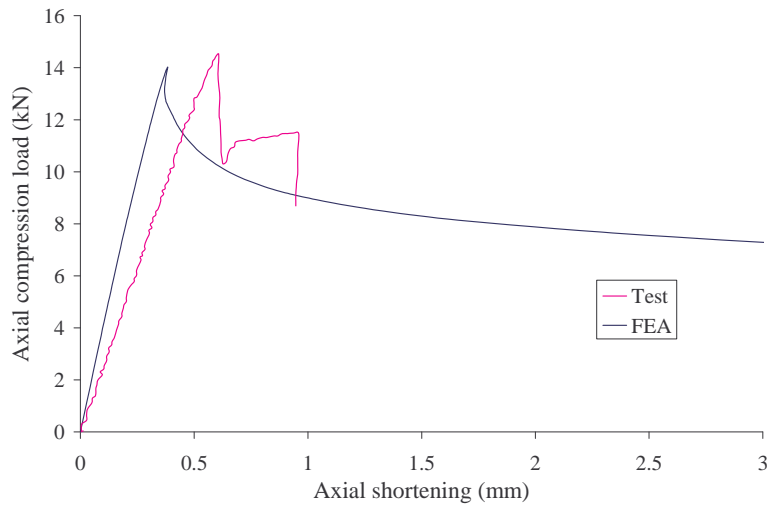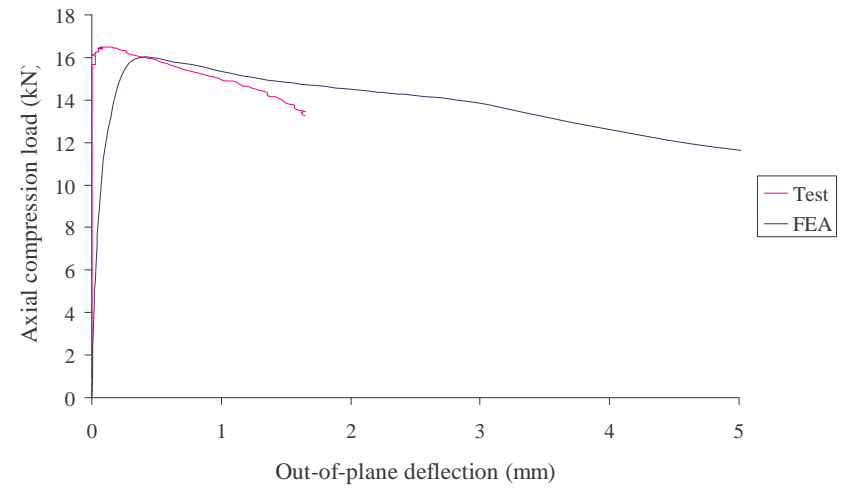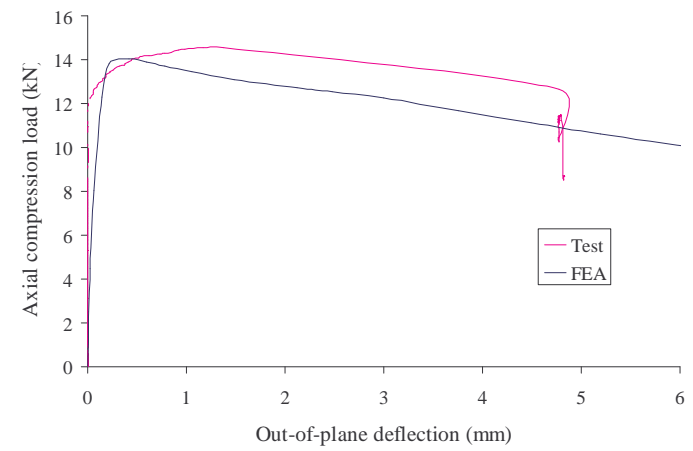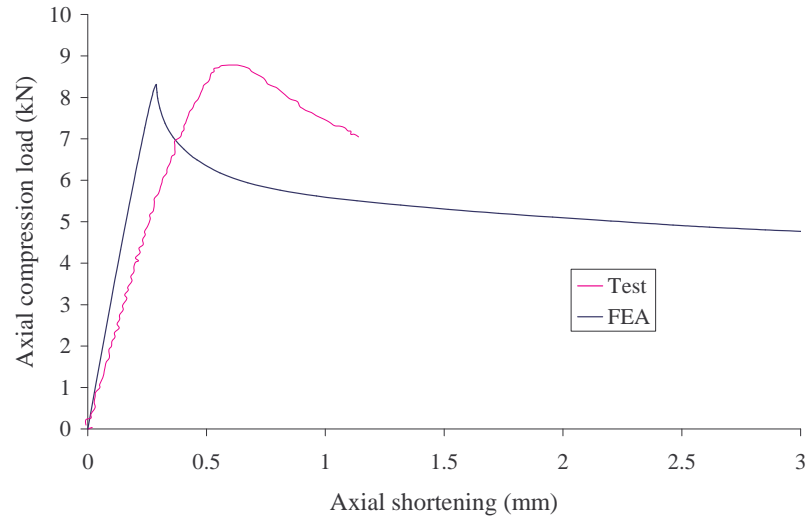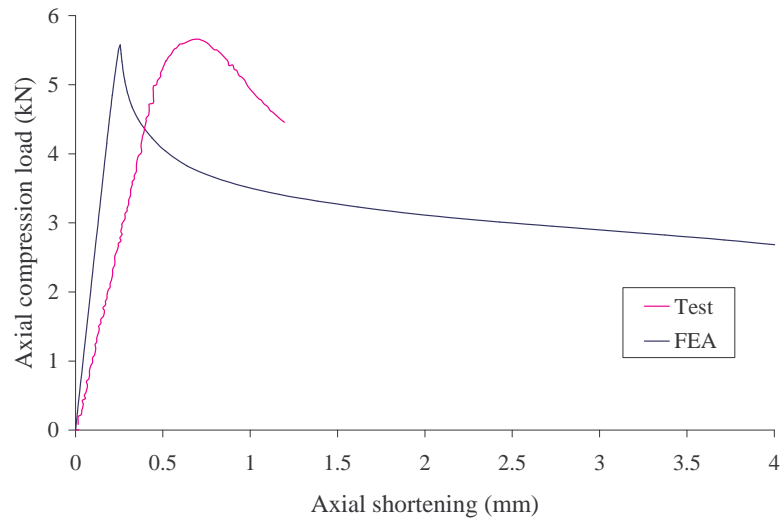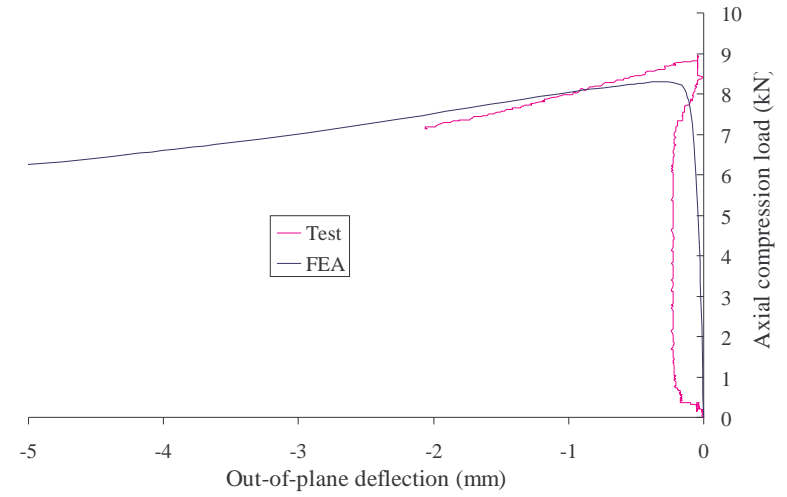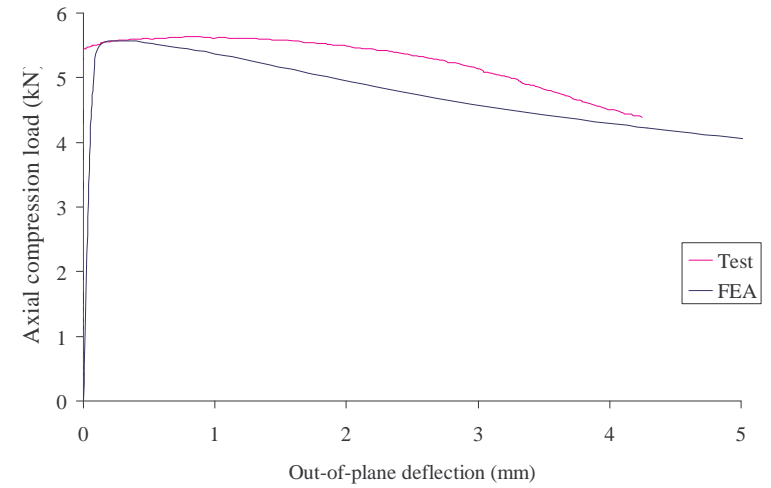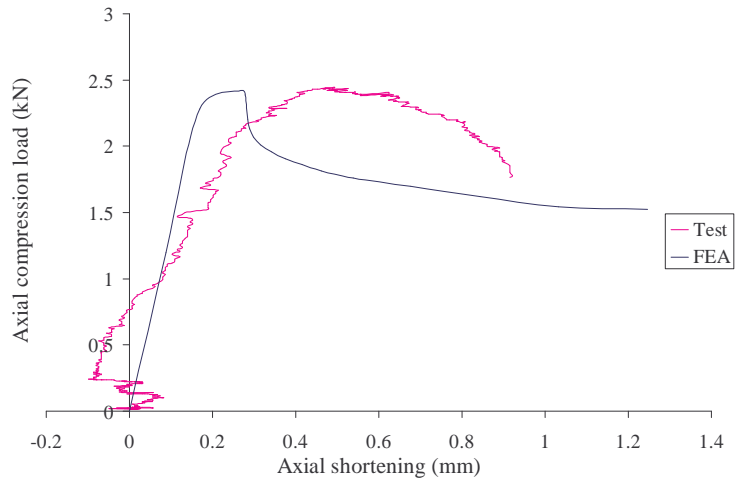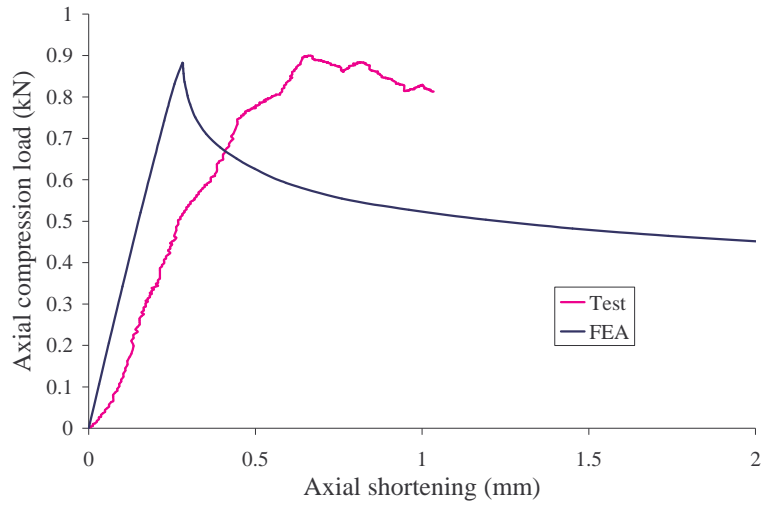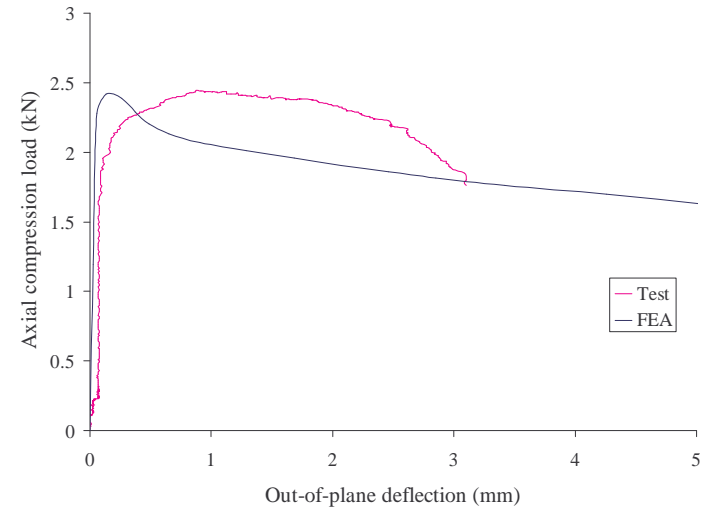
200°C
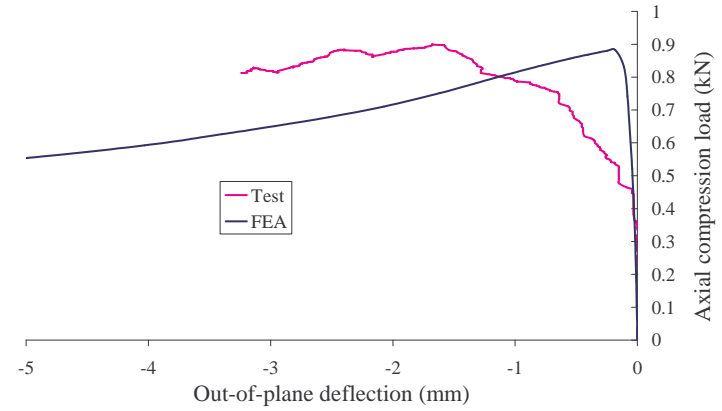
350°C

500°C

650°C

800°C

0.6mm G550 Type B Sections

20°C
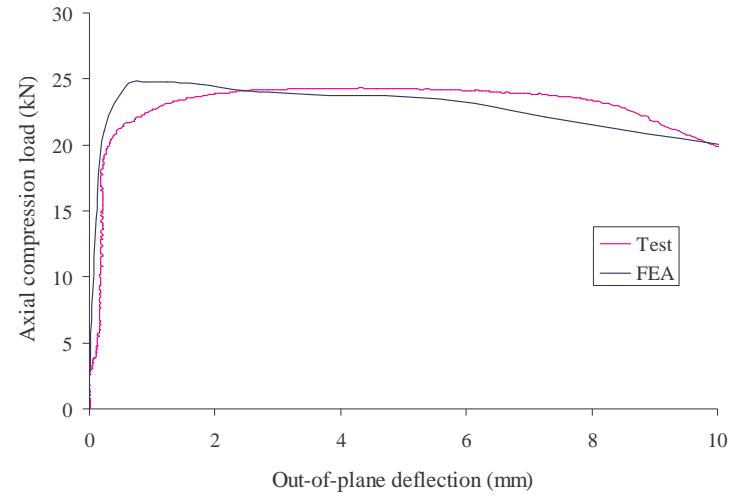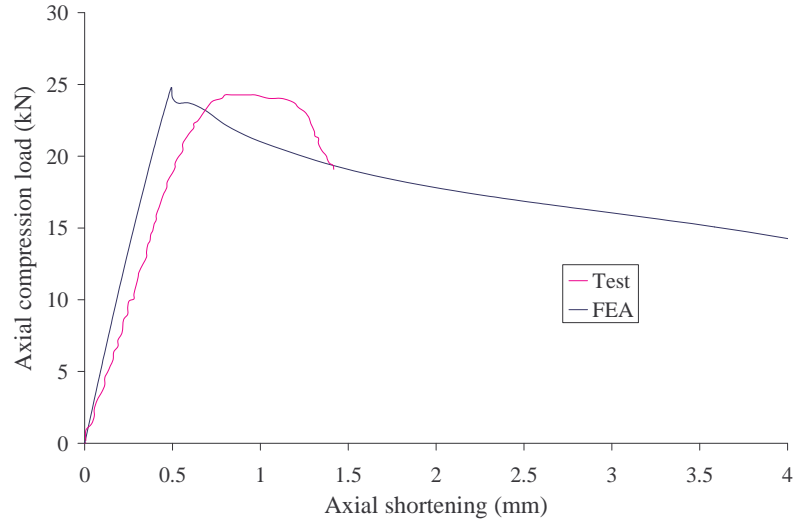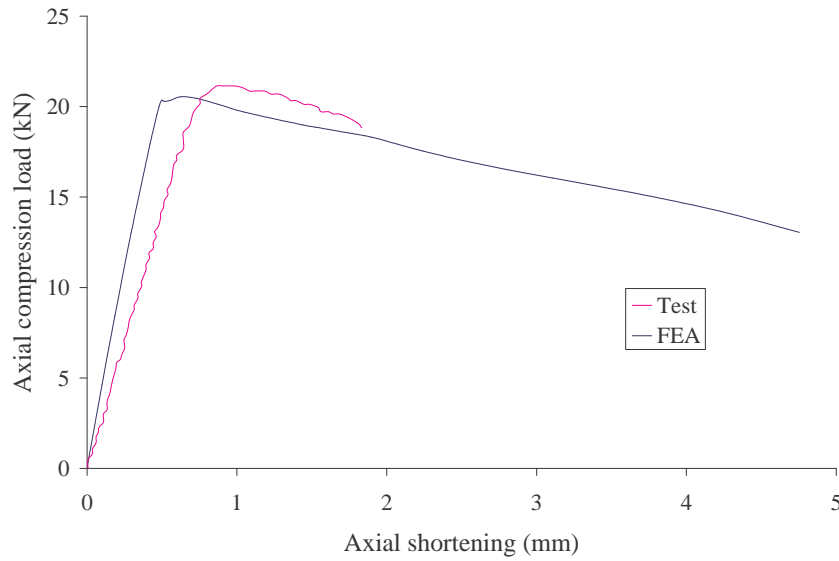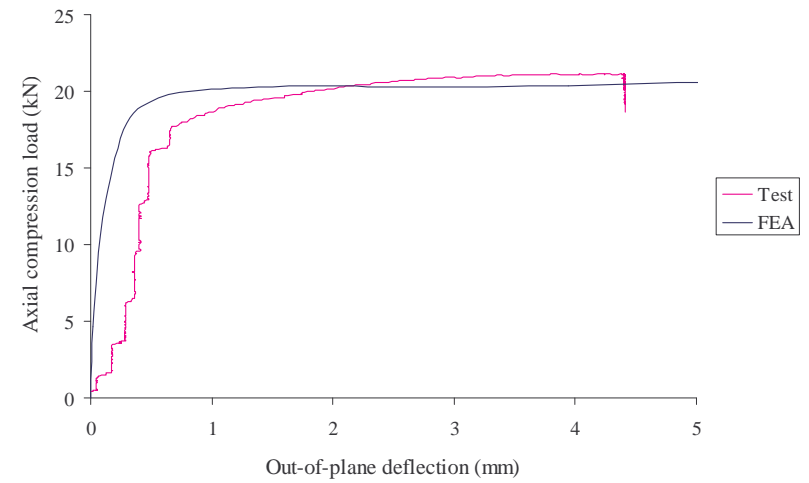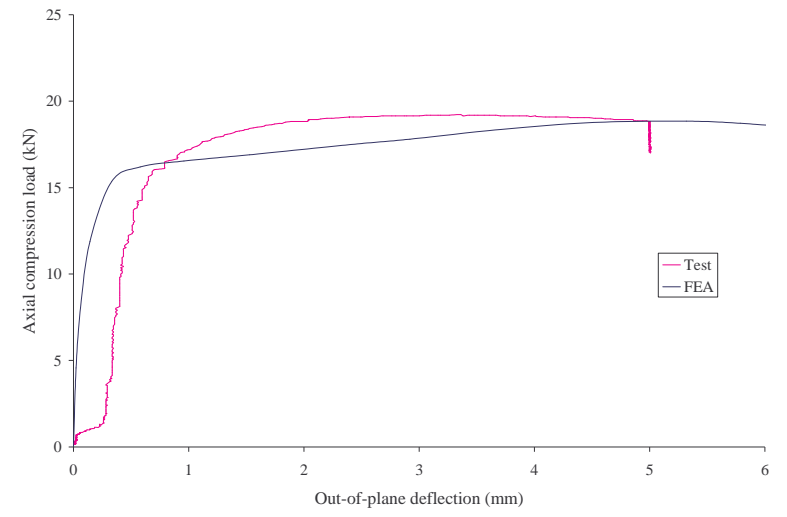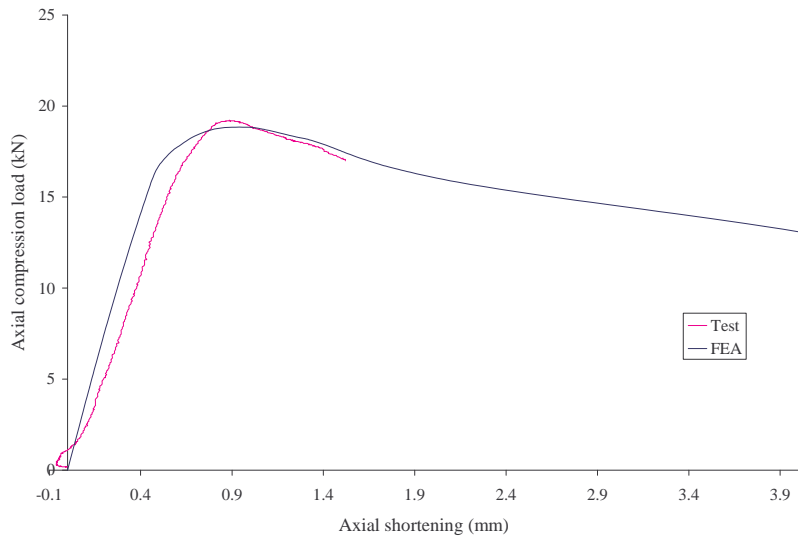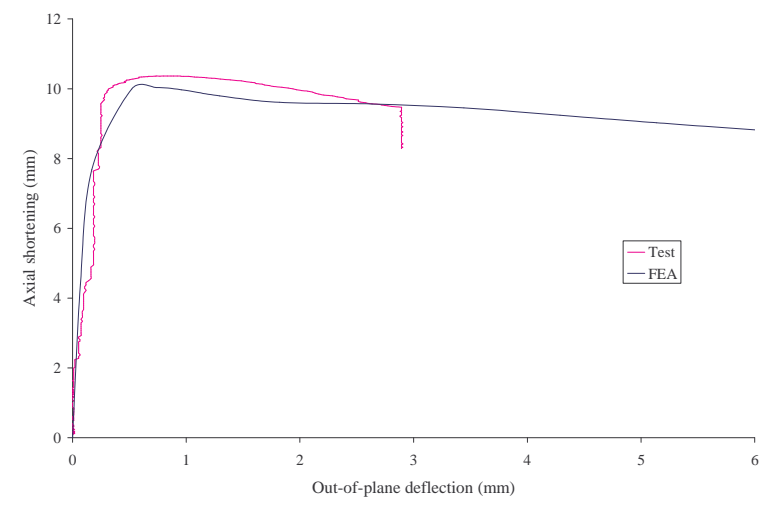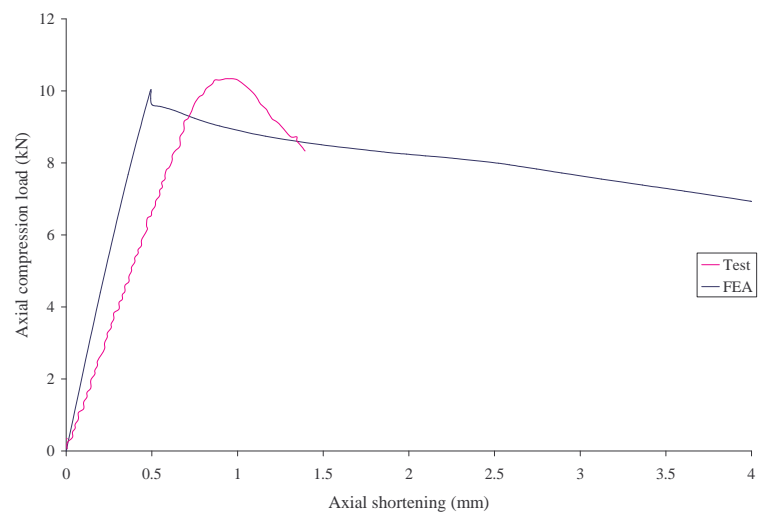
200°C
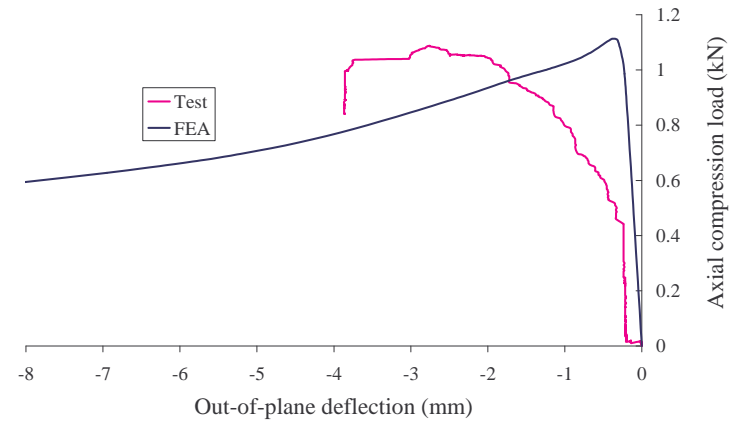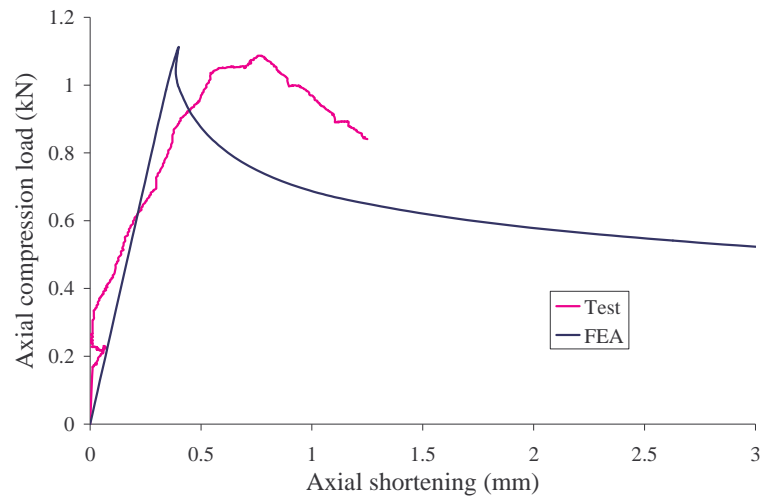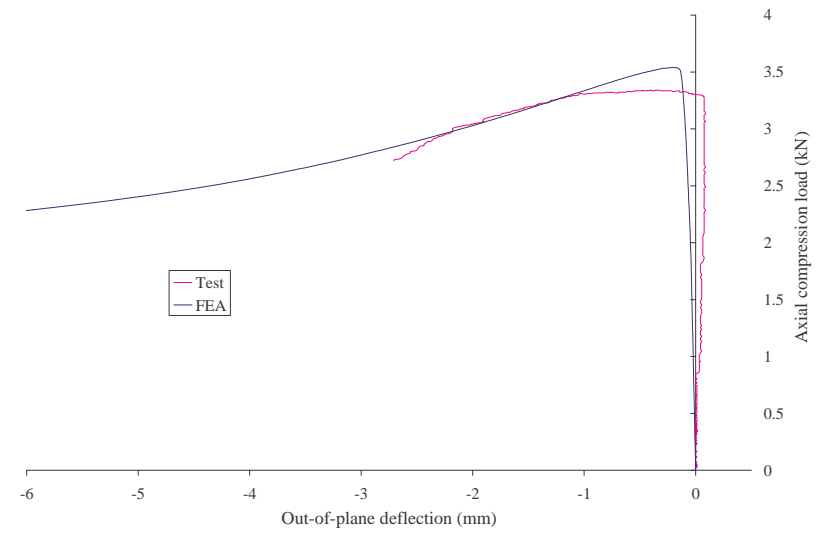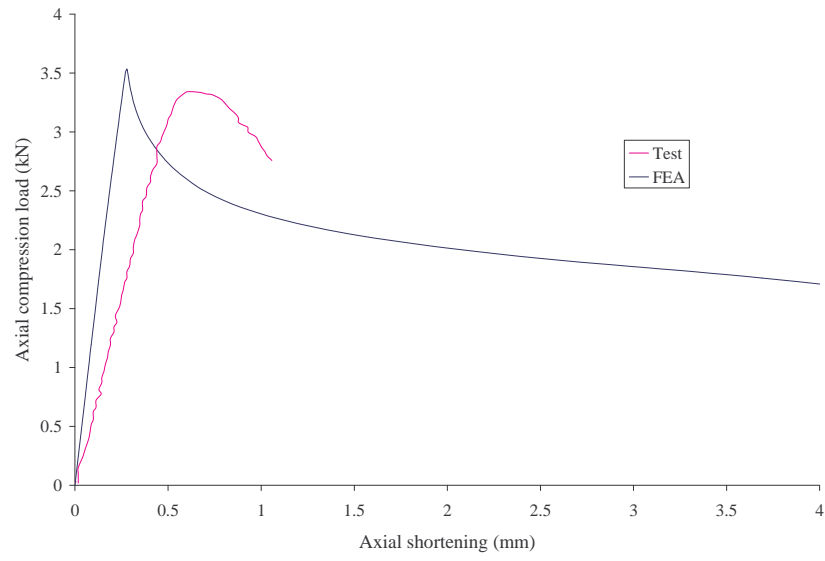
350°C

500°C

650°C

800°C

0.8mm G250 Type A Sections

$20^{o}C$

$200^{o}C$
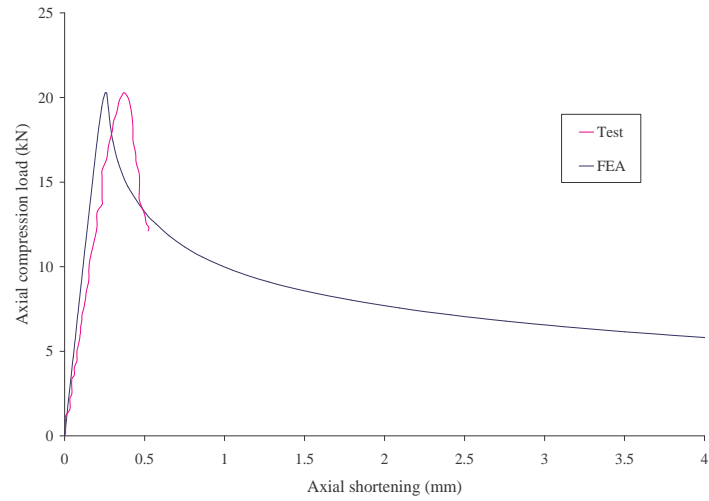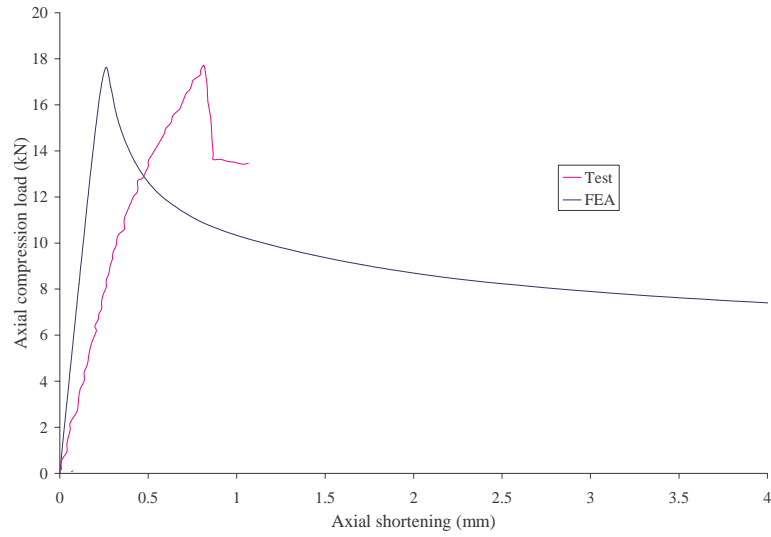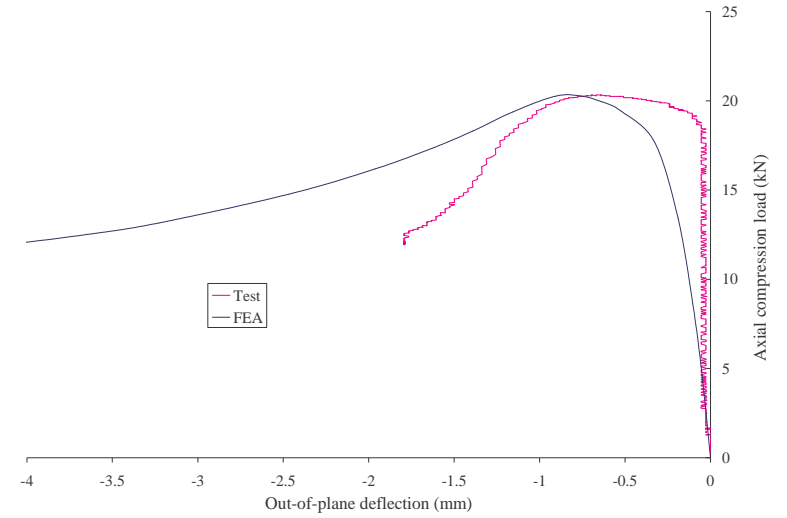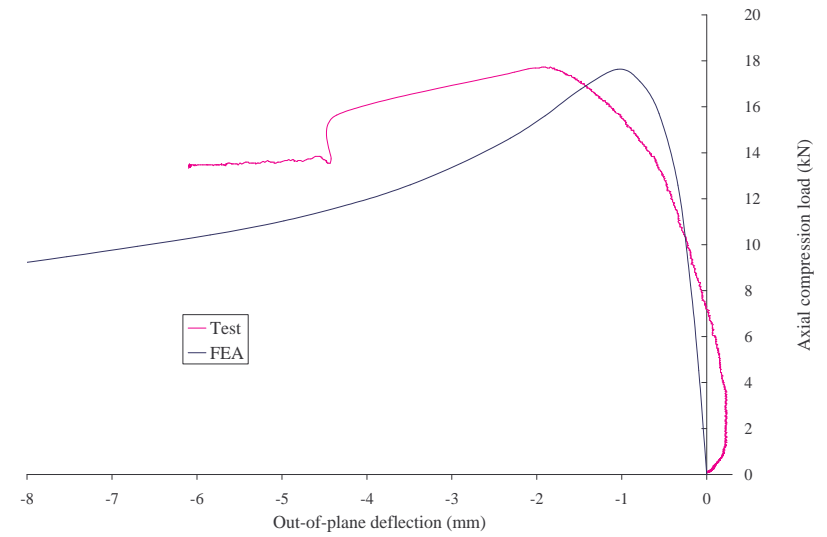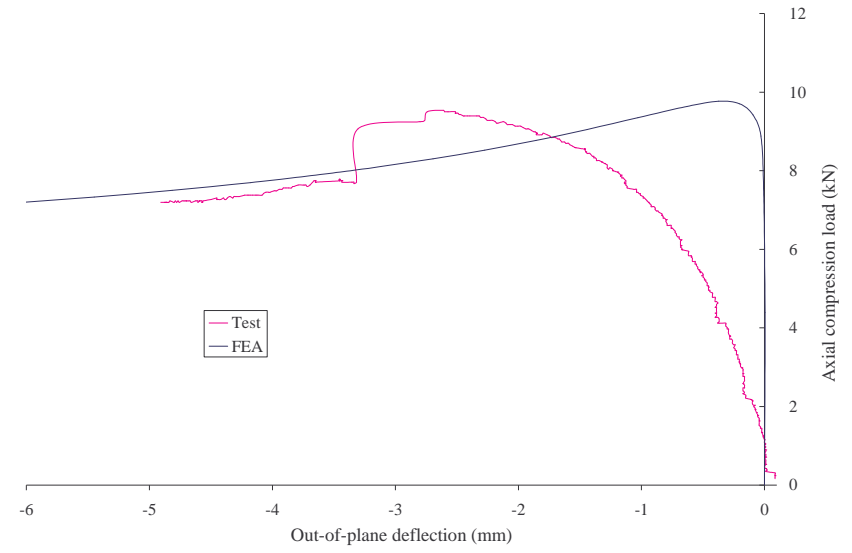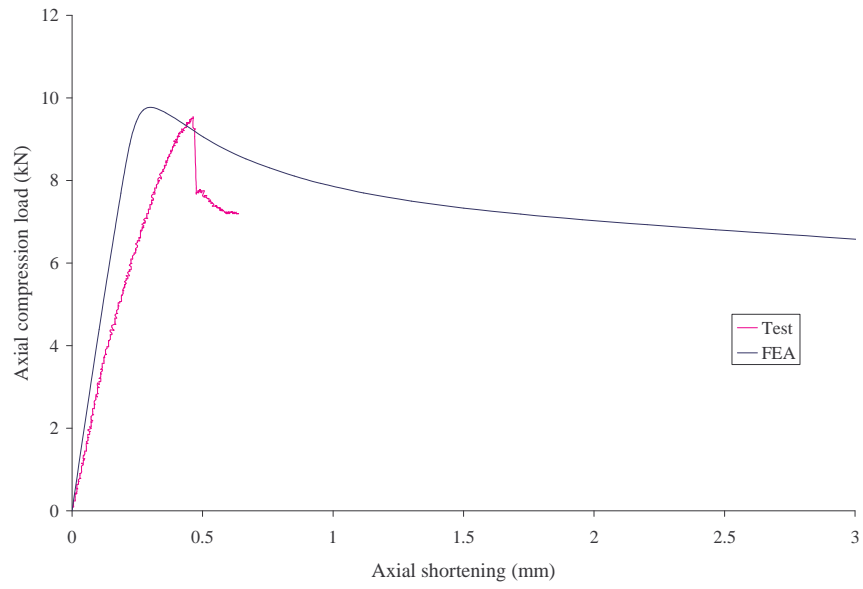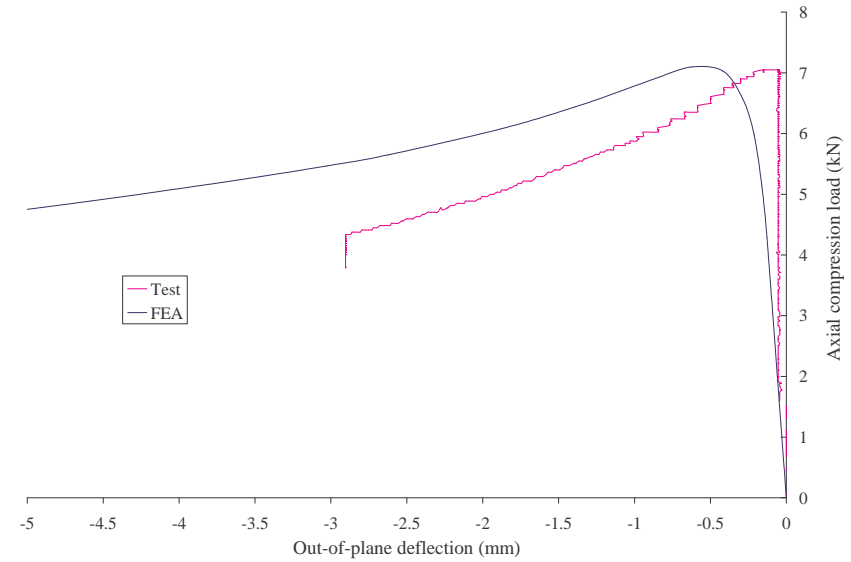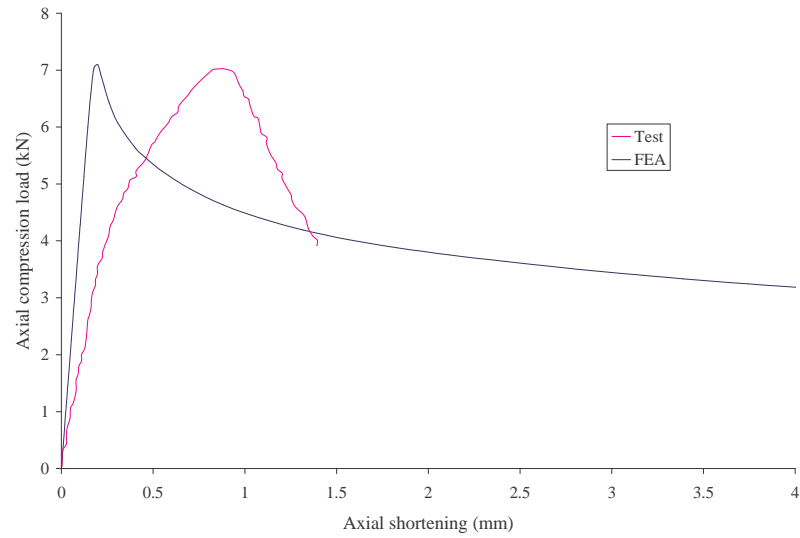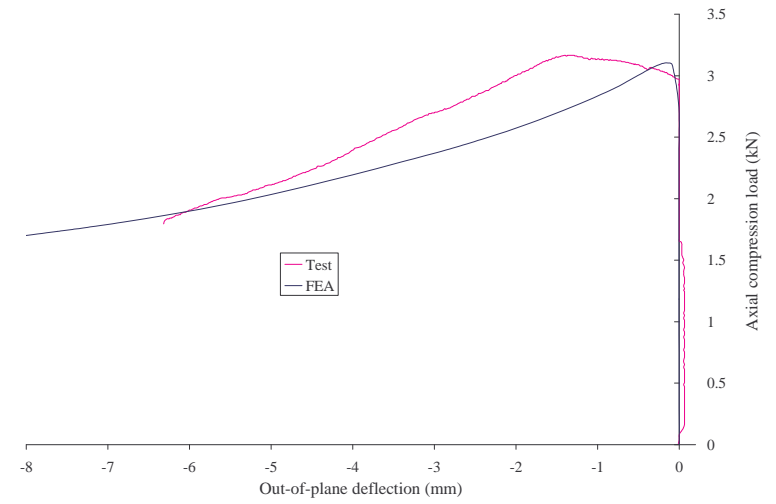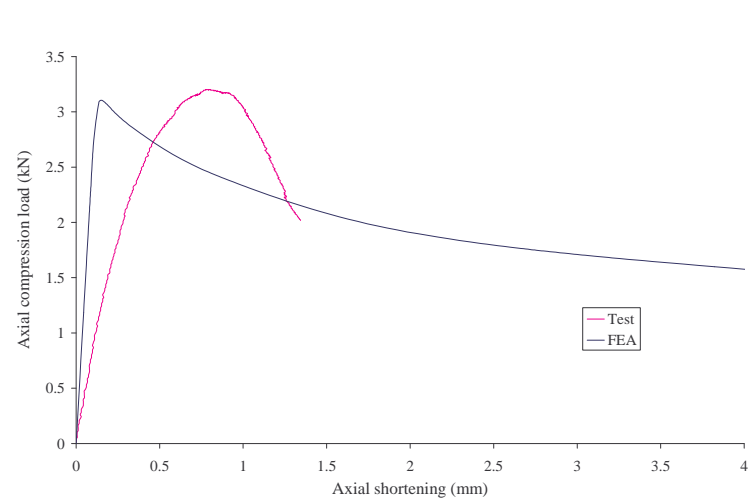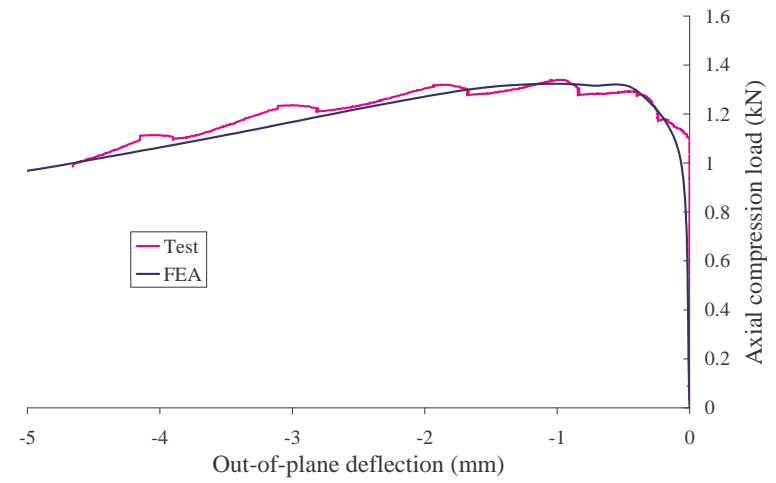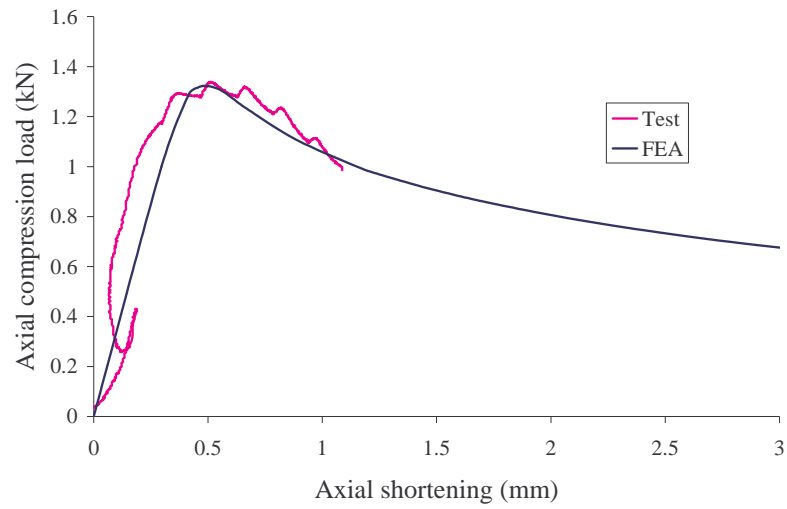
350°C

500°C

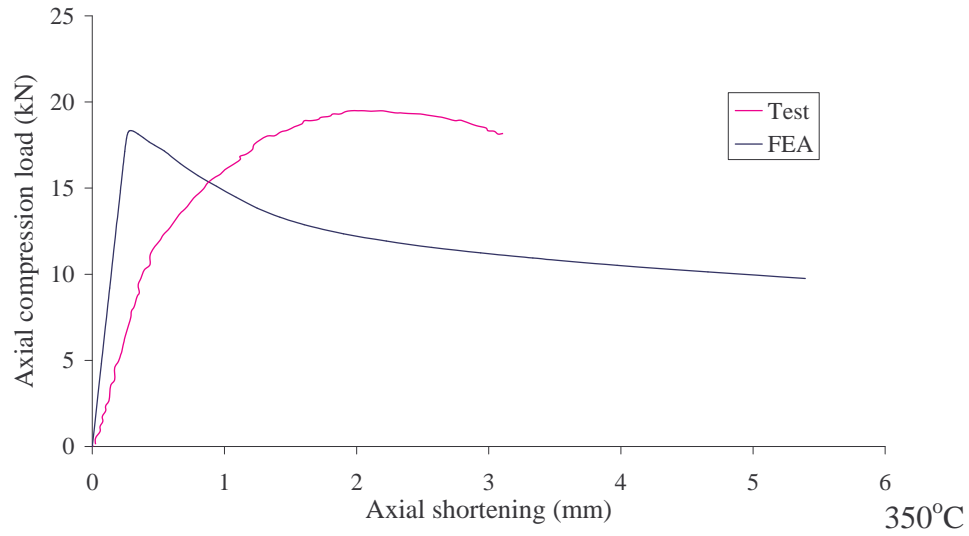650°C

800°C

0.8 mm G550 Type A section
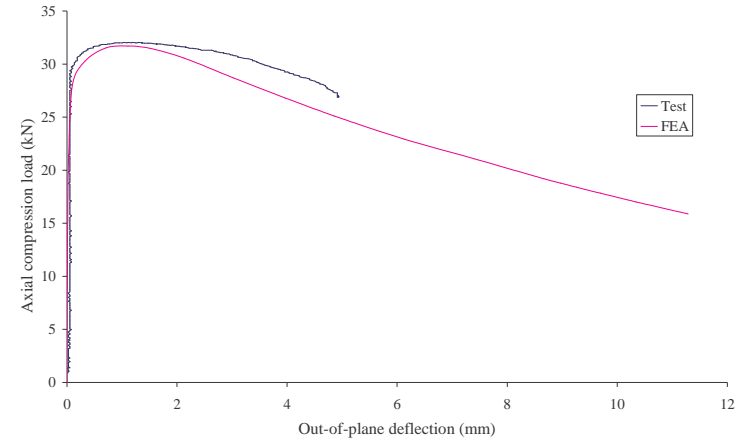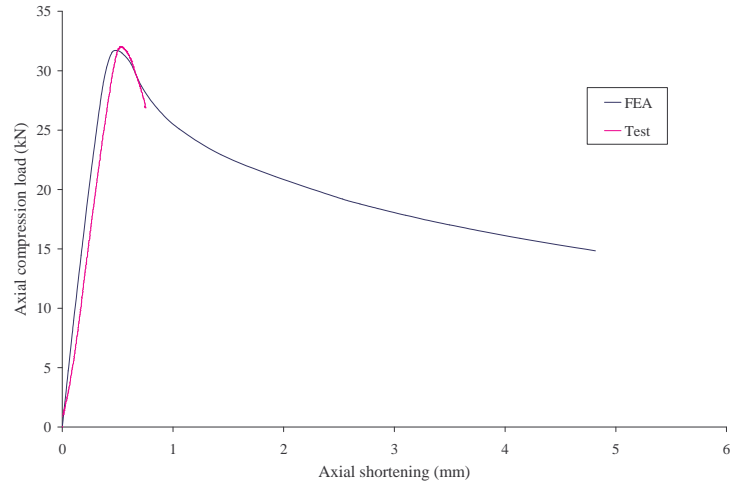
20^oC

200^oC

350°C

500°C

650°C

800°C

0.8 mm G250 Type B section

20°C

200°C

Distortional Buckling Behaviour of Cold-Formed Steel Compression Members at Elevated Temperatures
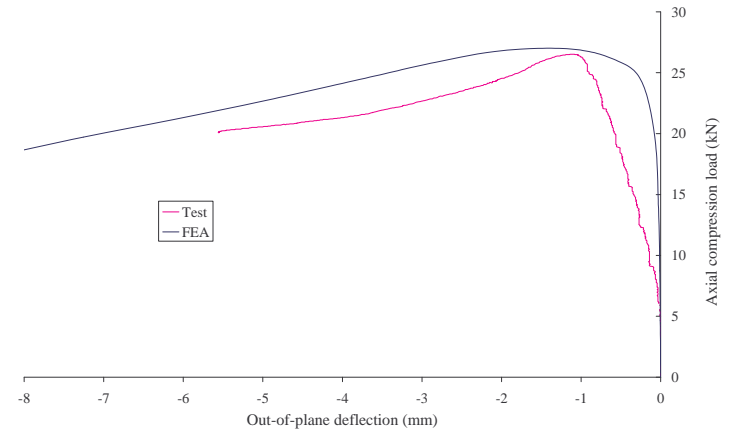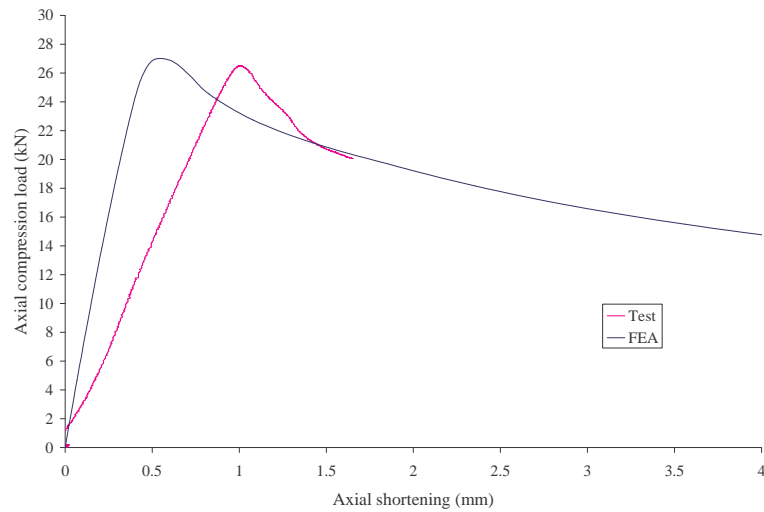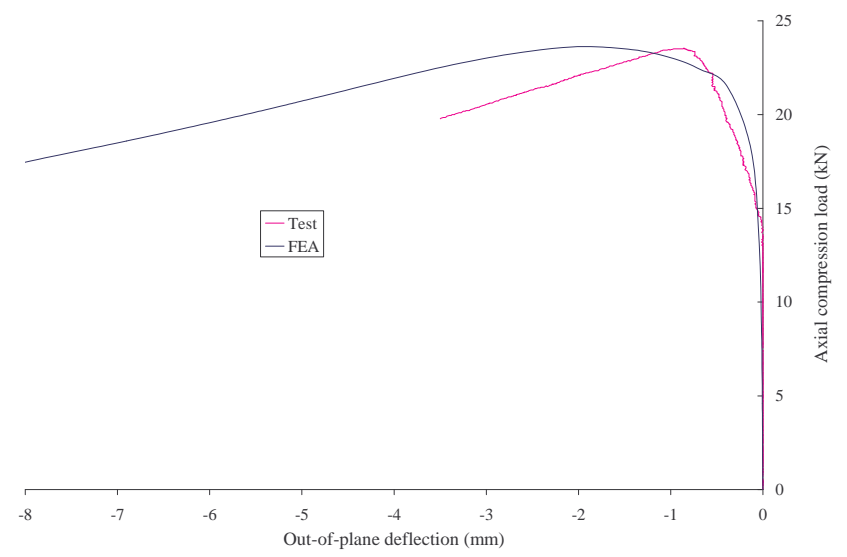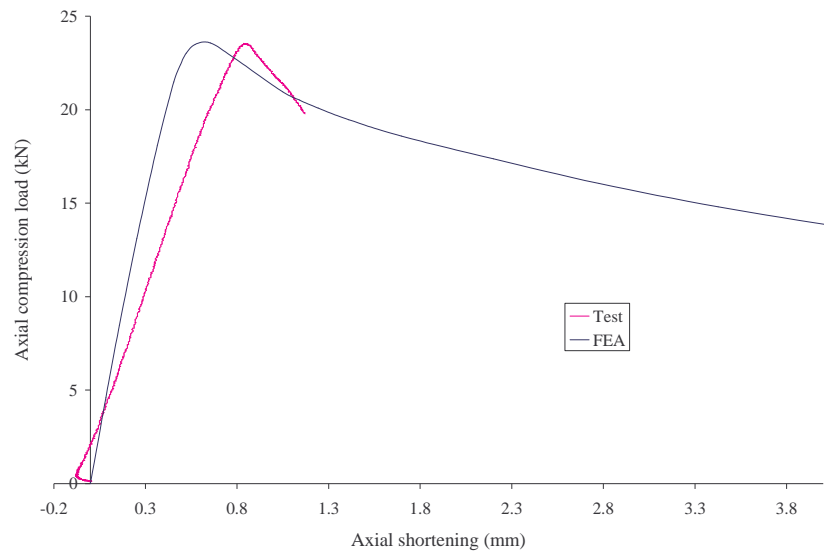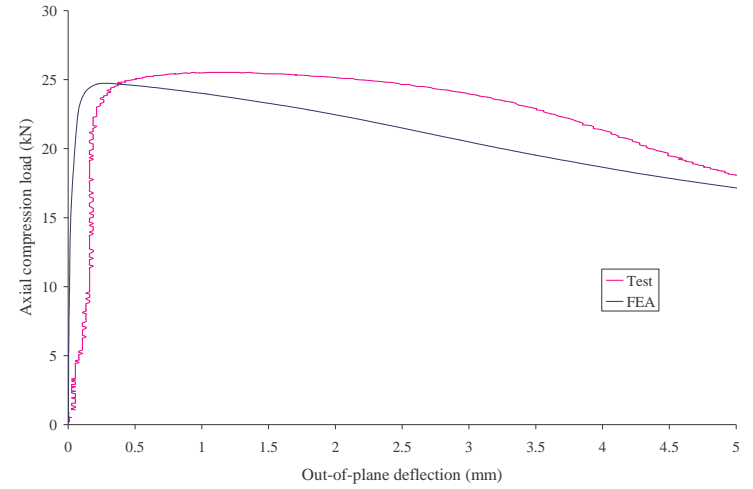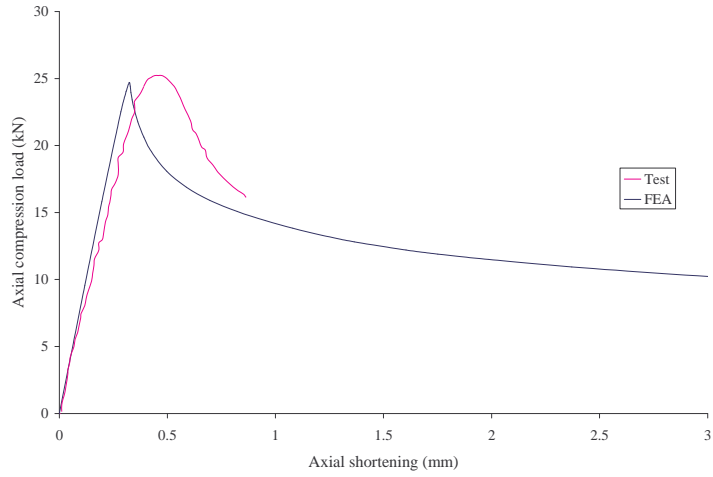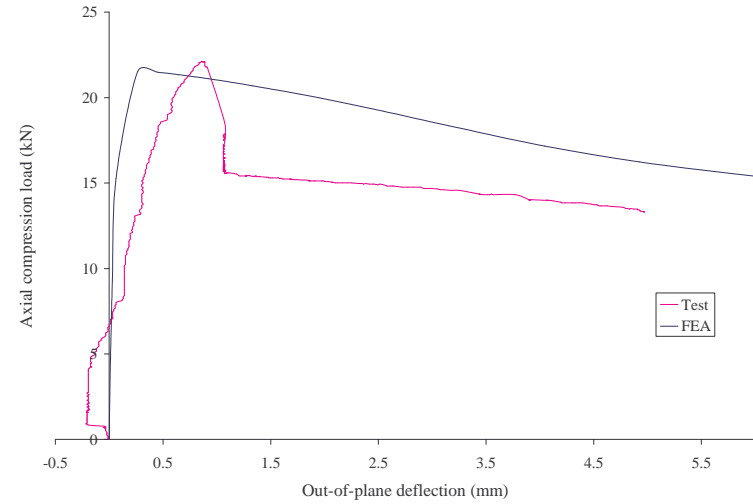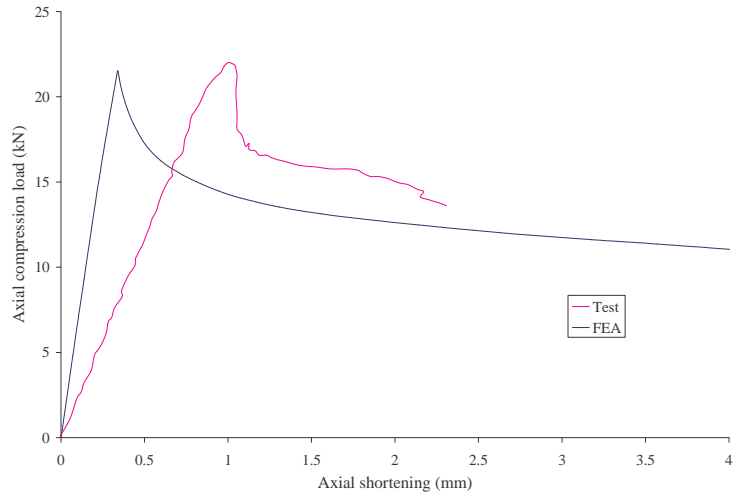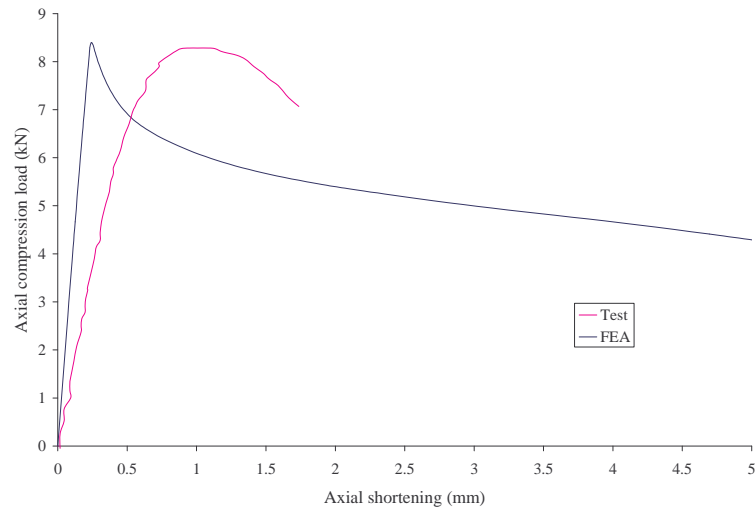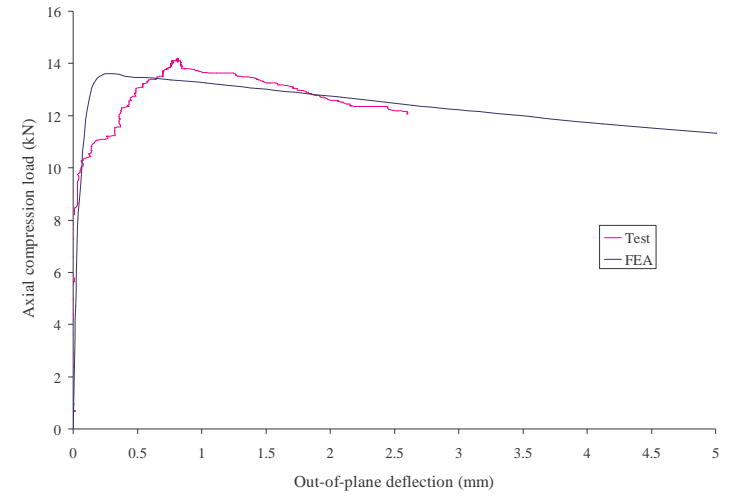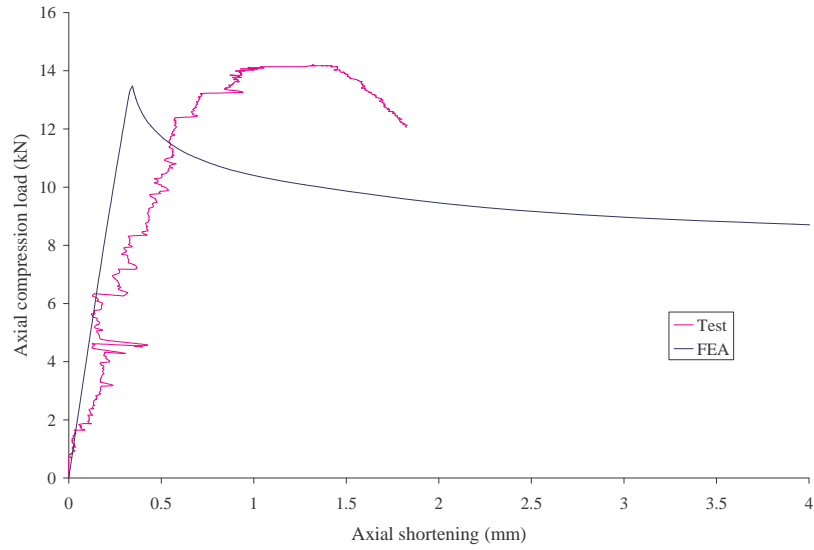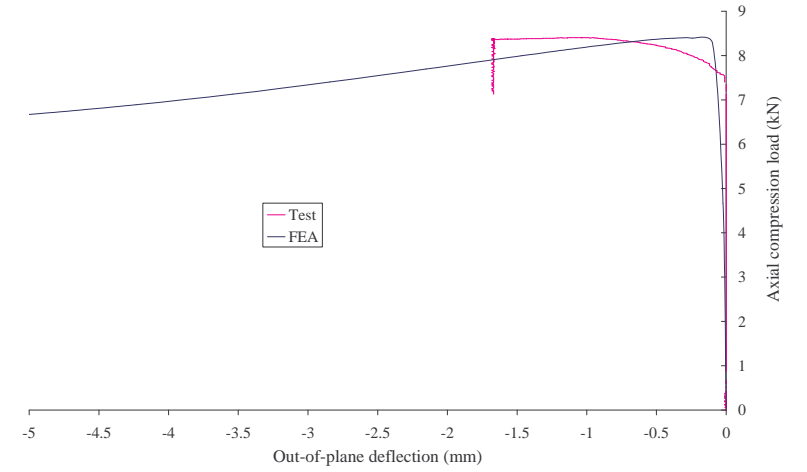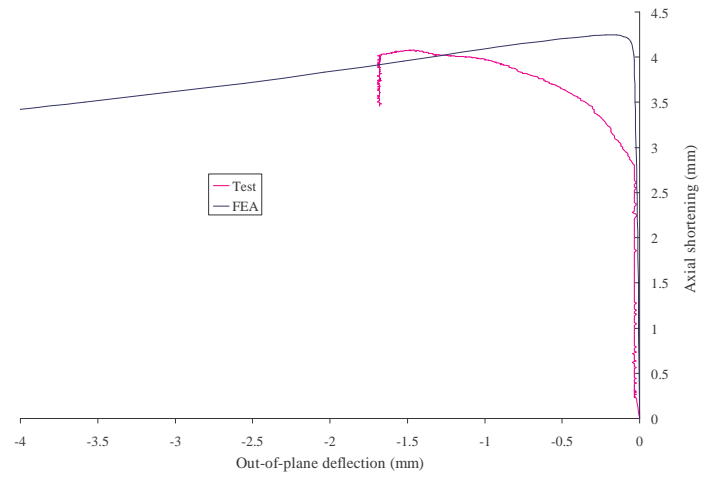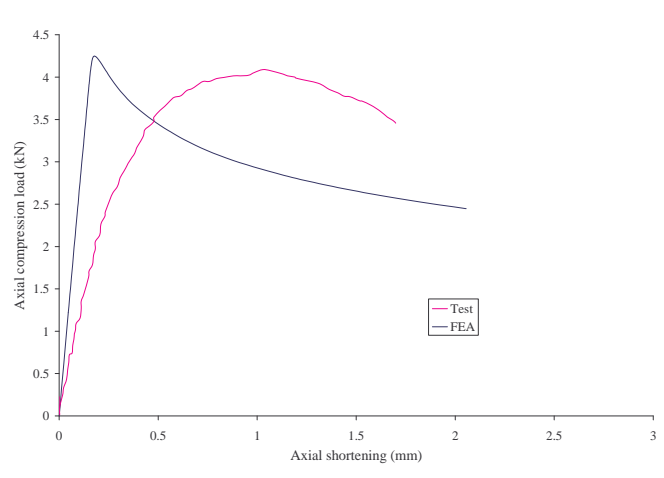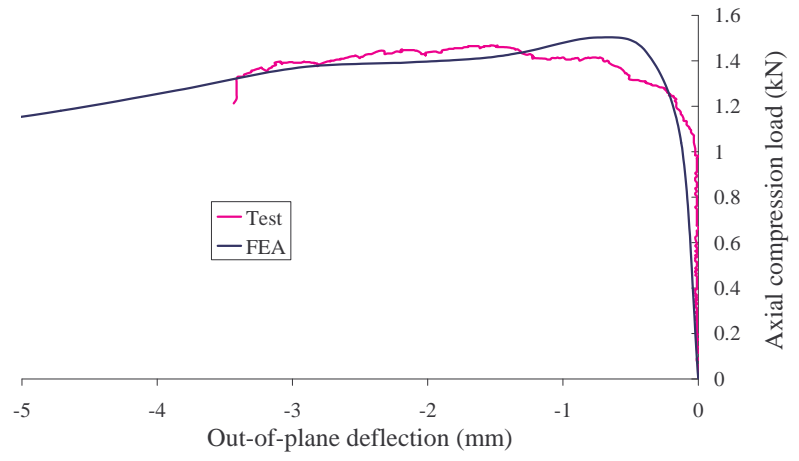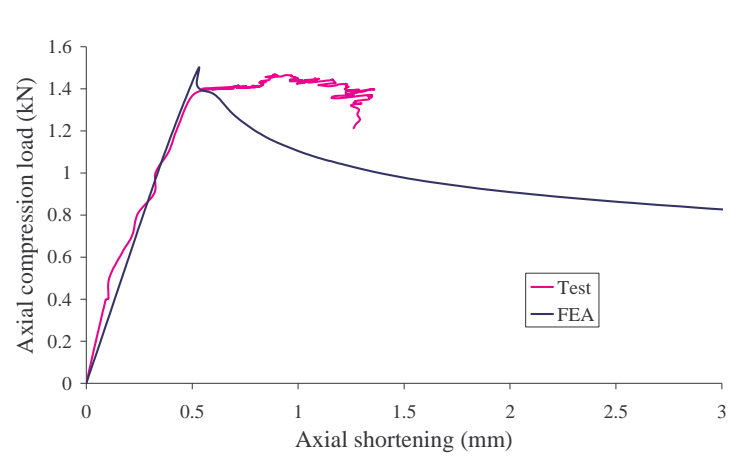
350°C

500°C

650°C

800°C

0.8 mm G550 Type B section

20°C
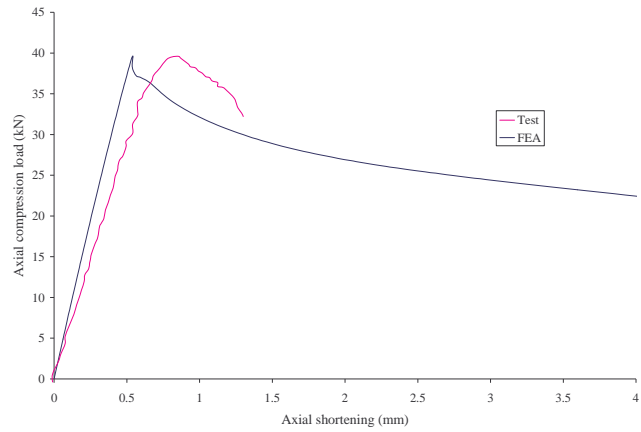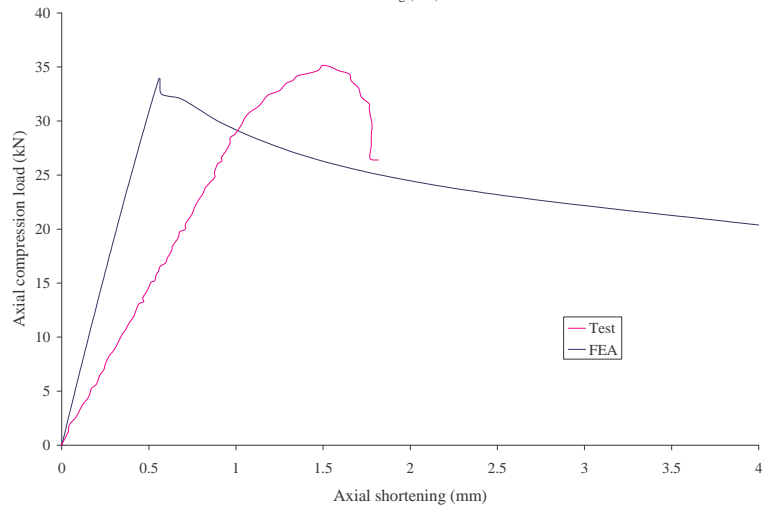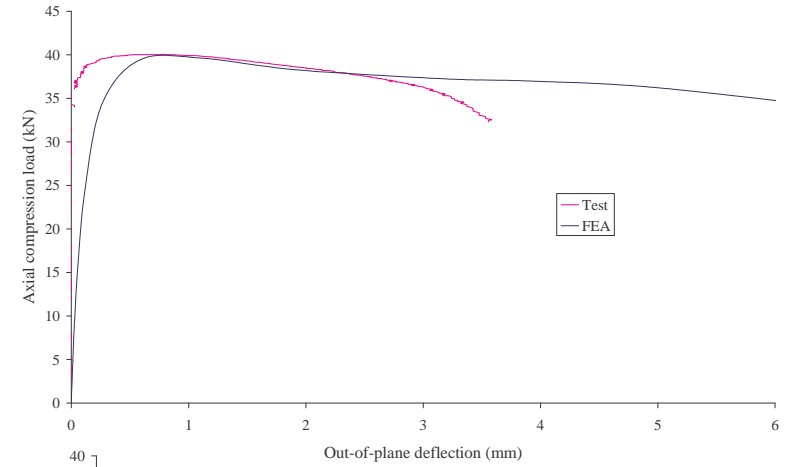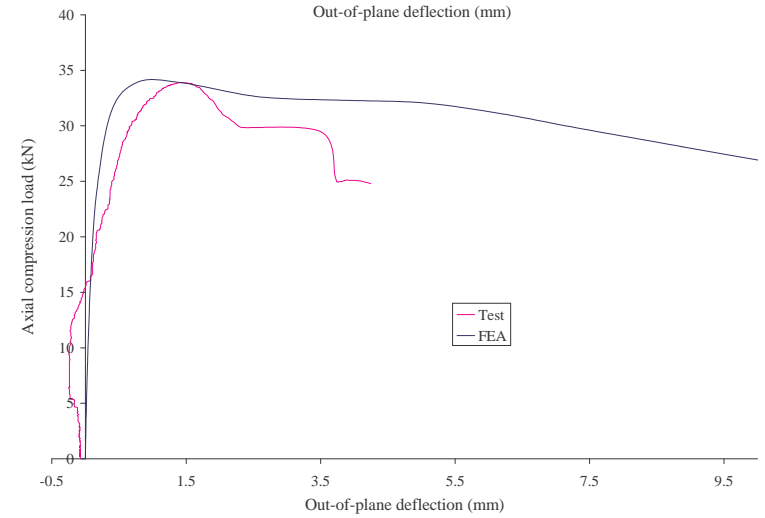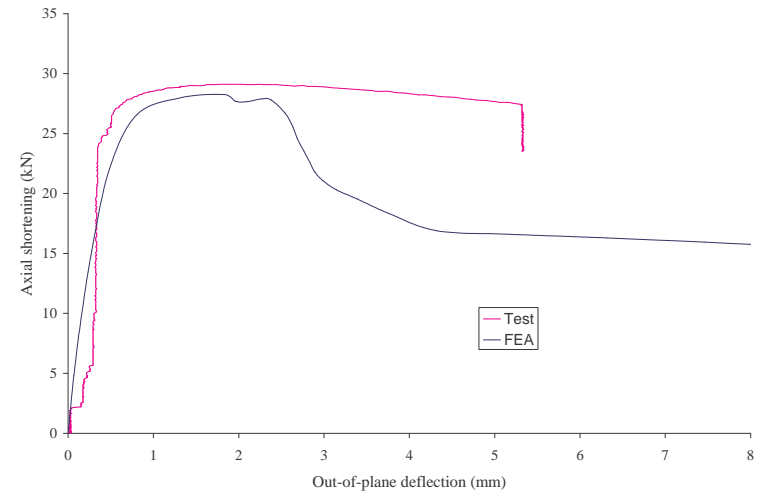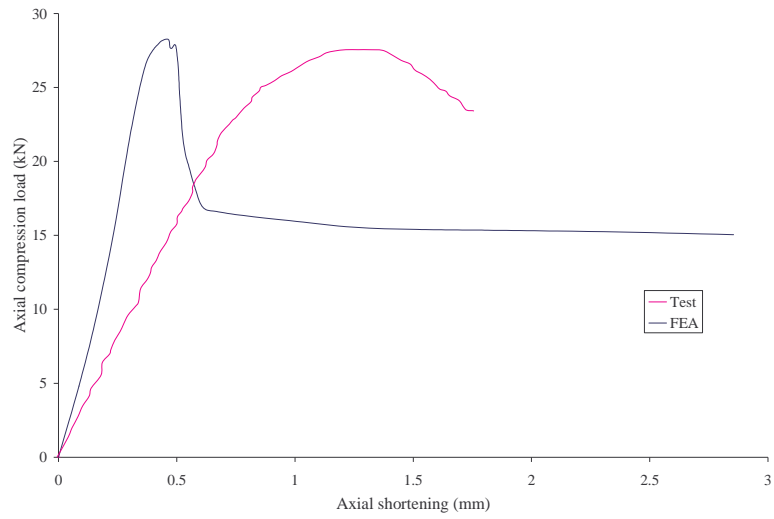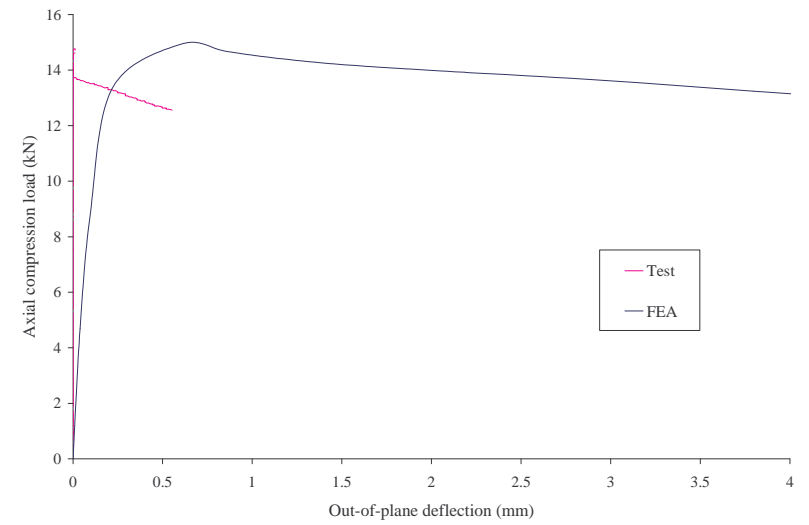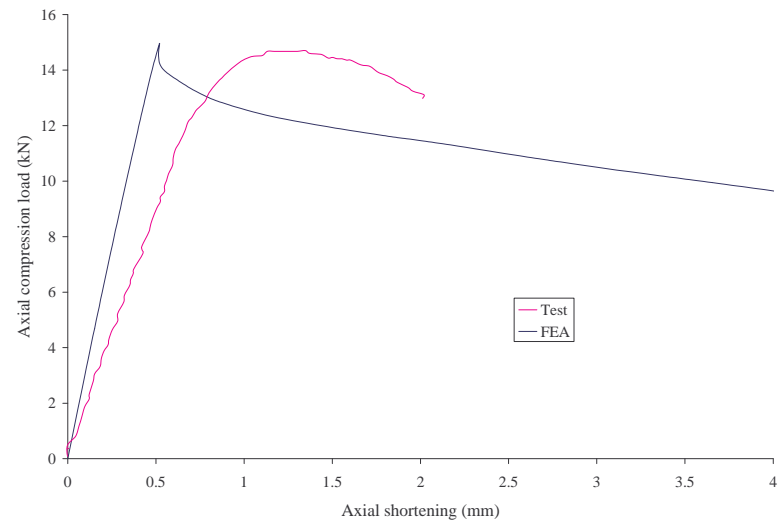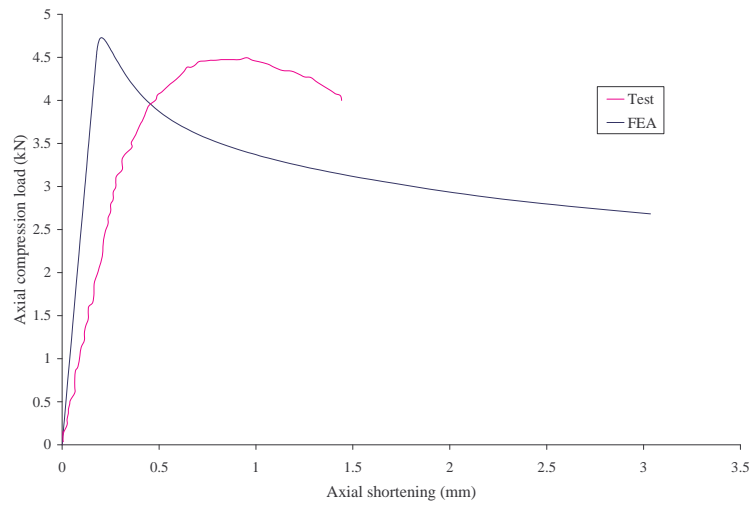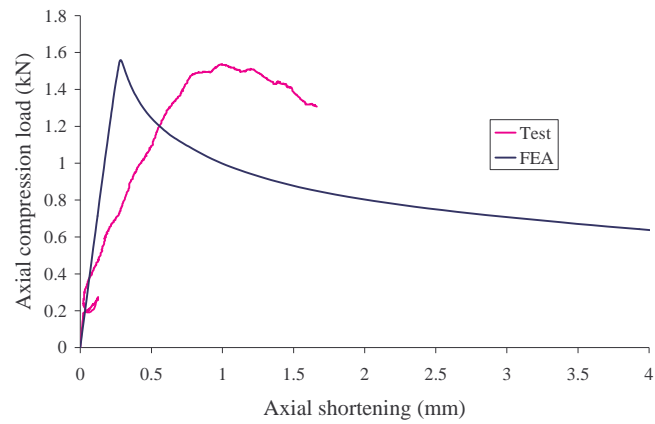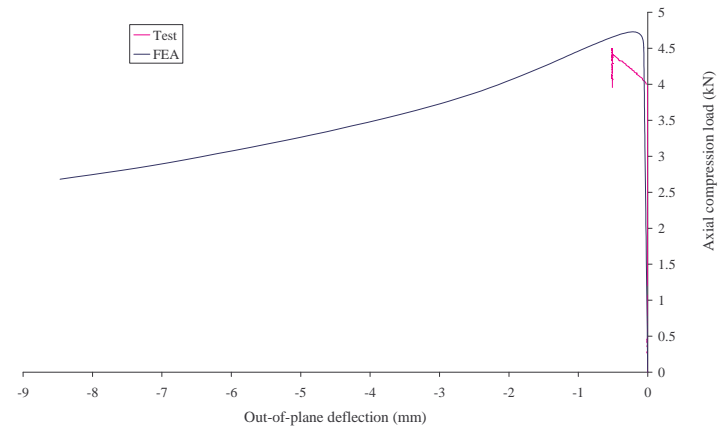
200°C
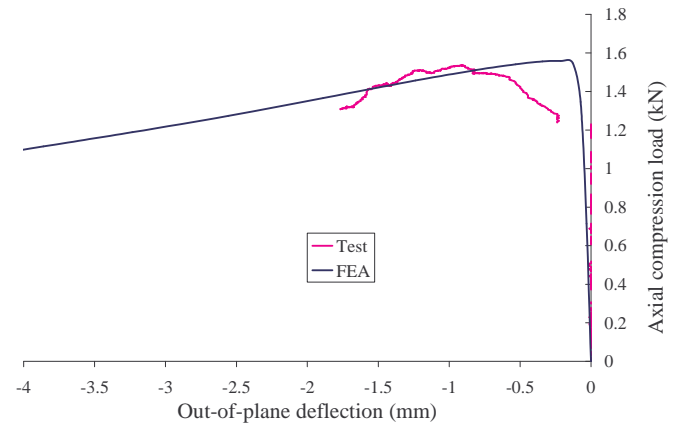
350°C

500°C

650°C

800°C

0.95 mm G250 Type A section

$20^{o}C$

$200^{o}C$
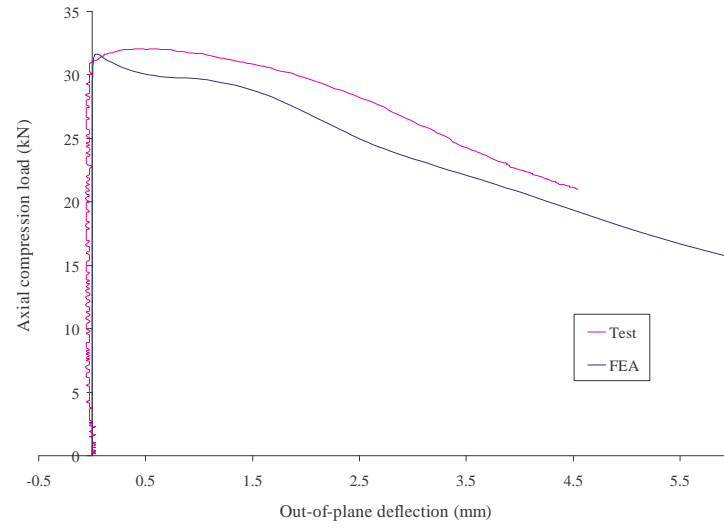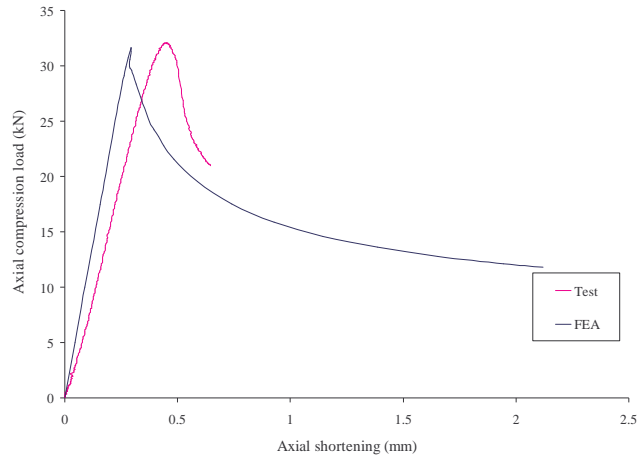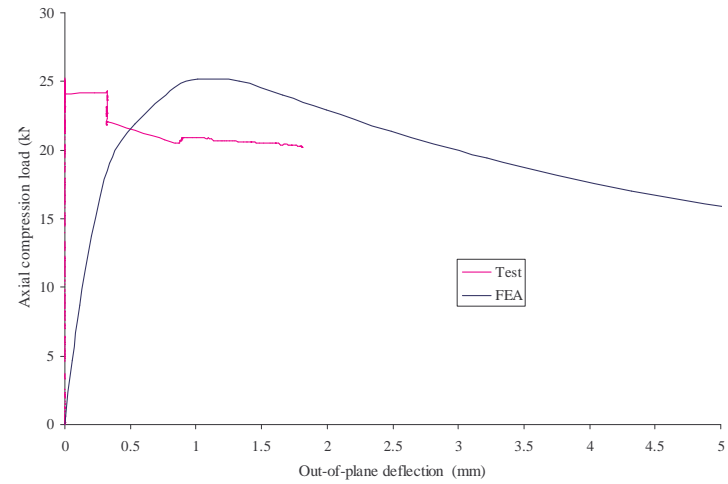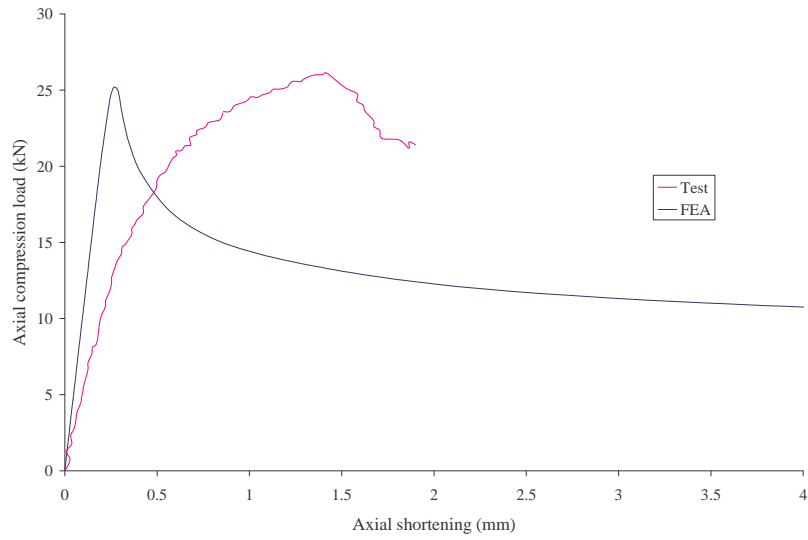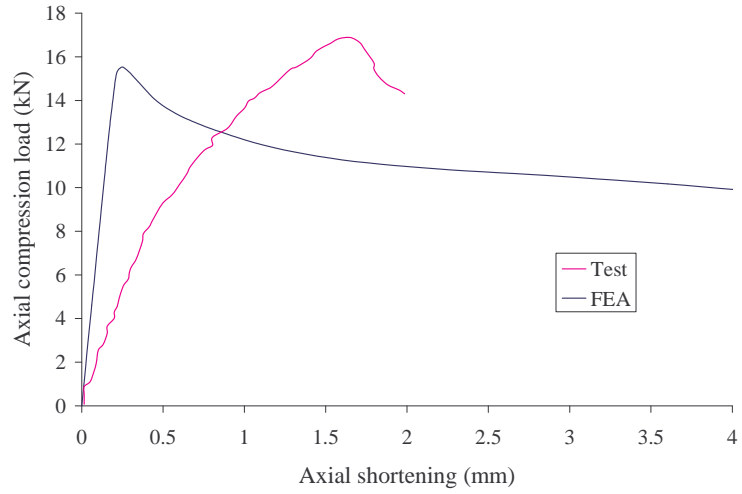
350°C

500°C

650°C

800°C

0.95 mm G550 Type A section

20°C
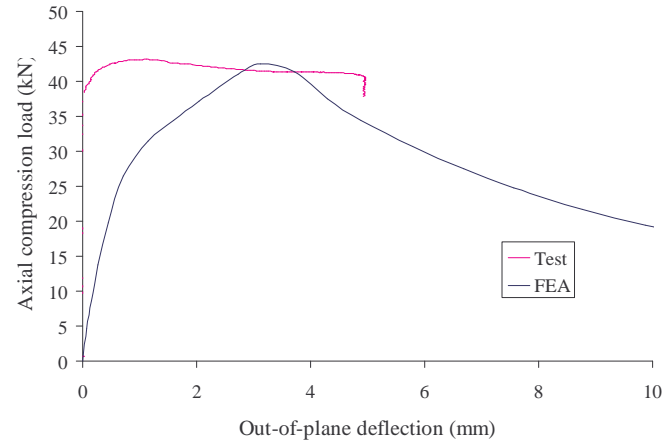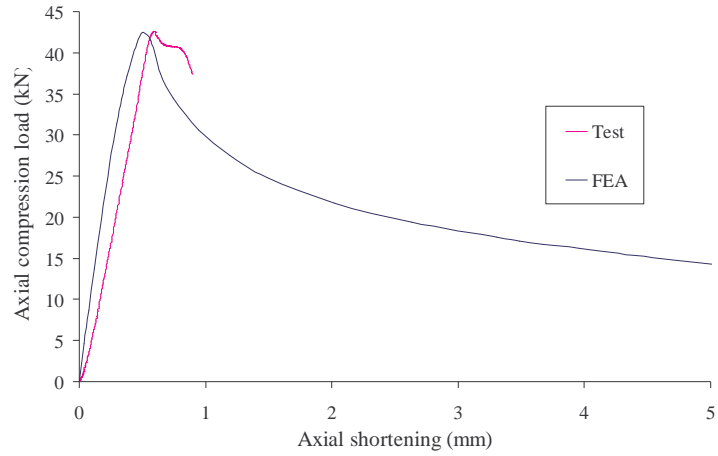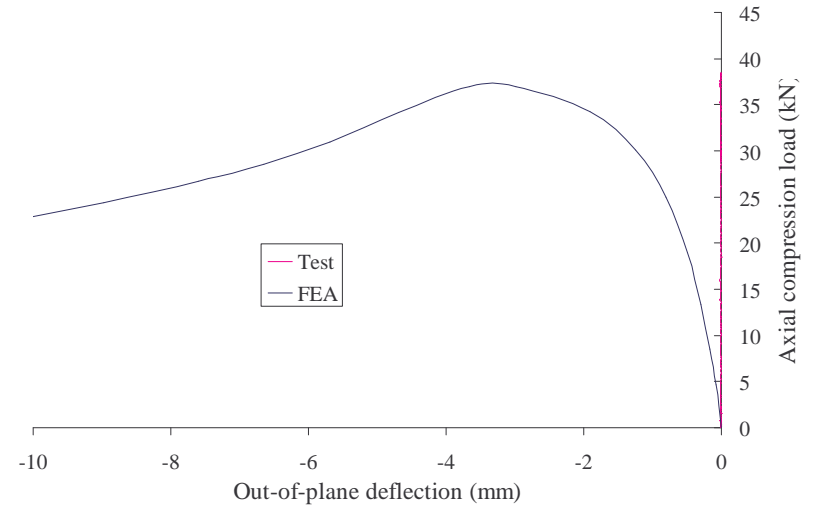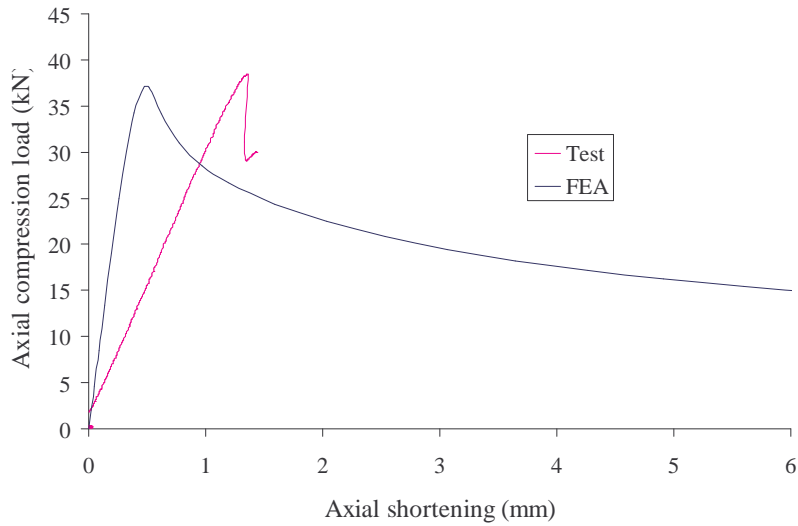
200°C
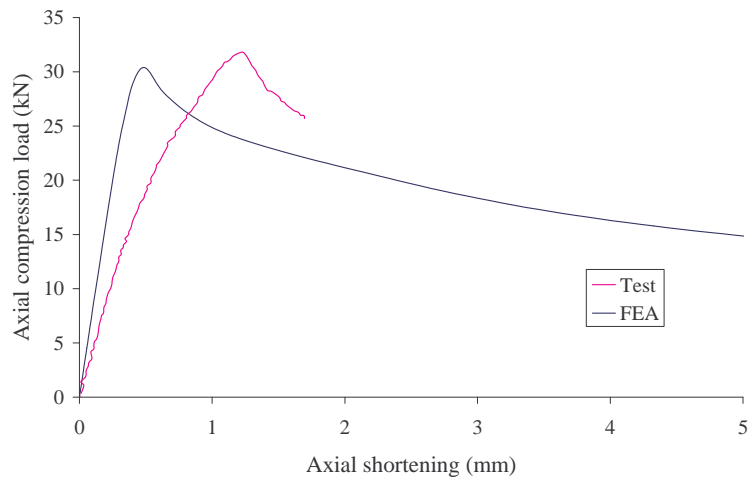
350°C
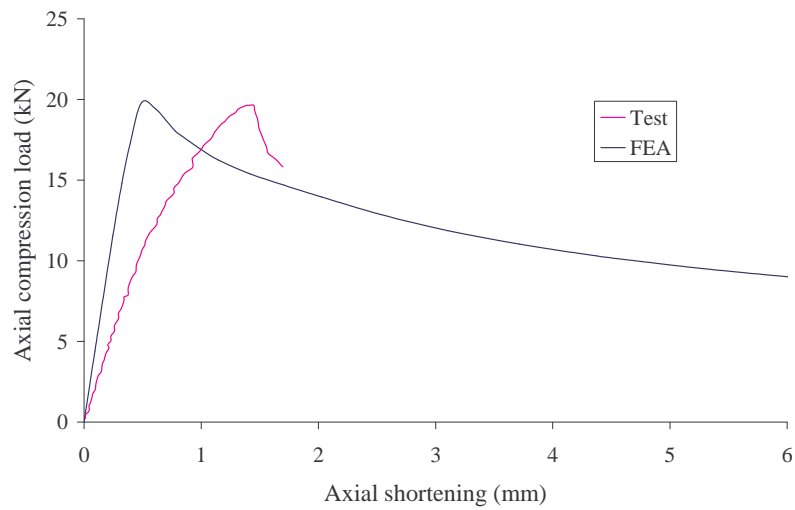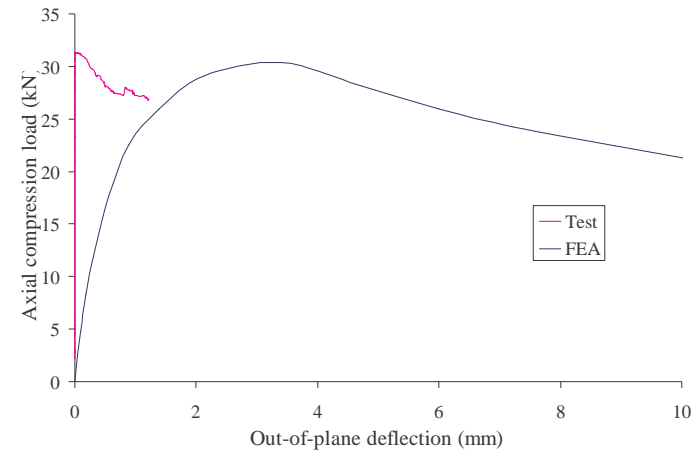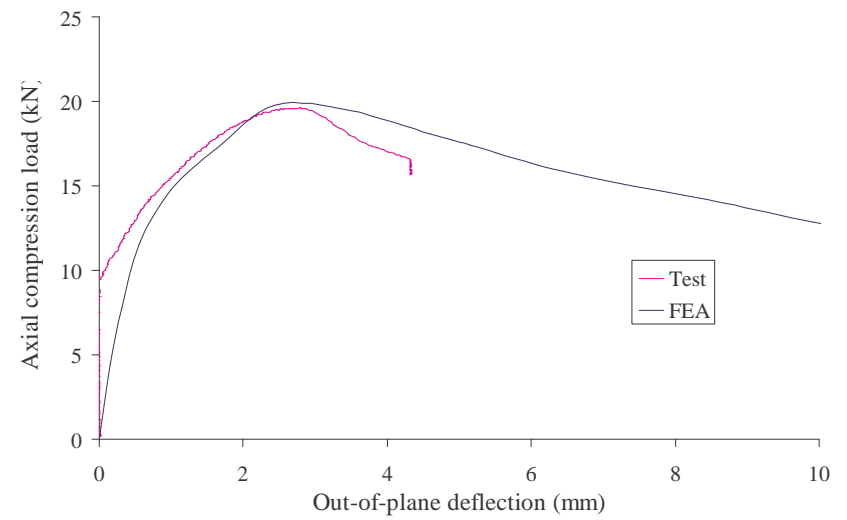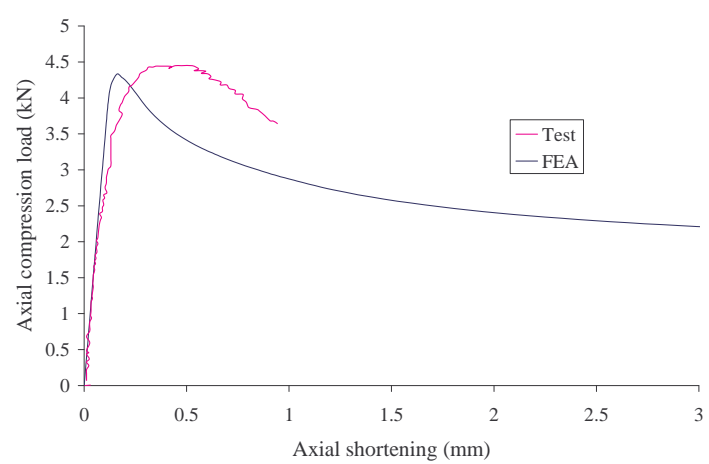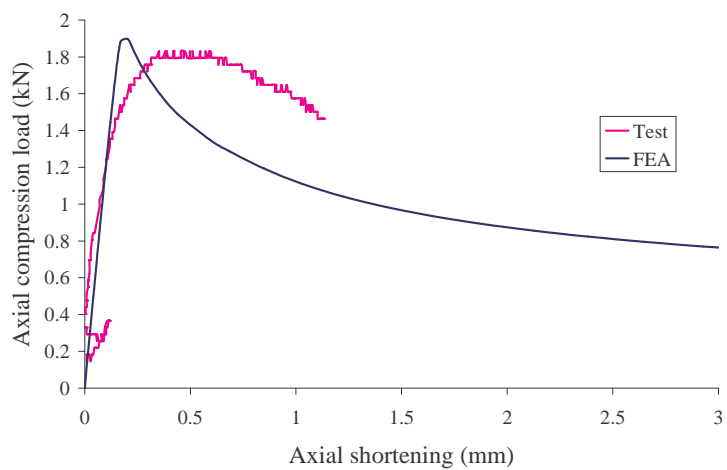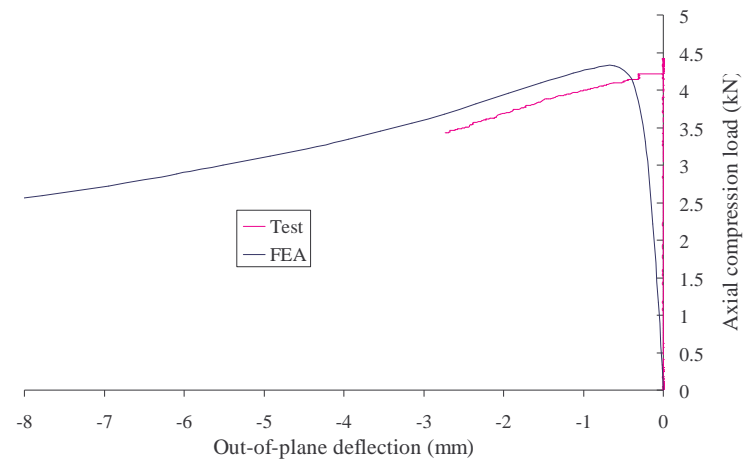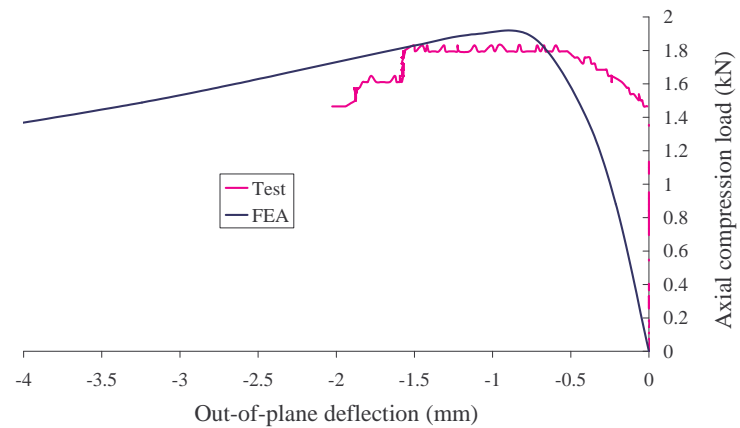
500°C

650°C

800°C

0.95 mm G250 Type B section

20°C
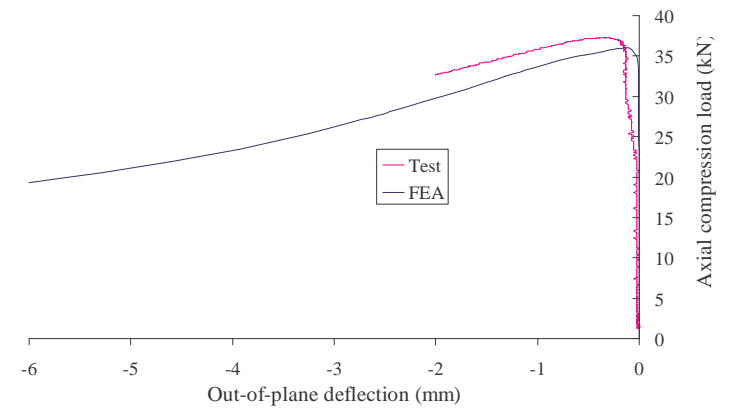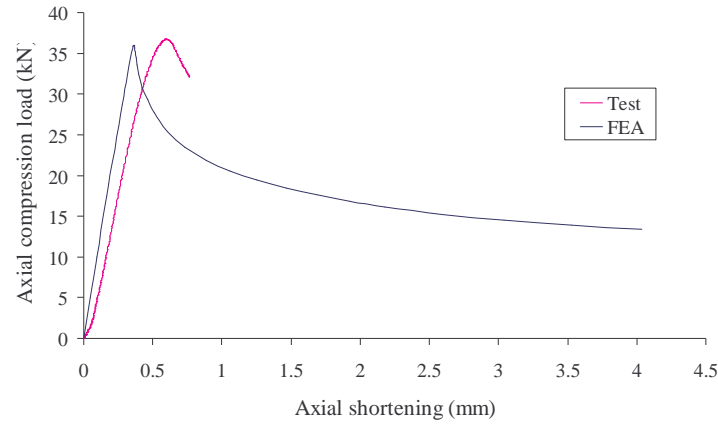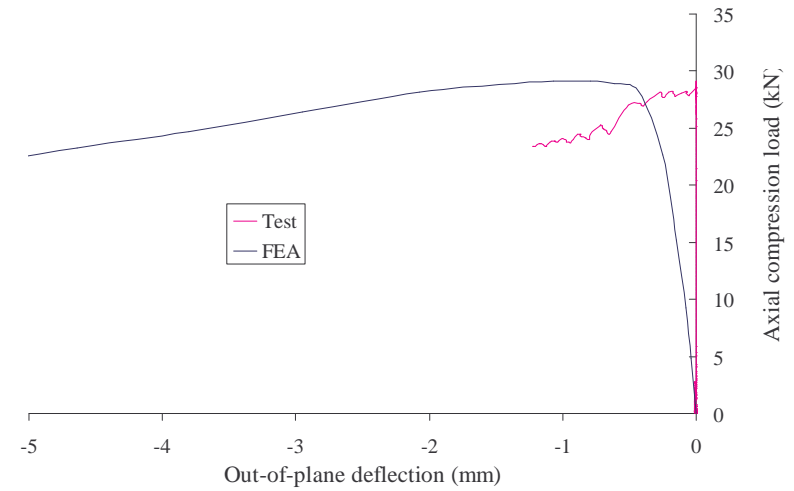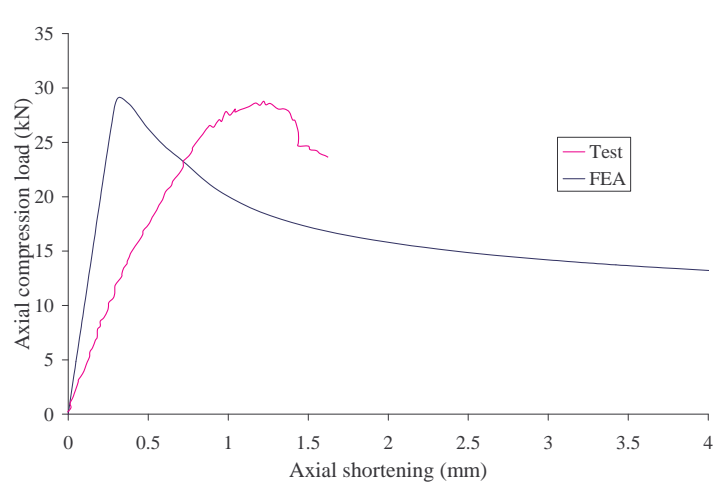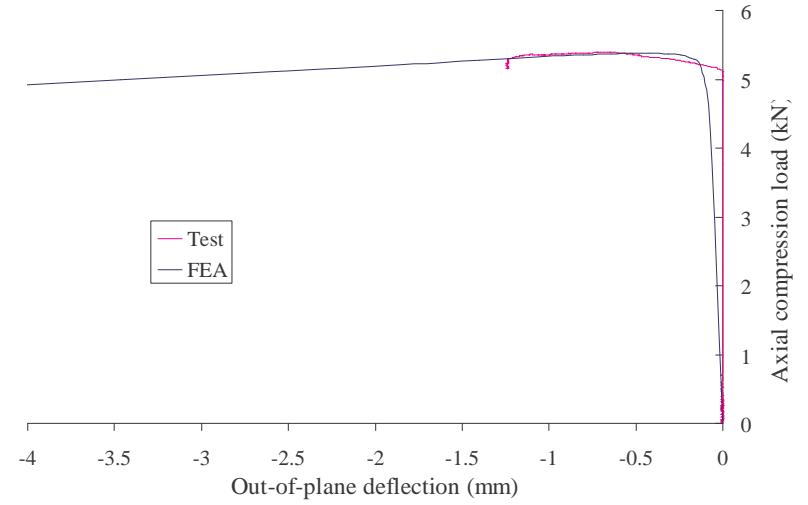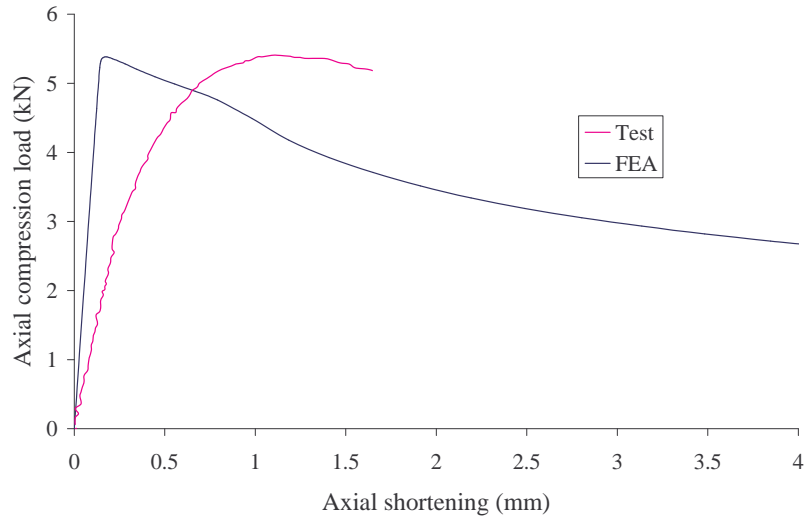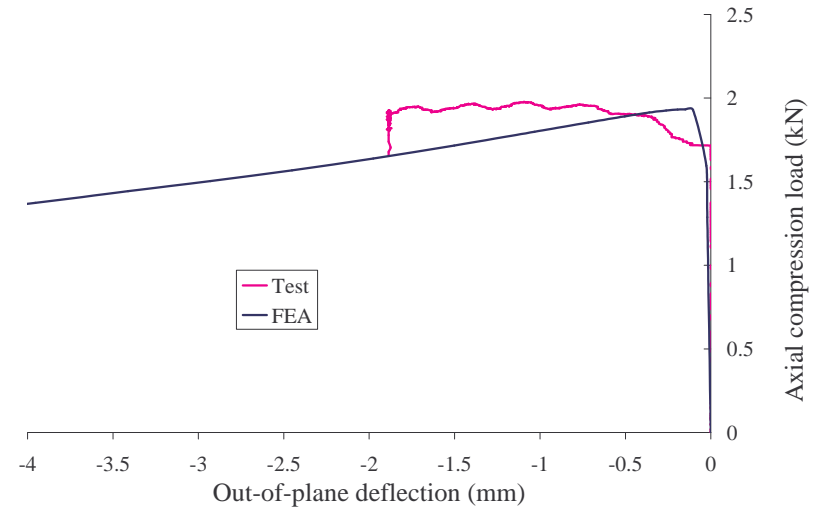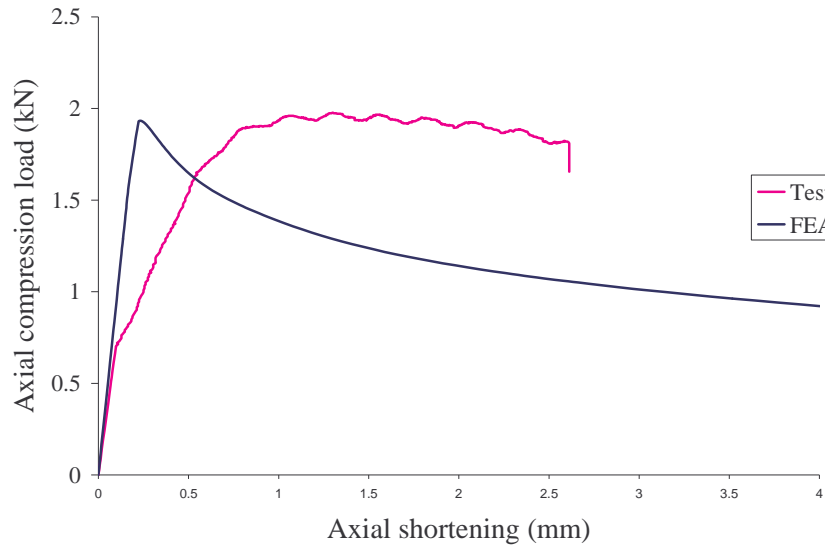
200°C

350°C

500°C

650°C

800°C

0.95 mm G550 Type B section

20°C
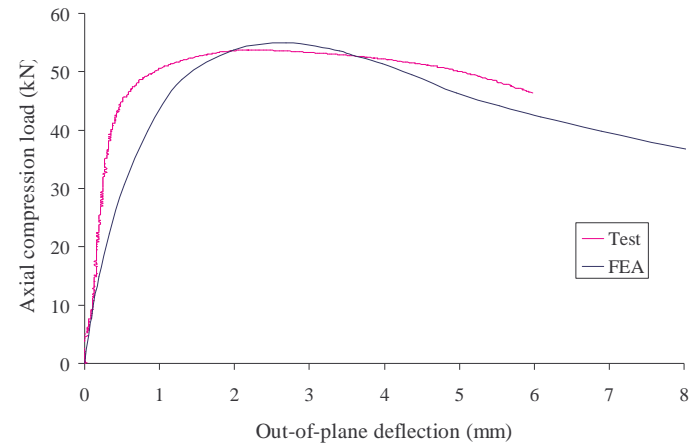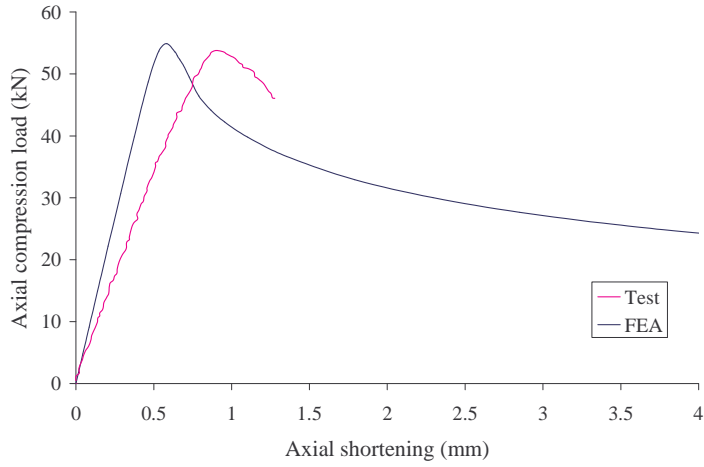
200°C

350°C
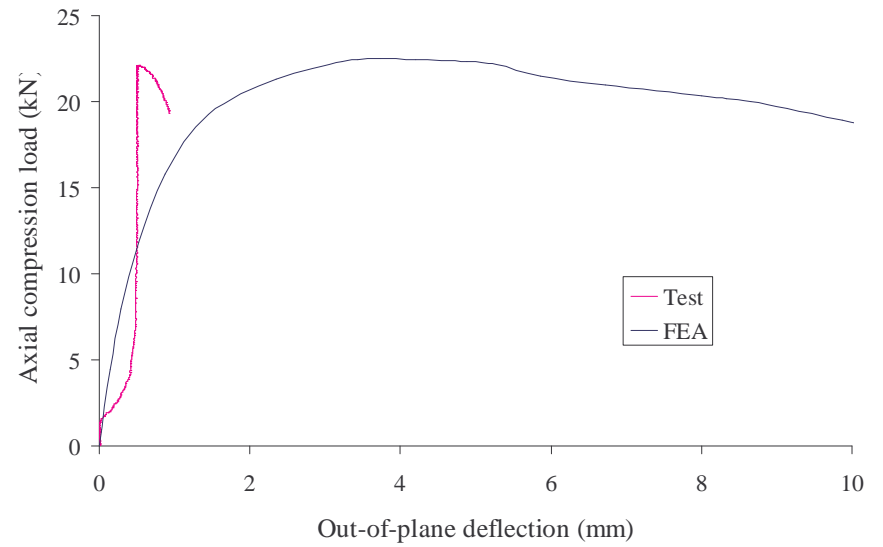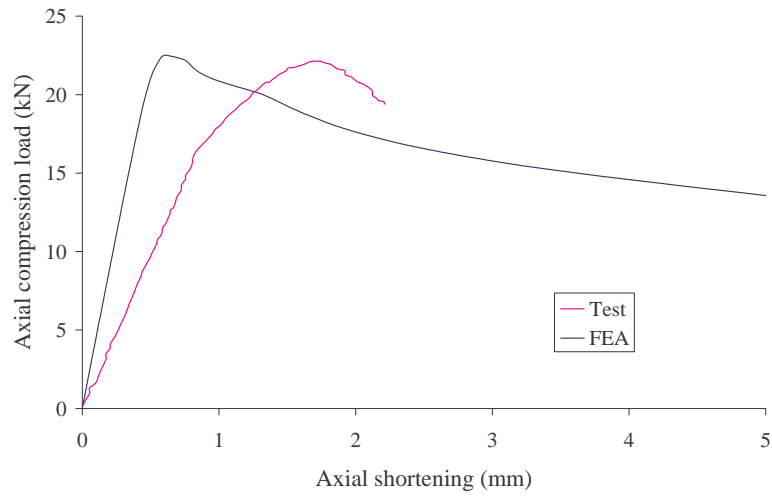
500°C
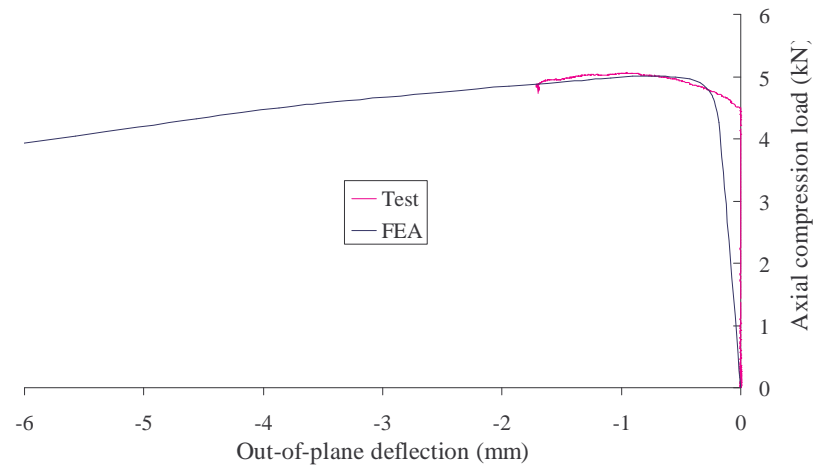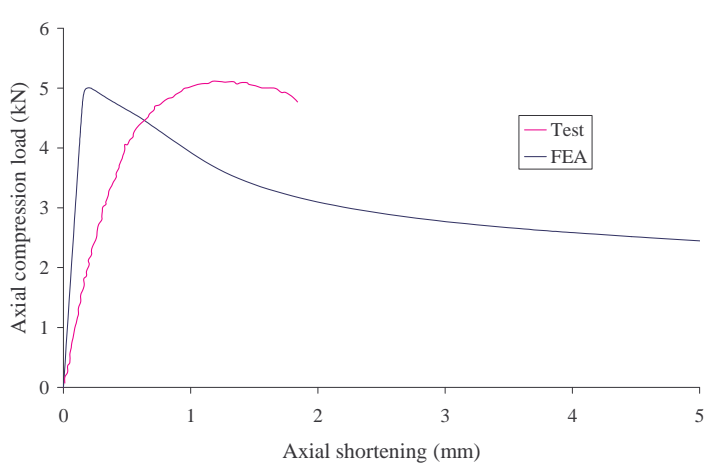
650°C
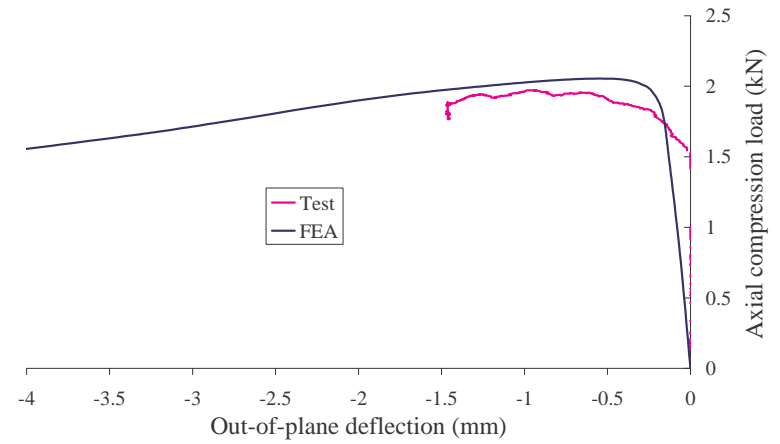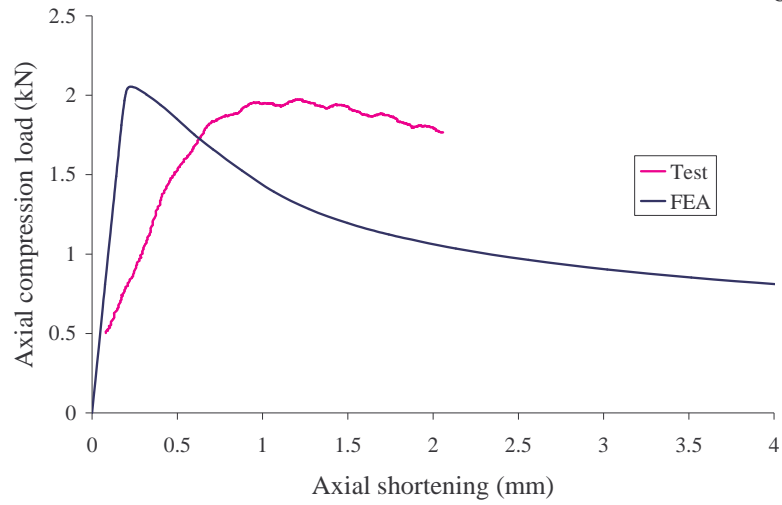
800°C

APPENDIX C

Sample Calculations

Sample Calculations Based on AS/NZS 4600 Design Rules

Ultimate load

G550-0.8-20-A specimen – based on measured dimensions and yield stresses

$A = 80 \text{ mm}^2$

f_y actual $= 610$ MPa
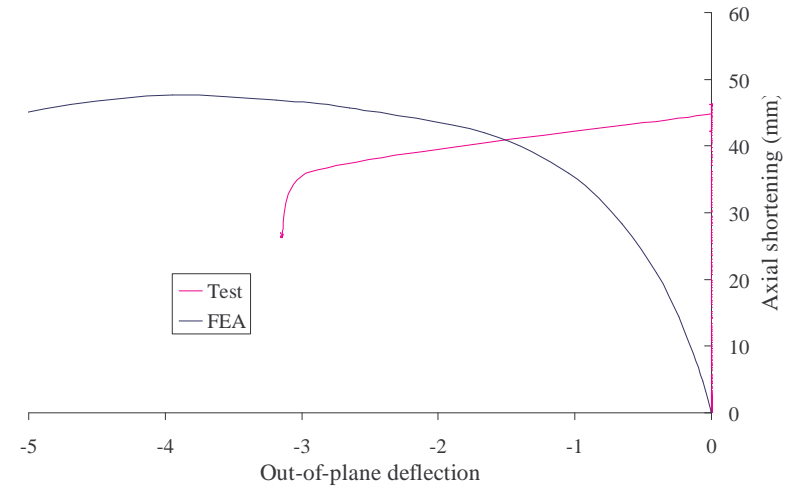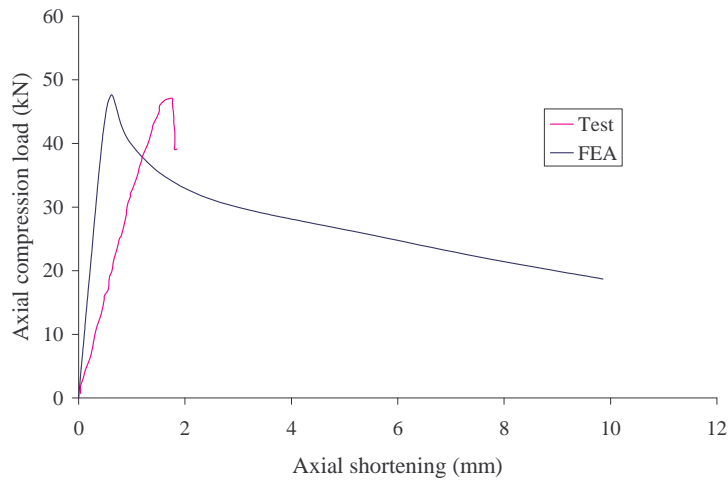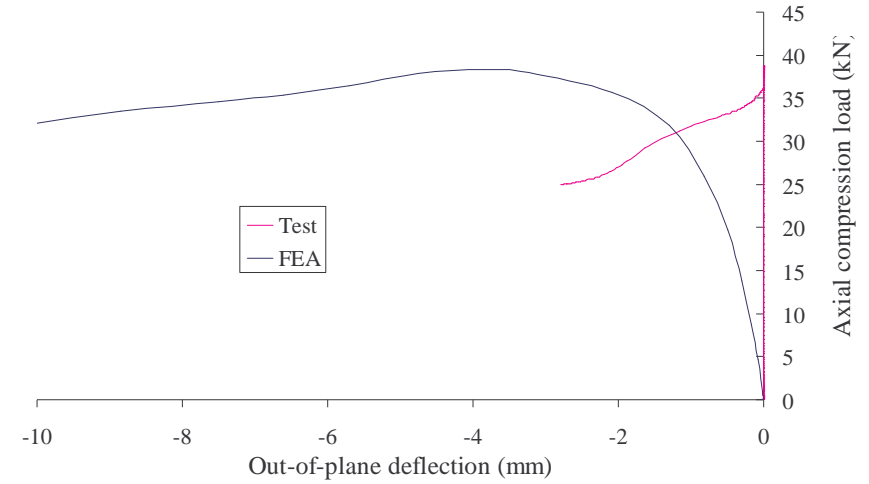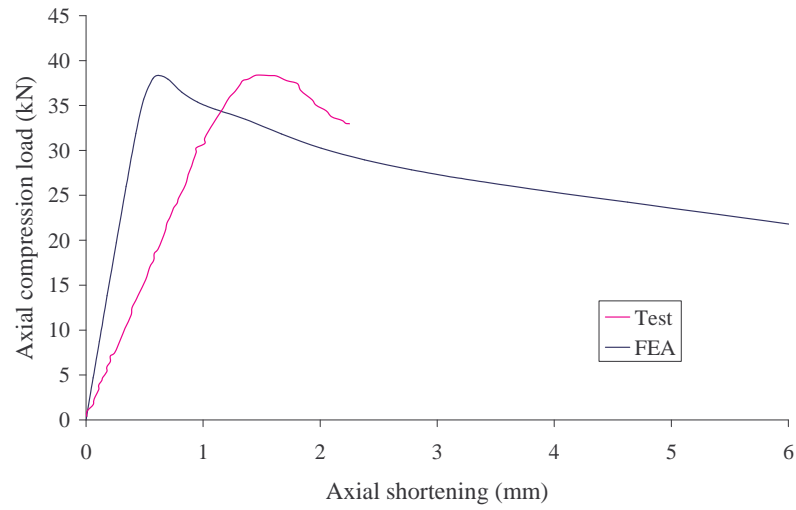
$f_y = 610 \times 0.9$ or 495 MPa whichever is

the lesser $= 495$ MPa

$f_{od} = 550.45$ MPa from ABAQUS

- For $f_{od} > f_y/2$: $P_n = Af_n = Af_y \left(1 - \dfrac{f_y}{4f_{od}} \right)$ clause 3.4.6(1)

- For $f_y/13 \leq f_{od} \leq f_y/2$: $P_n = Af_n = Af_y \left[0.055 \left(\sqrt{\dfrac{f_y}{f_{od}}} - 3.6 \right)^2 + 0.237 \right]$ clause 3.4.6(2)

$f_y/2 = 495/2 = 247.5$ MPa

$\therefore f_{od} > f_y/2$

$P_n = 80 \times 495 \times \left(1 - \dfrac{495}{4 \times 550.45} \right) = 30.7$ kN

G550-0.60-500-A specimen – based on measured dimensions and yield stresses

$A = 60 \text{ mm}^2$

f_y actual $= f_y = 283$ MPa

$f_{od} = 137.68$ MPa from ABAQUS

$f_y/2 = 141.5$ MPa

$\therefore f_{od} < f_y/2$

$$P_n = 60x283x \left| 0.055x \left(\sqrt{\frac{283}{137.68}} - 3.6 \right)^2 + 0.237 \right| = 8.407 \text{ kN}$$

G550-0.8-800-A specimen – based on measured dimensions and yield stresses

A = 80 mm^2

f_y actual = f_y = 31 MPa

f_{od} = 67.75 MPa from ABAQUS

$f_y/2$ = 15.5 MPa

$\therefore f_{od} > f_y/2$

$$P_n = 80x31x \left(1 - \frac{31}{4x67.75} \right) = 2.20 \text{ kN}$$

Sample Calculations Based on Direct Strength Method

$\lambda \leq 0.561$ 　　　　　　$P_n = Af_n = Af_y$

and

$\lambda > 0.561$ 　　　$P_n = Af_n = Af_y \left[1 - 0.25 \left(\frac{f_{od}}{f_y} \right)^{0.6} \right] \left[\frac{f_{od}}{f_y} \right]^{0.6}$

where, 　　　　　$\lambda = \sqrt{\frac{f_y}{f_{od}}}$

G550-0.8-20-A specimen – based on measured dimensions and yield stresses

A = 80 mm^2

f_y actual = 610 MPa

f_y = 610x0.9 or 495 MPa whichever is the lesser = 495 MPa

f_{od} = 550.45 from ABAQUS

$$\lambda = \sqrt{\frac{495}{550.45}} = 0.948$$

$\therefore \lambda > 0.561$

$$P_n = 80x495 \left[1 - 0.25 \left(\frac{550.45}{495} \right)^{0.6} \right] \left[\frac{550.45}{495} \right]^{0.6} = 30.96 \text{ kN}$$

APPENDIX D

Residual Stresses for G550 Type A 0.6 mm Specimen

```
SUBROUTINE SIGINI(SIGMA,COORDS,NTENS,NCRDS,NOEL,NPT,LAYER,KSPT)
INCLUDE'ABA_PARAM.INC'
REAL X,Y,Z,nipt,ipt,fy,fn
DIMENSION SIGMA(NTENS),COORDS(NCRDS)
C
nipt=5.
fy=647
X=COORDS(1)
Y=COORDS(2)
Z=COORDS(3)
C
IF(KSPT.EQ.1)THEN
                                    ipt=1.
ELSEIF(KSPT.EQ.2)THEN
                                    ipt=2.
ELSEIF(KSPT.EQ.3)THEN
                                    ipt=3.
ELSEIF(KSPT.EQ.4)THEN
                                    ipt=4.
ELSEIF(KSPT.EQ.5)THEN
                                    ipt=5.
ENDIF
C
IF((NOEL.GE.1).AND.(NOEL.LE.40))THEN
                                    fn=0.08*0.76*fy
ELSEIF((NOEL.GE.401).AND.(NOEL.LE.440))THEN
                                    fn=0.08*0.76*fy
ELSEIF((NOEL.GE.41).AND.(NOEL.LE.400))THEN
                                    fn=0.17*0.76*fy
ELSE
                                    fn=0.
ENDIF
C
IF(fn.NE.0.)THEN
                                    SIGMA(2)=fn*(1.-2.*(nipt-ipt)/(nipt-
                                    1.))
ELSE
                                    SIGMA(2)=0.
ENDIF
C
SIGMA(1)=0.
SIGMA(3)=0.
RETURN
END
```

Residual Stresses for G550 Type B 0.6 mm Specimen

```
        SUBROUTINE SIGINI(SIGMA,COORDS,NTENS,NCRDS,NOEL,NPT,LAYER,KSPT)
        INCLUDE'ABA_PARAM.INC'
        REAL X,Y,Z,nipt,ipt,fy,fn
        DIMENSION SIGMA(NTENS),COORDS(NCRDS)
C
        nipt=5.
        fy=647
        X=COORDS(1)
        Y=COORDS(2)
        Z=COORDS(3)
C
        IF(KSPT.EQ.1)THEN
                                        ipt=1.
        ELSEIF(KSPT.EQ.2)THEN
                                        ipt=2.
        ELSEIF(KSPT.EQ.3)THEN
                                        ipt=3.
        ELSEIF(KSPT.EQ.4)THEN
                                        ipt=4.
        ELSEIF(KSPT.EQ.5)THEN
                                        ipt=5.
        ENDIF
C
        IF((NOEL.GE.1).AND.(NOEL.LE.56))THEN
                                        fn=0.08*0.76*fy
        ELSEIF((NOEL.GE.729).AND.(NOEL.LE.784))THEN
                                        fn=0.08*0.76*fy
        ELSEIF((NOEL.GE.57).AND.(NOEL.LE.728))THEN
                                        fn=0.17*0.76*fy
        ELSE
                                        fn=0.
        ENDIF
C
        IF(fn.NE.0.)THEN
                                        SIGMA(2)=fn*(1.-2.*(nipt-ipt)/(nipt-
                                        1.))
        ELSE
                                        SIGMA(2)=0.
        ENDIF
C
        SIGMA(1)=0.
        SIGMA(3)=0.
        RETURN
        END
```

APPENDIX E

Sample Calculations

Ultimate Load

Type A Section of G550-0.6-25-25-5

Sample Calculations Based on AS/NZS 4600 Design Rules
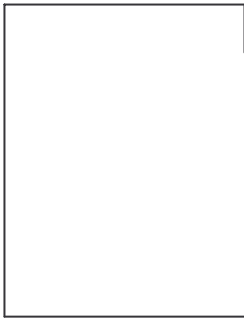
$A = 51 \text{ mm}^2$

$f_y = 678 \text{ MPa}$

$f_{od} = 608 \text{ MPa from ABAQUS}$

- For $f_{od} > f_y/2$: $P_n = Af_n = Af_y\left(1 - \dfrac{f_y}{4f_{od}}\right)$ clause 3.4.6(1)

- For $f_y/13 \leq f_{od} \leq f_y/2$: $P_n = Af_n = Af_y\left[0.055\left(\sqrt{\dfrac{f_y}{f_{od}}} - 3.6\right)^2 + 0.237\right]$ clause 3.4.6(2)

$f_y/2 = 339 \text{ MPa}$

$\therefore f_{od} > f_y/2$

$P_n = 51x678x\left(1 - \dfrac{678}{4x608}\right) = 24.9 \text{ kN}$

$\dfrac{f_n}{f_y} = \dfrac{24.9x1000}{51x678} = 0.720$

$\sqrt{\dfrac{fy}{fod}} = \sqrt{\dfrac{678}{608}} = 1.056$

Sample Calculations Based on Direct Strength Method

$\lambda \leq 0.561$

$$P_n = Af_n = Af_y$$

$\lambda > 0.561$

$$P_n = Af_n = Af_y\left[1 - 0.25\left(\frac{f_{od}}{f_y}\right)^{0.6}\right]\left[\frac{f_{od}}{f_y}\right]^{0.6}$$

where,

$$\lambda = \sqrt{\frac{f_y}{f_{od}}}$$

$$\lambda = \sqrt{\frac{f_y}{f_{od}}} = \sqrt{\frac{678}{608}} = 1.056 > 0.561$$

$$P_n = 51x678\left[1 - 0.25\left(\frac{608}{678}\right)^{0.6}\right]\left[\frac{608}{678}\right]^{0.6} = 24.8 \text{ kN}$$

Sample Calculations Based on Equation 6.10 at 100°C

$\lambda < 0.55$ $\quad P_{nT} = Af_{nT} = Af_{yT}$

$\lambda \geq 0.55$ $\quad P_{nT} = Af_{nT} = Af_{yT}\left(1 - 0.31\left(\frac{f_{odT}}{f_{yT}}\right)^{0.4}\right)\left(\frac{f_{odT}}{f_{yT}}\right)^{0.58}$

Where, $\quad \lambda = \sqrt{\frac{f_{yT}}{f_{odT}}}$

$A = 51 \text{ mm}^2$

$f_{yT} = 667 \text{ MPa}$

$f_{odT} = 608 \text{ MPa from ABAQUS}$

$$\lambda = \sqrt{\frac{f_{yT}}{f_{odT}}} = \sqrt{\frac{667}{608}} = 1.047 > 0.55$$

$$P_{nT} = 51x667\left(1 - 0.31\left(\frac{608}{667}\right)^{0.4}\right)\left(\frac{608}{667}\right)^{0.58} = 22.6 \text{ kN}$$

Sample Calculations Based on Equation 6.11 at 800°C

$\lambda < 0.43 \qquad P_{nT} = Af_{nT} = Af_{yT}$

$\lambda \geq 0.43 \qquad P_{nT} = Af_{nT} = Af_{yT}\left(1 - 0.37\left(\frac{f_{odT}}{f_{yT}}\right)^{0.31}\right)\left(\frac{f_{odT}}{f_{yT}}\right)^{0.58}$

Where, $\quad \lambda = \sqrt{\dfrac{f_{yT}}{f_{odT}}}$

$A = 51 \text{ mm}^2$

$f_{yT} = 27 \text{ MPa}$

$f_{odT} = 55 \text{ MPa from ABAQUS}$

$\lambda = \sqrt{\dfrac{f_{yT}}{f_{odT}}} = \sqrt{\dfrac{27}{55}} = 0.7 > 0.43$

$P_{nT} = 51 x 27\left(1 - 0.37\left(\dfrac{55}{27}\right)^{0.31}\right)\left(\dfrac{55}{27}\right)^{0.58} = 1.12 \text{ kN}$

REFERENCES

Ala-Outinen and Myllymaki, J. (1995) The Local Buckling of RHS members at Elevated Temperatures, Technical Research Centre of Finland, Espoo

American Iron and Steel Institute (AISI) (1996) Specification for the Design of Cold-Formed Steel Structural Members, Washington DC, USA.

American Iron and Steel Institute (AISI) (2004), Specification for the Design of Cold-Formed Steel Structural Members, American Iron and Steel Institute, Washington, D.C.

American Iron and Steel Institute. (2003). Cold-Formed Steel Design. Retrieved July 18, 2003, from   http://www.steel.org/construction/design/gallery

BSI (1990a), British Standard, BS 5950, Code of Practice for Design of Cold-formed Thin gauge Sections, Structural Use of Steelwork in Building, Part 5, London, UK

BSI (1990b), British Standard, BS 5950, Code of Practice for Fire Resistance Design, Structural Use of Steelwork in Building, Part 8, London, UK.

Buchanan, A.H. (2001), Structural Design for Fire Safety, John Wiley & Sons, New York.

Callister, W.D. (2000). Materials and science and engineering, John Wiley & Sons, USA.

Camotim, D., Silvestre, N. and Dinis, P.B., (2005), Numerical analysis of cold-formed steel members, Journal of Steel Structures, pp. 63-78.

Chen, J. and Young, B. (2004) Mechanical Properties of Cold-formed Steel at Elevated Temperatures, Proceeding of Seventeenth International Speciality

Conference on Cold-formed Steel Structures, University of Missouri-Rolla, Orlando, Florida, USA, pp. 437-465

Chen, J. and Young, B. (2006) Stress–strain curves for stainless steel at elevated temperatures, Engineering Structures, Vol. 28, Issue 2, pp. 229-239

Collapse. (2003). September 11 Twin Towers Memorial Photos Videos & News Archive of the WTC Attack. Retrieved July 18, 2003 from http://www.twin-towers.net/collapse.htm

Davies, J. M. (2000) Recent Research Advances in Cold-formed Steel Structures, Journal of Constructional Steel Research, Vol. 55, No. 1-3, pp. 267-288.

Davies, J. M. and Jiang, C. (1998) Design for Distortional Buckling, Journal of Constructional Steel Research, Vol. 46, No. 1-3, 6 pp. 174-175.

Davies, J.M. and Jiang, C. (1996) Design of Thin-walled Columns for Distortional Buckling, Proceedings of the 2nd International Conference on Coupled Instabilities in Metal Structures, Liege. London: Imperial College Press, pp. 141-148

Dubina, D. and Ungureanu, V. (2002), Effect of Imperfections on Numerical Simulation of Instability Behaviour of Cold-formed Steel Members, Thin-Walled Structures, 40(3):239-262.

Eurocode 3 (1996) CEN ENV 1993-1-2, Design of steel structures, General rules, Structural Fire Design, Brussels.

Eurocode 3 (2001) CEN ENV 1993-1-2, Design of steel structures, General rules, Structural Fire Design, Brussels.

Eurocode 3: (1996) CEN ENV 1993-1-3 Design of Steel Structures, General rules-Supplementary rules for Cold-formed Thin gauge Members and Sheeting, Brussels.

Feng, M., Wang, Y. C. and. Davies J. M. (2003a) Structural Behaviour of Cold-formed Thin-walled Short Steel Channel Columns at Elevated Temperatures, Part 1: Experiments, Thin-Walled Structures, Vol. 41, No. 6, pp. 543-570.

Feng, M., Wang, Y.C. and Davies, J.M. (2003b) Structural Behaviour of Cold-formed Thin-walled Short Steel Channel Columns at Elevated Temperatures. Part 2: Design Calculations and Numerical Analysis, Thin-Walled Structures, Vol. 41, No. 6, pp. 571-594.

Feng, M., Wang, Y.C. and Davies, J.M. (2004) A Numerical Imperfection Sensitivity Study of Cold-formed Thin-walled Tabular Steel Columns at Uniform Elevated Temperatures, Thin-Walled Structures, Vol. 42, pp. 533-555.

Gardner, L. and nethercot, D.A. (2006) Structural stainless steel design: A New Approach, The Structural Engineer, Vol. 82, Issue 21, pp. 21-28.

Gerlich, J.T. (1995) Design of Load Bearing Light Steel Frame Walls for Fire Resistance, Fire Engineering Research Report 95/3, School of Engineering, University of Canterbury, Christchurch, NZ

Hancock, G. J. (2003) Cold-formed Steel Structures, Journal of Constructional Steel Research, Vol. 59, No. 4, pp. 473-487.

Hancock, G. J. (1998) Design of Cold-Formed Steel Structures, Australian Institute of Steel Construction, 3rd Edition, Sydney, NSW, Australia

Hancock, G. J. and Rogers C. A. (1998) Design of Cold-Formed Steel Structures of High Strength Steel, Journal of Constructional Steel Research, Vol. 46, No. 1-3, 6 pp. 167-168.

Hancock, G.J. (1985) Distortional Buckling of Steel Storage Rack Columns, Journal of Structural Engineering ASCE, Vol. 111, pp. 2770-2783.

Hancock, G.J., Young, B. and Bernard, E.S. (1994) Strength Design Curves for

Thin-walled Sections Undergoing Distortional Buckling, Journal of Constructional Steel Research, Vol. 31, No. 2-3, pp. 169-186.

Hibbitt, Karlsson & Sorensen, Inc. (2002), ABAQUS/Standard User's Manual, Version 6.1.

ISO 834-1 (1999), Fire-Resistance Tests-Elements of Building construction, Part 1-General Requirements, International Organisation for Standardisation, Switzerland.

Kaitila, O. (2002) Imperfection sensitivity analysis of lipped channel columns at high temperatures, Journal of Constructional Steel Research, Volume 58, Issue 3, pp. 333-351

Kesti, J. (2000) Local and Distortional Buckling of Perforated Steel Wall Studs, Laboratory of Steel Structures Publications 19, Helsinki University of Technology, Finland.

Kesti, J. and Davies, J.M. (1999) Local and Distortional Buckling of Thin-walled Short Columns, Thin-Walled Structures, Vol. 34, No. 2, pp. 115-134.

Klippstein, K.H. (1978) Strength of Cold-formed Steel Studs Exposed to Fire, Int Spec Conference, 4th, St Louis, Mo, University of Montana, Rolla, Mo, US, pp 513-555

Kwon, Y.B. and Hancock, G.J. (1992b). "Design of Channels Against Distortional Buckling", Research Report no. R660, University of Sydney, Sydney, Australia

Kwon, Y. B. and Hancock, G. J. (1993) Post-Buckling Analysis of Thin-walled Channel Sections Undergoing Local and Distortional buckling, Computers & Structures, Vol. 49, No. 3, pp. 507-516.

Kwon, Y.B., and Hancock, G.J. (1992a) Strength Tests of Cold-Formed Channel Sections undergoing Local and Distortional Buckling, Journal of Structural Engineering, ASCE, pp. 1786 – 1803.

Lau, S. C. W. and Hancock, G. J. (1987) Distortional Buckling Formulas for Channel Column, Journal of Structural Engineering, Vol. 113, pp. 1063-1078.

Lau, S. C. W. and Hancock, G. J. (1988) Distortional Buckling Tests of Cold-formed Channel Sections, Ninth International Speciality Conference on Cold-formed Steel Structures, pp. 45-73.

Lau, S. C. W. and Hancock, G. J. (1990) Inelastic Buckling of Channel Columns in the Distortional Mode, Thin-Walled Structures, Vol. 10, No. 1, pp. 59-84.

Lecce, M. and Rasmussen, K. (2004) Experimental Investigation of Distortional Buckling of Cold-formed Stainless Steel Sections, Proceeding of Seventeenth International Speciality Conference on Cold-formed Steel Structures, University of Missouri-Rolla, Orlando, Florida, USA, pp. 437-465

Lee, J., (2004), Local Buckling Behaviour and Design of Cold-Formed Steel Compression Members at Elevated Temperatures, PhD thesis, Queensland University of Technology, Brisbane, Australia.

Lee, J., Mahendran, M. and Makelainen, P. (2003) Prediction of Mechanical Properties of Light Gauge Steels at Elevated Temperatures, Journal of Construction Steel Research, pp. 1517-1532

Macadam, J. N. Brockenbrough, R. L. LaBoube, R. A. Pekoz. T. and Schneider, E. J. (1988) Low-Strain-Hardening Ductile Steel Cold-formed Members, Ninth International Speciality Conference on Cold-formed Steel Structures, pp. 459-488

Mistakidis, E.S. (1999)Evaluation of the Total Ductilityin Steel Structures through a Nonconvex Energy Optimization Approach, Journal of Engineering Structures, pp. 810-822

Narayanan, S. and Mahendran, M. (2002) Ultimate Capacity of Innovative Cold-formed Steel Columns, Journal of Constructional Steel Research, Vol. 59, pp. 489-508

North American Specification, NAS (2001) specification for the Design of Cold-formed Steel Structural Members, North American Cold-formed Steel Specification, American Iron and Steel Institute, Washington, D.C.

Olawale, A.O. and Plank R.J. (1988), The Collapse Analysis of Steel Columns in Fire Using a Finite strip Method, International Journal for Numerical Methods in Engineering, 26, 2755-2764.

Outinen, J. (1999) Mechanical properties of structural steels at elevated temperatures, Licentiate Thesis, Helsinki University of Technology, Finland

Outinen, J. and Makelainen, P. (2001a) Effect of High Temperature on Mechanical Properties of Cold-formed Structural Steel, Tubular Structures IX, Proceeding of the Ninth International Conference on Tubular Structures, Dusseldorf, Germany, pp. 439-444

Outinen, J. Kaitila, O. and Makelainen, P. (2000) A Study for the Development of the Design of Steel Structures in Fire Conditions, First International Workshop of Structures in Fire, Copenhagen, Denmark

Papangelis, J.P. and Hancock, G.J. (2000), THIN-WALL 2.0, The University of Sydney, Sydney, Australia.

Pekoz T. (1999) Possible Future Developments in the Design and Application of Cold-formed Steel, Proceeding of the 4th Int. Conf. Light-weight Steel and Aluminium Structures. Espoo, Finland

Ramberg, W. and Osgood, W.R. (1943) Description of Stress-strain Curves by Three Parameters, NACA Technical Note 902.

Ranby, A. (1998) Structural Fire Design of Thin-walled Steel Sections, Journal of Constructional Steel Research, Vol. 46, No. 1-3, 6 pp. 303-304.

Rasmessen, K.J.R. and Hancock, G.J. (1989) Compression Tests of Welded Channel section Columns, Journal of Structural Engineering, ASCE; 115 pp. 789-808

Rhodes, J. and Harvey, J. M. (1977), Interaction Behaviour of Plain Channel Columns under Concentric or Eccentric Loading, Preliminary Report, Stability of Steel Structures, Liege.

Robertson, A. (1925), Selected Engineering Papers No. 28, Institution Civil Eningeers, 1925.

Schafer, B.W. (1997) Cold-formed Steel Behaviour and Design: Analytical and Numerical Modelling of Elements and Members with Longitudinal Stiffeners, PhD Dissertation, Cornell University, Ithaca, N.Y.

Schafer, B.W. (2002) CUFSM Software Online home www.ce.jhu.edu/bschafer/cufsm

Schafer, B.W. (2000) Distortional Buckling of Cold-formed Steel Columns: Final Report (Online). Available: http:// www.ce.jhu.edu/bschafer/dist_columns.htm

Schafer, B.W. (2002) Local, Distortional and Euler Buckling of Thin-walled Columns, Journal of Structural Engineering, Vol. 128(3), pp. 289-299.

Schafer, B.W. and Pekoz, T. (1998) Computational Modelling of Cold-formed Steel: Characterising Geometric Imperfections and Residual Stresses, Journal of Constructional Steel Research, Vol. 47, pp. 193-210

Schafer, B.W. and Pekoz, T. (1998b) Direct Strength Prediction of Cold-formed Steel Members using Numerical Elastic Buckling Solutions, Proceedings of the Fourteenth International Specialty Conference on Cold-formed Steel Structures, Missouri, USA, 137-144.

Schafer, B.W. and Pekoz, T. (1999) Laterally Braced Cold-formed Steel Flexural Members with Edge Stiffened Flanges, Journal of Structural Engineering ASCE, Vol. 125, pp. 118-127

Schaefer, B.W., (2004), Residual Stresses in Cold-formed Steel Members, E-mail Communication

Schaefer, B.W., (2006), Distortional buckling of Cold-formed Steel Members, E-mail Communication

Sidey, M.P. and Teague, D.P. (1988) Elevated Temperature Data for Structural Grades of Galvanised Steel, British Steel (Welsh Laboratories) Report

Sivakumaran, K.S. and Rahman, N.A. (1998), A Finite Element Analysis Model for the Behaviour of Cold-formed Steel Members, Thin-walled Structures, 31, 305-324.

SNZ (1992), Code of Practice for General Structural Design and Design Loadings for Buildings, Standards New Zealand, Wellington, New Zealand.

Standards Australia , SA (1998), AS 4100, Steel Structures, Sydney, Australia.

Standards Australia, SA (1996), AS/NZS 4600 Cold-formed Steel Structures, Sydney, Australia.

Standards Australia, (SA, 2003-Draft), AS/NZS 4600 Cold-formed Steel Structures, Sydney, Australia.

Standards Australia (SA) (1991), AS 1391-1991, Methods for Tensile Testing of Metal, Sydney, Australia.

Standards Australia (1979), AS 2291-1979, Methods for Tensile Testing of Metals at Elevated Temperatures, NSW, Australia

Steel Construction Institute (SCI) (1993), Building Design Using Cold Formed Steel Sections: Fire Protection, Silwood Park, Ascot

Teng, J.G., Yao, J. and Zhao, Y. (2003) Distortional Buckling of Channel Beam-Columns, Thin-Walled Structures, Vol. 41, No. 7, pp. 595-617.

Thomasson, P. (1978) Thin-walled C-shaped Panels in Axial Compression, Swedish Council for Building Research, Stockholm, Sweden

Tide, R.H.R. (1998), Integrity of Structural Steel After Exposure to Fire, Engineering Journal, pp. 26-38.

Valente, J.C. and Neves, I.C. (1999), Fire Resistance of Steel Columns with Elastically Restrained Axial Elongation and Bending, Journal of Constructional Steel Research, 52(3), pp. 319-331.

Venkataramaiah, K. R. and Roorda, J. (1982) Analysis of Local Plate Buckling Experimental Data, Proceeding of Sixth International Speciality Conference on Cold-formed Steel Structures, pp. 45-74.

Walker, A.C. (1975), Design and Analysis of Cold-formed Section, Halsted Press, New York.

Yan, J. and Young, B. (2003) Design of Cold-formed Steel Channels Columns with Complex Stiffeners using Direct Strength Method, Proceeding of International Conference on Advances in Structures ASSCCA, Vol. 1, pp. 289-294.

Yang, D. and Hancock, G.J. (2003) Compression Tests of Cold-reduced High Strength Steel Channel Columns Failing in the Distortional Mode, Proceeding of International Conference on Advances in Structures ASSCCA, Vol. 1, pp. 303-307.

Young, B. and Hancock, G. J. (2003) Compression Tests of Channels with Inclined Simple Edge Stiffeners, Journal of Structural Engineering, Vol. 129, No. 10 pp. 1403-1411.

Young, B. and Rasmussen, K.J.R. (1999) Behaviour of Cold-formed Singly Symmetric Columns, Thin-Walled Structures, Vol. 33, No. 2, pp. 83-102.

Young, B. and Rasmussen, K.J.R. (1995) Compression Tests of Fixed-end and Pin-end Cold-Formed Lipped Channels, Research Report R715, School of Civil and Mining Engineering, University of Sydney, Australia.

Young, B. and Yan, J. (2000), Finite Element Analysis of Cold-formed Channel Columns, Proceedings of the Fifteenth International Specialty Conference on Cold-formed Steel Structures, Missouri, USA, 281-305.

Young, B. and Yan, J. (2004) Design of Cold-formed Steel Channels Columns with Complex Stiffeners using Direct Strength Method, Journal of Structural Engineering, Vol. 130 , Issue 11, pp.1756-1763

Yu, W. W. (2000), Cold-Formed Steel Design, John Wiley & Sons, New York, Third edition

Von Karman, T., Sechler, E.E., and Donnell, L.H. (1932), The Strength of Thin Plates in Compression, Transactions ASME, 54.

Winter, G. (1947), Strength of Thin Steel Compression Flanges, Transactions ASCE, 112:527-554.